Biogeochemical significance and biomarker potential of novel glycerolipids and respiratory quinones in the marine environment

Dissertation
zur Erlangung des Doktorgrades
der Naturwissenschaften
- Dr. rer. nat. -

Am Fachbereich Geowissenschaften
der Universität Bremen

vorgelegt von

Kevin W. Becker

Bremen
Juni 2015

Die vorliegende Arbeit wurde in der Zeit von November 2011 bis Juni 2015 in der Arbeitsgruppe Organische Geochemie am MARUM – Zentrum für Marine Umweltwissenschaften und dem Fachbereich Geowissenschaften der Universität Bremen angefertigt.

1. Gutachter: Prof. Dr. Kai-Uwe Hinrichs
2. Gutachter: Prof. Dr. Ann Pearson

Tag des Promotionskolloquiums: 13. August 2015

Contents

Abstract

Microorganisms catalyze processes which shape the chemistry of the biosphere, drive global element cycles, and ultimately influence the composition of Earth's surface and interior on geological timescales. In the mid-1980's, when the study of genetic material in environmental samples started, metagenomics revealed that the composition of microbial communities in the natural world is far more complex than culturing methods had suggested. Since then, the number of unexplored species has been continuously increasing, but to date our understanding of their physiology and ecology has remained fragmentary. The investigation of microbial membrane lipids provides an alternative culture-independent route of investigation to study microbial life in the environment, as membrane lipids carry taxonomic information on source organisms and in addition also reflect their adaptation to the habitat. The latter is due to the fact that lipids play an important role in the regulation of membrane fluidity in response to external pressure, temperature, and pH. Moreover, certain membrane lipids have fundamental physiological functions; for example respiratory quinones facilitate cellular electron transport processes. The goals of this PhD project were to *(i)* develop advanced chromatographic methods for lipid analysis, *(ii)* to expand the portfolio of lipid biomarkers for the characterization of microbial life in marine environments, and *(iii)* to investigate the proxy potential of novel lipids and respiratory quinones as chemotaxonomic markers and indicator for redox conditions.

The systematic work on analytical protocols resulted in a new chromatographic method which allows not only detection of a series of novel lipids but also better separation of established biomarker lipids (Chapter III). The improved method for lipid analysis is based on ultra-high performance liquid chromatography (UHPLC) multiple stage mass spectrometry (MS^n). Compared to conventional HPLC protocols it provides superior chromatographic separation of archaeal and bacterial glycerol dialkyl glycerol tetraethers (GDGT) core lipids: the previously co-eluting isomers of GDGTs can now be separated, and the analytical window has been extended to encompass the whole spectrum of ether core lipids found in environmental samples. The novel protocol further allows to determine the three organic geochemical sea surface temperature (SST) proxies $U^{K'}_{37}$ (based on long chain alkenones from phytoplanktonic haptophytes), LDI (based on long chain diols from phytoplanktonic eustigmatophytes) and TEX_{86} (based on GDGTs from planktonic archaea) with one single HPLC analysis. The new protocol does not only reduce analysis time and costs, but also achieves a one order of magnitude increase in sensitivity compared to the commonly applied methods. Application of the new analytical protocol to a sediment core from the Sea of Marmara revealed significant discrepancies in the SST reconstructed from the three different proxies, which might be related to differences in the ecology of the signal producers (Chapter IV). This finding underlines the need for multiproxy approaches in order to arrive at robust estimates of paleo SST. Furthermore, analysis of diverse environmental samples and identification of previously unresolved and unknown compounds lead to the discovery of fatty acid

substituted isoprenoid GDGTs (Chapter V). These compounds are likely of diagenetic origin rather than biologically produced and their abundance in marine sediments appears to depend on reactant availability as well as hydrolytic conditions.

In order to study benthic archaea and their life strategies in the deep subseafloor, a suite of new analytical protocols, which had been developed both within this PhD project and by colleagues, were applied to investigate core and intact polar lipids (IPLs) in concert with metagenomics and geochemistry at various sites in the Mediterranean, Marmara and Black Sea. This approach allowed us to identify distinct microbial communities in the hostile environment of the deep-sea hypersaline anoxic Discovery Basin in the Eastern Mediterranean Sea (Chapter VI). At the brine-seawater interface, the detection of intact polar and polyunsaturated archaeols that are only known to occur in extremely halophilic and methanogenic archaea as well as thaumarchaeal-specific intact GDGTs indicate an active participation of this community in carbon, and nitrogen cycling. Other diagnostic lipids include phospholipids containing diether and ether/ester core lipids, which are associated with sulfate-reducing bacteria. Several intact membrane lipids have been identified for the first time in environmental samples, such as (*N*-acetyl)-glucosamine-monoglycosyl and *N*-acetylglucosamine archaeol, which are associated with archaeal methanogens belonging to *Methanohalophilus*. We further identified for the first time intact forms of hybrid isoprenoid/branched GDGTs, lipids that combine archaeal and bacterial traits. Their biological sources remain unknown, while the stable carbon isotopic composition indicates chemolithoautotrophic growth of their producers.

The new analytical methods revealed a widespread occurrence of respiratory quinones in environmental samples and triggered our interest in their proxy potential. To examine their utility as chemotaxonomic markers for archaea, the quinone profiles of 25 cultivated strains including members of three different phyla *Crenarchaeota*, *Euryarchaeota*, and *Thaumarchaeota* were investigated (Chapter VII). The results demonstrate that the quinone inventories can be used to distinguish environmentally relevant archaea as well as metabolisms. For example, saturated and monounsaturated menaquinones containing side chains with six isoprenoid units are diagnostic for *Thaumarchaeota*, while thiophene-bearing quinones are specific for *Sulfolobales* and methanophenazines, which are functional quinone analogs, only occur in the *Methanosarcinales*. The obtained data have also implications for the evolution of respiratory quinone systems of archaea and bacteria and indicate that the highly divergent quinone distribution in *Euryarchaeota* may result from a combination of vertical inheritance, lateral gene transfer and gene loss. To showcase the utility of environmental quinone profiling, we studied the distribution of respiratory quinones and membrane lipids in a sequence of water column and sediment samples in the Black Sea (Chapter VIII). The Black Sea is separated into oxic, suboxic, and euxinic zones, each characterized by different biogeochemical processes and by distinct microbial communities, which respire through a succession of redox reactions. Depth distributions of diagnostic quinones and IPLs were well correlated with the zonation of microbial processes, demonstrating that the combined biomarker approach provides a valuable tool for tracking the abundances and metabolic processes of bacterial, archaeal, and eukaryotal organisms. Thus, the quinone composition carries valuable information on microbes involved in redox cycling of carbon, sulfur and nitrogen in the water column and sediments.

Zusammenfassung

Mikroorganismen spielen eine Schlüsselrolle für die Steuerung der globalen Stoffkreisläufe und katalysieren Prozesse, die grundlegend die Zusammensetzung der Erdoberfläche sowie des Erdinneren über geologische Zeiträume verändern. Mitte der 1980 Jahre, als man begann genetisches Material in Umweltproben zu untersuchen, haben metagenomische Studien gezeigt, dass die Zusammensetzung von Mikroorganismen in der Umwelt viel komplexer ist als mit Hilfe von kulturabhängigen Methoden angenommen wurde. Seitdem ist die Anzahl unerforschter Spezies stetig gestiegen, doch ihre Physiologie und Ökologie ist weitgehend unbekannt. Eine alternative kulturunabhängige Methode ist die Untersuchung mikrobieller Membranlipide, da sie zum einen taxonomischen Bezug zu ihren produzierenden Organismen besitzen und zum anderen die Adaption von Organismen an ihren Lebensraum widerspiegeln. Die Adaption von Membranlipiden spielt eine wichtige Rolle bei der Regulierung von Membranfluidität. So passen Organismen ihre Lipidzusammensetzung in Abhängigkeit von äußerem Druck, Temperatur und pH-Wert an, um eine definierte Fluidität der Membran aufrecht zu erhalten. Des Weiteren haben bestimmte Lipide grundlegende physiologische Funktionen. So ermöglichen z.B. respiratorische Chinone den Transport von Elektronen in der Atmungskette. Ziele dieser Dissertation waren *(i)* die Weiterentwicklung chromatographischer Methoden für die Analyse mikrobieller Lipide, *(ii)* die Identifizierung von neuen Lipidbiomarkern, die für die Charakterisierung von mikrobiellem Leben in marinen Lebensräumen geeignet sind, und *(iii)* das Untersuchen des Proxypotentials von neuentdeckten Lipiden und respiratorischer Chinone als chemotaxonomische Marker und Indikator für Redoxbedingungen.

Die systematische Arbeit an Analyseprotokollen resultierte in einer neuen chromatographischen Methode, die nicht nur die Detektion von neuen Lipiden ermöglicht, sondern auch eine bessere Trennung etablierter Biomarkerlipide (Kapitel III). Die verbesserte Methode zur Lipidanalyse basiert auf Ultra-Hochleistungs-Flüssigkeit-Chromatographie (UHPLC) gekoppelt mit Mehrfach-Massenspektrometrie (MS^n). Verglichen mit den konventionellen HPLC Protokollen ermöglicht sie deutlich verbesserte chromatographische Trennung von archaeellen und bakteriellen Glyceroldialkylglyceroltetraether (GDGT) Kernlipiden: die bisher koeluierenden Isomere von GDGTs können nun getrennt werden, und das analytische Fenster wurde um das gesamte Spektrum der Etherkernlipide, die in Umweltproben zu finden sind, erweitert. Das neue Protokoll ermöglicht außerdem, drei organisch-geochemische Proxies für die Rekonstruktion von Oberflächenwassertemperatur (SST) $U^{K'}_{37}$ (basierend auf langkettigen Alkenonen von phytoplanktonischen Haptophyten), LDI (basierend auf langkettigen Diolen von phytoplanktonischen Eustigmatophyten) und TEX_{86} (basierend auf GDGTs von planktonischen Archaeen) in einer einzigen HPLC-Analyse zu bestimmen. Das neue Protokoll reduziert dabei nicht nur die Analysezeit, sondern erhöht auch die Sensitivität um eine Größenordnung verglichen mit der herkömmlichen Methode. Die Anwendung des neuen analytischen Protokolls auf Proben eines Sedimentkerns vom Marmara Meer zeigte signifikante Unterschiede in der SST, die mithilfe der drei verschiedenen Proxies rekonstruiert wurde, was auf

Unterschiede in der Ökologie der lipidproduzierenden Organismen zurückzuführen ist (Kapitel IV). Diese Erkenntnis macht die Notwendigkeit von Multiproxy-Ansätzen für verlässliche Bestimmungen der Paläo-SST Proxies deutlich. Darüber hinaus führte die Analyse von diversen Umweltproben und die Identifizierung von bisher unbekannten Komponenten zur Entdeckung von fettsäuresubstituierten isoprenoiden GDGTs (Kapitel V). Diese Komponenten sind vermutlich diagenetischen und nicht biologischen Ursprungs, und ihre Häufigkeit in marinen Sedimenten scheint von der Verfügbarkeit von Reaktanten und hydrolytischen Bedingungen abzuhängen.

Um benthische Archaeen und ihre Überlebensstrategien im Meeresgrund der Tiefsee zu untersuchen, wurde eine Reihe von neuen analytischen Protokollen, die im Rahmen dieser Doktorarbeit und von Kollegen entwickelt worden sind, angewendet, um sowohl Kernlipide als auch intakte polare Lipide (IPLs) in Kombination mit Metagenomik und Geochemie an unterschiedlichen Standorten im Mittelmeer, Marmara Meer und dem Schwarzen Meer zu untersuchen. Dieser Ansatz ermöglichte es uns, unterschiedliche mikrobielle Gemeinschaften im lebensfeindlichen hypersalinen und anoxischen Tiefseebecken des Discovery Basin im westlichen Mittelmeer zu identifizieren (Kapitel VI). Die Identifizierung von intakten polaren und vielfach ungesättigten Archaeolen, die bisher nur in extrem halophilen und methanogenen Archaeen nachgewiesen wurden, sowie *Thaumarchaeen*-spezifischen intakte GDGTs an der Grenzfläche zwischen dem hypersalinen und normal salinen Meerwasser, deuten auf eine aktive Rolle dieser Mikroorganismen am Kohlenstoff- und Stickstoffkreislauf hin. Weitere diagnostische Lipide umfassten Phospholipid-diether und acylether, die mit sulfatreduzierenden Bakterien assoziiert sind. Mehrere intakte Membranlipide wurden zum ersten Mal in Umweltproben identifiziert, wie zum Beispiel (*N*-acetyl)-glucosamine-monoglycosyl und *N*-acetylglucosamine Archaeol, welche mit methanogenen Archaeen der Gruppe *Methanohalophilus* assoziiert sind. Wir haben außerdem zum ersten Mal intakte Formen von hybriden isoprenoid/verzweigten GDGTs identifiziert; diese Lipide kombinieren archaeelle und bakterielle Eigenschaften. Obgleich ihre biologischen Ursprünge noch unbekannt sind, weist ihre isotopische Zusammensetzung des Kohlenstoffs auf chemolithoautotrophisches Wachstum der Quellorganismen hin.

Die neuen analytischen Methoden zeigten ein weitverbreitetes Vorkommen von respiratorischen Chinonen in Umweltproben auf und weckten unser Interesse an ihrer möglichen Verwendbarkeit als Proxies. Um ihre Eignung als chemotaxonomische Marker für Archaeen zu überprüfen, wurden die Chinonprofile von 25 kultivierten Stämmen inklusive Vertretern der Phyla *Crenarchaeota*, *Euryarchaeota*, und *Thaumarchaeota* untersucht (Kapitel VII). Die Ergebnisse zeigen, dass die Chinonzusammensetzung genutzt werden kann, um umweltrelevante Archaeen und Metabolismen zu unterscheiden. Zum Beispiel sind gesättigte und einfachungesättigte Menachinone, die sechs Isoprenoideinheiten in ihrer Seitenkette enthalten, spezifisch für *Thaumarchaeota*, während Thiophen-enthaltene Chinone spezifisch für *Sulfolobales* sind und *Methanophenazine*, welche funktionale Chinonanaloge darstellen, nur in *Methanosarcinales* auftreten. Die gesammelten Daten weisen auch Implikationen für die Evolution des respirativen Chinonsystems von Archaeen und Bakterien auf und deuten zum Beispiel darauf hin, dass die hoch divergente Chinonverteilung in *Euryarchaeota* eine Folge aus einer Kombination von Vererbung, lateralem Gentransfer und Genverlust ist. Um die Nützlichkeit von Chinonprofilen für die Charakterisierung von mikrobieller Aktivität zu demonstrieren, haben wir die Verteilung von respiratorischen Chinonen und Membranlipiden in einer

Sequenz der Wassersäule und Sedimentproben im Schwarzen Meer untersucht (Kapitel VIII). Das Schwarze Meer ist in oxische, suboxische, und euxinische Zonen unterteilt, die sich jeweils durch unterschiedliche biogeochemische Prozesse und mikrobieller Gemeinschaften auszeichnen. Die Tiefenverteilung von spezifischen Chinonen und IPLs korrelierten mit der Zonierung der mikrobiellen Prozesse, was zeigt, dass der kombinierte Biomarkeransatz es ermöglicht, die Verteilung und metabolische Aktivität der bakteriellen, archaeellen, und eukaryotischen Organismen aufzuklären. Somit enthält die Chinonzusammensetzung wichtige Informationen über Mikroorganismen, die in biogeochemische Kreisläufe von Kohlenstoff, Schwefel und Stickstoff in der Wassersäule und im Sediment involviert sind.

Acknowledgements

I am sincerely and immensely grateful to my supervisor Prof. Kai-Uwe Hinrichs. His unconditional support, guidance and inspiring ideas built the foundation for this thesis. Thank you for getting me started in science and letting me develop my own thoughts and ideas. I would also like to thank Prof. Ann Pearson for serving on my thesis committee and agreeing to review my thesis. I am really honored that you came the long way to attend my defense. Many thanks also to Prof. Wolfgang Bach and Dr. Jan-Hendrik Hehemann for joining my PhD committee.

A great part of the work would not have been possible without the support from Dr. Julius Lipp. I am deeply grateful for your unconditional helpfulness, great patience and for teaching me in the noble arts of liquid chromatography and mass spectrometry. I deeply thank Felix Elling for sharing countless ideas that significantly contributed to writing this thesis.

I particularly want to thank Drs. Verena Heuer and Marcus Elvert for the continuous support and answering countless questions throughout the years. I kindly thank Dr. Marcos Yoshiunaga, Dr. Frauke Schmidt, Dr. Martin Könneke, Dr. Lars Wörmer, Nadine Goldenstein, Jan Schröder, Miriam Sollich, Dr. Matthias Kellermann, Dr. Florence Schubotz, Thomas Evans, and Dr. Xiaolei Liu for sharing ideas, data, and extensive discussions that contributed to many projects of this thesis.

I am indebted to Birgit Schmincke, Xavi Prieto Moller, Jenny Wendt, Dr. Heidi Taubner, Evert Kramer, and Jessica Arndt for keeping the labs running smoothly and supporting all kinds of analyses that form the foundations of this thesis. Thank you to all the Hinrichs lab members that are not mentioned here for creating a wonderful and collaborative working atmosphere. I would also like to thank my student assistants Susanne Alfken, Tim Stoltmann, Nadine Smit, and Christopher Vogel who greatly supported my work.

I thank all my Bremen and non-Bremen friends for all the social distraction and continuous support.

I deeply thank my parents, Petra and Wolfhard, and my brother, Bennet, for unconditional support and encouragement and for inspiring me to prove my worth and to do my best whatever I do.

Jana, I sincerely thank you for all your love and for always inspiring, supporting, encouraging, entertaining, and helping me get through this sometimes strenuous time in the most positive way.

List of Abbreviations

1G	Monoglycosyl
2G	Diglycosyl
3G	Triglycosyl
m/z	Mass to charge ratio
AEG	Acyletherglycerol
Anammox	Anaerobic ammonium oxidation
ANME	Anaerobic methanotrophic archaea
AOA	Ammonia-oxidizing archaea
AOM	Anaerobic oxidation of methane
APCI	Atmospheric pressure chemical ionization
AR	Archaeol
B-GDGT	Branched glycerol dialkyl glycerol tetraether
BDGT	Butantriol dibiphytanyl glycerol tetraether
BDTQ	Benzodithiophenoquinone
BL	Betaine lipid
Cer	Ceramide (sphingosine)
ChQ	Chlorobiumquinone
CQ	Caldariellaquinone
DA	Dalton
DAG	Diacylglycerol
DCM	Dichloromethane
DEG	Dietherglycerol
deoxyG	Deoxyhexose
DHAB	Deep-sea hypersaline anoxic basin
DIC	Dissolved inorganic carbon
DMK	Demethylmenaquinone
DMMK	Dimethylmenaquinone
DPG	Diphosphatidylglycerol
EIC	Extracted ion chromatogram
ESI	Electrospray ionization
Ext-AR	Extended archaeol
FID	Flame ionization detector

GC ..... Gas chromatography
GDD ..... Glycerol dialkanol diether
GDGT ..... Glycerol dialkyl glycerol tetraether
GTGT ..... Glycerol trialkyl glycerol tetraether
HPH ..... Hexose-phosphohexose
HPLC ..... High performance liquid chromatography
IB-GDGT ..... Hybrid isoprenoid/branched glycerol dialkyl glycerol tetraether
IP-AR ..... Intact polar archaeol
IP-GDGT ..... Intact polar glycerol dibiphytanyl glycerol tetraether
IPL ..... Intact polar lipid
irMS ..... Isotope ratio mass spectrometry
LDI ..... Long chain diol index
Me-GDGT ..... Methylated glycerol dibiphytanyl glycerol tetraether
MeO-GDGT .... Methoxy glycerol dialkyl glycerol tetraether
MeOH ..... Methanol
MG-I/II ..... Marine Group I/II
MK ..... Menaquinone
MMK ..... Methylmenaquinone
MP ..... Methanophenazine
MS ..... Mass spectrometer/spectrometry
MS^1 ..... Primary order mass spectrometry stage
MS^2 ..... Secondary order mass spectrometry stage
MS^n ..... Higher order mass spectrometry stage
MTK ..... Methionaquinone
MUC ..... Multicore
NP ..... Normal phase
OB-GDGT ..... Overly branched glycerol dialkyl glycerol tetraether
OH-AR ..... Hydroxyarchaeol
OH-GDGT ..... Hydroxylated glycerol dibiphytanyl glycerol tetraether
OH-MP ..... Hydroxymethanophenazine
OL ..... Ornithine lipid
PC ..... Phosphatidylcholine
PDGT ..... Pentantriol dibiphytanyl glycerol tetraether
PDME ..... Phosphatidyldimethylethanolamine
PE ..... Phosphatidylethanolamine
PG ..... Phosphatidylglycerol
PH ..... Phosphohexose
PI ..... Phosphatidylinositol

PME ..... Phosphatidylmethylethanolamine
PQ ..... Plastoquinone
qToF-MS ..... Quadrupole time-of-flight mass spectrometer
RI ..... Ring index
RP ..... Reversed phase
SB-GDGT ..... Sparsely branched glycerol dialkyl glycerol tetraether
SQ ..... Sulfolobusquinone
SST ..... Sea surface temperature
TCA ..... Trichloroacetic acid
TEX_{86} ..... Tetraether index of tetraethers consisting of 86 carbon atoms
TEX_{86}^{H} ..... TEX index for high temperatures
TLE ..... Total lipid extract
TOC ..... Total organic carbon
$U_{37}^{K'}$ ..... Unsaturated Ketones with 37 carbon atoms
UHPLC ..... Ultra high performance liquid chromatography
Uns ..... Monounsaturated
UQ ..... Ubiquinone
VPDB ..... Vienna Pee Dee Belemnite

Chapter I

Introduction

I.1. Microbial life in the oceans

Microorganisms drive globally important biogeochemical cycles and they have shaped the elemental composition of Earth's surface environments and interior (see review by Falkowski et al., 2008). Within the marine carbon cycle, they are involved in both, a large fraction of primary production and turnover of organic carbon through mineralization processes. Thus, the oxygen we breathe is to a large extent produced by microbes, but they also play an important role for the regulation of greenhouse gases, such as CO_2 and CH_4, and are consequently involved in processes that drive climate at geological time scales. Microbial life on Earth has further adapted to a wide range of environments including some of the most hostile imaginable, exhibiting for example extreme pressures, temperatures, acidity and alkalinity, and limited energy and nutrient availability (e.g., Rothschild and Mancinelli, 2001; Pikuta et al., 2007). The introduction provides an overview about the importance of microbial life in natural environments and its role within carbon and nutrient cycling. Additionally, a detailed introduction on the role of microbial membrane lipids as biological marker molecules is presented as well as the research approaches to study present and past microbial activity based on lipid biomarkers. Finally, the utilized analytical methods are introduced.

I.1.1. The three domains of life

All of life on Earth is divided into the three domains: *Bacteria*, *Archaea* and *Eukarya* (Figure I.2; Woese et al., 1990). The classification is based on the relatedness of small subunit ribosomal RNA (SSU rRNA), which occurs in all organisms (e.g., Woese et al., 1990; Pace, 1997). The current view of evolutionary relationships was established

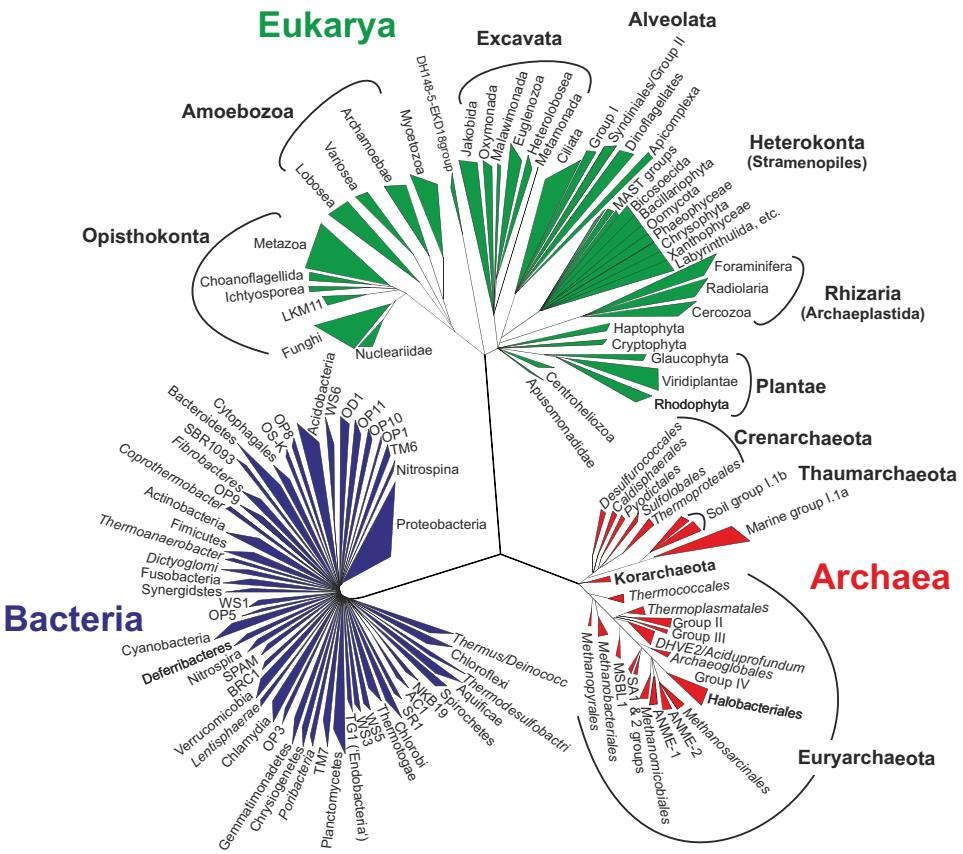

Figure I.1. Schematic and simplified phylogenetic tree of life based on SSU rRNA and other molecular evidence. The bacterial domain is colored in blue, the eukaryotal in green and the archaeal in red. Figure adapted from López-García and Moreira (2008).

by (Woese and Fox, 1977), who first recognized the *Archaea* as a separate domain; traditionally, archaea had been classified as archaebacteria within the *Bacteria*. Despite their visual similarity, the archaea and bacteria are not closely related. Instead, it appears that archaea possess genes and some metabolic pathways that are more closely related to eukarya (Woese et al., 1990). Recently, the identification and genomic characterization of a novel archaeal group that shares a common ancestry with eukaryotes by Spang et al. (2015) further "bridged the gap" between archaea and eukaryotes. However, one of the most pronounced differences between the domains is the high metabolic versatility of archaea and bacteria compared to eukaryotes. Their outstanding metabolic properties include the use of inorganic electron donors for energy generation, anaerobic growth, and the fixation of molecular nitrogen, whereas in eukaryotes these properties are either restricted to a few species or completely lacking. Today's microbial diversity results from almost 4 billion years of evolution (Madigan et al., 2011) and the development of diverse metabolic strategies allows microbes to not only survive but to grow and thrive under a large range of environmental conditions, including environmental extremes, such as low (<5 °C) and high (>50 °C) temperatures, acidic or alkaline pH values, high

salinities, energy limitation as well as high pressures that are present in the deep ocean and sediments (e.g., Mesbah and Wiegel, 2008). Particularly archaea have long been thought to be restricted to extreme environments due to their distinct physiologies, but since the early 1990s mesophilic archaea have been recognized to be an ubiquitous component of marine plankton (DeLong, 1992; Fuhrman et al., 1992; Karner et al., 2001) and they appear to be key players in the global nitrogen cycle and control nutrient levels in the ocean (e.g., Wuchter et al., 2006). The distinct physiologies of prokaryotes and their ubiquity in a wide range of habitats emphasizes their crucial role within global biogeochemical cycles.

I.1.2. Biogeochemical cycles in the ocean and sediments

> *The environment not only determines the conditions under which life exists, but the organisms influence the conditions prevailing in their environment. (Redfield, 1958)*

Euphotic zone. Oceans cover almost 70 % of the Earth's surface and host half of the global primary production (ca. 50 Pg C yr^{-1}; Falkowski, 1998; Field, 1998). Most of the organic carbon in the marine environment is produced by photosynthetic activity in the illuminated, upper 200 m of the water column by cyanobacteria (e.g., *Prochlorococcus*, *Synechococcus*) and eukaryotic algae (e.g., diatoms and coccolithophorids; e.g., DeLong, 2006; Boyd et al., 2010). Besides the oxygenic photolithotrophs, anoxygenic photolithotrophs and chemolithotrophs contribute 0.5 to 1.0 % to autotrophic inorganic carbon assimilation of the net primary productivity (Raven, 2009; Hügler and Sievert, 2011). Primary production is further strongly dependent on the availability of nutrients, such as nitrate and phosphorous, which are supplied for example by upwelling, bacterial nitrogen fixation, terrestrial input, and the decomposition of organic matter (cf. Arrigo, 2005). Although the organic carbon produced in the photic zone is mostly remineralized to CO_2 by aerobic heterotrophs (e.g., diverse *Proteobacteria*), a small portion (ca. 20 %) escapes respiration and is exported in the form of particulate and dissolved organic matter to the deep ocean (e.g., Ducklow, 1995).

Meso- and bathypelagic zones. In the deep waters below the photic zone, life is independent from sunlight. Thus, microbes living in this largest continuous habitat on Earth need alternative energy sources. We still have only limited knowledge about the microbial diversity and the response of microbes to changes in the distribution, composition, and flux of organic carbon in the deep ocean (Azam, 1998; Arístegui et al., 2009). It was generally assumed that the degradation of sinking organic matter from the

photic zone is the major microbial activity in the deep ocean, which is an important process for the re-supply of inorganic nutrients to the photic layer and the concomitant release of CO_2 (e.g., Vidal et al., 1999; Arístegui et al., 2005, 2009). However, more recent studies revealed evidence that planktonic *Crenarchaeota* belonging to the Marine Group I (MG-I) dominate prokaryotic cell numbers in the mesopelagic zone of the Pacific Ocean (Karner et al., 2001). They catalyze the first and rate-limiting step of nitrification, the oxidation of ammonia to nitrite, and are well adapted to the oligotrophic conditions commonly found in the open and deep ocean (Martens-Habbena et al., 2009; Stahl and de la Torre, 2012; Könneke et al., 2014). The most recent studies have affiliated MG-I *Crenarchaeota* with the *Thaumarchaeota*, a recently proposed novel phylum of the domain Archaea (Brochier-Armanet et al., 2008; Spang et al., 2010) and they have been found to be the predominant ammonium oxidizers in the marine environment (e.g., Schattenhofer et al., 2009) depicting their importance not only in nitrogen but also in carbon cycling (Herndl et al., 2005; Wuchter et al., 2006). However, their contribution to total biomass is generally small due to the small cell size of these organisms (Schattenhofer et al., 2009). Other ubiquitously occurring archaea in the oceans belong to the MG-II (Karner et al., 2001), but the function and metabolisms of these planktonic *Euryarchaeota* remain unknown due to their resistance against cultivation. Besides the ammonia oxidizing archaea (AOA), ammonium oxidizing bacteria (AOB) are abundant in the meso- and bathypelagic zones (cf. Hügler and Sievert, 2011). AOBs typically occur in association with nitrite oxidizing bacteria, providing their energy source (Abeliovich, 2006). Nitrite oxidation is the second step of the nitrification process, which is oxidation of nitrite to nitrate. Remarkably, this process results in the dissolution of carbonate in exchange for CO_2, which is they assimilate (Abeliovich, 2006).

Oxygen minimum zones. The mesopelagic waters may become anoxic if the flux of detrital organic matter and its subsequent decomposition exceeds the available quantity of dissolved oxygen, resulting in the formation of oxygen minimum zones (OMZ) between ca. 100-1000 m, which occur widespread in the modern oceans (Karstensen et al., 2008; Paulmier and Ruiz-Pino, 2009). It is assumed that these areas will significantly expand as a result of ocean warming and increased water column stratification (Keeling et al., 2010; Stramma et al., 2010), and thus OMZs have received increased attention during the last decade. Generally, two types of OMZ environments can be distinguished: *(i)* open ocean OMZs, which are located enclosed between oxygenated water layers and *(ii)* OMZs that are characterized by a transition from oxic to anoxic (euxinic) marine bottom waters. In the sulfidic waters, sulfur-oxidizing microorganisms, including anaerobic phototrophs, particularly *Chlorobiales*, can play important roles for element cycling, while they are absent from most open ocean OMZs (cf. Hügler and Sievert, 2011).

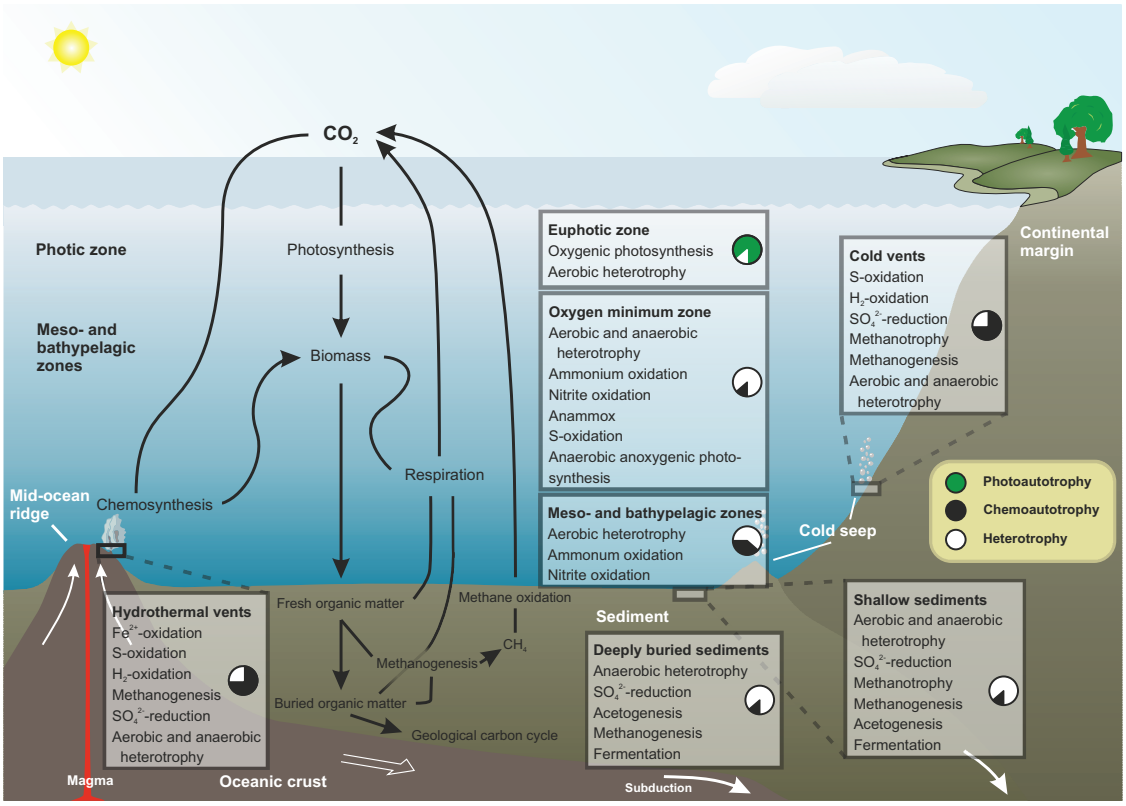

Figure I.2. Schematic diagram illustrating the major oceanic microbial habitats including the water body and different environments in the subseafloor as well as the major biogeochemical processes the microbes are mediating in each habitat. The importance of the major microbial processes is shown in the pie charts. Additionally, the major fluxes of the marine carbon cycle are shown. The largest fraction of organic carbon is produced by photosynthetic activity in the euphotic zone and is subsequently remineralized by heterotrophic activity while sinking with debris to the seabed. With increasing water depth, the importance of organic matter as carbon source is decreasing, whereas in the sediments organic matter is again the major carbon source. Ecosystems that rely predominantly on inorganic carbon and chemical energy sources, thus being independant of photosynthesis, are abundant in the deep ocean and occur for example at hydrothermal and cold vents. Figure modified after Bach et al. (2006), Jørgensen and Boetius (2007), Wefer (2010), Hügler and Sievert (2011), and Kellermann (2012).

Open ocean OMZs contain diverse communities of bacteria and archaea whose metabolisms control key steps in marine biogeochemical cycling and strong vertical oxygen gradients (oxyclines) structure biological assemblages and the associated processes (Wright et al., 2012). Similarly to the oxygenated deep waters, heterotrophic processes, i.e., the oxidation of sinking phototrophic organic matter by aerobic respiration and denitrification coupled to the concomitant release of CO_2, were thought to predominate in OMZs. However, extensive surveys of the microbial ecology in several of the ocean's OMZs revealed abundant and widespread chemoautotrophic assemblages that fix CO_2 rather than release it. Along the oxycline, microaerophilic assemblages, which include ammonia- and nitrite-oxidizing communities, and anaerobic communities

co-occur (Stewart et al., 2012). Particularly, AOA have been shown to be abundant at marine oxyclines (e.g, Coolen et al., 2007; Schouten et al., 2012; Hernández-Sánchez et al., 2014; Xie et al., 2014) and to dominate over AOB (e.g., Stewart et al., 2012). The community structure in the anoxic OMZ core is dominated by anaerobic heterotrophic and autotrophic organisms (Wright et al., 2012). The organic carbon mineralization occurs according to a defined order of terminal electron acceptors. The major autotrophic process is the anaerobic oxidation of ammonium (anammox) by a specific group of *Planctomycetes*, which may be responsible for the majority of nitrogen loss in OMZs (Kuypers et al., 2003; Dalsgaard et al., 2005; Kuypers et al., 2005; Thamdrup et al., 2006). The required ammonium for the anammox bacteria is supplied by the mineralization processes. Anammox as well as the denitrification process that occurs in the upper oxycline regenerate N_2, while denitrification also produces N_2O and thus contribute to a loss in fixed nitrogen and to the production of greenhouse gases. Nitrogen cycling was generally thought to dominate the biogeochemistry and microbial ecology of OMZs, but recent studies also identified sulfur oxidizing bacteria that use nitrite as alternate electron acceptor as important community members as well as sulfate-reducing heterotrophs (Stevens and Ulloa, 2008; Lavik et al., 2009; Walsh et al., 2009; Canfield et al., 2010; Stewart et al., 2012). Thus, although OMZs have long been seen as "dead zones", metabolic activities in these oceanographic features significantly affect nitrogen, sulfur and carbon cycling within the global ocean.

Subseafloor sediments. Diverse populations of microorganisms, utilizing a variety of electron acceptors, are responsible for the oxidation of organic matter in marine sediments. Organic material is deposited on the seafloor principally as aggregates which sink down through the water column as a continuous particle rain. This particulate organic flux is related to the primary productivity of the overlying plankton community and to the water depth through which the detritus sinks while being gradually decomposed as described in the previous paragraph.

The order of the utilized electron acceptors for organic matter degradation in the sediments – oxygen, nitrate, manganese and iron cations or sulfate anions, which diffuse into sediments from the seawater, is determined by their abundance and energy yield (Figure I.3; Froelich et al., 1979). Aerobic respiration is the most efficient pathway for organic matter degradation and O_2 is thus depleted first, followed by respiration using nitrite, iron(III), manganese(IV), sulfate, and finally CO_2. When all inorganic electron acceptors are depleted, organic matter can only be mineralized by fermentation. The degradation of organic matter via fermentative pathways to small organic molecules such as lactate, butyrate, propionate, acetate, formate, H_2 and CO_2 is important in marine sediments, since these compounds are the main substrates for sulfate reduction and

partly for methane formation (e.g., Fry et al., 2008). Consequently, chemoautotrophy in the sediments is primarily fuelled by anaerobic organic matter degradation.

The last step in the sedimentary metabolic pathway succession is methanogenesis. This process is performed exclusively by strictly anaerobic archaea and the most prominent pathways are the reduction of carbon dioxide with molecular hydrogen (hydrogenotrophic methanogenesis) and the transformation of acetic acid into methane and carbon dioxide (acetoclastic methanogenesis). Since methanogens are outcompeted for acetate and H_2 by sulfate-reducing bacteria, the archaea using these two pathways are restricted to the sulfate-free zone (e.g., Abram and Nedwell, 1978; Oremland and Polcin, 1982; Lin et al., 2012). Non-competitive substrates that can be utilized only by methanogens from the order *Methanosarcinales* are several methylated compounds, such as methanol, methylated amines and methylated sulfides, allowing these archaea to co-occur with the sulfate reducers (methylotrophic methanogenesis; e.g., Oremland and Polcin, 1982), but in contrast to hydrogen and acetate, quite limited information is available on those methylated methanogenic substrates in marine sediments (Zhuang, 2014).

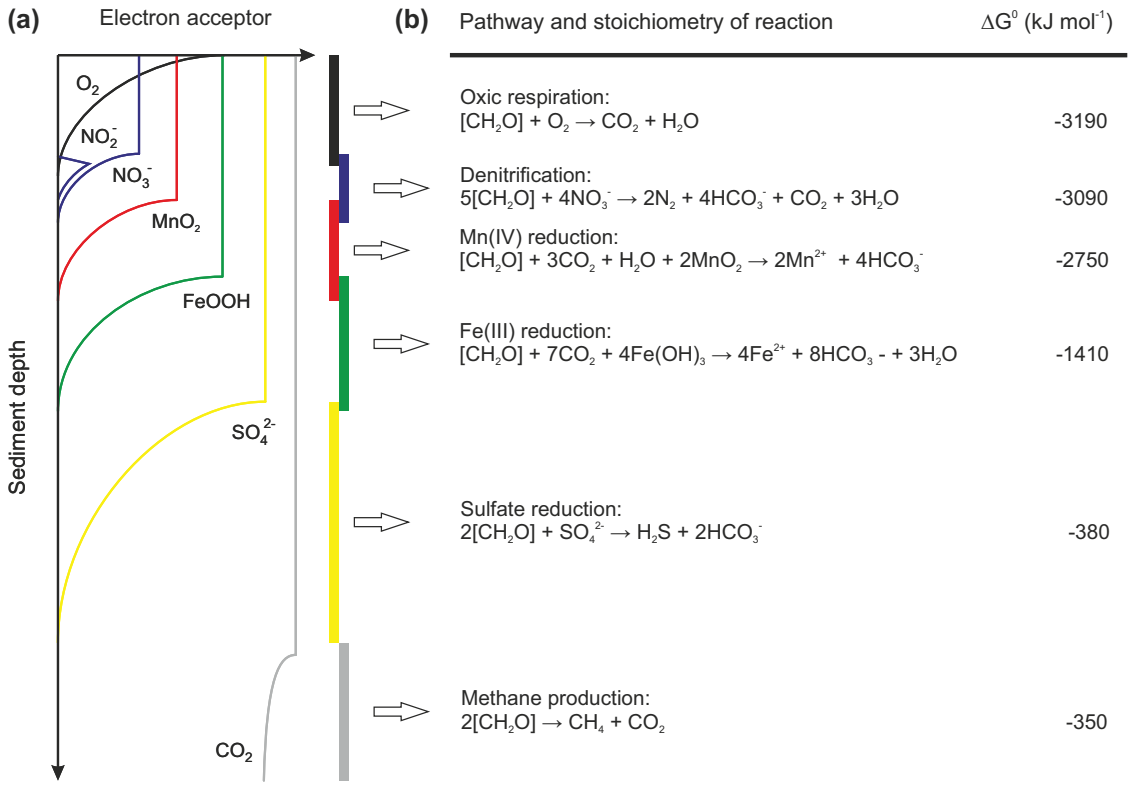

Figure I.3. (a) Schematic representation of redox–active compounds in marine sediments (modified after Froelich et al., 1979; Canfield and Thamdrup, 2009). (b) Simplified oxidation reactions of sedimentary organic matter with different electron acceptors and associated free energy yield (ΔG^0; Froelich et al., 1979). Organic matter of unspecified composition is symbolized by $[CH_2O]$. The ΔG^0 are presented as kilojoules per mole of glucose ($C_3H_{12}O_6$).

Another important process that occurs ubiquitously in marine sediments is the anaerobic oxidation of methane (AOM), which is also exclusively performed by members of the Archaea. This process is a major sink for methane that is produced in the sediments either by biotic or abiotic processes and thus plays a crucial role of maintaining a sensitive balance of our atmosphere's greenhouse gas content. AOM usually occurs at sulfate methane transition zones, where both methane (from below) and sulfate (from above) are simultaneously consumed by a consortium of autotrophic sulfate reducing bacteria and methane oxidizing archaea according to the equation $CH_4 + SO_4^{2-} \rightarrow HCO_3^- + HS^- + H_2O$ (Hoehler et al., 1994; Hinrichs et al., 1999; Boetius et al., 2000; Hinrichs and Boetius, 2002).

Deeply buried sediments. Of the ca. 50 Pg C yr^{-1} (Field, 1998; Dunne et al., 2007) that is produced in the euphotic zone, only 0.2 to 0.79 Pg C yr^{-1} (ca. 1 %) is buried in marine sediments (Hedges and Keil, 1995; Duarte et al., 2005; Burdige, 2007; Dunne et al., 2007), implying that almost all net marine primary production is recycled. Still, a small fraction escapes respiration and reaches deeper sediments and this flux continuously fuels the largest reservoir of organic carbon on Earth.

The deep sediments can be considered as extreme environment due to the prevailing high pressures, low pore space, extreme energy limitation as well as high temperatures at depth. However, it is suggested that Earth's subsurface environments provide ubiquitous microbial habitats (Jørgensen and Boetius, 2007; Fry et al., 2008) containing a multitude of different physicochemical settings from completely oxidized sediments in oligotrophic deep-sea sediments (D'Hondt et al., 2009) to highly reduced systems typically found in coastal and shelf sediments, (Parkes et al., 1990). Yet, we have only fragmentary understanding of the abundance, diversity and function of microbial life in these hardly accessible systems (e.g., Hinrichs and Inagaki, 2012; Orcutt et al., 2013). Based on geochemical analysis of marine pore waters, it was suggested that microbial life in the deep sediments is involved in the slow degradation of organic matter (e.g., D'Hondt et al., 2004) and thus, most microbial subsurface communities would indeed be ultimately – though indirectly – dependent on photosynthesis. Although microbial activity typically concentrates at geochemical interfaces, such as sulfate methane transition zones, it was generally observed that with increasing sediment depth the microbial abundance is exponentially decreasing (e.g., Parkes et al., 1994; Parkes et al., 2000). In the deepest subseafloor samples investigated to date (IODP Expedition 337, Shimokita Deep Coalbed Biosphere, sampled down to 2,466 mbsf, Inagaki et al., 2013), this trend did not continue at depth >1.5 kmbsf. However, the lower margin of the deep subseafloor biosphere has not been found yet and to date it is unclear which factors (energy, temperature, pore space) are ultimately limiting life at depth. There is an ongoing debate whether archaea or bacteria are numerically more abundant in

subseafloor sediments. Different approaches even on the same sediments (e.g., Peru Margin; Mauclaire et al., 2004; Schippers et al., 2005; Biddle et al., 2006; Sørensen and Teske, 2006; Webster et al., 2006; Lipp et al., 2008) have yielded contradictory results, while most of them detected similar bacterial as well as archaeal molecular markers. Since most of the organisms of the so called deep biosphere belong to uncultivated species, their metabolisms still remain largely unconstrained. However, recent studies based on lipid biomarker and genomic approaches suggested that uncultured subseafloor archaea are mainly heterotrophs (Biddle et al., 2006) and involved in the degradation of detrital proteins (Lloyd et al., 2013). Moreover, when inorganic electron acceptors other than CO_2 are depleted and thus not available in the deep subsurface (e.g., nitrate, ferric iron and sulfate), subsequent consumption of H_2 mediated by methanogenic archaea and acetogenic bacteria has been shown to be a major metabolic process (e.g., Conrad, 1999; Hoehler et al., 1999; Drake et al., 2006; Heuer et al., 2009). The substrates for these reactions are mainly provided by fermenting bacteria or by radiolysis of water, of which the latter supports life independent of photosynthesis (Lin et al., 2005; D'Hondt et al., 2009).

Hydrothermal vents and cold seeps. Microbial hot-spot ecosystems on the ocean floor are hydrothermal vents, cold seeps and gas-hydrate systems, which are characterized by high or special biodiversity compared to the surrounding larger area of low or normal biodiversity. Hydrothermal vent sites occur in all of the World's oceans at all active mid-ocean ridges and back-arc spreading centers, while cold seeps are found at passive and active continental margins, with the largest number occurring at active margins where the oceanic plates are being subducted beneath continents (cf. Campbell, 2006). At hydrothermal vents and cold seeps chemical-rich fluids emanate from the seafloor and often provide energy to sustain diverse microbial communities in some very harsh environments (e.g., Kelley et al., 2002; Schrenk et al., 2010). The two environments differ from one another in the underlying conditions that form and drive these ecosystems, but both predominantly support chemolithoautotrophic growth of the inhabiting microbes, while microbial heterotrophy seems to be of only minor importance (Hügler and Sievert, 2011).

In hydrothermal systems, hot fluids altered from seawater-rock interactions and rich in reduced chemicals, such as H_2, H_2S, Fe^{2+}, or methane, depending on the geological setting (Kelley et al., 2002), are discharged and provide the basis for microbial growth. Thus, a large variety of redox reactions available to chemolithoautotrophic microorganisms occur in these systems and the predominant microbial processes include sulfur oxidation, methanotrophy, sulfate reduction, methanogenesis and metal reduction (cf. Fisher et al., 2007). At cold vents, methane-rich interstitial fluids of non-hydrothermal origin migrate

along faults and fractures from deeper sedimentary sources to the seafloor and thus, methane serves as major source of energy in these systems (cf. Jørgensen and Boetius, 2007). The methane either derives from biogenic sources, i.e. archaeal methanogenesis, or from abiogenic production during rock-water interactions, thermogenic sources from pyrolysis of organic matter, or the dissociation of gas hydrates (e.g., Claypool and Kaplan, 1974; Schoell, 1988; Bohrmann and Torres, 2006; McCollom and Seewald, 2007). The key microbial metabolic process at cold seep sites is the anaerobic oxidation of methane coupled to sulfate reduction (Hinrichs et al., 1999; Boetius et al., 2000; Orphan et al., 2001). Hence, both cold and hot vents support vast amounts of microbial biomass and the estimated carbon production at deep-sea vents is in the range of 5 Tg C yr^{-1}, which is ca. $0.02\,\%$ of marine primary production by photosynthesis (McCollom and Shock, 1997).

I.2. How to study microbes in the environment? – The lipid biomarker concept

Molecular techniques are powerful tools for studying microbial life in both molecular biology and organic geochemistry. While the former discipline targets genetic information that is encoded in DNA and RNA molecules, the latter investigates the translation of this information into building blocks of cells. Molecular biomarkers are compounds that can be unambiguously linked to specific precursor molecules produced by living organisms (Eglinton et al., 1964; Eglinton and Calvin, 1967). Among these compounds are lipids from eukaryotic and prokaryotic cell membranes serving as source of information on the biogeochemistry and microbial ecology of natural ecosystems in modern (White et al., 1979; Harvey et al., 1986) and in ancient environments (e.g.; Brocks and Summons, 2003). The application of a biomarker to reconstruct (paleo)environments depends for example on knowledge about the biogeochemistry of such compounds, both within and outside the precursor organisms, the detailed chemical structure, and valid methods to accurately identify and quantify the concentration of appropriate compounds in a variety of samples including different sediment matrices, waters and cells (Poynter and Eglinton, 1991).

I.2.1. Membrane lipids – structure, chemotaxonomy and function

All cells are surrounded by membranes that ensure the individuality and integrity of cells and mediate their interactions with the surrounding environment (Madigan et al., 2011; Killops and Killops, 2013). The cytoplasmic membrane forms a diffusion barrier and constitutes a physical barrier between the cytoplasm and the external medium. This

barrier function regulates the flux of ions and other solutes, including nutrients and metabolic products, in and out of the cell. Moreover, the restricted ion-permeability involves a variety of ion transport systems, such as the electron transport chain, that can generate electrochemical ion and proton gradients across the membrane. This results for example in the so called 'proton motive force' and is essential for energy conservation and biosynthesis of ATP (Madigan et al., 2011). The building blocks of every cell membrane are lipids, which can represent up to 7 % of the cell dry weight and form a matrix in which various membrane proteins float. An essential general feature that is required for lipid membrane function is the capacity to persist in the liquid crystalline phase. In order to keep the cell integrity intact and to maintain the liquid crystalline state, membrane fluidity is carefully regulated by adapting the lipid composition to external variations in pressure, temperature, pH or other environmental factors (e.g.; Cronan and Gelmann, 1975; Hazel and Williams, 1990; Russell et al., 1995). The functional properties of the cytoplasmic membrane are thus crucial factors that determine whether an organism is capable of coping with and surviving in its continuously changing and often hostile environment.

I.2.1.1. Structure and chemotaxonomy

Membrane-building lipids are typically composed of a hydrophilic polar head group and a hydrophobic tail, and they separate the inside of the cell from the outside environment by arranging in a mono- or bilayer (Figure I.4; e.g.; Madigan et al., 2011). While organisms from all domains produce glycerol-based lipids, intrinsic differences occur in the biosynthetic pathways of membrane formation. Archaeal membrane lipids can be unequivocally differentiated from the other domains based by the glycerol backbone stereochemistry (Kates et al., 1965; Koga and Morii, 2005). In the *Archaea*, hydrophobic side chains are bound at *sn*-2 and *sn*-3 positions of the glycerol and linked to a head group attached to the *sn*-glycerol-1 position (Figure I.4b). Bacterial and eukaryotal membranes share the same lipid biochemistry and contain head groups attached to the *sn*-glycerol-3 position and core lipids bound at *sn*-1,2-positions (Figure I.4c). The synthesis of polar head groups is similar among all domains. The head groups are typically phosphate-based, but membranes with glycosidic-, amino-or sulfate-based head groups are also widely distributed (Dembitsky, 1996; Hölzl and Dörmann, 2007).

Bacterial and eukaryotal lipids. Intact polar lipids (IPLs) of bacteria and eukarya mainly form bilayer membranes and the core lipids typically consist of *n*- or methyl-branched fatty acids (diacylglycerols) with variable length of carbon chains and degrees of unsaturation. However, mixed ether/ester (acyletherglycerol) and dietherglycerols

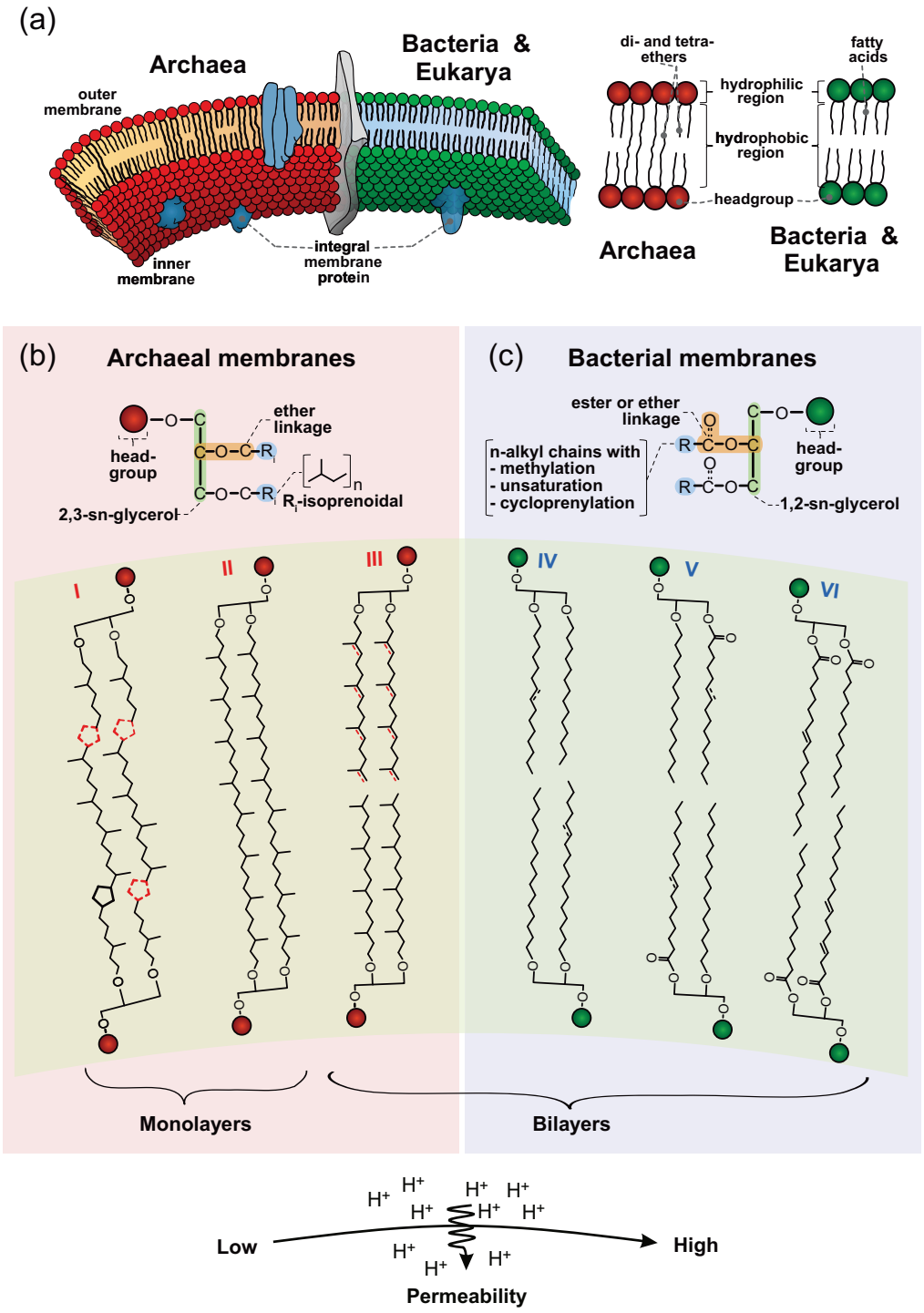

Figure I.4. Schematic structure of lipid membranes from *Archaea*, *Bacteria* and *Eukarya*. (a) General structure of the cytoplasmic membrane showing lipid molecules, forming either a mono- or a bilayer, and embedded proteins. The general structures of archaeal (red) and bacterial/eukaryotal lipids (green) are also shown. (b) Detailed structures of archaeal and bacterial membrane lipids including stereochemistry of the glycerol backbone and side chain linkage for Archaea and Bacteria/Eukarya. Structures of archaeal lipids: I, cyclopentane ring-containing glycerol dibiphytanyl glycerol tetraether (GDGT); II, Acyclic GDGT; III, fully saturated and unsaturated archaeol. Structures of bacterial lipids: IV, dietherglycerol, V, acyletherglycerol; VI, diacylglycerol. Bacterial lipids contain variable chain lengths and degrees of unsaturation. The general trend of increasing permeability to ions is indicated by the arrow at the bottom of the figure. Figure adapted from Valentine (2007), Madigan et al. (2011), and Kellermann (2012).

are widespread among anaerobic and microaerophilic bacteria (see Pearson, 2014, and references therein). For example, ether lipids are common in thermophiles (e.g., Langworthy et al., 1983; Huber et al., 1992) as well as in some sulfate-reducing species (Kamio et al., 1969; Rütters et al., 2001; Sturt et al., 2004). Another exception is the synthesis of diglycerol tetraether and tetraester lipids in some species from the order *Thermotogales* (Sinninghe Damsté et al., 2007; Sinninghe Damsté et al., 2011). Although ether lipid-containing lipids have been mainly reported from thermophilic bacteria, there seems to be no strict temperature-based association. Eukaryotes and some bacteria can also synthesize sphingolipids, which are composed of an alkyl chain and a fatty acid linked via an amide-bond to the alkyl chain (Olsen and Jantzen, 2001) as well as betaine lipids (BL), such as diacylglyceryl-*N,N,N*-trimethylhomoserine (DGTS). Other amino-based lipids, which seem to be restricted to the bacterial domain, are ornithine-containing (OL) lipids. They have been shown to be widespread among Gram-negative bacteria (Makula and Finnerty, 1975; Geiger et al., 2010). Additionally, hopanoids and steroids occur in bacteria and eukaryotes, respectively, which are suggested to act as membrane rigidifiers and are thus involved in membrane ordering (Ourisson et al., 1987; Dowhan and Bogdanov, 2002; Sáenz et al., 2012).

Archaeal diether lipids. In contrast to bacteria and eukaryotes, archaeal membranes are comprised of C_{15} to C_{40} isoprenoid alkyl chains bound to the glycerol exclusively through ether linkages (e.g.; Goldfine and Langworthy, 1988; Kates, 1993b; Koga and Morii, 2005). The most common archaeal core lipids are glycerol diethers (archaeols), which are composed of two C_{20} isoprenoids ether-linked to the glycerol and they predominantly occur in *Euryarchaeota*, although *Cren-* and *Thaumarchaeota* are also known to synthesize archaeols (Koga and Morii, 2005; Schouten et al., 2008). Diether core lipids comprise a diverse array of structures, including C_{15} to C_{25} isoprenoid chains (e.g.; de Rosa et al., 1982; De Rosa et al., 1983; Mancuso et al., 1985; Kates, 1993b), hydroxylated side chains (*sn*-2 hydroxyarchaeol), which are distinct for methanogenic and methanotrophic archaea (Koga et al., 1993a; Sprott et al., 1993; Koga et al., 1998; Hinrichs et al., 1999; Stadnitskaia et al., 2008), macrocyclic structures, which were identified in the methanogens *Methanococcus jannaschii* and *Methanococcus igneus* (Comita et al., 1984; Sprott et al., 1991; Trincone et al., 1992) as well as unsaturated phytanyl chains (Franzmann et al., 1988; Gibson et al., 2005; Dawson et al., 2012).

Archaeal tetraether lipids. Other unique structures of archaeal membrane lipids are glycerol dibiphytanyl glycerol tetraethers (GDGTs or caldarchaeols), which were first discovered in the thermoacidophilic archaeon *Thermoplasma acidophilum* by Langworthy (1977). Isoprenoid GDGTs contain two C_{40} biphytane molecules ether-linked to two glyc-

erols and are mainly found in thermophilic archaea, some mesophilic methanogenic *Euryarchaeota*, as well as *Thaumarchaeota* (see reviews by Koga and Morii, 2005; Schouten et al., 2013a). Whereas archaeols are incorporated into a bilayer within the archaeal cell membrane (de Rosa et al., 1982; De Rosa et al., 1983), the bipolar isoprenoid GDGT lipids span the whole cell membranes and build a monolayer (see Figure I.4; Langworthy, 1982; Gliozzi et al., 2002). Tetraether lipids can be found in large variety of structures. For instance, GDGTs with up to eight cyclopentane rings (De Rosa et al., 1977; De Rosa et al., 1983), glycerol trialkyl glycerol tetraethers (GTGT; de Rosa et al., 1986), H-shaped GDGTs (Morii et al., 1998) as well as hydroxylated (OH; Liu et al., 2012b) and methylated (Me; Knappy et al., 2009; Knappy et al., 2011) GDGTs have been identified in various mainly thermophilic archaeal isolates. However, in mesophilic *Thaumarchaeota*, GTGTs as well as OH-GDGTs have also been identified (Schouten et al., 2008; Elling et al., 2014). A unique GDGT structure represents crenarchaeol, which contains of four cyclopentane and one cyclohexyl ring (Sinninghe Damsté et al., 2002). This lipid has so far only been found in *Thaumarchaeota* and seems diagnostic for this phylum (e.g., Pitcher et al., 2011a). Additionally, glycerol dialkanol diethers (GDDs), which appear to be derivatives of GDGTs lacking one glycerol moiety, have been reported to represent minor compounds in some archaea (Knappy and Keely, 2012; Liu et al., 2012a; Elling et al., 2014; Bauersachs et al., 2015). A variety of archaeal lipids that have not been identified in cultures, but appear to be abundant in the environment have recently been reported. These orphan lipids include tetraether lipids in which one glycerol moiety has been substituted by butanetriol (BDGT) or pentanetriol (PDGT; Knappy et al., 2014; Zhu et al., 2014a), and GDGTs with unsaturated biphytanyl moieties (Zhu et al., 2014b). The former molecules have been tentatively linked to members of the Miscellaneous Crenarchaeotal Group (MCG) archaea (Meador et al., 2014a), while the latter are potentially associated with *Euryarchaeota* affiliated with the Marine Benthic Group D (Yoshinaga et al., 2015b). Both archaeal groups are globally distributed in subseafloor environments (e.g., Teske, 2006).

I.2.1.2. Function of microbial membrane lipids and adaptation to environmental conditions

Function of apolar side chains. In general, the isoprenoid ether lipids of archaea are considered to be more stable and less permeable to ions than bacterial and eukaryotal ester lipid, and tetraether-based membranes are less permeable than diether-based membranes (Figure I.4; Yamauchi et al., 1993; Elferink et al., 1994; Mathai et al., 2001). The distinctive lipid-membrane composition among archaea is further considered as a primary adaptation to energy stress. Physiological advantages of the low-permeability

membranes in archaea are *(i)* that less energy is lost during the maintenance of a chemiosmotic potential and *(ii)* that the high stability of the ether lipids results in less energy requirement for cellular repair (see review of Valentine, 2007). All these properties demonstrate why archaea are able to thrive at very harsh and energy-starved conditions and generally outcompete bacteria in many extreme environments. Although the classical view that archaea are exclusively extremophiles seems obsolete due to their high abundance in mesophilic environments (DeLong, 1998), such as AOA in the open ocean (Karner et al., 2001), they still seem to inhabit ecological niches and probably face chronic energy stress in the form of energy flux (Valentine, 2007). For example, marine AOA outcompete AOB in the open ocean, where concentrations of ammonium are generally one to two orders of magnitude lower than in nutrient replete regions (Pester et al., 2011; Stahl and de la Torre, 2012), as well as in suboxic waters such as the Black Sea chemocline (Coolen et al., 2007; Lam et al., 2007), which is likely due to their high affinity to ammonia and potentially, low oxygen requirement (Martens-Habbena et al., 2009).

Function of polar head groups. Different head group structures also significantly vary in their properties and functions. For example, the size of polar head groups differs considerably between different structural types, which has implications for the packing and organization and consequently for the physical properties of the membrane (Dowhan, 1997; Dowhan and Bogdanov, 2002). When small head groups are bound to large hydrophobic side chains, nonbilayer lipids are formed that are involved in generating membrane curvature. Other functions of nonbilayer forming lipids are stabilization of proteins, providing nonleaky discontinuity in the bilayer structure, supporting movement of macromolecules through the membrane, and to enable membrane vesicle formation during cell division (see review by Dowhan, 1997). Moreover, different polar head groups have different ionic characters, i.e., zwitterionic or anionic, at physiological pH. Of the phosphate-based head groups, phosphatidylethanolamine (PE), phosphatidyl-(*N*)-methylethanolamine (PME), phosphatidyl-(*N,N*)-dimethylethanolamine (PDME), and phosphatidylcholine (PC) represent zwitterionic lipids, while others such as phosphatidylglycerol (PG), diphosphatidylglycerol (DPG), and phosphatidyl inositol (PI) are anionic. The type of ionic head group influences the physiological and physical membrane properties and helps to maintain the optimal activity of major integral proteins (Dowhan, 1997).

Membrane lipid adaptation. An intriguing feature of bacteria and archaea is their ability to grow and thrive under a wide range of environmental conditions. In order to regulate membrane functioning under different conditions, such as variations in

temperature, salinity, pH and hydrostatic pressure, microorganisms adapt both the polar head group and the apolar core lipid composition (Beney and Gervais, 2001). For example, bacteria respond to growth at higher temperatures by increasing the length of the fatty acyl chains, changing the ratio of iso to anteiso branching, or by increasing the degree of unsaturation (cf. Zhang and Rock, 2008). Moreover, higher proportions of phosphatidylglycerol (PG) head groups in expense of phosphatidylethanolamine (PE) have been observed (e.g., Hasegawa et al., 1980), but changes in the polar head group composition are generally minor compared to changes in the core lipid composition at different temperatures (Russell et al., 1995). The increasing proportions of higher-melting lipids at higher temperatures result in a lower passive permeability of the membrane and keeps it in a liquid crystalline state (Suutari and Laakso, 1994). The response of archaeal membrane lipid compositions to temperature is also well studied. At increasing temperatures, thermophilic archaea increase the average number of cyclopentyl moieties in their isoprenoid side chains, while the temperature-cyclization relationship is distinct for different species (De Rosa et al., 1980; Gliozzi et al., 1983; Uda et al., 2001). Moreover, phospho-based head groups are substituted by glycosidic compounds (e.g., Shimada et al., 2008). These adaptations result in tight and rigid lipid packing and induce extremely low proton permeation required at high temperatures (Komatsu and Chong, 1998). In contrast, at cold temperatures, the psychrophilic methanogen *Methanococcoides burtonii* has been shown to increase the abundance of lipid unsaturation in order to keep the membrane in a liquid crystalline state and to help maintaining normal membrane function (Nichols et al., 2004). In acidic environments both archaea and bacteria use adaptations similar to those at high temperatures (Gabriel and Chong, 2000; Shimada et al., 2008; Zhang and Rock, 2008).

At high salt concentrations, adaptation of the polar head group and core lipids seems to be of equal importance. In order to keep cell integrity and fluidity intact under high ionic strength, halophilic archaea as well as bacteria increase the amount of anionic lipids such as phosphatidylglycerol phosphate (PGP), methylated-PGP (Me-PGP), PG and sulfated glycosidic based intact polar lipids in their membranes, while neutrally charged species, such as PE and PC decrease in concentration (Kushwaha et al., 1982; Vreeland, 1987; Russell, 1989; Kates, 1993a; Ventosa et al., 1998; Oren, 2002b). The synthesis of a high density of negative charges on the surface of membranes at high salt concentrations brings the advantage that the negative charges on the polar head groups are shielded by the high ionic concentration. This prevents disruption of the lipid bilayers due to charge-repulsive forces and provides a charge-stabilized lipid bilayer (Kates, 1993a). Besides head group adaptations, structural modifications of the apolar core lipids have been shown to be important adjustments in halophiles as the interaction of polar head groups and apolar side chains significantly influences the geometry and size of the IPLs

(Russell, 1989). For example, Dawson et al. (2012) showed higher degrees of unsaturation in archaeal isolates that have higher salinity optima. Similarly, bacteria increase the relative proportions of unsaturated fatty acids at high salt concentration, which enhances membrane fluidity as well as permeability (Russell, 1989).

Additionally, nutrient limitation affects lipid compositions, which is well known for bacteria and eukaryotes (e.g., Suutari and Laakso, 1994; Van Mooy et al., 2006). For instance, in cyanobacteria grown under phosphate limitation, phosphate based head groups have been shown to be substituted by either phosphate-free sulfate-based or amino-based head groups (e.g., Benning et al., 1995). The influence of nutrient limitation on lipid composition in archaea is less constrained. However, recent studies revealed that the thermophilic methanogen *Methanococcus thermautotrophicus* accumulates glycolipids relative to phospholipids during nutrient-limited growth (Yoshinaga et al., 2015a).

I.2.2. Membrane lipids as proxies for modern and ancient environments

I.2.2.1. Microbial lipids as life markers

Structural lipid diversity in natural samples (Figure I.5) is linked to both species diversity and the community's adaptation to certain environmental conditions. For IPLs outside living cells, it is generally assumed that they are quickly degraded (White et al., 1979; Harvey et al., 1986), which, generally, makes them good indicators for living cells. In a variety of aquatic environments, microbial IPLs have been successfully used for the study of microbial ecology and biogeochemistry. These environments include marine sediments (e.g., Rütters et al., 2002; Zink et al., 2003; Sturt et al., 2004; Biddle et al., 2006; Lipp et al., 2008; Lipp and Hinrichs, 2009; Seidel et al., 2012), cold seeps (Rossel et al., 2008; Yoshinaga et al., 2015b), hot springs (e.g., Schubotz et al., 2013), and the marine water column (e.g., Schubotz et al., 2009; Van Mooy et al., 2009; Popendorf et al., 2011; Schouten et al., 2012; Basse et al., 2014). Based on IPL analysis of globally distributed samples from deeply buried sediments, it has for example been proposed that archaea are the dominant prokaryotes in the marine deep biosphere (Lipp et al., 2008), which contradicts earlier gene-based investigations (e.g., Schippers et al., 2005). However, recent studies revealed evidence that the turnover time of the lipids outside living cells is strongly dependent on their structural properties (Logemann et al., 2011). Whereas intact lipids containing ester-bound moieties are rapidly degraded by microbes, ether-bound moieties, such as archaeal and bacterial diether and archaeal tetraether lipids, can even survive early diagenesis and thus contribute to the recalcitrant organic matter in deeply buried sediments (Logemann et al., 2011; Xie et al., 2013). Thus, the differentiation between intact and fossil signal in marine sediments is a fine line (cf. Pearson, 2008) and especially

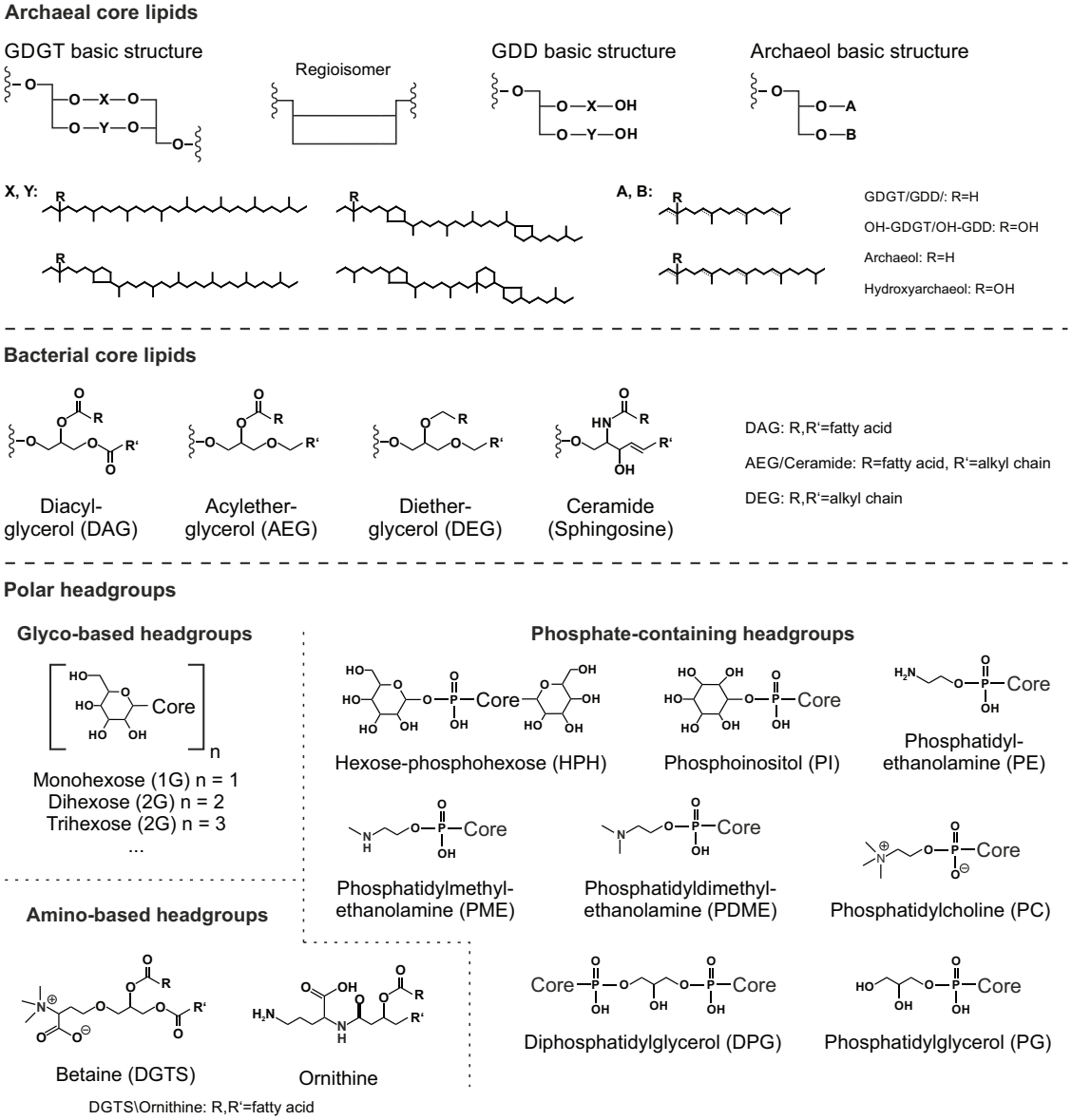

Figure I.5. Structures of archaeal and bacterial core lipids and associated polar head groups typically found in the marine environment. For archaeal ether lipids the different basic structures are composed of two isoprenoid units X and Y or A and B, which may be interchanged with respect to their positions at *sn*-2 and *sn*-3 of glycerol. For the basic structure of a GDGT both the anti-parallel and parallel configurations (regioisomer) are drawn. The vast number of combinations of these components gives rise to many structural isomers. More structures are possible. For bacterial core lipids the diversity is even higher due to highly variable chain lengths and degrees of unsaturations in the fatty acid and alkyl side chains.

the sedimentary IPL signal has to be carefully evaluated in order to distinguish signals of live and fossil microbial communities. Environmental IPL studies therefore benefit from complementary biomarker approaches as well as from the search for new biomarkers that can be applied as rigorous life markers.

I.2.2.2. From bio- to geomolecules – Microbial lipids as proxies for paleoenvironments

Organic matter of biogenic origin including lipids preserved in aquatic sediments can provide a record of planktonic productivity as well as the environmental conditions during deposition, since degradation products of intact lipid molecules are stable over geological timescales (e.g., Brocks and Summons, 2003). Lipid-based molecular fossils were found back to the late Archean (ca. 2.7 billion years; Waldbauer et al., 2009), demonstrating their exceptional preservation potential. Since structural modifications of the lipids over time are well studied, it is possible to utilize structures, functions, and phylogenetic distributions of modern biomolecules to predict their role in fossil ecosystems. Based on this knowledge, the biomarker-centric tree of life has been constructed, which provides an outstanding tool for the study of ancient microbial life and environmental conditions (Brocks and Pearson, 2005; Gaines et al., 2009). The most valuable biomarkers are taxonomically specific, carry environmental information and are resistant against degradation during early diagenesis. In paleoceanography, several proxies have been developed to reconstruct past environmental conditions such as ocean surface temperature, salinity, paleoproductivity, soil input, changes in vegetation, and precipitation patterns (e.g., Eglinton and Eglinton, 2008). These proxies use either lipid biomarker structures, abundances, ratios or stable isotope compositions. Sources of selected lipids used for paleoenvironmental reconstructions are shown in Figure I.6.

A prime concern in paleoceanography is the reconstruction of sea surface temperature (SST). The oceans influence climate on a global scale and heat exchange between the ocean's surface and the atmosphere is crucial to both oceanic and atmospheric circulation patterns. Moreover, it is essential to understand past climate variability in order to predict future climate change, which is highly debated at present (IPCC, 2014). Two established biomarker SST proxies have been developed: the $U^{K'}_{37}$ index (Unsaturated Ketones with 37 carbon atoms), which is based on the relative distribution of long chain alkenones mainly produced by the haptophyte algae *Emiliania huxleyi* (Brassell et al., 1986; Prahl and Wakeham, 1987) and the TEX_{86} (Tetraether IndeX with 86 carbon atoms), based on the relative abundance of core isoprenoid GDGTs biosynthesized by planktonic AOA (Schouten et al., 2002). While the general concept of GDGT cyclization as adaptation to temperature is well established for cultivated thermophilic archaea (see section I.2.1.2.), the role of alkenones in haptophyte physiology is still uncertain, although energy storage has been suggested (Eltgroth et al., 2005). These lipid based proxies bring the advantage that they provide SST estimates independent of initial seawater chemistry and, compared with carbonate microfossils, are less subjected to overprinting effects of diagenesis. Both paleothermometers are based on the observation that differences in the

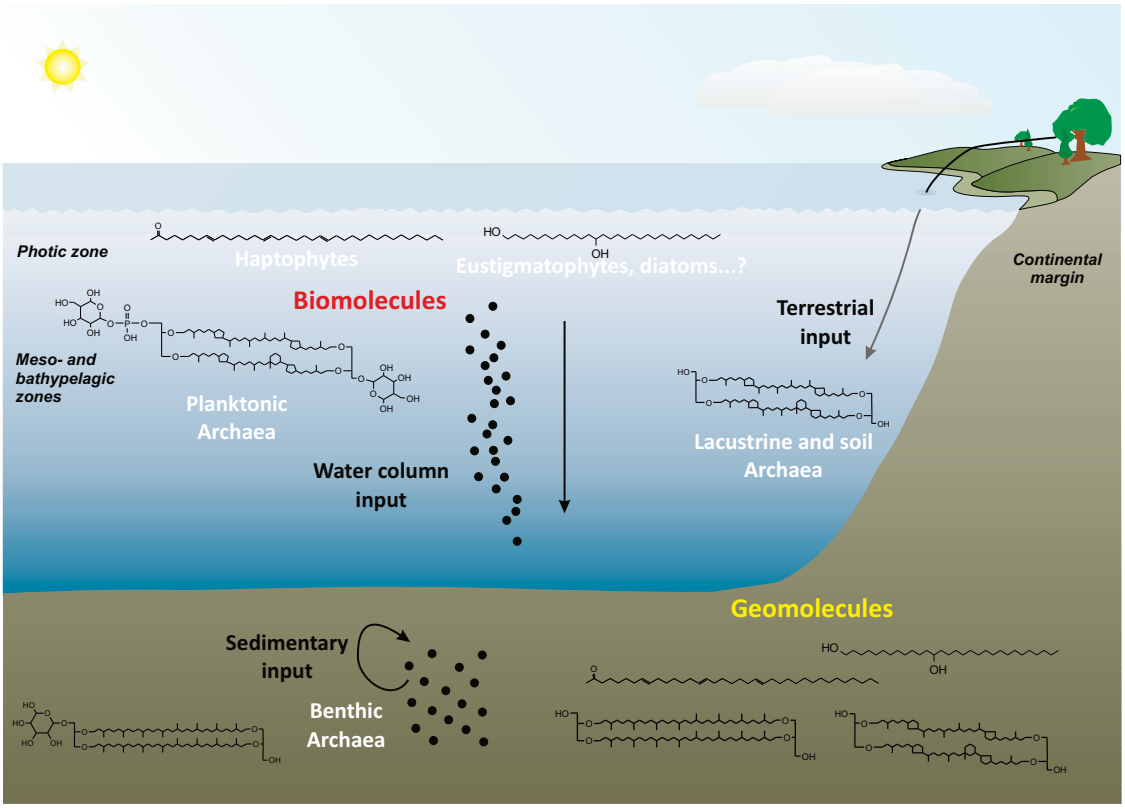

Figure I.6. Sources of selected archaeal and eukaryotal lipids in the marine environment used for the reconstruction of paleoenvironmental conditions. Figure modified after Liu (2011), landscape modified after Jørgensen and Boetius (2007).

relative abundances of the proxy relevant lipids are strongly correlated to sea surface temperature. The $U^{K'}_{37}$ SST proxy is expressed as:

$$U^{K'}_{37} = \frac{[C_{37:2}\text{alkenone}]}{[\text{GDGT-1}] + [C_{37:2}\text{alkenone}] + [C_{37:3}\text{alkenone}]} \quad \text{(Eq. 1)}$$

and converted into temperature using global (e.g., Müller et al., 1998a; Conte et al., 2006) or regional (e.g., Leider et al., 2010) core-top calibrations. The TEX_{86} SST proxy is expressed as:

$$TEX^{H}_{86} = \frac{[\text{GDGT-2}] + [\text{GDGT-3}] + [\text{GDGT-5'}]}{[\text{GDGT-1}] + [\text{GDGT-2}] + [\text{GDGT-3}] + [\text{GDGT-5'}]} \quad \text{(Eq. 2)}$$

where the number indicates the number of cyclopentyl rings in the GDGT and GDGT-5' corresponds to the crenarchaeol regioisomer. Similarly to $U^{K'}_{37}$, TEX_{86}, is converted into SST by using global or regional core-top calibrations (Figure I.7; e.g., Schouten et al., 2002; Kim et al., 2008). However, derivation of distinct calibration lines for high and low temperatures have been observed and separate calibrations were proposed (TEX^{H}_{86}, TEX^{L}_{86}; Kim et al., 2010). More recently, Tierney and Tingley (2014) developed a Bayesian

regression approach to the TEX_{86}-SST calibration, which considers uncertainties and likely provides best SST estimates.

Another SST proxy that was recently proposed is the long chain diol index (LDI Rampen et al., 2012), which is based on the relative distribution of long chain diols, presumably produced by eustigmatophyte algae (Volkman et al., 1992; Versteegh and de Leeuw, 1997):

$$\mathrm{LDI} = \frac{[\mathrm{C_{30}}1,15\ \mathrm{diol}]}{[\mathrm{C_{28}}1,13\ \mathrm{diol}] + [\mathrm{C_{30}}1,13\ \mathrm{diol}] + [\mathrm{C_{30}}1,15\ \mathrm{diol}]} \qquad \text{(Eq. 3)}$$

The empirical calibration of this ratio with sea surface seems promising, but due to the recent development the amount of available data is still limited (Rampen et al., 2012).

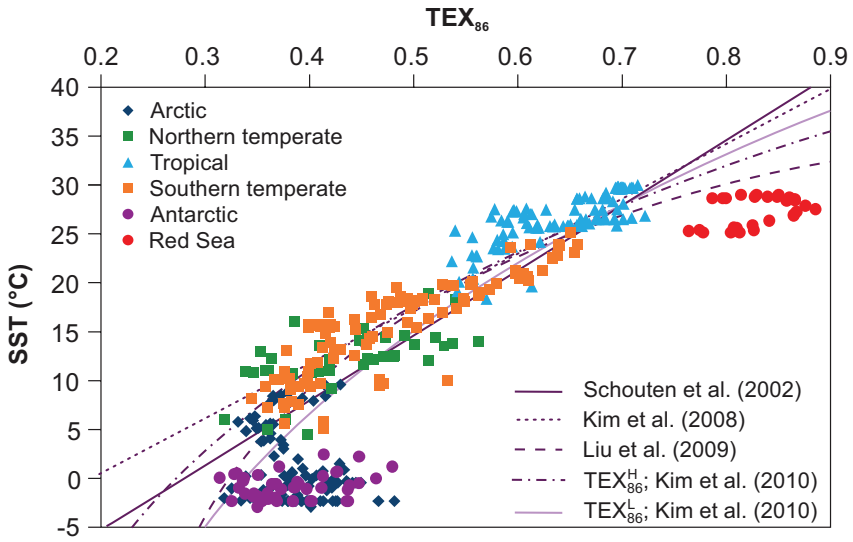

Figure I.7. Satellite derived sea surface temperature versus TEX_{86} from globally distributed sediment core-top data (Kim et al., 2010) separated by latitude after Pearson and Ingalls (2013). Additionally shown are the major TEX_{86} calibration lines. Since TEX_{86} uses different GDGT components than TEX_{86}, it was converted to fit on the TEX_{86} as described by Pearson and Ingalls (2013).

Although the SST proxies have been widely applied in various marine settings, each proxy has its limitations, such as alteration by selective degradation and diagenesis (e.g., Hoefs et al., 1998; Schouten et al., 2004; Kim et al., 2009) or vulnerability to transport and re-deposition (e.g., Ohkouchi et al., 2002; Mollenhauer et al., 2003). Moreover, culture experiments with different haptophytes revealed the alteration of the alkenone distribution with changing light intensity, cell division rate, salinity and nutrient concentration (Epstein et al., 1998; Versteegh et al., 2001; Prahl et al., 2003; Ono et al., 2012). The influence of physiology and environment on TEX_{86} in cultures of marine AOA has not been systematically studied, but likely influences the TEX_{86} signal as well (Pearson and

Ingalls, 2013). For example, a recent study by Elling et al. (2014) revealed that the TEX_{86} varies with growth phase of *Nitrosopumilus maritimus*, which is so far the only available marine AOA isolate, indicating that the metabolic state impacts the GDGT cyclization. Other largely unconstrained variables are contributions from other archaea to the GDGT pool, e.g., planktonic *Euryarchaeota* (Turich et al., 2007; Lincoln et al., 2014b) and benthic archaea (Lipp and Hinrichs, 2009; Xie et al., 2013). Age offsets between crenarchaeol, which is solely produced by AOA, and the crenarchaeol regioisomer observed by Shah et al. (2008) suggest a mixed origin of GDGTs in marine sediments. The mechanism behind the correlation between LDI and temperature, the exact biological source and the effect of environmental factors on the LDI is not constrained and requires further investigations (cf. Rampen et al., 2012). To overcome uncertainties of the proxies, the use of more than one paleotemperature proxy within a marine sediment record is recommended. This allows for example to verify the consistency of results between different methods and to overcome ecological biases of the signal producers.

I.2.3. Respiratory quinones – structure, function and biomarker potential

In addition to IPLs and core lipids, the analysis of respiratory quinone composition can be used as indicator for microbial biomass and community composition and additionally provides information on the redox state of the microbial community (Hedrick and White, 1986; Hiraishi and Kato, 1999). Respiratory quinones represent a diverse group of lipids that play essential roles in electron and proton transport. As part of the respiratory transport chain, they are for example involved in the generation of the proton motive force during both aerobic and anaerobic respiration and they are important components in photosynthetic transport systems (Madigan et al., 2011). Quinones are mainly located within the cytoplasmic membrane (Figure I.8; Quinn, 2012) and are composed of a cyclic polar head group containing two keto-groups and a head-to-tail linked apolar isoprenoid side chain, which usually comprises 4 to 14 isoprenoid units (Figure I.9; Collins and Jones, 1981). The polar head groups can interact with the hydrophilic parts of proteins, while the small size of quinone molecules and the lipid-soluble character of the isoprenoid side chain enables movement through the membrane. These properties enable the transfer of electrons and protons between protein complexes (Nowicka and Kruk, 2010). The transport occurs via reduction and oxidation of the quinone/quinol couple (Figure I.8). Substantial differences in the redox potentials of the different quinone types have been observed (Figure I.9), i.e., high potential ubi- (UQ), plasto- (PQ) or caldariellaquinones (CQ), low potential menaquinones (MK) as well as quinones of intermediate potential, such as demethylmenaquinones (DMK; Hedrick and White, 1986; Wissenbach et al., 1990; Bekker et al., 2007; Nowicka and Kruk, 2010). Besides central

roles in transport systems, quinones are suggested to contribute to membrane adaptation to physiological stress. For example, Sévin and Sauer (2014) observed the accumulation of UQ in Escherichia coli grown at increased salt concentration and suggest that UQs containing >8 isoprenoid units function to enhance membrane stability in response to osmotic stress. Thus, quinones appear essential for a holistic understanding of membrane properties in microorganisms.

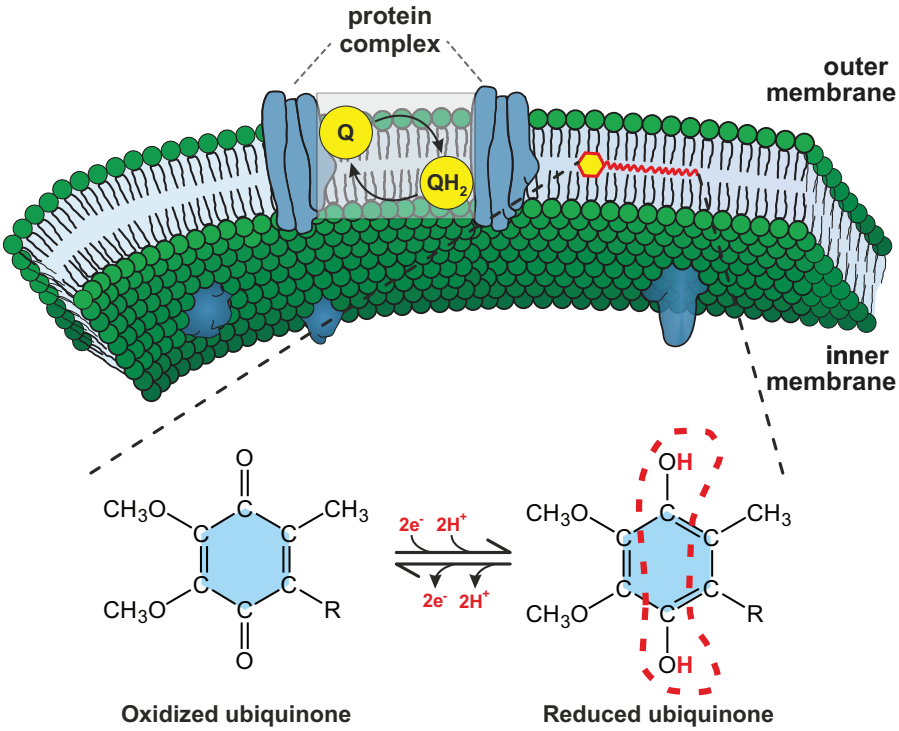

Figure I.8. Respiratory quinones in the cytoplasmic membrane. One respiratory protein complex transfers electrons and protons to the quinone (Q), which becomes reduced forming the quinol (QH_2). Another protein complex then accepts electrons and protons from QH_2. The yellow dot with the red tail within the phospholipid bilayer indicates the mobile character of quinones. UQs with ≥ 6 isoprenoid units have further been shown to be located in the mid plane of the membrane (Quinn, 2012) and they might be involved in membrane stabilization as response to osmotic stress (Sévin and Sauer, 2014). The structures of oxidized and reduced forms of a ubiquinone are shown at the bottom. The complete reduction of the quinone requires $2e^-$ and $2H^+$ (dashed red circle). R = isoprenoid side chain. Figure modified after Madigan et al. (2011), Kellermann (2012), and Clarke et al. (2014).

Respiratory quinones occur in almost all organisms, except for some obligatory fermentative bacteria (Collins and Jones, 1981) and methanogens (e.g., Thauer et al., 2008) and the type of quinone present in an organism is determined both by phylogeny and, due to their distinct redox potentials, also by the operating respiratory pathway (Collins and Jones, 1981; Bekker et al., 2007; Nowicka and Kruk, 2010). While microbes utilizing O_2 and nitrite mainly contain UQs, most anaerobic and facultative anaerobic prokaryotes predominantly synthesize MKs. Bacterial and eukaryotic photosynthetic organisms

contain neither UQs or MKs that are typically present in anaerobes, but phylloquinone (Vitamin K1), which is involved in electron transfer in photosystem I, and PQ, which is involved in in electron transfer in photosystem II. Besides the head groups, the side chain structures are of considerable value in classification, as they not only differ in length but also in the degree of unsaturation (Collins and Jones, 1981).

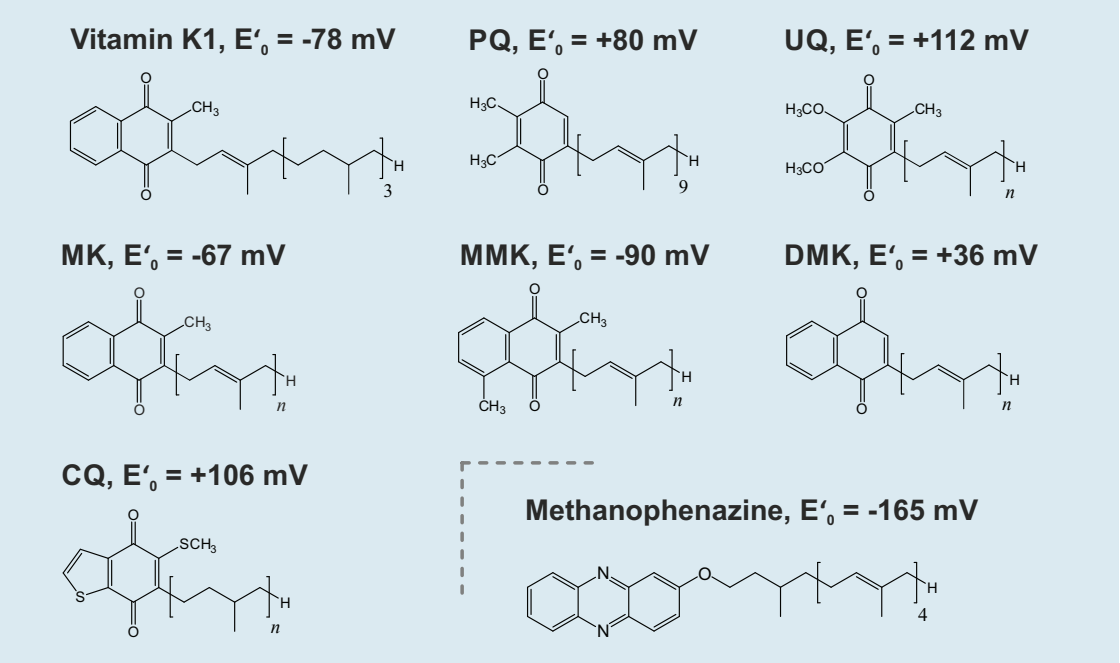

Figure I.9. Structures and midpoint redox potentials (E_0' at pH 7) of selected respiratory quinone classes as well as methanophenazine, an electron carrier in *Methanosarcinales*. The length and degree of unsaturation of the isoprenoid side chains of quinones may vary from 4 to 14 isoprenoid units and completely saturated to fully unsaturated, respectively. Abbreviations: DMK, Demethylmenaquinone; MK, Menaquinone; MMK, Methylmenaquinone; MP: Methanophenazine; CQ, Caldariellaquinone; PQ, Plastoquinone; UQ, Ubiquinone. Vitamin K1 = phylloquinone.

While the quinone composition in bacteria has been investigated in great detail (cf. Collins and Jones, 1981), the distribution of quinones in archaea is much less constrained (De Rosa et al., 1988). Studies on the quinone content in the archaeal domain have been restricted to halophiles, thermophiles and methanogens, while studies on the quinone content of the *Thaumarchaeota* has not been performed, although a central role of quinones in current models of the respiratory pathway for ammonia oxidation has been proposed (Walker et al., 2010; Stahl and de la Torre, 2012). In contrast to bacteria and eukaryotes, which contain polyunsaturated quinones (typically one double bond per isoprenoid unit or partially saturated compounds), many thermophilic archaea have been shown to produce fully saturated quinone compounds (Collins and Jones, 1981; Tindall et al., 1989; Hiraishi and Kato, 1999). However, the quinone composition of archaea revealed

a large structural diversity with specialized compounds in some lineages. For example, archaea from the order *Sulfolobales* contain quinones with an additional sulfur-containing heterocyclic ring, such as CQ, and it was suggested that its synthesis occurred as an adaptation to aerobic environments, due to the higher redox potential compared to MKs (Figure I.9; De Rosa et al., 1977). The thermoacidophile *Thermoplasma acidophilum* has further been shown to contain characteristic polyunsaturated methylated MKs (Shimada et al., 2001), while halophilic archaea exclusively contain polyunsaturated MKs (Collins and Jones, 1981), the latter likely having acquired quinone biosynthesis genes from bacteria via lateral gene transfer (Nelson-Sathi et al., 2012). In methanogens, respiratory quinones have not been detected; instead, representatives of the order *Methanosarcinales* contain the functional quinone analogue methanophenazine, an electron carrier directly involved in methanogenesis (Figure I.9; Abken et al., 1998).

Due to the physiological importance of isoprenoid quinones as well as their large structural diversity and taxonomic specificity, quinones likely provide valuable complementary information to other biomarker approaches, but applications of quinone analysis to marine environments are still very limited (Hedrick and White, 1986; Urakawa et al., 2000; Urakawa et al., 2001; Villanueva et al., 2010; Kunihiro et al., 2014) and are even lacking for the marine water column. Moreover, archaeal quinones have not been reported from any natural environment although their distribution patterns might help to constrain archaeal source organisms. Since additionally redox conditions and metabolism are major controls on the occurrence and relative abundance of specific quinones in microorganisms (Hedrick and White, 1986; Wissenbach et al., 1990; Bekker et al., 2007; Nowicka and Kruk, 2010), quinone-profiling likely contains an additional functional dimension to the quantitative aspects of for example IPL analysis.

The turnover times for respiratory quinones in marine environments have not been studied yet, although incubation experiments by Hedrick and White (1986) indicate rapid changes of the quinone distribution within a few days. This suggests that quinones represent reasonable life markers, but further investigations on the post-depositional behavior are required to use quinones as rigorous biomarkers especially in marine sediments.

I.2.4. Stable carbon isotopes of lipid biomarkers

The determination of compound-specific stable isotope ratios, especially those of carbon and hydrogen, of biologically produced organic molecules comprise an additional and important source of information for the reconstruction of modern and past environments. For carbon isotopes, the ratio of ^{12}C to ^{13}C depends on the isotopic composition of the utilized substrate, the isotopic fractionation associated with carbon assimilation,

metabolism and biosynthesis, and cellular carbon budgets (Hayes, 1993). Organisms typically discriminate against the heavier isotope since bonds formed by the lighter isotopes of an element are weaker, and thus react faster than bonds formed by the heavy isotopes. This results in progressive enrichment of ^{13}C in the precursor, while the end product, i.e., lipids, becomes depleted in ^{13}C (cf. Hayes, 2001). The extent of this kinetic isotope effect is further dependent on the carbon fixing enzymes used by an organism, and differences in the stable carbon isotope fractionation in different archaea and bacteria can be assigned to different carbon fixation pathways (Hayes, 2001; House et al., 2003; Pearson, 2010). Generally, organisms assimilating C1 compounds (CO_2, CH_4) have large fractionation effects, whereas only little fractionation is observed during heterotrophy, and the carbon isotopic composition of biomass and lipids broadly reflects its carbon source (DeNiro and Epstein, 1976; Hayes, 1993). This knowledge has been transferred

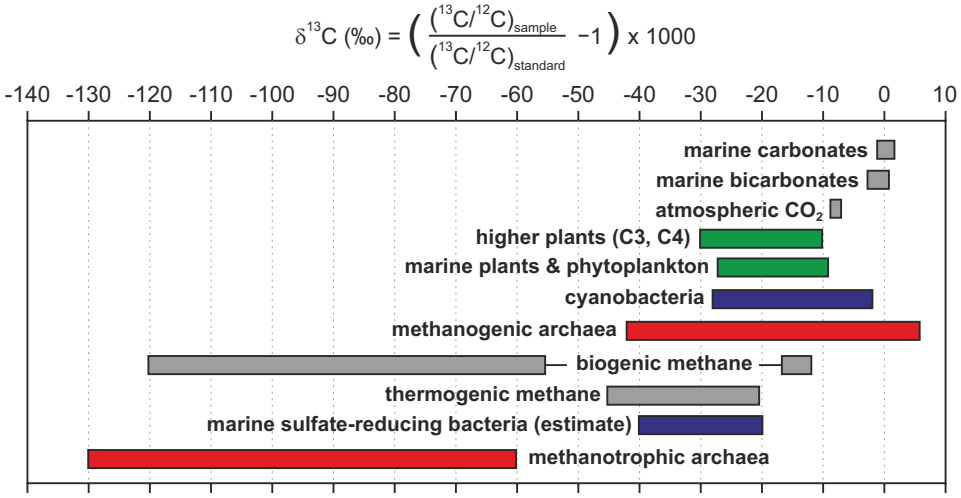

Figure I.10. Ranges of $\delta^{13}C$ values of selected archaeal (red), bacterial (blue), and eukaryotal (green) organisms as well as inorganic and organic carbon substrates (gray). Since stable isotope fractionations are small and for a better comparison they are expressed in per mil as the difference from the $^{13}C/^{12}C$ ratio of a standard, which is defined as 0 ‰ (usually Vienna PeeDee Belemnite). Figure adapted from Gaines et al. (2009) and Blumenberg (2010).

to the analysis of environmental samples, such as marine sediments. Carbon isotopic analysis of microbial biomolecules and their organic substrates has been used as a tool to reveal microbial metabolic pathways of carbon assimilation in modern systems and also helped to infer past microbial processes. The range of carbon isotopic compositions of different carbon reservoirs and organisms found in the marine environment is shown in Figure I.10. For example, the discovery of the elusive microbial communities that oxidize methane in anoxic marine sediments was based on the analysis of stable carbon isotopes, which revealed highly depleted $\delta^{13}C$ values of archaeal lipids (e.g., archaeol, OH-archaeol and crocetane) and were associated to strong fractionation during the uptake of methane (Elvert et al., 1999; Hinrichs et al., 1999).

I.3. Microbial lipid analysis

Microbial lipid analysis in this thesis was performed on samples obtained from marine sediments, the marine water column and pure cultures of archaea. All samples were immediately frozen at either −20 or −80 °C after recovery to avoid degradation of IPLs or post-collection growth of non-indigenous microorganisms (cf. Lin et al., 2010). Lipids were extracted using a modified Bligh and Dyer protocol, which has been developed to extract both archaeal and bacterial/eukaryotic IPLs (Sturt et al., 2004). For identification and quantification, the resulting total lipid extract (TLE) was either measured directly by high performance liquid chromatography coupled to mass spectrometry (HPLC–MS) or further separated into different lipid classes by semi-preparative HPLC before analysis. For intramolecular isotopic analysis of IPLs and tetraether core lipids, cleavage reactions were further necessary to obtain GC-amenable compounds (Figure I.11). In the following sections the different analytical techniques relevant for this thesis are described in detail.

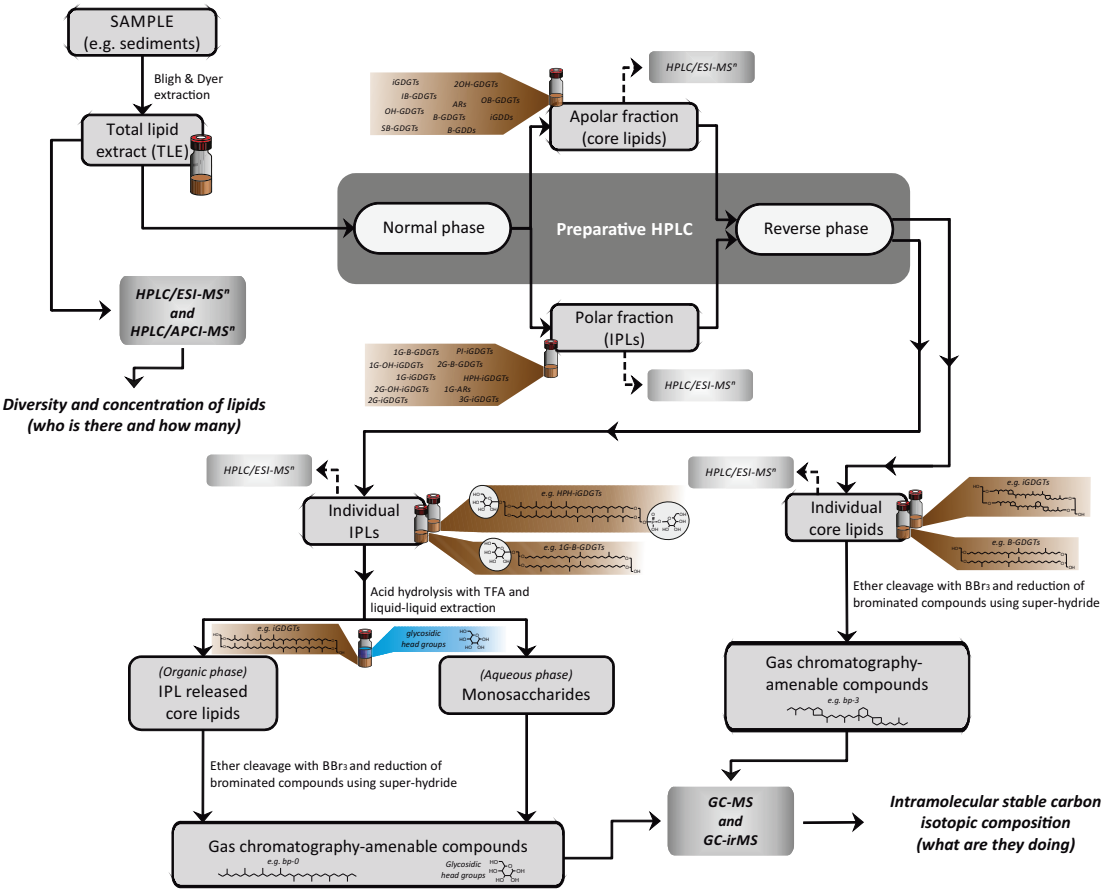

Figure I.11. Flow chart of the major laboratory steps. Bligh and Dyer extracted samples were measured by HPLC–MS to determine lipid concentration and distribution. For intramolecular stable carbon isotope analysis, the TLE was subjected to normal- and reverse phase semi-preparative HPLC to obtain individual core lipid and IPL fractions and break-down products were analyzed by GC after acid hydrolysis and/or ether cleavage reactions. Representative structures of target compounds and break-down products for each step are also shown (cf. Figure I.5).

I.3.1. Analytical techniques

Analytical techniques, such as gas and liquid chromatography-based methods, build the basis for lipid biomarker analysis and determine the amount of information that can be gleaned from a natural sample. The most important goal for chromatographic techniques, such as chromatography, is information per unit time at a resolution adequate to separate the components of interest. Moreover, in order to capture the full diversity of lipids, highly sensitive methods are required and for different target compounds different analytical protocols are to be used (Figure I.12). Mass spectrometry has emerged as a powerful tool for the quantitative and qualitative analysis of lipids and enables detailed structural elucidation of complex lipids when combined with gas or liquid chromatography–mass spectrometry.

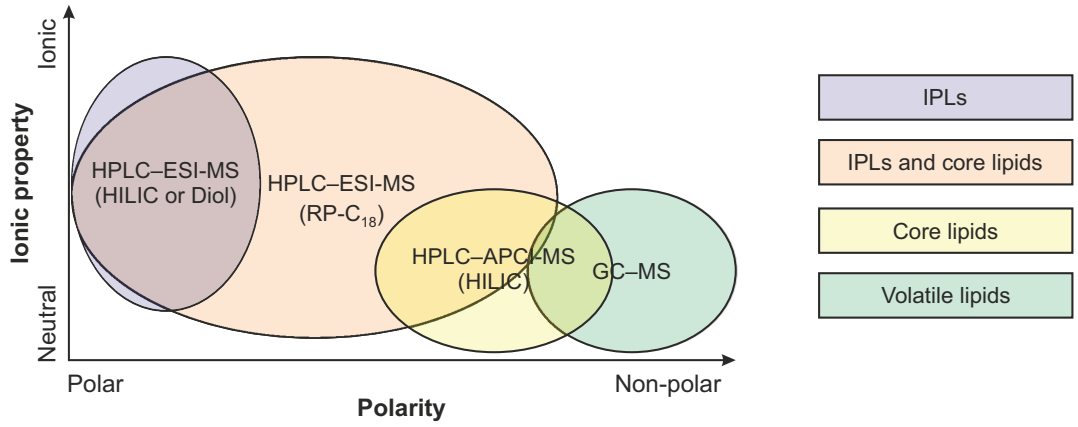

Figure I.12. Venn diagram showing the overlap of lipids detectable by GC–MS, HPLC–APCI-MS and HPLC–ESI-MS (modified after You et al., 2014). For HPLC–MS methods the separation column is denoted since the analytical window is strongly dependent on the choice of chromatographic conditions.

I.3.1.1. Gas chromatography-based methods

The most commonly used chromatographic technique in organic geochemistry is gas chromatography, which facilitates the separation, detection and quantification of individual compounds in complex mixtures such as extracts from marine sediments. One requirement for GC-based analysis is that the target compounds are easily transferred into the gaseous phase. The general principle of GC separation is the partitioning of analytes between a mobile gaseous phase and a liquid stationary phase at temperatures above their boiling points. Most GC-columns are used in a thermostat-regulated oven and can be heated up to 400 °C, which limits this techniques to analysis of analytes with lower boiling points. Detection of compounds is mainly achieved by either flame

ionization detection (FID) or mass spectrometry (MS). While FID provides quantities of target compounds but is indiscriminate of the type of analyte, MS-based detection additionally provides rich information on structure and molecular mass. GC-based methods are used for the quantification and identification of a diverse array of compounds, such as *n*-alkanes, fatty acids and alcohols including sterols and hopanols in a mass range of ca. 50-700 Da. The commonly applied methods allow chromatographic separation of compounds with minor structural differences such as *n*-alkyl lipids with different degrees of unsaturation as well as structural isomers, e.g., *cis*- and *trans*-isomers and *iso* and *anteiso* branching patterns of fatty acids analyzed as methyl esters, which are valuable biomarkers for chemotaxonomy (e.g., Volkman et al., 1998). However, GC-based methods are not suitable for high molecular weight compounds such as IPLs and GDGT core lipids and therefore alternative instrumental approach are required for their separation and identification in mixtures. Attempts to analyze more polar and high molecular weight compounds (e.g., core GDGTs) by GC were made in the past by using high-temperature GC (Nichols et al., 1993; Weijers et al., 2006; Pancost et al., 2008). However, such methods are not routinely applied because they are laborious and impacted by various constraints. For example, GDGTs containing OH groups in the biphytane chain are not thermostable if analyzed with GC and the chromatographic resolution is generally worse than that for HPLC methods.

I.3.1.2. Liquid chromatography-based methods

Liquid chromatography. Traditionally, the study of membrane lipids as biomarkers in modern prokaryotic ecosystems has focused on derivatives of the original membrane lipids formed by breakdown of the polar precursor (e.g., Langworthy et al., 1972; White et al., 1979; Guckert, 1985) largely through the application of GC. Consequently, the polar lipid sources of core lipids and fatty acids have largely escaped detailed examination, since IPLs are not amenable to GC analysis. However, IPLs are taxonomically more specific than their constituent fatty acids (Fang et al., 2000; Rütters et al., 2002) and hence, more comprehensive and specific information can be obtained by their direct analysis. The original methods for detecting and identifying such high molecular weight lipids mainly relied on thin layer chromatography (TLC) and the subsequent infrared or nuclear magnetic resonance (NMR) spectrometric analysis of the isolated compounds (e.g., Langworthy, 1977). However, this approach is not practicable for most samples from natural environments such as sediments due to complex sample matrices that complicates isolation of pure compounds. Moreover, large sample volumes are generally required, which is often not feasible for sample screening.

The development of high performance liquid chromatography–electrospray ionization-

mass spectrometry (HPLC–ESI-MS) for direct analysis of intact phospho- and glycolipids (Rütters et al., 2002; Sturt et al., 2004) revolutionized the use of IPLs as biomarkers for studying active microbial communities in samples from the natural environment. These methods separate IPLs of complex mixtures by their differing polar head groups and recent studies employing this technique have revealed a broad molecular diversity of IPLs for both eukaryotic and prokaryotic microbes (e.g., glycolipids, betaine lipids) in marine environments that extends far beyond the more commonly known phospholipids (Rütters et al., 2002; Zink et al., 2003; Sturt et al., 2004; Suzumura, 2005; Van Mooy et al., 2006; Schubotz et al., 2009; Van Mooy et al., 2009). However, in order to acquire detailed information on core lipid (e.g., cyclopentylation) and fatty acid side chain structure (e.g., *iso* and *anteiso* branching pattern), hydrolysis of IPLs and subsequent GC analysis are still necessary as such details cannot be resolved with HPLC–ESI-MS methods, and consequently individual identification and quantification is currently impossible.

Due to the large size of core GDGTs (>1000 Da), they were initially analyzed by GC–MS as biphytanes after ether cleavage of the molecules (e.g., Michaelis and Albrecht, 1979; Chappe et al., 1982; Schouten et al., 1998). Nowadays, the direct analysis of core GDGTs is achieved by HPLC–MS but instead of ESI, atmospheric pressure chemical ionization (APCI) is typically used. Hopmans et al. (2000) established HPLC–APCI-MS for direct analysis, and research on the environmental occurrence and geochemical importance of GDGTs greatly expanded since this important analytical advancement. For example, the detection and identification of crenarchaeol (Sinninghe Damsté et al., 2002) and non-isoprenoid branched GDGTs (B-GDGTs) of bacterial origin (Sinninghe Damsté et al., 2000) has been facilitated by HPLC–APCI-MS. Detailed studies on the distribution of these GDGTs in marine sediments and soils showed that they carry information on environmental parameters such as SST (Schouten et al., 2002), soil organic matter input (Hopmans et al., 2004), and soil pH and mean air temperature (Weijers et al., 2007). These proxies based on GDGT distributions are now widely applied in paleoenvironmental studies. Moreover, the extension and improvement of these methods aided further discovery of a multitude of novel GDGT compounds such as B-GDGTs containing higher (OB-GDGTs) and lower (SB-GDGTs) degrees of methylation (Liu et al., 2012c) as well as hybrid isoprenoid/branched GDGTs (IB-GDGTs; Schouten et al., 2000; Liu et al., 2012c). Although the biological source for many of these lipids is still unknown, their widespread occurrence in the marine environment suggests a significant role of the signal producers (Schouten et al., 2000; Liu et al., 2012c, 2014; Xie et al., 2014).

However, the methods for both IPL and core lipid analysis still have their limitations. Despite the recent advances, the diversity of structures, properties and the wide range of concentrations in environmental samples often requires a combination of complementary protocols to fully characterize a sample. The overall workflow is thus rather

complex, time-consuming and susceptible to errors induced by sample preparation steps necessary before analysis, such as separation of free core lipids from IPLs and hydrolysis of polar head groups. Another concern is the incomplete separation of isomers of core GDGTs by applying the conventional HPLC–APCI methods. The presence of several isomers of both B-GDGTs as well as isoprenoid GDGTs, which partly co-elute with the original compounds, have been widely observed (Weijers et al., 2007; Pitcher et al., 2009a; Sinninghe Damsté et al., 2012) and initiated the improvement of chromatographic separation of specific B-GDGT isomers (Zech et al., 2012; Becker et al., 2013; De Jonge et al., 2013).

The availability of new modes of separation, for instance separation columns containing sub-2 μm particles with alternative stationary phases, such as hydrophilic interaction liquid chromatography (HILIC) or reversed phase (RP) applied in ultra-high performance liquid chromatography (UHPLC), resulted in higher chromatographic separation and enables separation of previously co-eluting compounds. The latter method offers the unique possibility to analyze IPLs and core lipids in the same chromatographic run (Wörmer et al., 2013). This method is further suitable for separation of IPLs based on side chain length, degree of saturation and/or presence of acyl/ether bonds that were previously inaccessible using the initial normal phase methods for IPL analysis. Modifications of this RP method by using a different separation column (C_{18} RP column) even allows explicit determination of IPL-specific TEX_{86} and ring index and thus provides new insights into diagenetic and biological mechanisms inherent to these proxies (Zhu et al., 2013a). These developments have opened up new analytical avenues and revealed novel biomarkers valuable for proxy development, such as archaeal core and intact GDGTs containing unsaturations in the isoprenoid side chain, which are likely produced by uncultivated anaerobic planktonic and benthic archaea (Zhu et al., 2014b).

Mass spectrometry. In addition to the new modes of chromatographic separation the improved methods also employ state-of-the-art, high accuracy MS offering highly sensitive analysis as well as detailed structural information. A variety of different mass analyzers have been employed for lipid analysis, including quadrupole, ion-trap, time-of-flight and Fourier transform (FT) analyzers, which discriminate on the basis of the mass to charge ratio (m/z) of the detected analyte. Single quadrupole MS systems are well suited for routine analysis of known compounds at low detection limits, especially in selected ion monitoring (SIM) mode. This MS technique is most commonly applied for analysis of core GDGTs and is ideal for the determination of their related proxies (cf. Schouten et al., 2013b). One limitation of single quadrupole MS arises from the use of only a single stage of mass spectrometric analysis. Thus, the lipids are only assigned on the basis of their retention times and the m/z of protonated molecules, but structural

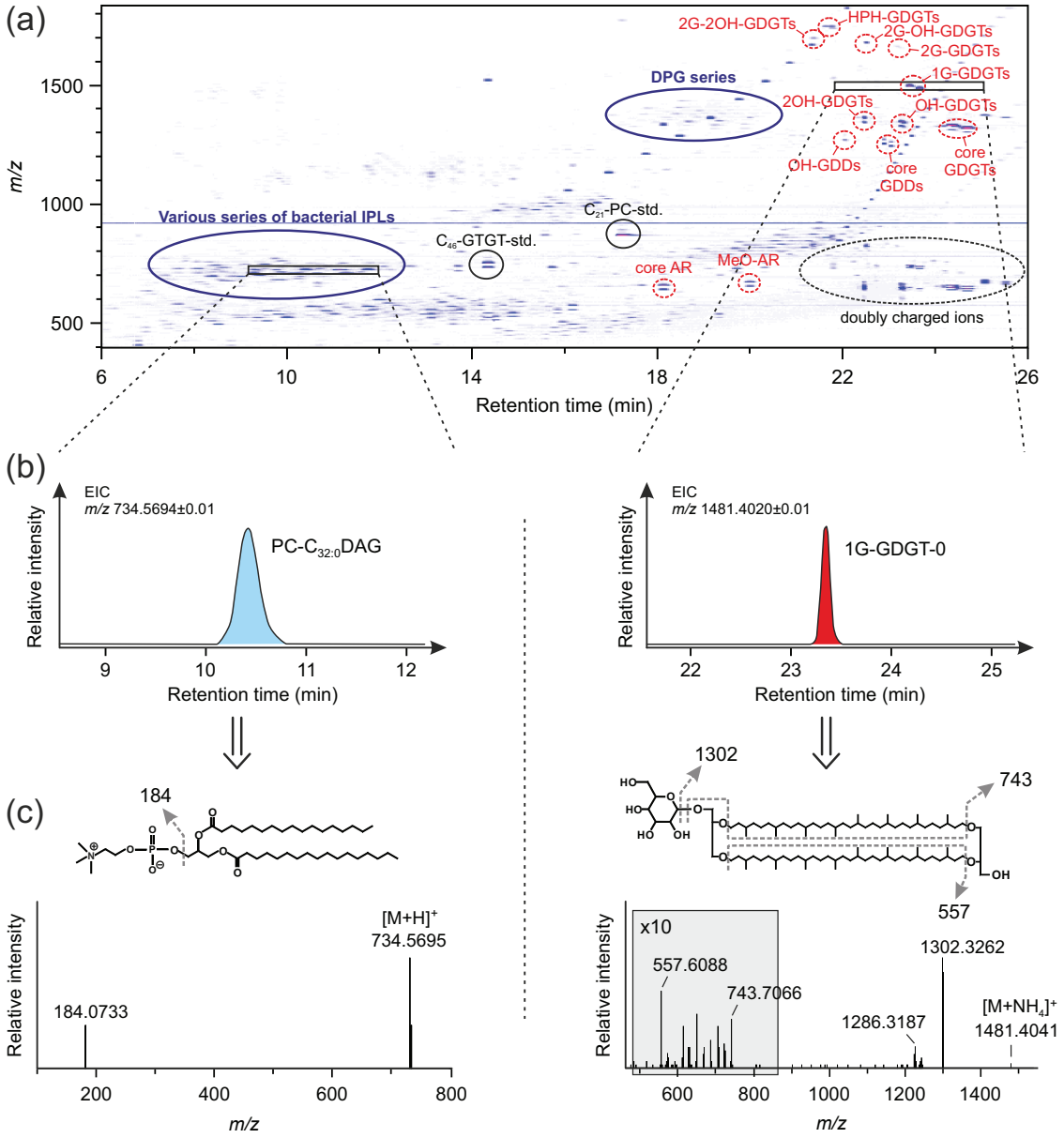

Figure I.13. Lipid analysis and identification. (a) RP-UHPLC–ESI-qToF-MS density map (x = time, y = *m/z*, z = intensity) showing elution order and *m/z* of archaeal (red) and bacterial (blue) lipids in positive ionization mode in sample M84/1, GeoB15102-3, 3570 mbsl. This sample originates from the brine-seawater interface from the deep-sea hypersaline Discovery Basin in the Eastern Mediterranean. IPLs and core lipids can be detected in one analysis. Compounds are mainly separated by chain hydrophobicity and most bacterial phospholipids elute closely together, but IPLs with the same head group are separated according to side chain structure (Wörmer et al., 2013, e.g., chain length, degree of saturation or the presence of ether instead of ester bonds; cf.). (b) Extracted ion chromatograms (EIC) of the bacterial IPL PC-$C_{32:0}$DAG and the archaeal IPL 1G-GDGT-0 using an isolation width of 10 mDa of their exact masses. (c) Multiple stage mass spectra (MS^2) of PC-$C_{32:0}$DAG and 1G-GDGT-0, respectively. Additionally, the corresponding structures and the formation of major product ions are shown. Note that the mass range between *m/z* 500-850 for the 1G-GDGT-0 spectrum is enlarged. Most IPLs typically lose their polar head group from which a diagnostic neutral mass loss can be calculated (e.g., 1G, neutral loss of 162 Da). Other IPLs show a major ion representing the polar head group (e.g., PC, *m/z* at 184 Da). For archaeal lipids additional information on side chain structures can be obtained from the MS^2 spectrum in positive ion mode, while for bacterial IPLs, negative ion mode is required for information on fatty acid compositions.

information from fragmentation of parent ions cannot be obtained. For IPLs, structure elucidation by multiple stage MS (MS^n) is extremely useful due to their large diversity and high complexity and a widely applied technique for analysis of environmental samples is ion trap-based MS^n. The main advantage of the ion trap is the possibility of performing data-dependent MS^n where several consecutive fragmentation steps on a selected ion are performed. This allows detailed structural characterization of IPLs by combining information gained in positive and negative ionization modes (Figure I.13) by combining information gained in positive and negative ionization modes (e.g., Rütters et al., 2002; Sturt et al., 2004; Yoshinaga et al., 2011). Triple quadrupole MS probably provides the most sensitive and selective method for targeted analysis currently available and thus brings many advantages for quantitative analysis (e.g., lower limit of quantification in the fg range on column). This MS technology further offers specialized scan modes such as the ability to perform multiple reaction monitoring, neutral loss-, and precursor ion-scanning experiments, which not only provides quantification at very high sensitivity but also helps with identification of structures. However, quadrupole-based MS is usually limited to a mass accuracy of 0.1 Da and unit resolution. In contrast, instruments such as the time-of-flight (ToF) MS and the Fourier transform orbitrap MS typically provide mass accuracies on the order of <5 ppm and a mass resolution in the range of tens to hundreds of thousands, which can be obtained in both MS^1 full scan and MS^2 fragment spectra. Therefore, these systems are ideal for screening and characterization of unknown compounds. The recent advancements in MS technologies provide innovative analytical solutions for different tasks in environmental lipid profiling, especially in environments with low biomass concentration and complex sample matrices, and will expand the dynamic range of lipidome observations ultimately leading to a better understanding of microbial life in the marine realm.

Chapter II

Scope and Outline

This PhD thesis is connected with the interdisciplinary project 'Deep subsurface Archaea: carbon cycle, life strategies, and role in sedimentary ecosystems' (DARCLIFE) which started in April 2010 and was granted by the European Research Council (ERC) for five years as Advanced Investigator grant to Professor Kai-Uwe Hinrichs. The main objectives of this project are to get detailed information about the factors that control the distribution of benthic archaea in marine sedimentary systems and their role within the carbon cycle. This frontier research aimed to constrain the role of benthic archaea in the Earth system and to examine the fundamental properties of life at minimum energy. Within the framework of DARCLIFE, this thesis focused on the information encoded in the distribution and isotopic composition of microbial membrane lipids in environmental samples and archaeal cultures. The major goals were to develop advanced chromatographic methods for lipid analysis as well as to investigate the biological origin and fate of microbial lipids in the marine environment.

In a variety of aquatic environments, microbial membrane lipid analysis has been successfully applied as markers in microbial ecology and biogeochemistry, including marine sediments, cold seeps, hot springs and the marine water column. Additionally, fossil lipids preserved in the sedimentary record are widely used for the reconstruction of paleoenvironmental conditions such as the TEX_{86} for past SSTs, as the lipid distributions reflect the conditions of the time when community members have existed. In general, however, most of the lipids are common to several phylogenetically related organisms within a domain and lipid distribution patterns are a response to multiple environmental variables and depend on the physiology of their producers. Consequently, their use as biomarker molecules is often limited. Moreover, the degradation kinetics of IPLs are not well constrained and the transition between bio- and geomolecules is blurry.

This especially applies to marine sediments where deposits serve as an archive for paleoenvironmental reconstructions, and at the same time provide habitat for a vast number of active microbes. Hence the identification of new biomarkers – which may offer greater taxonomic specificity or additional information about life strategies – would provide substantial advantage for the study of both modern microbial ecology and past environmental conditions. Analytical techniques, such as HPLC–MS-based methods, are the foundation for lipid biomarker analysis and essential for the discovery of new biomarkers and the subsequent development of new proxies. However, the detection of microbial life in systems with very low microbial activity and abundances, such as the deep marine biosphere, is challenging, since existing methods often do not provide the required low limit of detection. To overcome these problems and to capture the full diversity of microbial lipids in the environment, highly sensitive and precise methods are required.

II.1. Objectives

This thesis is guided by the following objectives:

1. **To improve existing analytical methods for the analysis of ether core lipids in environmental samples by using novel modes of chromatographic separation, to drastically lower limits of detection, to increase sensitivities, and to determine the structures of previously inaccessible compounds by multiple stage mass spectrometry.**

   Chromatographic co-elution of core GDGTs isomers was observed in many HPLC chromatograms when using existing methods. The incomplete separation likely results from the similarity in the structures, so that component quantification is problematic, which is of particular concern for GDGT-based proxies, such as the TEX_{86}. Chromatographic separation of these compounds would allow a more nuanced exploration of the distribution of these lipids in the environment and might provide previously hidden clues regarding source organisms.

2. **To validate the novel protocol for the determination of paleoenvironmental proxies and to significantly simplify the overall analytical workflow for these proxies.**

   The reconstruction of SSTs is a primary concern in paleoclimate research and a variety of organic and inorganic proxies exist. The organic geochemical SST proxies are organism-based and thus affected by the ecology of the signal producers. Consequently, other environmental variables than temperature, e.g., nutrient availability, influence lipid distributions. Multiproxy approaches have been widely applied to verify the consistency of results from different proxies, but they typically require more investment in time and resources, while being susceptible to errors induced by sample preparation steps necessary before analysis. To reduce sources of errors, simple and fast protocols are needed that additionally allow high sample throughput in relatively short time.

3. **To study the microbial ecology of the deep-sea hypersaline anoxic Discovery Basin and underlying sediments, to determine signatures for distinct membrane lipid adaptations to this hostile environment, to examine what additional information can be gained from IPL and core lipid analysis compared to other molecular techniques, and to investigate the development of microbial life.**

   The Discovery Basin is one of the most extreme environments on our planet exhibiting the highest concentration of Mg^{2+} found so far in the natural environment in addition to anoxia, high hydrostatic pressure and no light. The conditions in the Discovery Basin likely limit microbial life to the brine-seawater interface but still, several studies revealed that microbial metabolism can proceed even at significant Mg^{2+} levels of up to 2.3 M in this system. Besides known halophilic archaea and bacteria, the identified microbial populations include distantly related microbes to known phylogenetic clades, and thus this system provides a unique opportunity to study microbial membrane lipid adaptations and to discover new biomarkers. Distinct membrane lipid adaptation can be expected in response to the multiple extremes. The high Mg^{2+} concentrations in the sediments likely result in excellent preservation of molecular markers and sedimentary IPLs may thus provide a record of microbial life biosignatures from times prior to the brine formation to modern conditions.

4. **To examine the full potential of respiratory quinones as chemotaxonomic marker for environmentally relevant archaeal groups, by studying the quinone inventories in a range of cultivated archaea.**

   Quinones are membrane-bound lipids functioning as electron carriers in respiratory chains of almost all organisms. They have the potential to provide clues on both the taxonomy of their producers and the redox processes these are mediating. However, the quinone composition particularly in archaea is still fragmentary limiting their use as rigorous biomarkers for organisms of this domain.

5. **To examine the proxy potential of quinones for studying microbial respiration in the marine environment by determining the abundance and diversity of microbial quinones in suspended particulate matter and sediment samples from the Black Sea and by interpreting the quinone data in the context of complementary information on geochemistry and IPLs.**

   The Black Sea is the World's largest stratified marine basin and is separated into oxic, suboxic, and euxinic zones and thus serves as redox gradient in which microorganisms respire through a succession of redox reactions. Concerning this distinct zonation and the well-studied microbial community composition, the Black Sea serves as an ideal model ecosystem for studying microbial life. Thus, the utility of quinones as proxies for the study of microbial ecology and biogeochemistry can be ideally investigated at this site.

These objectives were addressed in total in six chapters. **Chapters III and IV** focus on the improvement of analytical protocols for environmental lipid profiling and its application to paleobiomarker studies and address objectives 1 and 2. **Chapter V** describes novel presumably diagenetically produced compounds and their distribution in diverse marine environments. **Chapter VI** addresses objective 3 and provides a comprehensive study of microbial membrane lipids in the deep-sea hypersaline Discovery Basin. In **Chapter VII**, we investigate the quinone inventories of 25 archaeal species belonging to the archaeal phyla *Eury-* , *Cren-*, and *Thaumarchaeota* and in **Chapter VIII**, we performed an in-depth analysis of respiratory quinones in the different redox zones of the Black Sea, to address objectives 4 and 5, respectively.

II.2. Contributions to publications

This PhD thesis includes the complete versions of six first-author manuscripts for publication in international journals (chapters III - VIII) of which two are shared first-author manuscripts (chapters VII and VIII). All other co-author contributions are summarized in the appendix together with manuscript abstracts.

Chapter III

An improved method for the analysis of archaeal and bacterial ether core lipids.

Kevin W. Becker, Julius S. Lipp, Chun Zhu, Xiao-Lei Liu and Kai-Uwe Hinrichs

Published in *Organic Geochemistry*, 2013, Vol. 61, pages 34-44.
doi: 10.1016/j.orggeochem.2013.05.007

J.S.L. and K.-U.H designed the project; K.W.B. developed the method with help from J.S.L and C.Z.; K.W.B. extracted, analyzed and evaluated lipid data with help from J.L.S.; K.W.B. wrote the manuscript with contributions from all co-authors.

Chapter IV

Rapid and simultaneous analysis of three molecular sea surface temperature proxies and application to sediments of the Sea of Marmara.

Kevin W. Becker, Julius S. Lipp, Gerard J.M. Versteegh, Lars Wörmer and Kai-Uwe Hinrichs

Published in *Organic Geochemistry*, 2015, Vol. 85, pages 42-53.
doi: 10.1016/j.orggeochem.2015.04.008

K.W.B. and K.-U.H. designed the project; K.W.B. optimized the method with help from J.L.S. and L.W.; K.W.B. and G.J.M.V. provided the samples; K.W.B. extracted, analyzed and evaluated lipid data with help from J.S.L; K.W.B. wrote the manuscript with contributions from all co-authors.

Chapter V

Identification, formation and distribution of fatty acid-substituted glycerol dialkyl glycerol tetraethers in marine sediments.

Kevin W. Becker, Felix J. Elling, Julius S. Lipp, Jan M. Schröder, Thomas W. Evans, Marcus Elvert, Martin Könneke and Kai-Uwe Hinrichs

In preparation for *Organic Geochemistry*

K.W.B. and K.-U.H. designed the project; K.W.B., F.J.E., J.M.S., M.K. and T.W.E provided samples and extracted, analyzed and evaluated lipid data with help from J.S.L. and M.E.; K.W.B. wrote the manuscript with contributions from all co-authors.

Chapter VI

Record of microbial life in the deep-sea hypersaline anoxic Discovery Basin and sediments.

Kevin W. Becker, Marcos Y. Yoshinaga, Cassandre Lazar, Julius S. Lipp, Marcus Elvert, Verena B. Heuer, Matthias Zabel, Tobias Goldhammer, Ivano W. Aiello, Andreas P. Teske, Yuki Morono, Fumio Inagaki and Kai-Uwe Hinrichs

In preparation for *Geochimica et Cosmochimica Acta*

K.U.-H. designed the project; K.W.B. extracted, analyzed and evaluated lipid data with help from M.Y.Y., J.S.L. and M.E.; C.L., Y.M. and F.G. provided cell count data; V.B.H. provided bulk parameters of organic carbon; M.Z. and T.G. provided inorganic geochemistry data; K.W.B. wrote the manuscript with contributions from all co-authors.

Chapter VII

Respiratory quinones in *Archaea*: phylogenetic distribution and application as biomarkers in the marine environment.

Felix J. Elling*, Kevin W. Becker*, Martin Könneke, Jan M. Schröder, Matthias Y. Kellermann, Michael Thomm and Kai-Uwe Hinrichs
*equal contribution

Under review at *Environmental Microbiology*

F.J.E., K.W.B., and K.-U.H. designed the research; M.T. provided samples; F.J.E., K.W.B., J.M.S., and M.Y.K. performed lab work; F.J.E. and K.W.B. analyzed data with contributions from J.M.S., M.Y.K., M.K., and K.-U.H.; F.J.E., K.W.B. and M.K. wrote the manuscript with contributions from all co-authors.

Chapter VIII

Sources, distribution and fate of respiratory quinones in the water column and sediments of the Black Sea.

Kevin W. Becker*, Felix J. Elling*, Jan M. Schröder, Julius S. Lipp, Matthias Zabel and Kai-Uwe Hinrichs
*equal contribution

In preparation for *Geochimica et Cosmochimica Acta*

K.W.B., F.J.E., and K.-U.H. designed the research; K.W.B., F.J.E., and J.M.S performed lab work; M.Z. provided data; K.W.B., F.J.E., and J.M.S. analyzed data with contributions from J.S.L., M.Z., and K.-U.H.; K.W.B. and F.J.E. wrote the manuscript with contributions from all co-authors.

Chapter III

An improved method for the analysis of archaeal and bacterial ether core lipids

Kevin W. Becker*, Julius S. Lipp, Chun Zhu, Xiao-Lei Liu and Kai-Uwe Hinrichs

Published in *Organic Geochemistry*
Vol. 61 (2013), pages 34-44. doi: 10.1016/j.orggeochem.2013.05.007

Organic Geochemistry Group, MARUM - Center for Marine Environmental Sciences &
Department of Geosciences, University of Bremen, 28359 Bremen, Germany

*Corresponding author. E-mail: k.becker@uni-bremen.de

Abstract

In recent decades, microbial membrane lipids have become focus of geoscientific research because of their proxy potential. The aim of this study was to develop new methods for ultra high performance liquid chromatography (UHPLC) separation of isomers of archaeal and bacterial membrane ether lipids, in particular glycerol dialkyl glycerol tetraethers (GDGTs), because of their tendency to co-elute with related but incompletely characterized derivatives. Our newly developed protocol, involving analysis using two Acquity BEH HILIC amide columns in tandem, enables chromatographic separation of several of these co-eluting compounds, such as the isoprenoid GDGT with four cyclopentyl moieties and other chromatographic shoulders often observed in GDGT analysis. Additionally, resolved peaks were observed for isoprenoid GDGTs, branched GDGTs and isoprenoid glycerol dialkanol diethers (GDDs); these have typically the same molecular mass as the corresponding major compound. Multiple stage mass spectrometry MS^2 indicated that the shoulder peaks represent either regioisomers or other structural isomers with different ring or methyl positions. In some samples, these isomers can be even more abundant than their regular counterparts, suggesting that previously hidden clues regarding source organisms and/or community response to environmental forcing factors may be encoded in the distributions.

III.1. Introduction

Archaeal and bacterial glycerol ether lipids are widespread in marine and terrestrial environments (Schouten et al., 2000, 2002; Weijers et al., 2007; Lipp et al., 2008; Liu et al., 2012c). The prominent glycerol dialkyl glycerol tetraethers (GDGTs) and glycerol dialkyl diethers (e.g. archaeol) provide information on the biogeochemistry and microbial ecology of natural ecosystems in modern and in ancient environments (e.g. Hoefs et al., 1997; Hinrichs et al., 1999; Kuypers et al., 2001; Biddle et al., 2006; Lipp et al., 2008; Lipp and Hinrichs, 2009). The respective core glycerol ether lipids are preserved in sediments on geological timescales and enable study of past archaeal activity (e.g. Bolle et al., 2000; Kuypers et al., 2001). Core GDGTs are used for a variety of paleoceanographic proxies such as TEX_{86} for sea surface temperature (SST) reconstruction (Schouten et al., 2002). It utilizes isoprenoid GDGTs from planktonic archaea and is based on the observation that an increasing number of cycloalkyl moieties in the GDGT distribution corresponds to increasing mean annual sea surface temperature. Moreover, proxies for the reconstruction of soil input to the ocean (BIT index; Hopmans et al., 2004), mean annual air temperature (MAAT) and soil pH (Weijers et al., 2007) were developed on the basis of branched GDGTs (*br*GDGTs), which originate partly from anaerobic soil bacteria. These proxies, in particular for MAAT and soil pH reconstruction, measure the degree of methylation (MBT) and cyclization (CBT) of *br*GDGTs, respectively. Another ubiquitous series of ether lipids in marine sediments is glycerol dialkanol diethers (GDDs), which have recently been identified (Liu et al., 2012a). Due to their recent discovery, the exact source of these lipids and their biogeochemical significance, as well as their significance as biomarkers, requires further exploration.

Conventional analytical methods, in particular gas chromatography (GC), are unsuitable for direct analysis of GDGTs because they are non-volatile high molecular weight compounds. For a long time analysis had to target the GC-amenable products of the ether cleavage reaction (e.g. De Rosa et al., 1977; Michaelis and Albrecht, 1979). The introduction of protocols utilizing high performance liquid chromatography-atmospheric pressure chemical ionization-mass spectrometry (HPLC-APCI-MS) for direct analysis of GDGT core lipids Hopmans et al., 2000 facilitated the identification and quantification of these compounds. More recently, modified protocols for this method have been published, which on the one hand improved analysis speed and reduced solvent amount (Escala et al., 2007; Schouten et al., 2007) and on the other hand improved the chromatographic separation of specific GDGT isomers (Zech et al., 2012; De Jonge et al., 2013). However, in many chromatograms, GDGT peaks still showed shoulders due to co-elution with largely uncharacterized compounds. For example, lipids with the same molecular mass as the GDGTs used for TEX_{86}, but with slightly earlier elution times

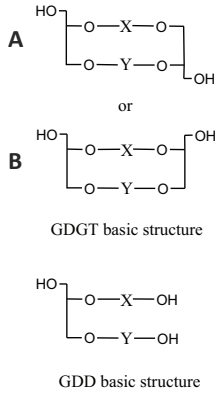

GDGT no.	X	Y	GDGT basic structure	Number of isomers
0	a	a	A, B	2
1	a	b	A, B	4
1	b	a	A, B	
2	b	b	A, B	8
2	b	b'	A, B	
2	b'	b	A	
2	a	c	A, B	
2	c	a	B	
3	b	c	A, B	12
3	b'	c	A	
3	c	b	B	
3	a	d	A, B	
3	d	a	A, B	
3	a	e	A, B	
3	e	a	A, B	
5	c	f	A, B	4
5	f	c	A, B	

GDD no.	X	Y	Number of isomers
0	a	a	1
1	a	b	4
1	a	b'	
1	b	a	
1	b'	a	
2	b	b	6
2	b	b'	
2	b'	b	
2	b'	b'	
2	a	c	
2	c	a	
3	b	c	12
3	b'	c	
3	c	b	
3	c	b'	
3	a	d	
3	a	d'	
3	d	a	
3	d'	a	
3	a	e	
3	a	e'	
3	e	a	
3	e'	a	
5	c	f	4
5	c	f'	
5	f	c	
5	f'	c	

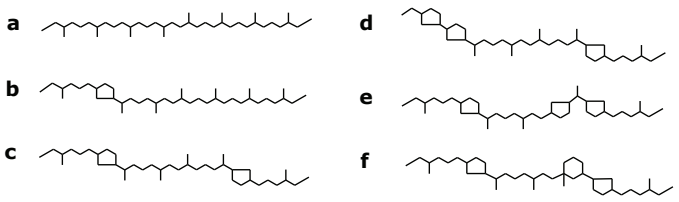

Figure III.1. Structures of biphytanyl di- and tetraether membrane lipids. The basic structure of a GDGT is composed of two biphytanyl units X and Y, which may be interchanged with respect to their positions at *sn*-2 and *sn*-3 of glycerol. For the basic structure of a GDGT both the anti-parallel (A) and parallel configurations (B) are drawn. In addition, the basic structure of a GDD is shown, which is ether bound to isoprenoid chains containing 0 to 3 rings. The tables provide structural combinations for the different GDGT and GDD isomers arising from different biphytanyl moieties and, for GDGTs, from the parallel and anti-parallel configuration. Primed biphytanyl moieties (e.g., b') refer to the vertical mirror images of the non-primed versions shown. Only published and commonly detected biphytanes were taken into account for constructing possible isomer structures (Schouten et al., 1998, 2000). More structural combinations are possible.

have been observed in different studies (Pitcher et al., 2009b, 2011a; Sinninghe Damsté et al., 2012). They tentatively represent GDGT isomers based on different combinations of biphytane chains in two basic sterical arrangements (cf. Figure III.1 for structures of isoprenoid GDGT and GDD isomers). With existing methods the similarity in the structures results in incomplete separation, so component quantification is problematic. In addition, detailed characterization of the compounds has not been performed. The lack of such knowledge is largely due to a lack of chromatographic resolution, which prevents the compounds being examined individually without co-elution using MS^2 experiments. Additionally, chromatographic shoulders can potentially affect quantification of proxies for both SSTs (TEX_{86}) and terrestrial input into the oceans (BIT index). In some soils and hot springs the shoulders on the isoprenoid GDGTs were even more abundant than the well-characterized GDGTs (Pitcher et al., 2009b), indicating their proxy potential. In this study we present improved protocols for an increased separation of archaeal and

bacterial membrane ether lipids and tentatively assign previously co-eluting compounds by way of APCI-MS^2 with ultra HPLC (UHPLC).

III.2. Materials and Methods

III.2.1. Sample collection, homogenization and extraction

Samples were collected during RV Meteor cruise M84/1 ("DARCSEAS 1") from different depositional environments (Table III.2). Site GeoB15103 is in the eastern Mediterranean and the sample is from sapropel S1; site GeoB15104 is in the Sea of Marmara, representing a location with high terrestrial input and site GeoB15105 in the Black Sea represents a methane-rich site (Zabel and Cruise Participants, 2013). After recovery, the samples were immediately frozen and stored at $-80\,^{\circ}\mathrm{C}$ until further treatment. In addition, biomass from the archaeal culture *Nitrosopumilus maritimus* was used. Growth conditions have been described by Könneke et al. (2005). Cells were harvested in the late exponential phase and stored at $-20\,^{\circ}\mathrm{C}$.

All frozen sediment samples were homogenized at $-198\,^{\circ}\mathrm{C}$ using a Retsch Cryomill, which was operated as follows: two cycles of pre-cooling for 2 min each, with a speed of the impactor of 5 impacts s^{-1} and homogenizing and fragmenting for 2 min with 25 impacts s^{-1}. Homogenized sediment samples and the archaeal biomass were spiked with an internal standard (C_{46}GDGT; Huguet et al., 2006) and extracted, using a modified Bligh and Dyer protocol as described by Sturt et al. (2004). The wet weight of each sediment sample was 25 ± 0.5 g. The sediments were ultrasonically extracted (4 x 10 min) with CH_2Cl_2/MeOH/buffer (1:2:0.8, v:v:v) using 4 ml solvent g^{-1} sediment per extraction step. A phosphate buffer ($8.7\,\mathrm{g\,l^{-1}}$ KH_2PO_4, pH 7.4) was used for the first two steps, and a Cl_3CO_2H buffer ($50\,\mathrm{g\,l^{-1}}$, pH 2) for the final two steps. After each step, the sample was centrifuged at 800 x g for 10 min and the supernatant collected in a separation funnel. The combined supernatants were washed 3 x with deionized MilliQ water allowing separation into an organic phase and an aqueous phase, the organic phase being collected as the total lipid extract (TLE). The solvent was gently removed under a stream of N_2 and stored at $-20\,^{\circ}\mathrm{C}$.

Table III.1. Sample site characteristics.

Cruise	Site	Location	Position	Water depth (m)	Sampling interval (cmbsf)
M84/1	GeoB15103	Eastern Mediterranean	34°01.65'N/32°37.80'E	1367	21-34
M84/1	GeoB15104	Sea of Marmara	40°47.97'N/27°43.49'E	600	360-375
M84/1	GeoB15105	Black Sea	41°31.71'N/30°53.07'E	1266	420-435

III.2.2. Semi-preparative LC

In order to obtain cleaner fractions before further analysis, the TLE was subjected to semi-preparative HPLC for separation into an apolar fraction (containing core lipids) and a polar fraction (containing the more polar IPLs). A semi-preparative LiChrospher Diol-100 column (250 x 10 mm, 5 µm, Alltech, Germany) was connected to a ThermoFinnigan Surveyor HPLC instrument equipped with a Gilson FC204 fraction collector. The flow rate was $1.5\,\mathrm{ml\,min^{-1}}$ and the eluent gradient was: $100\,\%$ A to $65\,\%$ B in 90 min, held at $65\,\%$ B for 30 min, then 30 min column re-equilibration with $100\,\%$ A, where A was n-hexane/isopropanol (90:10, v:v) and B isopropanol/MilliQ water (90:10, v:v). The apolar fraction was collected from 0 to 30 min and the polar fraction from 30 to 90 min. Solvents were removed under a stream of N_2 and the fractions stored at $-20\,^{\circ}\mathrm{C}$ until further analysis.

III.2.3. Hydrogenation

To ca. 10 mg PtO_2 in a homemade glass ampoule were added $50\,\mu\mathrm{l}$ n-hexane. The mixture was saturated with H_2 and a sample aliquot was added. After flushing with H_2, the ampoule was sealed and heated to $60\,^{\circ}\mathrm{C}$ for 1 h. Finally, the sample was transferred to a 2 ml vial, evaporated to dryness and prepared for UHPLC–APCI-MS.

III.2.4. Methodology for GDGT analysis

Separation was carried out with a Dionex Ultimate 3000RS UHPLC instrument. It was connected to a Bruker maXis ultra-high resolution quadrupole time-of-flight mass spectrometry (qToF-MS) instrument, equipped with an APCI II source.

In order to test and validate various protocols for GDGT analysis, $10\,\mathrm{microl}$ aliquots in *n*-hexane:isopropanol (99.5:0.5, v:v) were injected onto different HPLC columns. The columns were: *(i)* a Prevail Cyano column (2.1 x 150 mm, $3\,\mathrm{microm}$; Grace, Germany) maintained at $30\,^{\circ}\mathrm{C}$, *(ii)* a single Acquity BEH HILIC amide column (2.1 x 150 mm, 1.7 µm, Waters, Eschborn, Germany; cf. Wörmer et al., 2013) and *(iii)* two coupled Acquity BEH HILIC amide columns maintained at $50\,^{\circ}\mathrm{C}$. The solvent system and the gradients were adjusted for the BEH HILIC amide columns. Each sample was injected at least in duplicate, all samples analyzed according to the newly proposed protocol involving two coupled columns in triplicate.

With the Prevail Cyano column, GDGTs were eluted using the following gradient (modified after Schouten et al., 2007; Liu et al., 2012a) with eluent A [*n*-hexane:isopropanol (99:1, v:v)] and eluent B [*n*-hexane:isopropanol (90:10, v:v)] at $0.2\,\mathrm{ml\,min^{-1}}$: $100\,\%$ A, held isocratically for 5 min, linear gradient to $90\,\%$ A and $10\,\%$ B in 20 min, followed by a linear gradient to $100\,\%$ B at 35 min and then held isocratically at $100\,\%$ B for 10

min. Cleaning the column was achieved by back flushing with $100\,\%$ B for 5 min at $0.6\,\mathrm{ml\,min^{-1}}$. Finally, the column was equilibrated with $100\,\%$ A for 10 min.

With the Acquity BEH HILIC amide column (single and tandem), GDGTs were eluted using the following gradient with eluent A (*n*-hexane) and eluent B [*n*-hexane:isopropanol (90:10, v:v)] and a constant flow rate of $0.5\,\mathrm{ml\,min^{-1}}$: linear gradient from $3\,\%$ B to $5\,\%$ B in 2 min, linear gradient to $10\,\%$ B in 8 min, linear gradient to $20\,\%$ B in 10 min, linear gradient to $50\,\%$ B in 15 min and linear gradient to $100\,\%$ B in 10 min. In order to clean the column(s), $100\,\%$ B was held for 6 min. Finally, the column(s) was/were equilibrated with $3\,\%$ B for 9 min before the next injection. For all methods described above an UHPLC instrument is not necessarily needed because the LC pump pressure was generally below the maximum pressure allowed for many commonly used HPLC pumps.

Detection of GDGTs was achieved using positive ion APCI, while scanning a *m/z* range from 150 to 2000; source parameters were optimized during infusion of a mixture of GDGTs and finally were as follows: corona current 3500 nA, nebulizer gas 5 bar, drying gas $8\,\mathrm{l\,min^{-1}}$, drying gas $160\,^{\circ}\mathrm{C}$, vaporizer $400\,^{\circ}\mathrm{C}$. The same APCI settings were used for all columns tested. Only the scan rate needed to be adjusted because the peak width differed strongly between the different methods tested, while we opted to obtain 20 to 30 scans per peak. The scan rate for the analysis with the Prevail Cyano column was 1 Hz and for the Acquity BEH HILIC amide column(s) 2 Hz. MS^2 spectra of GDGT and GDD compounds were obtained in data dependent mode. For each MS full scan, up to three MS^2 experiments targeted the most abundant ions with N_2 as collision gas and a collision energy of 53 eV for isoprenoid GDGTs and GDDs and 45 eV for *br*GDGTs, respectively. The isolation width was 9 Da. Active exclusion limited how often a given ion was selected for fragmentation and thus allowed us to obtain MS^2 data for less abundant ions. The mass spectrometer was set to a resolution of 27000 (at *m/z* 1222) and exact mass calibration was performed by loop-injection of tune mixture at the end of each run. Additionally, every spectrum was corrected using a lock mass (*m/z* 922.0098), resulting in a final mass accuracy of typically <1 ppm. The chromatographic separation of individual protocols was validated on the basis of chromatographic resolution (Rs), which was calculated with Eq. (1) from the retention time difference of two adjacent peaks (ΔtR) divided by sum of their mean peak width at half peak height (W_{avg}):

$$\mathrm{RS} = \frac{\Delta \mathrm{tR}}{\mathrm{W}_{avg}} \qquad \text{(Eq. 1)}$$

TEX_{86}^{H} values were calculated using the most recent definition and calibration for high temperature regions by Kim et al. (2010):

$$TEX_{86}^{H} = log\frac{[GDGT\text{-}2] + [GDGT\text{-}3] + [GDGT\text{-}5']}{[GDGT\text{-}1] + [GDGT\text{-}2] + [GDGT\text{-}3] + [GDGT\text{-}5']} \quad \text{(Eq. 2)}$$

TEX_{86}^{H} was suggested to be the most appropriate index for reconstructing SST for (sub)tropical oceans (Kim et al., 2010) and is therefore reported here in order to validate if the new methods give comparable results and to estimate the influence of the co-eluting shoulder peaks. In order to estimate the reproducibility of the analysis we regularly analyzed a pooled environmental sediment sample from the Peru Margin (ODP Leg 201, Site 1227A-2H2-65-75 cm, 8.05 mbsf, 1227A-2H5-83-93 cm, 12.43 mbsf, 1227A-3H2-55-65 cm, 17.15 mbsf, 1227A-11H2-118-128 cm, 1227A-92.72 mbsf, 1227A-13H3-0-15 cm, 113.60 mbsf (D'Hondt et al., 2003).

III.3. Results and discussion

A reconstructed base peak chromatogram and the associated reconstructed density map of the sample GeoB15103-2, 21-34 cmbsf from the eastern Mediterranean obtained from the analysis using two Acquity BEH HILIC amide columns in tandem are shown in Figure III.2. The detected compounds include the well-established isoprenoid GDGTs, *br*GDGTs, GMGTs (glycerol monoalkyl glycerol tetraethers) and several recently identified classes: isoprenoid GDDs, brGDDs, OH-GDDs, OH-GDGTs. To further differentiate multiple series of non-isoprenoid *br*GDGTs, we have adopted the nomenclature of Liu et al. (2012c) in order to distinguish the major *br*GDGTs with four to six methyl that are used in the BIT index (Hopmans et al., 2004) from less abundant, chromatographically distinct compounds with higher or lower degrees of methylation, i.e., hybrid isoprenoid/branched (IB) GDGTs, overly branched (OB) GDGTs, and sparsely branched (SB) GDGTs.

III.3.1. Evaluation of different UHPLC–APCI-MS methods

The chromatographic resolution of critical GDGT and GDD pairs for the different methods is shown in Table III.2. The use of a single Acquity BEH HILIC amide column showed considerable chromatographic improvement relative to the conventional protocol with the Prevail Cyano column, in particular for the GDDs. However, shoulder peaks were still not completely separated for the isoprenoid GDGTs. These promising results with this column, as well as its demonstrated utility for the analysis of intact polar lipids

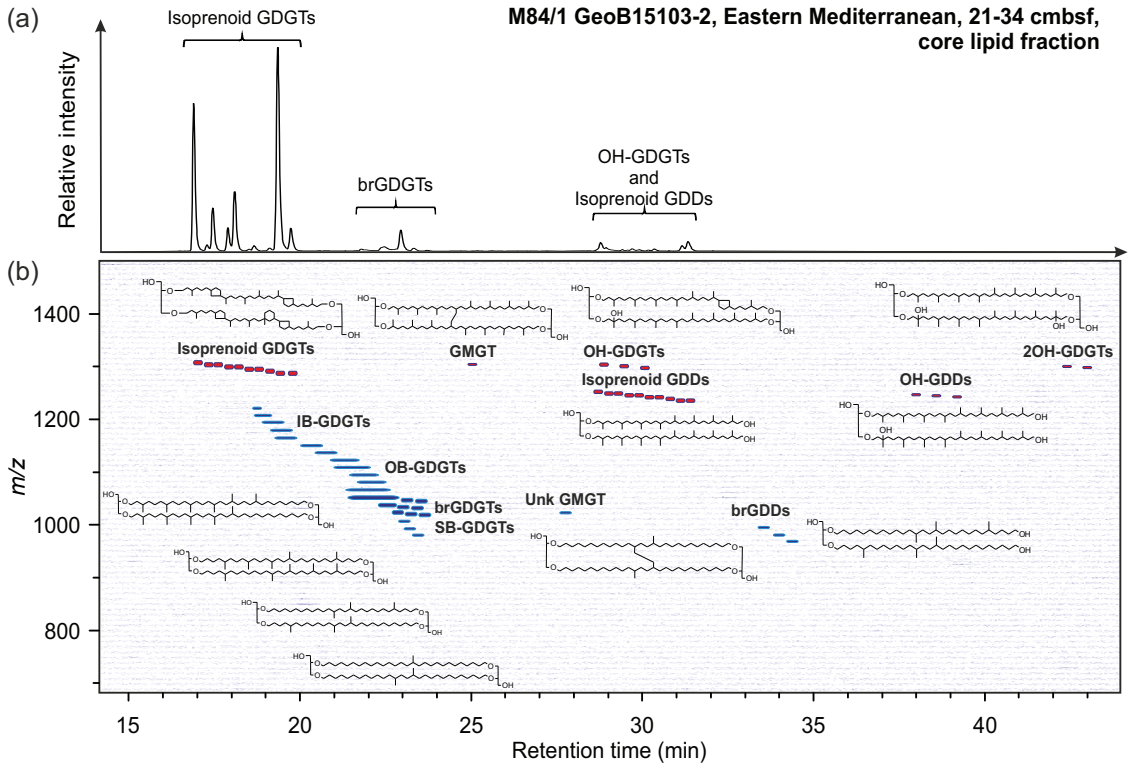

Figure III.2. (a) Reconstructed UHPLC–APCI-qToF-MS base peak chromatogram showing isoprenoid GDGTs, *br*GDGTs, isoprenoid GDDs and OH-GDGTs in the core lipid fraction of M84/1 GeoB15103-2, 21-34 cmbsf. The sample was analyzed using two Acquity BEH HILIC amide columns in tandem; (b) associated, reconstructed density map plot showing the major diagnostic ions of all archaeal and bacterial ether lipids in the core lipid fraction. Also shown are representative structures of the different compound groups. Abbreviations (according to Liu et al., 2012c): GDGT, glycerol dialkyl glycerol tetraether; GDD, glycerol dialkanol diether; GMGT, glycerol monoalkyl glycerol tetraether; OH, monohydroxy; 2OH, dihydroxy; br, branched; IB, hybrid isoprenoid/branched; OB, overly branched; SB, sparsely branched; Unk, unknown. More structural combinations are possible.

(Wörmer et al., 2013), led us to further invest time into optimizing its chromatographic separation. This resulted in a scheme with two Acquity BEH HILIC amide columns arranged in tandem, which vastly increased separation of the GDGT and GDD compounds (Figure III.3). One shoulder was baseline separated from GDGT-1, -2 and -3, respectively. These slightly earlier eluting compounds have the same molecular mass as each following GDGT and are therefore marked with an ‘a’; for example GDGT-1a.

The two column protocol offers additional advantages for detection of *br*GDGTs and recently identified series of GDDs. Their chromatographic resolution was increased substantially (Table 2). For example, for each compound belonging to the group of GDDs, except for GDD-0, one shoulder was chromatographically separated. These peaks had the same molecular mass as the later eluting GDD (Figure III.3). The separated shoulders were designated with an ‘a’, for example GDD-1a. As for the group of isoprenoid GDGTs, the compound containing four cyclopentane moieties (GDD-4) was separated. Remarkably,

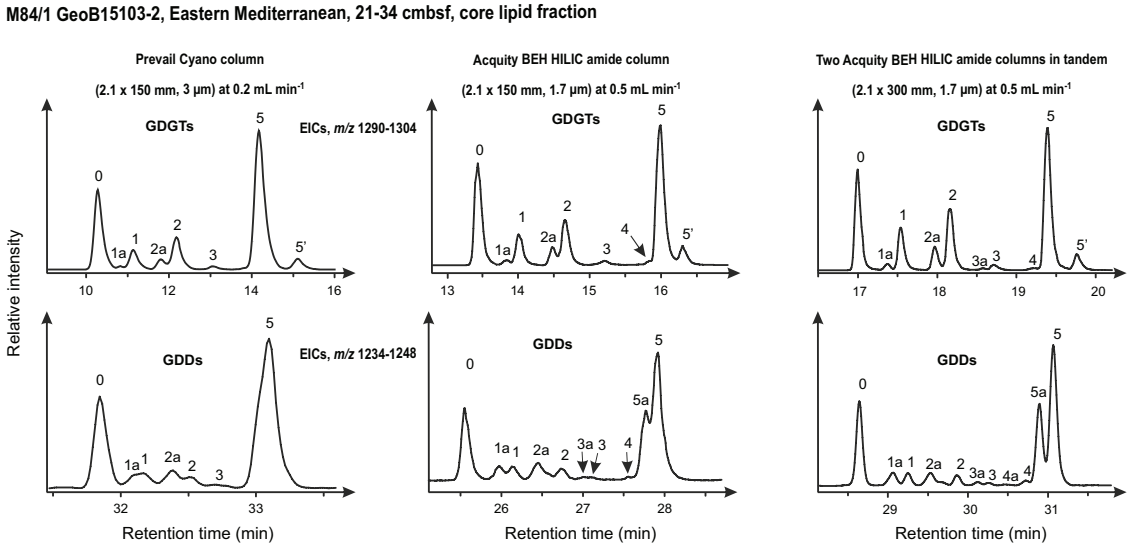

Figure III.3. UHPLC–APCI-MS chromatograms, shown as extracted ion chromatograms (EICs), illustrating isoprenoid GDGTs and GDDs in the apolar fraction of sample M84/1 GeoB15103-2, 21-34 cmbsf. Compounds labeled with an 'a' have the same molecular mass as the corresponding, later eluting compound. Numbers represent numbers of unsaturation (rings and/or double bonds). Chromatographic separation was greatly increased for the GDGTs and GDDs when two Acquity BEH HILIC amide columns in tandem were used. For further explanation, see text.

Table III.2. Chromatographic resolution calculated after Eq. (7) of critical pairs of isoprenoid GDGTs, *br*GDGTs and GDDs in sample GeoB15103-2, 21-34 cmbsf determined by replicate analysis with different columns. No values are reported for resolutions <0.5 (-) because peaks cannot be integrated correctly below this value.

Method	GDGT-1 and GDGT-1a	GDGT-2 and GDGT-2a	GDGT-3 and GDGT-3a	GDGT-4 and GDGT-5	GDGT-5 and GDGT-5'	*br*GDGT-I and *br*GDGT-Ia	*br*GDGT-Ia and *br*GDGT-Ib	GDD-1 and GDD-1a	GDD-2 and GDD-2a	GDD-3 and GDD-3a	GDD-4 and GDD-5a
1[a] (n=2)	0.69±0.01	0.73±0.02	0.59±0.04	-	1.85±0.14	1.24±0.06	1.47±0.13	-	0.51±0.02	-	-
2[b] (n=2)	0.73±0.01	0.73±0.02	0.60±0.02	0.55±0.03	1.36±0.10	1.62±0.02	1.96±0.05	0.67±0.06	1.10±0.01	-	0.83±0.09
3[c] (n=3)	1.08±0.06	1.16±0.03	0.65±0.01	0.83±0.05	2.04±0.08	1.83±0.06	1.98±0.03	0.81±0.12	1.17±0.08	0.51±0.04	0.84±0.12

[a] Prevail Cyano column, 3 µm particle size.
[b] Acquity BEH HILIC amide column, 1.7 µm particle size, 150 mm length.
[c] Two Acquity BEH HILIC amide columns in tandem, 1.7 µm particle size, 150 mm length each.

the shoulder peaks of the GDDs were as abundant as their later-eluting counterparts. This is in contrast to the shoulder peaks of the isoprenoid GDGTs, which account for only ca. 10 % compared with their counterpart. Among the *br*GDGTs, several previously co-eluting compounds with identical molecular mass were separated with the tandem method (Figure III.4). However, not all peaks could be baseline separated.

The tandem method also enabled separation of GDGT-4, which co-elutes with crenarchaeol (GDGT-5) with the conventional method. In the sediment samples the concentration of GDGT-4 was very low and it seemed to partly co-elute with crenarchaeol. However, the ion at *m/z* 1294 was slightly higher than the ion at *m/z* 1292 for the peak eluting just before crenarchaeol. Before this peak, an even smaller peak with a mass of 1294 Da eluted, which represents the chromatographic shoulder of GDGT-4. In order to further evaluate the separation of GDGT-4, the TLE of *N. maritimus* was analyzed.

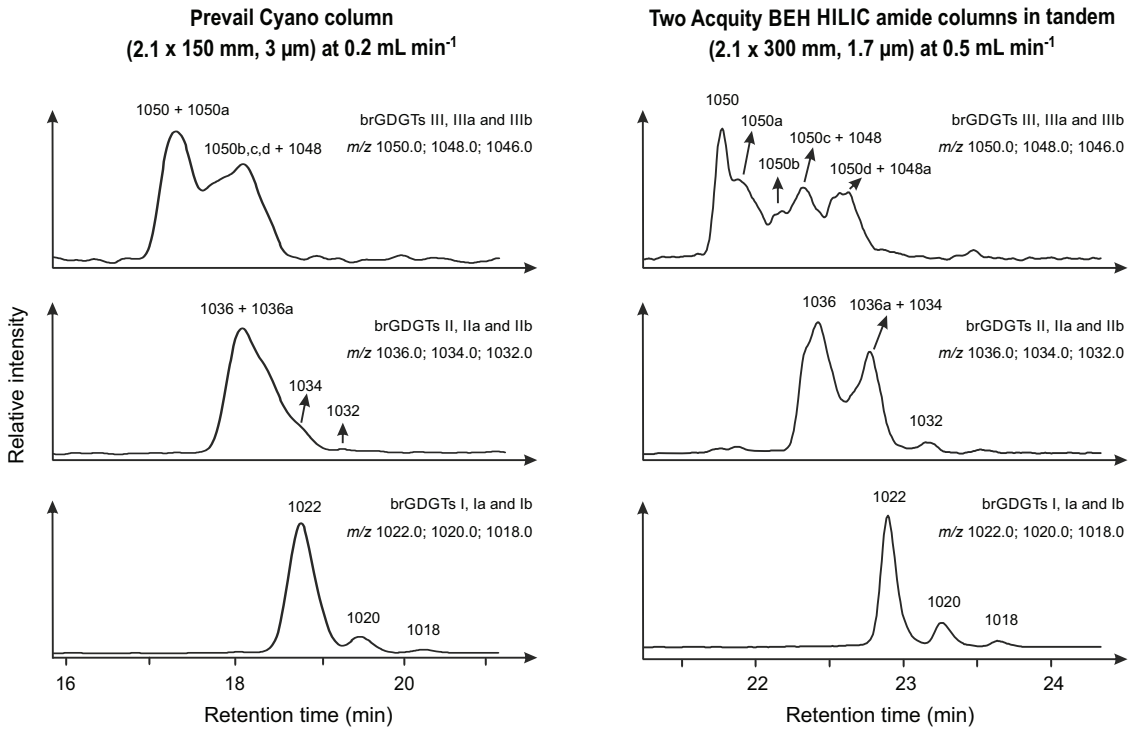

Figure III.4. UHPLC–APCI-MS chromatograms shown as EIC, illustrating *br*GDGTs in the apolar fraction of sample M84/1 GeoB15103-2, 21-34 cmbsf. Several additional compounds with the same molecular mass as the original *br*GDGTs are separated after analysis with the tandem method, but not all peaks are fully separated. Roman numbers refer to structures presented by Weijers et al. (2007). Compounds are labeled with *m/z* of the molecular ion.

Here, the relative abundance of the compound eluting slightly before crenarchaeol was relatively high and, based on the MS^2 spectra, was unambiguously assigned as GDGT-4 (Figure III.5).

In addition to the increased separation, we compared injections of identical extract aliquots; the results showed strongly improved peak shapes for all modified protocols. For example, the mean peak width at half peak height of crenarchaeol was 0.251 min for the Prevail Cyano column and 0.091 min for the two Acquity BEH HILIC amide columns in tandem, resulting in higher sensitivity. Moreover, the 50-minute analysis time for the new protocols was comparable with earlier methods using a single Prevail Cyano column (Hopmans et al., 2000; Schouten et al., 2007).

III.3.2. Assignment of unknown compounds

In order to study the fragmentation features of isoprenoid GDGTs, *br*GDGTs, as well as GDDs, in detail with exact mass and at high mass resolution, the samples were analyzed

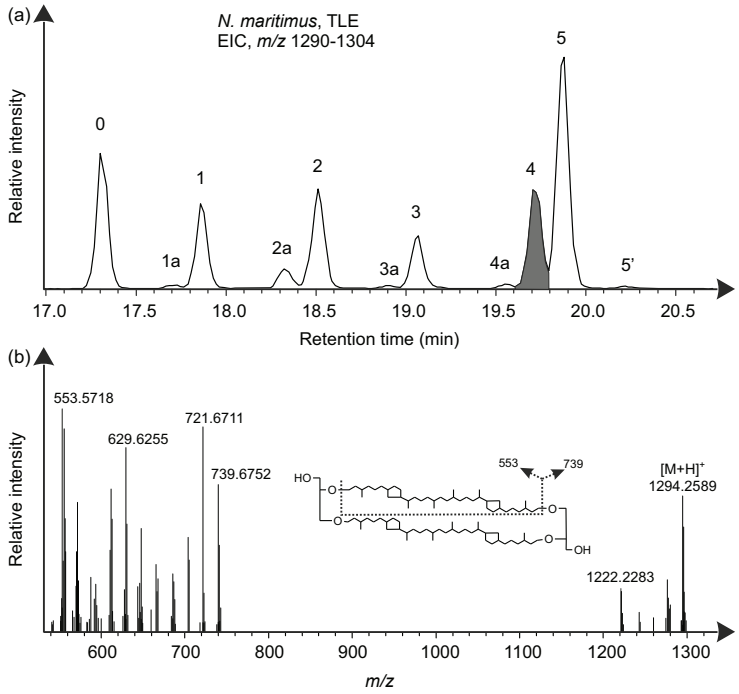

Figure III.5. (a) UHPLC–APCI-MS chromatograms, shown as extracted ion chromatogram (EIC), illustrating the isoprenoid GDGTs in the TLE of the archaeal culture textitN. maritimus; (b) product ion (MS^2) spectra of GDGT-4 ($[M+H]^+$ ion of *m/z* 1294.3, in the range *m/z* 540-1320), show the diagnostic product ions used to assign the structure. The major fragments at *m/z* 739 and 553 are formed from the loss of one biphytanyl chain with two cyclopentyl moieties. The structure and the formation of product ions from loss of the biphytanyl chain are also shown.

using UHPLC-qToF-MS^2 to compare the MS^2 spectra of the GDGTs and their previously co-eluting shoulders.

III.3.2.1. MS analysis of isoprenoid GDGTs

MS analysis of GDGT-1 and the corresponding chromatographic shoulder (GDGT-1a) showed one main cluster of fragment ions in the MS^2 experiment (Figure III.6). Both precursor ions were $[M+H]^+$ at *m/z* 1300.3. The main MS^2 fragments in the cluster were *m/z* 741.7 and 557.6, resulting from the neutral loss of the acyclic biphytanyl moiety (Figure III.7). The enlarged spectra show that both fragmentation patterns are almost identical. Both spectra were characterized by multiple losses of water after loss of one biphytane moiety and glycerol-derived $C_3H_6O_2$ units. This fragmentation pattern is in agreement with the observation by Knappy et al. (2009), Knappy et al. (2011), and Liu et al. (2012c), who discussed MS^2 spectra of tetraether core lipids in detail. The only slight difference between the spectra of GDGT-1a and GDGT-1 was the higher relative intensity of *m/z* 743.7 for the former, resulting from loss of a monocyclic biphytanyl moiety. Accordingly, GDGT-1 preferentially loses the acyclic biphytanyl moiety, while GDGT-1a does not show a preferential loss.

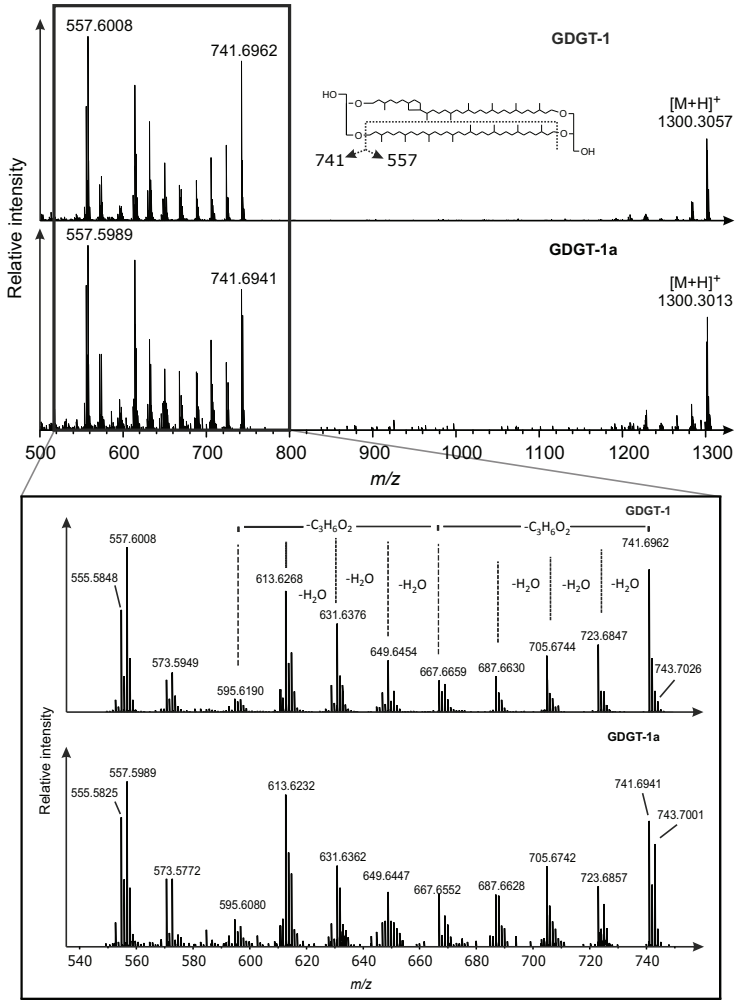

Figure III.6. UHPLC–APCI-MS^2 spectrum of GDGT-1 and GDGT-1a in sample M84/1 GeoB15103-2, 21-34 cmbsf. Shown are the MS^2 fragment ions of the tetraether core ($[M+H]^+$ at *m/z* 1300.3) in the range *m/z* 500-1310. The structure of GDGT-1 and the formation of the major fragments are also shown. The enlarged area highlights the main cluster of fragments. The cluster is characterized by multiple losses of water (18.0 Da) and glycerol-derived $C_3H_6O_2$ units (74.0 Da).

MS analysis of GDGT-2 and GDGT-2a ($[M+H]^+$ at *m/z* 1296.3) revealed similar patterns (Fig. 7). Here, the MS^2 fragments are formed from the loss of monocyclic alkyl chains (*m/z* 741.7; neutral loss 555.6 Da), indicative of the presence of one cycloalkyl moiety in each biphytane chain. Interestingly, additional product ions resulting from loss of alkyl chains containing zero (*m/z* 739.7; loss of 557.6 Da) and two (*m/z* 743.7; loss of 553.6 Da) rings are also evident in the resulting MS^2 spectrum (Fig. 7).

The nearly identical mass spectra of the two GDGT pairs suggests that the core structures of GDGT-1 and GDGT-1a, as well as GDGT-2 and GDGT-2a, are very similar. Possible structural differences are *(i)* double bonds instead of cycloalkyl moieties, *(ii)* other structural isomers resulting from a combination of biphytanes with different ring combinations, which can partially be resolved with MS data, e.g. zero ring/two ring or

one ring/one ring in case of GDGT-2 (Figure III.7), *(iii)* different ring positions within one biphytanyl moiety, or *(iv)* regioisomers, i.e. isomers with parallel and anti-parallel arrangement of glycerol units, as for crenarchaeol and its later eluting regioisomers (Sinninghe Damsté et al., 2002).

MS analysis cannot distinguish whether a double bond or a ring is present in the biphytane chain because it is not fragmented at these positions. Furthermore, regioisomers and different positions of rings within one biphytanyl moiety cannot be identified. However, such isomers could result in chromatographically separable peaks.

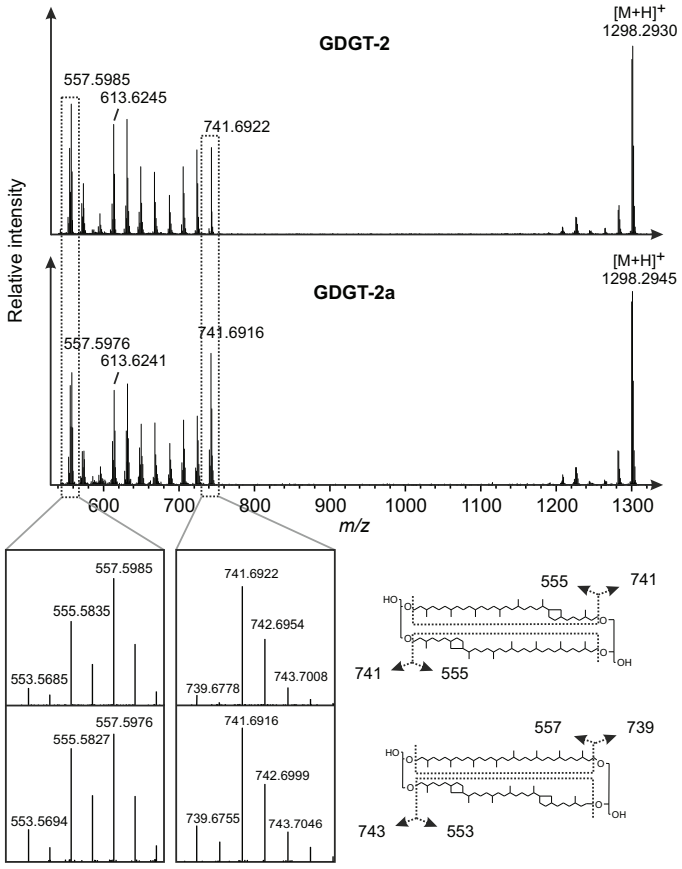

Figure III.7. UHPLC–APCI-MS^2 spectrum of GDGT-2 and GDGT-2a in sample M84/1 GeoB15103-2, 21-34 cmbsf. Shown are the MS^2 fragment ions of the tetraether core ([M+H]$^+$ at *m/z* 1298.3) within the *m/z* range 500-1310. The enlarged area shows fragments produced by losing one biphytanyl moiety. Both spectra show fragments of a combination of two monocyclic biphytanes vs. an acyclic/bicyclic biphytane combination. The structure and the formation of product ions by loss of one biphytanyl moiety are also shown.

In order to test for the presence of double bonds, an aliquot of the TLE was hydrogenated, but in no case did the mass spectra or retention times of the components change. This suggested that the chromatographic shoulders were not double-bond bearing compounds. Schouten et al. (1998), Pancost et al. (2001) and Knappy et al. (2011) showed structural isomers for isoprenoid GDGTs, in which the position of rings differed,

e.g. GDGT-2 with an acyclic and a bicyclic biphytane moiety vs. GDGT-2 with two monocyclic biphytane moieties. However, these isomers were not chromatographically resolved (see Figure III.7) because both the major GDGT peaks and the shoulder peaks showed mixed ring combinations in their MS^2 spectra, which excludes shoulder peaks being such structural isomers. Therefore, these compounds represent either regioisomers or isomers with different positions of rings within one biphytanyl moiety. Sinninghe Damsté et al. (2012) detected co-eluting compounds in a thaumarchaeal soil isolate and suggested the compounds to be regioisomers. This assumption was based on an earlier study by Sinninghe Damsté et al. (2002) who used NMR analysis to show that compounds eluting later than the regular GDGTs 4 and 5 represent their regioisomers with a parallel arrangement of glycerol units. GDGT-0, not associated with shoulders, appeared to be present as a single structural isomer. Hence, for this compound the regioisomerism does not result in chromatographically resolvable peaks using the commonly applied, as well as our newly implemented protocols. We cannot exclude the separation efficiency of the tandem method still being insufficient for the separation of all isomers; alternatively not all possible combinations are necessarily present in nature. Further information on the nature of the less abundant shoulder peaks could be gained via chemical degradation, such as regiospecific ether cleavage. For example, Gräther and Arigoni (1995) showed that GDGT-0 from three archaeal species is in fact a 1:1 mixture of the regular, anti-parallel compound and its regioisomer with the parallel arrangement of glycerol units.

III.3.2.2. MS analysis of isoprenoid GDDs

MS analysis of GDDs and corresponding shoulder peaks revealed no discernible difference between the two groups, suggesting close structural similarity. All GDD MS^2 spectra were characterized by loss of one biphytanyl moiety, multiple losses of water and one glycerol-derived $C_3H_6O_2$ unit. For example, the main fragment ions for GDD-2, as well as for GDD-2a (each with the $[M+H]^+$ at *m/z* 1242.3), have *m/z* values of 667.6, 649.6, 631.6, 613.6, 593.6, 573.6 and 557.6/555.6 (Figure III.8); these ions are also observed during fragmentation of the isoprenoid GDGTs after they have lost one biphytanyl moiety and a $C_3H_6O_2$ unit. Regioisomerism can be excluded as a source of multiple peaks because GDDs contain only one glycerol. Therefore, the shoulder peaks must represent other structural isomers. Different biphytane moiety combinations can be excluded because they do not appear to be chromatographically resolved, e.g. fragments for both combinations, an acyclic and a bicyclic biphytane moiety vs. two monocyclic biphytane moieties, were observed in the spectra of GDD-2 and GDD-2a, indicating that the two peaks were mixtures of these two isomers. It remains to be resolved why only

one shoulder peak was associated with each major GDD because, as for the isoprenoid GDGTs, for most GDDs several additional structural isomers are possible (see Figure III.1).

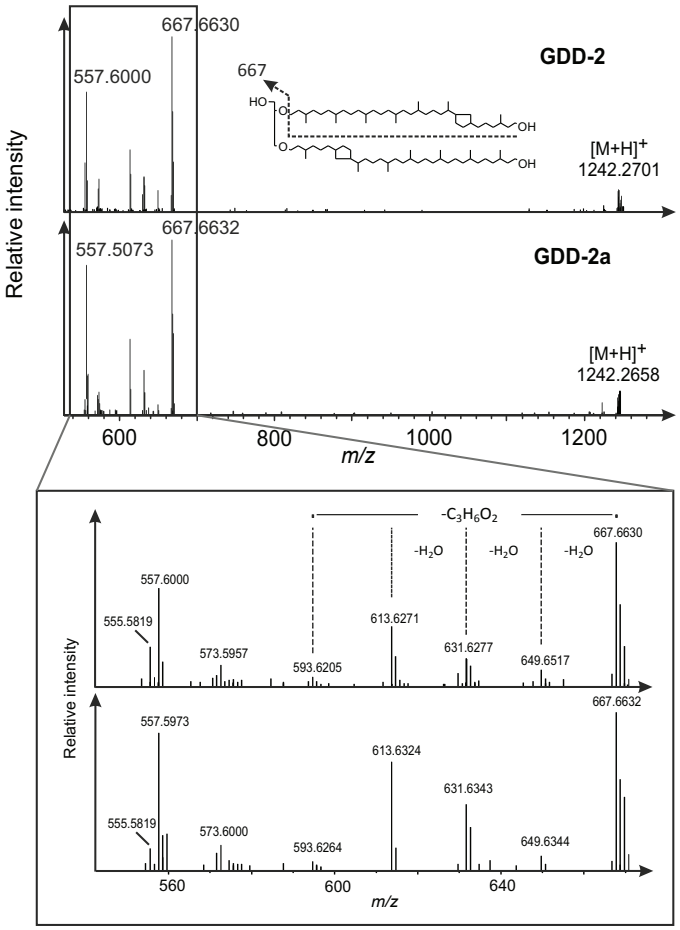

Figure III.8. UHPLC–APCI-MS^2 spectrum of GDD-2 and GDD-2a in sample M84/1 GeoB15103-2, 21-34 cmbsf. Shown are the MS^2 fragment ions of the diether core ($[M+H]^+$ at *m/z* 1242.3) within the *m/z*range 500-1310. The structure of GDD-2 and the formation of the major fragment are also shown. The enlarged area highlights the main cluster of fragments. The cluster is characterized by multiple losses of water (18.0 Da) and glycerol-derived $C_3H_6O_2$ units (74.0 Da). Both spectra show fragments of a combination of two monocyclic biphytanes vs. an acyclic/bicyclic biphytane combination

Interestingly, GDD shoulder peaks were relatively more abundant than the corresponding compound with the same molecular mass as the GDGT shoulder peaks in the three samples (see Figure III.3, Table III.4). The reason for this could be that, in the case of the GDGTs, the difference in polarity and/or steric configuration of some structural isomers with a different biphytane distribution is not large enough, leading to co-elution. For GDDs, however, where one glycerol unit is missing, a different biphytane distribution could result in larger differences that could be chromatographically well separated. This hypothesis could be tested in future studies employing NMR spectroscopy.

III.3.2.3. MS analysis of brGDGTs

A detailed analysis of mass spectra of *br*GDGTs was conducted on a purified *br*GDGT fraction of a sample from Aarhus Bay (56°07.06'N, 10°20.85'E, 15 m water depth, 6-7 m sediment depth). The fraction containing *br*GDGTs resulted as a byproduct from the OH-GDGT isolation Liu et al. (2012b). We detected six distinct peaks (a-f) with similar fragmentation patterns in the EIC of *m/z* 1050.0, corresponding to *br*GDGT-III (Figure III.9). All MS^2 spectra showed a fragment ion resulting from the loss of a glycerol-derived $C_3H_6O_2$ unit (*m/z* 976.0; neutral loss of 74.0 Da), while the main cluster of fragments involved the loss of one alkyl moiety, multiple losses of water after losses of one alkyl moiety and glycerol-derived $C_3H_6O_2$ units. This fragmentation behavior is analogous to that of archaeal GDGTs (Knappy et al., 2009; Knappy et al., 2011; Liu et al., 2012c) and has recently been described by De Jonge et al. (2013) for *br*GDGTs; these authors used a modified analytical setup that resulted in improved chromatographic separation and the identification of four *br*GDGT-III isomers in a peat sample. Interestingly, all six peaks except peak f showed a mixed signal of at least two compounds, which differed in the total carbon number of the alkyl chains. Fragments reflect a *br*GDGT with a combination of two C_{31} alkyl chains and another one with a combination of one C_{30} and one C_{32} alkyl chain (Figure III.9), consistent with findings by De Jonge et al. (2013). The isomers we observed could either differ in the degree of methylation in the two C_{28} base alkyl moieties or the two linear base alkyl moieties were of different length, which would result in different degrees of methylation. Based on the MS^2 spectra we cannot distinguish such structural differences. The position of the methyls in the alkyl chains can also not be determined using MS^2 analysis but different methyl group positions in the *br*GDGT molecule can result in chromatographically resolvable peaks (De Jonge et al., 2013). Nevertheless, our MS^2 experiments showed that the analyzed sample contains at least eleven *br*GDGT-III isomers, which cannot be chromatographically separated completely.

III.3.3. Validation of new protocols for determination of tetraether lipid proxies

The Peru Margin mix sample was analyzed during a three-month interval to estimate the reproducibility of the analysis. Results with the two-column protocol showed a standard deviation for the TEX_{86}^H of 0.0025 (relative standard deviation $0.72\,\%$). TEX_{86}^H values were calculated with and without chromatographic shoulders to evaluate the influence of incomplete separation, leading to possible overestimation of the peak area of individual GDGTs and therefore shifts in TEX_{86}^H. The calculated TEX_{86}^H values showed only minor differences between the different chromatographic methods, with a maximum difference

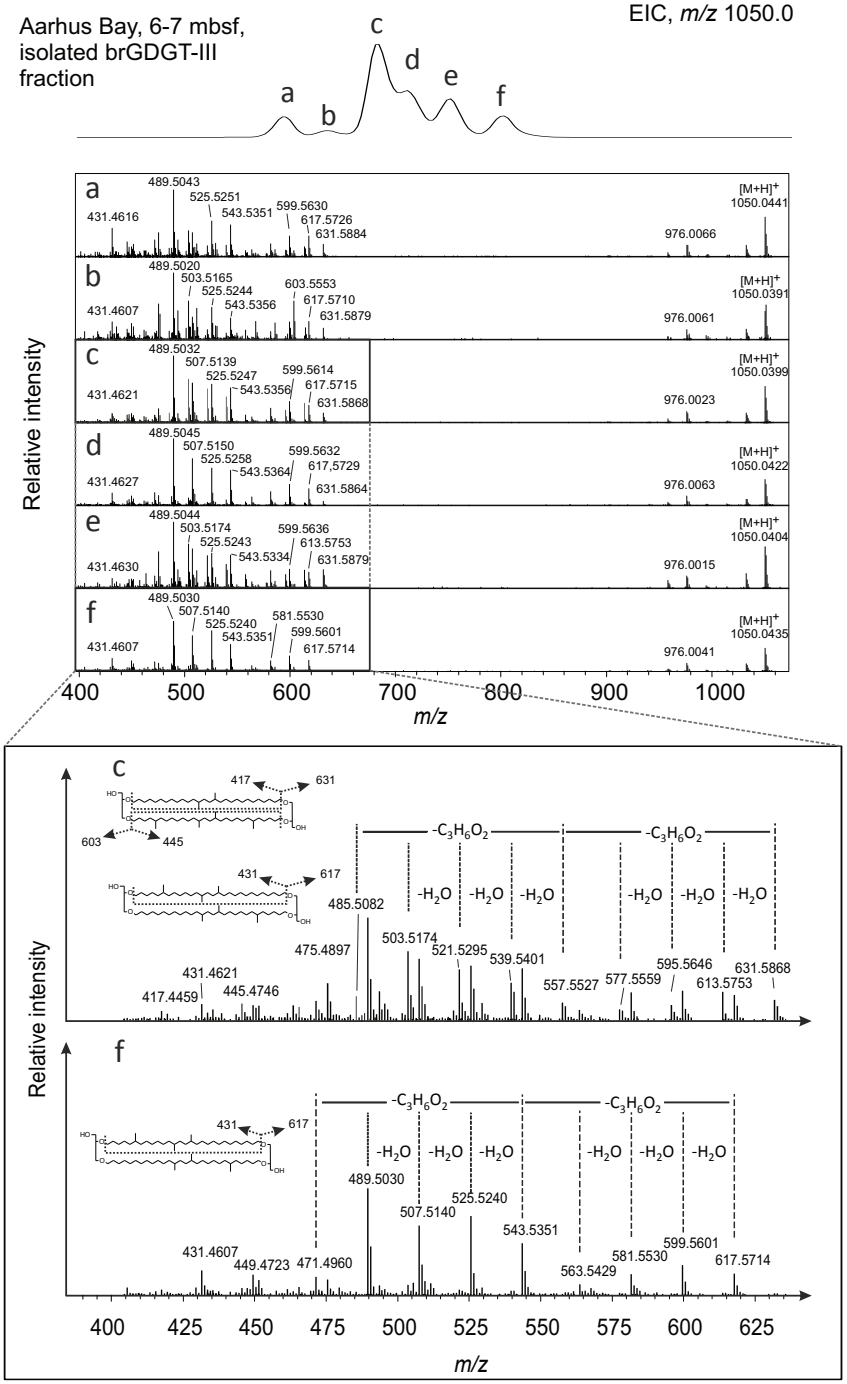

Figure III.9. EIC showing the distribution of *br*GDGT-III isomers in the sample from theAarhus Bay, 6–7 mbsf. Below: UHPLC–APCI-MS^2 mass spectra of *br*GDGT-III isomers (a–f) and the formation of the major product ions of the tetraether core ([$[M+H]^+$] + at *m/z* 1050.0) within the *m/z* range 400–1060 are shown. The enlarged area highlights the main cluster of fragments of the peaks c and f. Both spectra are characterized by the loss of an alkyl moiety and additional, multiple losses of water and glycerol-derived $C_3H_6O_2$ units (74.0 Da). Additionally, the MS^2 spectrum of peak c shows two major series of fragment ions indicating that the peak is a mixture of at least two compounds with different total carbon numbers in the alkyl chain, one having a combination of a CC_{30} and a C_{32} alkyl chain and one having a combination of two C_{31} alkyl chains, whereas the MS^2 spectrum of peak f only shows one series of fragments indication a structure with identical total carbon numbers in the alkyl chains (C_{31}). Also shown are possible structures for the isomers and the formation of their major product ions.

of 0.03. This suggests that the new methods are suitable for SST determination, but a larger set of samples needs to be analyzed to fully validate their applicability.

Table III.3. TEX_{86}^{H} obtained from the different methods.

Method	Site, sample	TEX_{86}^{H} excluding shoulders	TEX_{86}^{H} including shoulders
1[a]	GeoB15103-2,	-0.16±0.0043	-0.10±0.0026
2[b]	21-34 cmbsf	-0.16±0.0041	-0.09±0.0042
3[c]		-0.16±0.0029	-0.10±0.0013
1[a]	GeoB15104-2,	-0.39±0.0007	-0.39±0.0040
2[b]	360-375 cmbsf	-0.38±0.0016	-0.37±0.0010
3[c]		-0.37±0.0006	-0.36±0.0029
1[a]	GeoB15105-2,	-0.28±0.0071	-0.27±0.0078
2[b]	420-435 cmbsf	-0.27±0.0050	-0.26±0.0035
3[c]		-0.26±0.0075	-0.25±0.0072

[a] Prevail Cyano column, 3 µm particle size.
[b] Acquity BEH HILIC amide column, 1.7 µm particle size, 150 mm length.
[c] Two Acquity BEH HILIC amide columns in tandem, 1.7 µm particle size, 150 mm length each.

The impact of inclusion of shoulder peaks appears to be generally low but naturally increases with their relative abundance (Table III.3). For the sample from site GeoB15103, with the highest relative abundance of shoulder peaks (Table III.4), the maximum TEX_{86}^{H} discrepancy between inclusion vs. exclusion of shoulders was 0.07. For the other two samples, with relatively small shoulder peaks, the difference in the TEX_{86}^{H} value was 0.01. The small influence of co-eluting isomers on TEX_{86}^{H} values is consistent with earlier observations from an interlaboratory study by (Schouten et al., 2009). However, the chromatographic shoulders can have an influence on the proxy when they are not separated and therefore included in the TEX_{86}^{H} calculation. In most commonly represented sediments, the abundance of the isomers is assumed to be low, but no study has focused on the quantification of these compounds in environmental samples.

The greater diversity of *br*GDGT isomers uncovered with the new protocol calls for further inspection and potential improvement in BIT index and CBT/MBT calculations since the specificity of selected isomers for the reconstruction process may be higher than that of the previously inseparable mixture.

III.4. Conclusions

The newly developed protocols, in particular the protocol using two columns in tandem, provides superior separation of archaeal and bacterial GDGT core lipids and opens a window to a more nuanced exploration of their distribution in the environment. The protocols feature reduced peak width at half peak height, higher peak height and

Table III.4. Relative abundance obtained with the tandem method for the major GDGT groups in the apolar fraction of the three samples (numbers in brackets represent % within the groups of isoprenoid GDGTs, *br*GDGTs and GDDs, respectively; n.d., not detected).

	GDGT or GDD	GeoB15103-2, 21-34 cmbsf	GeoB15104-2, 360-375 cmbsf	GeoB15105-2, 420-435 cmbsf
Relative abundance of isoprenoid GDGTs (%)	0	21.8 (26.2)	18.4 (27.7)	21.8 (30.1)
	1a	1.0 (1.2)	0.4 (0.6)	0.4 (0.6)
	1	6.8 (8.1)	7.2 (10.9)	8.7 (12.0)
	2a	3.4 (4.1)	0.3 (0.4)	0.4 (0.6)
	2	10.5 (12.6)	4.3 (6.5)	8.7 (12.1)
	3a	0.4 (0.4)	0.1 (0.2)	0.1 (0.2)
	3	1.1 (1.3)	0.6 (1.0)	1.3 (1.8)
	4a	0.1 (0.1)	n.d.	n.d.
	4	0.5 (0.6)	0.5 (0.8)	0.3 (0.5)
	5	34.2 (41.0)	34.3 (51.4)	30 (41.4)
	5'	3.6 (4.4)	0.4 (0.6)	0.5 (0.7)
Relative abundance of *br*GDGTs (%)	III	1.5 (15.1)	5.5 (33.2)	3.7 (27.0)
	IIIa	0.2 (1.9)	1.4 (8.6)	0.8 (5.6)
	IIIb	0.0 (0.3)	0.2 (1.4)	0.1 (1.0)
	II	2.4 (24.7)	3.7 (22.1)	2.9 (21.2)
	IIa	0.4 (4.4)	1.6 (9.7)	2.9 (21.0)
	IIb	0.1 (0.7)	0.2 (1.1)	0.5 (3.8)
	I	4.3 (44.4)	3.3 (19.9)	1.2 (8.5)
	Ia	0.6 (6.7)	0.5 (3.1)	1.1 (8.3)
	Ib	0.2 (1.8)	0.1 (0.9)	0.5 (3.5)
Relative abundance of isoprenoid GDDs (%)	0	1.4 (25.2)	1.7 (24.4)	1.5 (24.9)
	1a	0.2 (3.7)	0.4 (5.4)	0.4 (6.1)
	1	0.2 (3.9)	0.4 (5.5)	0.4 (5.9)
	2a	0.3 (5.9)	0.3 (4.0)	0.4 (5.9)
	2	0.2 (3.4)	0.2 (2.7)	0.3 (4.5)
	3a	0.1 (1.0)	0.1 (0.8)	0.1 (1.0)
	3	0.1 (1.0)	0.0 (0.7)	0.1 (1.1)
	4a	0.0 (0.3)	0.0 (0.4)	0.0 (0.4)
	4	0.1 (0.9)	0.1 (0.7)	0.1 (0.8)
	5a	1.0 (17.4)	1.5 (21.2)	1.1 (17.7)
	5	2.1 (37.2)	2.4 (34.3)	2.0 (31.8)

thus increased sensitivity. Previously partially co-eluting isoprenoid GDGTs can now completely separated and can be confidently quantified. Chromatographic shoulders were also separated within the group of the recently identified GDDs and, moreover, in the group of *br*GDGTs many additional peaks were revealed.

The exact structures of the compounds eluting as chromatographic shoulders of isoprenoid GDGTs and GDDs were not fully resolved. MS analysis showed the same fragmentation pattern for pairs comprising shoulder and major peak, suggesting a high degree of structural similarity. The substitution of cycloalkane moieties by double bonds in shoulder peaks was rejected on the basis of a hydrogenation experiment. Thus, the

isomers of the GDGTs likely represent either regioisomers or structural isomers with different biphytane moieties; verification is needed, however, to support this hypothesis. Since regioisomers do not exist for GDDs, their shoulder peaks must represent structural isomers, for example, isomers with exchanged biphytane chains or different ring positions within one biphytane chain.

Examination of MS^2 data for *br*GDGT-III isomers revealed similar fragmentation patterns for the six separated peaks and showed that most peaks were a mixture of isomers containing identical and different total carbon numbers in the two alkyl moieties. Therefore, the *br*GDGT isomers likely represent structural isomers with varying methyl positions and/or isomers with different base *n*-alkyl chain length. Identification of the exact structure of these isomers will be essential in future studies as the compounds may differ in their proxy potential, which could be further explored with the new protocol.

On a small set of samples we could show that the tandem method provides comparable TEX_{86}^{H} values as long as the chromatographic shoulder peaks were not included in the TEX_{86} in previous protocols.

Acknowledgements

We are grateful to the participating scientists and ship crews of the RV Meteor cruise M84/1 (DARCSEAS). We thank L. Wörmer for support with UHPLC analysis. One sample for this study was retrieved during the Ocean Drilling Program (ODP) Leg 201. We also thank F. Elling and M. Könneke for providing biomass of textitN. maritimus and B. Orcutt for providing marine sediment from Aarhus Bay. The study was funded by the European Research Council under the European Union's Seventh Framework Programme - "Ideas" Specific Programme, ERC grant agreement No. 247153 (Advanced Grant DARCLIFE; PI K.-U.H.) and by the Deutsche Forschungsgemeinschaft (DFG, Germany) through grants Inst 144/300-1 (LC-QToF system), HI616/10-1 (K.-U.H.), LI1901/1-1 (J.S.L) and the postdoctoral fellowship granted through the Cluster of Excellence/Research Center MARUM to C.Z. Further support was given by the Bremen International Graduate School for Marine Sciences (GLOMAR) funded by the DFG. We thank two anonymous reviewers for helpful comments and suggestions.

Chapter IV

Rapid and simultaneous analysis of three molecular sea surface temperature proxies and application to sediments from the Sea of Marmara

Kevin W. Becker[a,*], Julius S. Lipp[a], Gerard J.M. Versteegh[b], Lars Wörmer[a] and Kai-Uwe Hinrichs[a]

Published in *Organic Geochemistry*
Vol. 85 (2015), pages 42-53. doi: 10.1016/j.orggeochem.2015.04.008

[a]Organic Geochemistry Group, MARUM - Center for Marine Environmental Sciences & Department of Geosciences, University of Bremen, 28359 Bremen, Germany
[b]Heisenberg Group Marine Kerogen, MARUM - Center for Marine Environmental Sciences & Department of Geosciences, University of Bremen, 28359 Bremen, Germany

*Corresponding author. E-mail: k.becker@uni-bremen.de

Abstract

Reconstructing ocean temperature values is a major target in paleoceanography and climate research. However, most temperature proxies are organism-based and thus suffer from an "ecological bias". Multiproxy approaches can potentially overcome this bias but typically require more investment in time and resources, while being susceptible to errors induced by sample preparation steps necessary before analysis. Three lipid-based temperature proxies are widely used: $U^{K'}_{37}$ (based on long chain alkenones from phytoplanktonic haptophytes), TEX_{86} [based on glycerol dialkyl glycerol tetraethers (GDGTs) from pelagic archaea] and LDI (based on long chain diols from phytoplanktonic eustigmatophytes). So far, separate analytical methods, including gas chromatography (GC) and liquid chromatography (LC), have been used to determine these proxies. Here we present a sensitive method for determining all three with a single analysis using normal phase high performance LC coupled to atmospheric pressure chemical ionization mass spectrometry (NP-HPLC–APCI-MS). Each of the long chain alkenones and long chain diols was separated and unambiguously identified from their accurate masses and characteristic fragmentation during multiple stage MS analysis (MS^2). Comparison of conventional GC and HPLC-MS methods showed similar results for $U^{K'}_{37}$ and LDI, respectively, using diverse environmental samples and an Emiliania huxleyi culture. Including the three sea surface temperature (SST) proxies, the NP-HPLC–APCI-MS method allows simultaneous determination of nine paleoenvironmental proxies. The extent to which the ecology of the source organisms (ecological bias) influences lipid composition and thereby the reconstructed temperature values was demonstrated by applying the new method to a sediment core from the Sea of Marmara, covering the last 21 kyr BP. Reconstructed SST values differed considerably between the proxies for the last glacial maximum (LGM) and the period of sapropel S1 formation at ca. 10 kyr BP, whereas the trends during the late Holocene were similar. Changes in the composition of alkenone-producing species at the transition from the LGM to the Bølling/Allerød (B/A) were inferred from unreasonably high $U^{K'}_{37}$-derived SST values (ca. $20\,^{\circ}C$) during the LGM. We ascribe discrepancies between the reconstructed temperature records during S1 deposition to habitat change, e.g. a different depth due to changes in nutrient availability.

IV.1. Introduction

Past ocean temperatures are an essential parameter for reconstructing the Earth's climate. Several organic and inorganic proxies for reconstructing sea surface temperature (SSTs) exist. Amongst these is the lipid based alkenone unsaturation index ($U_{37}^{K'}$), expressing the relative abundance of long chain alkenones biosynthesized by some haptophytes, in particular *Emiliania huxleyi* (Brassell et al., 1986), and the tetraether index with 86 carbon atoms (TEX_{86}), based on the relative abundance of isoprenoid glycerol dialkyl glycerol tetraethers (*i*GDGTs) biosynthesized by planktonic archaea (Schouten et al., 2002). Both proxies are widely used since they appear robust and applicable in most marine settings, and their analysis is inexpensive and requires only small amounts of sample of ≤ 1 g (e.g. Prahl et al., 1988; Müller et al., 1998b; Schouten et al., 2002; Kim et al., 2008). More recently, the long chain diol index (LDI) has been proposed as an additional SST proxy (Rampen et al., 2012). It is based on the relative distribution of long chain diols, presumably produced by eustigmatophyte algae (Volkman et al., 1992; Versteegh and de Leeuw, 1997).

In paleoclimatology, a multiproxy approach is often used because each proxy has its limitations, such as alteration by selective degradation and diagenesis (e.g. Hoefs et al., 1998; Schouten et al., 2004; Kim et al., 2009) or vulnerability to transport and redeposition (e.g. Ohkouchi et al., 2002; Mollenhauer et al., 2003). Additionally, the ecology of the different organisms and the resulting discrepancies between different SST proxies are not completely understood (e.g. Grauel et al., 2013; Lopes dos Santos et al., 2013; Smith et al., 2013). In order to minimize sources of errors and to allow high sample throughput in a relatively short time, simple and fast protocols are needed. At present, $U_{37}^{K'}$, LDI and TEX_{86} are obtained via separate analytical methods. $U_{37}^{K'}$ is conventionally obtained through gas chromatography (GC) coupled with either flame ionization detection (GC-FID) or mass spectrometry (GC–MS) operated in chemical ionization mode (CI; Rosell-Mele et al., 1995) or by fast GC–time-of-flight mass spectrometry (ToF-MS; Hefter, 2008). LDI is determined via GC–MS, while TEX_{86} is acquired using normal phase high performance liquid chromatography coupled to atmospheric pressure CIMS (NP-HPLC–APCI-MS; Hopmans et al., 2000; Schouten et al., 2007). TEX_{86} can either be determined directly from the total lipid extract (TLE) or after fractionation over a silica gel or alumina column, whereas determination of $U_{37}^{K'}$ and LDI usually requires additional sample preparation steps, e.g. base hydrolysis to eliminate co-eluting alkenoates (Villanueva et al., 1997) or derivatization of hydroxyl groups of long chain diols. Other protocols for analyzing archaeal GDGTs and long chain alkenones with one instrument exist. For example, Nichols et al. (1993) reported the analysis of *i*GDGTs using high temperature GC and, using an adapted method, Pancost et al. (2008) detected *i*GDGTs and long chain

alkenones in the same analytical window. However, such methods are not routinely applied because they are laborious and impacted by various constraints. For example, *i*GDGTs containing OH groups in the biphytane chain are not thermostable if analyzed with GC and the chromatographic resolution is generally worse than for HPLC methods.

Here, we present an extension of the NP-HPLC–APCI-MS method recently described by Becker et al. (2013) to a dedicated protocol for the detection of long chain diols, long chain alkenones and core *i*GDGTs in a single analysis. As a proof of concept, we applied the method to sediments deposited since 21 kyr BP in the Sea of Marmara. The interval covers large shifts in climate and environment, like the Last Glacial Maximum (LGM), the Bølling/Allerød (B/A), the Younger Dryas (YD), sapropel S1 formation and the late Holocene. Furthermore, the Sea of Marmara has oscillated between lacustrine and marine stages following glacial and interglacial global sea level changes, respectively (Stanley and Blanpied, 1980; Ryan et al., 1997; Aksu et al., 1999; Çağatay, 1999; Çağatay et al., 2000; Aksu et al., 2002; Ryan et al., 2003). The current marine state was established ca. 14.7 kyr BP (e.g. Vidal et al., 2010). This oceanographic history makes the Sea of Marmara an ideal location for studying multiproxy records.

IV.2. Material and methods

IV.2.1. Samples and extraction

Sediment samples were collected during RV Meteor cruise M84/1 ("DARCSEAS I") from different depositional environments (Table IV.1). Site GeoB15103 is in the Eastern Mediterranean where organic-rich sediments (sapropels) alternate with organic-lean, coccolith-rich sediments. Site GeoB15104 in the Sea of Marmara experiences high terrigenous input and Site GeoB15105 in the Black Sea provides CH4-rich and organic-rich sediments. After recovery, the samples were immediately frozen and stored at $-80\,^{\circ}\mathrm{C}$ until further treatment (Zabel and Cruise Participants, 2013). Additionally, for analysis of alkenones, biomass of an *E. huxleyi* culture was used, which has been grown at $23\,^{\circ}\mathrm{C}$ in f/2 medium (Guillard and Ryther, 1962) with a 12h/12h light/dark cycle and harvested at exponential growth phase. For analysis and isolation of long chain diols, surface sediment samples from Aarhus Bay were used (56°07.06'N, 10°20.85'E, 15 m water depth, 10-12 cm and 0-60 cm sediment depth).

The sediment samples (25±0.5 g wet w), as well as the *E. huxleyi* culture, were extracted using a modified Bligh and Dyer protocol (Sturt et al., 2004): ultrasonication was performed for 10 min in four steps with a mixture of dichloromethane (DCM)/MeOH/buffer (1:2:0.8, v:v:v) using 4 ml solvent g_{-1} sediment and extraction step. A phosphate buffer ($8.7\,\mathrm{g\,l^{-1}}$ KH_2PO_4, pH 7.4) was used for the first two steps, and a Cl_3CO_2H buffer ($50\,\mathrm{g\,l^{-1}}$

Table IV.1. Sampling site characteristics.

Cruise	Site	Location	Position	Water depth (m)
M84/1	GeoB15103	Eastern Mediterranean	34°01.65'N/32°37.80'E	1367
M84/1	GeoB15104	Sea of Marmara	40°47.97'N/27°43.49'E	600
M84/1	GeoB15105	Black Sea	41°31.71'N/30°53.07'E	1266

Cl_3CO_2H, pH 2) for the final two. After each extraction step, the samples were centrifuged at 800 x g for 10 min and the supernatants collected in a separation funnel. The combined supernatants were then washed 3x with de-ionized MilliQ water. After separation into organic phase and water-soluble phase, the organic phase was collected as the total lipid extract (TLE). The solvent was gently removed under a stream of N2 and the extract stored at $-20\,°C$.

IV.2.2. Age model for sediment cores from the Sea of Marmara

The 39 samples from the Sea of Marmara were derived from a 704 cm long gravity core (GeoB15104-1) and a 52 cm multi-core (GeoB15104-2). The sampling interval for the multi-core was 2 cm (26 samples). The gravity core sediments were sampled every ca. 50 cm and covered prominent lithologies, for example the organic rich sediments from the Sapropel S1. The detailed lithology is described by Zabel and Cruise Participants (2013). The age model for the cores was based on sedimentation rates according to Vidal et al. (2010) for the nearby core MD01-2430. Matching lithologies and interfaces were adjusted, such as the top (7 kyr BP) and bottom (11.5 kyr BP) of S1 and the transition from the marine to the lacustrine sediments (14.7 kyr BP; Supp. Fig. IV.1). Based on this model, the gravity core covered the last ca. 21 kyr.

IV.2.3. Instrumentation

IV.2.3.1. NP-HPLC–APCI-MS

The *i*GDGTs, long chain diols and long chain alkenones were analyzed according to Becker et al. (2013) with a Dionex Ultimate 3000RS UHPLC instrument coupled to a Bruker maXis ultra-high resolution quadrupole time-of-flight mass spectrometer (qToF-MS), equipped with an APCI II ion source. Aliquots of the TLE (typically 10 µL) in n-hexane:propan-2-ol (99.5:0.5, v:v) were injected onto two coupled Acquity BEH amide columns (each 2.1 x 150 mm, $1.7\,\mu m$; Waters, Eschborn, Germany) kept at $50\,°C$. Compounds were eluted using the following gradient (after Becker et al., 2013) with eluent A (n-hexane) and eluent B [n-hexane:propan-2-ol (90:10, v:v)] and constant flow of $0.5\,m/permin$: 3 % B to 5 % B in 2 min, to 10 % B in 8 min, to 20 % B in 10 min, to 50 %

in 15 min and to 100 % in 10 min. Columns were washed with 100 % B for 6 min and equilibrated with 3 % B for 9 min before the next injection. Compounds were detected in positive ionization mode, scanning from *m/z* 150 to 2000 at 2 scans/s; source parameters were as described by Becker et al. (2013). MS^2 spectra were obtained in data dependent mode. For each MS full scan, up to three MS^2 experiments targeted the most abundant ions with N2 as collision gas and a collision energy of 35 eV. The isolation width was 6 Da. Active exclusion limited how often a given ion was selected for fragmentation and thus allowed us to obtain MS^2 data for less abundant ions. The mass spectrometer was operated at a resolution of 27,000 at *m/z* 1222 and mass accuracy after calibration by loop injection at the end of each run and by lock mass calibration was typically $\leq 1 - 2$ ppm (cf. Becker et al., 2013). Compounds were assigned from their exact masses and isotope pattern in full scan (MS^1) mode and their characteristic fragmentation in MS^2 spectra. Integration of peaks was performed on extracted ion chromatograms of ±10 mDa width of the $[M+H]^+$ ion in MS^1 spectra. Accurate mass, high resolution and MS^2 fragment spectra are not essential for quantification of GDGTs, alkenones and diols once the retention time is established; thus, conventional single quadrupole HPLC–MS systems are suitable. Lipid quantification was achieved by injecting an internal standard (C_{46} GTGT; Huguet et al., 2006) along with the samples. The abundances of *i*GDGTs, alkenones and diols were averaged from duplicate measurements; *i*GDGTs and alkenones were corrected for the response factors of GDGT-0 (caldarchaeol), purified from extracts of Archaeoglobus fulgidus, and authentic $C_{37:2}$ and $C_{37:3}$ alkenone standards vs. the C_{46}-GTGT standard. The lower limit of quantification (LLOQ) for *i*GDGTs and long chain alkenones was <10pg. The relative response factor (RRF) between the $C_{37:2}$ and $C_{37:3}$ alkenone was determined to be 1.3 with the higher response for the $C_{37:2}$ alkenone (RF $C_{37:2}$ = 1.3 x RF $C_{37:3}$). For our instrument, the RF values were linear in the range between 10 pg and 10 ng. Since authentic standards for long chain diols are not available, response factor correction and determination of LLOQ was not possible. To determine concentrations of diols we assumed a RRF of 1 vs. the C_{46}-GTGT. By assuming this RRF, the LLOQ was <10 pg.

IV.2.3.2. GC-FID

Alkenoates were removed via base hydrolysis of the TLE fraction following the procedure described by Elvert et al. (2003). GC was performed using a Trace Gas Chromatograph (ThermoFinnigan GmbH, Bremen, Germany) with a Rxi-5ms column (30 m × 0.25 mm × 0.25 µm; Restek GmbH, Bad Homburg, Germany) equipped with FID. He served as carrier gas at a constant 1 mmin. The GC temperature program was: 60 °C (1 min) to 150 °C at 15 °C/min, then to 300 °C (held 28 min) at 4 °C/min. The injector was at 310 °C

and the detector at 300 °C. Assignment of di- and triunsaturated C_{37} alkenones ($C_{37:2}$ and $C_{37:3}$) was based on retention times and comparison with parallel GC–MS runs. All samples were analyzed in quadruplicate.

IV.2.3.3. GC–MS

Long chain diols were analyzed using GC–MS with a Trace gas chromatograph system interfaced to a Trace MS instrument (both from ThermoFinnigan) after derivatization with bis(trimethylsilyl)-trifluoroacetamide in pyridine at 60 °C for 1 h (Elvert et al., 2003). The mass spectrometer was operated in electron ionization mode (EI^+) at 70 eV over *m/z* 40 to 700. The ion source was at 200 °C, the interface at 300 °C and He was the carrier gas at a constant 1 ml/min. Samples were injected in splitless mode at 310 °C and analyte separation was achieved with an Rxi-5ms column (30 m × 0.25 mm × 0.25 µm; Restek GmbH, Bad Homburg, Germany) using the same temperature program as for GC-FID. Assignment of long chain diols was based on retention times and characteristic fragments in the GC–MS run (see Smith et al., 1983; Versteegh and de Leeuw, 1997). Relevant long chain diols were quantified using extracted ion chromatograms (EICs) of the characteristic fragment ions at *m/z* 299.4, 313.4, 341.4, 327.4, 341.4 and 355.4. All samples were analyzed in duplicate.

IV.2.3.4. Long chain diol isolation

For HPLC-based long chain diol assignment the compounds were isolated from the TLE of the Aarhus Bay sediment sample through reversed phase semi-preparative LC with an Agilent 1200 series HPLC instrument equipped with an Agilent 1200 series fraction collector and coupled to an Agilent 6130 MSD by active splitter. The diols were eluted using the chromatographic protocol of Zhu et al. (2013a). In brief, the TLE was fractionated with a semi-preparative Zorbax Eclipse XDB-C_{18} column (5 µm, 250 × 9.4 mm; Agilent Technologies Deutschland GmbH, Böblingen, Germany) operated at 45 °C. Samples were dissolved in MeOH:propan-2-ol (8:2, v:v) and eluted using a linear gradient from 80 % MeOH: 20 % 2-propanol to 60 % MeOH: 40 % propan-2-ol in 5 min and then to 35 % MeOH: 65 % propan-2-ol in another 40 min at 2.2 mmin. The column was washed with 100 % propan-2-ol for 15 min followed by column re conditioning with 100 % MeOH for another 15 min. The diols were collected in a time window of 8.6 to 12 min.

IV.2.3.5. Calculations

TEX_{86} was calculated using the definition of Schouten et al. (2002):

$$TEX_{86}^{H} = \frac{[\text{GDGT-2}] + [\text{GDGT-3}] + [\text{GDGT-5'}]}{[\text{GDGT-1}] + [\text{GDGT-2}] + [\text{GDGT-3}] + [\text{GDGT-5'}]} \quad \text{(Eq. 1)}$$

where numbers refer to number of rings in the GDGT and GDGT-5' to the crenarchaeol regio-isomer. TEX_{86} was converted to SST using the core top transfer function of Kim et al. (2008):

$$SST = -10.78 + 56.2 \times (TEX_{86}) \quad \text{(Eq. 2)}$$

$U_{37}^{K'}$ was calculated according to Prahl and Wakeham (1987):

$$U_{37}^{K'} = \frac{[C_{37:2}\text{alkenone}]}{[\text{GDGT-1}] + [C_{37:2}\text{alkenone}] + [C_{37:3}\text{alkenone}]} \quad \text{(Eq. 3)}$$

It was converted to SST by applying the core top transfer function of Conte et al. (2006):

$$SST = 29.876 \times (U_{37}^{K'}) - 1.334 \quad \text{(Eq. 4)}$$

LDI was calculated using Eq. 5 as described by Rampen et al. (2012):

$$LDI = \frac{[C_{30}\text{1,15 diol}]}{[C_{28}\text{1,13 diol}] + [C_{30}\text{1,13 diol}] + [C_{30}\text{1,15 diol}]} \quad \text{(Eq. 5)}$$

SST values were estimated using the global core top calibration from the same study:

$$SST = \frac{\text{LDI-0.095}}{0.033} \quad \text{(Eq. 6)}$$

Mean deviations for duplicate NP-HPLC–MS runs were ±0.01 $U_{37}^{K'}$ units (±0.32 °C), ±0.006 TEX_{86} units (±0.31 °C) and ±0.01 LDI units (±0.23 °C), respectively, and ±0.004 $U_{37}^{K'}$ units (0.14 °C) and ±0.003 TEX_{86} units (0.11 °C), respectively, for HPLC–MS runs. Mean standard deviation for quadruplicate GC-FID runs was ±0.02 $U_{37}^{K'}$ units (±0.62 °C) and for duplicate GC–MS runs ±0.01 LDI units (±0.28 °C). The chromatographic resolution (Rs) was calculated from the retention time difference between two adjacent peaks (ΔtR) divided by the sum of their mean peak width at half peak height (W_{avg}):

$$RS = \frac{\Delta tR}{W_{avg}} \quad \text{(Eq. 7)}$$

IV.3. Results and discussion

The NP-HPLC–APCI-MS method (Becker et al., 2013) allows simultaneous determination of nine paleoenvironmental proxies (Figure IV.1): the SST proxies TEX_{86} (Schouten et al., 2002), $U^{K'}_{37}$ (Brassell et al., 1986) and LDI (Rampen et al., 2012), the proxy for terrestrial input to the ocean using the branched isoprenoid tetraether index (BIT; Hopmans et al., 2004), proxies for annual mean air temperature (MAT) and soil pH using the cyclisation (CBT) and methylation ratio of branched tetraethers (MBT; Weijers et al., 2007), a proxy for paleosalinity using the archaeol and caldarchaeol ecometric (ACE; Turich and Freeman, 2011), a proxy for past methane hydrate dissociation using the methane index (MI; Zhang et al., 2011) and a SST proxy for high latitudes via hydroxylated *i*GDGT-based indices (Huguet et al., 2013). Additionally, the whole suite of recently identified tetraether core lipids from Liu et al. (2012c) and Zhu et al. (2014a), such as *br*GDGTs with a higher and lower degree of methylation than the regular compounds, and butane- and pentanetriol dialkyl glycerol tetraethers, could be detected (Fig. 1b). Their ecological and environmental significance still needs, however, to be clarified. We demonstrate below the extension of the HPLC–MS protocol of Becker et al. (2013) to the analysis of $U^{K'}_{37}$ and LDI, i.e. to simultaneous analysis of three molecularly independent SST proxies in a single analysis (see Figure IV.1), which is not possible with the conventional protocols due to inadequate chromatographic separation of the proxy-relevant alkenones and diols, respectively.

IV.3.1. Detection of long chain alkenones using HPLC—MS

In the NP-HPLC base peak chromatogram (BPC) of the TLE of the *E. huxleyi* culture (Figure IV.2a) the long chain alkenones eluted between 1.8 and 2.5 min. They were unambiguously assigned from their exact mass in full scan (MS^1) spectra and their characteristic fragmentation in MS^2 spectra. The major product ion of the $C_{37:2}$ alkenone ($[M+H]^+$ at *m/z* 531.5499) is *m/z* 513.5394 (-18.0 Da), formed by loss of water (Figure IV.2b). The remaining larger fragments form a series with 14.0 Da difference between the product ions, resulting from cleavage between different carbons after initial loss of water. For example, the fragment at *m/z* 317.3203 results from cleavage between C-23 and C-24 and that at *m/z* 331.3359 from cleavage between C-24 and C-25. The C=C locations cannot be determined using MS without derivatization, because they can migrate when the alkyl chain is ionized (López and Grimalt, 2004; Rontani et al., 2006). The C_{38} and C_{39} Et ketones elute before the C_{37} and C_{38} Me ketones and the $C_{37:2}$ and $C_{37:3}$ alkenones are well separated (see Figure IV.2a) and can be quantified readily for computation of $U^{K'}_{37}$. The chromatographic resolution according to Eq. (7) between the two peaks is 1.12. Resolving them is necessary, since otherwise the $^{13}C_2$ isotope

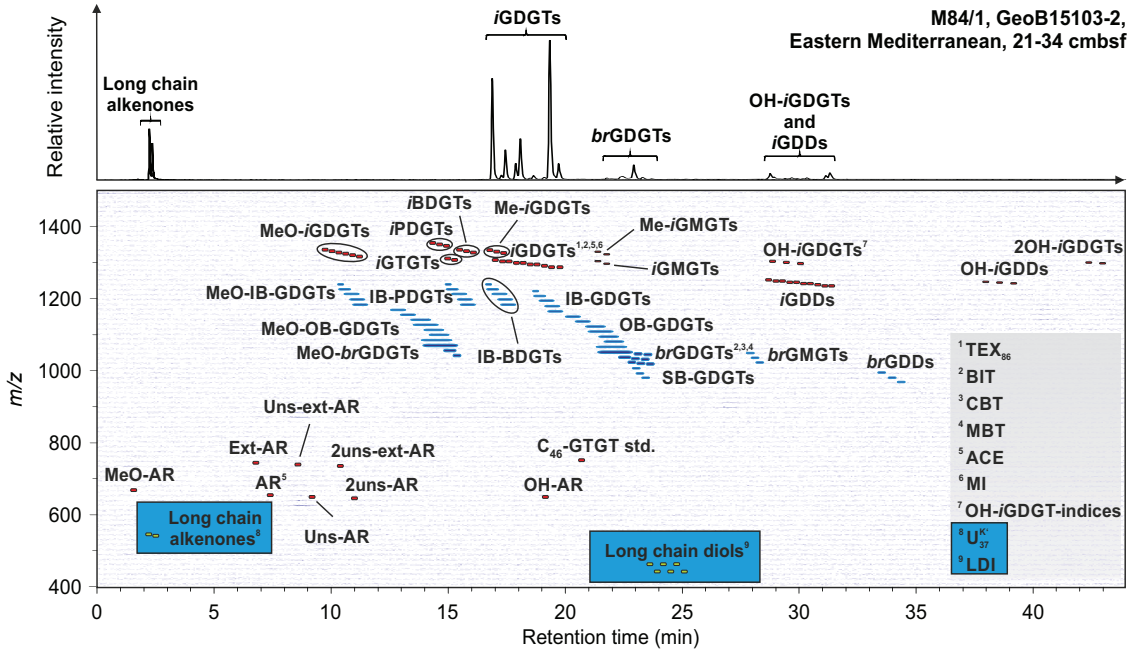

Figure IV.1. (a) Reconstructed NP-UHPLC–APCI-qToF-MS base peak chromatogram showing long chain alkenones, *i*GDGTs, *br*GDGTs, *i*GDDs and OH-*i*GDGTs in sample M84/1, GeoB15103-2, 21-34 cmbsf. (b) Associated, reconstructed density map plot showing whole range of lipid biomarkers detectable with the NP-HPLC–APCI-MS protocol, as well as long chain alkenones and diols (blue boxes). Superscripts indicate proxies that can be determined from specific lipids or lipid groups. Abbreviations according to Liu et al. (2012c) and Zhu et al. (2014a): GDGT, glycerol dialkyl glycerol tetraether; GDD, glycerol dialkanol diether; GMGT, glycerol monoalkyl glycerol tetraether; BDGT, butanetriol dialkyl glycerol tetraether; PDGT, pentanetriol dialkyl glycerol tetraether; GTGT, glycerol trialkyl glycerol tetraether; AR, archaeol; OH, monohydroxy; 2OH, dihydroxy; Uns, monounsaturated; 2uns, diunsaturated; Ext, extended; Me, methylated; MeO, methoxy; *i*, isoprenoid; *br*, branched; IB, hybrid isoprenoid/branched; OB, overly branched; SB, sparsely branched.

peak from $C_{37:3}$ would contribute to the monoisotopic peak of the $C_{37:2}$ alkenone. The co-elution of the C_{37} and C_{38} Me ketones does not influence their quantification because of the MS-based detection and a difference of 14.0 Da between the C_{37} and C_{38} alkenones. The $C_{37:4}$ alkenone was not detected in the *E. huxleyi* culture, presumably because of the relatively high culture temperature (23 °C), at which only small amounts of the $C_{37:4}$ alkenones are produced (Prahl et al., 1988).

Having demonstrated the detection of alkenones with NP-HPLC–MS, we are able to measure TEX_{86} and $U^{K'}_{37}$ in a single analysis (e.g. Figure IV.2c). This brings the advantages of eliminating sample preparation steps, e.g. base hydrolysis to remove alkenoates, highly reduced time for analysis, and increased sensitivity of one order of magnitude compared with conventional GC based methods. The limit of quantification for the new method is <10 pg, whereas for GC-FID it is generally in the ng range (e.g. Villanueva and Grimalt, 1997). Potential disadvantages of analyzing alkenones with HPLC–MS could be changes in the relative sensitivity between the di- and triunsaturated compounds and non-linear

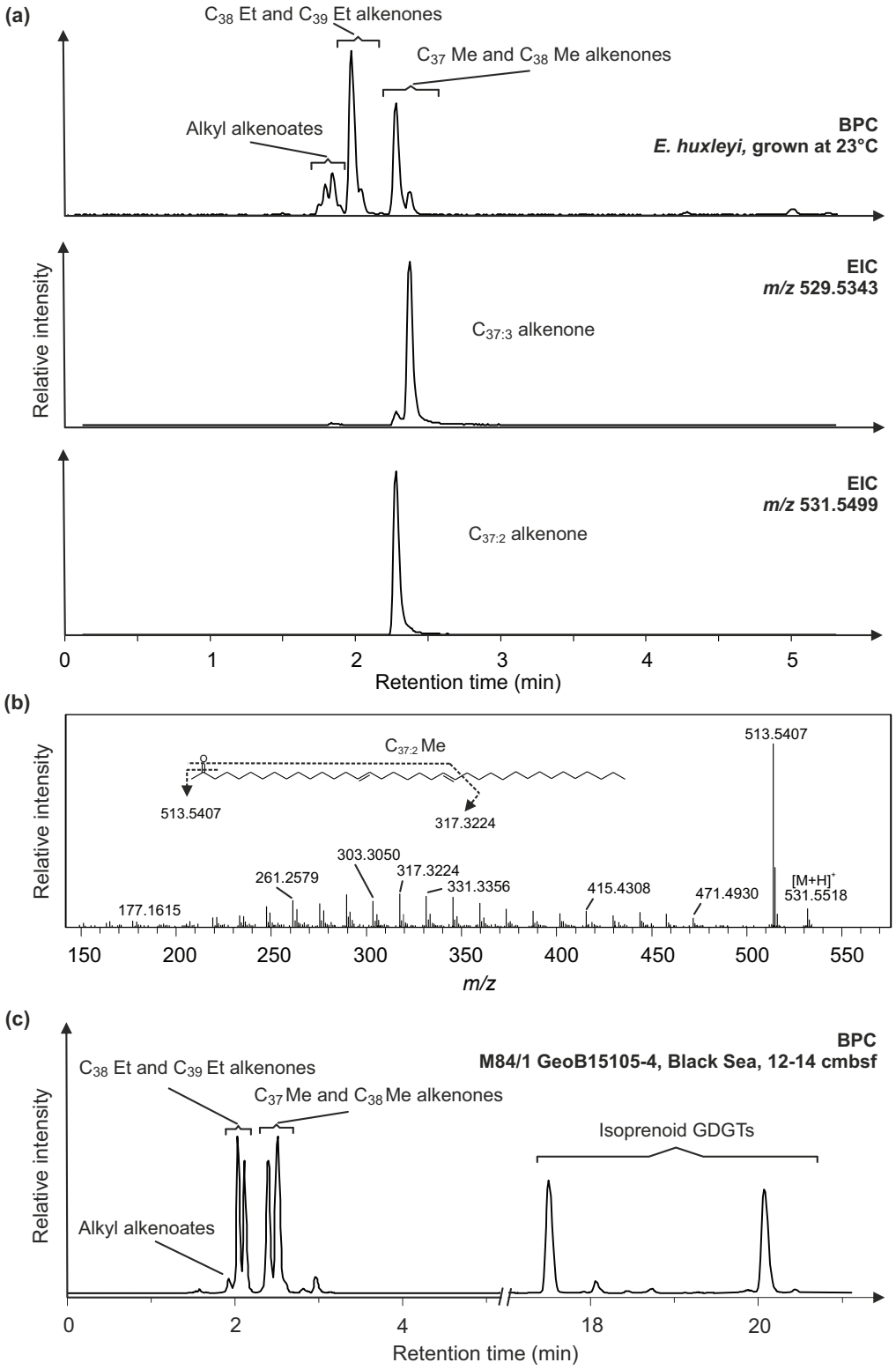

Figure IV.2. (a) NP-HPLC–APCI-MS base peak chromatogram (BPC) showing long chain alkenones and alkyl alkenoates, and extracted ion chromatograms (EICs) showing the triunsaturated (*m/z* 529.5) and diunsaturated (*m/z* 531.5) alkenones in the TLE of *E. huxleyi*. (b) NP-HPLC–APCI-multiple stage mass spectrum (MS^2) of the diunsaturated alkenone ($[M+H]^+$ at *m/z* 531.5). Shown are the MS^2 fragment ions within the range *m/z* 150-570. The structure and formation of the major product ions are also indicated. (c) NP-HPLC–APCI-MS BPC showing long chain alkenones and *i*GDGTs in the TLE of the marine sediment M84/1 GeoB15105-4, Black Sea, 12-14 cmbsf.

response factors, as observed with other MS methods, e.g. GC-CI-MS (Chaler et al., 2000; Chaler et al., 2003), GC-EI-MS (Versteegh et al., 2001) and GC-qToF-MS (Hefter, 2008). In order to quantify such effects, we calibrated our instruments with the $C_{37:2}$ and $C_{37:3}$ alkenone standards. The RRF values slightly differed between the two compounds but were linear for our instrument. Thus, the monitoring of RRF is recommended for the use of the presented protocol, which applies for MS-based detection in general.

IV.3.2. Detection of long chain diols using HPLC—MS

Detection of long chain alkenones with NP-HPLC–MS led us to further inspect the protocol for the detection of long chain diols, which are used for the LDI SST proxy. Their greater polarity than the long chain alkenones results in a longer retention time in the NP-HPLC chromatogram. Indeed, in the BPC of the isolated long chain diol fraction from the Aarhus Bay sediment, the diols eluted between 24 and 27 min (Figure IV.3). They were tentatively assigned from the exact mass in full scan (MS^1), the characteristic fragmentation in MS^2 spectra and by comparison of the relative distributions of the major diol isomers with that obtained through conventional GC–MS. The diols are subject to in source dehydration during the protocol for NP-HPLC–APCI-MS, with the resulting dehydrated fragment (-18.0 Da). For example, the major MS^1 signal for the C_{30} diols was at *m/z* 437.4171 and for the C_{28} diols at *m/z* 409.4404. For accurate quantification, we therefore propose to use the dehydrated fragments.

In the MS^2 spectrum of the C_{30} 1,15 diol ($[M+H]^+$-18.0 Da at *m/z* 437.4171) the major fragment was at *m/z* 419.4611 (Figure IV.3b), representing loss of the second OH group (-18.0 Da). The remaining larger fragments form a series with 14.0 Da difference between the product ions resulting from cleavage between different carbons after loss of the OH groups. Like the fragmentation of the long chain alkenones, C=C positions in the diol derivatives, obtained via loss of the OH groups, cannot be determined with MS^2. Therefore, the identity of the isomers with the same chain length cannot be determined using this method. However, comparison of the relative abundance of the major diol isomers between the conventional GC–MS method and the NP-HPLC protocol (Table IV.2) indicates that retention is based on compound polarity, so the earliest eluting major peak was the C_{30} 1,15 diol, the second with the same mass the C_{30} 1,14 diol and the third the C_{30} 1,13 diol, i.e. in order of increasing polarity. The major C_{28} diols were (early to late eluting): C_{28} 1,14, C_{28} 1,13 and C_{28} 1,12. The isomers used for LDI were baseline separated (see Figure IV.3a) and could be quantified readily for determination of LDI. The NP-HPLC protocol therefore enables the determination of the three proxies - TEX_{86}, $U^{K'}_{37}$ - and LDI from a single analysis (Figure IV.3c, Figure IV.4a).

The simultaneous detection of the three SST proxies might also be possible with con-

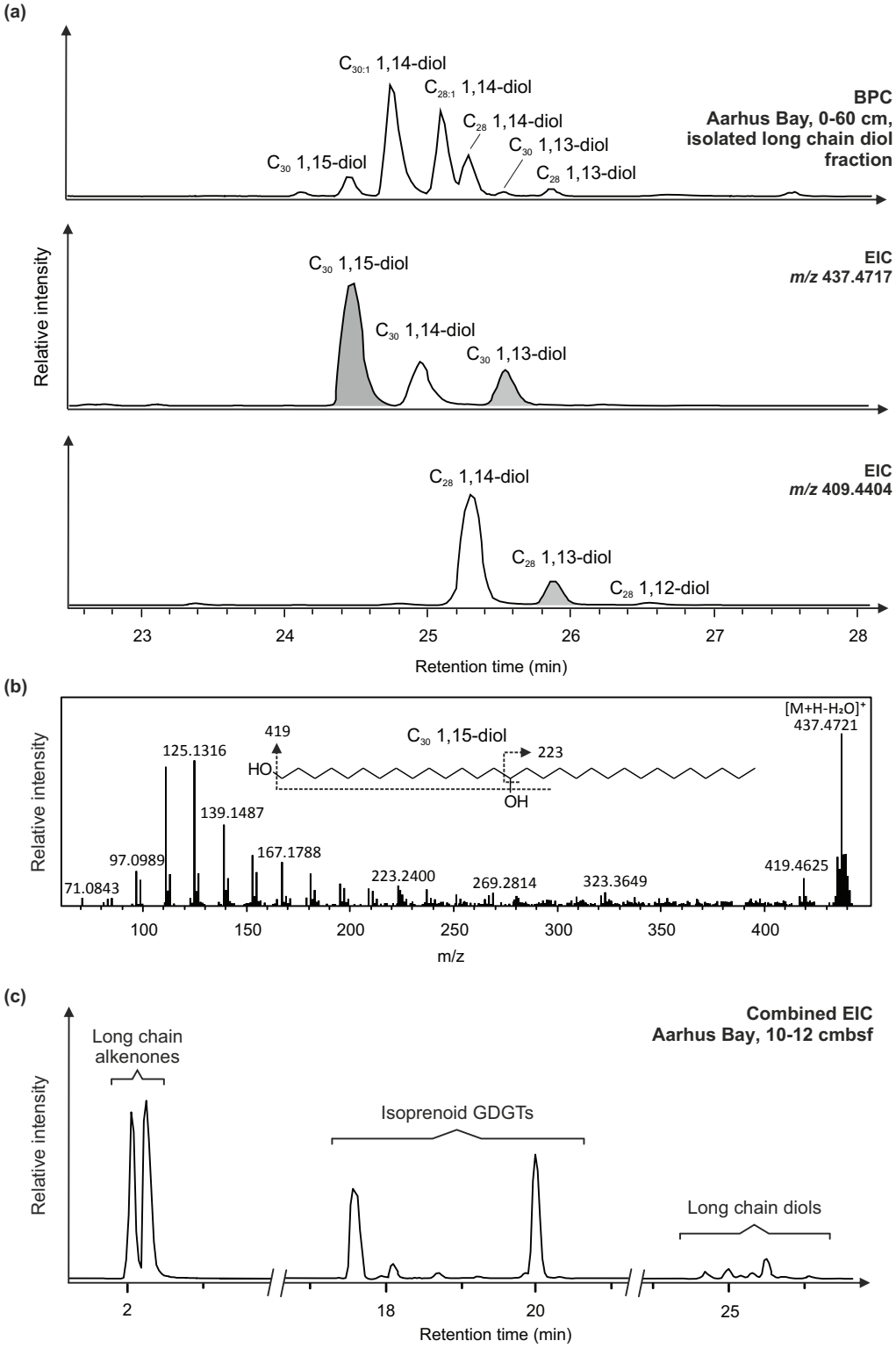

Figure IV.3. (a) NP-HPLC–APCI-MS BPC showing long chain diols, and EICs showing the C_{30} (*m/z* 437.4) and the C_{28} (*m/z* 409.4) diols in the isolated long chain diol fraction from the Aarhus Bay sediment sample, 0-60 cmbsf. Gray shaded peaks indicate the diols used for the LDI SST proxy. (b) NP-HPLC–APCI-multiple stage mass spectrum (MS^2) of the C_{30} 1,15 diol ($[M+H]^+$-18 Da at *m/z* 437.4). Shown are the MS^2 fragment ions within the range *m/z* 60-450. The structure and the formation of the major product ions are also shown. (c) NP-HPLC–APCI-MS BPC showing long chain alkenones, long chain diols and *i*GDGTs in the TLE of the marine sediment from Aarhus Bay, 10-12 cmbsf.

Table IV.2. Fractional abundance (%) of major long chain diols and LDI in isolated diol fraction from Aarhus Bay sediment determined from GC–MS and NP-HPLC–MS, respectively.

	C_{28} 1,12 diol	C_{28} 1,13 diol	C_{28} 1,14 diol	C_{30} 1,13 diol	C_{30} 1,14 diol	C_{30} 1,15 diol	LDI
GC–MS (n=3)	1.55±0.46	10.21±0.04	50.72±9.93	4.88±1.76	8.12±2.67	24.53±5.99	0.62±0.03
NP-HPLC–MS (n=3)	1.35±0.32	9.78±0.79	50.03±0.77	5.46±0.57	10.16±1.89	23.23±3.20	0.60±0.04

ventional single quadrupole HPLC–MS systems, since the pressure using the presented method is below the upper limit for most HPLC instruments (600 bar), but would require method development including the adjustment of ionization parameters as well as of the gradient system for the columns used here. Alternatively to the two coupled amide columns, the use of a single column results in adequate separation of alkenones and diols (data not shown) and the maximum pressure is <400 bar. However, *i*GDGT and *i*GDD isomers cannot be fully resolved under these conditions (Becker et al., 2013). The establishment of the retention times of long chain diols and alkenones should be based on standard compounds or isolated fractions as described here (i.e. alkenones from an *E. huxleyi* culture or long chain diols from marine sediments). The high sensitivity of the qToF-MS enables detection of the relevant compounds in full scan mode, which is likely not possible with a single quadrupole MS instrument. As for GDGTs, detection should be performed in selective ion monitoring (SIM) mode scanning only for the masses of alkenones (as $[M+H]^+$ ions; see Figure IV.2) and diols (as $[M+H-H_2O]^+$; see Figure IV.3).

IV.3.3. Comparison of $U_{37}^{K'}$ determined from GC–FID and HPLC–MS

The GC-FID-based $U_{37}^{K'}$ values for samples from the Eastern Mediterranean, the Black Sea and selected samples from the Sea of Marmara core varied between 0.21±0.05 and 0.82±0.05 (providing SST between 5.4±1.7 and 23.4±1.5 °C) and thus cover a wide range of the possible $U_{37}^{K'}$ scale (Figure IV.4a, b; Table IV.3). The relatively large error for quadruplicate GC-FID runs (precision of 0.02 $U_{37}^{K'}$ units) might result from the low amounts of the $C_{37:2}$ and $C_{37:3}$ alkenones injected on-column especially for the sediment samples (Grimalt et al., 2001). In contrast, standard deviation for quadruplicate runs of the *E. huxleyi* culture, which contained alkenones at considerably higher abundance, was 0.004 and thus within the range generally obtained (Herbert, 2003). The maximum discrepancy between NP-HPLC and GC for $U_{37}^{K'}$ was 0.12±0.03 (sample GeoB15103-2, 21-43 cm below sea floor, cmbsf), representing a temperature difference of 3.5±0.8 °C. For most samples, the discrepancy was within the standard error for most calibrations (±0.7-1.6 °C). The mean $\Delta_{U_{37}^{K'}}$ between GC and NP-HPLC analysis was ±0.05. The linear relationship between NP-HPLC and GC $U_{37}^{K'}$ (r^2 0.93, slope 0.95; Figure IV.4b) shows that the protocol provides reliable and reproducible results for $U_{37}^{K'}$.

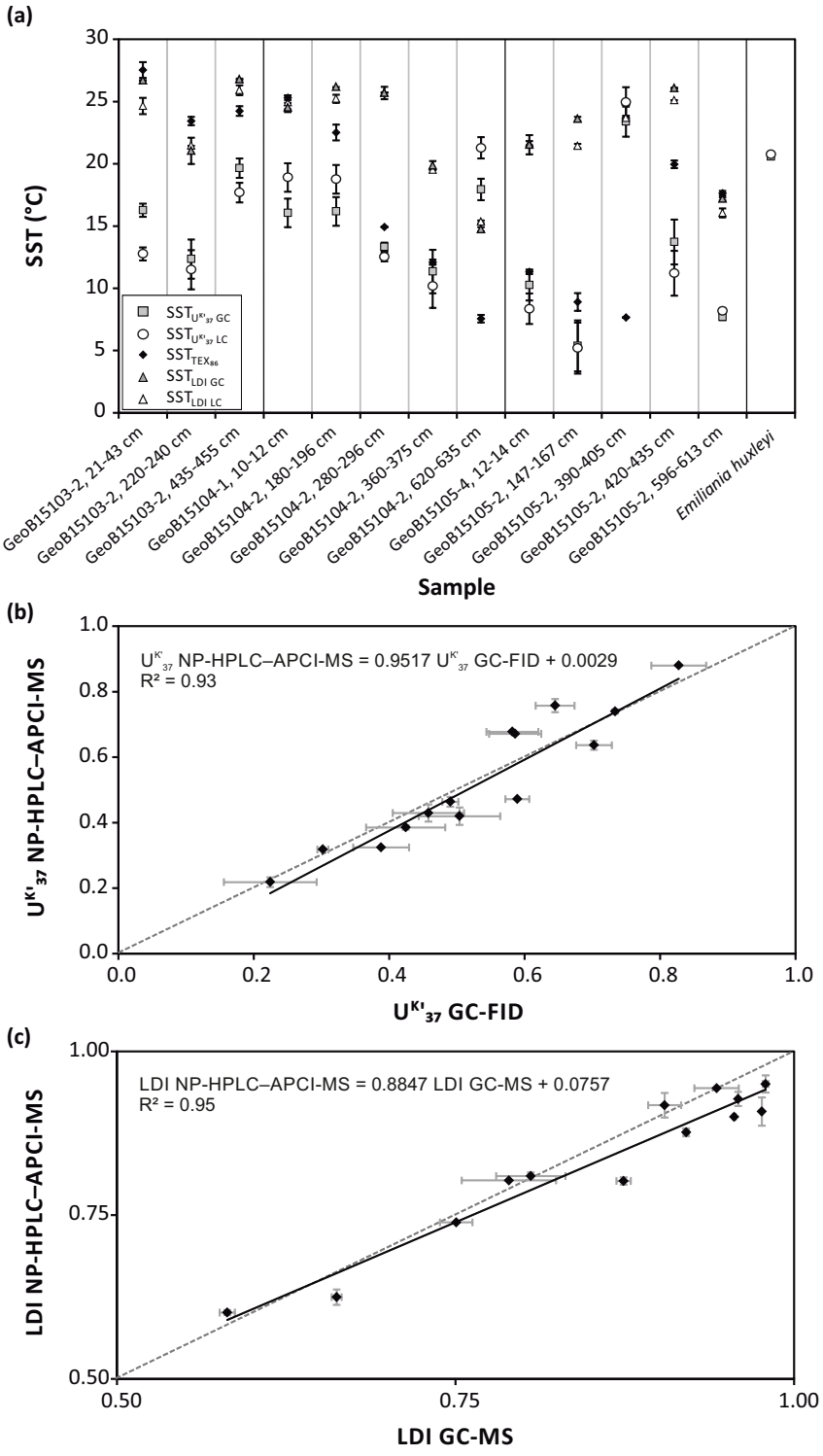

Figure IV.4. (a) SST values for different marine sediments and *E. huxleyi* culture. Shown are the alkenone-based temperatures determined from GC-FID ($SST_{U^{K'}_{37}\ GC}$) and NP-HPLC–APCI-MS ($SST_{U^{K'}_{37}\ LC}$), the diol-based temperatures determined from GC–MS ($SST_{LDI\ GC}$) and NP-HPLC–APCI-MS ($SST_{LDI\ LC}$) and archaeal GDGT-derived temperature ($SST_{TEX_{86}}$) determined from NP-HPLC–APCI-MS. Error bars indicate deviation for replicate analysis. (b) Cross plot of $U^{K'}_{37}$ values determined using GC-FID and NP-HPLC–APCI-MS. (c) Cross plot of LDI values determined using GC–MS and NP-HPLC–APCI-MS. Dashed lines in each cross plot indicates the 1:1 line.

IV.3.4. Comparison of LDI determined from GC–MS and HPLC–MS

LDI values determined from GC–MS in the sample set as above varied between 0.58±0.01 and 0.98±0.0007, providing SST values between 14.7±0.2 and 26.8±0.06 °C (Table IV.3, Figure IV.4a). LDI values from NP-HPLC and GC–MS show a clear linear relationship (r^2 0.95, slope 0.88; Figure IV.4c), demonstrating that the NP-HPLC protocol provides robust results for LDI. For most samples, the discrepancy between NP-HPLC and GC LDI was within the standard error for the most recent calibration (±2 °C, Rampen et al., 2012). The mean Δ_{LDI} for the samples was ±0.03 and the mean Δ_T±0.88 °C. The maximum discrepancy between NP-HPLC and GC LDI was 0.07±0.01 for GeoB15105-2, 147-167 cmbsf, representing a difference of 2.2±0.3 °C.

Table IV.3. $U_{37}^{K'}$, LDI, TEX_{86} and corresponding SST values obtained from the different methods.

		GC–FID		GC–MS		NP-HPLC–APCI-MS					
Core (GeoB)	Depth interval (cmbsf)	$U_{37}^{K'}$	SST	LDI	SST	$U_{37}^{K'}$	SST	TEX_{86}	SST	LDI	SST
15103-2	21-34	0.59±0.02	16.27±0.58	0.98±0.007	26.70±0.02	0.47±0.001	12.76±0.03	0.68±0.01	27.53±0.63	0.91±0.02	24.64±0.65
15103-2	220-240	0.46±0.05	12.35±1.57	0.79±0.03	21.04±1.05	0.43±0.03	11.49±0.79	0.61±0.01	23.44±0.33	0.80±0.001	21.45±0.001
15103-2	435-455	0.70±0.03	19.65±0.91	0.98±0.002	26.79±0.06	0.64±0.02	17.69±0.51	0.62±0.01	24.24±0.39	0.95±0.01	25.92±0.40
15104-1	10-12	0.58±0.04	16.05±1.25	0.90±0.01	24.53±0.37	0.68±0.03	18.9±0.84	0.64±0.003	25.3±0.17	0.92±0.02	24.93±0.56
15104-2	180-196	0.59±0.04	16.17±1.25	0.96±0.001	26.17±0.01	0.67±0.003	18.79±0.10	0.59±0.01	22.51±0.63	0.93±0.01	25.23±0.33
15104-2	280-296	0.49±0.02	13.3±0.35	0.94±0.02	25.69±0.50	0.46±0.01	12.51±0.19	0.46±0.002	14.93±0.01	0.94±0.001	25.72±0.003
15104-2	360-375	0.42±0.06	11.34±1.70	0.75±0.01	19.86±0.36	0.39±0.03	10.18±0.76	0.41±0.003	12.10±0.21	0.74±0.001	19.51±0.01
15104-2	620-635	0.65±0.05	17.94±0.97	0.58±0.01	14.74±0.17	0.76±0.001	21.29±0.01	0.33±0.01	7.56±0.30	0.61±0.004	15.34±0.08
15105-4	8-10	0.39±0.04	10.26±1.19	0.81±0.03	21.53±0.78	0.32±0.001	8.36±0.02	0.39±0.003	11.31±0.18	0.81±0.01	21.66±0.16
15105-2	147-167	0.22±0.06	5.37±1.71	0.87±0.01	23.61±0.16	0.22±0.01	5.19±0.34	0.35±0.01	8.90±0.71	0.80±0.01	21.43±0.17
15105-2	390-405	0.83±0.05	23.39±1.52	0.92±0.001	25.01±0.06	0.88±0.002	24.95±0.07	0.33±0.002	7.65±0.01	0.88±0.01	23.68±0.18
15105-2	420-435	0.50±0.06	13.72±1.85	0.96±0.001	26.08±0.03	0.42±0.03	11.21±0.78	0.55±0.01	19.96±0.30	0.90±0.001	25.10±0.001
15105-2	596-613	0.30±0.01	7.69±0.22	0.66±0.003	17.19±0.11	0.32±0.001	8.17±0.02	0.51±0.003	17.64±0.18	0.60±0.02	16.05±0.66
Emiliania huxleyi		0.73±0.01	20.58±0.15	-	-	0.74±0.01	20.75±0.26	-	-	-	-

IV.3.5. SST estimates from different proxies

The substantially higher TEX_{86} than $U_{37}^{K'}$ SST estimates for most samples obtained from the NP-HPLC analysis (Figure IV.4a, Table IV.3) might be explained by differences in ecology of the relevant haptophyta and archaea, such as production season or water depth. A similar pattern has been observed for the Mediterranean Gulf of Taranto, where the $U_{37}^{K'}$ signal corresponds to winter SST and the offshore TEX_{86} signal to summer SST (Leider et al., 2010). Only two samples showed the opposite behavior, i.e. higher $U_{37}^{K'}$ than TEX_{86} SST estimates. One originates from the Black Sea sapropel, an interval of strong (upper) water-column stratification, and the anomalous signal at this site could be explained by a strong contribution of deeper dwelling planktonic archaea that thrive in the colder chemocline, an explanation also suggested by Menzel et al. (2006). However, this is in contrast to studies of modern subsurface GDGT distributions, which showed a warm bias for the TEX_{86} signal (Schouten et al., 2012; Basse et al., 2014; Hernández-Sánchez et al., 2014; Xie et al., 2014). The LDI-derived temperature values are generally higher than those from $U_{37}^{K'}$ and TEX_{86} for corresponding samples

(Figure IV.4a), except for the Eastern Mediterranean, where TEX_{86}-derived temperatures are equal to or slightly higher than those derived from the LDI. This warm bias of LDI-derived temperatures was also observed by Lopes dos Santos et al. (2013). The authors compared LDI-inferred and foraminiferal assemblage-derived temperature values for the Southern Ocean and suggested that the LDI reflects SST of the warmest month. The ecological factors that might influence the lipid distribution of the signal producers and therefore the proxies are discussed in the next section. Lateral sediment transport and selective aerobic degradation during early diagenesis may also contribute to differences between SST from alkenones and *i*GDGTs (e.g. Huguet et al., 2009; Kim et al., 2009).

IV.3.6. Past SST variation in the Sea of Marmara determined with the new protocol

Alkenones, diols and *i*GDGTs were detected in all samples in sufficiently adequate concentration for proxy estimations (Figure IV.5a, b; Supp. Table IV.1; Supp. Table IV.2).Total *i*GDGT concentration varied between 0.44 and $8.58\,\mu g\,g^{-1}$ sediment dry wt (sed. dw) all along the record. The maximum concentration occurred within S1. A second peak was observed in the sample from the B/A with a concentration of $5.81\,\mu g\,g^{-1}$ sed. dw. Total diol concentration followed a similar pattern but absolute values were one to two orders of magnitude lower than for *i*GDGTs. In contrast, total alkenone concentration showed no distinct peak in S1. The maximum concentration occurred in the sample from the B/A at $4.45\,\mu g\,g^{-1}$ sed. dw. Lowest concentration was in samples from the lacustrine stage (0.02-$0.7\,\mu g\,g^{-1}$ sed. dw). For these samples, alkenones characteristic of freshwater environments (Thiel et al., 1997; Schulz et al., 2000) were not detected. For the Holocene samples, alkenone concentration ranged between 2.22 and $0.8\,\mu g\,g^{-1}$ sed. dw in the top 15 cm of the record, whereas it was ca. $0.41\,\mu g\,g^{-1}$ sed. dw for the deeper samples Supp. Table IV.2. The alkenone and diol concentration profiles are in line with previous studies (Vidal et al., 2010) and suggest that haptophytes were important in the phytoplanktonic community before the sapropel formation right after the marine connection of the Sea of Marmara. The high concentration of total *i*GDGTs and diols in S1 can be attributed to both increased primary production and preservation of organic matter (e.g. Sperling et al., 2003).

$U_{37}^{K'}$, TEX_{86} and LDI-derived temperature estimates are similar for the Late Holocene (7 to 0 kyr BP) with high and largely invariable values, although absolute values for the $U_{37}^{K'}$ derived SSTs are consistently lower than those derived from TEX_{86} and LDI (Figure IV.5b). Reconstructed temperature values from $U_{37}^{K'}$ ($SST_{U_{37}^{K'}}$) are 17.0 to $20.5\,°C$, from TEX_{86} ($SST_{TEX_{86}}$) 22.2 to $26.0\,°C$ and from LDI (SST_{LDI}) 23.2 to $25.4\,°C$ (Table IV.4). Between the LGM and S1, the temperature records differ. In the LGM, the $SST_{U_{37}^{K'}}$ shows

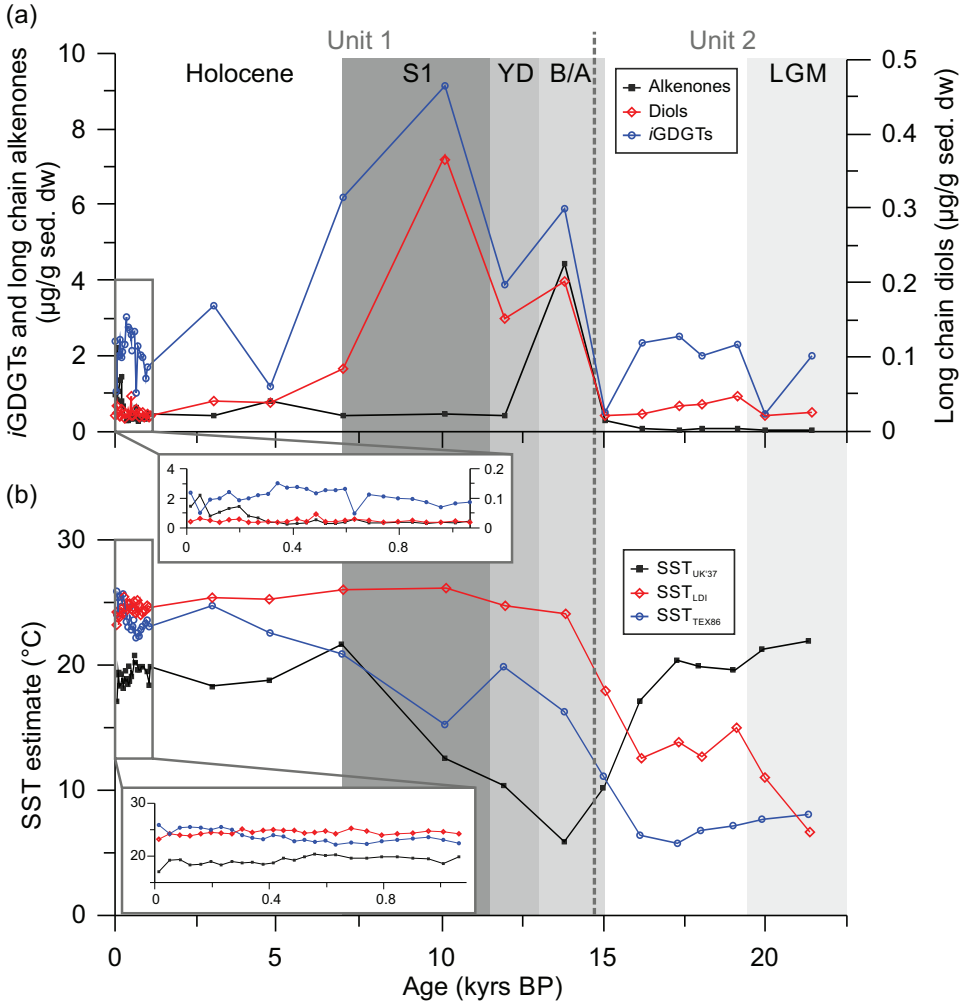

Figure IV.5. (a) Total *i*GDGT, diol and alkenone concentrations (µg g^{-1} sed. dw) vs. age. (b) SST estimates for cores GeoB15104-2 and -4 from the Sea of Marmara based on alkenones ($SST_{U^{K'}_{37}}$), diols (SST_{LDI}) and archaeal *i*GDGTs ($SST_{TEX_{86}}$) determined from NP-HPLC–APCI-MS. The timing of the Younger Dryas (YD), Bølling/Allerød (B/A), Sapropel S1 (S1), Last Glacial Maximum (LGM), Holocene and marine (Unit 1) and lacustrine (Unit 2) units are denoted.

its highest temperature (21.9 °C) which decreases during the transition from the LGM to the B/A, reaching 5.9 °C in the B/A. From the B/A to S1, $SST_{U^{K'}_{37}}$ increases again, reaching 21.7 °C at the top of S1. In contrast to $SST_{U^{K'}_{37}}$, SST_{LDI} and $SST_{TEX_{86}}$ are relatively low for the last glacial, with constant $SST_{TEX_{86}}$ of ca. 7 °C and TLDI between 6.6 (at 21.3 kyr) and 15.3 °C. $SST_{TEX_{86}}$ and SST_{LDI} increase during the transition from the glacial to the B/A. SST_{LDI} reaches modern Holocene values during the B/A. However, the warming trend for $SST_{TEX_{86}}$ starting at ca. 15.2 kyr is interrupted in S1, where temperatures decreases by 4.7 °C and relative to the YD (19.9 °C). Modern $SST_{TEX_{86}}$ is not reached before 4.7 kyr BP.

$SST_{TEX_{86}}$ suggests an LGM to late Holocene warming of ca. 18 °C, ca. 8 °C larger than for the Mediterranean Sea (Castañeda et al., 2010) and Black Sea (Ménot and Bard, 2010).

Table IV.4. $U_{37}^{K'}$, LDI, TEX_{86} and corresponding SST values for sediment cores from the Sea of Marmara.

Core (GeoB)	Coring device	Depth interval (cmbsf)	Estimated age (kyr BP)	$U_{37}^{K'}$	$SST_{U_{37}^{K'}}$ (°C)	TEX_{86}	$SST_{TEX_{86}}$ (°C)	LDI	SST_{LDI} (°C)
15104-1	MUC	0-2	0.01	0.62±0.02	17.09±0.59	0.65±0.02	25.95±0.86	0.86±0.05	23.2±1.42
15104-1	MUC	2-4	0.05	0.69±0.001	19.24±0.01	0.62±004	24.25±0.20	0.89±0.02	24.22±0.49
15104-1	MUC	4-6	0.09	0.69±0.03	19.35±0.87	0.64±0.01	25.33±0.47	0.88±0.02	23.91±0.47
15104-1	MUC	6-8	0.12	0.66±0.06	18.34±1.82	0.65±0.01	25.49±0.69	0.88±0.04	23.84±1.06
15104-1	MUC	8-10	0.16	0.66±0.01	18.39±0.16	0.64±0.01	25.37±0.41	0.89±0.05	24.18±1.45
15104-1	MUC	10-12	0.2	0.68±0.03	18.9±0.84	0.64±0.003	25.3±0.17	0.92±0.02	24.93±0.56
15104-1	MUC	12-14	0.23	0.66±0.03	18.26±0.84	0.65±0.02	25.51±1.29	0.90±0.02	24.39±0.72
15104-1	MUC	14-16	0.27	0.68±0.01	19.02±0.31	0.64±0.003	25.02±0.15	0.89±0.01	24.17±0.23
15104-1	MUC	16-18	0.31	0.67±0.02	18.75±0.51	0.62±0.01	23.94±0.33	0.93±0.02	25.15±0.54
15104-1	MUC	18-20	0.34	0.67±0.03	18.77±0.95	0.61±0.01	23.51±0.76	0.90±0.01	24.53±0.16
15104-1	MUC	20-22	0.38	0.66±0.02	18.47±0.71	0.61±0.01	23.22±0.44	0.91±0.01	24.84±0.15
15104-1	MUC	22-24	0.41	0.67±0.01	18.71±0.28	0.62±0.01	23.96±0.29	0.92±0.01	24.97±0.16
15104-1	MUC	24-26	0.45	0.70±0.01	19.66±0.41	0.61±0.01	23.69±0.42	0.92±0.01	24.91±0.26
15104-1	MUC	26-28	0.49	0.69±0.01	19.27±0.16	0.60±0.01	22.77±0.74	0.92±0.02	24.88±0.56
15104-1	MUC	28-30	0.52	0.71±0.01	19.88±0.38	0.60±0.01	23.02±0.51	0.90±0.01	24.34±0.44
15104-1	MUC	30-32	0.56	0.73±0.05	20.41±1.57	0.60±0.01	22.64±0.63	0.90±0.01	24.54±0.19
15104-1	MUC	32-34	0.6	0.72±0.01	20.14±0.38	0.60±0.003	22.99±0.19	0.91±0.01	24.74±0.42
15104-1	MUC	34-36	0.63	0.72±0.03	20.30±0.83	0.59±0.01	22.15±0.77	0.89±0.001	24.20±0.12
15104-1	MUC	36-38	0.69	0.70±0.01	19.58±0.27	0.59±0.005	22.51±0.28	0.93±0.02	25.20±0.61
15104-1	MUC	38-40	0.74	0.70±0.02	19.60±0.51	0.59±0.01	22.32±0.82	0.91±0.01	24.67±0.36
15104-1	MUC	40-42	0.79	0.71±0.02	19.90±0.67	0.60±0.01	22.86±0.32	0.89±0.01	24.02±0.34
15104-1	MUC	42-44	0.85	0.71±0.01	19.89±0.25	0.60±0.01	23.12±0.49	0.90±0.01	24.25±0.19
15104-1	MUC	44-46	0.9	0.7±0.003	19.55±0.08	0.61±0.03	23.35±1.43	0.90±0.02	24.40±0.67
15104-1	MUC	46-48	0.96	0.7±0.02	19.49±0.69	0.61±0.002	23.54±0.11	0.91±0.03	24.75±0.81
15104-1	MUC	48-50	1.01	0.67±0.07	18.56±1.98	0.6±0.009	23.08±0.49	0.91±0.03	24.65±0.76
15104-1	MUC	50-52	1.06	0.71±0.01	19.82±0.17	0.59±0.02	22.48±0.95	0.89±0.003	24.16±0.09
15104-2	GRC	116-130	3.01	0.66±0.01	18.29±0.33	0.63±0.01	24.73±0.59	0.93±0.01	25.35±0.44
15104-2	GRC	180-196	4.76	0.67±0.003	18.79±0.10	0.59±0.01	22.51±0.63	0.93±0.01	25.23±0.33
15104-2	GRC	222-236	6.95	0.77±0.02	21.70±0.67	0.56±0.01	20.94±0.39	0.95±0.01	25.97±0.34
15104-2	GRC	280-296	10.1	0.46±0.01	12.51±0.19	0.46±0.0002	14.93±0.01	0.94±0.001	25.72±0.003
15104-2	GRC	310-325	11.91	0.39±0.02	10.34±0.63	0.55±0.02	19.88±1.12	0.91±0.01	24.76±0.37
15104-2	GRC	340-355	13.76	0.24±0.01	5.86±0.22	0.48±0.01	16.3±0.401	0.89±0.03	24.12±0.85
15104-2	GRC	360-375	14.99	0.39±0.03	10.18±0.76	0.41±0.003	12.10±0.21	0.74±0.001	19.51±0.01
15104-2	GRC	420-435	16.12	0.62±0.03	17.12±0.88	0.31±0.01	6.38±0.78	0.51±0.05	12.57±1.47
15104-2	GRC	480-495	17.24	0.73±0.03	20.41±0.97	0.29±0.02	5.69±0.94	0.55±0.04	13.80±1.31
15104-2	GRC	517-532	17.94	0.71±0.04	19.89±1.33	0.31±0.02	6.71±1.01	0.51±0.05	12.59±1.503
15104-2	GRC	575-588	19.01	0.70±0.02	19.54±0.52	0.32±0.01	7.13±0.64	0.59±0.01	14.95±0.29
15104-2	GRC	620-635	19.87	0.76±0.001	21.29±0.01	0.33±0.01	7.56±0.30	0.61±0.012	15.34±0.08
15104-2	GRC	690-704	21.29	0.78±0.03	21.94±0.96	0.33±0.01	8.02±0.29	0.31±0.02	6.58±0.63

SST_{LDI} suggests a LGM to Holocene warming of 13 °C on average, but the maximum amplitude is almost 20 °C between 6.96 kyr BP and the LGM (21.29 kyr BP). The $SST_{U_{37}^{K'}}$ difference between the youngest Holocene and the YD is ca. 14 °C and in good agreement with other $SST_{U_{37}^{K'}}$ records from the Sea of Marmara (Sperling et al., 2003; Ménot and Bard, 2010; Vidal et al., 2010). Our $SST_{U_{37}^{K'}}$ record is closely similar to that of Sperling et al. (2003) for the time interval where both records overlap (YD to modern Holocene). This supports the novel protocol. There is an offset of ca. 2 °C between the two records during the Holocene. Sperling et al. (2003) determined $SST_{U_{37}^{K'}}$ from the total lipid extract without removing coeluting alkenoates, which may explain the offset. The novel MS-based protocol circumvents such potential bias caused by elevated levels of alkenoates. Other potential explanations are the slightly different core locations or differences in instrument performance. It has for example been shown in an interlaboratory study that absolute values can differ by up to 2 °C for exactly the same sample (Rosell-Melé et al., 2001).

The high $SST_{U_{37}^{K'}}$ values during the last glacial are unrealistic and indicate that the transfer function is not valid for the lacustrine setting in the Sea of Marmara during that time. In lacustrine settings, alkenone-producing taxa occur with $U_{37}^{K'}$ – SST relationships

very different from that of *E. huxleyi* (e.g. Versteegh et al., 2001; Zink et al., 2001; Toney et al., 2010). Coccolith analysis shows that *E. huxleyi* was only abundant during the marine phase (0 to 14.7 kyr BP) but not during the lacustrine phase (14.7 to 21 kyr BP), when overall abundance and diversity of coccoliths was low (Aksu et al., 2002). The change in coccolith species coincides with a change in salinity, which was low during the last glacial and increased after the marine connection in the Sea of Marmara was established (e.g. Sperling et al., 2003; Vidal et al., 2010). *E. huxleyi* likely "invaded" the Sea of Marmara after this flooding by Mediterranean water during deglaciation, as also suggested for the Black Sea (Hay et al., 1991). Our $SST_{U^{K'}_{37}}$ record, as well as evidence for hydrological and ecological changes (e.g. Aksu et al., 1999; Aksu et al., 2002; Sperling et al., 2003; Vidal et al., 2010), strongly suggests that SST reconstruction based on alkenones is not suitable for the lacustrine phase in the Sea of Marmara using the current transfer function.

In contrast, SST_{LDI} and $SST_{TEX_{86}}$ are low during the last glacial and, as expected, show warming at the transition to the B/A. Clearly, the ecological and hydrological changes in the Sea of Marmara had less influence on the relationship between temperature and the distributions of *i*GDGTs and long chain diols. This is in agreement with mesocosm incubations of enriched *Thaumarchaeota* under different salinity conditions (Wuchter et al., 2004). In S1, a significant cooling of ca. $5\,^{\circ}C$ occurs in $SST_{TEX_{86}}$. Cooling during sapropel formation based on TEX_{86} has also been reported for Pliocene sapropels from the Black Sea (Menzel et al., 2006). This observation has been explained by a strong contribution from marine Crenarchaeota, thriving at the deeper and colder chemocline. At the time of the sapropel formation in the Sea of Marmara, a similar effect could have led to a change in the distribution of *i*GDGTs. A chemocline could have developed as a result of higher primary productivity and reduced mixing of the water masses, leading to O_2 depletion and bottom water anoxia (e.g. Sperling et al., 2003; Vidal et al., 2010). Therefore, *Thaumarchaeota* could have been driven to a different ecological niche. In modern nutrient-replete nearshore and oceanic upwelling environments, such a cold bias has also been observed (Huguet et al., 2007; Lee et al., 2008; Leider et al., 2010; Wei et al., 2011) and been interpreted as a shift in the depth of GDGT production (Kim et al., 2008; Taylor et al., 2013). However, these interpretations have to be revised since more recent studies showed a bias towards higher TEX_{86} temperature estimates for subsurface waters (Schouten et al., 2012; Basse et al., 2014; Hernández-Sánchez et al., 2014; Xie et al., 2014), which indicates a distinct relationship between *i*GDGT biosynthesis and temperature from subsurface archaea. The influence of physiology and environment on TEX_{86} in cultures of marine planktonic *Thaumarchaeota* has not been systematically studied. The only exception is a study of *Nitrosopumilus maritimus* (Elling et al., 2014), where the *i*GDGT distribution and conversely TEX_{86} changed with growth phase, independent of

temperature. One trigger for the sapropel formation in the Sea of Marmara is enhanced primary productivity due to the inflow of Mediterranean water (Sperling et al., 2003; Vidal et al., 2010), also suggesting increased nutrient influx. Such a change in nutrient availability could have changed the *i*GDGT-temperature relationship (cf. Turich et al., 2007; Elling et al., 2014), but further studies are needed to assess the impact of factors other than temperature influencing *i*GDGT distribution.

The expected warming during the B/A and the cooling during the YD are not reflected in any of the SST records. This has also been observed by others using $U^{K'}_{37}$ in the Sea of Marmara (Sperling et al., 2003; Vidal et al., 2010). Sperling et al. (2003) argued that warmer water originating from the Mediterranean Sea or the incorporation of 'old' alkenones from the preceding B/A interstadial might have distorted the temperature signal. This is in contrast to records from the western (Rodrigo-Gámiz et al., 2014) and eastern Mediterranean Sea (Castañeda et al., 2010), where climate change during the YD and the B/A was documented by the (SS)T proxies. In our case, the limited number of samples at the transitions of the different climatic events might explain why the changes were not observed. The incongruent changes of $SST_{U^{K'}_{37}}$ and SST_{LDI} from the B/A to the termination of S1 further suggest that other environmental factors such as nutrient availability, salinity and O_2 availability affected the proxy temperature relationship for diols and alkenones. For example, beside changes in species composition that can lead to erroneous $U^{K'}_{37}$ temperature reconstructions (see above), culture experiments with different haptophytes revealed the alteration of the alkenone distribution with changing light intensity, cell division rate, salinity and nutrient concentration (Epstein et al., 1998; Versteegh et al., 2001; Prahl et al., 2003; Ono et al., 2012). Accordingly, the environmental changes that occurred in the Sea of Marmara since the last glacial (e.g. Vidal et al., 2010) have potentially impacted the alkenone distribution in addition to changes in temperature. The mechanism behind the correlation between LDI and temperature, the exact biological source and the effect of environmental factors on the LDI needs to be constrained (cf. Rampen et al., 2012), but adaptations in lipid composition to multiple environmental variables can be expected for most organisms (e.g. Hazel and Williams, 1990). The differences in absolute temperature between the three proxies, particularly for the Holocene, might be explained by differences in the growing season of the source species (e.g. Castañeda et al., 2010; Leider et al., 2010; Lopes dos Santos et al., 2013; Rodrigo-Gámiz et al., 2014). However, absolute temperatures have to be interpreted with caution, since the differences could simply be within the uncertainties in the temperature calibrations for the individual proxies. As a complementary approach to the global core-top calibration to convert TEX_{86} to temperature, we used the BAYSPAR calibration model (Supp. Fig. IV.2), which produces meaningful uncertainty estimates (Tierney and Tingley, 2014). We applied the "standard prediction" mode and used the default settings. The SST

estimates based on this calibration showed the same trend as those obtained from the global core-top calibration, but absolute values were consistently lower (between 1.3 and 4 °C). The 90 % uncertainty intervals (Fig. S2, light blue area) extend about 10 °C for a single sample. Considering additionally the standard errors for the calibrations of the other two SST proxies, which do not fully account for uncertainties, it becomes apparent that speculation on absolute temperature differences is problematic.

IV.4. Conclusions

For reconstructing climate and environment, reliable and rapid assessment of past temperature is essential. We have demonstrated a rapid and reliable method for determination of the lipid based $U_{37}^{K'}$, LDI and TEX_{86} temperature proxies within a single NP-HPLC–MS analysis. The method permits the direct analysis of TLEs, saving time-consuming and error-prone clean up procedures. The reduction in analytical processing time is at least one day for eliminating the saponification, derivatization and fractionation steps, whereas the measurement time is reduced to 60 min/sample for all the compounds for the NP-HPLC–APCI-MS method. $U_{37}^{K'}$ values obtained with HPLC–MS and GC-FID as well as LDI values obtained with HPLC–MS and GC–MS were similar and showed almost a 1:1 linear relationship. To monitor the stability of the method and to further assess the validity of a correction function, the use of reference samples is recommended, for $U_{37}^{K'}$ preferably based on pure alkenone standards with known $U_{37}^{K'}$ values. The application of the new method to a sediment core from the Sea of Marmara was in agreement with literature data on lipid based paleo SST proxies from the region. The discrepancies between the SST proxies in the sediment record likely derive from parameters other than temperature affecting the distributions of the relevant lipids. However, the different ecologies of the organisms are poorly understood. In particular, more insight into the physiological responses of the organisms to a changing environment and their effects on the proxies are needed. The proposed NP-HPLC–APCI-MS protocol allows determination of nine paleoenvironmental proxies within a single analysis. Since in most modern organic chemical laboratories HPLC systems are available, the protocol could be established for routinely use as a tool for environmental reconstruction.

Acknowledgements

We thank the crew, chief scientist, M. Zabel, and the scientific shipboard party of the RV Meteor cruise M84/1 (DARCSEAS I). We further thank I.D. Bull for providing alkenone standards, R. Himmelsbach for growing *E. huxleyi*, S. Alfken, C. Vogel and T. Stoltmann for help with sample preparation for lipid analysis and lipid quantification, and F. Schmidt

and M. Elvert for stimulating discussions. We would also like to thank M. A. Lever, H. Røy and B.B. Jørgensen from the Center for Geomicrobiology at Aarhus University, and the crew of Aarhus University's research vessel Tyra, for support in the sampling and processing of Aarhus Bay sediment samples. The study was funded by the European Research Council under the European Union's Seventh Framework Programme - "Ideas" Specific Programme, ERC grant agreement No. 247153 (Advanced Grant DARCLIFE; PI K.-U.H.) and by the Deutsche Forschungsgemeinschaft (DFG, Germany) through grants Inst 144/300-1 (LC-qToF system), VE486/3 (GJMV). Further support was given by the Bremen International Graduate School for Marine Sciences (GLOMAR) funded by the DFG through MARUM Center for Marine Environmental Sciences. We thank J.E. Tierney and an anonymous reviewer for constructive comments and suggestions.

IV.5. Supporting Information

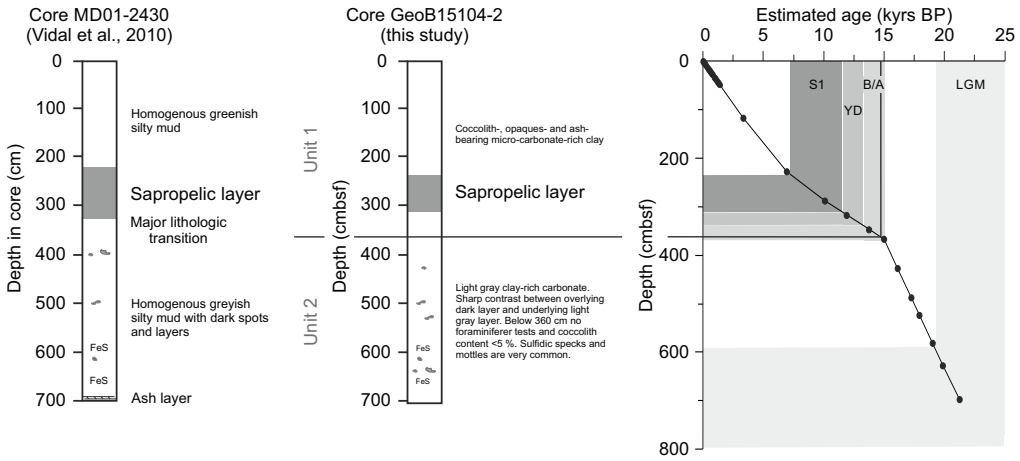

Supplementary Figure IV.1 Lithological description and the age-depth relationship for core GeoB15104-2. The age model is based on sedimentation rates according to Vidal et al. (2010). Matching lithology and interfaces were adjusted. Shaded areas correspond to sapropel (S1, dark gray), the Younger Dryas (YD) (medium/dark gray), the Bølling/Allerød (B/A) (medium gray) and the last glacial maximum (LGM) (light gray). For comparison, core MD01-2430 from (Vidal et al., 2010) is shown.

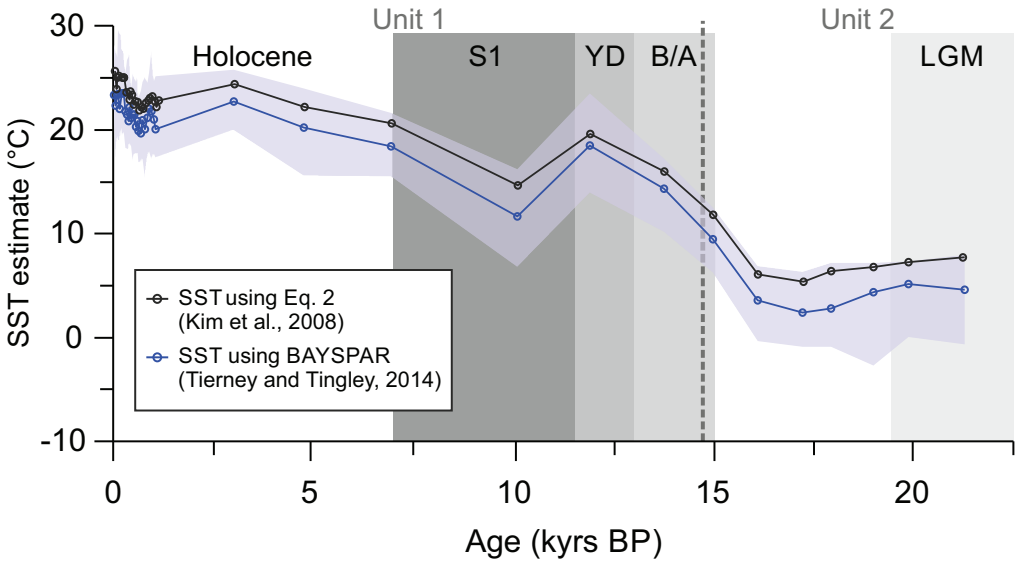

Supplementary Figure IV.2 Comparison of SST estimates for the Sea of Marmara based on archaeal *i*GDGTs determined from NP-HPLC–APCI-MS using the global core-top calibration from (Kim et al., 2008) and the BAYSPAR calibration Tierney and Tingley (2014). The light blue area indicates the 90 % uncertainty interval. The timing of the Younger Dryas (YD), Bølling/Allerød (B/A), Sapropel S1 (S1), Last Glacial Maximum (LGM), Holocene and marine (Unit 1) and lacustrine (Unit 2) units are denoted.

Supplementary Table IV.1 Concentrations from triplicate analysis of individual *i*GDGTs (ng sed. dw), and total concentration of this compound group (µg sed. dw). Stars indicate average concentration and deviation for n = 2.

Core (GeoB)	Depth interval (cmbsf)	Estimated age (kyr BP)	*i*GDGT-0	*i*GDGT-1	*i*GDGT-2	*i*GDGT-3	*i*GDGT-4	*i*GDGT-5	*i*GDGT-5'	Total *i*GDGTs
15104-1	0-2	0.01	613.12±17.94	150.704±27.701	181.44±19.64	20.69±6.54	22.21±1.79	1262.97±19.82	82.53±23.52	2.33±0.02
15104-1	2-4	0.05	328.47±32.83*	86.699±4.16	95.08±6.44	11.98±0.8	11.04±0.98	389.25±65.19*	36.56±0.904	0.96±0.02*
15104-1	4-6	0.09	477.79±80.79	132.54±34.06	151.89±41.82	18.77±7.28	20.44±0.06	1060.42±79.34	69.04±18.74	1.93±0.04
15104-1	6-8	0.12	509.77±3.38	131.23±32.96	149.302±30.15	20.604±4.43	17.25±3.51	1076.09±32.33	67.46±11.98	1.97±0.02
15104-1	8-10	0.16	634.49±47.56	165.59±39.47	184.22±44.6	24.99±7.51	22.03±5.11	1305.91±32.196	89.95±19.58	2.43±0.03
15104-1	10-12	0.2	513.45±2.61	178.21±116.69	192.84±131.19	26.799±19.02	27.91±10.99	990.46±15.84	93.89±58.26	2.02±0.05
15104-1	12-14	0.23	538.52±6.603	135.18±32.602	149.84±32.94	21.03±4.76	17.23±5.56	1046.64±72.43	75.04±14.86	1.98±0.02
15104-1	14-16	0.27	572.403±10.93	141.62±25.66	151.35±29.07	21.55±4.97	19.56±1.27	1215.47±184.86	75.94±9.93	2.198±0.04
15104-1	16-18	0.31	654.05±5.89	158.796±47.34	161.27±52.38	23.598±8.19	18.19±5.85	1218.99±91.11	72.301±16.89	2.31±0.03
15104-1	18-20	0.34	870.56±110.87	177.84±17.21	170.41±8.56	26.81±2.24	27.18±8.13	1592.79±136.44	80.98±8.08	2.95±0.04
15104-1	20-22	0.38	777.56±53.16	178.18±30.57	169.199±34.21	24.75±6.86	22.65±5.395	1448.86±45.12	80.02±12.28	2.701±0.03
15104-1	22-24	0.41	758.59±43.82	168.53±29.88	163.87±32.42	25.33±6.36	26.16±3.39	1525.26±54.33	84.68±15.57	2.75±0.03
15104-1	24-26	0.45	756.07±15.897	176.95±37.204	173.86±37.43	24.62±8.03	28.56±3.03	1404.04±47.97	83.55±20.25	2.65±0.02
15104-1	26-28	0.49	711.38±83.22	258.75±214.28	236.73±187.36	34.17±28.81	20.34±4.802	1222.98±24.95	103.02±74.05	2.59±0.09
15104-1	28-30	0.52	727.66±40.19	167.55±35.91	154.92±24.66	22.43±6.42	19.11±1.29	1360.64±63.102	74.71±13.01	2.53±0.03
15104-1	30-32	0.56	754.27±72.84	180.56±34.77	161.73±28.29	24.29±5.65	21.65±4.35	1331.11±91.15	79.35±16.28	2.55±0.04
15104-1	32-34	0.6	735.34±39.67	180.73±35.27	164.99±27.64	25.62±7.66	23.23±3.64	1418.41±45.099	81.403±14.53	2.63±0.02
15104-1	34-36	0.63	326.21±27.65*	95.39±1.36	86.16±0.25	13.74±2.06	11.91±3.78	381.04±31.89*	35.49±7.28	0.95±0.01*
15104-1	36-38	0.69	659.38±13.93	158.79±36.74	143.902±32.01	21.48±7.36	18.83±4.06	1192.48±2.66	65.74±15.39	2.26±0.02
15104-1	38-40	0.74	636.003±32.03	146.84±36.92	128.38±31.82	20.01±7.06	16.404±3.59	1113.05±123.09	62.28±15.96	2.12±0.04
15104-1	40-42	0.79	562.28±8.86	136.88±40.37	121.32±38.95	21.14±7.803	18.801±3.36	1090.81±16.15	62.495±16.41	2.01±0.02
15104-1	42-44	0.85	539.96±34.902	128.17±24.22	116.47±22.59	19.59±5.59	16.62±0.97	1067.38±97.89	60.05±16.47	1.95±0.03
15104-1	44-46	0.9	495.38±8.59	112.28±27.36	102.599±15.83	16.71±3.88	17.22±2.65	944.37±54.24	53.37±12.73	1.74±0.02
15104-1	46-48	0.96	406.18±10.51	91.33±22.24	88.23±21.47	14.66±3.96	14.301±4.57	745.97±23.26	40.38±8.43	1.4±0.01
15104-1	48-50	1.01	474.23±68.58	120.62±50.73	111.33±48.2	17.65±7.87	15.87±1.65	915.26±200.202	54.11±19.91	1.71±0.06
15104-1	50-52	1.06	504.09±77.42	130.96±43.34	112.83±32.29	17.73±6.88	15.28±2.51	921.45±184.37	57.67±10.54	1.76±0.05
15104-2	116-130	3.01	353.498±56.67	72.01±13.35	65.12±12.03	10.72±2.49	12.09±2.51	660.25±265.71	33.595±6.27	1.21±0.05
15104-2	180-196	4.76	950.35±174.43	204.39±54.66	217.87±56.28	30.65±11.5	27.17±2.25	1769.74±332.98	102.2±24.13	3.302±0.09*
15104-2	222-236	6.95	386.87±233.28	123.08±16.98	108.64±6.17	17.59±1.12	16.25±1.38	411.26±410.39	43.63±3.53	1.11±0.096
15104-2	280-296	10.1	2117.08±321.14*	329.97±31.14	270.92±38.52	32.08±3.62	43.61±2.73	3157.58±484.88*	125.9±10.32	6.08±0.13*
15104-2	310-325	11.91	3699.37±262.38	391.65±320.55	233.71±187.82	40.54±31.25	70.32±2.34	4089.87±483.37	55.71±38.86	8.58±0.19
15104-2	340-355	13.76	1352.301±342.57	190.98±38.06	178.98±21.72	15.09±3.31	19.301±4.07	2022.799±506.04	34.02±2.28	3.81±0.13
15104-2	360-375	14.99	2417.07±297.63*	253.76±30.65	182.36±21.82	23.22±2.75	34.46±12.35	2865.84±236.68*	30.35±2.78	5.81±0.09*
15104-2	420-435	16.12	163.68±393.11	59.702±0.99	31.33±3.53	3.87±0.78	5.55±0.13	234.24±366.09	2.69±0.99	0.501±0.11
15104-2	480-495	17.24	636.49±413.13	160.62±74.33	54.01±27.61	10.12±5.38	21.58±13.16	1391.87±827.698	7.57±3.09	2.28±0.19
15104-2	517-532	17.94	734.601±472.74	179.25±103.75	53.999±27.39	9.83±4.99	20.197±9.91	1432.12±759.23	8.44±3.56	2.44±0.197
15104-2	575-588	19.01	562.33±354.904	139.92±69.41	45.53±20.98	8.71±4.02	24.01±18.801	1154.72±673.44	7.46±1.23	1.94±0.16
15104-2	620-635	19.87	676.59±401.26*	186.26±79.39	67.14±28.93	11.41±4.62	19.45±12.42	1320.03±864.16*	8.27±3.39	2.29±0.199*
15104-2	690-704	21.29	164.16±319.67	44.19±14.27	16.37±3.82	2.73±0.33	4.88±1.03	204.43±598.51	1.99±1.03	0.44±0.13

Supplementary Table IV.2 Concentrations from triplicate analysis of individual long chain alkenones and long chain diols (ng sed. dw), and total concentration of each compound group (µg sed. dw). Stars indicate average concentration and deviation for n = 2.

Core (GeoB)	Depth interval (cmbsf)	Estimated age (kyr BP)	$C_{37:2}$ alkenone	$C_{37:3}$ alkenone	C_{30} 1,15-diol	C_{30} 1,13-diol	C_{28} 1,13-diol	Total alkenones	Total diols
15104-1	0-2	0.01	868.11±91.32	539.57±57.95	18.41±0.92	1.3±0.25	1.76±1.13	1.41±0.07	0.021±0.001
15104-1	2-4	0.05	1525.29±97.47	689.71±83.46	29.14±12.52	1.88±0.47	1.45±0.42	2.22±0.09	0.032±0.004
15104-1	4-6	0.09	564.66±235.08	260.61±142.41	23.01±5.87	1.41±0.39	1.67±0.79	0.83±0.19	0.026±0.002
15104-1	6-8	0.12	713.45±278.53	350.53±78.32	17.01±2.17	1.28±0.29	1.05±0.803	1.06±0.18	0.019±0.001
15104-1	8-10	0.16	883.12±176.03	453.46±84.01	24.43±5.28	1.39±0.39	1.49±0.91	1.34±0.13	0.027±0.002
15104-1	10-12	0.2	980.38±264.26	478.83±190.398	25.75±8.74	1.5±0.43	1.22±0.702	1.46±0.23	0.028±0.003
15104-1	12-14	0.23	524.98±33.49	275.02±16.505	17.19±3.698	1.01±0.35	0.99±0.65	0.8±0.02	0.019±0.002
15104-1	14-16	0.27	458.85±101.196	215.04±50.76	15.85±3.94	1.3±0.27	0.59±0.21	0.67±0.08	0.018±0.001
15104-1	16-18	0.31	252.98±94.83	124.92±53.49	20.21±5.76	1.05±0.13	0.54±0.29	0.38±0.07	0.022±0.002
15104-1	18-20	0.34	264.23±36.06	127.37±1.46	17.35±4.18	1.4±0.62	0.44±0.27	0.39±0.02	0.019±0.002
15104-1	20-22	0.38	179.68±72.43	89.32±27.61	19.52±2.398	1.25±0.26	0.57±0.25	0.27±0.05	0.021±0.001
15104-1	22-24	0.41	189.01±32.99	93.02±20.08	26.87±2.68	1.67±0.14	0.698±0.22	0.28±0.03	0.029±0.001
15104-1	24-26	0.45	230.05±59.36	98.56±32.104	18.54±5.34	1.16±0.32	0.54±0.33	0.33±0.05	0.02±0.002
15104-1	26-28	0.49	370.68±296.88	168.47±138.04	43.55±28.73	2.42±0.68	1.17±0.67	0.54±0.22	0.047±0.01
15104-1	28-30	0.52	220.598±42.51	89.87±16.16	18.197±5.23	1.44±0.62	0.67±0.43	0.31±0.03	0.02±0.002
15104-1	30-32	0.56	228.09±59.62	84.09±23.51	19.36±3.76	1.43±0.21	0.62±0.31	0.31±0.04	0.021±0.001
15104-1	32-34	0.6	284.11±42.55	111.203±17.29	22.58±8.695	1.53±0.54	0.75±0.61	0.395±0.03	0.025±0.003
15104-1	34-36	0.63	436.79±114.001	169.91±66.81	26.84±10.204	2.04±0.82	1.13±0.27	0.61±0.09	0.03±0.004
15104-1	36-38	0.69	241.996±45.92	103.88±24.53	23.25±4.802	1.31±0.42	0.62±0.44	0.34±0.04	0.025±0.002
15104-1	38-40	0.74	219.902±65.96	94.57±31.89	17.196±2.19	1.15±0.05	0.56±0.16	0.31±0.05	0.019±0.001
15104-1	40-42	0.79	257.38±52.03	104.15±17.5	17.702±4.75	1.42±0.26	0.78±0.27	0.36±0.03	0.02±0.002
15104-1	42-44	0.85	261.42±52.45	107.13±25.43	22.27±8.71	1.76±0.78	0.89±0.48	0.37±0.04	0.025±0.003
15104-1	44-46	0.9	214.02±51.09	91.96±20.896	16.43±3.76	1.32±0.51	0.56±0.28	0.31±0.04	0.018±0.002
15104-1	46-48	0.96	255.44±44.95	110.68±16.91	17.92±4.85	1.15±0.57	0.699±0.39	0.37±0.03	0.02±0.002
15104-1	48-50	1.01	231.34±122.61	105.92±35.32	21.53±4.44	1.503±0.36	0.69±0.43	0.34±0.08	0.024±0.002
15104-1	50-52	1.06	326.297±64.36	134.99±30.23	16.93±4.99	1.23±0.29	0.803±0.25	0.46±0.05	0.019±0.002
15104-2	116-130	3.01	135.77±72.59	77.99±25.18	18.46±5.95	1.02±0.45	0.48±0.25	0.21±0.05	0.02±0.002
15104-2	180-196	4.76	260.103±129.94	136.14±70.65	37.45±3.995	1.897±0.32	0.82±0.21	0.396±0.103	0.04±0.002
15104-2	222-236	6.95	575.98±220.502	217.57±101.84	35.27±19.67	1.23±0.19	0.61±0.28	0.79±0.16	0.037±0.007
15104-2	280-296	10.1	324.51±26.097	97.23±20.48	78.63±16.56	2.68±0.78	1.303±0.46	0.42±0.02	0.083±0.006
15104-2	310-325	11.91	202.24±157.37	236.44±188.19	349.7±279.65	10.803±8.89	4.59±3.13	0.44±0.17	0.365±0.097
15104-2	340-355	13.76	169.74±71.03	261.07±100.36	136.86±51.53	11.26±3.76	1.61±0.62	0.43±0.09	0.15±0.019
15104-2	360-375	14.99	1071.91±43.01	3379.84±0.04	178.32±90.36	16.397±6.04	3.49±1.95	4.45±0.02	0.198±0.033
15104-2	420-435	16.12	106.16±32.63	172.78±70.46	14.32±9.61	2.31±1.41	3.88±1.98	0.28±0.05	0.021±0.004
15104-2	480-495	17.24	29.28±11.52	18.81±10.01	12.28±8.98	9.58±5.61	1.31±0.64	0.05±0.01	0.023±0.005
15104-2	517-532	17.94	34.24±24.84	12.61±8.52	19.12±15.33	13.03±9.85	1.97±1.27	0.05±0.02	0.034±0.009
15104-2	575-588	19.01	34.86±19.25	15.02±10.38	18.47±16.82	14.88±13.38	2.28±1.49	0.05±0.01	0.036±0.011
15104-2	620-635	19.87	45.98±15.43	20.21±8.44	27.2±12.62	15.54±6.79	3.46±2.06	0.07±0.01	0.046±0.007
15104-2	690-704	21.29	22.11±8.87	7.09±2.83	9.09±4.896	8.12±4.28	2.55±0.99	0.03±0.01	0.02±0.003

Chapter V

Identification, formation and distribution of fatty acid-substituted glycerol dialkyl glycerol tetraethers in marine sediments

Kevin W. Becker*, Felix J. Elling, Julius S. Lipp, Jan M. Schröder, Thomas W. Evans, Marcus Elvert, Martin Könneke and Kai-Uwe Hinrichs

In preparation for *Organic Geochemistry*

Organic Geochemistry Group, MARUM - Center for Marine Environmental Sciences & Department of Geosciences, University of Bremen, 28359 Bremen, Germany

*Corresponding author. E-mail: k.becker@uni-bremen.de

Abstract

Archaeal isoprenoid glycerol dialkyl glycerol tetraethers (*i*GDGTs) are abundant components of marine sedimentary organic matter and are used in paleoenvironmental reconstructions. During diagenesis, a significant fraction of free *i*GDGTs can be incorporated into macromolecules. However, the diagenetic reaction mechanisms involving *i*GDGTs remain unresolved. We identified a potential macromolecule precursor, fatty acid-substituted *i*GDGTs (FA-*i*GDGTs), in a globally distributed set of sediment samples and the archaeal culture *Nitrosopumilus maritimus* by high performance liquid chromatography–tandem mass spectrometry (HPLC–MS^2). Instead of a biosynthetic origin, a diagenetic origin of these compounds is proposed. First, a stable isotope probing experiment with *N. maritimus* did not reveal label uptake into the fatty acids and second, FA-*i*GDGTs in environmental samples appear to be in chemical equilibrium with *i*GDGTs. Moreover, the fatty acids connected to FA-*i*GDGTs are similar to the free fatty acids found in the investigated sediments. FA-*i*GDGTs are likely produced by esterification of free fatty acids and *i*GDGTs in sediments during early diagenesis and their formation seems to be dependent on reactant availability, hydrolytic conditions and water activity.

V.1. Introduction

Archaea occupy a wide range of environments and are particularly abundant in the marine water column and sediments (Lipp et al., 2008; Stahl and de la Torre, 2012). The lipid membranes of archaea are exclusively composed of isoprenoid hydrocarbons ether bound to one or two a glycerol moieties (Pearson, 2014). The most commonly observed archaeal membrane lipids in cultures and environmental samples are bilayer-forming diphytanyl glycerol diethers (archaeols) and membrane spanning isoprenoid glycerol dibiphytanyl glycerol tetraethers (*i*GDGTs; Pearson (2014). In contrast, the bilayer-forming lipids of bacteria and eukaryotes consist of a glycerol moiety linked to linear or branched hydrophobic fatty acids via ester or ether bonds (Koga, 2011). Beside these structural differences, archaea are distinct from bacteria and eukaryotes in the stereochemistry of the glycerol backbone. Whereas archaea utilize 2,3-*sn*-glycerol, bacteria and eukaryotes synthesize lipids with 1,2-*sn*-glycerol backbones (Koga, 2011). Thus, membrane lipids are among the most distinct chemotaxonomic markers for archaea. However, some studies reported straight chain fatty acids as well as phospholipid-derived fatty acids in archaea (Kates et al., 1968; Langworthy et al., 1974; Tornabene et al., 1979; Jones and Holzer, 1991; Carballeira et al., 1997; Nishihara et al., 2000; Gattinger et al., 2002). Additionally, homologs of enzymes involved in bacterial FA biosynthesis are found in most sequenced archaeal genomes (Peretó et al., 2004; Iverson et al., 2012) and have been interpreted as evidence for the existence of a fatty acid biosynthesis pathway in the cenancestor (Lombard et al., 2012). Therefore, the biosynthesis of fatty acids in archaea would have importance for current concepts of early evolution (Koga et al., 1998; Lombard et al., 2012; Sojo et al., 2014). However, the lack of acyl carrier protein homologs in archaea, cofactors that are responsible for binding all fatty acid intermediates during biosynthesis in bacteria and eukaryotes, implies that archaea might either not be able to synthesize fatty acids without this critical cofactor or possess a biosynthetic machinery that was already present in the cenancestor (Lombard et al., 2012). Moreover, unambiguous experimental evidence for the biosynthesis of fatty acids or ester-linked lipids in archaea is still lacking. In contrast, archaeal *i*GDGT membrane lipids occur ubiquitously in both marine and terrestrial environments (Schouten et al., 2000, 2002; Weijers et al., 2007; Lipp et al., 2008; Liu et al., 2012c). Their distribution, abundance and isotopic composition provide insights into the microbial ecology and biogeochemistry of archaea in natural ecosystems (e.g. Biddle et al., 2006; Ingalls et al., 2006; Schubotz et al., 2009, 2011). In the marine environment, *i*GDGTs are predominantly derived from planktonic and benthic archaea and can be preserved in the sediment record over geological timescales (Kuypers et al., 2001; Carrillo-Hernandez et al., 2003, e.g.). Analysis of these compounds is routinely applied to environmental samples for the

reconstruction of paleoenvironmental conditions, e.g. past sea surface temperature (SST) using the TEX_{86} proxy (Schouten et al., 2002). While *i*GDGTs are degraded in mature sediments (e.g. Michaelis and Albrecht, 1979), their diagenetic fate in the immature sediments commonly investigated in paleoclimatology, is less constrained (cf. Schouten et al., 2004; Pancost et al., 2008; Schouten et al., 2013a). Identifying diagenetic processes transforming the size and composition of the sedimentary *i*GDGT pool is imperative for accurately quantifying the microbial contribution to fossil organic matter (Kuypers et al., 2002, e.g.) and for the interpretation of *i*GDGT-based proxies (e.g. Huguet et al., 2008). In this study, we present the identification of novel compounds that combine characteristics of archaeal (ether bound isoprenoid side chains) and bacterial (ester bound fatty acids) membrane lipids. These lipids were detected in abundance in sediments from two deep-sea hypersaline anoxic basins, the Benguela upwelling region, and the southern Black Sea.

V.2. Methods

V.2.1. Cultivation

N. maritimus strain SCM1 was grown aerobically at 28 °C in 15-batch cultures in pH 7.5 HEPES-buffered Synthetic Crenarchaeota Medium amended with 1 mM NH_4Cl and 10 % ^{13}C-$NaHCO_3$ as described previously (Könneke et al., 2005; Martens-Habbena et al., 2009; Elling et al., 2014). Biomass was harvested in early stationary phase using cross-flow filtration and centrifugation.

V.2.2. Sample collection and extraction

Water column and sediment samples were collected using *in situ* pumps, a multicorer and a gravity corer during RV Meteor cruise M84/1 ("DARCSEAS I", Zabel and Cruise Participants, 2013) from the hypersaline anoxic Discovery Basin located in the Eastern Mediterranean Sea (Site GeoB15102, 35°16.43'N 21°41.50'E, 3615 m water depth) and the southern Black Sea (Site GeoB15105, 41°31.70'N 30°53.09'E, 1227 m water depth). Sediment samples from the hypersaline anoxic Orca Basin in the northern Gulf of Mexico were retrieved using a multicorer during RV Atlantis cruise AT18-2 (27°0'N 91°16.9'W, 2340 m water depth at). Sediment samples from the Benguela upwelling region were collected during RV Meteor cruise M76/1 (Zabel et al., 2008) using a multicorer and a gravity corer at sites GeoB12802 (25° 30'N 13° 27'E, 795 m water depth), GeoB12808 (26° 22.18'N 11° 53.50'E, 3794 m), GeoB12810 (24° 03.19'N 14° 15.69'E, 121 m) and GeoB12811 (26° 0.62' 12°N 34.39'E, 2975 m). Homogenized sediment samples were spiked with an internal standard (C_{46}-GTGT, Huguet et al., 2006) and ultrasonically extracted using

a modified Bligh and Dyer protocol with trichloroacetic acid buffer (cf. Sturt et al., 2004). In order to exclude the artificial production of fatty acid-substituted *i*GDGTs (FA-*i*GDGTs) by a trichloroacetic acid-catalyzed or methanol-induced esterification (Arpino and Ourisson, 1971), additional extraction protocols omitting the use of buffer solutions and methanol were tested (DCM:MeOH, 3:1, v:v; and pure DCM). Moreover, aliquots of the TLE were hydrolyzed using $50\,\%$ trifluoroacetic acid at 70 °C for 8 hours to induce the artificial production of fatty acid-substituted *i*GDGTs in environmental samples (Lin et al., 2010).

V.2.3. Analytical methodology for HPLC–APCI-MS

Compounds were analyzed on a Dionex Ultimate 3000RS UHPLC coupled to a Bruker maXis Ultra-High Resolution quadrupole time-of-flight mass spectrometer (qToF-MS), equipped with an APCI-II ion source using the same protocol as described by Becker et al. (2013). Briefly, TLE aliquots were dissolved in ßtextitn-hexane:2-propanol (99.5:0.5, v:v) and injected onto two coupled Acquity BEH Amide columns (2.1 x 150 mm, $1.7\,\mu m$ particle size, Waters, Eschborn, Germany) maintained at $50\,°C$. Lipids were eluted using a linear gradient of n-hexane (eluent A) to n-hexane:2-propanol (90:10, v:v; eluent B) at a flow rate of $0.5\,ml\,min^{-1}$. The initial gradient was $3\,\%$ B to $5\,\%$ B in 2 min, followed by increasing B to $10\,\%$ in 8 min, to $20\,\%$ in 10 min, to $50\,\%$ in 15 min and $100\,\%$ in 10 min, followed by 6 min at $100\,\%$ B to flush and 9 min at $3\,\%$ B to re-equilibrate the columns. FA-*i*GDGTs were identified by their exact mass measured in full scan mode (MS^1) and their characteristic fragmentation in MS^2 mode. The mass spectrometer was set to a resolution of 27,000 at *m/z* 1222.2 and exact mass calibration was performed by loop injections of calibrant solution (Agilent TuneMix) at the end of each run and the use of a lock mass, leading to mass accuracy typically <1-2 ppm (see Becker et al., 2013, for detailed parameters). The TLE of N. maritimus biomass was hydrolyzed with 1 M HCl in methanol for 3 h at $70\,°C$ to yield core lipids before analysis (Elling et al., 2014).

V.2.4. Semi-preparative LC

FA-*i*GDGTs were isolated from the TLE through reverse phase semi-preparative LC on an Agilent 1200 series HPLC equipped with and active splitter, Agilent 6130 single-quad MSD and fraction collector. We used the same column and gradient system as described in Zhu et al. (2013b) for archaeal intact lipid isolation. In brief, the TLE was subjected to a semi-preparative Zorbax Eclipse XDB-C_{18} column ($5\,\mu m$, 250 × 9.4 mm; Agilent Technologies Deutschland GmbH, Böblingen, Germany) operated at $45\,°C$. Samples were dissolved in MeOH:2-propanol (8:2, v:v) and eluted using a linear gradient from $80\,\%$ MeOH:$20\,\%$ 2-propanol to $60\,\%$ MeOH:$40\,\%$ 2-propanol in 5 min and then to $35\,\%$

MeOH:65 % 2-propanol in another 40 min at a flow-rate of $2.2\,\mathrm{ml\,min^{-1}}$. The column was washed with 100 % 2-propanol for 15 min followed by column re-conditioning with Zhu et al. (2013b) MeOH for another 15 min. FA-*i*GDGTs were collected in the time window of 60 to 66 min.

V.2.5. Fatty acid analysis

Fatty acids were released from *i*GDGTs by base hydrolysis according to the method described by Elvert et al. (2003). In brief, an aliquot of the polar fraction was dissolved in 2 mL of methanolic KOH (6 %KOH in MeOH, w:v) and the reaction took place for 3 h at $80\,^{\circ}\mathrm{C}$. After cooling down to room temperature, 2 mL of a 0.05M KCl solution were added and alcohols were extracted three times with 2 mL n-hexane. The pH value was adjusted to pH 1 with 25 % HCl and fatty acids were extracted three times with 2 mL *n*-hexane. After drying under a nitrogen stream, the reaction products were stored at $-20\,^{\circ}\mathrm{C}$ until derivatization and analysis.

Fatty acids were identified by coupled gas chromatography-mass spectrometry using an Agilent 5973 inert MSD system after derivatization with bis(trimethylsilyl)-trifluoroacetamide in pyridine at $60\,^{\circ}\mathrm{C}$ for 1 hour (Elvert et al., 2003). The mass spectrometer was operated in electron impact mode at 70 eV with a full scan mass range of *m/z* 40-700. Analyte separation was achieved on an Rxi-5ms column (30m × 0.25 mm × $0.25\,\mu\mathrm{m}$; Restek GmbH, Bad Homburg, Germany) using an oven temperature program of $60\,^{\circ}\mathrm{C}$ (held 1 min) to $150\,^{\circ}\mathrm{C}$ at $10\,^{\circ}\mathrm{C\,min^{-1}}$ and then to $310\,^{\circ}\mathrm{C}$ (held 20 min) at $45\,^{\circ}\mathrm{C\,min^{-1}}$.

V.2.6. Stable carbon isotope analysis of lipids

Stable carbon isotopic compositions of lipids were determined using a GC–isotope ratio-MS system (Trace GC Ultra coupled to a GC-IsoLink, ConFlow IV interface and a DeltaV Plus isotope ratio mass spectrometer, all from Thermo Scientific GmbH). GC conditions were the same as utilized for the GC–MS. Compounds were oxidized in a combustion interface at $90\,^{\circ}\mathrm{C}$. Stable carbon isotopic compositions are expressed as $\delta^{13}\mathrm{C}$ values in the per mil (‰) notation relative to VPDB standards. The analytical error was $<0.5\,\mathrm{permil}$ for non-labeled $\delta^{13}\mathrm{C}$ values, respectively.

V.3. Results and discussion

V.3.1. Detection of fatty acid substituted *i*GDGTs and identification via MS^2

In HPLC–APCI-MS analysis of diverse sediment samples, a group of novel compounds was detected. They eluted between 9 and 11 min in the HPLC chromatogram with a

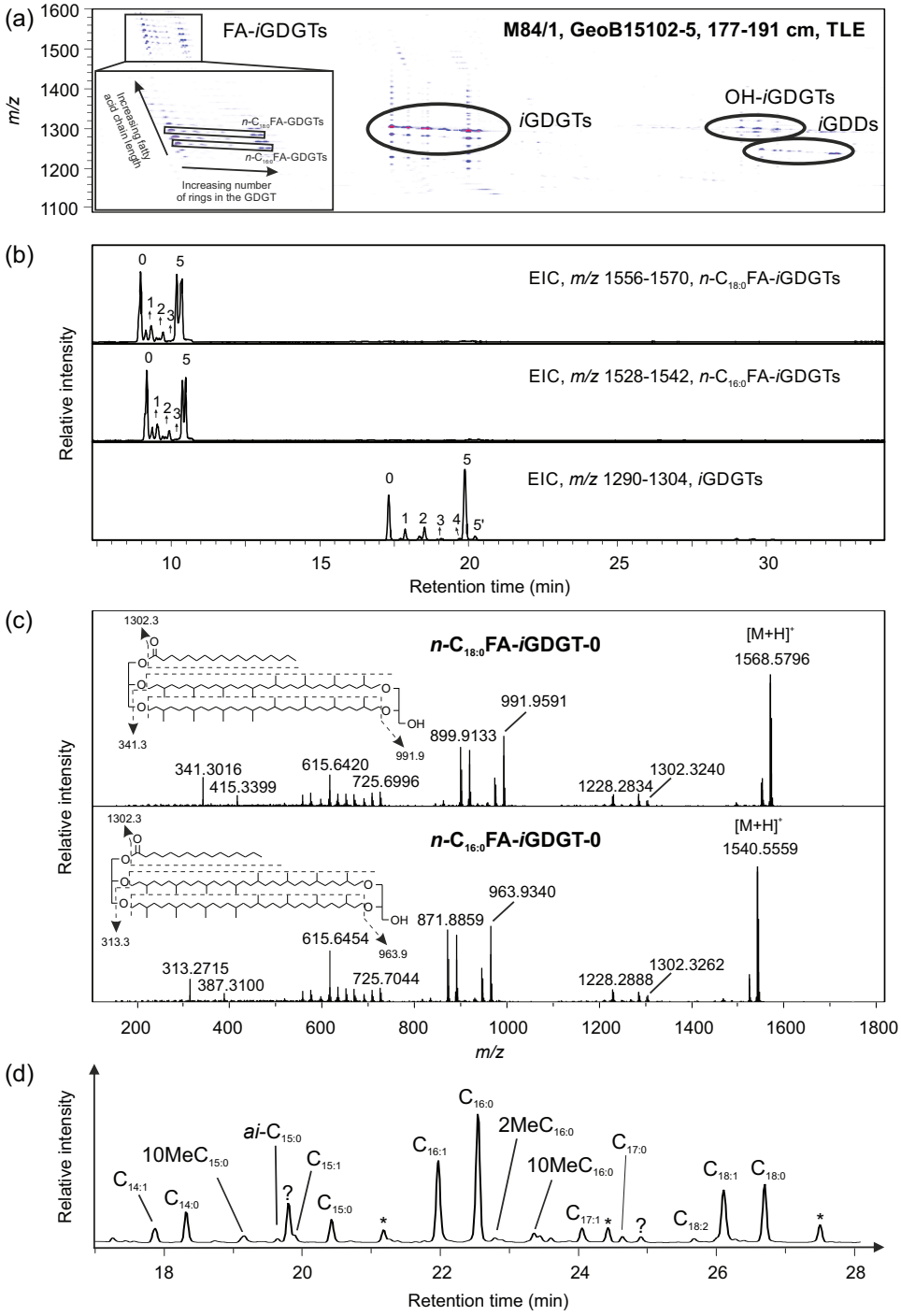

Figure V.1. (a) Density map plot showing the major diagnostic ions of archaeal ether lipids and FA-*i*GDGTs in the sample M84/1 GeoB15102-5, 177-191 cmbsf analyzed by HPLC–APCI-qToF-MS. The enlarged area shows the detailed elution order of FA-*i*GDGT. (b) HPLC–APCI-qToF-MS chromatogram shown as extracted ion chromatogram (EIC), illustrating *i*GDGTs (bottom chromatogram) and *n*-$C_{18:0}$ and *n*-$C_{16:0}$FA-*i*GDGTs in the TLE of sample M84/1 GeoB15102-5, 177-191 cmbsf. (c) HPLC–APCI-MS^2 spectrum of *n*-$C_{18:0}$FA-*i*GDGT-0 and *n*-$C_{16:0}$FA-*i*GDGT-0 in the same sample. Shown are the MS^2 fragment ions of the two compounds ($[M+H]^+$ ion of *m/z* 1568.6 and $[M+H]^+$ ion of *m/z* 1540.6) in the range *m/z* 100–1800. The structure of *n*-$C_{18:0}$FA-*i*GDGT-0 and the formation of the major fragments are also shown. (d) GC–MS total ion chromatogram of fatty acids released by saponification from isolated FA-*i*GDGTs. Stars indicate contamination peaks (polysiloxanes).

molecular mass ranging from *m/z* 1450-1650. The compounds appear as several nested series differing by 14 Da and 2 Da in the density map and chromatogram (Figure V.1a and b). The exact masses and the characteristic fragmentation behavior suggest that these compounds represent *i*GDGT molecules with additional fatty acids substituted at the s*n*-1 position of the glycerol (Figure V.1c). The MS^2 spectra of the protonated molecule ($[M+H]^+$) at *m/z* 1568.58 showed a major fragment at *m/z* 1302.32, which represents an *i*GDGT-0 molecule after the loss of a $C_{18:0}$ fatty acid. Another major cluster of fragment ions was observed between *m/z* 557 and 725, corresponding to the typical *i*GDGT fragmentation pattern (Knappy et al., 2009; Liu et al., 2012b). The fragment ions between *m/z* 863 and 1009 result from the loss of one biphytane, several losses of water and a glycerol based $C_3H_6O_2$ unit from the original molecule. The most abundant fragment ion at *m/z* 991.96 represents a combined loss of one biphytane and one water molecule, whereas the fragment ion at *m/z* 341.30 results from the loss of the two biphytanyl moieties including one glycerol unit, and a water molecule from the second glycerol. The MS^2 spectrum of the protonated molecule $[M+H]^+$ at *m/z* 1540.56 showed the same fragmentation behavior as the above described molecule. We also observed the typical fragment ions of a *i*GDGT-0 molecule, but the fragment ions after the loss of one and two biphytanes showed 28 Da lower masses than the fragment ions of the molecule $[M+H]^+$ at *m/z* 1568.58 (see Figure V.1c). This indicates that the difference in the structure between these two molecules is two methyl units in the fatty acid chain. Saponification further confirmed the structure of these compounds, since *i*GDGTs and free fatty acid were detected as reaction products (Figure V.1d). Therefore, the compounds were tentatively identified as fatty acid-substituted *i*GDGTs. The artificial production of FA-*i*GDGTs during extraction could be excluded since these compounds were detected in similar amounts for all applied extraction methods.

V.3.2. Stable isotope probing experiment with *N. maritimus*

To examine a potential biological origin of FA-*i*GDGTs, we analyzed the lipid composition of the thaumarchaeon *N. maritimus* and indeed, trace amounts of FA-*i*GDGTs were detected in the acid hydrolyzed TLE (Figure V.2a, b). FA-bearing membrane lipids are not known to occur in archaea even though there are a few studies reporting FAs in some archaea. For example, Carballeira et al. (1997) and Gattinger et al. (2002) detected phospholipid-derived FAs in several euryarchaeotal strains. In these studies, contamination from the medium was excluded as FAs were either not detected in the medium or the FA composition in biomass and medium differed significantly. Nevertheless, these findings only provide indirect evidence and contamination from other sources, such as other organisms, cannot be excluded. For instance, it has been shown that cyanobacterial

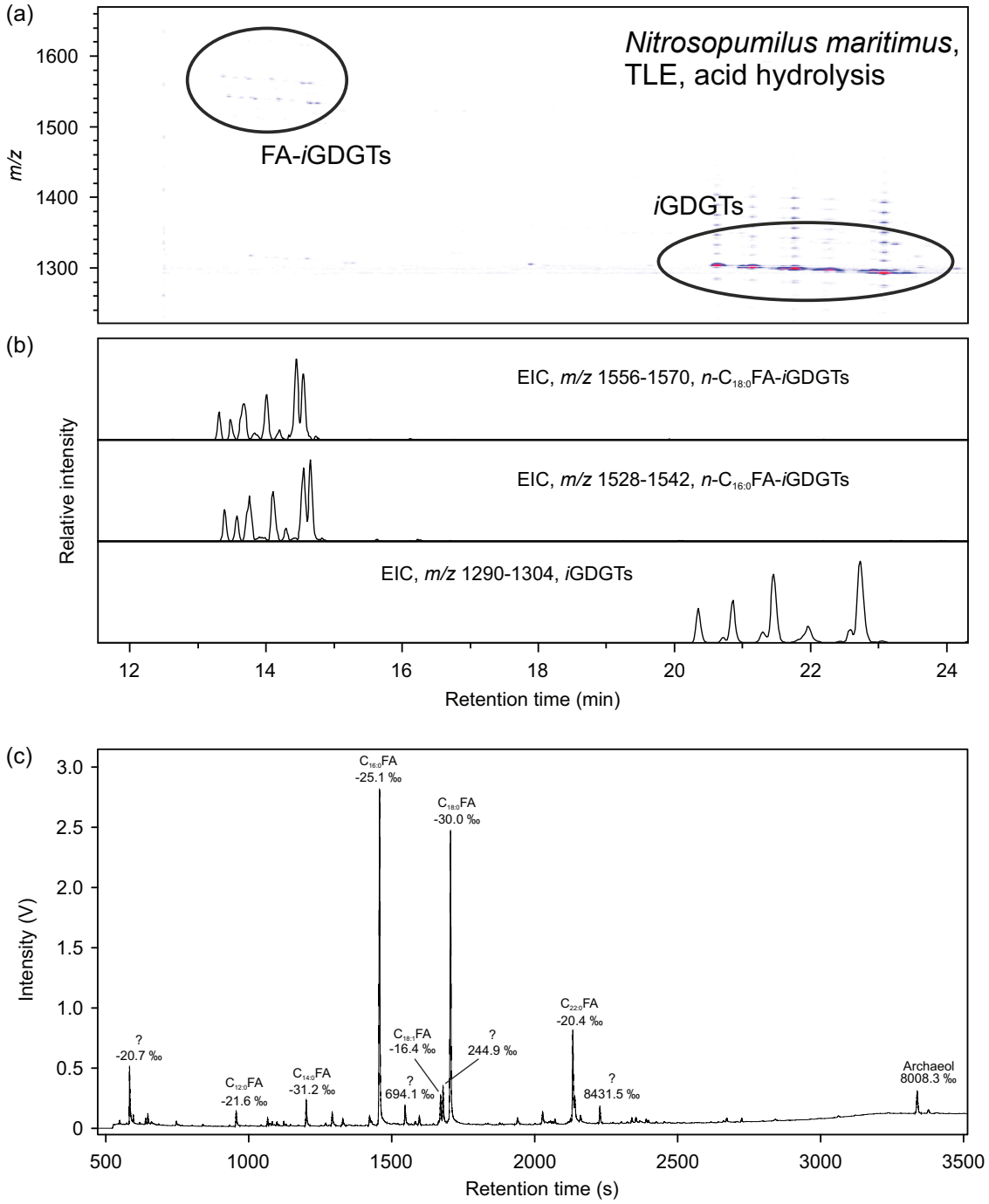

Figure V.2. (a) Density map plot showing the major diagnostic ions of *i*GDGTs and FA-*i*GDGTs in the acid hydrolyzed TLE of *Nitrosopumilus maritimus*, analyzed by HPLC–APCI-qToF-MS. (b) HPLC–APCI-qToF-MS chromatogram shown as extracted ion chromatogram (EIC), illustrating *i*GDGTs (bottom chromatogram) and *n*-$C_{18:0}$ and *n*-$C_{16:0}$FA-*i*GDGTs in the acid hydrolyzed TLE of *N. maritimus*. (c) GC–irMS chromatogram of fatty acids released by saponification from the same sample with $delta^13C$ values for each compound.

cultures are easily contaminated by sfungi (e.g. Summons et al., 2006). Another argument against FA synthesis in archaea is that they do not possess complete FA synthase machinery, at least for the known pathways (e.g. Lombard et al., 2012). To investigate potential biosynthetic production of fatty acids in archaea, we performed a stable isotope probing (SIP) experiment with *N. maritimus*. The free fatty acids detected after base hydrolysis of the TLE showed no label incorporation (Figure V.2c). In contrast, the archaeal lipids, such as archaeol, showed strong label incorporation. Therefore, the FAs detected in the TLE were not synthesized by *N. maritimus* and we thus suggest that detected FA-*i*GDGTs were likely artificially produced via esterification of free acids and *i*GDGTs during hydrolysis. The source of the FAs remains elusive but bacterial contamination is unlikely as bicarbonate was the only carbon source in the medium and thus growing bacteria would have to incorporate the label into their membranes. Moreover, microscopy did not reveal bacterial cells in the culture. Therefore, FAs might represent a contamination from glassware, consumables or the cross-flow harvesting system. Blank tests of solvents showed only minor amounts of C_{16} and C_{18} FAs, which is not sufficient to explain their abundance in *N. maritimus* in our experiment. FA contamination was thus most likely introduced during harvesting. The artificial production of FA-*i*GDGTs was further confirmed by acid hydrolysis experiments using trifluoroacetic acid, which resulted in increasing amounts of FA-*i*GDGTs in environmental samples (data not shown). As the used conditions were similar to described protocols for sugar cleavage reactions of glycosidic intact polar lipids (Lin et al., 2010), core lipids should not be analyzed after this procedure due to the production of artefacts.

V.3.3. Widespread occurrence and sources of FA-*i*GDGTs

FA-*i*GDGTs were detected in immature sediments from a variety of marine environments distributed over a large geographical area, including the hypersaline anoxic Orca Basin in the Gulf of Mexico, the hypersaline anoxic Discovery Basin in the Eastern Mediterranean, the Benguela upwelling region and the anoxic Black Sea. Concentrations of FA-*i*GDGTs were highest in sediments retrieved from the Discovery Basin and they were at least one order of magnitude lower in the sediments from the other regions. However, at all locations, the abundance of FA-*i*GDGTs was positively correlated to the abundance of *i*GDGTs ($n = 73$, $r^2 = 0.58$; Figure V.3a) and each location revealed a unique relationship of FA-*i*GDGT and *i*GDGT abundance with r^2 values between 0.82 and 0.94 (Figure V.3d-g).

The strong correlation of FA-*i*GDGT and *i*GDGT abundance in marine sediments suggests either a common biological source or diagenetic production of FA-*i*GDGTs from fatty acid and *i*GDGT precursors. As stated above, a biosynthetic origin of FA-*i*GDGTs seems unlikely, since fatty acid bearing membrane lipids are not known to

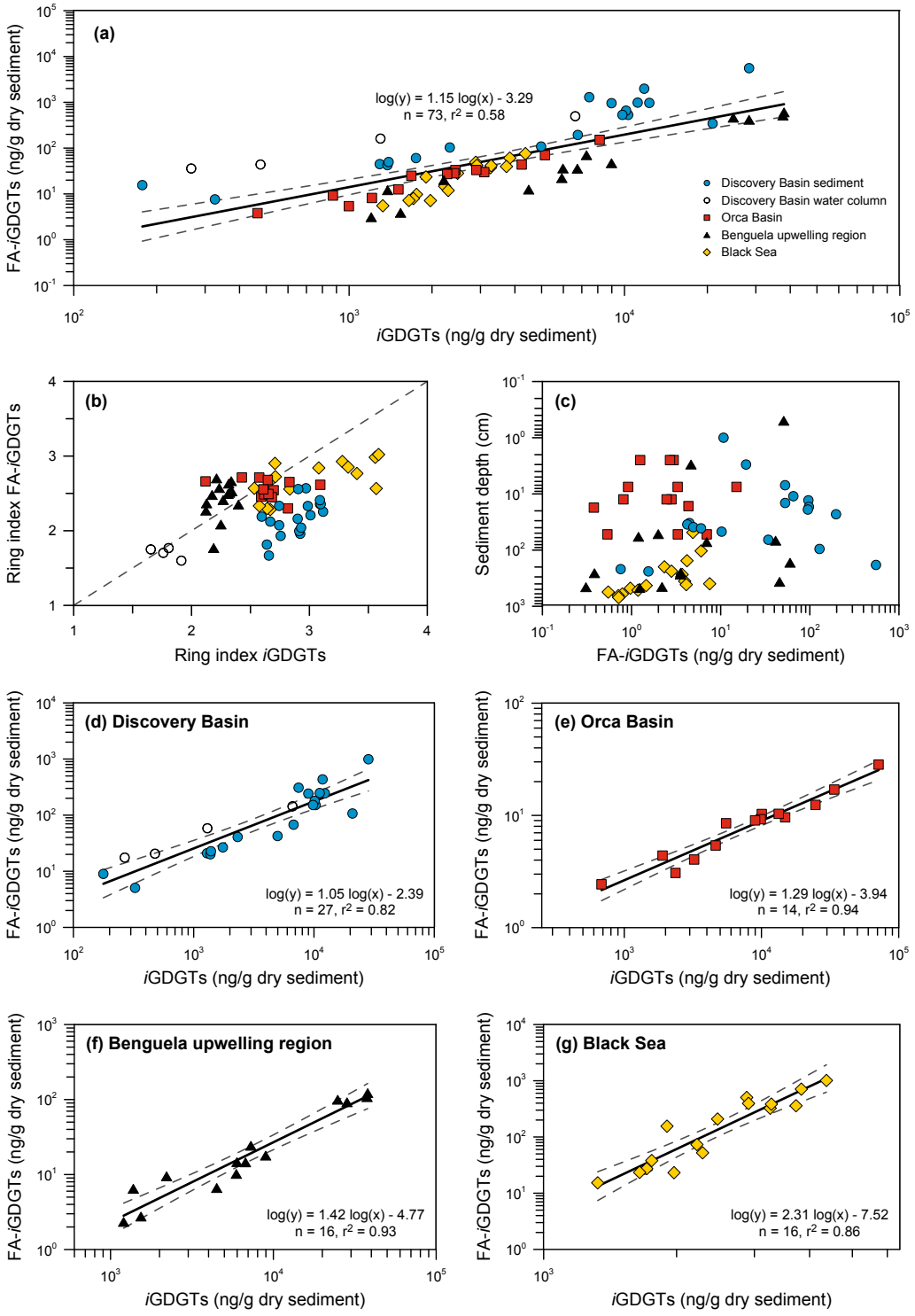

Figure V.3. Correlation between FA-*i*GDGTs and *i*GDGTs in marine sediments. (a) Cross plot of FA-*i*GDGT and *i*GDGT abundance in sediment and water column (brine) samples recovered from the hypersaline anoxic Discovery and Orca Basins as well as from the Benguela upwelling region and the Black Sea. Regression lines show total FA-*i*GDGTs (solid line) and the 95 % confidence interval (dashed lines). (b) Ring index (calculated after Pearson et al., 2004) of FA-*i*GDGTs and *i*GDGTs for all samples. Dashed line indicates 1:1 line. (c) Depth profile of FA-*i*GDGT concentrations in the investigated sediments. Panels (d) – (g) show cross plots of FA-*i*GDGTs and *i*GDGTs for each location. The regression lines show total FA-*i*GDGTs (solid lines) and the 95 % confidence interval (dashed lines).

occur in Archaea, while *i*GDGT biosynthesis is limited to this domain and we did not observe label uptake into FAs in the SIP experiment with *N. maritimus*. Additionally, the fatty acid composition and ring distribution of the FA-*i*GDGTs were similar to those of the free fatty acids and *i*GDGTs in the same samples (see Figure V.3b for ring indices of FA-*i*GDGTs and *i*GDGTs). Furthermore, the fatty acid distribution reflects a typical composition of marine sediments (e.g. Elvert et al., 2003). The possibility to artificially produce FA-*i*GDGTs under strong acidic conditions in the lab further suggests an abiogenic formation pathway in the sediments. Indeed, the strong correlation of FA-*i*GDGT and *i*GDGT abundance (see Figure V.3) and no correlation of FA-*i*GDGTs with sediment depth (Figure V.3c) indicate that these compounds are in a chemical equilibrium (Fatty acid + *i*GDGT $\leftrightarrow$ FA-*i*GDGT + H_2O). Hence, the abundance of FA-*i*GDGTs would primarily depend on the concentrations of the fatty acid and *i*GDGT reactants. This equilibrium might be shifted towards the reactants under most environmental conditions due to a high activity of water and hydrolytic enzymes (e.g. Boetius, 1995). However, Arpino and Ourisson (1971) showed that clay minerals, in particular montmorillonite, could act as catalyst for esterification. Since recent sediments typically contain high montmorillonite contents, FA-*i*GDGT production might be enhanced in these sediments as well. The elevated concentration of FA-*i*GDGTs in the sediments from the Benguela upwelling region are likely a result of both, high reactant concentrations and high clay mineral content. In the hypersaline basins, we additionally expect a low activity of water and hydrolytic enzymes (Litchfield, 1998) shifting the equilibrium further towards the FA-*i*GDGTs, explaining their high abundance in these samples, in particular in the samples from the Discovery Basin. Here, water activity is highly reduced (Hallsworth et al., 2007). The direct condensation of carboxylic acids with alcohols is generally avoided because the equilibrium between the substrates and the products require the elimination of water from the reaction mixture to shift the equilibrium in favor of the product. Diagenetic transformation of organic matter in marine sediments is commonly regarded as a series of condensation reactions of small molecules resulting in de-functionalization and the formation of macromolecules (Tissot and Welte, 1978). Indeed, Michaelis and Albrecht (1979), Kuypers et al. (2002), Schouten et al. (2004), and Pancost et al. (2008) demonstrated that *i*GDGTs are an integral part of the sedimentary macromolecular organic matter. The production of FA-*i*GDGTs by esterification of fatty acids and *i*GDGTs may serve as an example for the cross-linking reactions occurring during early diagenesis of these compounds leading to their de-functionalization and potential subsequent incorporation into geopolymers.

V.4. Conclusions

A novel group of compounds was detected in diverse environmental samples and *N. maritimus* biomass. They were assigned as fatty acid-substituted *i*GDGTs (FA-*i*GDGTs), which are likely produced from chemically free fatty acid and *i*GDGT precursors. A biosynthetic origin could be excluded based on a stable isotope probing experiment with *N. maritimus*, which revealed no label incorporation into the fatty acids. In the culture, FAs are likely a contamination from the harvesting system and FA-*i*GDGTs were artificially produced during hydrolysis. In the sediment samples, control experiments indicated that these compounds were not artificially produced during extraction. The observations that FA-*i*GDGTs appear to be in chemical equilibrium with *i*GDGTs and that the fatty acids connected to FA-*i*GDGTs were identical to the free fatty acids found in the sediment indicate a diagenetic origin. Since the ring distribution of FA-*i*GDGTs is broadly similar to that of the free *i*GDGTs, the effect of *i*GDGT diagenesis by fatty acid-substitution on lipid-based proxies, such as the TEX_{86}, is likely to be small. Still, the findings highlight the fact that *i*GDGTs may undergo diagenetic processes in immature sediments and thereby reduce the size of the free *i*GDGT pool, which is typically analyzed for TEX_{86} paleotemperature reconstructions. Fatty acid substitution of *i*GDGTs may therefore serve as an example for the largely unconstrained, initial steps of macromolecular organic matter formation.

Acknowledgements

We are grateful to the participating scientists and ship crews of the RV Meteor cruises M84/1 (DARCSEAS I) and M76/1. We would like to thank chief scientist S.B. Joye and the shipboard scientific party of cruise AT18-2 as well as the officers and crew of RV Atlantis. M. Yoshinaga, V. Heuer and L. Nigro are thanked for assistance during sampling. The study was funded by the European Research Council under the European Union's Seventh Framework Programme–"Ideas" Specific Programme, ERC grant agreement No. 247153 (Advanced Grant DARCLIFE; PI: K.-U.H.) and by the Deutsche Forschungsgemeinschaft through the Gottfried Wilhelm Leibniz Prize awarded to K.-U. Hinrichs and the Research Center/Cluster of Excellence MARUM.

Chapter VI

Records of microbial life in the deep-sea hypersaline anoxic Discovery Basin sediments

Kevin W. Becker[a,*], Marcos Y. Yoshinaga[a], Cassandre Lazar[b,+], Julius S. Lipp[a], Marcus Elvert[a], Verena B. Heuer[a], Matthias Zabel[c], Tobias Goldhammer[c], Ivano W. Aiello[d], Andreas P. Teske[b], Yuki Morono[e], Fumio Inagaki[e] and Kai-Uwe Hinrichs[a,*]

In preparation for *Geochimica et Cosmochimica Acta*

[a]Organic Geochemistry Group, MARUM - Center for Marine Environmental Sciences & Department of Geosciences, University of Bremen, 28359 Bremen, Germany
[b]Department of Marine Sciences, University of North Carolina at Chapel Hill, Chapel Hill, NC, USA
[c]Inorganic Geochemistry Group, MARUM - Center for Marine Environmental Sciences & Department of Geosciences, University of Bremen, 28359 Bremen, Germany
[d]Moss Landing Marine Laboratories, 8272 Moss Landing Road, Moss Landing, CA 95039-9647, USA
[e]Geomicrobiology Group, Kochi Institute for Core Sample Research, JAMSTEC, Monobe B200, Nankoku, Kochi 783-8502, Japan

*Corresponding author. E-mail: k.becker@uni-bremen.de

Abstract

Deep-sea hypersaline anoxic basins of the Eastern Mediterranean Sea are extreme and largely unexplored habitats. One of the most distinct hypersaline basins is the Discovery Basin, which is characterized by extremely high concentration of $MgCl_2$ (5 M), and considered incompatible with life as we currently know it. Thus, microbial life is likely limited to the brine-seawater interface, while the brine-influenced water column and sediments result in high preservation potential of biomolecules. The unique properties of the sediments provide thus an ideal opportunity to follow the development of microbial activity in the Discovery Basin from times prior to the brine to modern conditions. Three major phases of the basin formation were recorded: normal conditions before basin formation, basin formation and development of anoxia (35000 yr BP), and brine formation (<2000 yr BP). For this purpose, we studied the information encoded in the distribution and isotopic composition of intact polar membrane lipids (IPLs) as well as their core lipid derivatives. In the brine-seawater interface and in the sediments below the brine, we found intact polar and polyunsaturated archaeols that are only known to occur in extremely halophilic and methanogenic archaea. Interestingly, the composition of their head groups and unsaturated side chain structures differed distinctly between the brine-seawater interface and sediments, suggesting different haloarchaeal communities and/or adaptations to changing conditions since the development of the brine. Other taxonomically specific lipids indicated that archaeal ammonium oxidation and bacterial sulfate reduction occurs at the modern and past brine-seawater interface and implies intensive microbial carbon, nitrogen and sulfur cycles. After basin formation and before intrusion of high salt solution, methanogenesis and sulfate reduction were major microbial metabolic activities supporting the prevalence of anoxic conditions. Additionally, we identified for the first time intact forms of hybrid isoprenoid/branched tetraether lipids in sediments deposited prior to the basin collapse. These compounds combine attributes usually considered characteristic of either archaea (phytanyl moiety) or bacteria (methylated alkyl moiety) and were the major intact polar membrane lipids (IPLs) in sediments from before the basin formation. In conclusion, the membrane lipid biomarker approach allowed to detect records of distinct microbial communities as well as their membrane lipid adaptations to this hostile environment.

VI.1. Introduction

Deep-sea hypersaline anoxic basins (DHABs) represent some of the most unique and extreme environments on earth. They were found in several of the world's oceans, including the Eastern Mediterranean, the Gulf of Mexico and the Red Sea (Backer and Schoell, 1972; Shokes et al., 1977; De Lange and ten Haven, 1983; Jongsma et al., 1983). So far, eight DHABs have been discovered in the Eastern Mediterranean, most of them located west of Crete on the Western Mediterranean ridge at depths greater than 3000 m below sea level (mbsl). These basins were formed several thousand years ago by dissolution of ancient subterranean salt deposits (Messinian evaporites) exposed to seawater by tectonic activity and the downward flow of the dense brines into local abyssal depressions. This was followed by the progressive development of anoxia in the brine lakes (Belderson et al., 1978; Kastens and Spiess, 1984; De Lange et al., 1990a; Fusi et al., 1996). In addition to the high salt concentration, high sulfide concentrations are prevailing conditions in these habitats, dramatically limiting growth of any life form.

Each of the DHABs in the Eastern Mediterrnaean shows a disticnt geochemistry (van der Wielen et al., 2005). For example, the Discovery Basin (Figure VI.1) is characterized by the highest concentration of $MgCl_2$ (5 M) found so far in a marine environment and low concentration of Na^+ (Wallmann et al., 1997; Wallmann et al., 2002); such concentrations are considered uninhabitable for life (Hallsworth et al., 2007). In contrast, most other brine pools in this region are contain NaCl-rich brines. There exist several lines of evidence suggesting that life within the Discovery Basin hypersaline brine and underlying sediments is not favorable: *(i)* the high redox potential (10 mV) compared with three other anoxic brine sediments from the Eastern Mediterranean (l'Atalante, Bannock and Urania), which contain NaCl-rich brines (-82 to -136 mV; Polymenakou et al., 2007), *(ii)* undetectable mRNA from archaea and bacteria below the brine-seawater interface (Hallsworth et al., 2007), and *(iii)* lowest viable cell counts for bacteria and the highest endospore abundance among the different hypersaline basins of the Eastern Mediterranean (Sass et al., 2008).

Magnesium is well known for generating high osmotic potentials, strongly reducing the mole fraction of water, and its chaotropic properties. Especially chaotropic solutes are powerful inhibitors of cellular systems because they destabilize and dena-ture biological macromolecules, and induce a strong stress response (Hallsworth et al., 2003). However, based on cell counts, fluorescence *in situ* hybridization (FISH) and 16S rRNA, microbial life appears to flourish at the upper brine-seawater interface in the Discovery Basin. For instance, sulfate-reducing bacteria belonging to the *Desulfobacteraceae* and *Desulfohalobiaceae* were the dominant bacteria at the interface (Hallsworth et al., 2007). Detected archaea included Marine Group 1 Thaumarchaeota in the superficial brine-seawater

interface, Haloarchaea, which only occurred in a narrow window of the halocline, Euryarchaeota Mediterranean Sea Brine Lake Group 1 (MSBL1) and *Methanohalophilus*, which occurred in the anoxic deeper layers of the interface (van der Wielen et al., 2005; Hallsworth et al., 2007).

Halophilic organisms adapt to the high salt concentrations by using one of two substantially different strategies, both maintaining osmotic equilibrium with the environment (e.g., Oren, 2008). Most extremely halophilic archaea use the "salt-in" strategy, which involves accumulation of high concentrations of K^+ ions within their cytoplasm to maintain a positive water balance. Extremely halophilic bacteria mainly use the "salt-out" strategy, synthesizing and accumulating organic compatible solutes like glycine betaine within the cytoplasm while actively pumping (i.e., via ATP) Na^+ ions out. Given the high energy cost for the biosynthesis of large amounts of organic osmotic solutes, archaea are favored over bacteria in extremely hypersaline environments (Oren, 1999). Moreover, in order to keep cell integrity and membrane fluidity under high ionic strength intact, halophilic archaea as well as bacteria increase the amount of anionic lipids in their membranes (Russell, 1989; Oren, 2002b), including phosphatidylglycerol (PG), PG-phosphate (PGP), methylated-PGP (Me-PGP) and sulfated glycosidic-based intact polar lipids (IPLs; e.g., Kushwaha et al., 1982; Kates, 1993a). Beside this headgroup adaptation, structural modifications of the apolar core lipids have been shown to be important in halophiles, as the interaction of polar head groups and apolar side chains significantly influences the geometry and size of the IPLs (Russell, 1989). For example, Dawson et al. (2012) showed highest degrees of unsaturation in haloarchaeal isolates at their salinity optima.

The present study examined the microbial membrane lipid distributions in the brine-seawater interface, the anoxic brine and sediments of the deep-sea hypersaline anoxic Discovery Basin. Although osmoregulation and membrane lipid adaptations may be crucial to halophilic microbes in the Discovery Basin, they are still faced with the life-limit quandary. Thus, we consider two possibilities: (1) novel extremophilic life may proceed at Mg^{2+} concentrations of 5 M (cf. Sass et al., 2008) and (2), which is more conformable with the current knowledge about halophilic limits of life (Hallsworth et al., 2007; Yakimov et al., 2015), microbial activity is limited to the brine-seawater interface, where concentrations of Mg^{2+} are below 2.3 M (Hallsworth et al., 2007). While microbial cells are well preserved in sediments from the Discovery Basin (Sass et al., 2008), the extremely high Mg^{2+} concentrations in the sediments may impair microbial detection by DNA extraction/amplification (e.g., Edwards, 2004). In this case, the analysis of lipids could represent a unique opportunity providing taxonomic information in this extreme environment. Lipids are further amenable to carbon isotopic analysis, which may provide additional information on carbon metabolism mediated by the producers of the lipids in natural settings (Hinrichs et al., 1999; Lin et al., 2010; Schubotz et al., 2011). Since

the Mg^{2+} concentrations in the sediments are considered incompatible with life (e.g., Hallsworth et al., 2007), we propose that the sedimentary IPL record may reflect past microbial assemblages from the brine-seawater interface. We thus aimed to use lipids as tools to follow the development of microbial activity in the Discovery Basin from times prior to the brine to modern conditions (<2,000 years).

VI.2. Material and methods

VI.2.1. Sample collection

Suspended particulate matter and sediment samples were collected during RV Meteor cruise M84/1 ("DARCSEAS I") from the hypersaline anoxic Discovery Basin located in the Eastern Mediterranean Sea (Site GeoB15102, 35°16.43'N 21°41.50'E, 3615 m water depth, Figure VI.1) using *in situ* pumps, a multicorer and a gravity corer. After recovery, the samples were immediately frozen and stored at $-80\,^{\circ}\mathrm{C}$ until further treatment (Zabel and Cruise Participants, 2013). Suspended particulate matter samples (GeoB15102-3) were recovered at four depths (3570, 3575, 3580 and 3610 mbsl) by pumping 1.3 to 12.5 liters of water through double pre-combusted $0.7\,\mu\mathrm{m}$ pore-size GF/F glass fiber filters. The 23 sediment samples have been derived from a 411 cm long gravity core (GeoB15102-5) and a 48 cm long multi-core (GeoB15102-4). Pore water was extracted from sediment cores with Rhizon micro suction samplers ($0.1\,\mu\mathrm{m}$ filter width, Rhizosphere Research Products, Wageningen) and split into subsamples for onshore analysis (Zabel and Cruise Participants, 2013). Water column profiles of conductivity, temperature and depth as well as pressure and dissolved oxygen were measured with a vertical resolution of 1 m using a CTD (GeoB15102-2). The salinity was derived from conductivity, while the density was calculated from pressure and temperature measurements as well as salinity.

VI.2.2. Core description

The sediments of the Discovery Basin (Site GeoB15102) are very heterogeneous and characterized by prominent color variations, different types of sedimentary structures, such as soft sediment deformation, lamination and banding and trace fossils (see Figure VI.3 for core picture). The sediments also contained precipitates of gypsum and other authigenic minerals that formed crystals and nodules ranging from a few mm to more than 10 cm. The most common sedimentary component at this site is homogenous to laminated coccolith ooze that can occur mixed with various amounts of secondary components including clay, micro-carbonates, foraminifers, volcanic ash and framboidal pyrite (Unit II). Downcore, color changes of the coccolith ooze reflect changes in the relative amount of secondary components in the sediment. For instance, light gray sediments

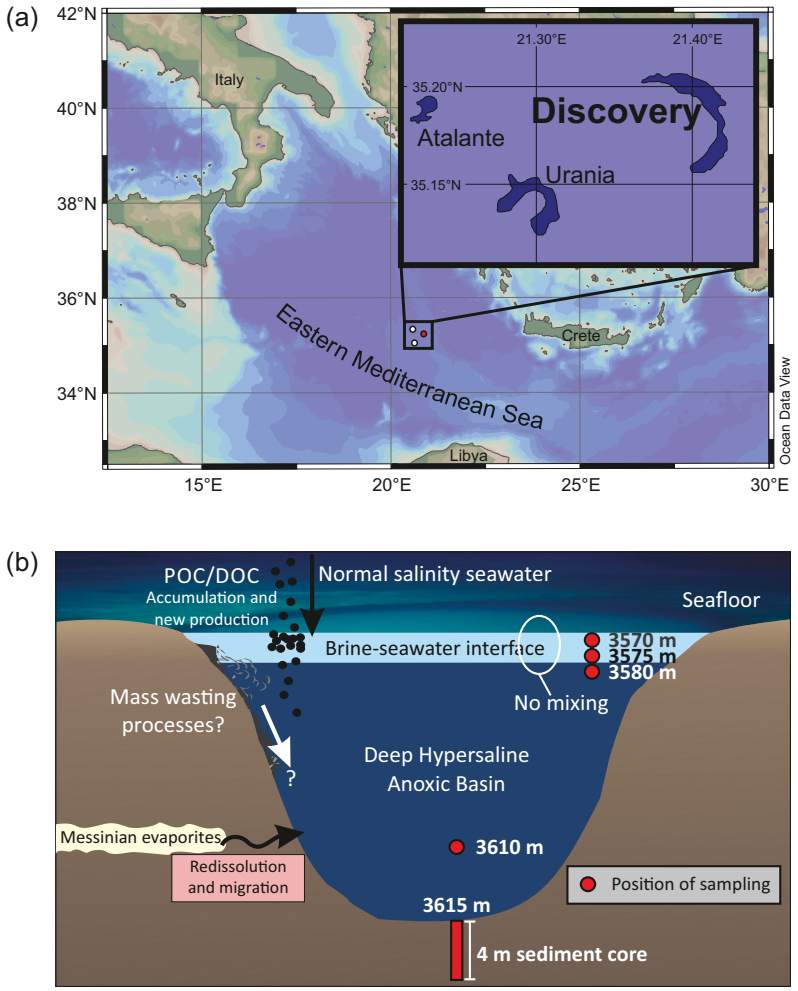

Figure VI.1. (a) Location of deep hypersaline anoxic basins in the Eastern Mediterranean Sea. The detailed locations of the Discovery, Urania and Atalante Basin are shown in the insert map. The maps were constructed with ocean data view software (http://odv.awi.de/). (b) Schematic of a brine including its major characteristics and the position of sampling for membrane lipid analysis. Samples were then obtained using in situ pumps from the brine-seawater interface and the brine as well as from the underlying sediments using multi and gravity cores.

are made almost entirely by coccoliths, while reddish brown sediments are composed of a subequal mix of coccoliths and clay. Components that are generally secondary in the bulk coccolith ooze sediment can occur concentrated in discrete laminae or bands characterized by prominent color changes including foraminifer sand and graded ash, and black sulfide-rich laminae and mottles. The second most prominent lithology at the site occurs mainly in the upper 50 cm of the gravity core (Unit Ia) and is a black, organic-rich diatom and coccolith ooze mixed with large volumes (>50 % sediment) of cm-size gypsum crystals. A third lithology occurs in discrete gray layers in the top 50 cm of the core. These layers are composed of a silicoflagellates- and radiolarian-rich diatom clay and match the description of sapropels by Wallmann et al. (2002). The interval of the above mentioned soft sediment deformation occurred between 50 and 200 cm

(Unit Ib) and indicates re-sedimentation probably triggered by tectonic activity of the accretionary wedge which is the main structural feature of the region.

VI.2.3. Pore water geochemistry

Dissolved chloride (Cl^-) was determined by ion chromatography (Metrohm Compact IC, METROSEP A Supp 5 column, conductivity detection after chemical suppression) in samples diluted 1:100 with Milli-Q grade H_2O. Dissolved magnesium (Mg), sodium (Na), potassium (K), and calcium (Ca) were quantified by inductively coupled plasma-optical emission spectroscopy (ICP-OES, Varian Vista Pro) in samples diluted 1:10 to 1:100 with $1\,\%$ ultrapure nitric acid.

VI.2.4. TOC

An aliquot ($\sim$3 g) of homogenized and freeze-dried sediment sample was decalcified by acidification with $10\,\%$ HCl. Between 10-30 mg sediment was weighted into tin capsules and analyzed for total organic carbon (TOC) content and its stable carbon isotopic composition $\delta^{13}C_{TOC}$. A Thermo Scientific Flash 2000 elemental analyzer interfaced to a Thermo Delta V Plus IRMS was used to conduct $\delta^{13}C_{TOC}$ and elemental concentration ($\%$ carbon) analysis. The $\delta^{13}C_{TOC}$ values are expressed relative to VPDB (Vienna Pee Dee Belemnite).

VI.2.5. Extraction of lipids

The *in situ* pump filters and homogenized sediment samples were spiked with an internal standard (phosphatidyl choline diacyl glycerol, C_{21}-PC-DAG). Then the samples (25±0.5 g wet weight for the sediments) were extracted using a modified Bligh and Dyer protocol Sturt et al. (2004). The sediments were ultrasonically extracted for 10 min in four steps with a solvent mixture of dichloromethane/methanol/buffer (1:2:0.8, v:v:v) using $4\,\mathrm{ml}$ solvent per gram of sediment and extraction step. A phosphate buffer ($8.7\,\mathrm{g\,l^{-1}}$ KH_2PO_4 pH 7.4) was used for the first two steps, and a trichloroacetic acid buffer ($50\,\mathrm{g\,l^{-1}}$ CCl_3COOH, pH 2) for the final two steps. After each extraction step, the samples were centrifuged at 800 x g for 10 min and the supernatants were collected in a separation funnel. The combined supernatants were then washed three times with de-ionized MilliQ water. After separation into organic phase and water-soluble phase, the organic phase was collected as the total lipid extract (TLE). The solvent was gently removed under a stream of N_2 and the TLE was stored at $-20\,^\circ\mathrm{C}$.

VI.2.6. Analytical methods for membrane lipid analysis

VI.2.6.1. Intact polar lipid analysis

Intact polar lipids were analyzed on a Dionex Ultimate 3000 ultra-high performance liquid chromatography (UHPLC) system connected to a Bruker maXis Ultra-High Resolution quadrupole time-of-flight tandem mass spectrometer (qToF-MS) equipped with an electrospray ion source (ESI) operating in positive mode (Bruker Daltonik, Bremen, Germany). Compounds were also detected in negative ionization mode to obtain structural information on fatty acid side chains. The mass spectrometer was set to a resolving power of 27,000 at *m/z* 1222 and every analysis was mass-calibrated by loop injections of a calibration standard and correction by lock mass, leading to a mass accuracy of <1-3 ppm. Ion source and other MS parameters were as described by Wörmer et al. (2013).

Bacterial IPL separation was achieved using normal-phase (NP) HPLC on an Acquity UPLC BEH Amide column ($1.7\,\mu m$, 2.1 × 150 mm; Waters Corporation, Eschborn, Germany) maintained at $40\,°C$ as described by Wörmer et al. (2013). Aliquots of the TLE were dissolved in dichloromethane:methanol (9:1, v:v) and analytes were eluted at a flow rate of $0.5\,ml\,min^{-1}$ with $99\,\%$ eluent A (acetonitrile:dichloromethane, 75:25, with $0.01\,\%$ formic acid and NH_3, v:v:v:v) and $1\,\%$ eluent B (methanol:water, 50:50, with $0.4\,\%$ formic acid and NH_3) for 2.5 min, increasing B to $5\,\%$ at 4 min, to $20\,\%$ B at 22.5 min and $40\,\%$ B at 26.5 min. The column was then flushed with $40\,\%$ B for 1 min.

For archaeal IPL separation, the samples were additionally analyzed on the same system under different chromatographic conditions using reverse-phase (RP) chromatography as described by Wörmer et al. (2013). Briefly, $1\,\%$ TLE aliquots were dissolved in methanol:dichloromethane (9:1, v:v) and injected onto an Acquity UPLC BEH C_{18} column ($1.7\,\mu m$, 2.1 x 150 mm, Waters, Eschborn, Germany) maintained at $65\,°C$. Analytes were eluted at a flow rate of $0.4\,ml\,min^{-1}$ using linear gradients of methanol:water (85:15, v:v, eluent A) to methanol:isopropanol (50:50, v:v, eluent B) both with $0.04\,\%$ formic acid and $0.1\,\%$ NH_3. The initial condition was $100\,\%$ A held for 2 min, followed by a gradient to $15\,\%$ B in 0.1 min and a gradient to $85\,\%$ B in 18 min. The column was then washed with $100\,\%$ B for 8 min.

Lipids were identified by retention time, molecular mass, and MS^2 fragmentation. Integration of peaks was performed on extracted ion chromatograms of ±10 mDa width and included the $[M+H]^+$, $[M+NH_4]^+$, and $[M+Na]^+$ ions. Bacterial IPLs were quantified from NP-HPLC runs relative to the internal standard. Archaeal IPL quantification was achieved from RP-HPLC runs by injecting a standard (C_{46}-GTGT, Huguet et al., 2006) along with the samples. Given the lack of available IPL standards by the time of analysis, particularly for newly identified IPLs, we were unable to determine the response factors of individual IPLs relative to the internal and the injection standard.

VI.2.6.2. Core lipid analysis

Core lipids were analyzed on the same UHPLC-qToF-MS system, but equipped with an APCI II ion source using the protocol of Becker et al. (2013). Compounds were detected in positive ionization mode, while scanning a *m/z* range from 150 to 2000 at 2 scans per second.

Aliquots of the TLE (typically $10\,\mu l$, dissolved in *n*-hexane:isopropanol (99.5:0.5, v:v), were injected on two coupled Acquity BEH HILIC Amide columns (each 2.1 x 150 mm, $1.7\,\mu m$, Waters, Eschborn, Germany) kept at $50\,°C$. Compounds were eluted using the following gradient with eluent A (*n*-hexane) and eluent B [*n*-hexane:isopropanol (90:10, v:v)] and a constant flow of $0.5\,ml\,min^{-1}$: $3\,\%$ B to $5\,\%$ B in 2 min, to $10\,\%$ B in 8 min, to $20\,\%$ B in 10 min, to $50\,\%$ B in 15 min and to $100\,\%$ B in 10 min. Columns were washed with $100\,\%$ B for 6 min and equilibrated with $3\,\%$ B for 9 min before next injection.

Lipids were identified by their exact mass measured in full scan mode (MS^1) and their characteristic fragmentation in MS^2 mode. Integration of peaks was performed on extracted ion chromatograms of ±10 mDa width of the $[M+H]^+$ ion. Quantification was achieved by injecting C_{46}-GTGT standard along with the samples.

To evaluate GDGT cyclization we calculated the ring index according to Pearson et al. (2004):

$$\text{Ring index} = \frac{[\text{GDGT-1}]+2\times[\text{GDGT-2}]+3\times[\text{GDGT-3}]+4\times[\text{GDGT-4}]+5\times[\text{GDGT-5 + GDGT-5'}]}{[\text{GDGT-0}]+[\text{GDGT-1}]+[\text{GDGT-2}]+[\text{GDGT-3}]+[\text{GDGT-4}]+[\text{Cren + Cren'}]} \quad \text{(Eq. 1)}$$

Similarly, cyclization of glycerol dibiphytanyl diethers (GDDs) was calculated.

To evaluate the degree of unsaturation of archaeols we calculated the unsaturation index as follows:

$$\text{Unsaturation index} = \frac{[\text{monouns}]+2\times[\text{diuns}]+3\times[\text{triuns}]+4\times[\text{tetrauns}]+5\times[\text{pentauns}]+6\times[\text{hexauns}]}{[\text{monouns}]+[\text{diuns}]+[\text{triuns}]+[\text{tetrauns}]+[\text{pentauns}]+[\text{hexauns}]} \quad \text{(Eq. 2)}$$

VI.2.6.3. Semi-preparative HPLC - purification of individual core lipid and IPL groups for isotope analysis

To target the isotopic analysis of the apolar side chain of individual core lipids and IPLs, an aliquot of the TLE was subjected to two-dimensional (orthogonal) semi-preparative HPLC, involving the combination of normal- and reverse-phase HPLC. Normal-phase semi-preparative HPLC was used for separation into an apolar fraction (containing core lipids) and a polar fraction (containing the more polar IPLs). For this approach, a semi-preparative Inertsil Diol column ($5\,\mu m$, 150 × 10 mm, GL Sciences Inc., Tokyo, Japan)

was connected to an Agilent 1200 series HPLC instrument equipped with an Agilent 1200 series fraction collector. The flow rate was $3\,\mathrm{ml\,min^{-1}}$ and the eluent gradient was: $100\,\%$ A to $10\,\%$ B in 5 min, to $85\,\%$ B in 1 min, held at $85\,\%$ B for 9 min, then 6 min column re-equilibration with $100\,\%$ A, where eluent A was *n*-hexane:isopropanol (85:15, v:v) and eluent B isopropanol:MilliQ water (90:10, v:v). The apolar fraction was collected from 0 to 5 min and the polar fraction from 5 to 15 min. Fractions were evaporated under a stream of N_2 and stored at $-20\,^{\circ}\mathrm{C}$ until further analysis.

To further separate single core lipid and IPL groups, reverse-phase semi-preparative HPLC was used following the protocol from Zhu et al. (2013a). In brief: samples were dissolved in methanol:2-propanol (8:2, v/v) and separated by a Zorbax Eclipse XDB-C18 column (9.4 × 250 mm, $5\,\mu\mathrm{m}$ particle size; Agilent Technologies Deutschland GmbH, Böblingen, Germany) operated at $45\,^{\circ}\mathrm{C}$. Compounds were eluted by linear gradients from $80\,\%$ methanol: $20\,\%$ 2-propanol to $60\,\%$ methanol: $40\,\%$ 2-propanol in 5 min, and then to $35\,\%$ methanol: $65\,\%$ 2-propanol in another 40 min with a flow rate of $2.2\,\mathrm{ml\,min^{-1}}$. The column was washed by $100\,\%$ 2-propanol for 10 min followed by column re-equilibration with $100\,\%$ methanol for another 15 min.

Subsequently, individual core lipid and IPL fractions were subjected to ether cleavage using boron tribromide (BBr_3, Aldrich) according to the protocol from Bradley et al. (2009). In brief, $200\,\mu\mathrm{l}$ 1.0 M BBr_3 was added to individual lipid under a stream of argon. The vials were sealed and heated to $60\,^{\circ}\mathrm{C}$ for 2 h. The resulting bromides were reduced to hydrocarbons by adding $1\,\mathrm{ml}$ Super-Hydride solution (1.0 M lithium triethylborohydride in tetrahydrofuran, Aldrich) under a stream of argon. The reaction took place at $60\,^{\circ}\mathrm{C}$ for 2 h.

VI.2.6.4. GC–MS, GC–FID and GC–irMS

GC–MS analysis for identification of hydrocarbons was performed on an Agilent 5973 inert MSD system equipped with an Rxi-5ms capillary column (Restek GmbH, Bad Homburg, Germany; L = 30 m; ID = 0.25 mm; $0.25\,\mu\mathrm{m}$ film thickness) with He as carrier gas and a flow rate of $20\,\mathrm{ml\,min^{-1}}$. All samples were injected at $300\,^{\circ}\mathrm{C}$ in splitless mode. For hydrocarbon analysis, the oven temperature was set to $60\,^{\circ}\mathrm{C}$ at injection, held for 1 min, raised to $150\,^{\circ}\mathrm{C}$ at $10\,^{\circ}\mathrm{C\,min^{-1}}$, further increased to $320\,^{\circ}\mathrm{C}$ at $4\,^{\circ}\mathrm{C\,min^{-1}}$, and held isothermal for 27.5 min.

Stable carbon isotopic compositions of hydrocarbons were determined using a GC-isotope ratio-MS (Trace GC Ultra coupled to a GC-IsoLink, ConFlow IV interface and a DeltaV Plus isotope ratio mass spectrometer, all from Thermo Scientific GmbH). GC conditions were the same as utilized for the GC–MS. Compounds were oxidized in a combustion interface at $940\,^{\circ}\mathrm{C}$. Stable carbon isotopic compositions are expressed as

δ^{13}C values in the per mil (‰) notation relative to VPDB standards. The analytical error was <0.5 ‰.

VI.2.7. Cell counts

A volume of 0.5 ml of each subsample from the cores was fixed in 0.5 ml 4 % paraformaldehyde solution and incubated 4 hours at 4 °C, followed by washing with 0.5 ml 1X PBS, and addition of 0.5 ml 1X PBS:Ethanol (1:1) was added to the pellet. The fixed samples were stored at −20 °C. The samples were then prepared and stained with SYBR Green for automatic fluorescence microscope enumeration as described previously (Morono et al., 2009) at the JAMSTEC facility (Kochi, Japan). 50 µl of the fixed sample was used for sonication, and 20 µl of the prepared sample was filtered through the membrane. Cell abundance was only determined for the sediment samples, but not for the in situ pump filters. Based on total IPL and cell concentration, we calculated the IPL content per cell according to Lipp et al. (2008). A volume of 0.5 ml of each subsample from the cores was fixed in 0.5 ml 4 % paraformaldehyde solution and incubated 4 hours at 4 °C, followed by washing with 0.5 ml 1X PBS, and addition of 0.5 ml 1X PBS:Ethanol (1:1) was added to the pellet. The fixed samples were stored at −20 °C. The samples were then prepared and stained with SYBR Green for automatic fluorescence microscope enumeration as described previously (Morono et al., 2009) at the JAMSTEC facility (Kochi, Japan). 50 µl of the fixed sample was used for sonication, and 20 µl of the prepared sample was filtered through the membrane. Cell abundance was only determined for the sediment samples, but not for the in situ pump filters. The cellular lipid content was calculated from cell counts and IPL abundance.

VI.3. Results

VI.3.1. Geochemistry of Discovery Basin brine and sediments

Temperature, dissolved oxygen and salinity were determined from the water column overlying the Discovery Basin and the brine itself. The brine layer was located at a water depth of 3570 m and was 25 m thick. The depth measurement slightly varied for the different deployments (CTD rosette, rope length for *in situ* pumps and gravity corer, respectively). At the brine surface, the temperature slightly increased from 14 °C to 14.5 °C, oxygen concentration dropped from 140 µmol kg^{-1} to zero, fluorescence increased from –0.1 to almost 0.4 mg m^{-3} and salinity increased from 40 to more than 60 psu (Figure VI.2). Although the high salt concentration might has influenced the measurements, the interface was well documented. In the entire water column above the brine, salinity, temperature, oxygen and fluorescence showed only minor variations.

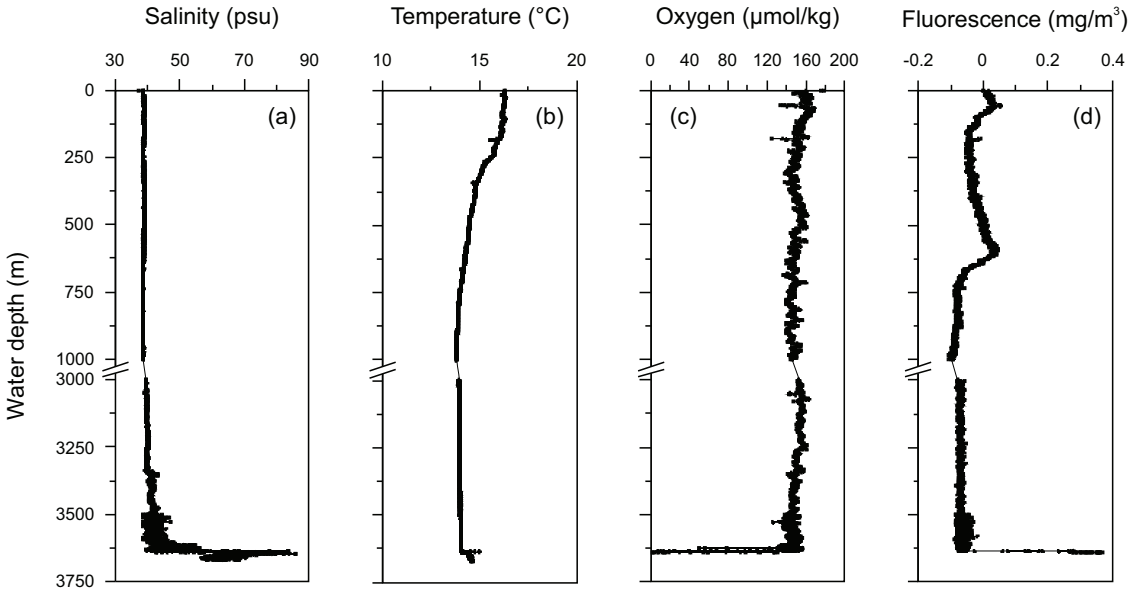

Figure VI.2. Depth profiles of (a) salinity, (b) temperature, (c) oxygen and (d) fluorescence from the water column overlying the Discovery Basin and the hypersaline brine obtained from CTD measurements. The brine showed an oily consistency, which probably led to a repeat failure of the oxygen and conductivity (salinity, density) sensor. All parameters show abrupt changes at the brine-seawater interface at ∼3570 mbsl, i.e., increase in salinity and fluorescence, slight increase in temperature and a decline in oxygen concentration.

The concentrations of selected ions were determined for samples collected above the brine (i.e., normal salinity seawater), at the brine seawater-interface, the brine and the pore waters of the sediments (Supp. Fig. VI.1). Magnesium concentration increased abruptly at the interface from 0.06 to more than 5.5 M in the brine. In sediments, Mg^{2+} concentration decreased with increasing depth, reaching values below saturation (<5 M) at 100 cm sediment depth. Similar to Mg^{2+}, K^{+} accumulated in the brine and in the sediments, they showed the opposite trend. Whereas Mg^{2+} decreased with increasing sediment depth, K^{+} linearly increased. While in the normal salinity seawater Na+ concentrations were 0.5 M, considerably lower concentrations (0.07 M) were detected in the brine. In the sediments, Na^{+} concentrations increased from 0.07 to 0.26 M with depth. Calcium showed similar trends compared to Na^{+}, but profiles displayed much lower concentrations. Chloride concentrations were 0.9 M in the seawater above the brine and increased towards 100 fold higher values in the brine. In the sediments, Cl^{-} concentrations decreased form ca. 10 M to values around 8 M with increasing sediment depth.

Total organic carbon (TOC) content varied between 0.065 and 1.32 wt% in the investigated sediment core. Higher TOC concentrations occurred in the first 2 m of the sediment (Unit I) with the maximum at 201.5 cm below sea floor (cmbsf), whereas relatively low concentrations (<0.25 wt%) were found in the deeper samples (Unit II, Figure VI.3a). The

stable carbon isotope composition of TOC ($\delta^{13}C_{TOC}$) showed little variation with values between -20.5 and $-21.7\,‰$ (Figure VI.3a).

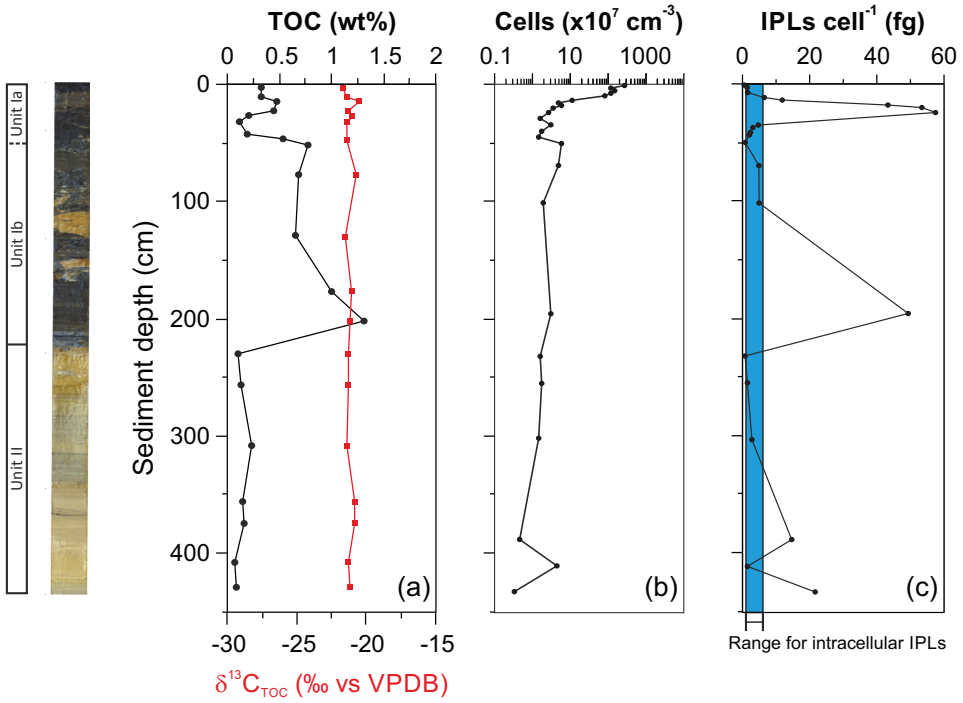

Figure VI.3. (a) TOC and $\delta^{13}C_{TOC}$, (b) cell concentrations and (c) Lipid quota per cell calculated after Lipp et al. (2008) for the sediments of the Discovery Basin. The blue shaded area (c) indicates in the hypothetic range for intracellular IPLs (from Lipp et al. (2008) for spherical cells with a diameter between 0.5 and 1 µm). On the left, a picture of the investigated gravity core GeoB15102-5 and the classification into units is shown. Classification of units is based on major lithological changes (see text).

VI.3.2. Microbial cell counts and total membrane lipid concentration

Microbial cell concentration was highest in the surface sediments with 277 x 10^7 cells cm^{-3}. Within the first 15 cmbsf, the cell concentration profile showed an exponential decrease reaching almost 100 times lower values (Figure VI.3b). Below 15 cmbsf, the cell concentration profile showed only minor changes, except for the samples at 386 cmbsf with 4.41 x 10^7 cells cm^{-3}. Here, the cell concentration was 10 times higher than in the samples located directly above and below this depth. For the water column samples, cell abundance was not determined.

The superficial layers of the brine-seawater interface (3570 mbsl) showed total IPL concentration of $1.9\,\mu g\,l^{-1}$ and a similar range was found at the deeper interface (3575 mbsl, Figure VI.4a). In contrast, more than five times lower values were observed in the brine water samples (3580 and 3610 mbsl). In the sediments, total IPL concentration showed highest values in the top 24 cmbsf (between 1.5 and $3\,\mu g\,g^{-1}$ sed. dw in samples

6-8 and 18-20 cmbsf, respectively). In the interval between 23 and 47 cmbsf, IPL concentration decreased and did not exceed $0.1\,\mu g\,g^{-1}$ sed. dw. Between 65.5 and 184 cm sediment depth (lithological Unit Ia), IPL concentration increased with a maximum at 184 cm sediment depth with $1.53\,\mu g\,g^{-1}$ sed. dw. Below 184 cm sediment depth, lowest IPL concentrations were measured (lithological Unit II). Calculated lipid content per cell in the sediments varied between 0.6 and 57.5 fg IPL cell^{-1}. Distinct maxima occurred at 23, and 184 cmbsf with the sample from 23 cmbsf showing the highest value (Figure VI.3b).

VI.3.3. Intact polar lipid composition

VI.3.3.1. Distribution of archaeal IPLs

Intact polar archaeal GDGTs (IP-GDGTs) and ARs (IP-ARs) were detected throughout the sediment cores. IP-GDGTs were always more abundant than IP-ARs, but the relative abundance of IP-ARs increased continuously with depth. Whereas they only comprised $5\,\%$ of total archaeal IPLs in the shallow sediments (0-34 cm), they reached $35\,\%$ in the sample from 386.5 cmbsf (Figure VI.4b). In the water column samples, IP-GDGTs were also detected at all depths, whereas IP-ARs were only present in noticeable amounts in the sample from 3570 mbsl.

IP-GDGTs were present as mono-, di- and triglycosidic lipids (1G-, 2G-, and 3G-GDGTs), and as phosphohexose (PH) and hexose-phosphohexose (HPH; see Figure VI.4b). Glycosidic GDGTs also included mono- and di-hydroxylated (1G-OH-GDGTs, 1G-2OH-GDGTs, 2G-OH-GDGTs, 2G-2OH-GDGTs, 3G-OH-GDGTs) isoprenoid chains as well as recently identified butanetriol-based core lipids (1G-BDGT; Zhu et al., 2014a). IP-GDGTs, except for IP-OH-GDGTs, occurred as acyclic to pentacyclic compounds. However, they could not be quantified individually, due to co-elution of different GDGT isomers with the same head group (Wörmer et al., 2013). IP-OH-GDGTs occurred only as acyclic to dicyclic compounds. The most abundant IP-GDGTs in all samples were 1G-GDGTs with a relative abundance of always >$50\,\%$ of total IP-GDGTs. Other abundant IP-GDGTs in the superficial layers of the brine-seawater interface were 2G-OH- and HPH-GDGTs comprising 10 and $9\,\%$ of the total IP-GDGT pool, respectively. In the deeper brine samples, 1G-GDGTs account for more than $92\,\%$, whereas the minor GDGTs were always below $3.3\,\%$. In the first 2m of the sediment column, 2G-GDGTs showed a relative abundance ranging from 6 and $26\,\%$, whereas 2G-OH- and 2G-2OH-GDGTs showed relative abundances between 1 and $11\,\%$ of total IP-GDGTs. PH- and HPH-GDGTs were only detected in the first 23 cmbsf, representing more than $20\,\%$ of total IP-GDGTs in some samples. Below 184 cmbsf 1G-GDGTs were the only detected intact tetraethers beside minor amounts of 1G-BDGTs.

IP-ARs were present as 1G-, 2G-, phosphatidyl-glycerol- (PG-), glycerol-pentose-

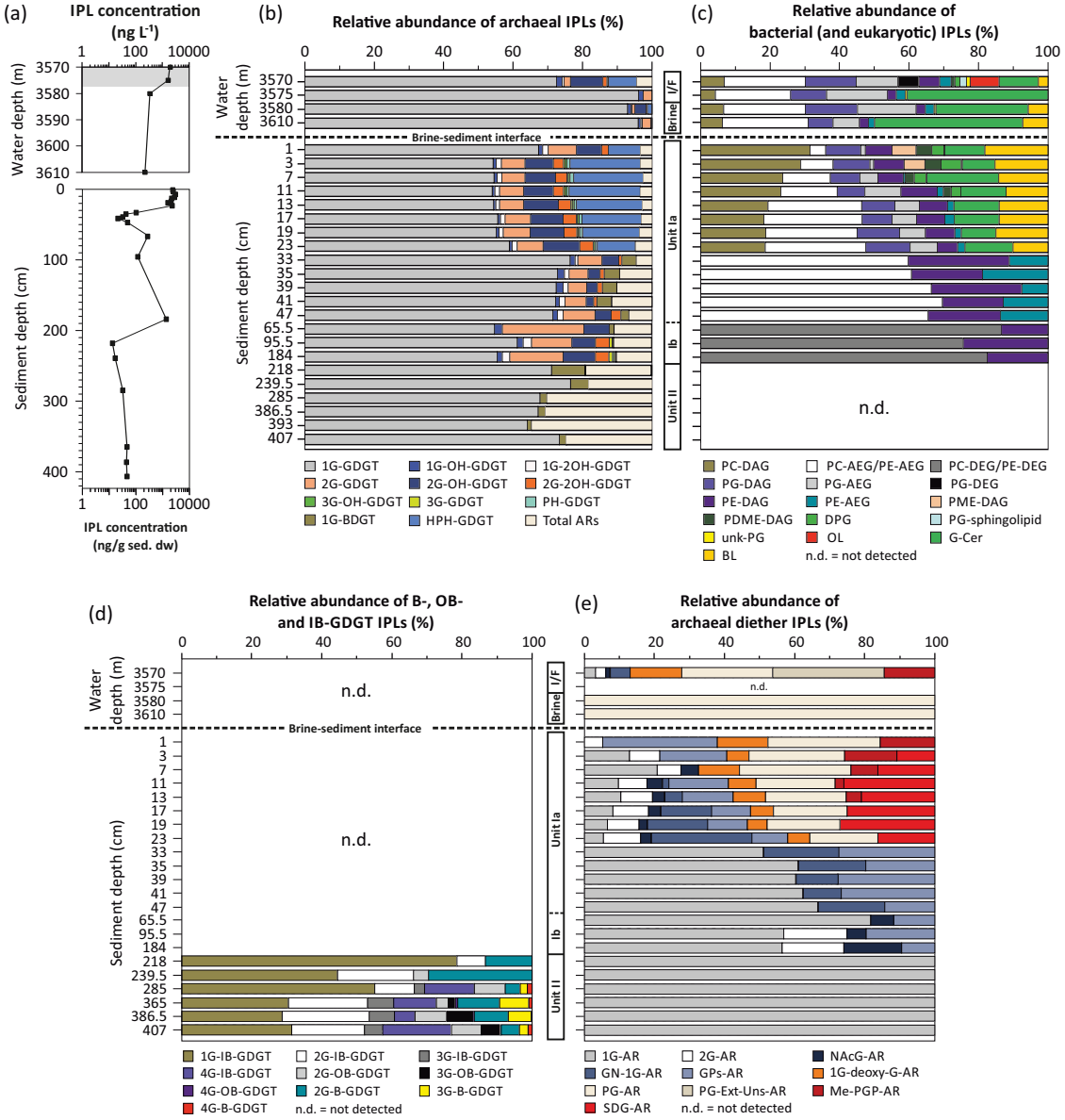

Figure VI.4. Distribution of intact polar lipids in samples from the brine-seawater interface (I/F), the brine and sediments of the Discovery Basin. (a) Total IPL concentration, (b) detailed distribution of archaeal IPLs, (c) detailed distribution of bacterial (and eukaryotic) IPLs, (d) detailed distribution of intact B-, OB- and IB-GDGTs. Note that sugars moieties of intact B-, OB- and IB-GDGTs include several derivatives of regular sugars, i.e., methoxylated and deoxylated sugars. (e) Relative abundances of intact archaeal diether lipids separately.

(GPs-), N-acetylglucosamine- (NAcG-), PG-extended-unsaturated- (Uns-Ext-), monoglycosyl-deoxy-glycosyl- (1G-deoxy-G-), (N-acetyl)-glucosamine-monoglycosyl- (GN-1G-), methylated-phosphatidylglycerolphosphate- (Me-PGP-) and sulphated diglycosyl (SDG-) ARs (for identification see supplementary information). In the upper brine-seawater interface sample, the most abundant IP-ARs were PG-Ext-Uns-, PG-, 2G-deoxy and Me-PGP-AR with 31.9, 25.9, 14.9 and 14.3 % of total IP-ARs, respectively (Figure VI.4b and e). Minor components were GN-1G-, 1G-, 2G- and NAcG-AR. In the sample from

3575 mbsl, no IP-ARs were detected, and in the other two brine water samples, only PG-AR was present. In the first 23 cm of the sediment, the diversity was as high as in the uppermost water column sample but the distribution considerably differed. Here, the major IP-ARs were PG- and GPs-AR, accounting for 32 % each of total IP-ARs in the surface sample. Other prominent IP-ARs within the first 23 cm of the sediment were 1G-deoxy-G-, 1G- and 2G-AR. While PG-Ext-Uns-AR was not detected in the sediments, Me-PGP-AR, which was also present in the sample from the upper brine-seawater interface, disappeared below 13 cm sediment depth. SDG-AR was first detected at 3 cm, NAcG-AR at 7 cm and GN-1G at 11 cm sediment depth. When detected, SDG- and GN-1G-AR represented major IP-ARs. For example, SDG-AR accounted for 27 % of total IP-ARs in the sample from 19 cmbsf and GN-1G-AR for 29 % in the sample from 23 cmbsf. The diversity decreased towards greater depths and 1G-AR was always the major IP-AR with more that 50 % of total IP-ARs. GPs-, and GN-1G-AR were detected between 33 and 65.5 cmbsf, whereas between 65.5 and 184 cmbsf, 2G- and NAcG-AR were also present. In the deepest samples from 218 to 407 cmbsf, the only detected IP diether was 1G-AR.

VI.3.3.2. Distribution of bacterial IPLs

Bacterial IPLs were detected as diacylglycerol (DAG) phosphatidylcholine (PC), phosphatidyl-(N,N)-dimethylethanolamine (PDME), phosphatidyl-(N)-methylethanolamine (PME), phosphatidylethanolamine (PE) and phosphatidylglycerol (PG). Acyletherglycerol (AEG) were present as PC, PG and PE, whereas dietherglycerols were only found with the polar head groups PC and PG. Other detected IPL classes included diphosphatidylglycerol (DPG), betaine lipids (BL), PG-sphingosines, glycerol ceramides (G-Cer) and ornithine lipids (OL; Figure VI.4c). The structure of G-Cer, which has not been reported in the literature, was tentatively identified based on accurate mass in MS^1 and fragmentation behaviour in MS^2.

The most abundant bacterial IPLs in the upper brine-seawater interface sample were PC-AEGs with 23 %, PG-DAGs with 15 %, PG-AEGs with 12 % and G-Cer with 11 % of total bacterial IPLs. Other detected IPLs included OLs, PC-DAGs, PG-DEGs, PE-DAGs, PE-AEGs and BLs with relative abundances between 3 and 8 %. Minor bacterial IPLs (<2 % relative abundance) were PG-sphingosines, DPGs, PDME-DAGs and PGs with unknown (unk) core lipid structure. In all deeper water column samples, the diversity of bacterial IPLs was comparably low. The most abundant in the sample from 3575 mbsl were G-Cer, PC-AEGs, PG-AEGs, and PG-DAGs. Minor bacterial IPLs in the same sample included PC-DAGs, PE-AEGs and unk PGs, contributing less than 5 % to the total bacterial IPL pool. This distribution remained relatively constant between the

samples from the lower layers of the brine-seawater interface and brine water. In the sediments, the distribution of bacterial IPLs differed from that of the water column. The major bacterial IPLs in the surface sediment sample were PC-DAGs, BLs, G-Cer and PG-DAGs contributing 31 %, 18 %, 12 % and 10 % to the total bacterial IPL pool, respectively. Other important bacterial IPLs were PE-DAGs, PME-DAGs, PDME-DAGs, DPGs, PC- and PG-AEGs with less than 10 % of total bacterial IPLs. Major trends in their relative abundance were the increase in relative abundance of AEGs lipids, particularly PC-AEG, whereas the relative abundance of most DAG lipids, such as PC-, PME- and PDME-DAGs, decreased within the first 23 cm of the sediment column. Below this depth, most common bacterial IPLs disappeared. PC-AEGs, PG-DAGs and PE-AEGs were the only detected bacterial IPLs between 33 and 47 cmbsf. Between 65.5 and 184 cmbsf, only PE-DEGs and PG-DAGs were detected, whereas in the samples below 184 cmbsf (Unit II), bacterial phospholipids were absent and the only bacterial IPL found were the branched and isoprenoid/branched tetraether (see below).

The structural composition of fatty acids from P-DAGs and P-AEGs as well as BLs were dominated by aliphatic tails with 15 to 18 carbons and they were either fully saturated or monounsaturated (Supp. Table VI.1). The combination of fatty acids included odd and even, even and even, and odd and odd carbon numbers. In the first 50 cm of the sediment, PC-DAGs additionally contained low amounts of $C_{22:6}$ and $C_{20:5}$. Dominant P-DEG core lipids were saturated and monounsaturated C_{30} to C_{32} compounds in the superficial brine-seawater interface and saturated C_{30} to C_{32} compounds in lithological Unit II.

VI.3.3.3. Intact branched and isoprenoid/branched tetraether IPLs

Intact polar hybrid isoprenoid/branched (IB-), overly branched (OB-) and branched (B-) GDGTs (for mass spectral identification see supplementary information) were detected the six samples from below 184 cmbsf (Unit II, Figure VI.4d). They occurred as mono- to tetraglycosidic IPLs, including methoxylated and deoxylated derivatives (Figure VI.4 and Supp. Fig. VI.6). Generally, the diversity increased with depth. Three IPL species were detected in the sample from 218 cm sediment depth, which were 1G- and 2G-IB-GDGTs as well as 2G-B-GDGTs, with 1G-IB-GDGT being dominant (79 % relative abundance). The highest diversity occurred in the three deepest samples, where ten different IPL species were detected. Here, 1G- to 4G-IB-GDGTs, 2G- to 4G-OB-GDGTs and 2G- to 4G-B-GDGTs were present. The intact IB-GDGTs represented the largest fraction within this IPL group.

VI.3.4. Distribution of isoprenoid ether core lipids

Although core lipids are generally associated with degradation products of archaeal intact polar lipids (Schouten et al., 2013a), they are frequently found in cultured archaea (e.g., Elling et al., 2014; Meador et al., 2014b; Yoshinaga et al., 2015a). Thus, the absence of a head group might not necessarily mean that core lipids are not structural components, although their function in the membranes has not yet been systematically studied.

The concentration profile of total core lipids decreased exponentially in the water column, from $7.2\,\mu g\,l^{-1}$ in the uppermost brine-seawater interface to less than $0.5\,\mu g\,l^{-1}$ in the deepest brine water sample (Figure VI.5c). In the sediments, concentrations showed a similar trend as the total IPLs, with highest concentrations in the first 23 cmbsf and between 59 and 184 cmbsf, and lowest concentrations between 33 and 47 cm and below 184 cmbsf.

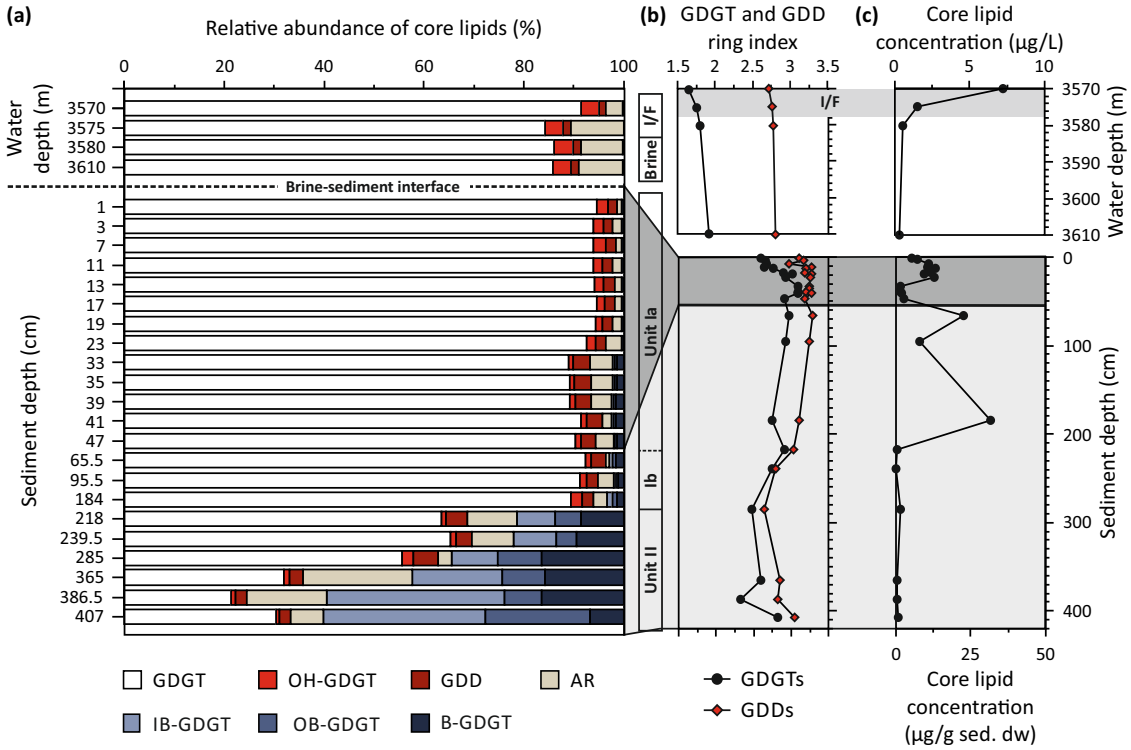

Figure VI.5. (a) Relative abundances of di- and tetraether core lipids, (b) ring indices of core GDGTs and GDDs and (c) total core lipid concentration in samples from the brine-seawater interface, the brine and sediments of the Discovery Basin.

In the water column samples and in the first two-meter of the sediments, isoprenoid GDGTs represented the largest fraction with more than $80\,\%$ of total core lipids (Figure VI.5a). OH-GDGTs and GDDs represented minor components at all depths examined. Archaeal diethers (ARs), including archaeol and its extended (ext), unsaturated (uns), a combination of extended and unsaturated (Ext-Uns), hydroxylated (OH) and methoxylated (MeO) analogues, were abundant components in the water column samples, par-

ticularly in the three samples from the brine water and in the sediments below 184 cm, where they comprised >8 % of total core lipids. The concentration of total archaeal core ARs (Figure VI.6d) decreased almost linearly from the superficial brine-seawater interface to upper brine sample and stayed low through the brine from more than 200 to 20 ng l^{-1}. In the sediments, two concentration maxima were observed. The first occurred at 23 cmbsf with 319 ng g^{-1} sed. dw and the second at 184 cmbsf with 672 ng g^{-1}. Below 184 cm sediment depth, concentrations declined to ten times lower values without significant changes to the bottom of the core. IB-GDGT core lipids were only detected in trace amounts in the water column samples, whereas OB- and B-GDGTs were absent. In the first two meters of the sediment, all three branched GDGT species were detected but they represented minor components. Below 184 cmbsf, the core lipid distribution is substantially different. Here, IB-, OB- and B-GDGTs showed highest relative abundances, which increased with increasing depth. Whereas their sum contributes 21 % to the total core lipid pool in the sample from 218 cmbsf, they comprise more than 60 % in the deepest sample from 407 cmbsf.

Cyclization of GDGTs showed two major trends indicated by the ring index (Eq. 1). Cyclization was low (ring index of 1.7-1.9) and slightly increased with depth in the water column samples and comparatively higher in the sediments (ring index of 2.3-3.3; Figure VI.5b). Whereas an increase in cyclization was observed in the first 40 cm of the sediment, cyclization showed an overall decreasing trend downcore. GDD cyclization was generally higher than GDGT cyclization and differences between the brine and the sediments are much less pronounced (see Figure VI.5b).

The detailed distribution of core ARs revealed changes between water column, surface and deep sediments (Figure VI.6). Saturated AR was the most abundant core ARs in all samples with relative abundances >35 %. MeO-AR was detected in all samples. The highest relative abundance of MeO-AR occurred in the samples from the brine water, where it contributes up to 40 % to the total core AR pool. In the sediments, the abundance of MeO-AR is slightly lower (20 %) and it almost disappeared in the deepest sediment samples. In the superficial brine-seawater interface, Uns- and Ext-Uns-ARs were abundant components with 11 and 18 % of total core ARs, respectively, whereas they are only minor compounds in the deeper brine samples (Figure VI.6a). In the top 24 cm of the sediment column, uns-ARs are major contributors to the total AR pool (25-30 %). OH-ARs, which include two isomers and a monounsaturated species, showed relatively low relative abundances in the samples from the water column and first two meters of the sediment. In the deeper sediment samples (212-411 cmbsf), their abundance increased reaching values between 9 and 25 %. Ext-AR represents only a minor component in most samples, but Ext- and Ext-Uns-ARs increased in relative abundance

in the deepest sediments samples (365-407 cmbsf), comprising 6 and 21 % of total core diethers, respectively (Figure VI.6a).

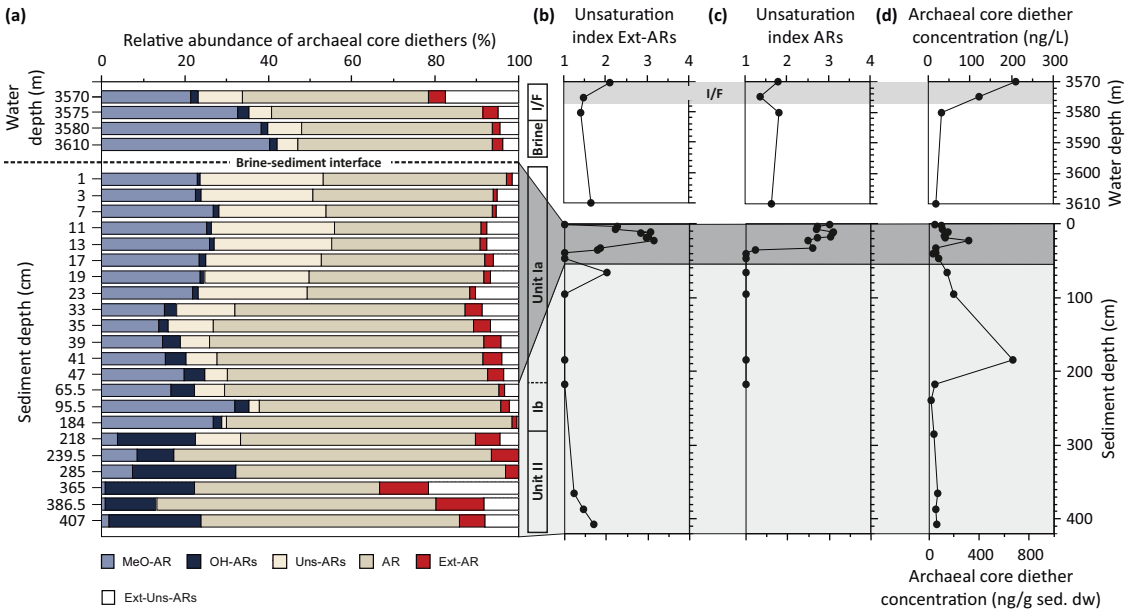

Figure VI.6. (a) Relative abundances of archaeal diether core lipids, (b) unsaturation index of extended archaeols (Ext-ARs), (c) unsaturation index of ARs, and (d) total archaeal core diether concentration in samples from the brine-seawater interface, the brine and sediments of the Discovery Basin.

The degree of unsaturation (unsaturation index; Eq. 2) of core Ext-ARs decreased with depth in the water column samples (Figure VI.6b). Whereas the index is higher than 2.0 in the brine-seawater interface, it is 1.5 in the brine samples. In the sediments, the unsaturation index showed maximum values (around 3.0) between 11 and 19 cmbsf. Lowest values of 1.0 occurred in the surface sediment sample and between 95.5 and 184 cmbsf. In the deepest three sediment samples, the unsaturation index of core Ext-ARs slightly increased again to 1.7. The unsaturation index of core ARs showed a similar range of 1.8 in the water column. In the sediments, between 1 and 35 cmbsf, the unsaturation index of ARs showed highest values around 3.0 and decreased towards 1.0 below this depth (Figure VI.6c).

VI.3.5. Carbon isotopes of ether lipids

The ether cleavage products of various isolated intact polar and core lipid groups from selected samples were analyzed for their stable carbon isotopic composition (δ^{13}C). Samples included the brine-seawater interface sample from 3570 mbsl and six sediment samples covering the complete investigated core interval (Figure VI.7 and Supp. Tables VI.2 and VI.3). Archaeal core lipids that could be isolated from the TLEs included AR, GDGTs, GDDs and OH-GDGTs. The δ^{13}C of archaeal IPLs could only be determined

from IP-GDGT derived biphytanes (bp). Isolated species for δ^{13}C analysis were 1G- and 2G-GDGTs as well as their hydroxylated analogues. HPH-GDGTs could not be separately isolated as they co-elute with 2G-2OH-GDGTs with the used semi-preparative HPLC protocol. The δ^{13}C determination of AR was obtained from phytane, whereas GDDs and GDGT species were obtained from average δ^{13}C values of acyclic to tricyclic biphytanes (Supp. Tables VI.2 and VI.3). Similarly, δ^{13}C values for B-, OB- and IB-GDGT core and intact lipids were determined. For the B-GDGT stable carbon isotopic composition, the average δ^{13}C value of octacosanyl chains containing two and three methylations was determined. For δ^{13}C values representative for OB-GDGTs, octacosanyl chains containing four to six methylations as well as co-eluting isomers were averaged. The ether cleavage products of IB-GDGTs only revealed one peak in the GC chromatogram that could be clearly assigned to a triacontanyl chain as basic structure with five methylations, which is likely composed of coupled phytane and iso-pentadecane (Schouten et al., 2000; Liu et al., 2012c).

In the superficial brine-seawater interface, the bp-0 of core GDGTs was depleted in ^{13}C compared to the sediments with δ^{13}C values of $-31.4\,‰$ (Figure VI.7. In the sediments, δ^{13}C values of GDGTs showed little variability throughout the sediment core, ranging from -23.3 to $-17.7\,‰$, which were similar to OH-GDGTs and GDDs. The δ^{13}C values of AR-derived phytanes ranged from -37.2 to $-23.4\,‰$ and they became more depleted with increasing sediment depth.

The B-, OB- and IB-GDGT core lipid derived hydrocarbons showed δ^{13}C value between -36.6 and $-25.2\,‰$ and they generally became more enriched in ^{13}C with increasing sediment depth (Figure VI.7). In contrast to the archaeal GDGTs, the compounds released from these different precursors had an offset in their isotopic composition. For example, in the sample from 285 cmbsf, δ^{13}C values of hydrocarbons released from OB-GDGTs showed values of $-36.6\,‰$, whereas B-GDGT derived compounds were more enriched in 13C with values of $-25.2\,‰$. The hydrocarbons released from intact B-, OB- and IB-GDGTs present only in depths >184 cmbsf (Figure VI.4) revealed similar isotopic compositions for all three precursors. At 285 cm sediment depth δ^{13}C values were more depleted in ^{13}C ($-33\,‰$) than in the deeper sample from 393 cmbsf where values of $-27\,‰$ were observed.

VI.4. Discussion

VI.4.1. Geochemical evidences for sediments spanning pre-basin to post-brine conditions

The obtained pore water profiles of Mg^{2+}, Ca^{2+} and Cl^{-} are in good agreement with those reported in the literature and show that the brine solution is penetrating into the

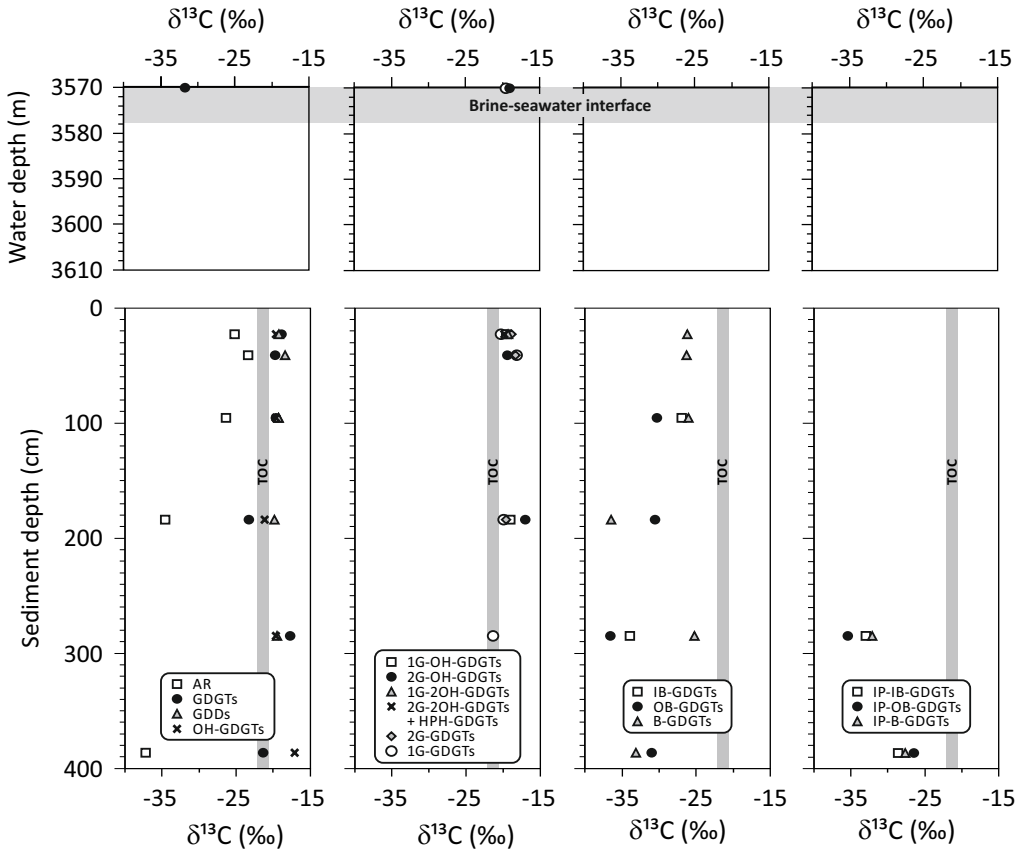

Figure VI.7. Carbon isotopic composition of core and intact di- and tetraether lipid-cleavage products in selected samples from the Discovery brine-seawater interface and the sediments underlying the brine pool. The δ^{13}C values of AR were obtained from phytane. The carbon isotopic composition of isoprenoid and branched GDGT compounds were obtained from average values of biphytanes containing 0 to 3 rings and non-isoprenoid alkyl chains, respectively. Similarly, δ^{13}C values were generated for the GDDs.

sediments by advection and diffusion (Wallmann et al., 1997; Wallmann et al., 2002). Interestingly, absolute concentrations of Mg^{2+} and Cl^{-} were ca. 1 M higher higher than those reported by Wallmann et al. (1997). This observation suggests that the brine was recently refilled with a $MgCl_2$-rich solution between 1993 and 2011, when the samples were taken. To increase the $MgCl_2$ concentration, inflow of brine solution must be higher than advection and diffusion into the sediments. Since the Discovery Basin was formed by residual brine that migrated along faults and entered the basin at its flanks (Wallmann et al., 1997), tectonic activity in this region potentially resulted in the increased inflow by opening new paths. The similar concentrations between our measurements and the ones reported by Wallmann et al. (1997) in greater depth can be explained by an increase of density-driven convection.

Surface enrichment of TOC (lithological Unit I) results from enhanced preservation of organic matter due to anoxia in the overlying brine (De Lange and ten Haven, 1983; Wallmann et al., 2002). The combination of anoxic conditions together with the high

salt concentration additionally reduces benthic microbial activity and therefore the degradation of deposited organic material. Wallmann et al. (1997) and Wallmann et al. (2002) suggested based on transport modeling experiments and sedimentation rates that the Discovery Basin was filled with a $MgCl_2$-rich brine only since the past ca. 700-2000 yr and by assuming a sedimentation rate of 6 cm ky^{-1} (Wallmann et al., 2002), only the top 12 cm represent brine sediments. Dark-colored anoxic sediments were observed down to ca. 2 mbsf (Figure VI.3, indicating that the basin was anoxic before the brine formation as previously shown by Wallmann et al. (2002). The low TOC content in lithological Unit II indicates oxygenated sediments deposited under oligotrophic conditions, like the present situation for the Eastern Mediterranean (e.g., Fontugne and Calvert, 1992). The drastic change in sedimentology between the two major lithologies recorded in the Discovery Basin has been interpreted as a result of a sudden collapse that formed the depression, followed by progressive development of basin anoxia (Fusi et al., 1996). The sedimentary features, such as sediment deformation and local re-sedimentation between 50 and 200 cmbsf indicate sliding from the steep side walls of the basin delivering sediments resulting in high sedimentation rates during this interval, similar to other brine pools in the Eastern Mediterranean (e.g., Camerlenghi and McCoy, 1990). Other sediment cores from the Discovery Basin (Fusi et al., 1996; Wallmann et al., 2002) showed distinct TOC maxima within the anoxic sediment (ca. 7 wt%), which were associated with the deposition of sapropels. We have not observed such pronounced TOC contents in our core, although smear slide analysis revealed a composition that matches the description of sapropels in two discrete layers in the top 50 cm. Constant $\delta^{13}C_{TOC}$ values of ca. -21 ‰ through the whole sediment core indicated a major marine phytoplanktonic origin of the deposited organic matter. These observations indicate that the Discovery Basin has been a highly dynamic system since its formation. Figure VI.8 summarizes our hypothesis concerning the development of the Discovery basin from pre-basin to post-brine conditions.

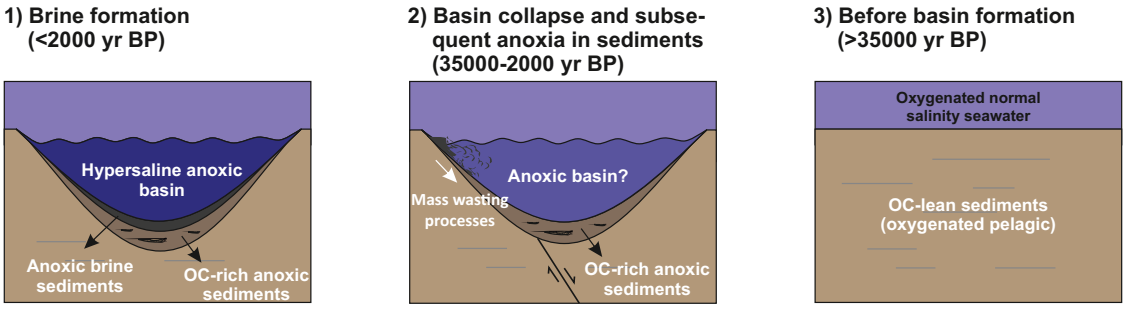

Figure VI.8. Sketch illustrating the development of the Discovery Basin from before the basin collapse to modern conditions.

VI.4.2. Indications of microbial biomass in Discovery Basin

Total IPL concentration was considerably higher in the brine-seawater interface than in the underlying brine. This is in line with DNA-based studies from the Discovery Basin as well as other deep-sea brines (Hallsworth et al., 2007; Yakimov et al., 2007) and suggests inhibition of microbial life in the brine body of the Discovery Basin. Most halophilic microorganisms studied in the laboratory can grow under NaCl concentrations that approach saturation but not under high $MgCl_2$ concentrations (Oren, 2002b). The record holder so far is the archaeon Halobacterium sodomense, which grows fairly at 2.5 M $MgCl_2$, but requires 0.5 M NaCl to compensate the chaotropic effects of magnesium (Oren, 1983). Hallsworth et al. (2007) proposed that the limit for life in $MgCl_2$-rich systems is 2.3 M in the absence of compensating kosmotropes, such as sodium and sulfates. These authors attributed the recovery of genetic biomarkers in the Discovery Basin at $MgCl_2$ concentrations above 2.3 M to preserved dead cells. Thus far, laboratory experiments to grow microbes under *in situ* salinities of the Discovery Basin have failed, indicating that *in situ* conditions do not favor microbial life as we currently know it (Hallsworth et al., 2007; Sass et al., 2008). Although indications for metabolically active microbes at concentrations above 3 M in the Kryos Basin were reported recently (Yakimov et al., 2015), these concentrations are still well below those encountered in the Discovery Basin brine. Based on these studies, it can be assumed that life in the Discovery Basin is limited to the upper interface whereas the brine body and underlying sediments appear inhospitable for microbial life. Therefore, we have considered the life markers (either lipids or cells) that we detected outside the upper interface as records of past microbial communities.

Total IPL and cell concentrations measured in sediments revealed similar downcore profiles, with a decreasing trend with increasing sediment depth. Importantly, calculated intracellular lipid content per cell falls into or is close to the hypothetic range of 1.4 to 6.5 fg IPL per cell for spherical cells with 0.5 to 1 μm diameter (Lipp et al., 2008) for most samples. This suggests that cells as well as IPLs are similarly well preserved in the sediments, with the exception of samples collected immediately below the surface sediments and at the transition between Unit I and II (Figure VI.3). Higher IPL content in cells observed in these samples likely indicates preservation of IPLs compared to cells, i.e. reflects accumulation of extracellular IPLs (e.g., Xie et al., 2013). In the following sections we provide a detailed characterization of lipids detected at the seawater-brine interface in comparison with the few DNA-based studies that have been performed in the Discovery Basin (van der Wielen et al., 2005; Hallsworth et al., 2007). Based on the high preservation potential of cells both in brine and supposedly under anoxic conditions of Unit I, we proposed to use microbial lipids in the context of the hypothesized lithological

model for the development of the basin (Figure VI.8). Finally, we interpreted the sources of microbial lipids from Unit II to infer pre-basin environmental conditions.

VI.4.3. Sources of IPLs at the interface and in the brine

VI.4.3.1. Evidence for ammonia-oxidizing archaea (AOA), haloarchaea and methanogens

DNA-based studies retrieved a high number of Marine Group 1 sequences, which are affiliated with the recently proposed phylum *Thaumarchaeota* (Brochier-Armanet et al., 2008; Spang et al., 2010), in the superficial brine-seawater interface (van der Wielen et al., 2005; Hallsworth et al., 2007). Intact GDGTs in this layer likely originate from this thaumarchaeal community since the distribution is highly similar to that found in AOA cultures (Schouten et al., 2008; Pitcher et al., 2011a; Elling et al., 2014). For example, we detected the same headgroup types, i.e., 1G-GDGT, 2G-GDGT and HPH-GDGT, as well as 1G- and 2G-GDGTs with monohydroxylated isoprenoid core structures, in similar proportions as reported by Elling et al. (2014). The relatively high abundance of labile HPH-GDGTs further indicates growing and metabolically active cells rather than communities at steady state (Elling et al., 2014), even though a potential origin from the overlying water column and deposition with sinking debris cannot be excluded (e.g., La Cono et al., 2011; Yakimov et al., 2015). The measured stable carbon isotopic composition of the intact GDGT derived biphytanes of ca. $-20\,‰$ (Figure VI.7) supports a thaumarchaeal origin, assuming typical deep ocean $\delta^{13}C_{DIC}$ of ca. $0\,‰$ (e.g., Quay et al., 2003), as cultured AOA have been shown to have a carbon isotopic fractionation of $-20\,‰$ between DIC and biphytanes (Könneke et al., 2012). Moreover, we detected the methoxylated AR, an intact lipid that was first described by Elling et al. (2014) in the thaumarchaeon *Nitrosopumilus maritimus* and that might be specific for marine AOA. Thus far, MeO-AR has not been reported from the natural environment and we attribute the source organisms in our samples to AOA.

Ammonium, required as electron acceptor for AOA (Könneke et al., 2005), was shown to be present at high concentrations in many deep-sea brine pools (De Lange et al., 1990b; Van Cappellen et al., 1998; Daffonchio et al., 2006) and concentration profiles were interpreted to reflect biologically mediated redox cycling, further supporting actively growing AOA at deep-sea brine-seawater interfaces. In the deeper interface sample and in the brine, no HPH-GDGTs were detected and overall abundance and diversity of intact GDGTs was low suggesting that the thaumarchaeal community is restricted to the surface layers of the interface where dissolved oxygen is still present and salinity has not reached brine concentration. The oxygen requirement for growth of AOA has not been systematically studied yet, but there is circumstantial evidence based on lipids

as well as thaumarchaeal 16S rDNA and amoA (ammonia monooxygenase subunit A) gene biomarkers from various environments that these microbes are abundant at marine oxyclines (Coolen et al., 2007; Wakeham et al., 2007; Schouten et al., 2012; Basse et al., 2014; Xie et al., 2014). This suggests relatively low oxygen requirements for environmental AOA to perform nitrification as has been shown for the cultured strain *N. maritimus* (Martens-Habbena et al., 2009). The oxygen limitation in the brine-seawater interface as well as the high specific affinity for reduced nitrogen of AOA (Martens-Habbena et al., 2009) additionally favors AOA over ammonia-oxidizing bacteria (AOB), which were found to be absent in brine-seawater interfaces at other locations (Yakimov et al., 2007; Ngugi et al., 2015). Furthermore, the study from Ngugi et al. (2015) revealed specific adaptations of a halotolerant thaumarchaeon in the interfaces of Red Sea brine pools enabling these microbes to cope with osmotic stress. The clear predominance of thaumarchaeal lipids in the Discovery Basin interface suggests ammonium consumption by AOA via oxidation as an important microbially mediated metabolic process in these layers.

In our samples from the brine-seawater interface and the brine, the ring distribution of the core GDGTs differed significantly from the IPL signal. The core GDGTs were mainly composed of the acyclic isomer, which is also indicated by the low ring index (see Figure VI.5), whereas for HPH-, 1G- and 2G-GDGT cyclic compounds, including crenarchaeol, a GDGT containing four cyclopentane and one cyclohexane ring, occurred in significant amounts (data for IPLs not shown). Additionally, the GDGT core lipid derived acyclic biphytane showed a more negative stable carbon isotope signature than the biphytanes derived from the intact GDGTs (see Supp. Tables VI.2 and VI.3). These observations suggest that a substantial fraction of the core GDGTs is fueled by a source other than the degradation products of IPLs from AOA. Other archaea detected by 16S rRNA and mRNA gene sequences analyses in the Discovery Basin, particularly in the upper interface, are *Halobacteriales*, *Methanohalophilus* and MSBL1 (van der Wielen et al., 2005; Hallsworth et al., 2007). Both *Halobacteriales* and *Methanohalophilus* are not known to synthesize GDGTs (e.g., Kates, 1993b; Koga and Morii, 2005), suggesting that acyclic core GDGTs in the brine-seawater interface of the Discovery Basin could be sourced by MSBL1 archaea. Even though there is no cultured representative of MSBL1 members, on the basis of their phylogenetic relatedness to methanogens it was suggested that members of this group are involved in methanogenesis at high salinities (van der Wielen et al., 2005). Although the connection of MSBL1 to methanogenesis requires further experimental validation, we suggest that at least some of IP-ARs are in fact produced by methanogens. *Methanohalophilus* species (Koga et al., 1993b; Koga and Morii, 2005) are known to synthesize similar lipids as the detected 1G-GN- and NAcG-AR, and we considered members of this genus as likely sources of these lipids. In addition,

Methanohalophilus that belong to the order *Methanosarcinales* do not produce GDGTs, but are known to produce abundant OH-ARs (Koga et al., 1993b). Thus the presence of 1G-GN- and NAcG-AR as well as core OH-AR may indicate activity of *Methanohalophilus* in the anoxic portions of the seawater-brine interface of the Discovery Basin.

Beside the activity of AOA and methanogens, halophilic archaea have been shown to inhabit the brine-seawater interface in a narrow depth interval within this layer as suggested by DNA analysis (Hallsworth et al., 2007). Correspondingly, we detected specific IPLs such as Me-PGP-AR and PG-Ext-AR, which are diagnostic IPLs of extremely halophilic archaea (e.g., Kushwaha et al., 1982; Kates, 1993a). Archaeol-based core lipids additionally provide a chemotaxonomic link to haloarchaea. The combination of Ext-AR (C25) and Uns-ARs is a common lipid feature of most cultured halophiles belonging to *Halobacteriales* (de Rosa et al., 1982; De Rosa et al., 1983; Nichols and Franzmann, 1992; Kamekura and Kates, 1999; Gibson et al., 2005). It was further shown that the degree of unsaturation appears to be involved in membrane lipid adaptation to high salinities (Dawson et al., 2012). Based on the relative abundance of intact polar and core ARs, our data suggest that haloarchaea dominate over methanogens at the brine-seawater interface. However, the higher abundance of GDGTs from AOA relative to other archaeal lipids clearly indicated *Thaumarchaeota* as the dominant archaea in this environment. In summary, we suggest that archaea within the Discovery Basin interface are involved in nitrogen and carbon cycling.

VI.4.3.2. Evidence for bacterial heterotrophy and sulfate reduction

Most bacterial and eukaryotic IPLs, especially diacyl glycerol phospholipids, can have multiple sources and thus only partly be assigned to specific organisms. In contrast to ether-linked archaeal lipids, extracellular IPLs with fatty acid side chains are rapidly degraded (White et al., 1979; Harvey et al., 1986; Logemann et al., 2011), although degradation kinetics might differ between IPLs with different head groups. Thus, sources for P-DAGs from the overlying water column seem unlikely. This is also confirmed by the absence of glycosidic DAG lipids, which are typically the dominant planktonic IPLs (e.g., Van Mooy and Fredricks, 2010). An eukaryotic source of IPLs at the Discovery Basin cannot be completely excluded, since diverse assemblages of mainly unicellular protist plankton were reported for some of the Eastern Mediterranean deep brine basin interfaces (Alexander et al., 2009; Edgcomb et al., 2009; Stock et al., 2012; Filker et al., 2013). However, the fatty acid distribution of IPLs was dominated by saturated and C_{15} to C_{18} monounsaturated compounds (Supp. Table VI.1) and further suggests bacteria rather than eukaryotes as their major source at the brine-seawater interface. Eukaryotes typically contain significant proportions of polyunsaturated fatty acids (Brett and Müller-Navarra,

1997), . It has further been shown that dense populations of heterotrophic microorganisms inhabit brine-seawater interfaces, including the Discovery Basin interface (van der Wielen et al., 2005), likely reflecting the accumulation of organic matter in this effective particle trap (LaRock et al., 1979). For instance, PG- and PE-DAGs have long been shown to dominate the membranes of cultivated strains of marine heterotrophic bacteria (e.g., Oliver and Colwell, 1973), and PME and PDME headgroups have been attributed to heterotrophic *Gammaproteobacteria*, *Alphaproteobacteria* or *Bacteroidetes* in the water column of the Black Sea (Schubotz et al., 2009) or as in oil-impregnated sediments in the Gulf of Mexico (Schubotz et al., 2011). Moreover, PG and PE appeared to be derived primarily from heterotrophic bacteria in the water column of the eastern subtropical South Pacific (Van Mooy and Fredricks, 2010). With increasing salt concentration, bacteria tend to increase the amount of the negatively charged headgroups PG and DPG in their membranes at the expense of neutrally charged species, such as PE and PC (Vreeland, 1987; Russell, 1989; Ventosa et al., 1998; Oren, 2002a). However, PG and DPG contributed ca. 30 % to the total bacterial IPL pool in the superficial brine-seawater interface sample in the Discovery Basin, which is similar to other non-hypersaline environments, such as tidal flat sediment (Seidel et al., 2012).

Phospholipids containing mixed ester/ether and diether lipids are only known from anaerobic and microaerophilic bacteria, including thermophiles (e.g., Langworthy et al., 1983; Huber et al., 1992) as well as some sulfate reducing bacteria (SRB), which typically synthesize IPLs with mixed DAG, AEG and DEG core lipids (Rütters et al., 2001; Sturt et al., 2004). The detection of AEG and DEG-based IPLs have been attributed to SRB in anoxic environments, ranging from cold seeps (e.g., Sturt et al., 2004; Rossel et al., 2008), water column (Schubotz et al., 2009), tidal flats (Seidel et al., 2012) to hydrothermal vents (Bradley et al., 2009). The presence of AEG and DEG-based IPLs in the brine-seawater interface of the Discovery Basin is consistent with the detection of SRB in DNA-based studies and sulfate reduction rates measured in the interface as well as in the brine (van der Wielen et al., 2005; Hallsworth et al., 2007). In addition, we detected ornithine lipids, which have been shown to be major lipids in SRB (Makula and Finnerty, 1975; Seidel et al., 2012) and have been associated with sulfate reducers in the anoxic water column of the Black Sea (Schubotz et al., 2009). This further supports the presence of abundant SRB in the Discovery Basin interface.

Other lipids found at the interface included betaine lipids (BL) and ceramides. Betaine lipids were thought to be present only in eukaryotes (Dembitsky, 1996), but have been recognized to also be present in bacteria (Benning et al., 1995; Geiger et al., 1999; López-Lara et al., 2003; Geiger et al., 2010). In samples from the surface ocean, BLs have been shown to substitute phospholipids, especially PC, under phosphate limitation (Van Mooy et al., 2009) and BLs were mainly attributed to eukaryotic algae sources (Kato et al.,

1996; Van Mooy et al., 2009). However, based on detection of BLs below the photic and within the anoxic zone in the Black Sea water column and a fatty acid composition that is typical for bacteria, Schubotz et al. (2009) suggested these lipids to be additionally of anaerobic bacterial origin and the detection in our samples supports this hypothesis, although an allochthonous origin cannot be excluded. Moreover, betaine lipids have been found abundantly in anoxic and sulfate-reducing sediments of cold seeps (Rossel et al., 2011; Schubotz et al., 2011; Yoshinaga et al., 2015a). Sphingolipids (ceramides) are commonly distributed among some of the bacteria and almost all eukaryotic organisms (Kawahara et al., 1999). Glycosphingolipids from the surface ocean have been shown to be a biomarker for viral infection of natural phytoplankton assemblages (Vardi et al., 2009) and the detection of the ceramide analog in the anoxic water from the Black Sea has been associated with anaerobic bacteria (Schubotz et al., 2009). The ceramides that we tentatively identified contained a glycerol instead of glycosyl headgroup and the detection in our samples indicates that they might be part in the haloadaptation of certain bacteria (see above).

In contrast to the archaeal IPLs, most bacterial lipids penetrated into the brine body, which is unexpected since archaea are generally better adapted to more extreme conditions, i.e., higher salt concentrations (e.g., Valentine, 2007). Additionally, Hallsworth et al. (2007) found only archaeal sequences in the deeper interface layers. While sulfate reduction rates indicate active bacteria in the brine (van der Wielen et al., 2005), here we reported higher concentrations of $MgCl_2$ than those reported by Wallmann et al. (1997). Thus, we suggest that bacterial lipids in the brine originate from inactive cells, likely derived from the interface. Nevertheless, our results from comprehensive lipid analysis clearly support previous work that the brine-seawater interface of the Discovery Basin represents a microbial hot spot, in which microbes are adapted to high $MgCl_2$ concentrations and actively involved in carbon, nitrogen and sulfur cycling.

VI.4.4. Sources of microbial lipids in the sediments

Since the pore waters of the sediments are almost saturated with $MgCl_2$ (see Supp. Fig. VI.1), this environment can be considered anathema to life, whereas preservation of dead cells is assumed to be exceptionally high (Hallsworth et al., 2007; Sass et al., 2008). This can be also assumed for the IPLs and allows to investigate the history of microbial life in the Discovery Basin from brine formation to the modern conditions. The IPL composition showed three major changes largely following changes in the lithology (see Figure VI.4), which might be associated with changes in the paleo microbial communities. We suggest that those changes resulted from changing environmental conditions including brine formation, pre-brine anoxic conditions as well as oxic and

oligotrophic conditions during deposition of Unit II sediments. The first zone occurs in the top 23 cm of the sediment and is characterized by lipids of similar biological origin than we found at the modern interface. The second interval from 33-184 cmbsf is characterized by dark sediments indicating anoxic depositional environment, with a much lower diversity of IPL composed predominantly of methanogenic and SRB lipids. The deepest interval (between 2 and 4 mbsf) almost exclusively contained glycosidic tetraether lipids from both archaea and so far unknown bacteria as biological sources.

VI.4.4.1. Past microbial communities from the interface

Based on transport modeling experiments and sedimentation rates, it was suggested that the Discovery Basin was filled with a $MgCl_2$-rich brine for the past ca. 700-2000 yr (Wallmann et al., 1997; Wallmann et al., 2002). However, we detected haloarchaeal lipids within the top 24 cmbsf (Figure VI.4) and assuming an average sedimentation rate of 6 cm kyr^{-1} (Wallmann et al., 2002), the basin would have an age of 4000 yr. This discrepancy might be explained by variable sedimentation rates in the basin. The general IPL distribution in the top 24 cm is similar to that in the present brine-seawater interface and suggests a constant microbial community composition since the formation of the brine. For example, the archaeal signal is dominated by GDGTs associated with AOAs, with methanogenic and halophilic archaea also contributing significantly to the total lipid pool. However, the detailed lipid distribution revealed major changes.

The contrasting intact and core AR distribution we found in the sediments compared to the brine-seawater interface suggests either a different halophilic archaeal community in the early phase of the brine or haloarchaeal adaptation to changing conditions. Selective transport and/or selective degradation of the individual IP-ARs from the interface seems unlikely due to the similar chemical structure of the compounds that were detected in the two environments. Instead, the recent refill of the basin with a $MgCl_2$-rich solution, leading to concentrations of more than 5 M (see Supp. Fig. VI.1), shows that salinity can change abruptly in this system prompting adaptations of the microbial community. For instance, the fractional abundance of Ext-AR core lipids was higher in the interface than in the sediments (Figure VI.6). These differences might reflect a change of the halophilic community as Dawson et al. (2012) showed that C_{20-20} vs. C_{25-20} ARs appears to be primarily related to taxonomy rather than salinity or pH. These changes in haloarchaeal lipid biomarkers were also evident froms the composition of IPLs. While PG-Ext-Uns-AR was only detected in the superficial interface, SDG-AR were widely detected in sediments and absent at the interface (Figure VI.4). We are unable to pinpoint whether these distinct distributions of both intact and core AR at the interface and in the sediments are due to

community composition changes or reflect a membrane lipid adaptation of haloarchaea to higher or lower Mg^{2+} layers.

Coinciding with the extent of which haloarchaea biomarkers were found in the sediments, we observed the presence of HPH-GDGTs, which are commonly attributed to *Thaumarchaeota* in marine environments (Pitcher et al., 2011b; Schouten et al., 2012). Moreover, in contrast to the brine-seawater interface, the carbon isotopic composition of core GDGT derived bp-0 showed the same signature as the other biphytanes (ca. -20 ‰) and thus all biphytanes have likely the same source. The substantially higher ring index of core GDGTs in the sediments compared to the brine-seawater interface and the brine is more typical for *Thaumarchaeota* and additionally indicates little or no contribution from methanogens to the GDGT pool. However, the occurrence of NAcG- and GN-1G-AR in both interface and sediments indicates that similar methanogenic communities inhabited the brine interface since its formation. The preservation and relative abundance of intact polar and core ARs indicate the presence of haloarchaea, AOA and methanogens biomarkers within the top 24 cmbsf (Figure VI.4). This finding supports the idea that the development of the brine might have selected this archaeal community composition since its formation in the Discovery Basin.

Corroborating our findings with archaeal lipids, bacterial IPLs in the sediments revealed a similar distribution compared to the overlying brine-seawater interface, indicating that sulfate reducers as well as heterotrophic bacteria might have been also active throughout the brine history. Some differences included a higher abundance of DAG relative to ether-bound lipids. This distribution seems more representative for aerobic bacteria and thus suggests an at least partially planktonic source from the normal salinity seawater of the lipids for example by sedimentation with debris, even though this is contradicted by the limited exchange of the brines with the overlying seawater (e.g., De Lange et al., 1990b). However, the fatty acid composition of PC-DAGs revealed minor amounts of $C_{22:6}$ and $C_{20:5}$ compounds, which typically occur in eukaryotic algae and Cyanobacteria (e.g., Brett and Müller-Navarra, 1997) and support a contribution of planktonic lipids to the IPL signal. An alternative explanation for the different lipid composition in the interface and sediments might be lateral transport of lipids. For instance, sediments from the flanks of the basin might be transported to its center by resuspension, but as mentioned above, mass wasting processes as have been shown to occur in other deep-sea hypersaline basins (Tompkins and Shephard, 1979; Camerlenghi, 1990). However, as mentioned above, mass wasting processes were unlikely to occur in the top 24 cmbsf since no sedimentary features indicative for such processes were observed in these layers.

Potentially, changes in sedimentary archaeal and bacterial IPL signals relative to the interface could be related to a relict benthic community from conditions when

$MgCl_2$ concentrations were far below 5 M. The "refill" we observed between the cruises in 1993 and 2011 indicates that the Discovery Basin is highly dynamic system and potentially, the $MgCl_2$-saturation conditions occurred late in the formation of the brine by successive inflow of the $MgCl_2$-rich solution. Thus, benthic microbes could have been active in the past and their lipids might have been preserved when $MgCl_2$ concentrations reached hostile values incompatible with life. In natural sediments dead microbial cells are usually decomposed by their own autolysins and by enzymes from neighboring microbes (Novitsky, 1986; Ferris et al., 1988). However, under high salt concentrations the activity of hydrolytic enzymes is strongly reduced (Litchfield, 1998), which enhances the preservation of intact cellular structures such as IPLs.

VI.4.4.2. Evidences for methanogenesis and sulfate reduction after the basin collapse

The sediments between 33 and 184 cmbsf were likely deposited after the collapse of the basin (ca. 35 kyr BP), but before it was filled with $MgCl_2$-rich brine. Comparably high organic carbon content and sediment lithology (Figure VI.3) suggest anoxic conditions during this time (Fusi et al., 1996; Wallmann et al., 2002). Sediment accumulation in this interval largely results from sliding from the steep adjacent walls of the basin, which is supported by sedimentary features such as deformation and obviously re-deposited material (see core picture in Figure VI.3). Thus, the sediments were deposited as turbidity currents, debris flows, and slumpings as has been shown for the nearby Bannock Basin (Camerlenghi and McCoy, 1990; Ziveri et al., 1995). In the Bannock basin, a sedimentation rate of up to 14 cm 100 yr^{-1} was estimated. This rapid accumulation including high amounts of biogenic material (Ziveri et al., 1995) likely resulted in anoxia at least in the sediments.

The change from anoxic normal salinity to anoxic brine conditions was also reflected in the lipid composition, i.e., no intact lipids indicative for halophilic bacteria or archaea were detected (e.g., as anionic PG-DAG bacterial lipids, and the *Halobacteriales*-specific SDG- and Me-PGP-ARs). Instead, the detected IPL signals are associated with methanogenic archaea and SRB. While SRB are likely the sources of abundant PC- and PE-AEG in these sediment horizons, since they produce significant amounts of diether or mixed ether/ester side chains in the phospholipids (e.g., Rütters et al., 2001; Sturt et al., 2004; Grossi et al., 2015), the relatively depleted $\delta^{13}C$ value of core AR derived phytane (-35 ‰) in the sample from 184 cmbsf indicates a contribution of methanogenic biomass (Londry et al., 2008). Sulfate reduction and methanogenesis are widespread in anaerobic settings, such as anaerobic marine sediments, where the microbes are involved in the degradation of organic matter (e.g., Wellsbury et al., 1997). Given that SRB are known to

outcompete methanogens for substrates such as H_2 and acetate (e.g., Oremland et al., 1982; Valentine, 2011), we suggest that methanogens from the Discovery Basin likely rely on non-competitive substrates such as methylated compounds . Detection of NAcG- and GN-1G-AR exclusively found in *Methanosarcinales* (Koga et al., 1993a) further supports the possibility for methylotrophic methanogenesis throughout the development of the Discovery Basin.

The change from anoxic normal salinity to anoxic brine conditions is also reflected in the lipid composition, i.e., no intact lipids indicative for halophilic bacteria or archaea were detected (e.g., as anionic PG-DAG bacterial lipids, and the *Halobacteriales*-specific SDG- and Me-PGP-ARs). Instead, the detected IPL signals are associated with methanogenic archaea and SRB. While SRB are likely the sources of abundant PC- and PE-AEG in these sediment horizons, since they produce significant amounts of diether or mixed ether/ester side chains in the phospholipids (e.g., Rütters et al., 2001; Sturt et al., 2004; Grossi et al., 2015), the relatively depleted δ^{13}C value of core AR derived phytane (-35 ‰) in the sample from 184 cmbsf indicates a contribution of methanogenic biomass. Sulfate reduction and methanogenesis have been shown to occur widespread in anaerobic settings, such as anaerobic marine sediments, where the microbes are involved in the degradation of organic matter (e.g., Wellsbury et al., 1997). Given that SRB are known to outcompete methanogens for substrates such as H_2 and acetate, we suggest that methanogens from the Discovery Basin likely rely on non-competitive substrates such as methylated compounds (e.g., Oremland et al., 1982; Valentine, 2011). Detection of NAcG- and GN-1G-AR exclusively found in *Methanosarcinales* (Koga et al., 1993a) further supports the possibility for methylotrophic methanogenesis throughout the development of the Discovery Basin.

An additional evidence for methanogenesis in the depth interval from 33-184 cmbsf was the detection of Uns-ARs, with much lower degree of unsaturation compared to the overlying sediments (Figure VI.6). Uns-ARs have been reported in the methanogen *M. burtonii*, which was isolated from Ace Lake, Antarctica, and the incorporation of unsaturations has been demonstrated to be an adaptation to cold temperatures (Nichols et al., 2004). The low relative abundance and degree of unsaturation of Uns-ARs is in agreement with moderate temperatures in the modern brine (ca. 14 °C; Figure VI.2) and sea surface temperatures showed only little variability in the Eastern Mediterranean during the past ca. 10 kyr of the Holocene (Castañeda et al., 2010).

Other abundant IPLs in these depths were glycosidic GDGTs. The stable carbon isotopic composition of individual IP-GDGT derived biphytanes was similar to TOC and core lipids over the whole sediment core (Figure VI.7). This signal could either be explained by heterotrophic benthic archaea (Biddle et al., 2006) or by preserved planktonic biomass. We suggest that active *Thaumarchaeota* did not contribute significantly to the

archaeal lipid pool during anoxic conditions before the brine intrusion into the Discovery Basin. Our suggestion is based on the absence of HPH-GDGT, which is generally assumed to be quickly degraded while sinking through the water column (e.g., Schouten et al., 2013a). Although recent modeling and laboratory experiments indicate that archaeal ether lipids might be more stable than previously expected, especially under anoxic conditions (Bauersachs et al., 2010; Schouten et al., 2010; Logemann et al., 2011; Xie et al., 2013), we detect abundant bacterial PE-DAG which supposedly display a faster turnover of these lipids compared to ether-bound lipids (Logemann et al., 2011). These observations are in line with the hypothesis that prior to brine formation, the microbial community was basically composed of methanogenic archaea and SRB. In summary, our data indicate that the Discovery Basin underwent two phases since its formation: 1. Anoxic conditions after the collapse of the basin, and 2. Anoxic, brine-filled conditions in the last 2000 years. These two periods are clearly characterized by distinct microbial communities.

VI.4.4.3. Possible sources of microbial lipids in sediments before basin formation: Unit II

The sediments of Unit II represent normal pelagic sediments (Fusi et al., 1996; Wallmann et al., 2002) and the low TOC content (Figure VI.3) indicates that these layers were well oxygenated. Additionally, the Eastern Mediterranean is and was characterized by oligotrophic conditions and thus the low primary productivity in the surface waters results in low organic matter fluxes from the photic zone, except for episodic periods of enhanced productivity that resulted in the formation of organic-rich sapropels (e.g., Fontugne and Calvert, 1992). However, in our sediment core, we have not observed sapropel deposits in Unit II, which are generally characterized by TOC concentrations of >2 % (Calvert, 1983). It was further suggested that these sediments were deposited before the basin formation (Fusi et al., 1996; Wallmann et al., 2002) and thus, they represent a very different microbial habitat than the anoxic sediments observed after the basin collapse (Figure VI.8). These distinct characteristics are clearly reflected in the microbial lipid composition, which is fundamentally different compared to the overlying sediments.

In Unit II, intact bacterial phospholipids, which otherwise were widespread in Unit I sediments, were not detected. This finding likely reflect the rapid degradation of these bacterial phospholipids under oxic depositional environments of Unit II. The stable carbon isotopic composition of archaeal intact GDGT derived biphytanes was similar to that of TOC and core lipids (ca. −20 ‰ Figure VI.7) indicating an allochthonous source from planktonic archaea, although a contribution from GDGT-producing benthic archaea cannot be excluded (Biddle et al., 2006). Similar to the adjacent anoxic sediments,

the stable carbon isotopic composition of core AR derived phytanes showed δ^{13}C values of <-35 ‰ in Unit II (Figure VI.7), suggesting a methanogenic contribution. Moreover, increased relative abundances of core OH-ARs observed in these sediments (Figure VI.6) are indicative of methanogenesis by members of the order *Methanosarcinales* (Koga et al., 1998).

We further identified abundant intact as well as core B-, OB- and IB-GDGTs (Figures VI.4 and VI.5). The source of these lipids is still unknown, but their co-occurrence indicates a common biological origin, which is probably bacterial. Structural elucidation of core B-GDGTs isolated from a peat extract revealed 1,2-*sn*-glycerol configuration (Sinninghe Damsté et al., 2000), which strongly suggests a bacterial rather than an archaeal origin of these lipids. Thus far, intact and core B-, OB- and IB-GDGTs have so far not been detected in microbial cultures, except for small amounts of one B-GDGT core lipid in species belonging to the order *Thermotogales* (Sinninghe Damsté et al., 2007) and in a few species of *Acidobacteria* (Sinninghe Damsté et al., 2011). However, non-isoprenoid branched GDGT core lipids have been largely detected in natural environments ranging from peats and soils (e.g., Schouten et al., 2000; Sinninghe Damsté et al., 2000; Hopmans et al., 2004; Weijers et al., 2006) to marine (e.g., Hopmans et al., 2004; Peterse et al., 2009; Liu et al., 2012b) and lake sediments (e.g., Tierney and Russell, 2009). Intact polar B-GDGTs have only been reported in peats (e.g., Liu et al., 2010) and the detection of core B-GDGTs in marine sediments was initially interpreted as terrestrial signal (Hopmans et al., 2004). However, more recent studies revealed indications for the *in situ* production of B-GDGTs in various marine settings, such as in the oxygen minimum zone of the Eastern Tropical North Pacific Ocean (Xie et al., 2014) and the anoxic water columns of the Black Sea and the Cariaco Basin (Liu et al., 2014). While these latter observations indicate a similar anaerobic biological origin for marine B-GDGTs, their exact source remains elusive. We further identified abundant intact as well as core B-, OB- and IB-GDGTs (Figures VI.4 and VI.5). The source of these lipids is still unknown, but their co-occurrence indicates a common biological origin, which is probably bacterial. Structural elucidation of core B-GDGTs isolated from a peat extract revealed 1,2-*sn*-glycerol configuration (Sinninghe Damsté et al., 2000), which clearly confirms a bacterial rather than an archaeal origin of these lipids. Thus far, intact and core B-, OB- and IB-GDGTs have so far not been detected in microbial cultures, except for small amounts of one B-GDGT core lipid in species belonging to the order *Thermotogales* (Sinninghe Damsté et al., 2007) and in a few species of *Acidobacteria* (Sinninghe Damsté et al., 2011). However, non-isoprenoid branched GDGT core lipids have been largely detected in natural environments ranging from peats and soils (e.g., Schouten et al., 2000; Sinninghe Damsté et al., 2000; Hopmans et al., 2004; Weijers et al., 2006) to marine (e.g., Hopmans et al., 2004; Peterse et al., 2009; Liu et al., 2012b) and lake sediments (e.g.,

Tierney and Russell, 2009). Intact polar B-GDGTs have only been reported in peats (e.g., Liu et al., 2010) and the detection of core B-GDGTs in marine sediments was initially interpreted as terrestrial signal (Hopmans et al., 2004). However, more recent studies revealed indications for the *in situ* production of B-GDGTs in various marine settings, such as in the oxygen minimum zone of the Eastern Tropical North Pacific Ocean (Xie et al., 2014) and the anoxic water columns of the Black Sea and the Cariaco Basin (Liu et al., 2014). While these latter observations indicate a similar anaerobic biological origin for marine B-GDGTs, their exact source remains elusive.

The carbon isotopic composition of the alky chains derived from the intact B-, OB- and IB-GDGTs allows us to speculate on the metabolism of their producers. Depending on the utilized substrate, biosynthetic pathway and growth conditions, isotopic fractionation during lipid biosynthesis can range between -2 to $-8\,‰$ for this process (e.g., DeNiro and Epstein, 1977; Hayes, 1993; Hayes, 2001). The $\Delta\delta^{13}C$ between TOC and lipids was $>-10\,‰$ for most branched GDGT derived alkyl chains in most of our samples (Figure VI.7), slightly off the heterotrophic range considering the similar biomass and substrate $\delta^{13}C$ during heterotrophy (Blair et al., 1985). However, for some sulfate reducers grown heterotrophically, isotope fractionation between substrate and fatty acids has been shown to be between -11.9 and $-14.4\,‰$ and thus respiring heterotrophs as source for intact B-, OB-, and IB-GDGTs cannot be completely excluded. Alternatively, fractionation during chemoautotrophy might explain the depleted carbon isotopic composition. Assuming typical sedimentary $\delta^{13}C_{DIC}$ values of $-20\,‰$ in the past environment (e.g., Presley and Kaplan, 1968), we evaluated the possibility for chemoautotrophic assimilation of CO_2. Considering that lipids are depleted in ^{13}C compared to bulk biomass (e.g., Sakata et al., 1997), the Calvin-Benson-Bassham (CBB) cycle as well as the reductive acetyl-CoA by methanogens or acetogens seem to be of little or no relevance as both typically result in substantial $^{13}C/^{12}C$ fractionation (House et al., 2003). In contrast, the carbon isotopic fractionation from CO_2 to biomass by the reductive TCA cycle as well as the acetyl-CoA pathway in microbes that do not form methane or acetate typically results in much lower carbon isotopic fractionation (House et al., 2003), and would be the most plausible pathways resulting in the observed carbon isotopic signature of the branched GDGT derived alkyl chains.

The occurrence of intact B-, OB- and IB-GDGT in combination with a distinct archaeal lipid distribution fundamentally distinguished the benthic microbial community of Unit II from that after the basin formation. Based on this observation, we propose three possibilities for the exclusive detection of glycosidic ether lipids in these sediments. The first concerns the higher preservation potential of ether- relative to ester-bound lipids in marine sediments (Logemann et al., 2011; Xie et al., 2013), which might be even more pronounced under oxic conditions of Unit II sediments. Secondly, cell membranes

composed of sugar-based and ether lipids are less permeable to ions than phosphate-based and ester lipids, respectively (Yamauchi et al., 1993; Baba et al., 2001; Mathai et al., 2001). Based on the concept that membrane lipids dictate the microbial thermodynamic ecology in the environment (Valentine, 2007, 2009), we suggest that the detection of glycosidic tetraethers from both bacteria and archaea might reflect an adaptation to stress conditions in the sediments prior to basin formation (e.g., ultraoligotrophic conditions or high temperatures). A third possibility is related to past hydrothermally active sediments in the Discovery Basin, which is located at the tectonically active Mediterranean Ridge (Fusi et al., 1996). In addition, the formation of the brine pools in this area was suggested to result from tectonically induced fluid circulation through the Messinian deposits (Wallmann et al., 1997). Thus the solely detection of ether lipids, especially the glycosidic bacterial tetraethers, might be related to high temperature sediments during Unit II or a pyrolysis event during basin formation. While the exact mechanism leading to the occurrence and accumulation of those unusual bacterial tetraethers is uncertain, further geochemical and mineralogical analysis (X-ray analyses and electron microscope observations) might provide clues regarding the paleoconditions of sediments during Unit II.

VI.5. Summary

The results of this study provide insights into the identities of predominant microorganisms in the deep-sea hypersaline anoxic Discovery Basin as well as their development over time from the basin formation to the modern conditions evident from the sedimentary record (Figure VI.9). Given the extremely high $MgCl_2$ concentrations in the main brine body and sediments are incompatible with life, the sedimentary record provided an ideal archive to investigate changes in the microbial community composition. Taxonomic highly specific lipids indicate that methanogenesis, ammonium oxidation, heterotrophy and sulfate reducing activity occurs at the modern brine-seawater interface and implies intensive microbial activity on carbon, nitrogen and sulfur cycles.

Several intact membrane lipids have been identified for the first time in environmental samples, such as GN-1G- and NAcG-AR, which are likely associated with archaeal methanogens belonging to *Methanohalophilus*. Other distinct lipids could be assigned to *Halobacteriales*-like archaea, such as Me-PGP-, SDG- and PG-Ext-Uns-AR as well as core Uns- and Ext-ARs. We further identified intact forms of hybrid isoprenoid/branched tetraether lipids. These compounds combine attributes usually considered characteristic of either archaea (phytanyl moiety) or bacteria (methylated alkyl moiety) and were the major IPLs in the sediments deposited before the basin formation. Their stable carbon

isotopic composition suggests chemolithoautotrophic growth of the not yet identified source organisms.

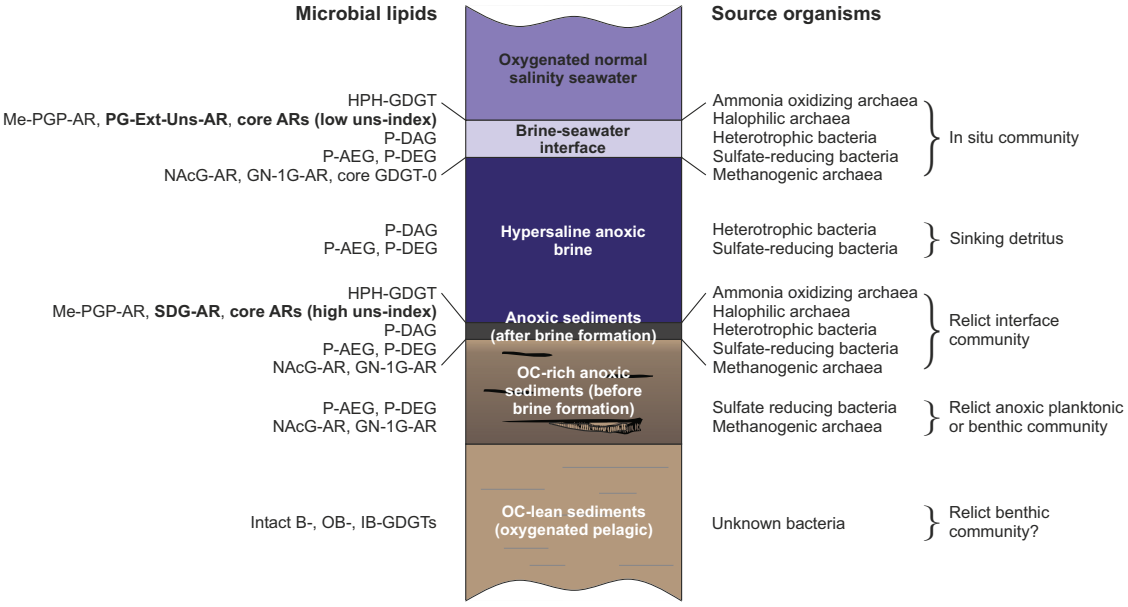

Figure VI.9. Schematic representation of the distribution of intact polar and associated microbial communities in the brine-seawater interface, brine body and underlying sediments of the Discovery Basin. The sediment column is divided into different zones according to the lithology representing different depositional environments.

The sediment record suggested changing environmental conditions as described in Fig. 8, which was consistently reflected in changes in lipid biomarker distribution. The detection of halophilic archaea- and AOA-specific IPLs only in the top 23 cmbsf matches DAN-based evidence for these archaea at the modern interface and is in agreement with modeling experiments for the development of the brine from other studies. Before the basin became brine-filled, conditions in the sediments were likely anoxic and the microbial community predominantly consisted of methanogenic archaea and sulfate reducing bacteria as indicated by the IPL composition. A sharp lithological transition recorded the collapse of the basin. The sediments below this transition, i.e. Unit II, were deposited under oligotrophic conditions and likely hosted distinct microbial communities as indicated by the IPLs. The detected lipids potentially originate from relict benthic communities and likely represent specific adaptations to so far unknown environmental variables but conditions, such as high temperatures together with anoxia could explain the presence of the intact bacterial tetraether lipids.

In conclusion, the unique properties of the sediments below the Discovery Basin allowed us to use IPLs as biomarkers for the reconstruction of past microbial communities and environmental conditions and demonstrated their biomarkers potential for assessing the taxonomic composition of microbial biomass.

Acknowledgements

We thank the crew and the scientific shipboard party of the RV Meteor cruise M84/1 (DARCSEAS I). We further thank J. Wendt and X. Prieto for help with δ^{13}C analysis of lipids and S. Alfken and J.-K. Gal for help with sample preparation for lipid analysis. The study was funded by the European Research Council under the European Union's Seventh Framework Programme - "Ideas" Specific Programme, ERC grant agreement No. 247153 (Advanced Grant DARCLIFE; PI K.-U.H.) and by the Deutsche Forschungsgemeinschaft (DFG, Germany) through grants Inst 144/300-1 (LC-qToF system). Further support was given by the Bremen International Graduate School for Marine Sciences (GLOMAR) funded by the DFG through MARUM Center for Marine Environmental Sciences.

VI.6. Supporting Information

Supplementary Table VI.1 Core lipid structures of bacterial IPL compound classes in the water column and sediments of the deep-sea hypersaline anoxic Discovery Basin. Core structures are depicted as combinations of fatty acids (e.g., 14:0/16:1) or ether-lipids (e.g., o-16:0).

Zonation	Bacterial IPL compound class	Major core structure
Superficial brine-sea water interface (3570 mbsl)	PC-DAG, PG-DAG, PE-DAG, PDME-DAG, DPG, PG sphingolipid, unk PG-DAG	15:0/15:0; 15:0/16:1; 15:0/16:0; 16:1/17:0; 15:0/17:0; 17:0/17:0
	PC-AEG, PG-AEG	15:0/o-15:0; o-15:0/16:1; o-15:0/16:0; o-16:1/17:0; o-17:0/17:0
	PG-DEG	o-30:0; o-30:1; o-31:0; o-31:1; o-32:0; o-32:1
	BL	16:1/18:1; 16:0/18:1; 17:0/17:0
Brine-sea water interface (3575 mbsl)	PC-DAG, PG-DAG, PE-DAG, unk PG-DAG	15:0/16:1; 15:0/16:0; 16:1/17:0; 15:0/17:0; 17:0/17:0
	PC-AEG, PG-AEG	o-15:0/16:1; o-15:0/16:0; 15:0/o-16:0; 16:1/o-17:0; o-17:0/17:0
Brine (3580-3610 mbsl)	PC-DAG, PG-DAG, PE-DAG, BL, unk PG-DAG	15:0/16:1; 15:0/16:0; 16:1/17:0; 15:0/17:0; 17:0/17:0
	PC-AEG, PG-AEG, PG-AEG	15:0/16:1; 15:0/16:0; 16:1/17:0; 17:0/17:0
Surface sediments (Unit Ia, 0-12 cmbsf)	PG-DAG, PE-DAG, PME-DAG; PDME-DAG, DPG, BL, unk PG-DAG	15:0/16:1; 15:0/16:0; 16:1/17:0; 17:0/17:0; 16:1/18:1; 16:1/18:0
	PC-DAG	16:1/17:0; 17:0/17:0; 16:1/18:1; 16:1/18:0; 18:1/22:6; 20:5/20:5
	PC-AEG, PG-AEG	o-15:0/16:1; o-15:0/16:0; 15:0/o-16:0; 16:1/o-17:0; o-17:0/17:0
Sediment (Unit Ia, 12-24 cmbsf)	PG-DAG, PE-DAG, BL	15:0/16:1; 15:0/16:0; 16:1/17:0; 15:0/17:0; 17:0/17:0; 16:1/18:1; 16:1/18:0
	PC-DAG	16:1/17:0; 17:0/17:0; 16:1/18:1; 16:1/18:0; 18:1/22:6; 20:5/20:5
	PC-AEG, PG-AEG	o-15:0/16:1; o-15:0/16:0; 15:0/o-16:0; 16:1/o-17:0; o-17:0/17:0
Sediment (Unit Ia, 32-48 cmbsf)	PE-DAG	15:0/16:1; 15:0/16:0; 16:1/17:0; 15:0/17:0; 17:0/17:0
	PC-AEG, PE-AEG	o-15:0/16:1; o-15:0/16:0; 15:0/o-16:0; 16:1/o-17:0; o-17:0/17:0
Sediment (Unit Ib, 59-191 cmbsf)	PE-DAG	15:0/16:1; 15:0/16:0; 16:1/17:0; 17:0/17:0; 16:1/18:1; 16:1/18:0
	PC/PE-DEG	o-30:0; o-31:0; o-32:0
Sediment (Unit II, 212-411 cmbsf)	n.d.	n.d.

Supplementary Table VI.2 Carbon isotopic composition from individual archaeal and bacterial ether core lipid derived alkyl chains.

		δ^{13}C (‰)						
Core lipid class	Ether cleavage product	3570 mbsl	23 cmbsf	41 cmbsf	95.5 cmbsf	184 cmbsf	285 cmbsf	386.5 cmbsf
AR	Phytane	n.d.	-25.2	-23.3	-26.4	-34.6	n.d.	-37.2
GDGTs	bp-0	-31.4	-18.9	-19.5	-19.5	-24.3	-17.9	-22.5
	bp-1	n.d.	-18.9	-19.9	-19.9	-23.5	-18.0	-22.0
	bp-2	n.d.	-18.5	-19.7	-19.3	-22.8	-17.7	-20.0
	bp-3	n.d.	-19.1	-19.8	-19.7	-22.6	-17.3	-20.9
	mean	-31.4	-18.9	-19.7	-19.6	-23.3	-17.7	-21.3
GDDs	bp-0	n.d.	-19.7	n.d.	-19.7	-20.7	-18.6	n.d.
	bp-1	n.d.	-18.6	n.d.	-17.9	-18.9	-19.9	n.d.
	bp-2	n.d.	-19.2	n.d.	-19.0	-19.5	-19.8	n.d.
	bp-3	n.d.	-19.4	n.d.	-20.5	-20.3	-19.5	n.d.
	mean	n.d.	-19.2	n.d.	-19.3	-19.8	-19.5	n.d.
OH-GDGTs	uns-bp-0	n.d.	n.d.	n.d.	n.d.	-19.34	n.d.	n.d.
	bp-0	n.d.	-20.1	n.d.	-21.9	-23.5	-23.6	-17.1
	bp-1	n.d.	-19.6	n.d.	-20.5	-22.4	-17.9	n.d.
	bp-2	n.d.	-19.2	n.d.	-17.7	-20.0	-18.8	n.d.
	bp-3	n.d.	n.d.	n.d.	-18.2	-20.6	-18.4	n.d.
	mean	n.d.	-19.6	n.d.	-19.6	-21.6	-19.7	-17.1
IB-GDGTs	I	n.d.	n.d.	n.d.	-27.0	n.d.	-33.9	n.d.
OB-GDGTs	I	n.d.	n.d.	n.d.	-27.0	-29.5	-34.9	n.d.
	II	n.d.	n.d.	n.d.	-32.9	-29.8	-35.4	n.d.
	III	n.d.	n.d.	n.d.	-31.0	-32.4	-39.5	-31.0
	mean	n.d.	n.d.	n.d.	-30.3	-30.6	-36.6	-31.0
B-GDGTs	I	n.d.	-26.2	n.d.	-26.0	-32.3	-25.2	-33.3
	II	n.d.	n.d.	n.d.	n.d.	-40.2	n.d.	-33.0
	III	n.d.	n.d.	n.d.	n.d.	-37.1	n.d.	n.d.
	mean	n.d.	-26.2	n.d.	-26.0	-36.5	-25.2	-33.2

n.d., not detected or below detection.

Supplementary Table VI.3 Carbon isotopic composition from individual archaeal and bacterial intact polar ether lipid derived alkyl chains.

Core lipid class	Ether cleavage product	δ^{13}C (‰)					
		3570 mbsl	23 cmbsf	41 cmbsf	184 cmbsf	285 cmbsf	386.5 cmbsf
2G-2OH-GDGT + HPH-GDGT	bp-0	n.d.	-20.72	n.d.	n.d.	n.d.	n.d.
	bp-1	n.d.	-19.91	n.d.	n.d.	n.d.	n.d.
	bp-2	n.d.	-18.29	n.d.	n.d.	n.d.	n.d.
	bp-3	n.d.	-20.52	n.d.	n.d.	n.d.	n.d.
	mean	n.d.	-19.86	n.d.	n.d.	n.d.	n.d.
1G-2OH-GDGT	bp-0	n.d.	-20.25	n.d.	n.d.	n.d.	n.d.
	bp-1	n.d.	-18.27	n.d.	n.d.	n.d.	n.d.
	bp-2	n.d.	-18.39	n.d.	n.d.	n.d.	n.d.
	bp-3	n.d.	-20.33	n.d.	n.d.	n.d.	n.d.
	mean	n.d.	-19.31	n.d.	n.d.	n.d.	n.d.
2G-OH-GDGT	bp-0	-19.05	-20.74	-19.62	-17.12	n.d.	n.d.
	bp-1	n.d.	-19.19	-20.87	-16.77	n.d.	n.d.
	bp-2	n.d.	-19.66	-18.43	-17.65	n.d.	n.d.
	bp-3	n.d.	-18.93	-18.37	-17.39	n.d.	n.d.
	mean	-19.05	-19.63	-19.32	-17.23	n.d.	n.d.
1G-OH-GDGT	bp-0	n.d.	-19.75	n.d.	-20.52	n.d.	n.d.
	bp-1	n.d.	-19.29	n.d.	-18.47	n.d.	n.d.
	bp-2	n.d.	-18.79	n.d.	-19.71	n.d.	n.d.
	bp-3	n.d.	-19.99	n.d.	-17.73	n.d.	n.d.
	mean	n.d.	-19.45	n.d.	-19.11	n.d.	n.d.
2G-GDGT	bp-0	n.d.	-18.85	n.d.	-22.98	n.d.	n.d.
	bp-1	n.d.	-18.09	n.d.	-19.19	n.d.	n.d.
	bp-2	n.d.	-19.21	n.d.	-18.77	n.d.	n.d.
	bp-3	n.d.	-20.34	n.d.	-18.25	n.d.	n.d.
	mean	n.d.	-19.12	n.d.	-19.8	n.d.	n.d.
1G-GDGTs	bp-0	-19.78	-19.35	n.d.	-19.89	-22.03	n.d.
	bp-1	-19.26	-20.26	n.d.	-19.49	n.d.	n.d.
	bp-2	-19.44	-20.45	n.d.	-20.24	-20.43	n.d.
	bp-3	-19.73	-21.03	n.d.	-20.18	-21.57	n.d.
	mean	-19.55	-20.27	n.d.	-19.95	-21.34	n.d.
Intact IB-GDGT	I	n.d.	n.d.	n.d.	n.d.	-32.96	-28.62
Intact OB-GDGT	I	n.d.	n.d.	n.d.	n.d.	-32.03	n.d.
	II	n.d.	n.d.	n.d.	n.d.	-37.7	-26.85
	III	n.d.	n.d.	n.d.	n.d.	-36.52	-26.12
	mean	n.d.	n.d.	n.d.	n.d.	-35.42	-26.48
Intact B-GDGT	I	n.d.	n.d.	n.d.	n.d.	-31.22	-26.2
	II	n.d.	n.d.	n.d.	n.d.	-31.42	-26.91
	III	n.d.	n.d.	n.d.	n.d.	-33.67	-29.82
	mean	n.d.	n.d.	n.d.	n.d.	-32.1	-27.64

n.d., not detected or below detection.

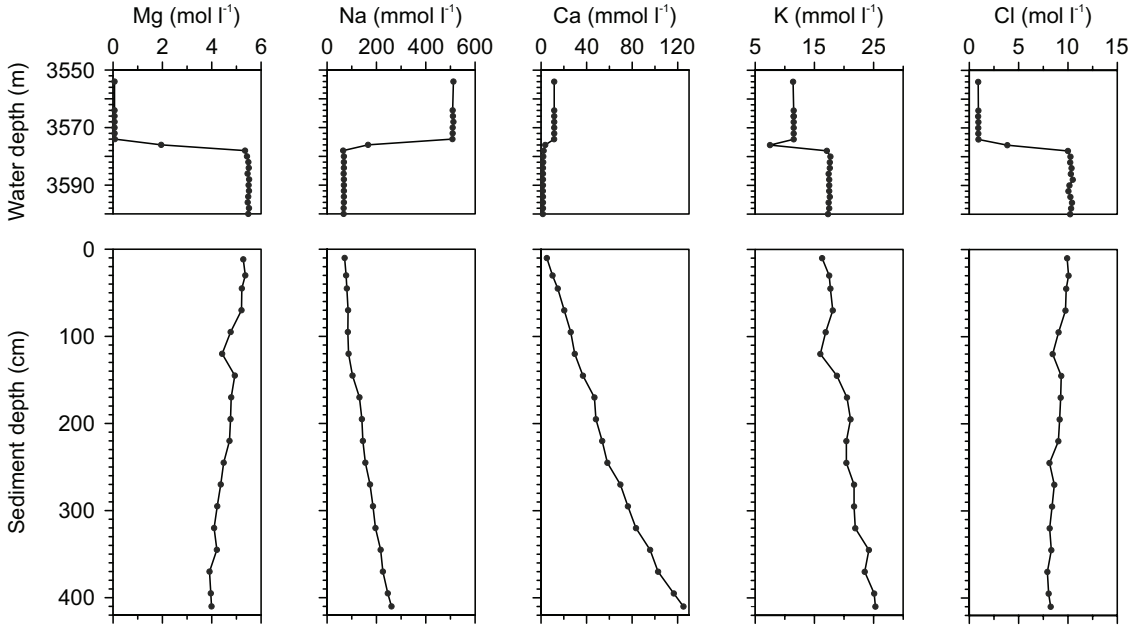

Supplementary Figure VI.1 Concentration profiles of Mg, Na, Ca, K and Cl in the in the water column and pore water fractions of the sediment at site GeoB15102.

VI.6.1. Mass spectral identification of novel compounds

Several novel compounds were identified in the sediments and water column of the Discovery Basin based on elution time, accurate mass/proposed sum formula and diagnostic fragments mainly based on Yoshinaga et al. (2011) in RP-HPLC-ESI-MSn. We identified five novel structures of intact polar archaeols, including glycerol-pentose- (GPs), N-acetylglucosamine- (NAcG), phosphatidylglycerol-unsaturated-extended (PG-Uns-Ext), monoglycosyl-deoxy-glycosyl (1G-deoxy-G) and (N-acetyl)-glucosamine-monoglycosyl (GN-1G) AR.

GPs-AR eluted at 16.0 min retention time (see Supp. Fig. VI.2 for extracted ion chromatograms of all identified intact archaeols) at *m/z* 862.7 ($[M+NH_4]^+$) in the RP-HPLC–MS chromatogram of sample GeoB15102-4, 22-24 cmbsf, using the protocol form Wörmer et al. (2013). Sum formula calculation from accurate mass and isotope pattern match indicated the stoichiometric formula $C_{50}H_{104}NO_9^+$ for the ammoniated molecule. The major product ions for this molecule during MS^2 fragmentation were at *m/z* 653.7, which is formed by the loss of the polar head group and represents a core AR fragment (Supp. Fig. VI.3a) and at *m/z* 373.3, resulting from the loss of the polar head group and one phytanyl group (as phytene).

1NAcG-AR eluted at 16.0 min retention time at *m/z* 856.7 ($[M+H]^+$) in sample GeoB15102-5, 177-191 cmbsf. Sum formula calculation from accurate mass and isotope pattern match indicated the stoichiometric formula $C_{51}H_{102}NO_8^+$ for the protonated molecule. The major product ion for this molecule during MS^2 fragmentation was at *m/z* 204.1, which represents the 1NAcG head group (Supp. Fig. VI.3b).

PG-Uns-Ext-AR eluted at 15.6 min retention time at *m/z* 875.7 ($[M+H]^+$) in sample GeoB15102-3, 3570 mbsl. Sum formula calculation from accurate mass and isotope pattern match indicated the stoichiometric formula $C_{51}H_{104}NO_8P^+$ for the ammoniated molecule. The major product ions for this molecule during MS^2 fragmentation were at *m/z* 595.4, resulting from the loss of the phytanyl chain (as phytene) and at *m/z* 527.4, resulting from the loss of the monounsaturated sesterterpenyl chain as a diunsaturated neutral fragment (Supp. Fig. VI.3c).

GN-1G-AR eluted at 15.5 min retention time at *m/z* 976.8 ($[M+H]^+$) in sample GeoB15102-4, 22-24 cmbsf. Sum formula calculation from accurate mass and isotope pattern match indicated the stoichiometric formula $C_{55}H_{110}NO_{12}^+$ for the protonated molecule. One major product ion for this molecule during MS^2 fragmentation was at *m/z* 653.7, which is formed by the loss of the polar head group and represents a core AR fragment (Supp. Fig. VI.3d). Another major fragment ion was at *m/z* 373.3, resulting from the loss of the polar head group and one phytanyl group (as phytene).

2G-Deoxy-AR eluted at 15.9 min retention time at *m/z* 978.8 ($[[M+NH_4]^+$) in sample

GeoB15102-4, 22-24 cmbsf. Sum formula calculation from accurate mass and isotope pattern match indicated the stoichiometric formula $C_{55}H_{112}NO_{12}^{+}$ for the ammoniated molecule. The major product ions for this molecule are the same as for GN-1G-AR (Supp. Fig. VI.3e).

A second group of novel compounds include intact polar branched, overly branched (OB) and hybrid isoprenoid/branched (IB) GDGTs (Supp. Fig. VI.5). These compounds were present in all samples from below 184 cmbsf. Based on MS properties during IPL analysis using RP-HPLC-ESI-MS^n, we found several distinct series of the different GDGT IPL groups differing in mass by 14 Da. For example, the molecular ions obtained from MS1 experiments of the most prominent cluster in the sample from 380 to 393 cmbsf showed dominant *m/z* ($[M+NH_4]^+$) values of 1501, 1515, 1529, respectively. The corresponding fragment ion from MS^2 experiments involving loss of the polar head group for the compound at *m/z* at 1515.3 was at *m/z* 1176, i.e. the characteristic ion of an IB-GDGT core lipid (Liu et al., 2012c). Another major fragment at *m/z* 1322 demonstrates the loss of one methoxylated (MeO) sugar moiety (neutral loss of 176 Da) from the original molecule. Consequently, the second sugar moiety represents a deoxylated (deoxy) sugar (*m/z* 1322˘146 Da loss; (Supp. Fig. VI.5b;Yoshinaga et al. (2011). Overall, we identified compound series with one to four sugar moieties, which can be present as regular hexoses (or inositol) but also as deoxy and MeO sugars, and branched, overly branched and hybrid isoprenoid/branched GDGT core lipids.

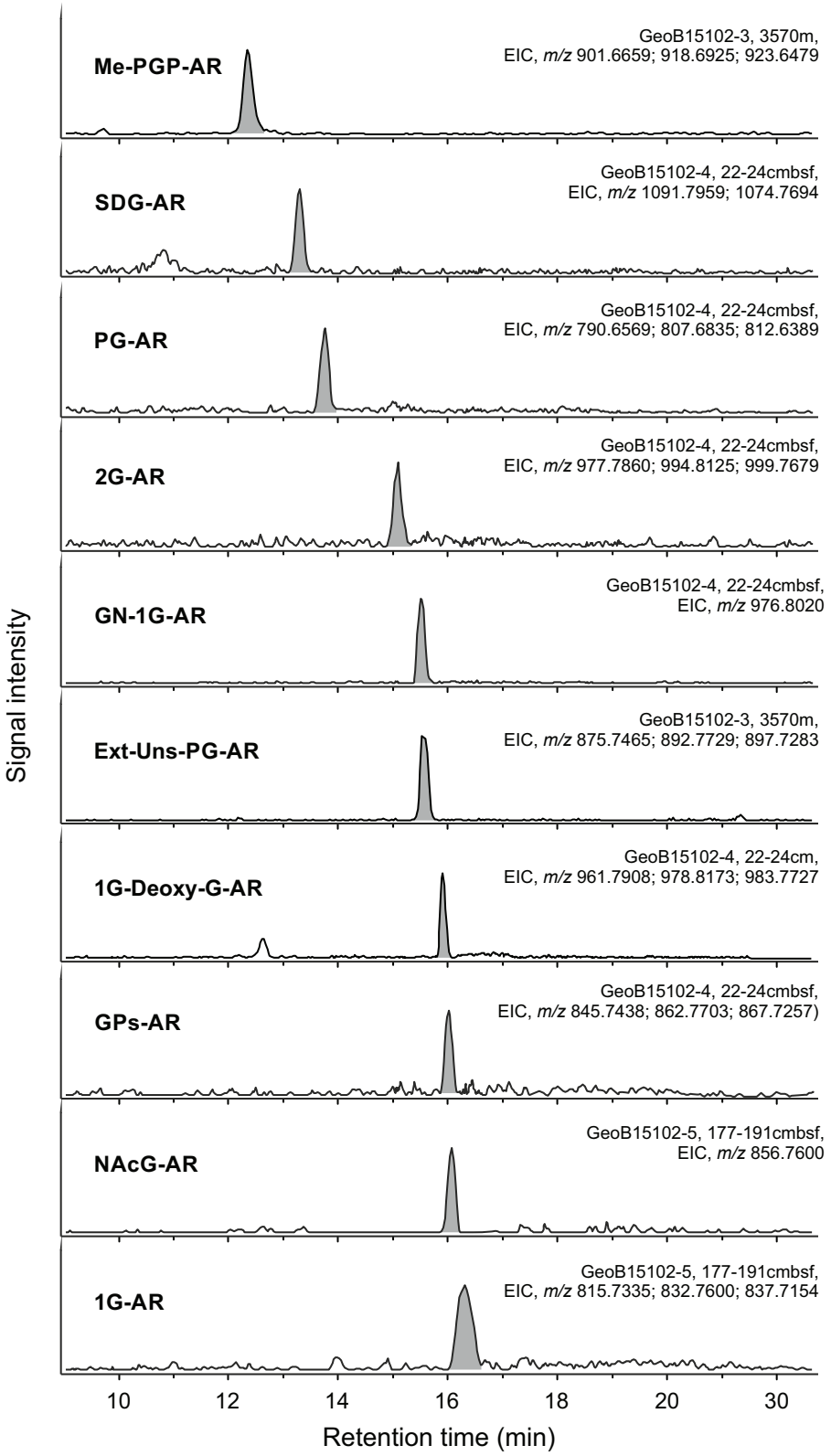

Supplementary Figure VI.2 UHPLC-qToF-MS chromatogram shown as extracted ion chromatogram (EIC) of identified intact polar archaeols in samples from the water column and sediments of the deep-sea hypersaline Discovery Basin. Abbreviations: AR, archaeol; 1G, monoglycosyl; 2G, diglycosyl; 1G-deoxy-G, monoglycosyl-deoxy-glycosyl; GN-1G, N-acetyl-glucosamine-monoglycosyl; GPs, glycerol-pentose; Me-PGP, methylated phosphatidylglycerolphosphate; NAcG, N-acetylglucosamine; PG, phosphatidylglycerol; PG-Uns-Ext, phosphatidylglycerol-unsaturated-extended; SDG, sulphated diglycosyl.

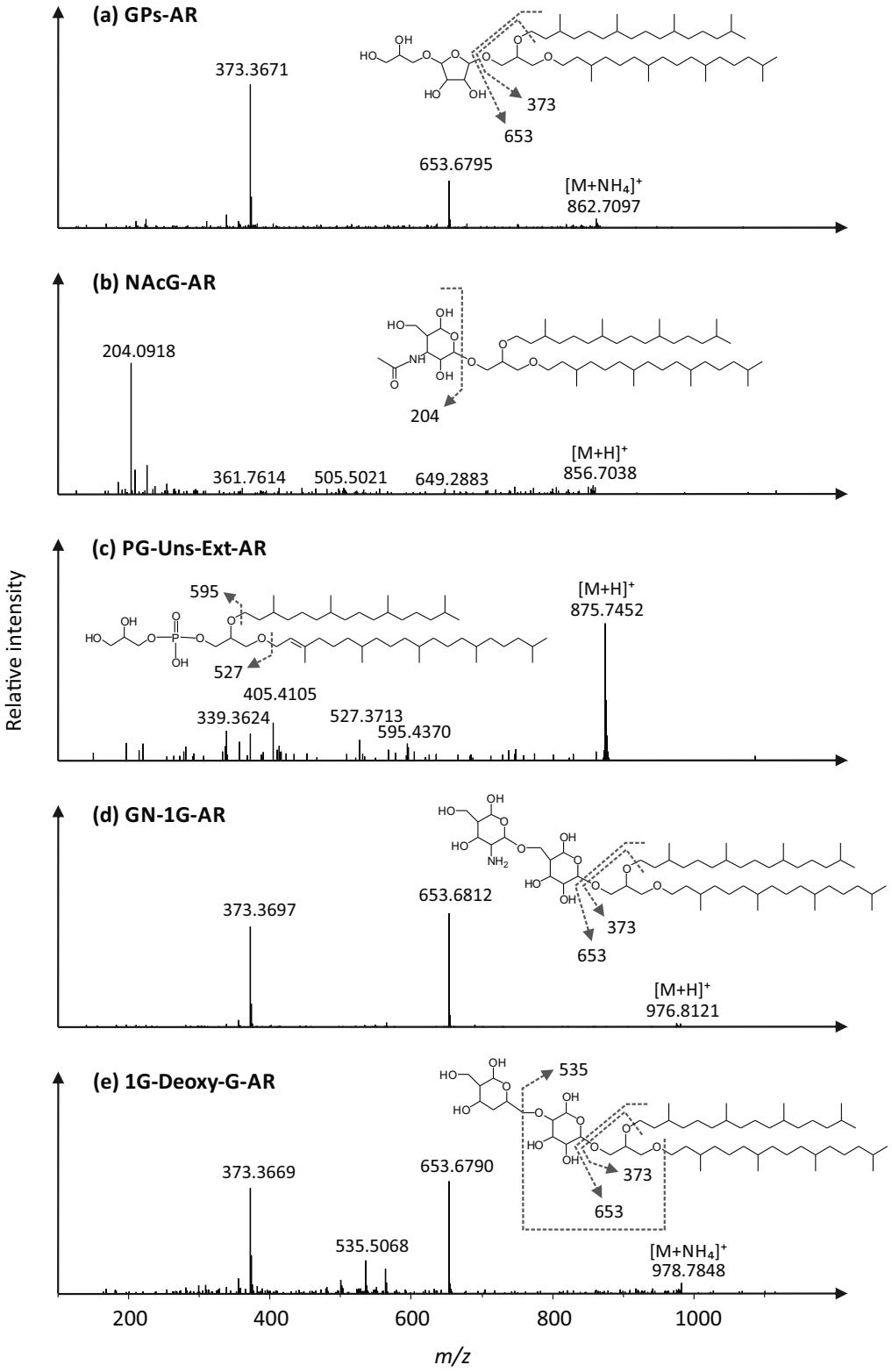

Supplementary Figure VI.3 MS^2 spectra of novel intact archaeols (ARs). (a) Glycerol-pentose-(GPs) AR, (b) N-acetylglucosamine-(NAcG) AR, (c) phosphatidylglycerol-unsaturated-extended-(PG-Uns-Ext) AR, (d) (N-acetyl)-glucosamine-monoglycosyl (GN-1G) AR and (e) 1G-deoxy-G-AR. Suggested structures and formation of major product ions are also drawn. For detailed mass spectral interpretation, see text.

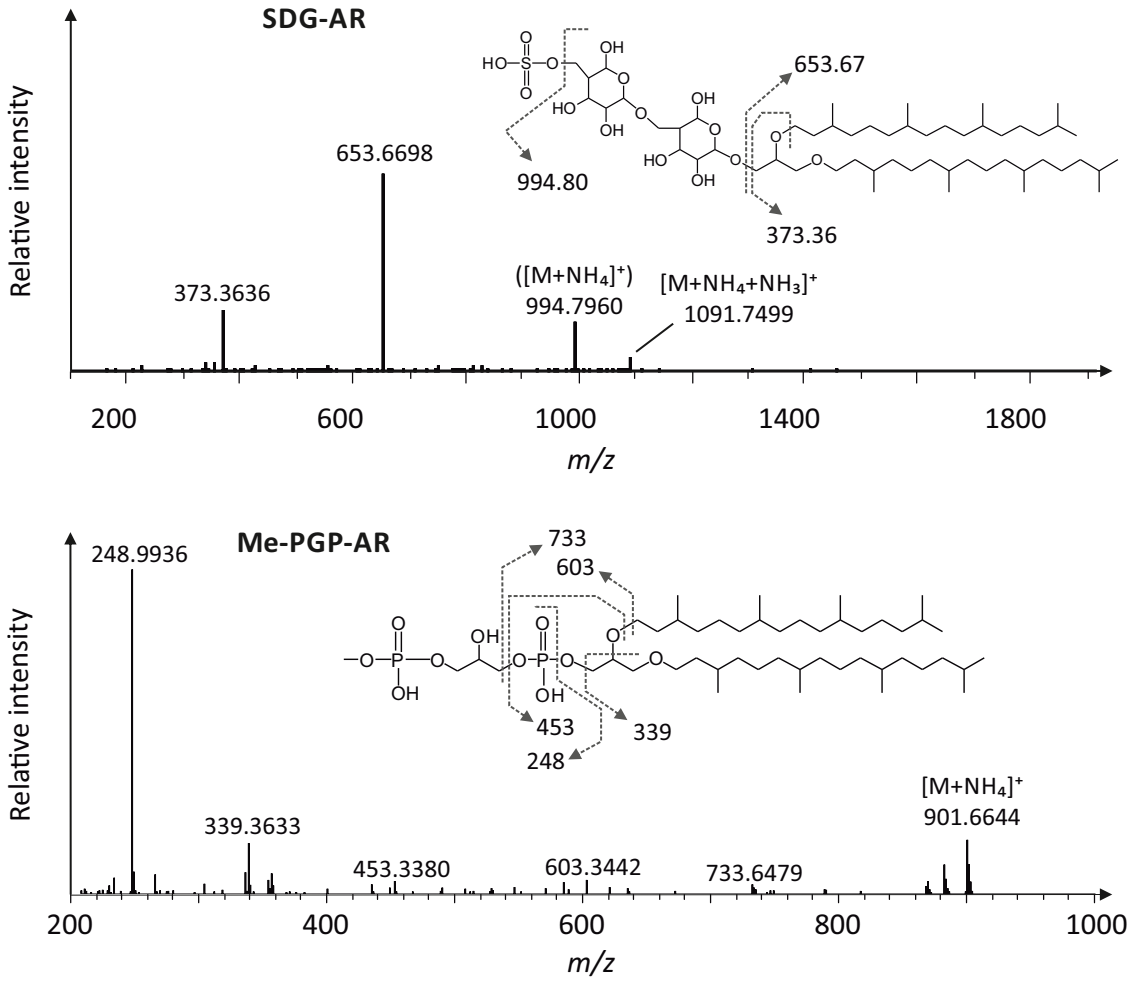

Supplementary Figure VI.4 MS^2 spectra of sulphated diglycosyl- (SDG) and methylated phosphatidylglycerolphosphate- (Me-PGP) archaeol (AR) in the samples from GeoB15102-4, 22-24 cmbsf and GeoB15102-3, 3570 mbsl, respectively. The chemical structure and formation of major product ions are also shown.

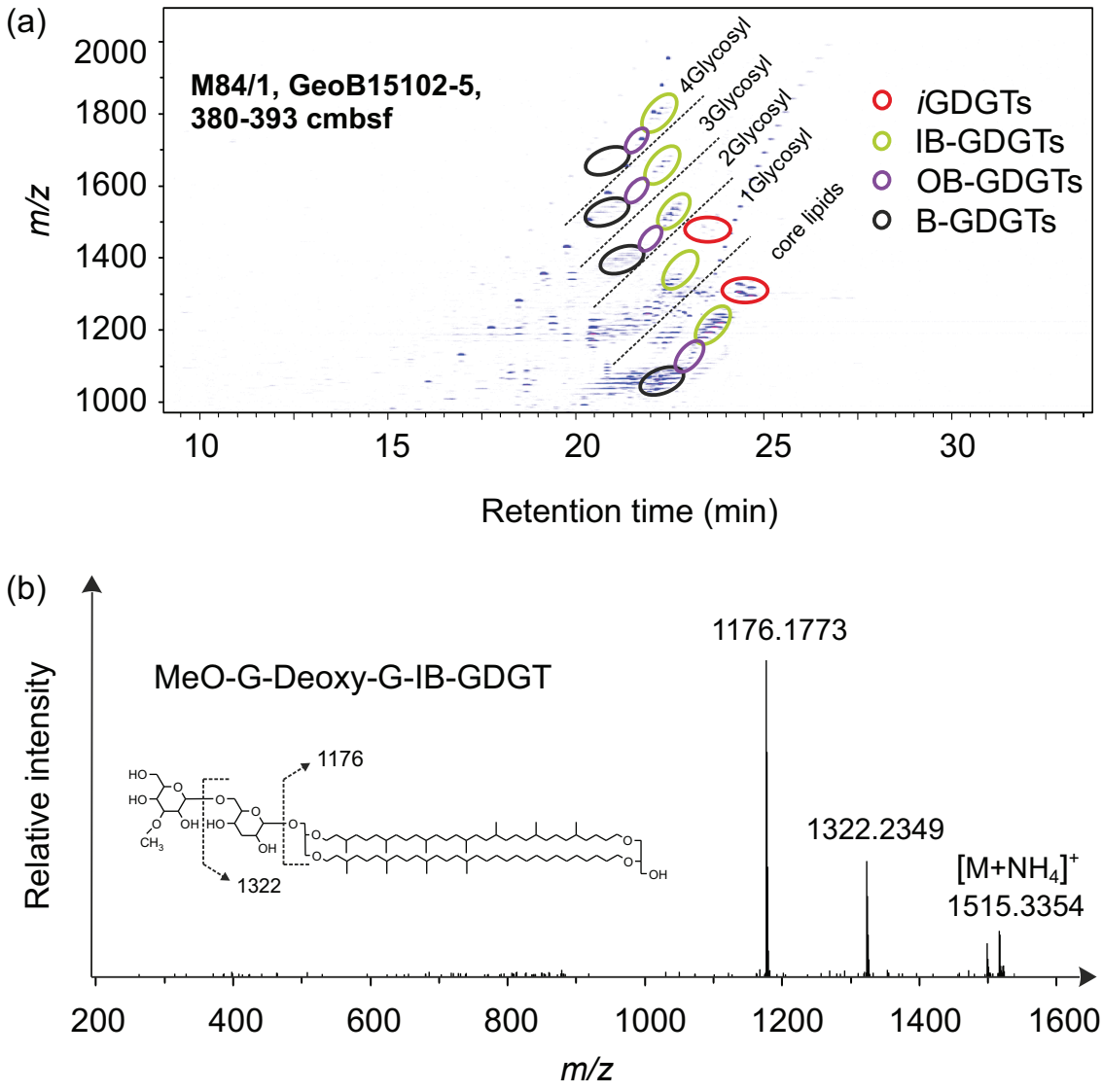

Supplementary Figure VI.5 (a) Density map of sample M84/1, GeoB15102-5, 380-393 cmbsf showing major core and intact tetraether lipids. (b) MS^2 spectrum of an intact IB-GDGT at *m/z* 1515.3. The spectrum indicates a structure containing one methoxylated (MeO) and one deoxylated (deoxy) sugar head group, and the major product ion at *m/z* 1176.2 suggests an IB-GDGT containing 11 methylations (cf. Liu et al., 2012c). Presumed structure and formation of major product ions are also shown.

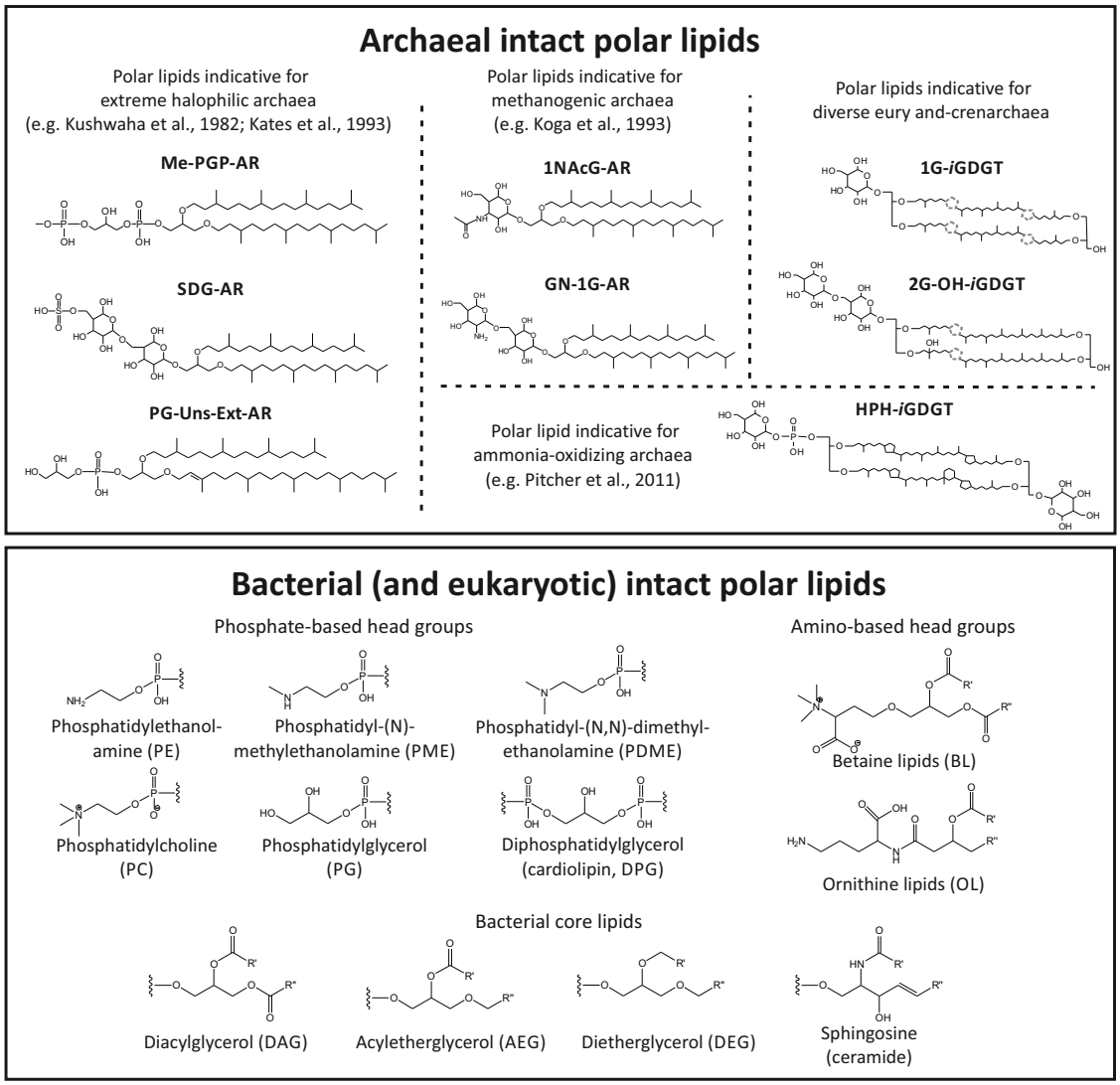

Supplementary Figure VI.6 Molecular structures and presumed biological origin (only for archaea, based on the works from Kushwaha et al. (1982), Kates (1993a), Koga et al. (1993b), and Pitcher (2011) of intact polar lipids identified in samples from the Discovery Basin.

Chapter VII

Respiratory quinones in *Archaea*: phylogenetic distribution and application as biomarkers in the marine environment

Felix J. Elling[a,+,*], **Kevin W. Becker**[a,+], Martin Könneke[a], Jan M. Schröder[a], Matthias Y. Kellermann[b], Michael Thomm[c] and Kai-Uwe Hinrichs[a]

Under review at *Environmental Microbiology*

[+]These authors contributed equally to this work.

[a]Organic Geochemistry Group, MARUM - Center for Marine Environmental Sciences & Department of Geosciences, University of Bremen, 28359 Bremen, Germany
[b]Department of Earth Science and Marine Science Institute, University of California, Santa Barbara, California, 93106 USA
[c]Lehrstuhl für Mikrobiologie und Archaeenzentrum, Universität Regensburg, 93053 Regensburg, Germany

[*]Corresponding author. E-mail: felling@marum.de

Abstract

Isoprenoid quinones are membrane-bound lipids functioning as electron carriers in respiratory chains of almost all organisms. However, knowledge of the quinone composition particularly in *Archaea* is still fragmentary. Using novel protocols that enable simultaneous detection of quinones and glycerol-based membrane lipids we investigated the quinone inventories of 25 species belonging to the archaeal phyla *Eury-*, *Cren-* and *Thaumarchaeota*. Saturated and monounsaturated menaquinones with six isoprenoid units forming the alkyl chain may represent chemotaxonomic markers for *Thaumarchaeota*. Other diagnostic biomarkers are thiophene-bearing quinones for *Sulfolobales* and methanophenazines as functional quinone analogs of the *Methanosarcinales*. The ubiquity of saturated menaquinones in the *Archaea* in comparison to *Bacteria* suggests that these compounds may represent an ancestral and diagnostic feature of the *Archaea*. Overlap between quinone compositions of distinct thermophilic and halophilic archaea and bacteria may indicate lateral gene transfer. The biomarker potential of thaumarchaeal quinones was exemplarily demonstrated on a water column profile of the Black Sea. Both, thaumarchaeal quinones and membrane lipids showed similar distributions with maxima at the chemocline. In conclusion, the structural variations of quinones and their distribution among the *Archaea* bear significant chemotaxonomic information and high biomarker potential for classification and quantification of distinct archaeal orders in the environment.

VII.1. Introduction

Isoprenoid quinones are a structurally diverse group of membrane-bound lipids that act as electron carriers in the respiratory chains of organisms from all domains of life (Nowicka and Kruk, 2010). Quinones are commonly classified based on the structure of a polar cyclic headgroup and can be further distinguished by the length and degree of unsaturation of the head-to-tail linked isoprenoid side chain (Collins and Jones, 1981; Hiraishi, 1999). The major classes of quinones include ubiquinones (UQs), plastoquinones (PQs) and derivatives (benzoquinones), which occur exclusively in *Bacteria* and mitochondria of *Eukarya*, as well as menaquinones (MKs, also known as vitamin K2) and related compounds (naphthoquinones), which occur only in *Archaea* and *Bacteria*, except for phylloquinone [$MK_{4:1}$, also known as vitamin K1; Quinone nomenclature ($Q_{m:n}$) indicates headgroup type (Q), number of isoprenoid units in the side chain (m) and number of double bonds (n)], which is involved in electron transferin the photosystem I of cyanobacteria and phototrophic eukaryotes (Collins and Jones, 1981; Hiraishi, 1999; Nowicka and Kruk, 2010). The side chains usually comprise 4 to 10 isoprenoid units and typically contain one double bond per isoprenoid unit in *Bacteria* (hereafter termed fully unsaturated), while in *Archaea* partially unsaturated and fully saturated side chains are more common (Collins and Jones, 1981; Tindall et al., 1989; Hiraishi, 1999).

The different quinone types have distinct redox potentials that depend on headgroup structures, while the influence of length of the side chain and degree of its unsaturation has not been systematically studied (Supp. Table VII.1; Nowicka and Kruk, 2010). The only organisms that do not contain quinones are fermentative *Bacteria* and methanogens. However, *Methanosarcina mazei* and potentially other representatives of the order *Methanosarcinales* synthesize methanophenazine as a substitute electron carrier (Supp. Fig. VII.1; Abken et al., 1998). Complementary to polar membrane lipid analysis, quinone profiling offers PCR-independent taxonomic characterization and quantification of microbial biomass in environmental samples (Collins and Jones, 1981; Hiraishi, 1999; Hiraishi et al., 2003). Furthermore, redox conditions and metabolism are major controls on the occurrence and relative abundance of specific quinones in microorganisms due to their distinct redox potentials (Supp. Table VII.1; Hedrick and White, 1986; Wissenbach et al., 1990; Bekker et al., 2007; Nowicka and Kruk, 2010). Therefore, quinone distributions in the environment likely contain an additional functional dimension related to microbial metabolisms and redox conditions.

In addition to their function in electron transport chains, quinones might contribute to membrane adaptation to physiological stresses similar to membrane lipids. For instance, Sévin and Sauer (2014) observed that sustained osmotic-stress tolerance in *Escherichia coli* depended on accumulation of ubiquinone. Therefore, characterization of the cellular

quinone pool appears essential for a holistic understanding of membrane properties in microorganisms.

Structural characterization and quantification of respiratory quinones facilitates the elucidationof microbial electron transport chains (Whittaker et al., 2000; Stams and Plugge, 2009; Coates et al., 2013). Similarly, interpretation of quinone profiles in environmental samples is facilitated by detailed description of quinone diversity in cultivated organisms (Collins and Jones, 1981; Hiraishi, 1999; Urakawa et al., 2000; Urakawa et al., 2005).Comprehensive analysis of the occurrence of respiratory quinones in *Archaea* furthermore supports genetic investigations on the evolutionary history of quinone biosynthesis (cf. Sousa et al., 2013; Zhi et al., 2014). However, the knowledge on the distribution of quinone structural types particularly in the *Archaea* remains fragmentary. For example, the quinone composition of representatives of the ammonia-oxidizing *Thaumarchaeota*, possibly among the most abundant *Archaea* on Earth (cf. Stahl and de la Torre, 2012), has not been explored yet, despite the presumed central role of quinones in current models of the respiratory pathway for ammonia oxidation (Walker et al., 2010; Stahl and de la Torre, 2012).

Conventional methods used for quinone analysis are based on thin-layer or high performance liquid chromatography (HPLC) coupled to UV spectrophotometric detection. These methods do not allow precise quantification of quinones in complex mixtures and structural identification of unknown compounds (Hiraishi, 1999). Moreover, UV-based techniques require work-intensive preparative steps such as the prior separation of ubiquinones from menaquinones (Hiraishi, 1999).The coupling of HPLC to mass spectrometry (MS) provides a powerful framework to explore the taxonomic and process-related information contained in the structural diversity and abundance ofquinones (Hiraishi, 1999; Geyer et al., 2004; Kaiser et al., 2012).

Here, we performed an in-depth analysis of respiratory quinones in cultured representatives of three archaeal phyla originating from a wide range of environments including soils, hypersaline lakes, geothermal systems, and the surface ocean. These analyses were facilitated by modifying recently developed HPLC–MS methods to feature simultaneous detection and quantification of archaeal and bacterial respiratory quinones as well as core and intact polar glycerol-based membrane lipids. We explored the phylogenetic implications of respiratory quinone distribution in *Archaea* and evaluated the potential of quinones as chemotaxonomic markers. For the first time, we report the quinone inventories of soil and planktonic representatives of the phylum *Thaumarchaeota* as well as the crenarchaeal species *Ignicoccus hospitalis*, *Pyrolobus fumarii*, and *Sulfolobus islandicus*. Additionally, *M. acetivorans* and *M. barkeri* were analyzed for their methanophenazine composition. In order to demonstrate the strength of simultaneous quinone and membrane lipid profiling in the environment, we investigated thaumarchaeal abundance

in suspended particulate matter samples from the southern Black Sea, where archaeal community composition is linked to the distinctly stratified water column chemistry (Coolen et al., 2007; Wakeham et al., 2007).

VII.2. Results

VII.2.1. Chromatographic separation and mass spectrometric characterization of respiratory quinones

Reversed phase (RP)-HPLC–MS analysis of different archaeal culture extracts yielded chromatographic separation of respiratory quinones as well as core and intact polar glycerol diphytanyl diether (archaeols) and glycerol dibiphytanyl glycerol tetraether lipids (GDGTs; Fig. VII.1). Retention of quinones was dependent on headgroup type and isoprenoid alkyl chain length and its degree of unsaturation (Fig. VII.1 & Supp. Fig. VII.2) to the effect that compounds of a given headgroup type were baseline-separated when they possessed a different number of isoprenoid units and/or double bonds in the alkyl chain. The retention time increased with increasing length of the isoprenoid chain but decreased with increasing number of double bonds. Similarly, archaeal membrane lipids were separated by headgroup type and side chain structures as described previously (Zhu et al., 2013a, Fig. VII.1). For quinones with identical side chain structure, the elution order was UQs, PQs, demethylmenaquinone (DMKs), MKs, methionaquinones (MTKs), and methylmenaquinones (MMKs; Supp. Fig. VII.2 & Supp. Fig. VII.6). Co-elution was observed for several structurally distinct quinones (e.g., $DMK_{7:7}$, $MTK_{6:5}$, $MMK_{6:6}$; Supp. Fig. VII.2) but did not interfere with their quantification due to the MS-based detection. Application of the RP-HPLC–MS method from Wörmer et al. (2013) to a marine sediment sample also yielded chromatographic separation of respiratory quinones, with the same elution order as described for the protocol by Zhu et al. (2013a). The method by Wörmer et al. (2013) additionally allowed the detection of bacterial intact polar membrane lipids and reduced analysis time from 90 to 30 min (Supp. Fig. VII.6). While archaeal lipids could be detected using this method, differences in tetraether side chain cyclization could not be fully resolved (Wörmer et al., 2013).

Respiratory quinones were identified based on exact molecular mass and fragmentation patterns in MS2 mode. The systematic fragmentation in MS^2 spectra was primarily related to the structural properties of the headgroup and in part to the isoprenoid side chain (Fig. VII.2, Fig. VII.3, Supp. Table VII.1). For example, saturated menaquinones (MKs) showed a dominant product ion at *m/z* 187. This ion represents the naphthoquinone moiety after loss of the isoprenoid side chain (Tindall et al., 1989). Similarly, the major product ions of demethylmenaquinones (DMKs), methylmenaquinones (MMKs,

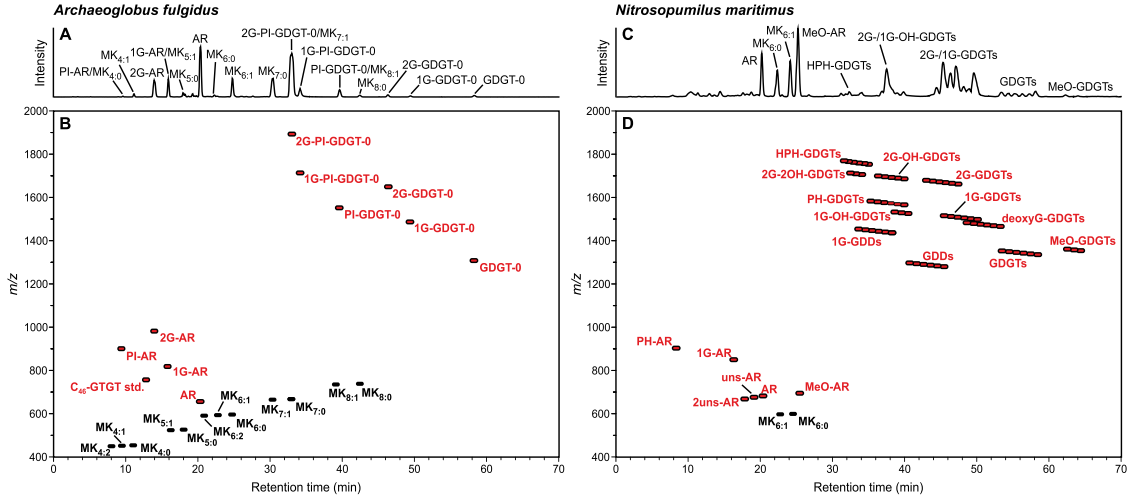

Figure VII.1. Reversed phase HPLC–MS analyses of archaeal cultures demonstrating simultaneous detection of respiratory quinones as well as core and intact polar lipids. Examples for reconstructed base peak chromatograms and density maps obtained from *Archaeoglobus fulgidus* (A, B) and *Nitrosopumilus maritimus* (C, D). Density map color code: red, glycerolipids; black, quinones. Lipid nomenclature designates combinations of core lipid types (GDGT-0, acyclic GDGT; OH-GDGT, hydroxy-GDGT; GDD, glycerol dialkanol diether; MeO-GDGT, methoxy GDGT; AR, archaeol; MeO-AR, methoxy AR) and headgroups (PI, phosphatidylinositol; PH, phosphohexose; HPH, hexose phosphohexose; 1G, monoglycosyl; 2G, diglycosyl). For chemical structures of lipids see Supp. Fig. VII.5.

i.e., thermoplasmaquinones), sulfolobusquinones (SQs), caldariellaquinones (CQs), benzodithiophenoquinones (BDTQs), UQs, PQs, and methanophenazine (MP) were also related to the loss of the quinone headgroup. Fragmentation of polyunsaturated quinones often showed additional product ions related to the loss of parts of the isoprenoid chain while methylthiol-based quinones produced fragments resulting from the loss of this moiety (Fig. VII.2, Supp. Table VII.1).

VII.2.2. Occurrence of respiratory quinones in distinct archaeal species

Respiratory quinones were analyzed in 25 cultured representatives of 14 archaeal orders spanning the three archaeal phyla *Euryarchaeota*, *Crenarchaeota*, and *Thaumarchaeota* (Table VII.1; Fig. VII.3). Seven respiratory quinone classes were identified in the investigated archaeal strains containing fully unsaturated to completely saturated side chains comprised of four to eight isoprenoid units. No respiratory quinones were detected in *Staphylothermus marinus*, *Thermococcus kodakarensis*, *Pyrococcus furiosus*, *Methanopyrus kandleri*, *Methanothermobacter thermautotrophicus*, and *Methanothermococcus thermolithotrophicus*.

Fully saturated quinones were dominant in most of the archaeal strains while partially unsaturated quinones were less abundant. Fully unsaturated side chains were only detected in the euryarchaeal acidophile *Thermoplasma acidophilum*, and the euryarchaeal

halophiles *Haloferax volcanii* and *Halorubrum lacusprofundi*. Menaquinones were detected in all quinone-producing strains except for members of the order *Sulfolobales*. Representatives of this order contained exclusively the sulfur-bearing quinones CQ, SQ and BDTQ with fully saturated, monounsaturated, or diunsaturated side chains comprised of five to six isoprenoid units (De Rosa et al., 1977; Thurl et al., 1986; Nicolaus et al., 1992).

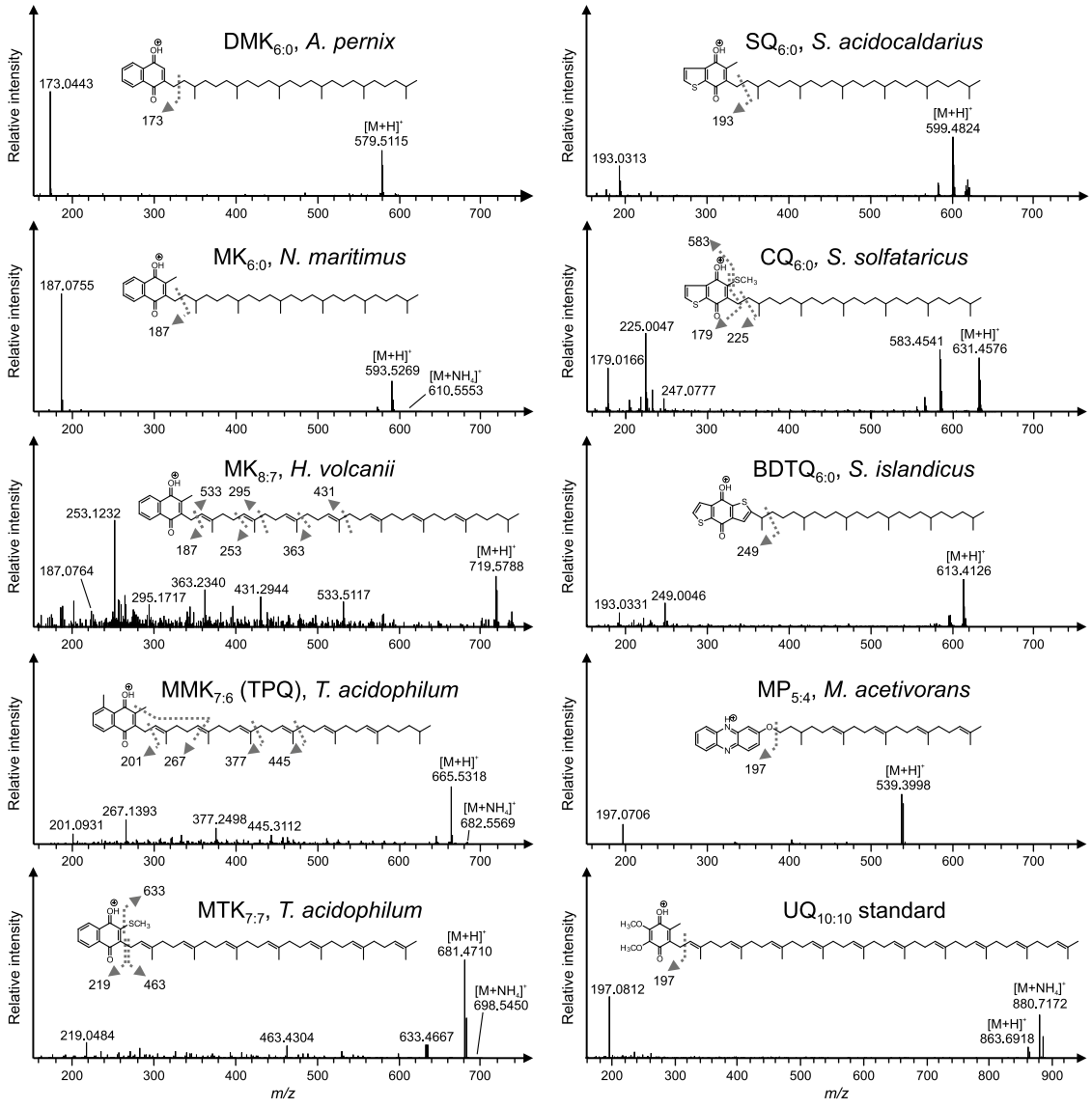

Figure VII.2. Structures and MS^2 spectra of protonated molecules of respiratory quinones (DMK, MK, MMK, MTK, SQ, CQ, BDTQ) and methanophenazine (MP), an electron carrier in Methanosarcinales, from lipid extracts of archaeal cultures and ubiquinone ($UQ_{10:10}$; available as commercial standard). The length and degree of unsaturation of the isoprenoid side chains of quinones may vary from 4 to 14 and completely saturated to fully unsaturated, respectively. Quinone nomenclature ($Q_{m:n}$) with headgroup type (Q), number of isoprenoid units in the side chain (m) and number of double bonds (n). DMK: Demethylmenaquinone. MK: Menaquinone. MMK: Methylmenaquinone. MTK: Methionaquinone. BDTQ: Benzodithiophenoquinone. SQ: Sulfolobusquinone. CQ: Caldariellaquinone. UQ: Ubiquinone.

Table VII.1. Occurrence and relative abundance (% of total quinones, quinone abundances below 0.1 % were rounded to 0.1 %) of respiratory quinones in archaeal strains investigated in this study. Quinone nomenclature ($Q_{m:n}$) indicates headgroup type (Q), number of isoprenoid units in the side chain (m) and number of double bonds (n). DMK: Demethylmenaquinone. MK: Menaquinone. MMK: Methylmenaquinone. MTK: Methionaquinone. BDTQ: Benzodithiophenoquinone. SQ: Sulfolobusquinone. CQ: Caldariellaquinone. MP: Methanophenazine. OH-MP: Hydroxymethanophenazine.

Phylum	Order/Group	Species	Strain	Habitat	Major quinones (relative abundance in %)	Minor quinones (relative abundance in %)
Thaumarchaeota	Group I.1a	*Nitrosopumilus maritimus*	SCM1	Marine water	$MK_{6:0}$ (91.0)	$MK_{6:1}$ (9.0)
	Group I.1b	*Nitrososphaera viennensis*	EN76	Soil	$MK_{6:0}$ (76.1), $MK_{6:1}$ (23.9)	-
		Nitrososphaera gargensis	Ga9.2	Terrestrial hydrothermal	$MK_{6:0}$ (68.0), $MK_{6:1}$ (32.0)	-
	SAGMCG-1	*Nitrosotalea devanaterra*	Nd1	Acidic soil	$MK_{6:0}$ (72.4), $MK_{6:1}$ (27.6)	-
Crenarchaeota	*Desulfurococcales*	*Ignicoccus hospitalis*	KIN4/1	Marine hydrothermal	$DMK_{6:0}$ (62.1), $DMK_{6:1}$ (14.1), $MK_{6:0}$ (13.7)	$MK_{6:1}$ (8.6), $DMK_{5:0}$ (0.5), $MK_{7:0}$ (0.2), $MK_{5:1}$ (0.2), $DMK_{6:2}$ (0.2), $MK_{7:1}$ (0.1), $MK_{5:0}$ (0.1), $DMK_{5:1}$ (0.1)
		Staphylothermus marinus	F1	Marine hydrothermal	-	-
		Aeropyrum pernix	K1	Marine hydrothermal	$MMK_{6:0}$ (74.8), $MK_{6:0}$ (15.0)	$MMK_{6:1}$ (5.7), $MK_{6:1}$ (1.6), $MMK_{5:0}$ (1.2), $MTK_{6:0}$ (1.0), $MK_{5:0}$ (0.3), $MTK_{6:1}$ (0.3), $DMK_{5:0}$ (0.1), $DMK_{5:1}$ (0.1)
		Pyrolobus fumarii	1A	Marine hydrothermal	$DMK_{6:0}$ (92.4)	$DMK_{5:0}$ (5.5), $DMK_{6:1}$ (1.1), $MK_{6:0}$ (0.6), $MK_{5:0}$ (0.1), $DMK_{7:0}$ (0.1), $DMK_{5:1}$ (0.1),
	Sulfolobales	*Metallosphaera prunae*	Ron 12/II	Heated mine tailings	$CQ_{6:0}$ (86.1), $CQ_{6:1}$ (12.2)	$CQ_{6:2}$ (1.4), $CQ_{5:0}$ (0.1), $SQ_{6:0}$ (0.1)
		Sulfolobus acidocaldarius	98-3	Terrestrial hydrothermal	$CQ_{6:0}$ (80.9)	$SQ_{6:0}$ (9.7), $CQ_{6:1}$ (9.2), $CQ_{6:2}$ (0.2)
		Sulfolobus solfataricus	P1	Terrestrial hydrothermal	$CQ_{6:0}$ (85.8), $CQ_{6:1}$ (13.7)	$SQ_{6:0}$ (0.5)
		Sulfolobus islandicus	Y.N.15.51	Terrestrial hydrothermal	$SQ_{6:0}$ (42.9), $CQ_{6:0}$ (36.4), $CQ_{6:1}$ (14.6)	$CQ_{6:2}$ (3.2), $SQ_{5:0}$ (1.5), $CQ_{5:0}$ (0.9), $BDTQ_{6:0}$ (0.4), $CQ_{5:1}$ (0.1)
Euryarchaeota	*Thermococcales*	*Pyrococcus furiosus*	Vc 1	Marine hydrothermal	-	-
		Thermococcus kodakarensis	KOD1	Terrestrial hydrothermal	-	-
	Methanopyrales	*Methanopyrus kandleri*	AV19	Marine hydrothermal	-	-
	Methanobacteriales	*Methanothermobacter thermautotrophicus*	Delta H	Terrestrial hydrothermal	-	-
	Methanococcales	*Methanothermococcus thermolithotrophicus*	SN-1	Marine hydrothermal	-	-
	Thermoplasmatales	*Thermoplasma acidophilum*	122-1B2	Terrestrial hydrothermal	$MK_{7:7}$ (40.1), $DMK_{7:7}$ (24.0), $MTK_{7:7}$ (17.3)	$MK_{7:6}$ (6.4), $DMK_{7:6}$ (3.4) $MK_{7:5}$ (3.2), $MMK_{7:7}$ (2.1), $DMK_{6:6}$ (1.0), $MK_{6:6}$ (0.7), $MTK_{7:5}$ (0.4), $MTK_{7:4}$ (0.2), $MTK_{7:6}$ (0.2), $MMK_{7:0}$ (0.1), $MMK_{7:1}$ (0.1), $MK_{7:4}$ (0.1), $MK_{6:5}$ (0.1), $MTK_{8:8}$ (0.1), $MTK_{6:4}$ (0.1), $MTK_{6:5}$ (0.1), $DMK_{7:4}$ (0.1), $DMK_{7:5}$ (0.1), $DMK_{6:5}$ (0.1)
	Archaeoglobales	*Archaeoglobus fulgidus*	VC-16	Marine hydrothermal	$MK_{7:0}$ (68.9), $MK_{7:1}$ (25.0)	$MK_{6:0}$ (2.1), $MK_{8:0}$ (1.1), $MK_{4:2}$ (1.1), $MK_{6:2}$ (0.9), $MK_{8:1}$ (0.2), $MK_{6:1}$ (0.2), $MK_{4:0}$ (0.2), $MK_{4:1}$ (0.2), $MK_{5:0}$ (0.1), $MK_{5:1}$ (0.1)
		Archaeoglobus profundus	AV18	Marine hydrothermal	$MK_{7:0}$ (61.1), $MK_{7:1}$ (36.5)	$MK_{5:1}$ (0.8), $MK_{6:0}$ (0.8), $MK_{5:0}$ (0.5), $MK_{5:1}$ (0.3)
	Halobacteriales	*Haloferax volcanii*	DS2	Terrestrial hypersaline	$MK_{8:7}$ (67.3), $MK_{8:8}$ (22.9)	$MK_{7:7}$ (7.1), $MK_{7:6}$ (0.7)
		Halorubrum lacusprofundi	ACAM34	Terrestrial hypersaline	$MK_{8:7}$ (54.4), $MK_{8:8}$ (45.1)	$MK_{7:6}$ (0.5), $MK_{7:7}$ (0.1)
	Methanosarcinales	*Methanosarcina acetivorans*	C2A	Marine sediment	$MP_{5:4}$ (57.0), OH-$MP_{5:4}$ (18.4), OH-$MP_{5:5}$ (12.6)	OH-$MP_{5:3}$ (7.9), $MP_{5:3}$ (4.2)
		Methanosarcina barkeri	MS	Terrestrial & marine sediment	$MP_{5:2}$ (67.2), $MP_{5:3}$ (25.1)	$MP_{5:1}$ (3.1), $MP_{5:0}$ (1.6), $MP_{5:4}$ (0.6), OH-$MP_{5:3}$ (1.1), OH-$MP_{5:5}$ (0.7), OH-$MP_{5:4}$ (0.5)
		Methanosarcina mazei	S-6	Soils & sediments	$MP_{5:4}$ (93.1)	$MP_{5:3}$ (2.7), OH-$MP_{5:4}$ (2.2), OH-$MP_{5:5}$ (1.5), OH-$MP_{5:3}$ (0.5)

The major quinone found in all investigated representatives of the phylum *Thaumarchaeota* was a fully saturated menaquinone with six isoprenoid units ($MK_{6:0}$) while a less abundant monounsaturated analog ($MK_{6:1}$) was also detected. Similarly, the major quinones in *Archaeoglobus fulgidus* and *Archaeoglobus profundus* were saturated and monounsaturated MKs with the dominant compounds containing seven isoprenoid units as their side chain. Fully unsaturated MKs occurred only in euryarchaeal species, the thermoacidophile *T. acidophilum* as well as the halophiles *H. volcanii* and *H. lacusprofundi*, while the length of the isoprenoid side chains differed. The halophiles contained predominantly $MK_{8:7}$ and $MK_{8:8}$, whereas *T. acidophilum* contained mainly $MK_{7:7}$ (Collins et al., 1981). Representatives of the crenarchaeal order *Desulfurococcales* contained minor amounts of MKs and in the case of *Aeropyrum pernix* also minor proportions of MTKs. The dominant quinone of *I. hospitalis* and *P. fumarii* were saturated MMKs with $MMK_{6:0}$ being most abundant in both strains. These saturated MMKs were not detected in other archaeal strains. In contrast, *A. pernix* was characterized by a high abundance of $DMK_{6:0}$. Minor amounts of DMKs but with seven isoprenoid units were exclusively detected in *T. acidophilum*. Additionally, *T. acidophilum* contained several polyunsaturated MMKs that were not detected in the *Desulfurococcales* or any other archaeal strain.

In contrast to the archaeal strains described above, respiratory quinones were not detected in the *Methanosarcinales*; instead, representatives of this order contained the functional quinone analogue methanophenazine, an electron carrier directly involved in methanogenesis (Abken et al., 1998). The degree of unsaturation of methanophenazine was specific for *M. acetivorans*, *M. barkeri*, and *M. mazei* (Table VII.1; Fig. VII.3). A previously not described compound in *Methanosarcinales* was tentatively identified as triunsaturated methanophenazine ($MP_{5:3}$), which occurred in all three analyzed strains. In M. barkeri, di- and monounsaturated MPs ($MP_{5:2}$, $MP_{5:1}$, respectively), and a fully saturated MP ($MP_{5:0}$) were additionally identified. Furthermore, novel hydroxymethanophenazines (OH-MP), i.e., methanophenazines with an hydroxylated isoprenoid side chain, were tentatively identified in *M. acetivorans* and *M. mazei* (Supp. Fig. VII.4).

VII.2.3. Chemotaxonomic patterns

Complementing the quinone distribution in the 25 investigated archaeal cultures with published distributions from 11 additional strains (Fig. VII.3; supplementary information) revealed several major chemotaxonomic groupings. The orders *Sulfolobales* and *Methanosarcinales* formed distinct clusters based on the exclusive occurrence of SQs, CQs and BDTQs, and MPs/OH-MPs, respectively. While menaquinones occurred in all quinone-producing archaeal orders, the menaquinone producing archaeal species could be separated into three groups based on the degree of side-chain unsaturation and the co-

occurrence of other quinone types. The first group comprised exclusively *Halobacteriales* strains and was characterized by polyunsaturated MKs with predominantly 7 or 8 isoprenoid units. In contrast, the two other groups, the *Thaumarchaeota* on the one hand and the *Thermoproteales* as well as most of the *Desulfurococcales* strains on the other hand, were characterized by fully saturated side chains. The *Thaumarchaeota* were further distinguished by the sole occurrence of $MK_{6:0}$ and $MK_{6:1}$, while menaquinone diversity in *Thermoproteales* and most *Desulfurococcales* strains was higher. The *Archaeoglobales* showed a similar quinone composition as *Thaumarchaeota*, *Thermoproteales* and *Desulfurococcales* but were the only *Euryarchaeota* containing saturated quinones. Similarly, *T. acidophilum* could be distinguished from other *Euryarchaeota* by the occurrence of a large range of unsaturated menaquinones and other naphthoquinone derivatives such as DMKs, MTKs, and MMKs.

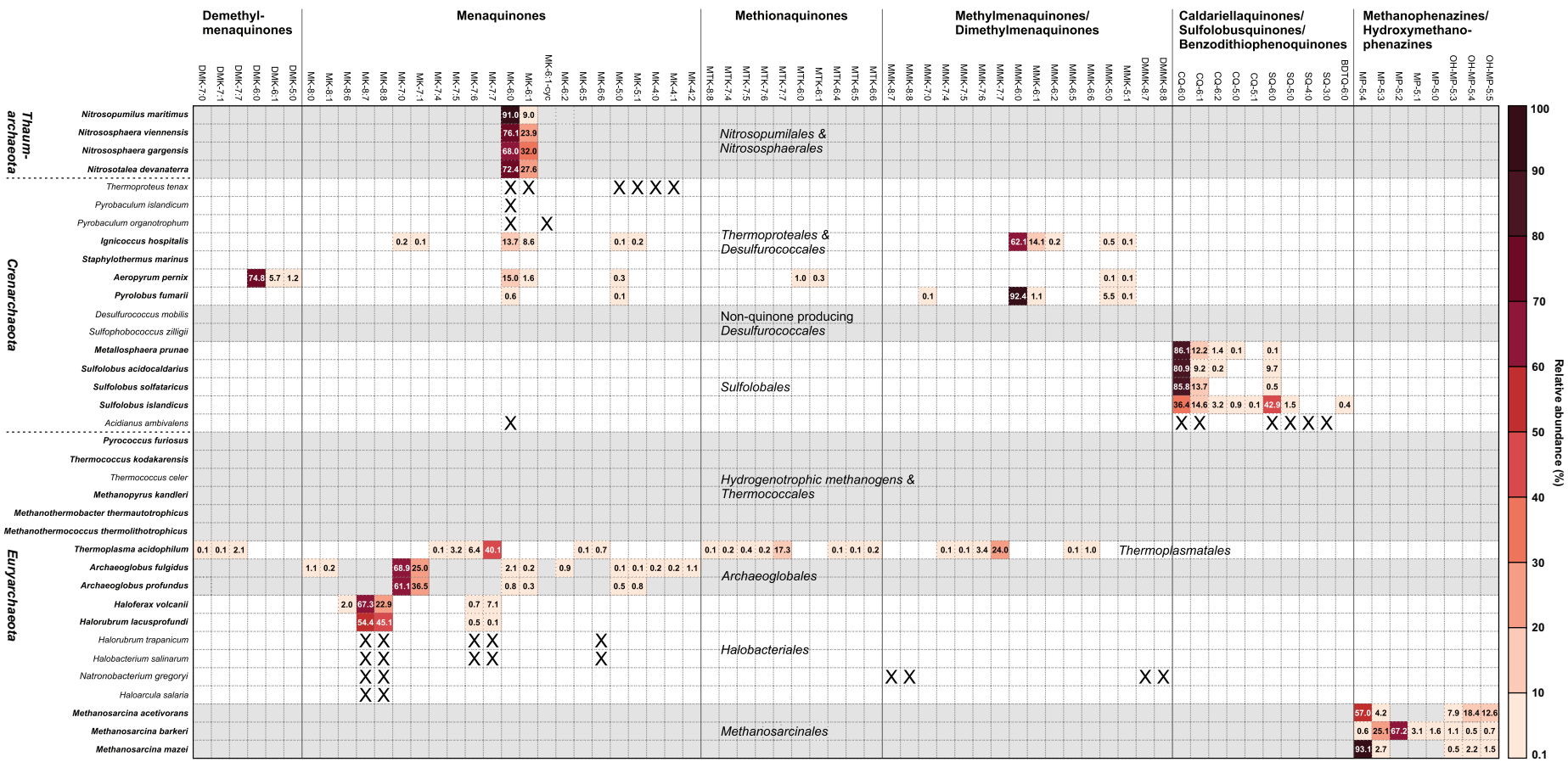

Figure VII.3. Relative abundances of respiratory quinones and methanophenazines in cultivated strains of the phyla *Thaumarchaeota*, *Crenarchaeota*, and *Euryarchaeota*. Major chemotaxonomic groupings are labeled and highlighted in grey/white. Compiled from strains investigated in this study (bold) and published data (indicating occurrence, (X) and absence/not reported (blank) of quinone types; sources listed in supplementary information). Quinone abundances below 0.1 % were rounded to 0.1 %.

VII.2.4. Thaumarchaeal quinones and glycerolipids in marine suspended particulate matter

In order to validate the biomarker potential of archaeal quinones, we investigated thaumarchaeal quinone in concert with membrane lipid abundances in the water column of the southern Black Sea (Supp. Table VII.2). Suspended particulate matter was sampled at nine depth intervals covering all major geochemical zones from oxic water (40 m water depth) to the suboxic chemocline (90, 120, 150 m) and the underlying anoxic (sulfidic) zone (300, 500, 700, 900, 1200 m).

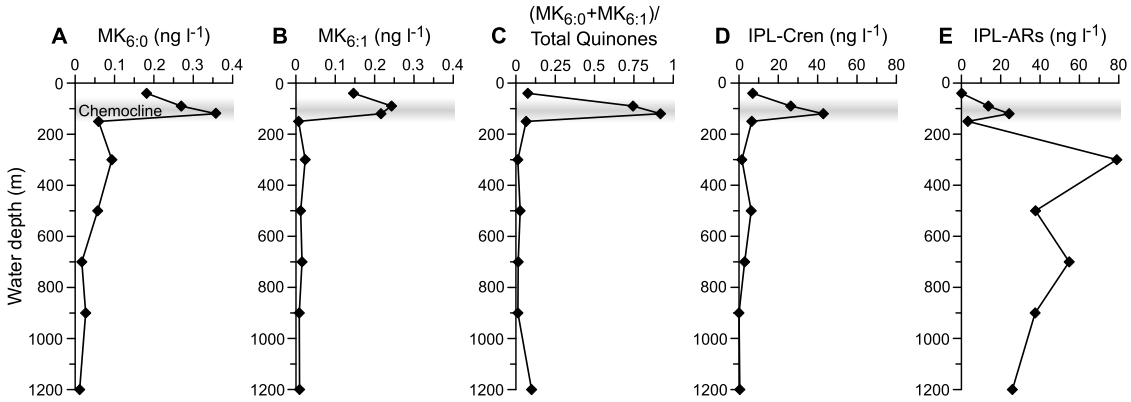

Figure VII.4. Distribution of $MK_{6:0}$ (**A**) and $MK_{6:1}$ (**B**), abundance of $MK_{6:0}$ and $MK_{6:1}$ relative to total quinones (**C**) intact polar crenarchaeol lipids (**D**), as well as intact polar archaeols (**E**) in the water column of the southern Black Sea. The location of the chemocline, indicating the transition from shallow oxic to deep anoxic water, is shaded in grey.

The concentrations of the *Thaumarchaeota*-specific quinones $MK_{6:0}$ and $MK_{6:1}$ were quantified in comparison to monoglycosidic, diglycosidic and hexose-phosphohexose crenarchaeol derivatives, i.e., major membrane lipids of marine *Thaumarchaeota* (Supp. Fig. VII.5). The concentration of $MK_{6:0}$ increased from oxic waters ($0.18\,\mathrm{ng\,l^{-1}}$) to the suboxic waters of the chemocline at 120 m ($0.36\,\mathrm{ng\,l^{-1}}$; Fig. VII.4a). $MK_{6:1}$ was similarly concentrated in the oxic waters ($0.14\,\mathrm{ng\,l^{-1}}$) but showed a shallower maximum at the chemocline at 90 m ($0.24\,\mathrm{ng\,l^{-1}}$; Fig. VII.4b). The concentrations of both $MK_{6:0}$ and $MK_{6:1}$ were one order of magnitude lower in the anoxic part of the water column below 150 m ($0.01\,\mathrm{ng\,l^{-1}}$). In contrast, total quinone concentrations, i.e., the sum of ubiquinones, menaquinones, plastoquinones, peaked in the oxic part (40 m, $4.3\,\mathrm{ng\,l^{-1}}$) as well as in the anoxic zone below the chemocline at 300 m ($9.4\,\mathrm{ng\,l^{-1}}$; Supp. Table VII.3) but were minimal between 90-150 m. The ratio of $MK_{6:0}$ to $MK_{6:1}$ relative to total quinones showed a sharp maximum between 90-120 m (Fig. VII.4c). Similar to the $MK_{6:0}$ and $MK_{6:1}$ profiles, the distribution of total intact polar crenarchaeol showed a peak between 90 and 120 m in the suboxic waters of the chemocline with $42.8\,\mathrm{ng\,l^{-1}}$ and minimal concentrations in the fully oxic and anoxic parts of the water column (Fig. VII.4d). Intact polar archaeols,

i.e., all glycolipids and phospholipids with an archaeol core structure (Supp. Fig. VII.5; Supp. Table VII.3), showed a maximum in the anoxic zone at 300 m water depth and below but were also detected in significant amounts in the chemocline.

VII.3. Discussion

VII.3.1. Phylogenetic significance of quinone biosynthesis in Archaea

A major taxonomic divide among the *Archaea* is the occurrence of menaquinones. Their presence in the archaeal phylum *Thaumarchaeota* (Table VII.1; Fig. VII.3) as well as other deeply branching archaeal (Table VII.1) and bacterial lineages (Supp. Table VII.1; Nitschke et al., 1995; Schütz et al., 2000; Schoepp-Cothenet et al., 2009) suggests that menaquinone biosynthesis was present in the last common ancestor of *Archaea* and *Bacteria* (Schoepp-Cothenet et al., 2013; Zhi et al., 2014). In particular, the low mid-point redox potentials of menaquinones ($-67\,\mathrm{mV}$; Wagner et al., 1974) support an origin of the last common ancestor in a reducing habitat (Nitschke et al., 1995; Schütz et al., 2000; Schoepp-Cothenet et al., 2009). However, the discovery of two independent biosynthetic pathways (Hiratsuka et al., 2008) suggests that menaquinone biosynthesis has evolved at least twice (Zhi et al., 2014). While the 'classical' pathway operates in most *Bacteria* and *Halobacteriales*, the alternative futalosine pathway is employed by other *Archaea* and some *Bacteria* (Sousa et al., 2013; Zhi et al., 2014). The respiratory quinone composition of the *Halobacteriales* is indeed remarkably similar to that of halophilic *Bacteria* (Collins et al., 1981; Schoepp-Cothenet et al., 2009) and appears to result from massive lateral gene transfer from bacterial donors to an ancestral methanogenic recipient (Boucher et al., 2003; Nelson-Sathi et al., 2012; Zhi et al., 2014). The acquisition of polyunsaturated menaquinone biosynthesis might have been advantageous in extremely saline habitats (cf. Sévin and Sauer, 2014), in analogy to the high abundances of unsaturated isoprenoid membrane lipids biosynthesized by *Halobacteriales* in response to high salinity (Gibson et al., 2005; Stiehl et al., 2005; Dawson et al., 2012). In contrast, saturated menaquinones occur in those archaeal clades (Table VII.1; Fig. VII.3) that have also predominantly saturated polar membrane lipids, such as the *Thaumarchaeota* and most thermophilic *Crenarchaeota* and *Euryarchaeota* (Thurl and Schäfer, 1988; Trincone et al., 1992; Völkl et al., 1993; Morii et al., 1999; Jahn et al., 2004; Tarui et al., 2007; Elling et al., 2014). Given the absence of saturated menaquinones in *Bacteria*, these compounds may represent an ancestral and diagnostic feature of the *Archaea*.

Methylated naphthoquinone derivatives (MMKs) are likely derived from methylation of menaquinones and are found in *Bacteria* (Collins and Jones, 1981), thermophilic *Archaea* (Fig. VII.3), and the haloalkaliphile *Natronobacterium gregoryi*, which also contains dimethylated menaquinones (DMMKs; Fig. VII.3; Collins and Tindall, 1987). Similar

to menaquinones, DMKs are found in *Bacteria* as well as *A. pernix* (Fig. VII.3; Nishida et al., 1999) and *T. acidophilum* (Fig. VII.3) and are precursors in menaquinone biosynthesis in the 'classical' pathway (Bentley and Meganathan, 1982) and potentially in the futalosine pathway (Hiratsuka et al., 2008). In addition to DMKs, *A. pernix* and *T. acidophilum* appear to be the only archaeal species to produce MTKs, methylthio-derivatives of naphthoquinones, which otherwise have only been observed in aerobic thermophilic, sulfur-metabolizing *Bacteria* belonging to the genera *Aquifex* and *Hydrogenobacter* (Hiraishi, 1999). The biosynthesis of MTKs in both *Aquificae* as well as *A. pernix* and *T. acidophilum* may represent either convergent development due to their shared preference for oxic, sulfur-rich geothermal habitats or may have been acquired via lateral gene transfer, which is thought to occur frequently among thermophiles (Nelson et al., 1999; Ruepp et al., 2000; Koonin et al., 2001).

As reduced menaquinones (menaquinols) may become spontaneously oxidized in the presence of oxygen (Kröger and Dadák, 1969), the biosynthesis of CQs, SQs and BDTQs featuring higher midpoint redox potentials (Supp. Table VII.1) by the *Sulfolobales* likely occurred as an adaptation to aerobic metabolism (Nitschke et al., 1995; Schütz et al., 2000; Schoepp-Cothenet et al., 2009, 2013) similar to the occurrence of ubiquinone biosynthesis in proteobacteria and plastoquinones in cyanobacteria (Schütz et al., 2000). This shift to a high-redox-potential bioenergetic chain does not seem to have occurred in the obligate aerobic, ammonia-oxidizing *Thaumarchaeota*. In addition to the high affinity of *Thaumarchaeota* to both oxygen and ammonium (Martens-Habbena et al., 2009), their menaquinone-based respiratory chains may facilitate persistence of *Thaumarchaeota* in oceanic redoxclines and other hypoxic environments compared to ubiquinone-utilizing ammonia-oxidizing bacteria (e.g. Stewart et al., 2012). Assuming that side chain length and unsaturation have only minor effects on quinone redox potentials, the large difference between the redox potentials of menaquinone/menaquinol ($MK_{6:6}$: $E'_0 = -67\,mV$; Wagner et al., 1974) and the NO_2/NH_3 redox couple ($E'_0 = +340\,mV$; Simon, 2002) suggests that thaumarchaeal respiratory chains differ fundamentally from those of ammonia-oxidizing bacteria.

Despite the central role of quinones in most studied archaeal respiratory chains, a considerable number of cultivated species does not synthesize quinones and hence appear to harbor distinct respiratory systems. The absence of quinones and functional quinone analogs as well as cytochromes in hydrogenotrophic methanogens (Thauer et al., 2008) in favor of a sole dependence on chemiosmosis appears to be a simpler, more ancient metabolic configuration than quinone-based energy metabolism and has been regarded as testimony for a methanogenic ancestor of the *Archaea* (Martin, 2012; Sousa et al., 2013). The occurrence of methanophenazines as quinone analogs as well as of cytochromes in *Methanosarcinales* thus appears to be a more recent evolutionary trait and might be

linked to the diversification of methanogenic substrates and increased substrate utilization efficiency of the *Methanosarcinales*. In contrast, a 'menaquinone-first' hypothesis of archaeal metabolism implies repeated loss of menaquinone-biosynthetic capacities during archaeal radiation after separation from the common ancestor of *Archaea* and *Bacteria* (Schoepp-Cothenet et al., 2013; Zhi et al., 2014), resulting in the patchy distribution of quinone biosynthesis in the crenarchaeal order *Desulfurococcales* (Fig. VII.3). Based on current phylogenetic models (Spang et al., 2010; Brochier-Armanet et al., 2011) and the occurrence of menaquinones in *Archaea* (Fig. VII.3), a 'menaquinone-first' scenario would imply the conservation of menaquinone biosynthesis in *Thaumarchaeota* and in a considerable fraction of (cultivated) *Crenarchaeota* as well as loss of biosynthetic capability in the ancestor of *Euryarchaeota*. Menaquinone biosynthesis in *Archaeoglobales* and *Thermoplasmatales* would then need to have been acquired through lateral gene transfer from other microbes, as evidently happened to the ancestor of the *Halobacteriales* (Nelson-Sathi et al., 2012). This scenario seems likely given the isolated occurrence of menaquinone biosynthesis in *Archaeoglobales* and *Thermoplasmatales* as well as high proportions of laterally acquired genes from *Bacteria* and other *Archaea* in these thermophilic archaeal orders (Ruepp et al., 2000; Boucher et al., 2001; Nelson-Sathi et al., 2014). Analysis of the occurrence of respiratory quinones in additional, especially basally branching, archaeal representatives may help to further resolve the evolutionary history of quinone biosynthesis.

In contrast to numerous thermophilic and halophilic archaeal cultures, only few non-methanogenic mesophilic isolates exist, which are exclusively ammonia-oxidizing archaea of the phylum *Thaumarchaeota*. Based on the high abundance and diversity of uncultured mesophilic planktonic (DeLong, 1992; Fuhrman et al., 1992; Karner et al., 2001) and benthic archaeal groups (Biddle et al., 2006; Teske and Sørensen, 2008), the majority of the archaeal quinone diversity currently remains unconstrained. The analysis of archaeal respiratory quinones in environmental samples could therefore yield additional insights into diversity and respiratory pathways of uncultured *Archaea*.

In conclusion, the heterogeneous taxonomic distribution of quinone types among the *Archaea* observed in this study yields insights into the evolutionary history of quinone biosynthesis. Specifically, the distribution of menaquinones in *Archaea* suggests an ancestral origin of menaquinone biosynthesis in *Cren-* or *Thaumarchaeota*. In contrast, the highly divergent quinone distribution in *Euryarchaeota* may result from a combination of vertical inheritance, lateral gene transfer and gene loss.

VII.3.2. Biomarker potential of archaeal respiratory quinones

In ecosystems that are not amenable to cultivation-dependent approaches, lipidomics and metagenomics are routinely applied to describe microbial community composition and potential function. The approach applied in this study provides streamlined analytical protocols for highly sensitive, detailed and simultaneous profiling of quinones and membrane lipids in environmental samples. This facilitates direct comparison of archaeal glycerolipids and quinone derivatives (Fig. VII.1, Supp. Fig. VII.6) to (*i*) estimate microbial biomass and (*ii*) to characterize microbial diversity and community structure. Overall, the high abundance of saturated and partially unsaturated quinones in *Archaea* observed in this study contrasts the dominance of fully unsaturated or terminally saturated side chains in *Bacteria* and *Eukarya* (e.g. Collins and Jones, 1981; Nowicka and Kruk, 2010). Even though some quinones occur in multiple archaeal species described here, the relative proportions of quinones are considerably different for each species. In particular, $MK_{6:0}$ and $MK_{6:1}$ in *Thaumarchaeota* are the first quinones to be described in mesophilic *Archaea* and are therefore promising biomarkers for tracing this globally abundant archaeal clade. Similarly, SQs, CQs and BDTQs are distinct for *Sulfolobales*, as are MPs and OH-MPs for *Methanosarcinales* (Fig. VII.3). Considering the widespread occurrence of *Methanosarcinales* in the marine environment, in particular subseafloor sediments (Lever, 2013), MPs and OH-MPs have potential to be used as biomarkers for this archaeal order. Additionally, methanophenazines might also be synthesized by uncultivated anaerobic methane-oxidizing *Archaea* (ANME-2), which are phylogenetically closely related to the *Methanosarcinales*.

The considerably different quinone inventories of the investigated archaeal strains may be attributed to different habitats, adaptive strategies and metabolism. For instance, cultured thaumarchaeal strains have a limited temperature and pH range, are obligate ammonia-oxidizing aerobes (Stahl and de la Torre, 2012) and contain only two respiratory quinones (Fig. VII.3). In contrast, the high diversity of quinones found in *T. acidophilum* may reflect the wide range of conditions to which this archaeon can adapt, such as aerobic and anaerobic growth as well as high temperature and low pH. Since the quinone composition in *Archaea* as well as *Bacteria* may change in response to growth conditions (Trincone et al., 1989; Nicolaus et al., 1992; Shimada et al., 2001; Sévin and Sauer, 2014), it is likely that the response to environmental properties such as oxygenation, abundance of electron acceptors, temperature, or salinity is also encoded in environmental quinone profiles. Exploring the environmental quinone diversity may therefore help to constrain redox conditions as well as adaptation pathways of microbes (cf. Hedrick and White, 1986; Hiraishi, 1999). This might be especially applicable to the study of environments with high microbial diversity and strong geochemical gradients such as microbial mats

and hydrothermal systems, and might complement membrane lipid-based and gene-based approaches.

VII.3.3. Tracing thaumarchaeal abundance in the Black Sea using quinones and intact polar lipids

The concentrations of intact polar crenarchaeol derivatives indicate a maximum in thaumarchaeotal abundance in the suboxic zone of the southern Black Sea. This result is in agreement with previous observations based on the abundances of thaumarchaeal 16S rRNA and *amoA* (ammonia monooxygenase subunit A) gene biomarkers (Coolen et al., 2007; Lam et al., 2007). The water column profiles of the menaquinones $MK_{6:0}$ and $MK_{6:1}$ trace the profile of intact polar crenarchaeol closely (Fig. VII.4), suggesting that these quinones are primarily sourced from *Thaumarchaeota* in the marine environment. This conclusion is supported by the observation that $MK_{6:0}$ and $MK_{6:1}$ abundances are not correlated with intact polar archaeols, which are the major archaeal lipids in the anoxic zone (Fig. VII.4e). These archaeols are likely sourced from Euryarchaeota such as methanogens (Koga and Morii, 2005) and ANME (Rossel et al., 2008), which are abundant in the anoxic zone of the Black Sea (Vetriani et al., 2003; Schubert et al., 2006; Wakeham et al., 2007). Among our selection of cultures including literature data, $MK_{6:0}$ and $MK_{6:1}$ are only abundant in *Thaumarchaeota* (Fig. VII.3) and may thus serve as biomarkers for tracing thaumarchaeal abundance in aquatic environments. Vertical offsets in quinone vs. lipid abundances such as observed in the oxic zone of the Black Sea (Fig. VII.4) may reflect adaptations to environmental conditions (e.g., oxygen and ammonia availability) or changes in thaumarchaeal community composition.

The ratio of $MK_{6:0}$ and $MK_{6:1}$ to total quinones indicates that *Thaumarchaeota* likely dominate the microbial assemblages in a narrow interval of 90-120 m at the chemocline but are not quantitatively important in the oxic and anoxic part of the water column (Fig. VII.4; Supp. Table VII.3). Previous studies suggested that crenarchaeol core lipid maxima in the anoxic zone are related to metabolically adapted thaumarchaeal communities (Coolen et al., 2007; Wakeham et al., 2007). However, our intact polar lipid and quinone profiles strongly suggest that *Thaumarchaeota* are confined to a narrow interval in the oxic and suboxic zone. Since crenarchaeol core lipids represent a predominantly fossil signal (Ingalls et al., 2012), quinone profiles appear to be better suited for tracing living Thaumarchaeota. Thus, the profiles of $MK_{6:0}$ and $MK_{6:1}$ suggest that previous crenarchaeol-based detection of Thaumarchaeota in the anoxic zone of the Black Sea may have been false positives. Considering the ubiquity of planktonic and benthic Thaumarchaeota in the oceans and other environments (Stahl and de la Torre, 2012), $MK_{6:0}$ and $MK_{6:1}$ may have a high potential to serve as biomarkers for thaumarchaeal activity.

VII.4. Experimental procedures

Archaeal strains described in this study were cultivated according to standard conditions. For detailed information please refer to supplementary information.

VII.4.1. Suspended particulate matter sampling

Suspended particulate matter samples were collected in the southern Black Sea (41°31.70'N, 30°53.10'E, 1227 m water depth) in February 2011 at GeoB15105 during cruise M84/1 of R/V *Meteor* ("DARCSEAS I"; Zabel and Cruise Participants, 2013). Particulate matter was recovered at nine depths (40, 90, 120, 150, 300, 500, 700, 900, 1200 m) by pumping 6 to 204 liters of sea water through double pre-combusted $0.7\,\mu m$ pore-size glass fiber filters using insitu pumps (for chemical zonation and corresponding CTD data refer to Supp. Table VII.2). Recovered filters were immediately wrapped in combusted aluminum foil and stored at $-20\,°C$. Due to the use of $0.7\,\mu m$ pore-size filters, membrane lipid and quinone concentrations should be regarded as minimum estimates (Ingalls et al., 2012).

VII.4.2. Lipid and quinone extraction and analysis

Lipids and quinones were ultrasonically extracted from filters and biomass pellets following a modified Bligh & Dyer protocol (Sturt et al., 2004) with dichloromethane: methanol:buffer (1:2:0.8, v:v:v) using phosphate and trichloroacetic acid (CCl_3CO_2H) buffers (each 2 times). The total lipid extract (TLE) was dried under a stream of N_2 and stored at $-20\,°C$ until measurement. Exposure to light was minimized during sample processing.

Respiratory quinones and intact polar membrane lipids were quantified by injecting an aliquot of the TLE dissolved in methanol on a Dionex Ultimate 3000 ultra-high performance liquid chromatography (UHPLC) system connected to a Bruker maXis Ultra-High Resolution quadrupole time-of-flight tandem mass spectrometer (qToF-MS) equipped with an ESI ion source operating in positive mode (Bruker Daltonik, Bremen, Germany). The mass spectrometer was set to a resolving power of 27,000 at *m/z* 1,222 and every analysis was mass-calibrated by loop injections of a calibration standard and correction by lock mass, leading to a mass accuracy of <1-3 ppm. Ion source and other MS parameters were optimized by infusion of standards into the eluent flow from the LC system using a T-piece. Analyte separation was achieved using RP-HPLC on an ACE3 C18 column (2.1 x 150 mm, $3\,\mu m$ particle size, Advanced Chromatography Technologies, Aberdeen, Scotland) maintained at $45\,°C$ as described previously (Zhu et al., 2013a). In brief, analytes were eluted at a flow rate of $0.2\,ml/\,min$ isocratically for 10 min with $100\,\%$ eluent A (methanol:formic acid:14.8 M NH_4^+, 100:0.04:0.10, v:v:v), followed by a

linear gradient to 24 % eluent B (2-propanol:formic acid:14.8 M NH_4^+, 100:0.04:0.10, v:v:v) in 5 min, followed by a gradient to 65 % B in 55 min. The column was then flushed with 90 % B for 10 min and re-equilibrated with 100 % A for 10 min.

In order to demonstrate the simultaneous analysis of bacterial and archaeal quinones and membrane lipids, the samples were additionally analyzed on the same UHPLC-qToF-MS system under different chromatographic conditions using RP chromatography as described by Wörmer et al. (2013). Briefly, 1 % TLE aliquots were dissolved in methanol:dichloromethane (9:1, v:v) and injected onto an Acquity UPLC BEH C18 column (1.7 µm, 2.1 x 150 mm, Waters, Eschborn, Germany) maintained at 65 °C. Analytes were eluted at a flow rate of 0.4 ml/ min using linear gradients of methanol:water (85:15, v:v, eluent A) to methanol:isopropanol (50:50, v:v, eluent B) both with 0.04 % formic acid and 0.1 % NH_3. The initial condition was 100 % A held for 2 min, followed by a gradient to 15 % B in 0.1 min and a gradient to 85 % B in 18 min. The column was then washed with 100 % B for 8 min.

Quinones and lipids were identified by retention time, molecular mass, and MS^2 fragmentation (cf. Yoshinaga et al., 2011). Integration of peaks was performed on extracted ion chromatograms of ±10 mDa width and included the $[M+H]^+$, $[M+NH_4]^+$, and $[M+Na]^+$ ions. Where applicable, doubly charged ions were included in the integration. Quantification was achieved by injecting an internal standard (C_{46}-GTGT) along with the samples. The quinone abundances were corrected for the relative response of commercially available menaquinone ($MK_{4:4}$) and ubiquinone ($UQ_{10:10}$) standards (Sigma Aldrich, St. Louis, MO, USA) versus the C_{46}-GTGT standard. Analysis of quinone standard mixtures showed elution of $MK_{4:4}$ at 6.2 and $UQ_{10:10}$ at 23.6 min (Supp. Fig. VII.7a). Calibration curves of $MK_{4:4}$ and $UQ_{10:10}$ standards were established by injecting 1 pg to 10 ng quinone on column (Supp. Fig. VII.7b). The lower limit of detection was determined as <1 pg, considering a signal-to-noise ratio of greater than 3. Archaeal lipid abundances were corrected for response factors of commercially available and purified standards. Purified standards were gained from extracts of *A. fulgidus* by orthogonal semi-preparative liquid chromatography as described by Zhu et al. (2013a). The abundances of mono- and diglycosidic crenarchaeol were corrected for the response of the purified acyclic analogs. Due to the lack of an identical standard, the abundances of hexose-phosphohexose crenarchaeol were corrected for the response of a commercially available phosphatidylglycerol-hexose GDGT standard (Matreya LLC, Pleasant Gap, PA, USA). The abundances of mono- and diglycosidic archaeol were corrected for the respective purified standard, while phosphatidylglycerol, phosphatidylinositol and phosphatidylethanolamine archaeol abundances were corrected for the response of a commercial phosphatidylethanolamine archaeol standard (Avanti Polar Lipids Inc., Alabaster, AL, USA).

Acknowledgements

We thank C. Schleper, M. Stieglmeier (University of Vienna) for providing *N. viennensis*, E. Spieck (University of Hamburg) for providing *N. gargensis*, and G.W.Nicol, J.I. Prosser, and J. Ross (University of Aberdeen) for providing *N. devanaterra*. R.J. Whitaker (University of Illinois), A. Treusch, and S. Jensen (University of Southern Denmark) are thanked for providing *S. islandicus* strain Y.N.15.51. H. Huber and E.J. Gagen (University of Regensburg), C. House (Pennsylvania State University), M.W. Bowles, T.B. Meador, M.Y.Yoshinaga, X.-L. Liu, and C.A. Peters (University of Bremen) are thanked for providing biomass samples and lipid extracts of crenarchaeal and euryarchaeal strains.We thank A.-L. Ducluzeau for helpful discussions. We are grateful to the crew, chief scientist M. Zabel, and the scientific shipboard party of R/V *Meteor* cruise M84/1 (DARCSEAS I). We thank L.Wörmer and J.S.Lipp for supporting HPLC–MS analysis. This study was funded by the European Research Council under the European Union's Seventh Framework Programme–'Ideas' Specific Programme, ERC grant agreement No. 247153 (Advanced Grant DARCLIFE; PI: K.-U.H.) and by the Deutsche Forschungsgemeinschaft through the Gottfried Wilhelm Leibniz Prize awarded to K.-U.H. (Hi 616-14-1) and instrument grant Inst 144/300-1 (LC-qToF system).

VII.5. Supporting Information

VII.5.1. Cultivation of thaumarchaeal strains

Nitrosopumilus maritimus strain SCM1 was grown aerobically at $28\,^{\circ}\mathrm{C}$ in 8.5-l batch cultures in pH 7.5 HEPES-buffered Synthetic Crenarchaeota Medium (SCM, 1.5 mM NH_4Cl) as described previously (Könneke et al., 2005; Martens-Habbena et al., 2009; Elling et al., 2014). Cultures were slightly shaken by hand twice a day when cultures reached a nitrite concentration of about 0.1 mM. Biomass was harvested in early stationary phase using cross-flow filtration and centrifugation.

Nitrososphaera gargensis strain (Hatzenpichler et al., 2008) was grown at $46\,^{\circ}\mathrm{C}$ in a 5-l batch culture in pH 7.8 SCM modified from Könneke et al. (2005) and Krümmel and Harms (1982) and harvested in early stationary phase. The medium contained $5\,\mathrm{g\,l^{-1}}$ NaCl, $1.5\,\mathrm{g\,l^{-1}}$ $CaCl_2$ x 2 H_2O, $1\,\mathrm{g\,l^{-1}}$ KCl, $0.5\,\mathrm{g\,l^{-1}}$ $MgCl_2$ x 6 H_2O, $0.5\,\mathrm{g\,l^{-1}}$ $MgSO_4$ x 7 H_2O, $2\,\mathrm{g\,l^{-1}}$ KH_2PO_4, $2\,\mathrm{mM}$ $NaHCO_3$, $7.5\,\mu\mathrm{M}$ FeNaEDTA, $1\,\mathrm{mM}$ NH_4Cl and $1\,\mathrm{ml\,l^{-1}}$ of a trace element solution (Widdel and Bak, 1992).

Nitrososphaera viennensis strain EN76 was grown at $37\,^{\circ}\mathrm{C}$ in a 15-l batch culture in pH 7.5 HEPES-buffered freshwater medium modified from Tourna et al. (2011) by addition of $1.5\,\mathrm{mM}$ pyruvate and $3\,\mu\mathrm{M}$ NH_4Cl and slight shaking (150 rpm). *N. viennensis* biomass was harvested in late exponential phase using centrifugation.

Nitrosotalea devanaterra strain Nd1 was grown $25\,^{\circ}\mathrm{C}$ in a 6-l batch culture and pH 5.4 modified from Lehtovirta-Morley et al. (2013) by addition of $0.08\,\mathrm{g\,l^{-1}}$ of CAS amino acids and $1\,\mu\mathrm{M}$ phthalate buffer solution. Cells were harvested in stationary phase using centrifugation.

VII.5.2. Cultivation of crenarchaeal and euryarchaeal strains

Methanosarcina mazei (DSM 2053) and *Methanosarcina barkeri* (DSM 800) were grown at $35\,^{\circ}\mathrm{C}$ in 100 ml of a freshwater medium (Widdel and Bak, 1992) supplemented with methanol, acetate and yeast extract. *Methanosarcina acetivorans* (DSM 2834) was grown at $35\,^{\circ}\mathrm{C}$ in DSMZ medium 304 with methanol as the carbon source. All strains were harvested in stationary phase using centrifugation. *Sulfolobus islandicus* strain Y.N.15.51 (Reno et al., 2009) was grown at $80\,^{\circ}\mathrm{C}$ and pH 4.2 in 1.5 L of DSMZ medium 182 amended with $5\,\mathrm{g\,L^{-1}}$ glucose. *S. islandicus* biomass was harvested by centrifugation at OD600 1.68, corresponding to stationary phase, and lyophilized before lipid extraction. *Haloferax volcanii* strain DS2 (ATCC 29605) and *Halorubrum lacusprofundi* strain ACAM34 (ATCC 49238) were grown at $17\,^{\circ}\mathrm{C}$ using ATCC medium 974. *Methanothermococcus thermolithotrophicus* (DSM 2095) and *Methanopyrus kandleri* (DSM 6324) were grown at $85\,^{\circ}\mathrm{C}$ in enamel-protected fermentors with stirring (400 rpm) and contin-

uous gassing (H_2/CO_2, 80/20). *Thermococcus kodakarensis* strain KOD1 (JCM 12380) was grown at 85 °C in JCM medium 280 as described previously (Meador et al., 2014b). *Methanothermobacter thermautotrophicus* strain Delta H (DSM 1053) was grown at 65 °C in 65-l bioreactors containing 50 l medium as described previously (Yoshinaga et al., 2015a). Biomass of *M. thermolithotrophicus*, *M. thermautotrophicus*, *M. kandleri*, and *T. kodakarensis* were harvested using centrifugation and subsequently lyophilized.

Freeze-dried biomass samples of *Aeropyrum pernix*, *Archaeoglobus fulgidus*, *Ignicoccus hospitalis*, *Metallosphaera prunae*, *Sulfolobus acidocaldarius*, *Sulfolobus solfataricus*, *Pyrococcus furiosus*, *Pyrolobus fumarii*, *Staphylothermus marinus*, and *Thermoplasma acidophilum* were provided by M. Thomm, E.J. Gagen, and H. Huber from the Archaeenzentrum, University of Regensburg, Germany. *A. pernix* (DSM 11879) was grown at 90 °C and pH 7 in Bacto Marine Broth (Difco 2216) amended with 0.1 % sodium thiosulfate and harvested in stationary phase. *A. fulgidus* (DSM 4304) was grown at 85 °C and pH 7 in MGG-Medium (Huber et al., 1982) amended with 0.1 % lactate and yeast extract and harvested in late logarithmic phase. *I. hospitalis* (DSM 18386) was grown at 90 °C and pH 5.5 in 1/2 SME-Ignicoccus medium (Paper et al., 2007) and harvested in stationary phase. *M. prunae* (DSM 10039) was grown at 70 °C and pH 2 in "Allen medium" (Allen, 1959) modified by addition of 0.1 % yeast extract (Brock et al., 1972) and harvested in logarithmic phase. *S. acidocaldarius* (DSM 639) and *S. solfataricus* (DSM 1616) were grown at 75 °C and 80 °C, respectively, and pH 2 in the same medium as *M. prunae* and harvested in stationary phase. *P. furiosus* (DSM 3638) was grown at 95 °C and pH 7 in SME medium supplemented with 0.1 % yeast extract, peptone, and starch (Huber and Stetter, 2006) and harvested in logarithmic phase. *P. fumarii* (DSM 11204) was grown at 106 °C and pH 6 in 1/2 SME medium amended with 0.1 % $NaNO_3$ (Blöchl et al., 1997) and harvested in logarithmic phase. *S. marinus* (DSM 3639) was grown at 85 °C and pH 7 in "Marine-Medium" supplemented with 0.1 % yeast extract and peptone (Keller et al., 1995) and harvested in logarithmic phase. *T. acidophilum* (DSM 1728) was grown at 55 °C and pH 2.5 in Darland's medium containing 0.1 % yeast extract and 1 % glucose (Darland et al., 1970). An extract of *Archaeoglobus profundus* (DSM 5631) harvested in late exponential phase was provided by C. House (Pennsylvania State University).

VII.5.3. Literature data

The distribution of quinone types in *Archaea* reported in this study was complemented with literature data compiled from the following sources: Collins et al. (1981), Thurl et al. (1985), Thurl et al. (1986), Collins and Tindall (1987), Tindall et al. (1989, 1991), Hensel et al. (1997), and Namwong et al. (2011).

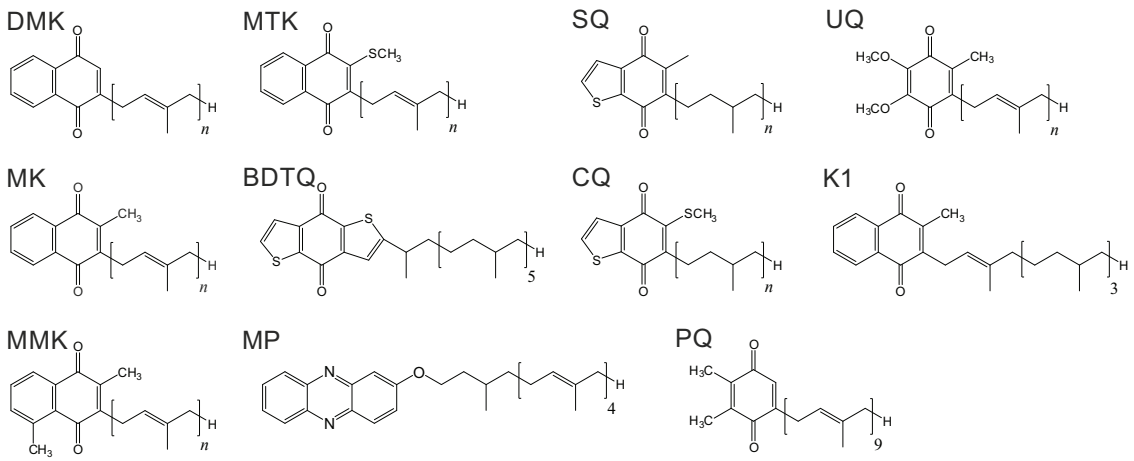

Supplementary Figure VII.1 Structures of respiratory quinone classes detected in cultivated archaea (DMK, MK, MMK, MTK, BDTQ, SQ, CQ) and bacteria (DMK, MK, MMK, MTK, UQ, K1, PQ) as well as methanophenazine, an electron carrier in *Methanosarcinales*. The length and degree of unsaturation of the isoprenoid side chains of quinones may vary from 4 to 14 and completely saturated to fully unsaturated, respectively. DMK: Demethylmenaquinone. MK: Menaquinone (vitamin K2). MMK: Methylmenaquinone. MTK: Methionaquinone. BDTQ: Benzodithiophenoquinone. MP: Methanophenazine. SQ: Sulfolobusquinone. CQ: Caldariellaquinone. PQ: Plastoquinone. UQ: Ubiquinone. K1: Vitamin K1 (synonyms: phylloquinone, $MK_{4:1}$).

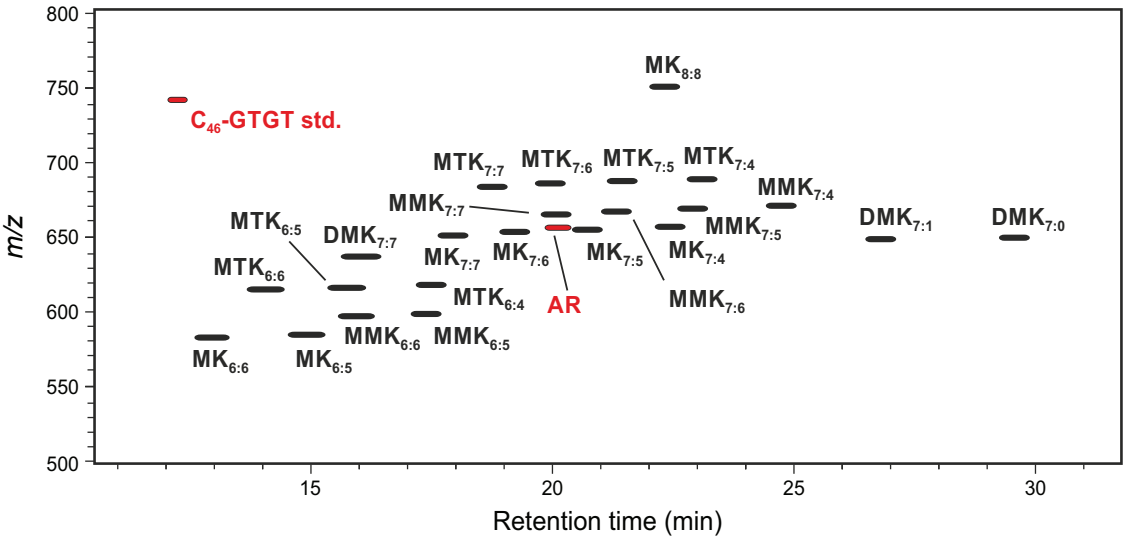

Supplementary Figure VII.2 Reconstructed density map obtained by reversed phase HPLC–MS showing elution of respiratory quinones (black) in an extract of *Thermoplasma acidophilum* relative to the C_{46}-GTGT standard and core archaeol (AR, red).

Supplementary Table VII.1 Diagnostic fragment ions in MS^2 mode (related to loss of the headgroup) and midpoint redox potentials (E'_0 at pH 7, ordered by redox potential) of archaeal quinones and methanophenazine as well as bacterial ubiquinone (UQ) and eukaryotal plastoquinone (PQ). NA: not available.

Quinone	Diagnostic ions in MS^2	E'_0 (mV)	Citation (E'_0)
UQ	197.1	+112 ($UQ_{10:10}$)	(Schnorf, 1966)
SQ	193	NA	-
CQ	179.0, 225.0	+106 ($CQ_{6:0}$)	(Schäfer et al., 1993)
PQ	151.1	+80 ($PQ_{9:9}$)	(Okayama, 1976)
BDTQ	249	NA	-
MTK (sat./polyuns.)	219	NA	-
DMK (polyuns.)	173	+36 ($DMK_{8:8}$)	(Holländer, 1976)
MK (sat.)	187.1	NA	-
MK (partially unsat.)	187.1	-78 ($MK_{4:1}$)	(Wagner et al., 1974)
MK (polyuns.)	187.1, 253.1	-67 ($MK_{6:6}$)	(Wagner et al., 1974)
MMK (sat.)	201.1	NA	-
MMK (polyuns.)	201.1, 267.1	-90 ($MMK_{6:6}$)	(Dietrich and Klimmek, 2002)
MP (partially unsat.)	197.1	-165 ($MP_{5:4}$)	(Tietze et al., 2003)

Supplementary Table VII.2 Sampling depth and pumped volume of *in situ* pumps inferred chemical zonation as well as density, salinity, and temperature obtained from CTD casts.

Water depth (m)	Pumped volume (l)	Chemical zone	Density (σ_θ)	Salinity (PSU)	Temperature (°C)
40	4.3	Oxic	14.2	17.8	8.5
90	6.1	Suboxic	15.4	18.7	8.5
120	23	Suboxic	15.9	19.8	8.4
150	204	Anoxic	16.4	20.5	8.5
300	10.8	Anoxic	16.8	21.7	8.8
500	11.4	Anoxic	17	22	8.9
700	21.3	Anoxic	17.1	22.2	8.9
900	9	Anoxic	17.2	22.3	9
1200	73.2	Anoxic	17.2	22.3	9

Supplementary Table VII.3 Menaquinone $MK_{6:0}$ and $MK_{6:1}$, and intact polar membrane lipid (IPL) concentrations ($ng\,l^{-1}$) in the Black Sea water column (n.d., not detected). IPL-Cren is the sum of IPLs with monoglycosidic, diglycosidic and hexose-phosphohexose headgroups attached to a crenarchaeol core lipid. Total IPL archaeols include archaeols with glycosidic and phosphatidic headgroups. Total quinones include menaquinones, ubiquinones, vitamin K1, and plastoquinones.

Water depth (m)	$MK_{6:0}$	$MK_{6:1}$	IPL-Cren	Total IPL-archaeols	Total quinones
40	0.18	0.15	7	10.4	4.3
90	0.27	0.24	26	8.8	0.7
120	0.36	0.22	43	8.2	0.6
150	0.06	0.01	6.5	3.3	1
300	0.09	0.02	1.5	79	9.4
500	0.06	0.01	6.2	38	2.6
700	0.02	0.02	2.9	85	2.2
900	0.03	0.01	n.d.	37	2.7
1200	0.01	0.01	0.4	33	0.2

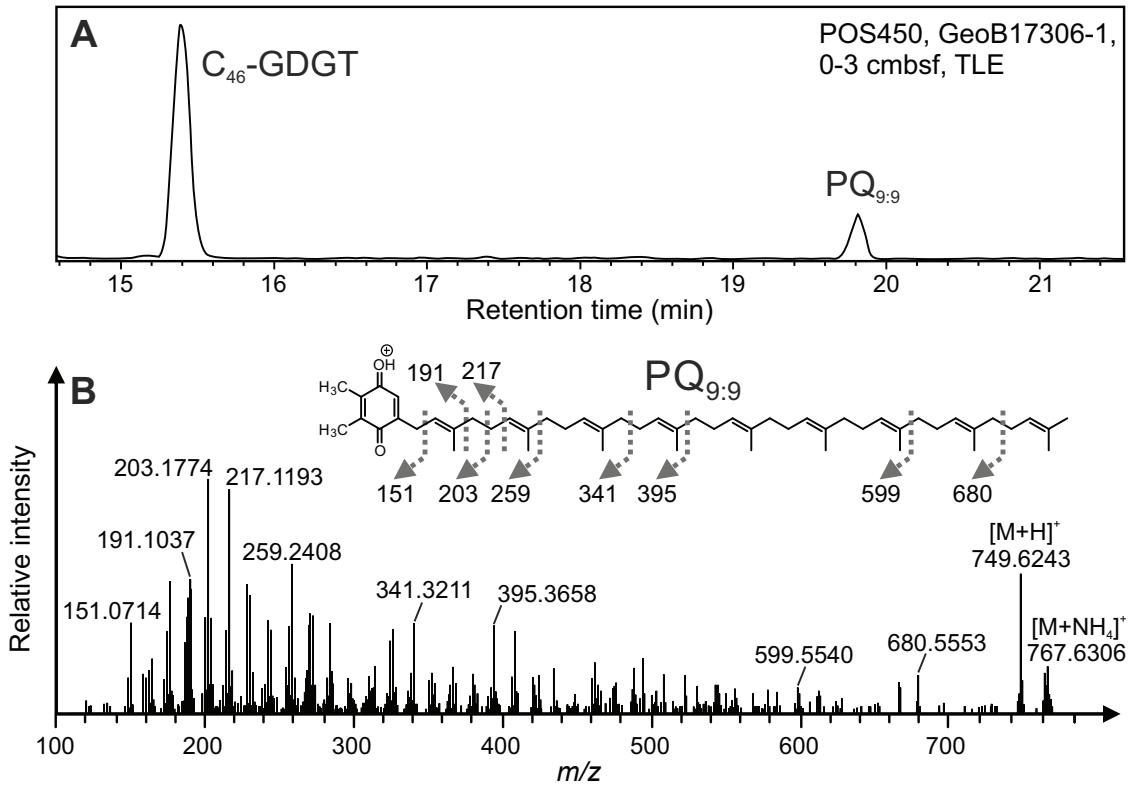

Supplementary Figure VII.3 Extracted ion chromatogram of C_{46}-GTGT and plastoquinone-9 ($PQ_{9:9}$; A) and MS^2 spectrum of $PQ_{9:9}$ obtained from a total lipid extract (TLE) of a marine sediment sample from the western Mediterranean Sea using the reversed phase HPLC-ESI-MS protocol of Wörmer et al. (2013).

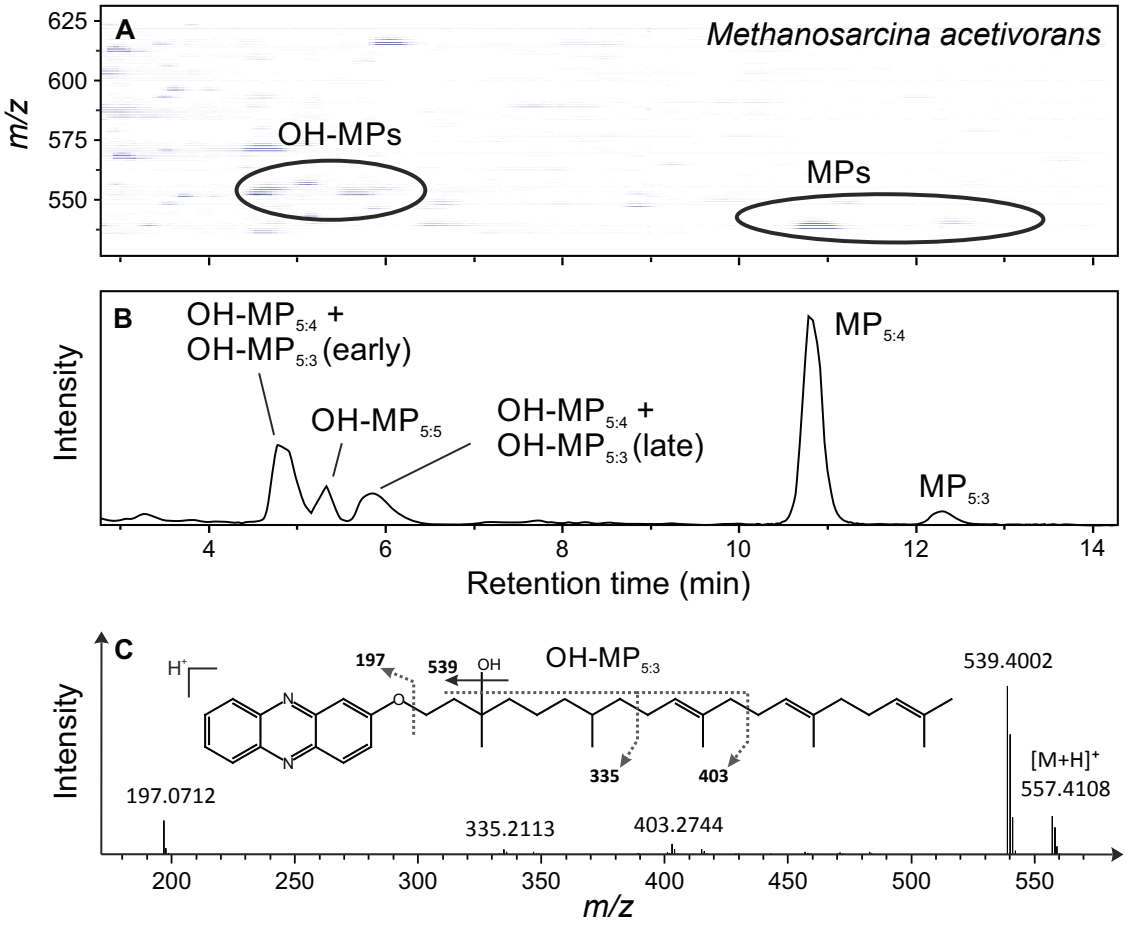

Supplementary Figure VII.4 Density map (A) and extracted ion chromatogram (B) obtained by reversed phase HPLC–MS showing elution of methanophenazines (MPs) and hydroxymethanophenazines (OH-MPs) in an extract of *M. acetivorans*. OH-$MP_{5:4}$ and OH-$MP_{5:3}$ show elution of two isomers. Panel (C) shows the tentative structure (position of double bonds and hydroxyl group not constrained) and MS^2 spectrum of OH-$MP_{5:3}$.

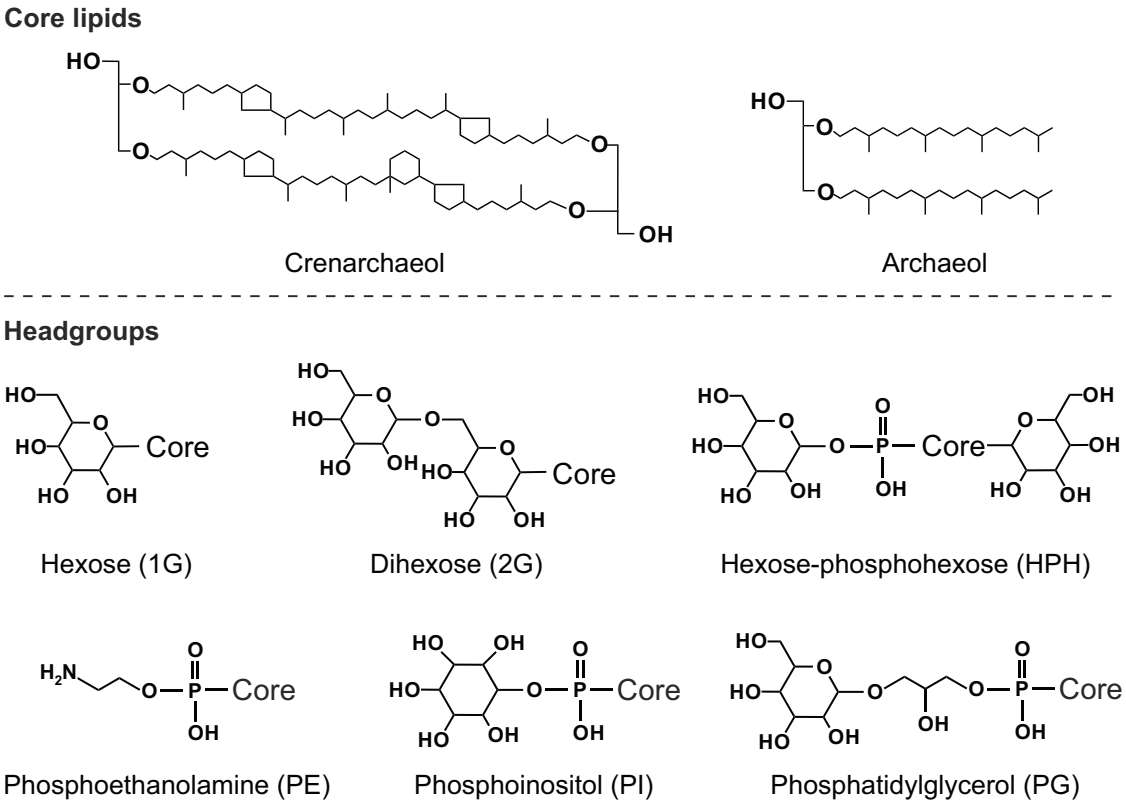

Supplementary Figure VII.5 Structures of archaeal core lipids and polar headgroups used for the calculation of total intact polar crenarchaeal and total intact polar archaeols (Fig. VII.4, Supp. Table VII.2). Intact polar lipids are combinations of a core lipid and one (GDGT, archaeol) or two headgroups (only GDGT).

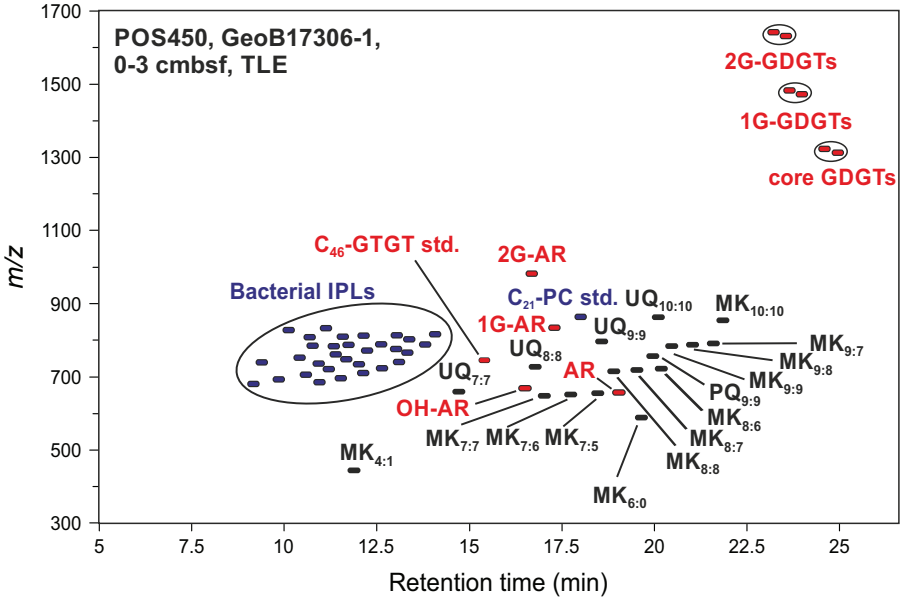

Supplementary Figure VII.6 Reconstructed density map showing elution of archaeal and bacterial respiratory quinones (black) and bacterial (blue) and archaeal (red) intact polar lipids from a marine sediment sample from the western Mediterranean Sea using the reversed phase HPLC-ESI-MS protocol of Wörmer et al. (2013).

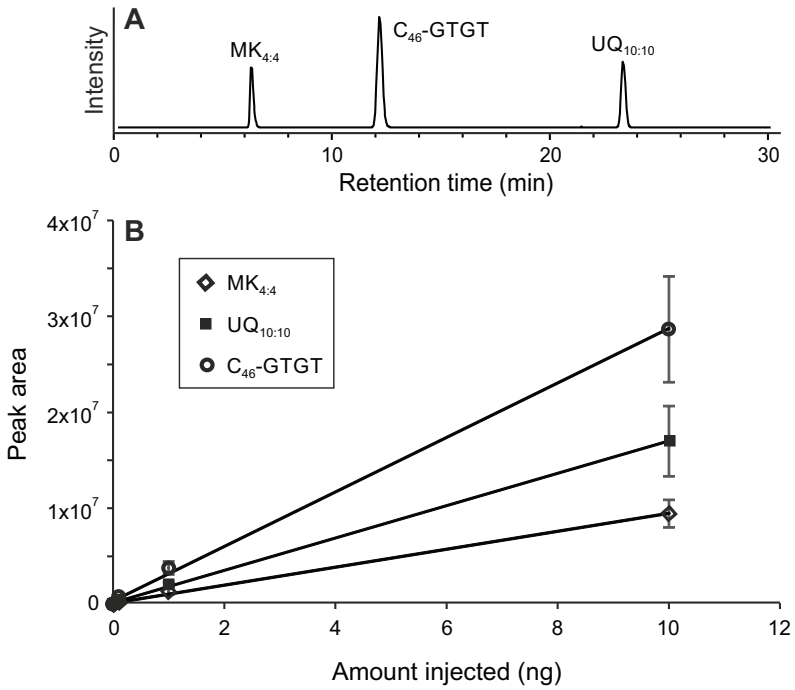

Supplementary Figure VII.7 Base peak chromatogram (**A**) and calibration curve (**B**) of a standard mixtures (0.001 ng, 0.1 ng, 1 ng, 10 ng on column) of C_{46}-GTGT, $MK_{4:4}$ and $UQ_{10:10}$ obtained by reversed phase HPLC-ESI-MS. Coefficient of correlation (r^2) of C_{46}-GTGT, $MK_{4:4}$ and $UQ_{10:10}$ was always >0.99. Error bars represent standard deviation of triplicate analyses.

Chapter VIII

Sources, distribution and fate of respiratory quinones in the water column and sediments of the Black Sea

Kevin W. Becker[a,+,*], Felix J. Elling[a,+], Jan M. Schröder[a], Julius S. Lipp[a], Matthias Zabel[b] and Kai-Uwe Hinrichs[a]

In preparation for *Geochimica et Cosmochimica Acta*

[+]These authors contributed equally to this work.

[a]Organic Geochemistry Group, MARUM - Center for Marine Environmental Sciences & Department of Geosciences, University of Bremen, 28359 Bremen, Germany
[b]Inorganic Geochemistry Group, MARUM Center for Marine Environmental Sciences & Department of Geosciences, University of Bremen, 28359 Bremen, Germany

[*]Corresponding author. E-mail: k.becker@uni-bremen.de

Abstract

Isoprenoid quinones are a diverse group of membrane-bound lipids serving as electron carriers in the respiratory chains of almost all organisms. Complementary to the quantitative and phylogenetic information encoded in membrane lipid distributions, quinone compositions reflect specific metabolisms and source organisms. Recent analytical advances enable simultaneous profiling of quinones and membrane lipids in environmental samples. In order to demonstrate the utility of coupled environmental quinone and membrane lipid profiling, we investigated a vertical section of the water column and sediment in the Black Sea, the world's largest anoxic marine basin which is characterized by its pronounced physical, chemical, and microbial stratification. Depth distributions of diagnostic quinones and membrane lipids were correlated with zones of distinct microbial processes: In the oxic photic zone of the water column, high abundances of quinones and membrane lipids were associated with oxygenic photosynthesis and aerobic respiration. Maximum abundances of thaumarchaeal saturated menaquinones and isoprenoid tetraether lipids at the chemocline and the low abundances of other quinone types indicate that archaeal mediated ammonia oxidation was a major respiratory process occurring in the suboxic zone. A distinct peak in abundance of chlorobiumquinone and the characteristic pigment isorenieratene in the deeper anoxic part of the chemocline indicated the occurrence of sulfur-oxidizing anoxygenic photosynthetic green sulfur bacteria. High abundances and diversity of specific quinones and membrane lipids in the dark anoxic zone indicated high respiratory activity and biomass of denitrifying, ammonium-oxidizing, sulfur-oxidizing and sulfate-reducing bacteria as well as archaeal-mediated anaerobic oxidation of methane. Sulfate reduction as well as anaerobic oxidation of methane and/or methylotrophic methanogenesis were the major processes identified in the upper sediment based on geochemical data, high abundances of bacterial polyunsaturated menaquinones and phospholipid containing ester and ether lipids as well as *Methanosarcinales*-specific methanophenazines and archaeal diether lipids. The sapropel layer located at $4\,\mathrm{m}$ sediment depth was associated with a peak of dissolved ammonium concentration as well as maximum abundances of bacterial and archaeal IPLs and quinones, suggesting intense microbial heterotrophic activity in this organic-matter rich layer. High abundances of biogenic methane in the deeper sediment and the disappearance of methanophenazines near and below the sapropel indicated that methanogenesis in the deep sediment is not driven by *Methanosarcinales* but by other hydrogenotrophic methanogens. Our findings show that the simultaneous analysis of membrane lipids and respiratory quinones permits a reconstruction of the stratification of microbial communities in the water column and sediments of the Black Sea. This approach may therefore be a valuable tool for improving quantitative membrane lipid analyses by providing process-related information from respiratory quinones.

VIII.1. Introduction

Microbial mediated redox-reactions ultimately drive the global cycling of carbon, nitrogen, sulfur and other biologically active elements (Newman and Banfield, 2002; Dietrich et al., 2006; Falkowski et al., 2008). On a cellular level, these redox reactions are utilized to maintain electron transport and proton gradients across the cytoplasmic membrane, which enable the generation of ATP and thus form the basis of the cellular economy in almost all organisms (Mitchell, 1961; Anraku, 1988; Schäfer et al., 1999). An essential component of the electron transport chain are respiratory quinones, which are isoprenoid lipids that shuttle electrons and protons between membrane-bound protein complexes (Anraku, 1988; Gray and Ellis, 1994). Respiratory quinones are commonly classified based on the structure of a polar cyclic headgroup and can be further distinguished by the length and degree of unsaturation of the head-to-tail linked isoprenoid side chain (Collins and Jones, 1981; Hiraishi, 1999). The distribution of structurally distinct quinones among eukaryotes and prokaryotes is determined both by phylogeny and, due to their distinct redox potentials, also by the operating respiratory pathway (Fig. VIII.1; Table VIII.1; Collins and Jones, 1981; Bekker et al., 2007; Nowicka and Kruk, 2010).

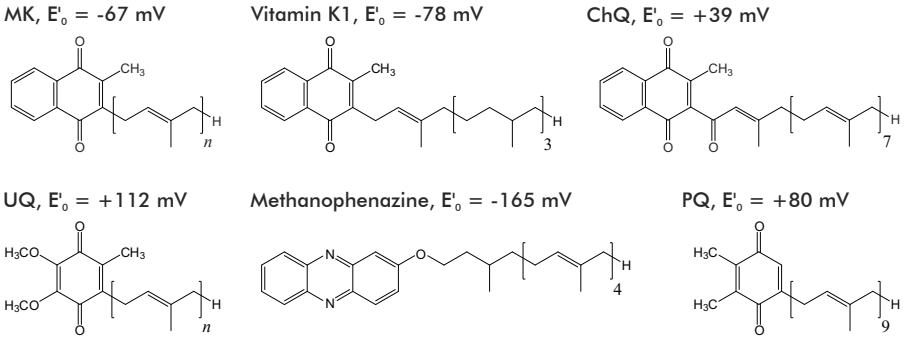

Figure VIII.1. Structures and midpoint redox potentials (E_0', at pH 7) of archaeal (MK), bacterial (MK, UQ, PQ, ChQ), and eukaryotal (UQ, PQ, K1) respiratory quinone classes and the *Methanosarcinales*-specific functional quinone analog methanophenazine detected in water column and sediment samples from the southern Black Sea. The length and degree of unsaturation of the isoprenoid side chains of quinones may vary from 4 to 14 and completely saturated to fully unsaturated, respectively, while known methanophenazines comprise exclusively four isoprenoid units. MK: Menaquinone (vitamin K2). UQ: Ubiquinone. PQ: Plastoquinone. K1: Vitamin K1 (synonyms: phylloquinone, $MK_{4:1}$). Redox potentials compiled from Schnorf (1966), Redfearn and Powls (1968), Wagner et al. (1974), Okayama (1976), and Tietze et al. (2003).

The major classes of quinones in bacteria are polyunsaturated ubiquinones (UQs) and menaquinones (MKs), which operate in aerobic and anaerobic metabolisms, respectively. UQs typically contain six ($UQ_{6:6}$) to ten ($UQ_{10:10}$), but in some organisms also up to 14 isoprenoid units and usually one double bond per isoprenoid unit, hereafter termed fully unsaturated (quinone nomenclature $Q_{m:n}$ indicates headgroup type Q, number of

isoprenoid units in the side chain m and number of double bonds n). They are involved in electron transport in the mitochondria and other compartments of eukaryotes (Nowicka and Kruk, 2010). Quinones that are specific for oxygenic photosynthetic eukaryotes and bacteria are vitamin K1 (also known as phylloquinone or $MK_{4:1}$) and plastoquinones (predominantly $PQ_{9:9}$), which occur in photosystems I and II, respectively (Fig. VIII.1; Amesz, 1973; Brettel and Leibl, 2001; Nowicka and Kruk, 2010).

In contrast to bacteria and eukaryotes, polyunsaturated quinones exclusively occur in two archaeal lineages, the *Thermoplasmatales* and the *Halobacteriales* (Chapter VII; Collins et al., 1981; Shimada et al., 2001), the latter having acquired quinone biosynthesis genes from bacteria via lateral transfer (Nelson-Sathi et al., 2012). Most archaea produce saturated or partially unsaturated MKs with four to eight isoprenoid units (cf. Chapter VII), while specialized compounds are synthesized by some lineages such as sulfur-containing quinones in *Sulfolobales*. The only organisms that have been suggested not to produce quinones are fermentative bacteria and some representatives of the *Crenarchaeota* and *Euryarchaeota*, including methanogens (cf. Chapter VII). However, methanogenic *Euryarchaeota* of the order *Methanosarcinales* are known to substitute quinones with the functional analog methanophenazine (Fig. VIII.1; Chapter VII); Abken et al., 1998).

Table VIII.1. Diagnostic fragment ions in MS^2 mode (related to loss of the headgroup; from Chapter VII and Fig. VIII.4) and midpoint redox potentials (E'_0, at pH 7, ordered by redox potential) of archaeal quinones and methanophenazine as well as bacterial and eukaryotal ubiquinone (UQ), plastoquinone (PQ), and chlorobiumquinone (ChQ). NA: not available.

Quinone	Diagnostic ions in MS^2	E'_0 (mV)	Citation (E'_0)
UQ	197.1	+112 ($UQ_{10:10}$)	Schnorf (1966)
PQ	151.1	+80 ($PQ_{9:9}$)	Okayama (1976)
ChQ	201.1	+39 ($ChQ_{7:7}$)	Redfearn and Powls (1968)
MK (sat.)	187.1	NA	-
MK (partially unsat.)	187.1	−78 ($MK_{4:1}$)	Wagner et al. (1974)
MK (polyuns.)	187.1, 253.1	−67 ($MK_{6:6}$)	Wagner et al. (1974)
MP (partially unsat.)	197.1	−165 ($MP_{5:4}$)	Tietze et al. (2003)

Given the large structural diversity of respiratory quinones, detailed knowledge of their phylogenetic distribution and their distinct redox-potentials, quinones offer a high potential as process-specific biomarkers in environmental studies (Chapter VII; Hiraishi, 1999; Urakawa et al., 2000; Kunihiro et al., 2014). In contrast to the increasing use of intact polar membrane lipid (IPL) analysis in environmental samples (e.g. Lipp et al., 2008; Schubotz et al., 2009; Popendorf et al., 2011), respiratory quinone analysis has been rarely employed in microbial community profiling (e.g. Hiraishi and Kato, 1999; Urakawa et al., 2000; Urakawa et al., 2001; Urakawa et al., 2005; Kunihiro et al.,

2014). However, tracing living microbial cells by IPL profiling may prove challenging in some environments (Lipp and Hinrichs, 2009; Schouten et al., 2010; Liu et al., 2011), particularly due to the largely unconstrained degradation rates of intact lipids (Xie et al., 2013). Environmental IPL-profiling therefore benefits from complementary biomarker approaches (e.g. Schubotz et al., 2013). Novel high-performance liquid chromatography-mass spectrometry (HPLC–MS) protocols enable simultaneous profiling of quinones and membrane lipids in a single analysis (cf. Chapter VII), thus opening new avenues for complementing the quantitative and phylogenetic information contained in membrane lipid distributions with process-specific quinone distributions.

To demonstrate the utility of coupled environmental quinone and membrane lipid profiling, we studied a sequence of water column and sediment samples in the southern Black Sea (Fig. VIII.2). Here, aerobic respiration depletes oxygen in the upper 40 to 200 m of the water column, while a shallow halocline leads to permanent water column stratification and thus prevents oxygenation of deeper waters (Sorokin, 2002). This oxic-anoxic interface is associated with a multilayered chemocline. The depth of this chemocline is temporally and spatially variable (Murray et al., 1989; Jørgensen et al., 1991; Coolen et al., 2007). The oxic zone is separated from the anoxic zone by a 20-40 m thick suboxic transition zone with no detectable sulfide (Murray et al., 1989; Sorokin, 2002). Chemoautotrophic carbon fixation supports high standing stocks of microbial biomass at the chemocline, accounting for 10 to 32 % of photoautotrophic productivity at the surface (Karl and Knauer, 1991; Sorokin et al., 1995).

Within the transition zone, microbes mediate a cascade of redox processes that can be traced by the sequence of nitrogen-, sulfur-, and metal species (Jannasch, 1991; Sorokin et al., 1995) and associated microbial biomarkers (e.g. Schubert et al., 2006; Wakeham et al., 2007; Schubotz et al., 2009; Fuchsman et al., 2011). Quantitatively important processes include ammonium and nitrite cycling by nitrifying archaea and bacteria as well as anaerobic ammonia oxidizing bacteria (Kuypers et al., 2003; Coolen et al., 2007; Lam et al., 2007), sulfide and thiosulfide oxidation e.g. by phototrophic green sulfur bacteria and *Shewanella* spp. (Jannasch et al., 1991; Jørgensen et al., 1991; Perry et al., 1993), aerobic methane oxidation by *Proteobacteria* (Schubert et al., 2006) as well as bacterial Fe and Mn cycling (e.g. Nealson et al., 1991; Fuchsman et al., 2011). In the anoxic zone, sulfate reduction and anaerobic oxidation of methane are major microbial metabolisms (Reeburgh et al., 1991; Albert et al., 1995; Schubert et al., 2006; Wakeham et al., 2007), which extend into the sediment.

While the depth distribution of the major sedimentary geochemical zones varies spatially, microbial processes form a continuum from the water column to the sediment of the Black Sea (Jørgensen et al., 2004; Knab et al., 2009). Sulfate reduction is the major carbon-remineralizing process in the surface sediments (Jørgensen et al., 2001), since

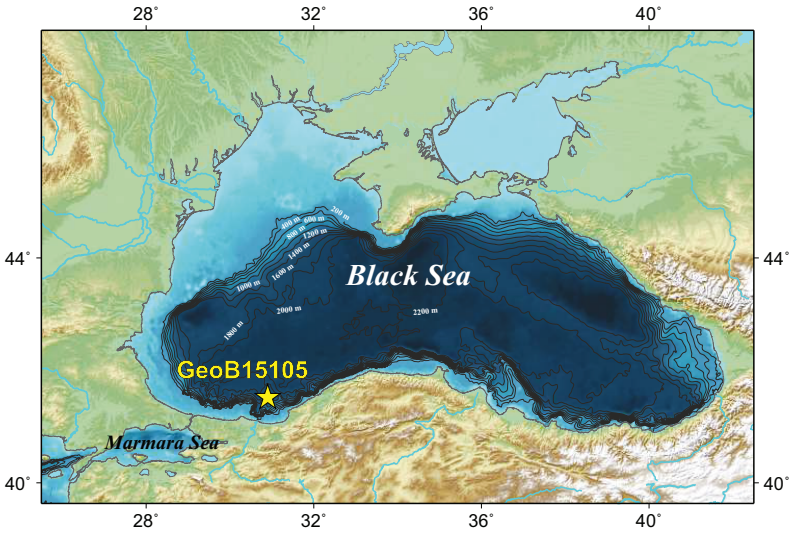

Figure VIII.2. Location of the study site at the southern continental slope of the Black Sea (GeoB15105, 41°31.70'N, 30°53.10'E, 1227 m water depth) sampled during R/V Meteor cruise M84/1.

other common electron acceptors such as oxygen and nitrate are either depleted at the chemocline (Murray and Yakushev, 2006) or settle at the seafloor in reduced form such as iron and manganese (Konovalov et al., 2004). The sulfate reduction zone extends up to 4 m into the sediment and partially overlaps with the underlying methanogenic zone (Jørgensen et al., 2001, 2004; Leloup et al., 2007). Anaerobic oxidation of methane occurs both within the surface sediment (Reeburgh et al., 1991; Riedinger et al., 2010) as well as within the comparatively broad sulfate methane transition zone (Jørgensen et al., 2001).

In this study, we applied novel HPLC–MS protocols to investigate the quinone and lipid distribution in the water column and sediments in the southwestern Black Sea which allowed the detection of a significantly larger variety of compounds compared to previous techniques (Urakawa et al., 2000; Kunihiro et al., 2014). The depth distributions of diagnostic quinones and membrane lipids in the water column were correlated with the zonation of microbial processes, such as nitrification and sulfur oxidation. Based on the distribution of quinones in water and sediment samples, we suggest that, while some sedimentary quinones may be derived from the water column, a plethora of compounds is being produced *in situ* and may therefore be used to characterize and quantify the benthic microbial community.

VIII.2. Materials and Methods

VIII.2.1. Suspended particulate matter and sediment sampling

Suspended particulate matter and sediment samples were collected in the southern Black Sea in February 2011 at site GeoB15105 (Fig. VIII.2; 41°31.70'N, 30°53.10'E, 1227 m water

depth) during R/V Meteor cruise M84/1 ('DARCSEAS I'; Zabel and Cruise Participants, 2013). Suspended particulate matter was recovered at nine depths (40, 90, 120, 150, 300, 500, 700, 900, 1200 m) by pumping 6 to 204 liters of sea water through double pre-combusted 0.7 µm pore-size glass fiber filters using *in situ* pumps. Recovered filters were immediately wrapped in combusted aluminum foil and stored at −20 °C. Due to the use of 0.7 µm pore-size filters, membrane lipid and quinone concentrations should be regarded as minimum estimates (cf. Xie et al., 2014). Pore water was extracted from sediment cores with Rhizon micro suction samplers (0.1 µm filter width, Rhizosphere Research Products, Wageningen) and split into subsamples for onshore analysis. Sediments were recovered using a multi-corer (GeoB15105-4) and a gravity corer (GeoB15105-2), sampled in a cold room at 4 °C and stored at −20 °C in brown glass bottles until extraction. At the study site, sedimentary units in the sampled upper 8 m comprise laminated coccolith ooze (Unit I, ca. 4 % dry weight TOC) deposited during the last 3 ka as well as an organic-rich sapropel (Unit II, up to 15 % dry wt. TOC) deposited from 7.5 to 3 ka before present (Brumsack, 1989; Bahr et al., 2005; Kwiecien et al., 2008), coeval to the development of water column anoxia in the Black Sea (Arthur and Dean, 1998; Eckert et al., 2013).

VIII.2.2. Water column and pore water chemistry

Water column profiles of temperature, fluorescence and depth as well as pressure and dissolved oxygen were measured with a vertical resolution of 1 m using a CTD rosette (GeoB15105-5). The salinity was derived from conductivity, while the density was calculated from pressure and temperature measurements as well as salinity.

Water column samples (10 to 20 mL) were directly filtered from the Niskin bottle (0.2 µm syringe micro filter) after the recovery of the CTD-equipped rosette. Pore water samples were taken from closed MUC cores and gravity cores and through rhizon micro suction samplers (5 cm length, 0.2 µm porous polymer). Dissolved sulfate (SO_4^{2-}) was determined by ion chromatography (Metrohm Compact IC, METROSEP A Supp 5 column, conductivity detection after chemical suppression) in samples diluted 1:100 with Milli-Q grade H_2O. Concentrations of dissolved phosphate (PO_4^{3-}) were measured photometrically. One mL of sample was placed in a disposable polystyrene (PS) cuvette (2.5 ml) containing 50 µl ammonium molybdate solution, and amended with 50 µl of an ascorbic acid solution. The extinction of the phosphomolybdenum blue complex was measured after 10 min at a wavelength of 820 nm (Hach Lange DR 5000 photometer). Dissolved ammonium (NH_4^+) was measured using a flow injection, PTFE tape gas separator technique after Hall and Aller (1992). About 200 to 300 µl of plain sample were injected into a 100 µl loop of a Rheodyne valve and mixed with an alkaline solution (0.01 M NaOH + 0.2 M sodium citrate) to form gaseous NH_3 that passed a PTFE membrane and caused a

conductivity signal in a receiving acid solution (0.001 M HCl). The resulting conductivity was determined using a temperature-compensated conductivity meter (Amber Scientific 1056) with a micro flow-through cell (Amber Scientific 529) and recorded on a strip chart recorder. Dissolved hydrogen sulfide (HS^-) was determined in samples fixed with $ZnCl_2$ using the photometric methylene blue method (Cline, 1969).

VIII.2.3. Hydrocarbon gases

Concentrations of dissolved methane were determined according to previously reported protocols (Kvenvolden and McDonald, 1986; D'Hondt et al., 2003). Two to three ml of wet sediment were enclosed in a gas-tight 22-ml glass vial with a Teflon septum and heated for 20 min at $60\,^{\circ}\mathrm{C}$. After heating, 100 to $500\,\mu\mathrm{l}$ sub-samples were taken from the headspace gas with a gas-tight syringe and analyzed on board by gas chromatography-flame ionization detection (GC-FID). The GC-FID was calibrated on a daily basis using hydrocarbon gas standards (Scotty Specialty Gases). Based on the partial pressure of methane in the headspace gas and the headspace volume, the total amount of released methane was quantified and normalized to the pore-water volume of the extracted sediment sample, using the sample volume and corresponding porosity data of solid phase samples.

The stable carbon isotopic composition of methane ($\delta^{13}CH_4$) was determined from duplicate GC-isotope ratio mass spectrometry (GC–irMS) analyses using a ThermoFinnigan Trace GC Ultra coupled to a DELTA Plus XP mass spectrometer equipped with via a ThermoFinnigan GC Combustion III interface. An aliquot of $200\,\mu\mathrm{l}$ of the headspace gas was injected into the GC using a split ratio of 1:3. The components were separated isothermally at $40\,^{\circ}\mathrm{C}$ for 8 min using a Carboxen-1006 PLOT fused-silica capillary column (30 m x 0.32 mm ID; Supelco, Inc, USA) at a constant Helium flow of $3\,\mathrm{ml\,min^{-1}}$. The system was calibrated at the start and end of the run using a reference gas with known carbon isotopic composition. Carbon isotope ratios are reported in the δ-notation as per mil deviation from the Vienna Pee Dee Belemnite standard. Analytical precision was determined by repeated injections of commercially available standards (methane 100 ppm; C_1 to C_6 mixture, 1000 ppm, Air Liquide) and was typically better than $1‰$.

VIII.2.4. Quinone and membrane lipid extraction and analysis

Respiratory quinones and membrane lipids were ultrasonically extracted from filters and sediments after addition of an extraction standard (phosphatidylcholine (PC) $C_{21:0}$) following a modified Bligh & Dyer protocol (Sturt et al., 2004) with dichloromethane: methanol: buffer (1:2:0.8, v:v:v) using phosphate and trichloroacetic acid (CCl_3CO_2H) buffers (each 2x). After each extraction step, the samples were centrifuged at 800 x g for

10 min and the supernatants were collected in a separation funnel. The combined supernatants were then washed three times with de-ionized MilliQ water. After separation into organic phase and water-soluble phase, the organic phase was collected as the total lipid extract (TLE). The TLE was dried under a stream of N_2 and stored at $-20\,°C$ until measurement.

Quinones and archaeal IPLs were analyzed by injecting an aliquot of the TLE dissolved in methanol on a Dionex Ultimate 3000RS high performance liquid chromatography (UHPLC) system connected to a Bruker maXis Ultra-High Resolution quadrupole time-of-flight tandem mass spectrometer (qToF-MS) equipped with an ESI ion source operating in positive mode (Bruker Daltonik, Bremen, Germany). The mass spectrometer was set to a resolving power of 27,000 at *m/z* 1222 and every analysis was mass-calibrated by loop injections of a calibration standard and correction by lock mass, leading to a mass accuracy of <1-3 ppm. Ion source and other MS parameters were optimized by infusion of standards into the eluent flow from the LC system using a T-piece.

Analyte separation was achieved using reversed phase (RP) HPLC on an ACE3 C_{18} column (2.1 x 150 mm, $3\,\mu m$ particle size, Advanced Chromatography Technologies, Aberdeen, Scotland) maintained at $45\,°C$ as described previously (Zhu et al., 2013a). In brief, analytes were eluted at a flow rate of $0.2\,ml\,min^{-1}$ isocratically for 10 minutes with $100\,\%$ eluent A (methanol:formic acid:14.8 M NH_4^+, 100:0.04:0.10, v:v:v), followed by a linear gradient to $24\,\%$ eluent B (2-propanol:formic acid:14.8 M NH_4^+, 100:0.04:0.10, v:v:v) in 5 minutes, followed by a gradient to $65\,\%$ B in 55 minutes. The column was then flushed with $90\,\%$ B for 10 minutes and re-equilibrated with $100\,\%$ A for 10 minutes. Quinones and lipids were identified by retention time, accurate molecular mass, and MS^2 fragmentation (Table VIII.1; cf. Chapter VII; Sturt et al., 2004; Yoshinaga et al., 2011). Integration of peaks was performed on extracted ion chromatograms of $\pm$10 mDa width and included the $[M+H]^+$, $[M+NH_4]^+$, and $[M+Na]^+$ ions. Where applicable, double charged ions were included in the integration.

Additionally, selected samples were analyzed for low-abundance methanophenazines and archaeal lipids under the same chromatographic conditions on a Dionex Ultimate 3000RS UHPLC system connected to an ABSciEX QTRAP4500 Triple Quadrupole/Ion Trap MS equipped with an ESI ion source operating in positive mode. Target compounds were detected by multiple reaction monitoring of diagnostic MS/MS transitions. Ion source, multiple reaction monitoring transitions and other MS parameters were optimized by direct infusion of commercially available lipid and quinone standards as well as total lipid extracts of *Nitrosopumilus maritimus* and *Methanosarcina acetivorans*.

Bacterial IPLs were analyzed by injecting 1-10 % of the TLE dissolved in dichloromethane:methanol (9:1, v:v) on a Dionex Ultimate 3000RS UHPLC system connected to a Bruker maXis Ultra-High Resolution qToF-MS equipped with an ESI ion source

operating in positive mode as described above. Analyte separation was achieved using normal phase HPLC on an Acquity UPLC BEH Amide column ($1.7\,\mu m$, 2.1 x 150 mm; Waters Corporation, Eschborn, Germany) maintained at $40\,°C$ as described by Wörmer et al. (2013). In brief, analytes were eluted at a flow rate of $0.4\,ml\,min^{-1}$ with $99\,\%$ eluent A (acetonitrile:dichloromethane, 75:25, with each $0.01\,\%$ formic acid and NH_3) and $1\,\%$ eluent B (methanol:water, 50:50, with $0.4\,\%$ formic acid and NH_3) for 2.5 min, increasing B to $5\,\%$ at 4 min, to $20\,\%$ B at 22.5 min and $40\,\%$ B at 26.5 min. The column was then flushed with $40\,\%$ B for 1 min.

Archaeal IPL and quinone quantification was achieved by injecting a known amount of an internal standard (C_{46}-GTGT) along with the samples. Bacterial IPLs were quantified by comparing their peak areas with the peak area of the extraction standard. The quinone abundances were corrected for the relative response of commercially available menaquinone ($MK_{4:4}$, for MKs, chlorobiumquinone (ChQ), vitamin K1) and ubiquinone ($UQ_{10:10}$, *trans*-isomer, for UQs, PQs) standards (Sigma Aldrich, St. Louis, MO, USA) versus the C_{46}-GTGT standard. Due to a lack of an authentic standard, MP concentrations were not corrected for their relative response and are thus not included in total quinone abundance and distribution patterns as well as calculations of diversity indices. The detection limit for quinones, intact polar and neutral lipids as detected for authentic standards using the qToF-MS was approximately 1 pg, depending on compound class and considering a signal-to-noise ratio of greater than 3.

Archaeal lipid abundances were corrected for response factors of commercially available and purified standards. Purified standards were obtained from extracts of *Archaeoglobus fulgidus* as described in Elling et al. (2014). The abundances of mono- (1G) and diglycosidic (2G) glycerol dibiphytanyl glycerol tetraethers (GDGTs) and hydroxylated GDGTs were corrected for the response of purified acyclic 1G- and 2G-GDGT standards, respectively. Due to the lack of an identical standard, the abundances of hexose phosphohexose (HPH) GDGTs were corrected for the response of a commercially available phosphatidylglycerol-hexose GDGT standard (Matreya LLC, Pleasant Gap, PA, USA) as described in Elling et al. (2014). The abundances of mono- and diglycosidic archaeol were corrected for the respective purified standard, while phosphatidylglycerol (PG), phosphatidylinositol (PI) and phosphatidylethanolamine (PE) archaeol abundances were corrected for the response of a commercial phosphatidylethanolamine archaeol standard (Avanti Polar Lipids Inc., Alabaster, AL, USA).

The abundances of isorenieratene were corrected by the relative response of a commercial β-carotene standard (Sigma Aldrich). Similarly, the abundances of cholesterol and alkenones were corrected by the relative response of a commercial cholesterol standard (Sigma Aldrich) and synthetic $C_{37:2}$ and $C_{37:3}$ alkenone standards (Rechka and Maxwell, 1988). The abundances of diacylglycerol (DAG) and dietherglycerol (DEG) lipids with

phosphatidylglycerol (PG), PE, monomethyl PE (PME) and dimethyl PE (PDME), were corrected by the relative responses of commercial DAG-$C_{16:0/16:0}$ standards with the respective headgroup (Avanti). The abundances of intact polar acyletherglycerol (AEG) lipids were corrected for the response of the respective DAG standard. The abundances of diphosphatidylglycerol (DPG), PC-DEG, 1G- and 2G-DAG lipids were corrected by the relative responses of DPG-$C_{18:1}$, PC-DEG-$C_{16:0/16:0}$ standards, 1G-DAG-$C_{16:0/16:0\text{-cyclopropyl}}$ (Avanti) and 2G-DAG-$C_{18:0/18:0}$ (Matreya) standards, respectively. Abundances of monoglycosidic Ceramides (1G-Cer) and hydroxylated PG (PG-OH)-Cer were corrected for the relative response of a 1G-Cer-$C_{18:1/18:0}$ standard (Avanti). Due to a lack of appropriate standards, ornithine and betaine lipids as well as DAG lipids with PI headgroups were not corrected for their relative response.

Microbial (MD_q) and bioenergetic divergence indices (BD_q) were calculated after Iwasaki and Hiraishi (1998):

$$MD_q = \left(\sum_{k=1}^{p} \sqrt{x_k} \right)^2 \qquad \text{(Eq. 1)}$$

where x_k indicates the abundance of quinone k relative to total quinones.

$$BD_q = \left(\sqrt{UQ} + \sqrt{PQ + K1} + \sqrt{polyuns\ MK} + \sqrt{sat + monouns\ MK} + \sqrt{ChQ} \right)^2 \qquad \text{(Eq. 2)}$$

where UQ, PQ, vitamin K1, polyunsaturated (polyuns) MK, saturated (sat) MK, monounsaturated (monouns) MK and ChQ indicate the relative abundance of UQs, PQs, vitamin K1, polyuns MKs, sat MKs, monouns MKs and ChQ of total quinones as 1, respectively.

VIII.3. Results

VIII.3.1. Water column and sediment chemistry

Geochemical data of the Black Sea water column revealed a strong vertical stratification (Fig. VIII.3). The salinity increased from 17.7 at the surface to 22.3 in deep waters (Fig. VIII.3A). The steepest increase occurred between 80 and 150 meters below sea level (mbsl). The temperature profile behaved similarly and ranged between 8.5 and 9 °C (Fig. VIII.3A). A minimum in fluorescence was detected at 70 mbsl (Fig. VIII.3B). Dissolved oxygen concentrations decreased in a narrow depth interval between 70 and 150 mbsl from more than $250\,\mu mol\,kg^{-1}$ to below detection (Fig. VIII.3C). Hydrogen sulfide was first detected below a depth of 100 mbsl and slightly increased in concen-

tration to $11.5\,\mu mol\,l^{-1}$ at ca. 1100 mbsl (Fig. VIII.3C). In the sample from 1205 mbsl, HS^- concentration showed a strong increase to $38.6\,\mu mol\,l^{-1}$. Both, dissolved phosphate (PO_4^{3-}) and ammonium (NH_4^+) first appeared at 150 mbsl. While PO_4^{3-} showed a distinct peak at this depth, NH_4^+ increased towards the seafloor. Phosphate concentrations followed this trend between 200 and 1200 m (Fig. VIII.3D). The suboxic zone is located at approximately 70 to 150 m water depth at the boundary between the oxic surface and anoxic deep layers. In this zone O_2 and HS^- co-occur and the concentrations of both are low. Thus, we defined the zonation of the water column at site GeoB15105 as follows: oxic zone from 0 to 70 mbsl, suboxic zone (chemocline) from 70 to 150 mbsl, and anoxic zone from 150 mbsl to the seafloor.

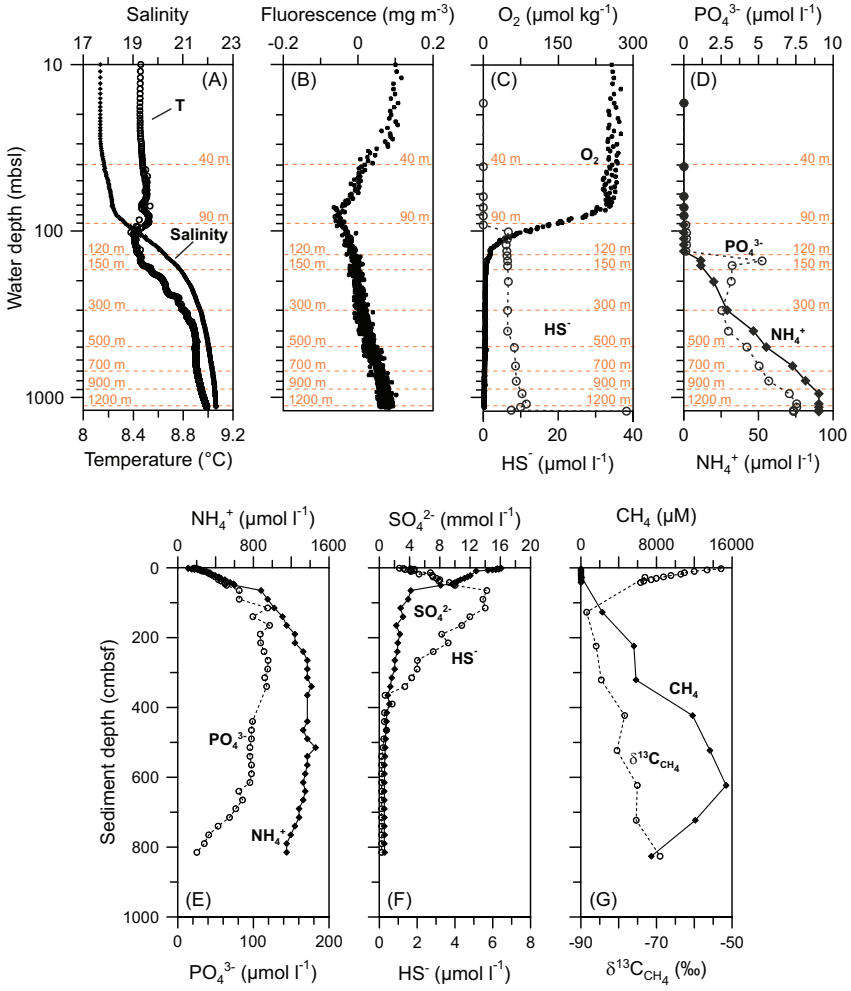

Figure VIII.3. Chemistry for the Black Sea water column and pore waters of the sediment. For the water column salinity and temperature (A), fluorescence (B), dissolved oxygen and hydrogen sulfide (C), and phosphate and ammonium (D) are shown. Additionally, sampling depth for lipid and quinone analysis are indicated by horizontal dashed lines. The depth is shown on a logarithmic scale (10 to 1200 mbsl) to emphasize the suboxic zone. For the pore waters phosphate and ammonium (E), sulfate and hydrogen sulfide (F), and methane and $\delta^{13}C$ of methane (G) are shown.

The pore water profiles of dissolved PO_4^{3-} and NH_4^+ followed similar trends with increasing concentrations within the first $2\,\mathrm{m}$ of the sediment (Fig. VIII.3E). Ammonium concentrations were ca. eight to ten times higher than phosphate concentrations. While NH_4^+ concentrations stayed fairly constant below 200 cm below seafloor (cmbsf), PO_4^{3-} concentrations slightly decreased towards the deepest sample. Dissolved sulfate decreased with sediment depth, reaching minimum values at 400 cmbsf. Hydrogen sulfide concentrations showed a maximum at approximately 100 cmbsf. Below 400 cmbsf, concentrations were close to zero (Fig. VIII.3F). Methane concentrations were low (<$75\,\mu\mathrm{mol}$) in the top 30 cm of the sediment, but increased to almost 15.4 mM at 623 cmbsf. The $\delta^{13}C_{CH_4}$ values significantly decreased from $-53‰$ to $-88.5‰$ within the top 127 cmbsf. Below this depth, $\delta^{13}C_{CH_4}$ values increased to $-69‰$ in the deepest investigated sample (Fig. VIII.3G).

VIII.3.2. Detection of novel quinones

Quinones detected in the Black Sea suspended particulate matter and sediment samples comprised vitamin K1, $PQ_{9:9}$, $ChQ_{7:7}$, polyunsaturated UQs and MKs with variable chain lengths and degrees of unsaturation, fully saturated and monounsaturated MK_6 as well as the functional quinone analogs $MP_{5:4}$ and $MP_{5:3}$ (Fig. VIII.5A). $ChQ_{7:7}$ was detected here for the first time in environmental samples. The structure of $ChQ_{7:7}$ was confirmed by comparing MS^2 spectra of $ChQ_{7:7}$ in the samples (Fig. VIII.4) with literature data (Powls et al., 1968).

We additionally tentatively identified several novel UQ and MK isomers based on accurate molecular mass in full scan (MS^1) mode and characteristic fragmentation in MS^2 mode (Fig. VIII.5). The quinones $UQ_{7:7}$ to $UQ_{10:10}$ each showed one early ($UQ_{m:n}$(a)) and one late ($UQ_{m:n}$(b)) eluting isomer and the two associated compounds for each UQ revealed highly similar MS^2 fragmentation (Fig. VIII.3B). The major product ion at *m/z* 197.1 represented the UQ head group. Minor fragments resulted from fragmentation of the isoprenoid side chain. Up to four isomers ($MK_{m:n}$(a-d)) were detected In the extracted ion chromatograms of fully unsaturated MKs. In this study, these isomers are numbered consecutively from 'a' to 'd' from early to late eluting (Fig. VIII.5). As for UQ isomers, MK isomers showed highly similar fragmentation patterns characterized by dominant product ions at *m/z* 187.1 (head group) and fragments of the isoprenoid side chain (Fig. VIII.5C). In total, 43 different quinone structures were identified in the water column and sediment samples. Due to the lack of authentic standards for MPs, these compounds could not be corrected for their relative response and are thus not included in total quinone abundance and distribution patterns as well as MD_q and BD_q calculations.

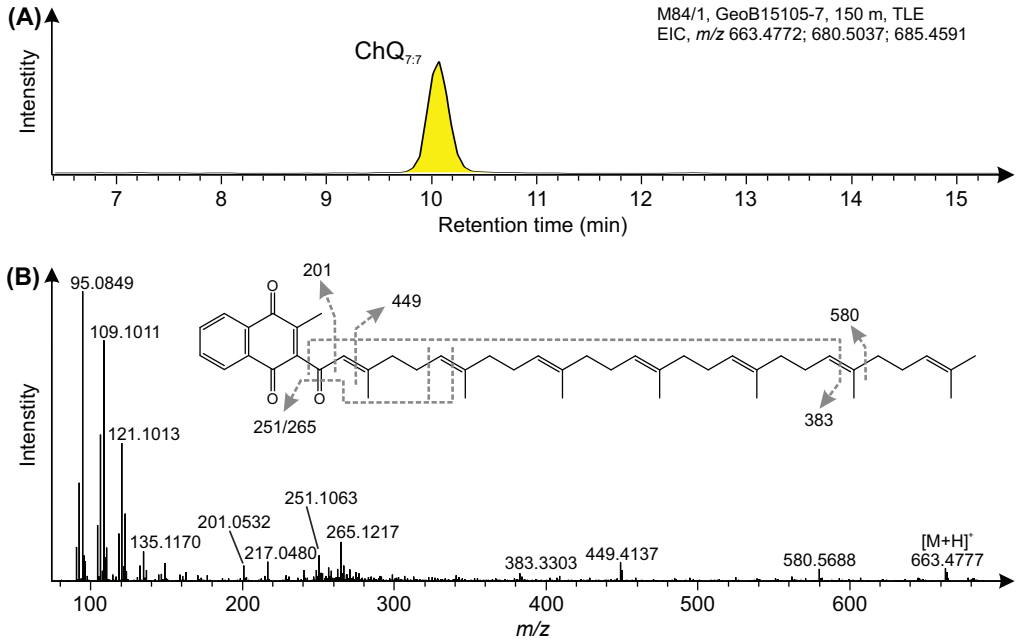

Figure VIII.4. (A) Extracted ion chromatogram (EIC), obtained by RP-UHPLC–ESI-MS, showing elution of chlorobiumquinone ($ChQ_{7:7}$) in a Black Sea suspended particulate matter sample from 150 m water depth. (B) MS^2 spectrum and structure of $ChQ_{7:7}$ ($[M+H]^+$ ion of *m/z* 663.5) as well as major product ions in the range *m/z* 50-700.

VIII.3.3. Relative abundances of quinone groups in the Black Sea water column and sediments

Total quinone concentrations in the water column ranged between 0.21 and $9.44\,\mathrm{ng\,l^{-1}}$ (Fig. VIII.6). The highest concentrations in the water column were measured at 40 mbsl within the oxic zone and at 300 mbsl within the anoxic part of the water column. From the oxic zone to the chemocline, concentrations decreased seven-fold. The lowest concentrations occurred in the deepest water column sample at 1200 mbsl. In the sediments, concentrations were highly variable and ranged from 1.7 ng to more than $1000\,\mathrm{ng\,g^{-1}}$ sediment dry weight (sed. dw.). The highest concentrations were measured in the surface sediment and the sapropel layer. Below the sapropel (lithological Unit II), concentrations were lowest and showed little variability.

The relative distribution of quinone groups showed large differences in the different redox zones of the Black Sea water column (Fig. VIII.6). At 40 mbsl (oxic zone), UQs and PQs were the major components, with UQs contributing more than $50\,\%$ and PQs more than $30\,\%$ to the total quinone pool, respectively. Archaeal menaquinones ($MK_{6:0}$ and $MK_{6:1}$) and vitamin K1 accounted for ca. $8\,\%$ each in the same sample. At the chemocline, archaeal menaquinones were the major contributors, whereas UQs were minor compounds with $2.6\,\%$ and $8\,\%$ relative abundance in 90 and 120 mbsl, respectively. At the lower boundary of the chemocline (150 mbsl), UQs were again the dominant com-

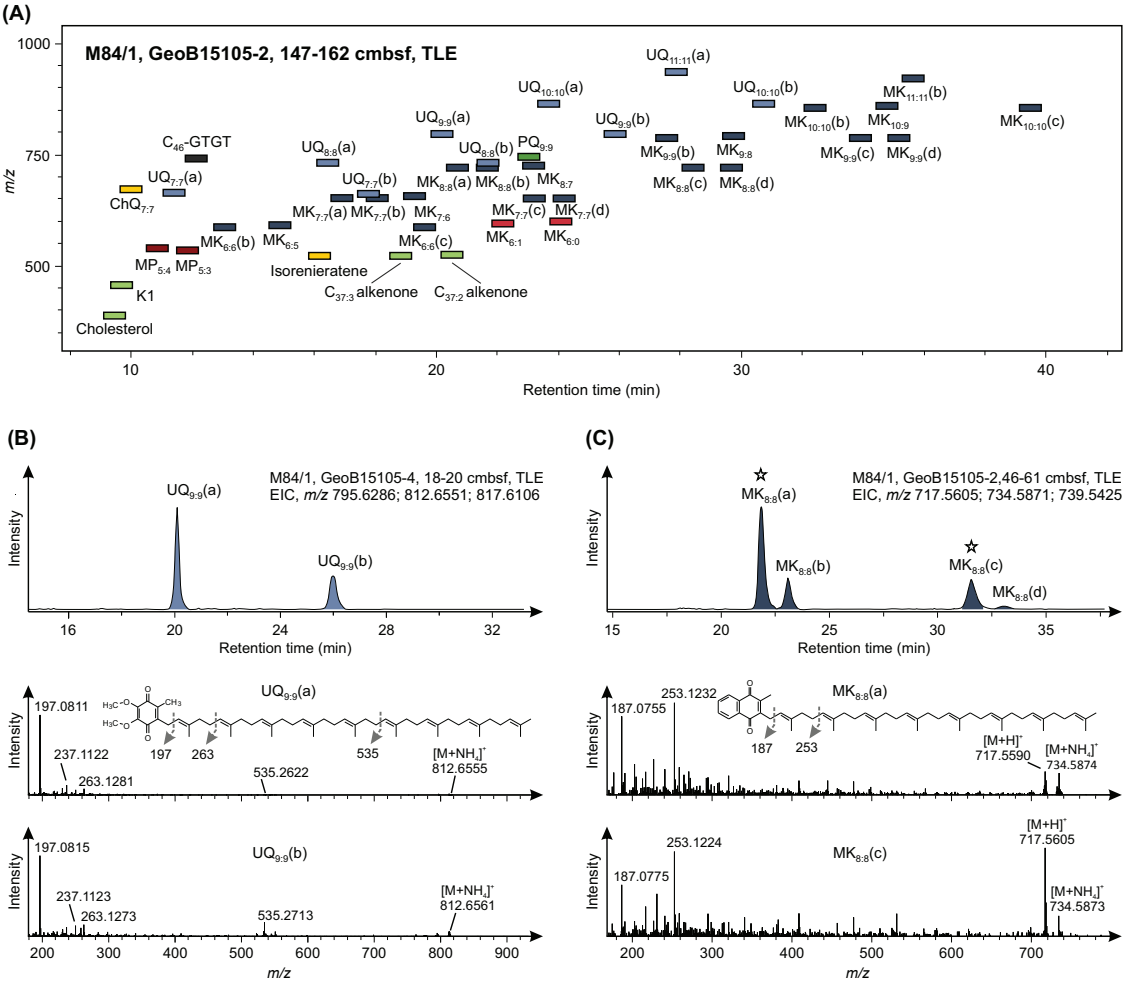

Figure VIII.5. (A) Reconstructed RP-UHPLC–ESI-MS density map showing elution order and *m/z* of all identified quinones, methanophenazines and the C_{46}-GTGT standard in sample M84/1, GeoB15105-2, 147-162 cmbsf. Colors indicate different quinone structures associated with distinct microbial metabolisms: green = photosynthetic quinones vitamin K1 (light green) and PQ (dark green), red = archaeal quinones (saturated and monounsaturated MKs) and *Methanosarcinales*-specific functional quinone analog MPs (dark red), light blue = aerobic bacterial quinones (UQs), dark blue = anaerobic bacterial quinones (polyunsaturated MKs) and yellow = the green sulfur bacterial ChQ. Quinones labeled with characters, e.g. $UQ_{9:9}$ (a) and (b) or $MK_{8:8}$(a), (b), (c) and (d), have the same molecular mass. Elution of eukaryotic apolar lipids cholesterol and C37 alkenones as well as isorenieratene, a biomarker pigment specific for green sulfur bacteria. (B) EIC of $UQ_{9:9}$ in sample M84/1, GeoB15105-4, 18-20 cmbsf illustrating an early and late eluting isomer ($UQ_{9:9}$(a) and $UQ_{9:9}$(b), respectively), and their corresponding MS^2 spectra. Both compounds revealed highly similar fragmentation patterns. (C) EIC of $MK_{8:8}$ in sample M84/1, GeoB15105-2 46-61 cmbsf showing four isomers ($MK_{8:8}$(a-d)). MS^2 spectra of two representatives ($MK_{8:8}$(a) and (c), indicated by star in the EIC) revealed highly similar product ions. Structures of $UQ_{9:9}$ and $MK_{8:8}$ and the formation of major product ions are also shown. MK, menaquinone; UQ, ubiquinone; K1, vitamin K1 (synonyms: phylloquinone, $MK_{4:1}$); PQ, plastoquinone; ChQ, chlorobiumquinone; MP, methanophenazine; GTGT, glycerol trialkyl glycerol tetraether.

pounds (46 % relative abundance). Polyunsaturated MKs and $ChQ_{7:7}$ were also detected in significant amounts in this sample, each contributing 22 % to the total quinone pool. In the deeper anoxic water column samples (300-1200 mbsl), polyunsaturated MKs and UQs occurred in similar proportions and account for more than 80 % of total quinones in the samples, whereas saturated and monounsaturated MKs as well as PQs were only minor components. Vitamin K1 was detected in trace amounts in the same samples. $ChQ_{7:7}$ occurred in trace amounts at 300 and 500 mbsl, but was absent in the deeper water column.

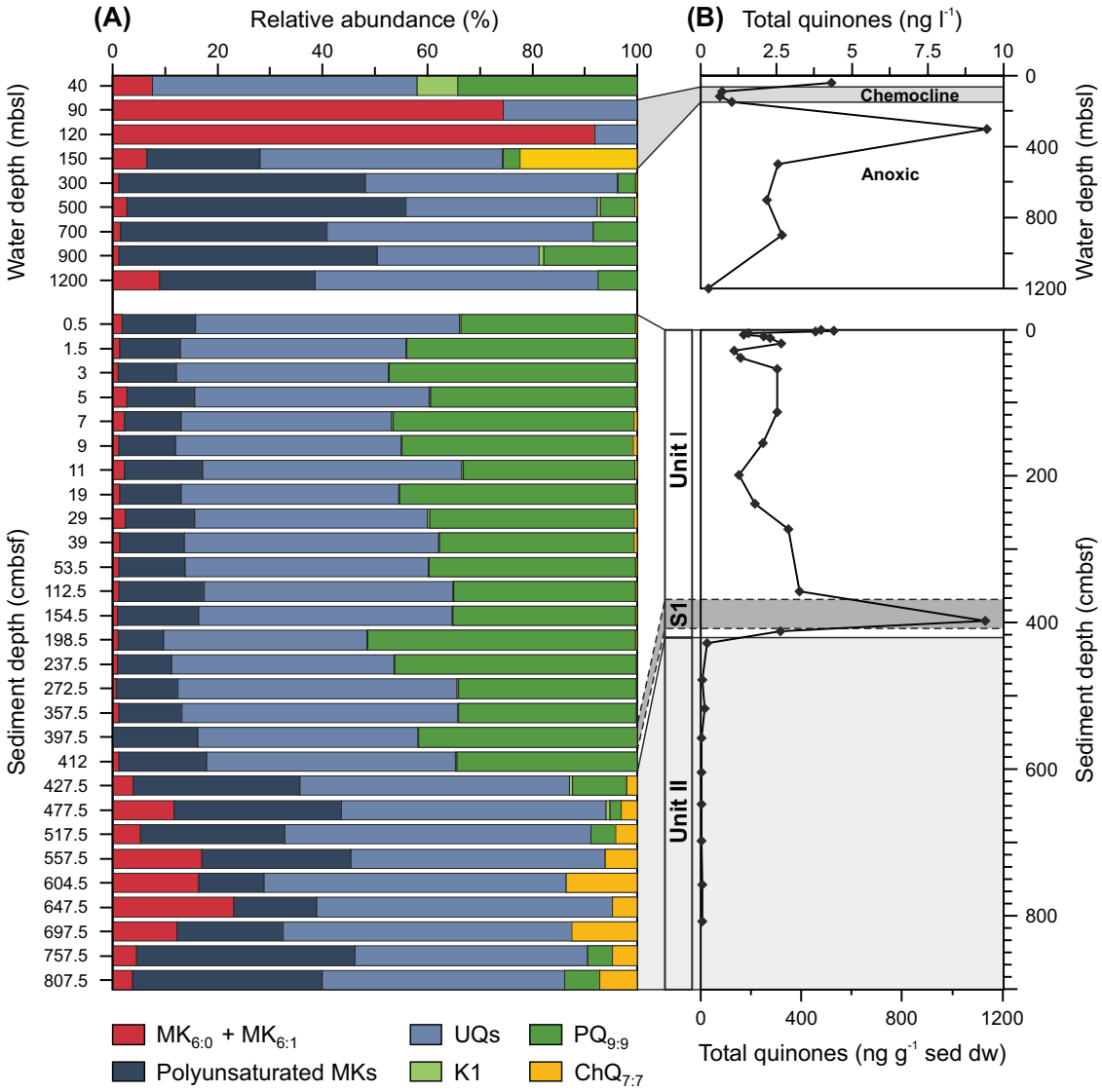

Figure VIII.6. Relative abundances of major quinones (A) and absolute quinone abundance (B) in the water column and sediments of the southern Black Sea (cruise M84/1, station GeoB15105). Shaded area in the water column profile corresponds to the chemocline. In the sediment, the marine (Unit I, white) and lacustrine (Unit II, light grey) units, as well as the sapropel (S1, dark grey) are denoted.

In the top 400 cmbsf (lithological Unit I), UQs and PQs were the dominant quinone types, contributing in sum to more than 80 % of total quinones (Fig. VIII.6A). Here, polyunsaturated MKs were also detected in significant amounts with relative abundances between 9 % and 17 %, whereas $MK_{6:0}$ and $MK_{6:1}$ were only minor components. Similarly, vitamin K1 and $ChQ_{7:7}$ were minor compounds in Unit I sediments. Below 400 cmbsf (lithological Unit II), the quinone distribution showed a different pattern: UQs were still the dominant quinone group, but PQs were almost absent (Fig. VIII.6). $MK_{6:0}$ and $MK_{6:1}$ increased in relative abundance with a maximum at 647.5 cmbsf, accounting for 23 % of total quinones. The abundance of polyunsaturated MKs also increased and $ChQ_{7:7}$ contributed significantly to the total quinone pool with relative abundances of up to 14 % in the deeper sediment (cmbsf).

VIII.3.4. Relative abundances of quinone isomers

The distribution of the 'regular' menaquinones and ubiquinones compared to the later eluting isomers showed large differences between the oxic and anoxic water column and the sediments (Fig. VIII.7). Based on the retention time of the commercially available standard ($UQ_{10:10}$), UQs labeled with '(a)' were referred to as regular compounds and the later eluting UQs (labeled with '(b)') were defined as isomers. Similarly, based on the retention time difference of the $MK_{4:4}$ standard relative to the compounds with longer isoprenoid side chains, MKs labeled with '(b)' were defined as regular MKs and other quinones with the same molecular mass were assigned as isomers (a, c, d; Fig. VIII.7).

The samples from the oxic zone and the chemocline contained only regular UQs, whereas regular UQs and MKs as well as their isomers occurred in the anoxic zone (Fig. VIII.7a). While UQ isomers were only minor constituents compared to the regular compounds, MK isomers were almost as abundant as the corresponding regular MKs in the water column. In the sediments, this pattern shifted towards higher relative abundances of the UQ and MK isomers compared to the respective regular compounds, and the distribution pattern of total isomers showed little variability (Fig. VIII.7a). However, analysis of the detailed distribution of isomers of individual quinones revealed major changes in the water column and sediment samples (Fig. VIII.7b). For example, the late eluting $UQ_{10:10}$(b) only occurred in two water column samples (150 and 300 mbsl) and showed a low relative abundance compared to the early eluting $UQ_{10:10}$(a) (Fig. VIII.7b), whereas $UQ_{10:10}$(b) was of greater abundance in the sediment, especially in lithological Unit I.

Differences in the distribution of isomers was even more pronounced for the four $MK_{8:8}$ isomers (Fig. VIII.7c). In the samples from the anoxic water column, the most abundant $MK_{8:8}$ isomer was $MK_{8:8}$(b). Similar to the distribution of $UQ_{10:10}$, the other

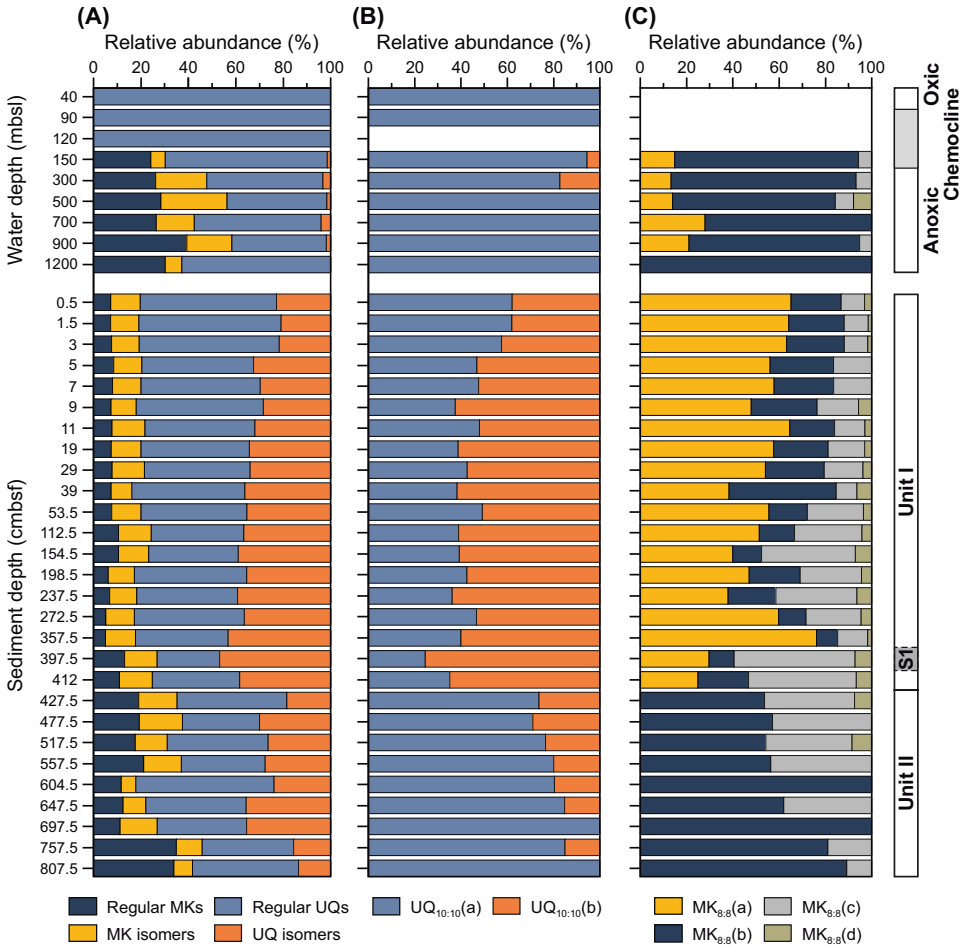

Figure VIII.7. Relative abundances of summed menaquinone and ubiquinone isomers (A), isomers of $UQ_{10:10}$ (B), and isomers of $MK_{8:8}$ (C) in the water column and sediments of the southern Black Sea (cruise M84/1, station GeoB15105).

MK isomers became dominant over the regular compound in lithological Unit I. Here, $MK_{8:8}$(a) was the most abundant isomer with up to $60\,\%$ relative abundance. In Unit II, $MK_{8:8}$(a) was not detected and $MK_{8:8}$(b) was the dominant isomer. With increasing sediment depth, the relative abundance of $MK_{8:8}$(c) increased to a maximum in the sapropel. $MK_{8:8}$(d) was a minor compound in all samples with relative abundances lower than $10\,\%$ of total $MK_{8:8}$.

VIII.3.5. Absolute abundances of individual quinones

Concentration profiles of the quinones associated with oxygenic photosynthesis, i.e., vitamin K1 and $PQ_{9:9}$, showed a distinct maximum in the oxic zone with concentrations of 0.3 and $1.5\,\mathrm{ng\,l^{-1}}$, respectively, and a decrease to below the detection limit in the chemocline (Fig. VIII.8A, B). In the anoxic part of the water column, both compounds showed more than five-fold lower concentrations compared to the oxic zone. $ChQ_{7:7}$ was not detected at shallower water depths and showed concentration maximum at

150 mbsl ($0.23\,ng\,l^{-1}$), below which concentrations were one order of magnitude lower (<$0.03\,ng\,l^{-1}$; Fig. VIII.8C). $UQ_{7:7}$(a) showed a similar depth trend (Fig. VIII.8D), while concentration maxima for other UQs were observed in the anoxic water column mainly at 300 mbsl (Fig. VIII.8E-J).

The concentration of $MK_{6:0}$ increased from oxic waters ($0.18\,ng\,l^{-1}$) to the suboxic waters of the chemocline at 120 m (0.36 ng l-1; Fig. VIII.8K). Concentrations of $MK_{6:1}$ were similar in the oxic waters ($0.14\,ng\,l^{-1}$) but showed a shallower maximum at the chemocline at 90 m ($0.24\,ng\,l^{-1}$; Fig. VIII.8L). The concentrations of both $MK_{6:0}$ and $MK_{6:1}$ were one order of magnitude lower in the anoxic part of the water column below 150 m ($0.01\,ng\,l^{-1}$) as compared to the oxic and suboxic zones. Concentrations of polyunsaturated MKs with different length and degree of unsaturation of the isoprenoid side chain varied between $10\,pg\,l^{-1}$ and ca. $1\,ng\,l^{-1}$ (Fig. VIII.8M-Ai). All MKs containing six isoprenoid units, including partially saturated compounds, showed a distinct maximum in the anoxic zone at 300 mbsl. The only other quinone that showed a similar concentration profile was $MK_{10:8}$. Many other MKs showed two concentration maxima, one at 300 mbsl and a deeper one at 700 mbsl. For example, $MK_{7:7}$ isomers, $MK_{8:8}$ isomer (except for $MK_{8:8}$(d)), $MK_{8:7}$ and $MK_{8:6}$, $MK_{9:9}$(b), $MK_{9:8}$, $MK_{10:10}$(a) and $MK_{10:9}$. $MK_{9:9}$(c) and $MK_{10:10}$(b) were the only MKs that showed a single maximum at 700 mbsl. $MK_{7:5}$ and $MK_{11:11}$(b) showed a deeper concentration maximum at 900 mbsl.

In the sediment, depth profiles of individual quinones were more uniform compared to the water column (Fig. VIII.9) and mainly tracked total quinone concentrations (see Fig. VIII.6B). Most quinones showed a pronounced concentration maximum in the sapropel layer at 397.5 cmbsf, with the exceptions of $ChQ_{7:7}$, $MK_{6:0}$, $MK_{6:1}$, $UQ_{11:11}$(a) and (b) as well as a few fully unsaturated and partially saturated MKs. Vitamin K1, $PQ_{9:9}$, $ChQ_{7:7}$; $MK_{6:0}$, most fully unsaturated MKs and all regular UQs additionally showed high concentrations in the surface sediments, which rapidly decreased within the first 20 to 30 cm sediment depth. For the late eluting UQ isomers as well as several fully unsaturated MKs, elevated concentrations in surface sediments were not observed. In Unit II, concentrations of individual quinones were more than one order of magnitude lower that in Unit I. Highest concentrations in the sediments were observed for $PQ_{9:9}$ with values of up to $470\,ng\,l^{-1}$ sed. dw. in the sapropel layer. The concentrations of vitamin K1, $ChQ_{7:7}$, and $MK_{6:1}$ and $MK_{6:0}$ were approximately two orders of magnitude lower as compared to $PQ_{9:9}$. Within the UQs, compounds with seven to ten isoprenoid units revealed similar concentrations, which were about ten-fold higher than concentrations for vitamin K1, $ChQ_{7:7}$, and $MK_{6:0}$ and $MK_{6:1}$ as well as $UQ_{11:11}$. The concentrations of the different polyunsaturated MKs showed large variability. While concentrations of partially saturated MKs were mainly below $1\,ng\,g^{-1}$ sed. dw., concentrations of some fully unsaturated $MK_{6:6}$, $MK_{7:7}$ and $MK_{8:8}$ isomers were at least one order of magnitude

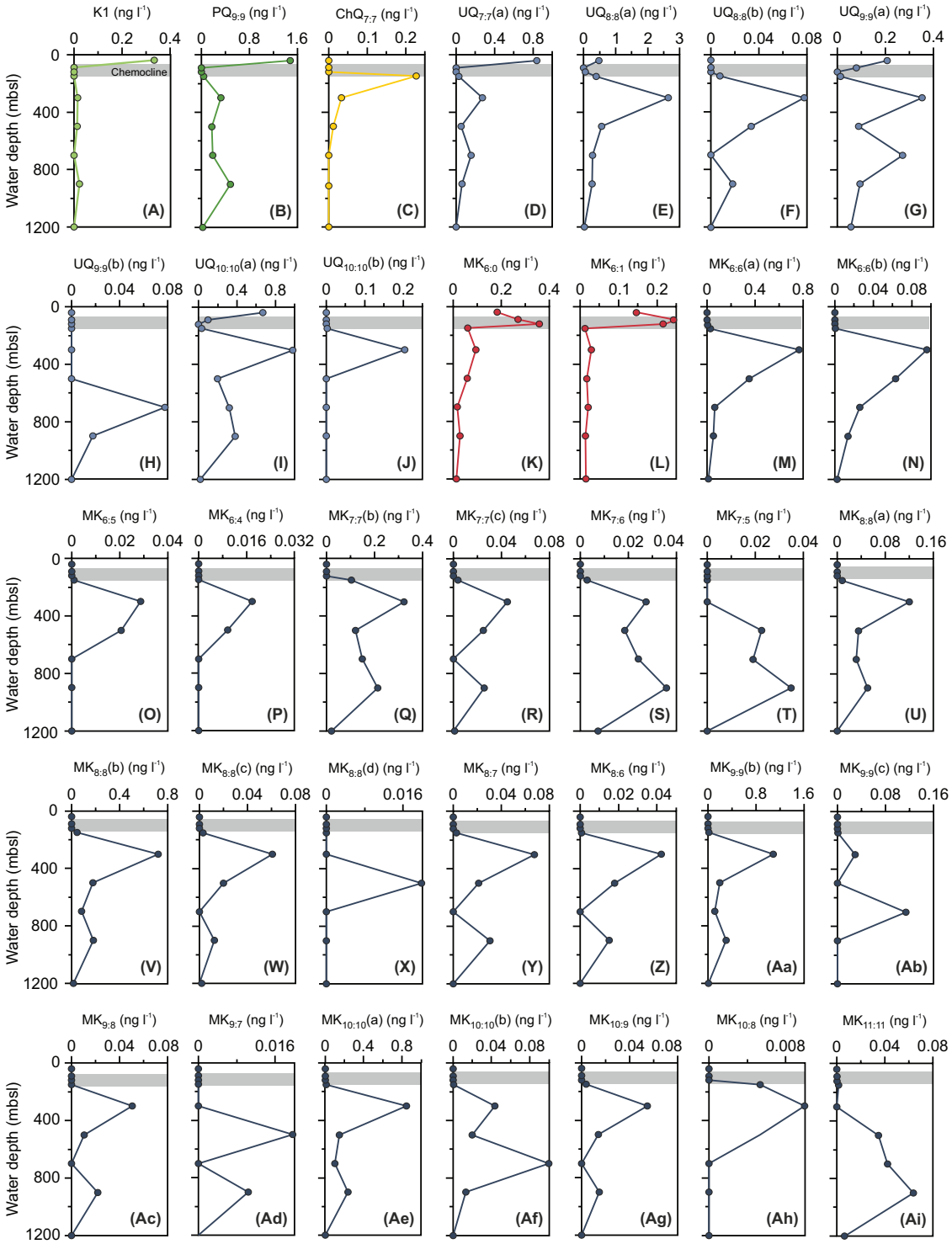

Figure VIII.8. Depth profiles of all quinones detected in the Black Sea water column. Shaded areas correspond to the chemocline. Colors indicate different quinone structures associated with distinct microbial metabolisms: green = photosynthetic quinones vitamin K1 (light green) and PQ (dark green), red = archaeal quinones (saturated and monounsaturated MKs, light red), light blue = aerobic bacterial quinones (UQs), dark blue = anaerobic bacterial quinones (polyunsaturated MKs) and yellow = the green sulfur bacterial ChQ. MK, menaquinone; UQ, ubiquinone; K1, vitamin K1; PQ, plastoquinone; ChQ, Chlorobiumquinone.

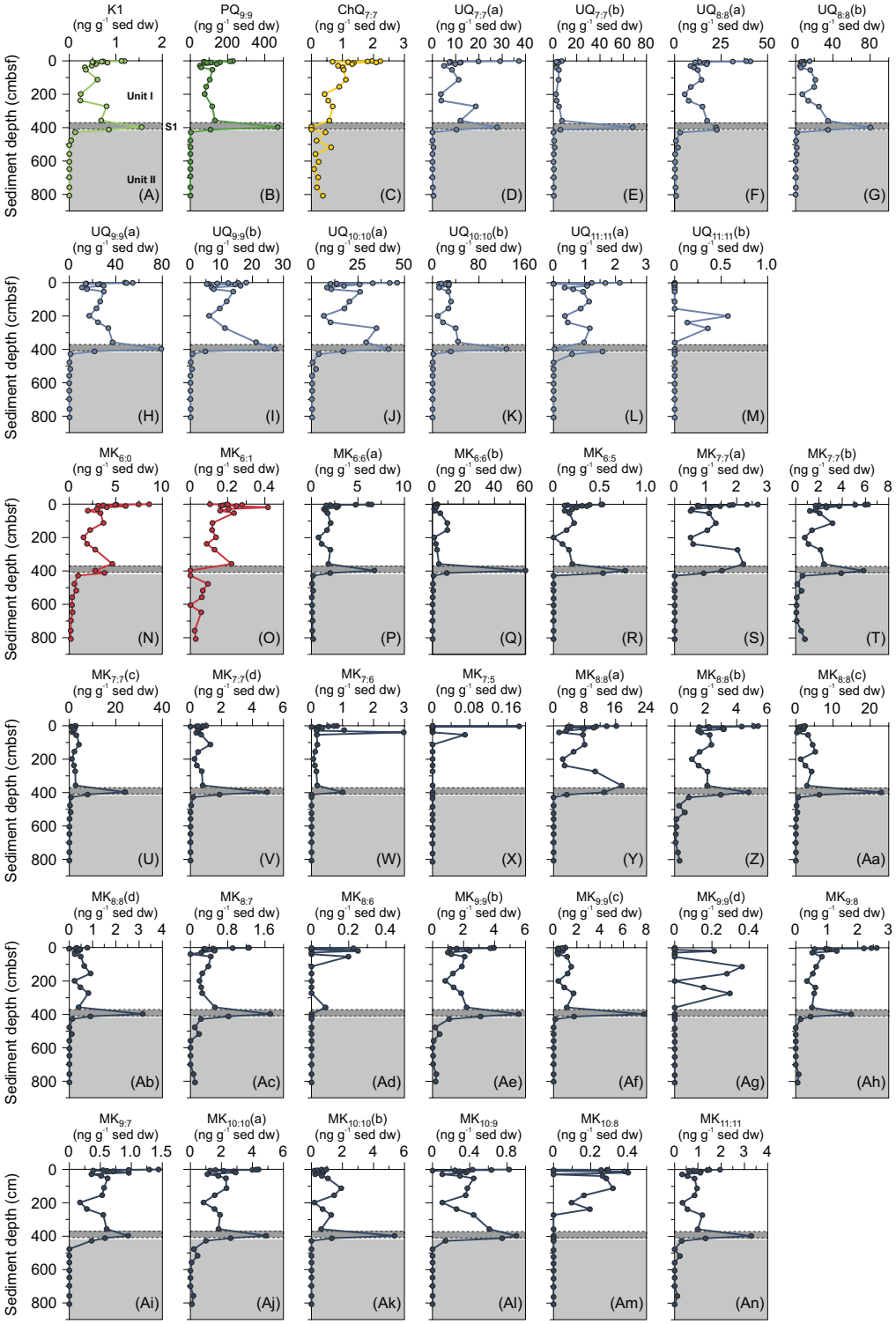

Figure VIII.9. Depth profiles of all quinones detected in Black Sea sediments. Marine (Unit I, light grey) and lacustrine (Unit II, intermediate grey) lithological units as well as the sapropel (S1, dark grey) are denoted. Colors indicate different quinone structures associated with distinct microbial metabolisms: green = photosynthetic quinones vitamin K1 (light green) and PQ (dark green), red = archaeal quinones (saturated and monounsaturated MKs), light blue = aerobic bacterial quinones (UQs), dark blue = anaerobic bacterial quinones (polyunsaturated MKs), and yellow = green sulfur bacterial ChQ. MK, menaquinone; UQ, ubiquinone; K1, vitamin K1; PQ, plastoquinone; ChQ, Chlorobiumquinone.

higher. Highest concentrations within the polyunsaturated MKs were observed for $MK_{6:6}$(b), $MK_{7:7}$(c), $MK_{8:8}$(a) and $MK_{8:8}$(c).

VIII.3.6. Microbial diversity and bioenergetic divergence (MD_q and BD_q)

Microbial diversity (MD_q) and bioenergetic divergence (BD_q) indices were calculated from quinone abundances using equations (1) and (2) and grouped according to the water column redox zones and the lithological units (Fig. VIII.10). Note that MD_q represents overall quinone diversity based on relative abundances of all individual quinones, while BD_q describes headgroup type richness, i.e., functional diversity.

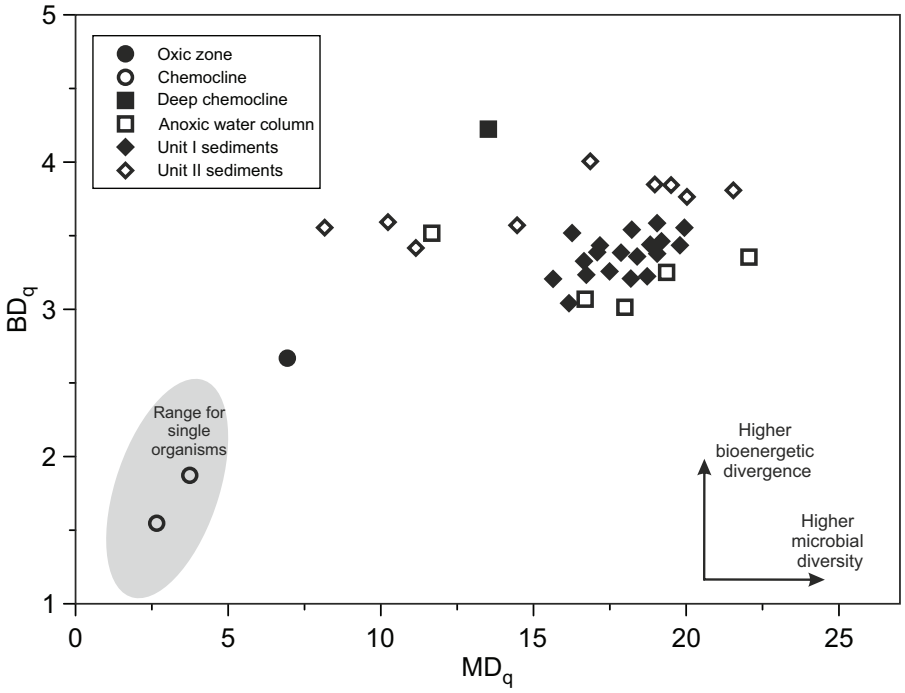

Figure VIII.10. Cross plot of microbial divergence (MD_q) and bioenergetic divergence (BD_q) indices after Iwasaki and Hiraishi (1998) for water column and sediment samples from the southern Black Sea (M84/1, GeoB15105). The range for single organisms is indicated by the grey area (based on the distribution of quinones in 24 archaeal strains shown in Chapter VII.

Samples from the same water column zones and sedimentary units showed similar BD_q values, whereas MD_q values were divergent. The lowest BD_q and MD_q indices were observed in samples from the chemocline at 90 and 120 mbsl, with MD_q values below 5 and BD_q values below 2. Low MD_q and BD_q values distinguish the sample from the oxic (photic) zone from the rest of the obtained dataset. The deep chemocline sample (150 mbsl) showed the highest BD_q values of all samples (4.2), while MD_q values were intermediate with 13.5. The samples from the anoxic zone showed BD_q values between 3 and 3.5, whereas the MD_q values were in a broad range from 11.6 to 22. All samples

from Unit I showed relatively high values but little variability for both indices (15.6-20 MD_q, 3-3.6 BD_q). A similar pattern was observed for the samples from sediment Unit II, albeit with a higher BD_q index (3.4-4) for most samples.

VIII.3.7. Methanophenazines

Methanophenazines were absent in the oxic part of the water column and the chemocline but were detected in the anoxic part of the water column, except at 1200 mbsl (Fig. VIII.11). Highest concentrations occurred at 300, 500 and 900 mbsl with values between 13 and 17 $pg\,l^{-1}$. The concentrations of methanophenazine decreased strongly with depth from 9 cmbsf (311 $pg\,g^{-1}$ sed. dw.) towards 400 cmbsf (below detection limit).

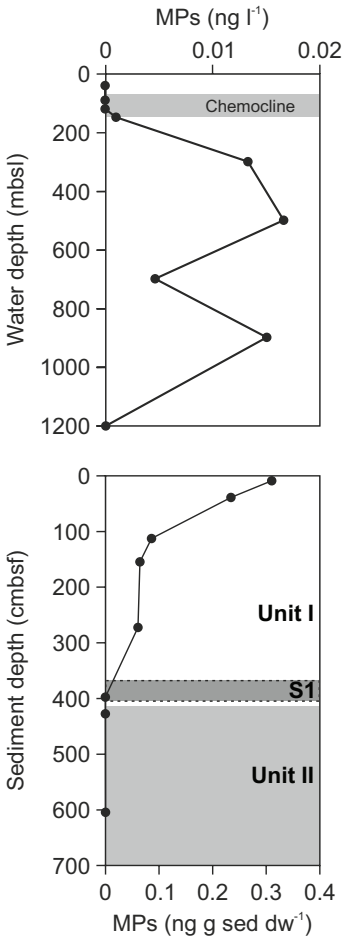

Figure VIII.11. Profile of total methanophenazines ($MP_{5:4}$ and $MP_{5:3}$) in the water column and sediments of the southern Black Sea (cruise M84/1, station GeoB15105).

VIII.3.8. Relative abundances of IPLs

For examining their distribution in the water column and sediments, IPLs (see Fig. VIII.12 for chemical structures) were grouped by headgroup and core lipid type irrespective of side chain structure into intact polar archaeols (IP-AR), GDGTs (IP-GDGTs), glycosidic (G-) and phosphatidic (P-) DAG, AEG, and DEG, as well as DPG, 1G-Cer, PG-(OH)-Cer, Ornithines (OL), and Betaines (BL).

The profiles of total quinones (Fig. VIII.6) and total IPLs (Fig. VIII.13) were similar in the water column and within the sediment. In the water column, IPL concentrations decreased from the oxic zone to the chemocline and showed maxima at 300 and 900 mbsl similar to quinone concentrations (Fig. VIII.13). In comparison to quinone concentrations, IPL concentrations in the surface sediments showed a steeper decrease towards deeper sediments and a less distinct maximum in the sapropel layer. Overall, IPL concentrations were approximately one order of magnitude higher than quinone concentrations in both the sediment and the water column.

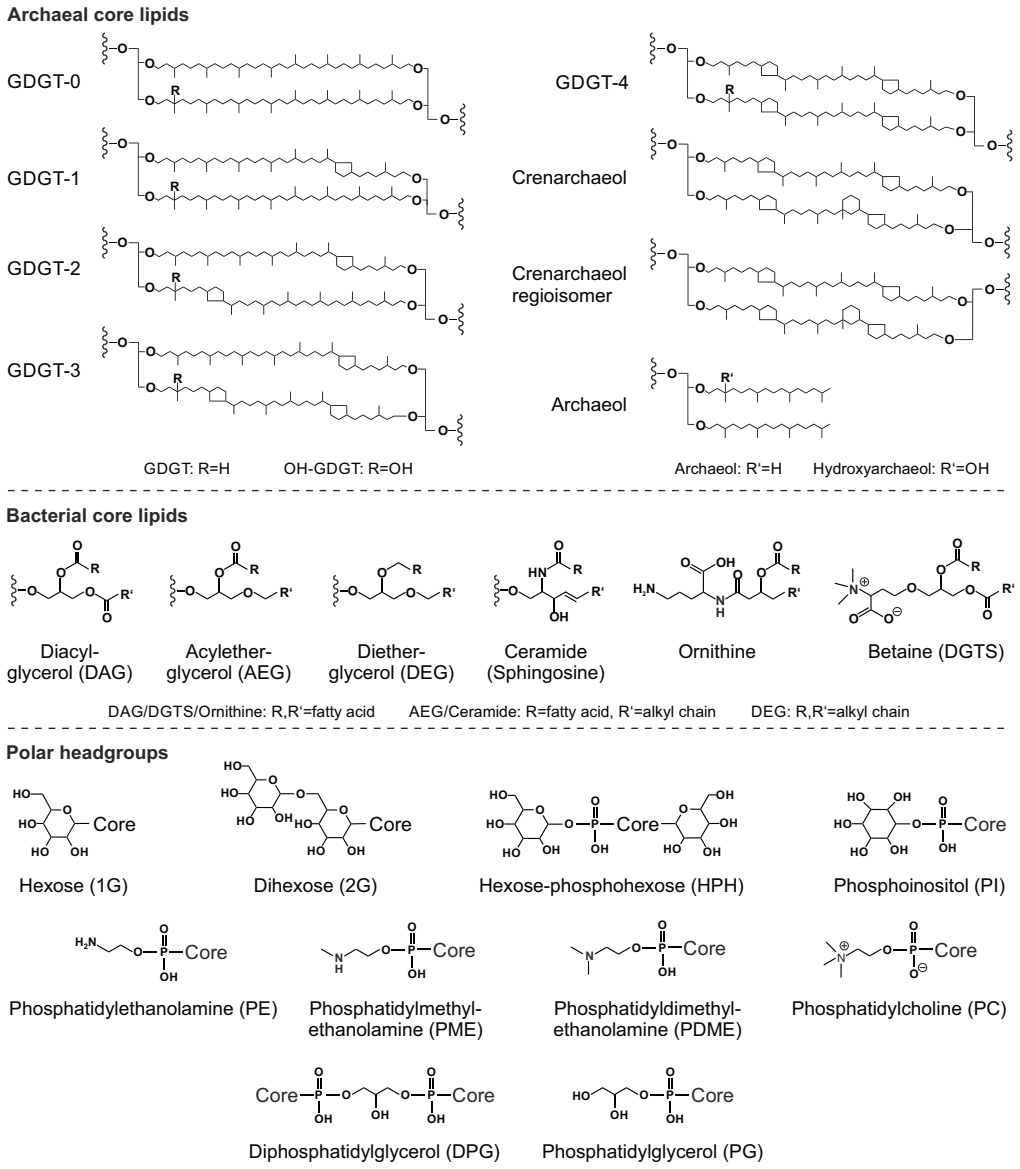

Figure VIII.12. Structures of archaeal and bacterial core lipids and associated polar headgroups detected in Black Sea water column and sediment samples.

Similar to the distribution of major quinone groups, specific IPL classes were associated with distinct geochemical zones. In the oxic zone, G-DAGs were the dominant IPLs, contributing almost 80 % to the total IPL pool. Minor IPL groups were P-DAG and BL, which were detected in similar amounts throughout the water column. Small amounts of IP-GDGTs and IP-ARs as well as P-AEG and P-DEG were also detected in the oxic zone. In the upper chemocline P-DAGs and IP-GDGTs increased in relative abundance. Here, archaeal IPLs accounted for about 10 % of total IPLs, which was the highest relative abundance of these compounds in the water column. Relative abundances of G-DAGs at the chemocline and in the anoxic zone were lower than in the oxic zone but still accounted for up to 30 % of the IPLs. 1G-Cer and DPG first appeared within the

chemocline (120 mbsl) and were detected throughout the anoxic water column. In the deepest part of the chemocline (150 mbsl), P-AEG and especially P-DEG increased in relative abundance, the latter accounting for more than 25 % of total IPLs. The combined relative abundance of these two groups was about 40 % throughout the anoxic zone. In contrast, concentrations of P-DAG decreased from the chemocline to the deep anoxic zone. Ornithine lipids (OL) and PG-(OH)-Cer were detected in low abundance only in the anoxic zone, where archaeal IPLs showed very low relative abundances.

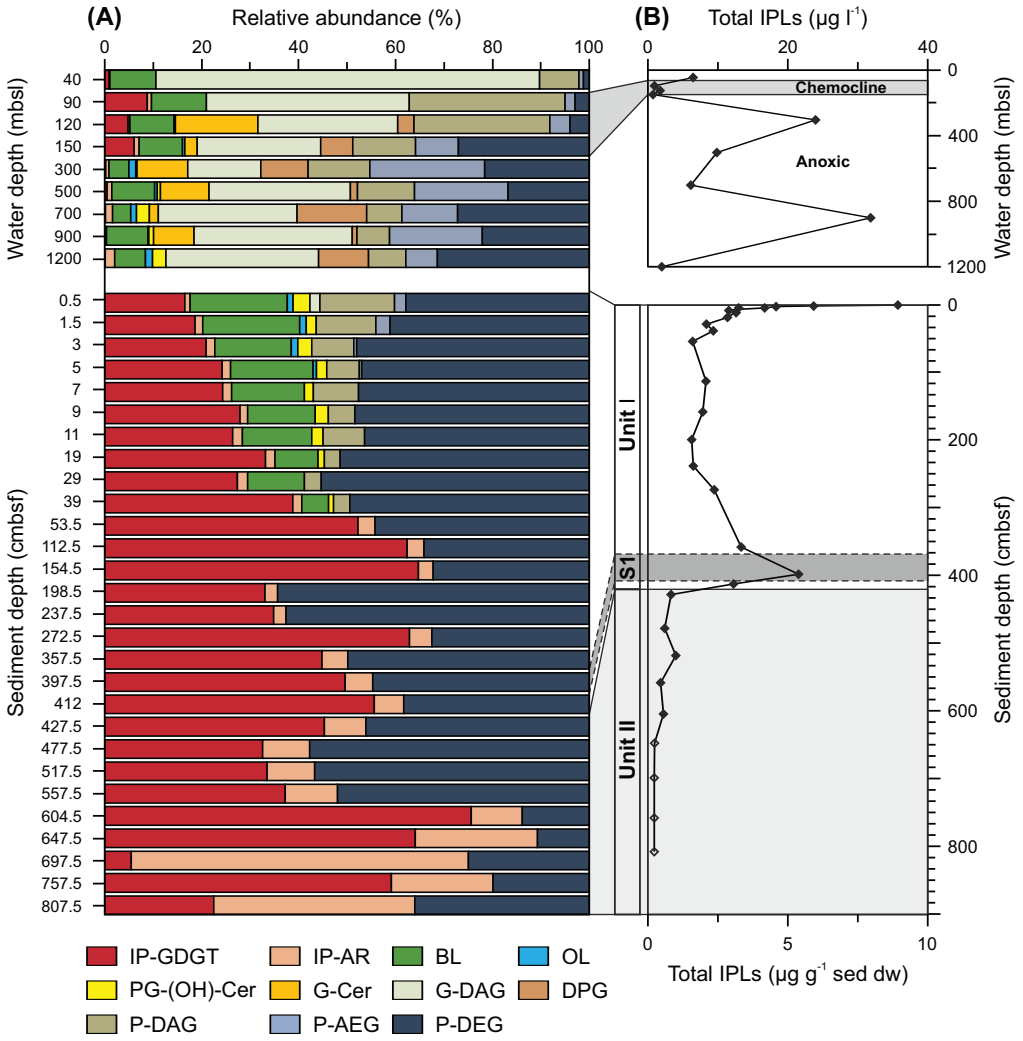

Figure VIII.13. Relative abundances of IPL groups (A) and absolute IPL abundance (B) in the water column and sediments of the southern Black Sea (cruise M84/1, station GeoB15105). Shaded area in the water column profile corresponds to the chemocline. In the sediment, the marine (Unit I, white) and lacustrine (Unit II, light grey) units, as well as the sapropel (S1, dark grey) are denoted. IPL data except for water column samples from 150 m, 300 m, 500 m, and 900 m depth from Schröder (2015).

The IPL composition of the sediments differed strongly from that of the water column (Fig. VIII.13). P-DEG was the dominant IPL group with almost 40 % relative abundance in surface sediments. Other major groups in surface sediments were BL, IP-GDGTs

and P-DAG. G-DAG were detected only in trace amounts and disappeared below the surface. DPG and 1G-Cer were not detected in the sediments and OL, P-AEG PG-(OH)-Cer and IP-ARs only occurred in very low relative abundance (<3.5 %). Within the upper 39 cmbsf, acyl side chain containing IPLs steadily decreased in relative abundance with depth, whereas relative abundances of ether-based lipids such as IP-GDGTs and P-DEG increased. Only IP-GDGTs, P-DEG and IP-AR were detected below 39 cmbsf in lithological Unit I, where either IP-GDGTs or P-DEG dominated the total IPL pool. The relative abundance of IP-ARs was low (∼5 %) but progressively increased with depth in sediment Unit I. IPL distributions in the upper part of Unit II (427.5-557.5 cmbsf) closely resembled the distribution of the lower part of Unit I. However, below 557.5 cmbsf, archaeal IPLs clearly dominated over bacterial P-DEG, although P-DEG still accounted for about 25 to 36 % of total IPLs. IP-ARs showed highest relative abundances of all samples below 557.5 cmbsf and were the dominant IPL group at 697.5 and 807.5 cmbsf.

VIII.3.9. Absolute abundances of IPLs and apolar lipids relative to quinones

The concentrations of the different IPL groups showed significant variations in the water column and, in part, within the sediment (Fig. VIII.14). Depth-dependent concentrations of G-DAG, BL and P-DAG (Fig. VIII.14A-C) strongly resembled each other. They showed a decrease from the oxic water column to the chemocline and a maximum at 900 mbsl (G-DAG and BL; Fig. VIII.14A, B) and at 300 mbsl (P-DAG; Fig. VIII.14C). The G-DAG depth profile was similar to the profiles of $PQ_{9:9}$ and vitamin K1, whereas the P-DAG profile was more similar to those of $UQ_{8:8}$(a), $UQ_{9:9}$(a) and $UQ_{10:10}$(a) (Figs. VIII.9 and VIII.14), although the distribution in the anoxic waters also matched some MK profiles. P-AEG, PE-DEG and 1G-Cer followed largely the same trend as P-DAG in the anoxic water column and concentrations were in a similar range. However, they were absent in the oxic zone and the chemocline (Fig. VIII.14D, E, and H). DPG, OL, and PG-(OH)-Cer were minor components or absent within the chemocline and the oxic zone (Fig. VIII.14F, G and I).

The concentrations of both DPG and OL peaked in the anoxic water column at 300 mbsl, which coincided with peaks in abundance in most other IPL groups, whereas the secondary maximum occurred slightly shallower at 700 mbsl instead of 900 mbsl observed e.g. for G-DAG, BL or P-DEG (Fig. VIII.14F and G). The concentration of PG-(OH)-Cer only peaked at 700 mbsl in the anoxic zone (Fig. VIII.14I). The concentration profiles of archaeal IP-GDGTs and IP-ARs were distinct from each other and bacterial IPLs in the water column: IP-GDGT concentrations increased from the oxic zone to the chemocline (Fig. VIII.14J), while they were low throughout the anoxic water column. This distinct maximum in the chemocline was not observed in the depth profile of IP-AR.

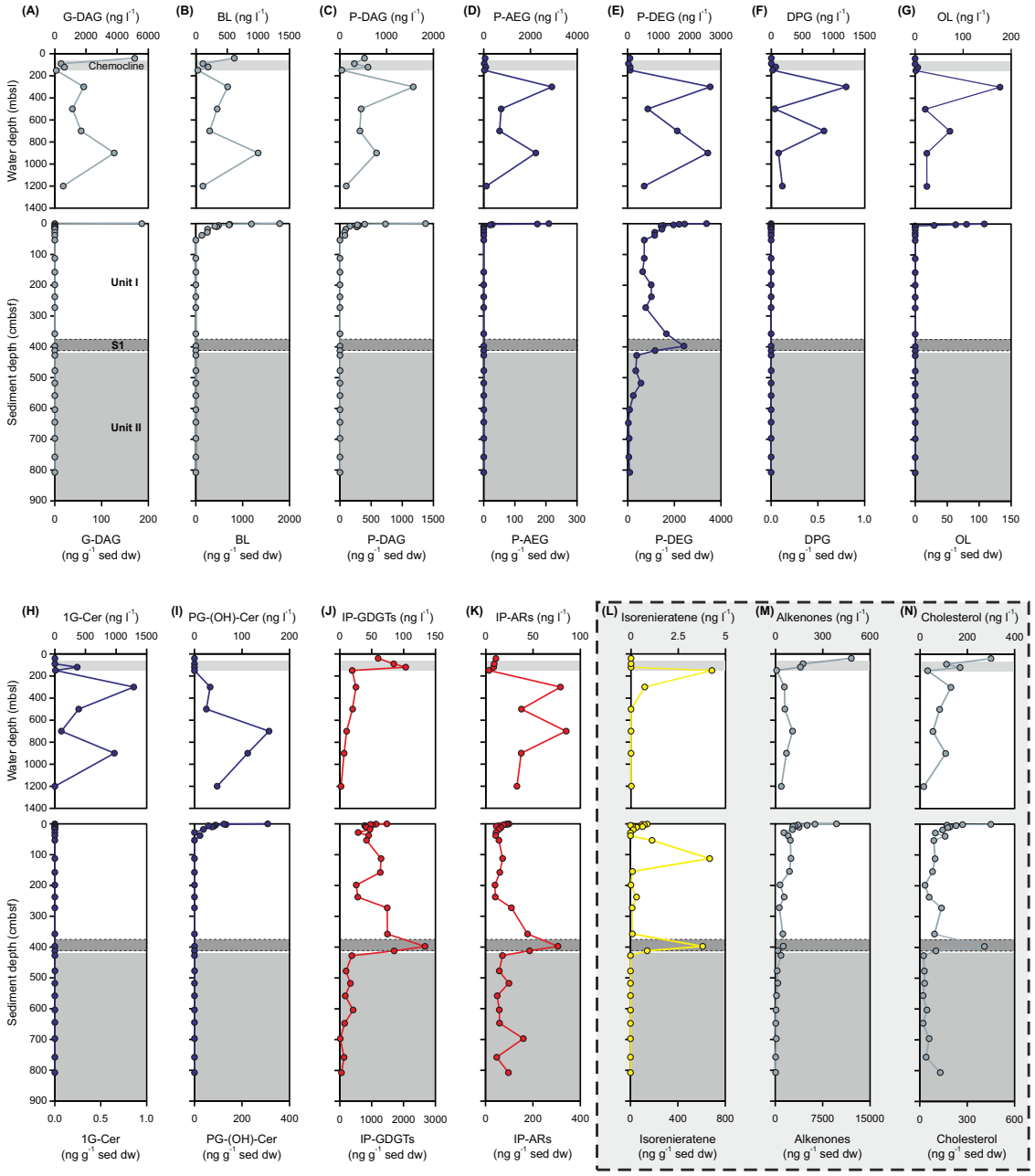

Figure VIII.14. Depth profiles of IPL groups, isorenieratene, alkenones and cholesterol detected in the water column and sediments of the Black Sea. Shaded areas in water column profiles correspond to the chemocline. Marine (Unit I, light grey) and lacustrine (Unit II, intermediate grey) lithological units as well as the sapropel (S1, dark grey) are denoted for sediment profiles. Color code: blue green, bacterial and/or eukaryotic lipids present in oxic waters; blue, bacterial and/or eukaryotic lipids only present in chemocline and anoxic waters; red, archaeal lipids. Abbreviations: G, glycosidic headgroup-bearing; P, phosphatidic headgroup-bearing; DPG, diphosphatidyl glycerol; BL, betaine lipids; OL, ornithine lipid; PG-(OH), hydroxy-phosphatidylglycerol; DAG, diacyl glycerol; AEG, acyl ether glycerol; DEG, diether glycerol; Cer, ceramide; IP, intact polar; GDGT, glycerol dibiphytanyl glycerol tetraether; AR, archaeol. IPL data except for water column samples from 150 m, 300 m, 500 m, and 900 m depth from Schröder (2015).

Within the chemocline and in the upper oxic water column, concentrations of IP-AR were low, whereas IP-AR concentrations were at least three times higher in the anoxic zone (Fig. VIII.14K). The depth profile of IP-GDGTs followed a similar trend as compared to $MK_{6:0}$ and $MK_{6:1}$ (Figs. VIII.1 and VIII.14), and IP-ARs largely followed the trend of MPs (Figs. VIII.11 and VIII.14). In the water column, the apolar lipid isorenieratene showed a distinct maximum at 150 mbsl and was absent in the rest of the water column except for minor abundances at 300 mbsl (Fig. VIII.14), and thus reflected the depth profile of $ChQ_{7:7}$ (Fig. VIII.8). The concentrations of cholesterol as well as summed $C_{37:2}$ and $C_{37:3}$ alkenones were highest in the oxic zone, decreased strongly with water depth within the chemocline and remained low throughout the anoxic water column.

In the sediment, the majority of IPL species were only detected in the surface (Fig. VIII.14). For example, the concentrations of BL, P-DAG, P-AEG, OL and PG-(OH)-Cer decreased exponentially with depth within the upper 50 cmbsf (Fig. VIII.14B-D, G, I). In contrast, the concentrations of P-DEG, IP-GDGTs and IP-ARs were relatively high within the sediment showing a slight decrease within the first 50 cmbsf, a pronounced peak within the sapropel layer (Fig. VIII.14E, J, and K), which was similar to most quinone profiles (cf. Fig. VIII.9) and invariably low concentrations in Unit II. Isorenieratene showed two concentration maxima, at 112.5 cmbsf and in the sapropel, but was otherwise low in concentration or absent (Fig. VIII.14L). In contrast to the water column, IP-AR and MP concentrations were decoupled in the sediments (cf. Figs. VIII.11 and VIII.14K). The concentrations of alkenones were highest at the sediment surface, decreased strongly within the upper 30 cmbsf and remained low throughout the rest of Unit I and Unit II. The concentration profile of cholesterol was similar but showed a peak in the sapropel layer.

VIII.4. Discussion

VIII.4.1. Structural elucidation of isomers

The almost identical MS^2 spectra of the various chromatographically resolved isomers of UQs and MKs suggest that they have highly similar structures, respectively, whose exact structural differences cannot be determined using the applied methods. However, isomers of MKs have already been reported. For example, two $MK_{9:8}$ peaks have been resolved by thin layer chromatography in the actinomycete *Mycobacterium phlei* and identified by NMR as *cis*- and *trans*-isomers, respectively (Dunphy et al., 1968). Similarly, *cis*- and *trans*-isomers of $MMK_{7:7}$ (methylated menaquinone) have been identified in the archaeon *Thermoplasma acidophilum* (Shimada et al., 2001). To the best of our knowledge, these are the only published descriptions of naturally occurring respiratory quinone isomers. For both $MK_{9:8}$ and $MMK_{7:7}$, the double bond of the isoprene unit that was

nearest to the menaquinone headgroup was suggested to be a *cis* configuration (Dunphy et al., 1968; Shimada et al., 2001). Based on comparison with the retention time of the commercially available $UQ_{10:10}$ (*trans*) standard, the early eluting UQ isomers (a-series) in our samples represent *trans*-isomers (cf. Fig. VIII.5). Thus, the late eluting isomers (b-series) potentially represent *cis*-isomers. The same might apply for the MK isomers, but here a maximum of four chromatographically separated isomers were detected. It seems unlikely that the four isomers represent compounds with *cis* configurations at different double bond positions or multiple *cis* configurations, since similar retention time patterns may be expected. Assuming the same retention time difference for *cis* and *trans*-isomers as for UQs, one early and one late eluting MK could represent a couple with *cis*- and *trans*-configuration, e.g., $MK_{8:8}$(a or b) and $MK_{8:8}$(c or d). Furthermore, the isomers may not represent variable double bond positions, since MK isomers were only detected for fully unsaturated (i.e., one saturation per isoprene unit) quinones. The structural differences of the MK and UQ isomers remain unconstrained and further investigation are needed in future studies to unambiguously identify their structure, for example by NMR.

VIII.4.2. Microbial stratification in the Black Sea water column and biomarker potential of respiratory quinones

Combined respiratory quinone and membrane lipid profiling resolved the stratification of microbial communities and metabolisms along the redox gradients of the southern Black Sea. Quinones, apolar lipids and intact polar lipids of similar biological origin were significantly correlated (Fig. VIII.15), which supports the utility of respiratory quinones as biomarkers for microbial community composition and associated respiratory processes.

The derived depth zonation and the potential sources of quinones and membrane lipids in the southern Black Sea are summarized in Table VIII.2. Microbial communities and metabolisms were separated into 1) the oxic (photic) zone supporting oxygenic photosynthesis, 2) the suboxic zone dominated by thaumarchaeal ammonia oxidation, 3) the anoxic photic zone inhabited by sulfur-oxidizing photosynthetic bacteria, and 4) (dark) anoxic zone which supports a diversity of bacterial and archaeal metabolisms such as methane oxidation, anammox and sulfate reduction.

The diversity of respiratory quinones in a sample (MD_q), as well as the BD_q, which reflects the mode of respiration that dominates in a sample, showed large variations between different geochemical zones (Fig. VIII.10), while samples from the same zone grouped in a close proximity in the MD_q versus BD_q coordinate system. The highest quinone diversities were observed in the anoxic water column as well as in the sediments. As most organisms contain only one to two abundant quinones (Collins and Jones,

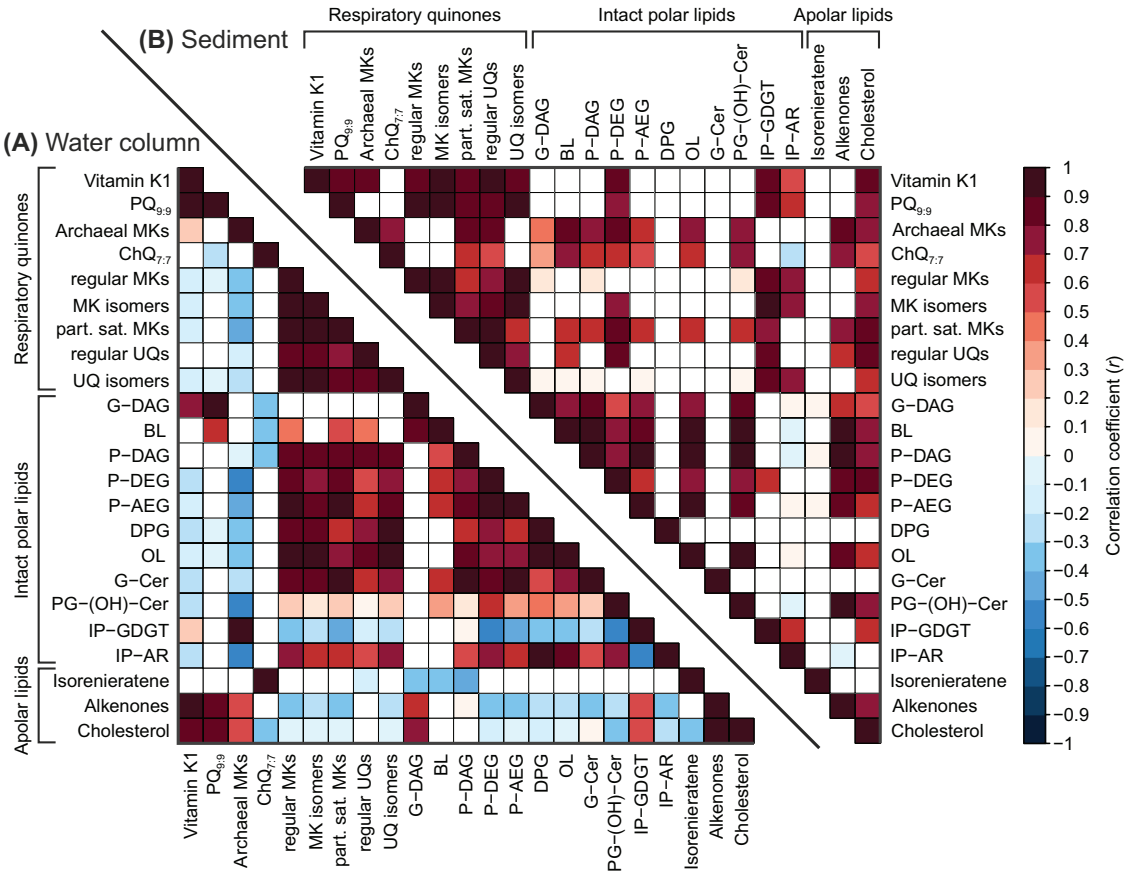

Figure VIII.15. Linear correlation coefficients (p <0.05) calculated from concentrations of respiratory quinones as well as apolar and intact polar lipids in the Black Sea water column (A) and sediments (B). Lipid nomenclature as described in Fig. VIII.14.

1981; Nowicka and Kruk, 2010), high quinone diversity translates to high microbial diversity in the anoxic zone. In contrast, low BD_q and MD_q values within the range for single organisms in the samples from the chemocline suggest that a single metabolism dominates respiratory activity in the suboxic zone. The oxic photic zone exhibited intermediate MD_q and BD_q values, which likely results from the predominance of oxygenic photosynthesis and a low diversity of aerobic respiration pathways. Highest bioenergetic divergence occurred within the photic anoxic zone, suggesting a high diversity of anaerobic metabolisms. The MD_q and BD_q values reported here are much higher as those previously reported for sewage sludge (Iwasaki and Hiraishi, 1998; Hiraishi, 1999) as well as shallow (Urakawa et al., 2001) and deep marine sediments (Cardace et al., 2006), and may be related to the larger diversity of quinones and isomers detectable by the improved analytical methods utilized in this study.

Table VIII.2. Geochemical zonation, source organisms of quinones and intact polar lipids as well as associated biogeochemical processes in the water column of the southern Black Sea. Quinone and lipid data compiled from Shively and Benson (1967), Goldfine and Hagen (1968), Hooper et al. (1972), Makula and Finnerty (1975), Makula (1978), Collins and Jones (1981), Knudsen et al. (1982), DiSpirito et al. (1983), Aleem and Sewell (1984), Collins and Green (1985), Sittig and Schlesner (1993), Harwood (1998), Brinkhoff et al. (1999), Hiraishi and Kato (1999), Rütters et al. (2001), Sturt et al. (2004), Koga and Morii (2005), Overmann (2006), Hölzl and Dörmann (2007), Sørensen et al. (2008), Schubotz et al. (2009), Nowicka and Kruk (2010), Pitcher et al. (2011a), Moore et al. (2013), Seidel et al. (2013), Ali et al. (2015), and Kulichevskaya et al. (2015); *not detected.

Zone	Quinone type	Lipid class	(Putative) source organism	Biogeochemical process
Oxic (0-90 m)	Vitamin K1, $PQ_{9:9}$, $UQ_{7:7}$, $UQ_{9:9}$, $UQ_{10:10}$	G-DAG, BL, P-DAG, Alkenones, Cholesterol	*Cyanobacteria*, eukaryotic algae	Oxygenic photosynthesis
	$UQ_{7:7}$, $UQ_{8:8}$, $UQ_{9:9}$, $UQ_{10:10}$	G-DAG, P-DAG, P-AEG, P-DEG	Diverse *Proteobacteria*	Bacterial autotrophy & heterotrophy
Suboxic (90-120 m)	$MK_{6:0}$, $MK_{6:1}$	IP-GDGTs, IP-ARs	*Thaumarchaeota*	Ammonia oxidation
	$UQ_{8:8}$, $UQ_{10:10}$	G-DAG, P-DAG, DPG	*α-Proteobacteria* (e.g. *Nitrobacter*, type II methanotrophs)	Nitrite, iron & aerobic methane oxidation
	$UQ_{8:8}$	P-DAG, DPG	*β-Proteobacteria* (e.g. *Nitrosomonas*, *Thiobacillus*)	Ammonia, iron & sulfur oxidation
	$UQ_{8:8}$, $UQ_{9:9}$	P-DAG, DPG	*γ-Proteobacteria* (e.g. (*Marinobacter*, *Thiomicrospira*, *Nitrosococcus*, *Nitrococcus*, type I methanotrophs)	Ammonia, sulfur, iron, nitrite & aerobic methane oxidation
Photic anoxic (120-150 m)	ChQ, $MK_{7:7}$	G-DAG, P-DAG, DPG, Isorenieratene	Green sulfur bacteria (*Chlorobiaceae*)	Anoxygenic photosynthesis
Dark anoxic (150-1200 m)	$MK_{6:6}$	P-DAG, P-AEG, P-DEG, OL	*δ-* (*Desulfomonas*, *Desulfovibrio*), *ϵ-Proteobacteria* (e.g., *Sulfurimonas*)	Sulfate reduction, Sulfur oxidation
	$MK_{7:7}$	P-DAG, P-AEG, P-DEG	*δ-Proteobacteria* (*Desulfobacter*, *Desulfococcus*, *Desulfosarcina*)	Sulfate reduction
	$MK_{6:6}$	P-DAG, OL, BL, (PC- & PE-ladderanes*)	*Planctomycetes*	Anaerobic ammonium oxidation
	$MK_{7:7}$, $MK_{8:8}$	IP-GDGTs, IP-ARs	Planktonic *Euryarchaeota* and *Crenarchaeota*	Unknown
	$MK_{8:8}$	P-DAG, P-AEG, P-DEG	*δ-Proteobacteria* (*Desulfuromonas*)	Sulfate reduction
	$MK_{7:7}$, $MK_{9:9}$	G-DAG, P-DAG, BL	*Firmicutes* (e.g., *Desulfotomaculum*)	E.g., sulfate reduction
	$MK_{8:8}$, $MK_{8:7}$, $MK_{8:6}$, $MK_{9:9}$, $MK_{9:8}$, $MK_{9:7}$, $MK_{10:9}$, $MK_{10:10}$, $MK_{11:11}$	G-DAG, P-DAG	*Actinobacteria*	E.g., nitrate reduction
	$MP_{5:4}$, $MP_{5:3}$	IP-ARs	*Methanosarcinales*, anaerobic methane oxidizing archaea (ANME)	*Methanogenesis*, anaerobic oxidation of methane
	Regular UQs	-	Unknown anaerobic source or fossil detritus	-
	UQ isomers	-	Unknown anaerobic source	-
	Vitamin K1, $PQ_{9:9}$	-	Unknown anaerobic source or fossil detritus	-

VIII.4.2.1. Oxic water column (0-90 mbsl): Oxygenic photosynthesis and bacterial aerobic respiration

The major quinone types in the oxic water column are associated with aerobic autotrophy and heterotrophy (UQs) as well as oxygenic photosynthesis (UQs, vitamin K1 and PQ9:9; Hiraishi, 1999). Sources for $UQ_{9:9}$, $UQ_{10:10}$, vitamin K1 and PQ9:9 are both cyanobacteria and eukaryotic algae (Table VIII.2; Amesz, 1973; Collins and Jones, 1981; Brettel and Leibl, 2001; Nowicka and Kruk, 2010), while UQs with side chain lengths of 7 to 10 are additionally produced by α-, β-, and γ-*Proteobacteria* (Table VIII.2; Hiraishi, 1999; Nowicka and Kruk, 2010). Only the *trans*-isomers (a-series) were detected in the oxic zone, indicating that aerobic organisms predominantly synthesize UQs with this specific stereochemical configuration.

The major IPLs in the oxic zone, G-DAGs, are widely distributed among cyanobacteria and phototrophic eukaryotes (Benning et al., 1995; Sanina et al., 2004; Hölzl and Dörmann, 2007) but are also produced by heterotrophic bacteria (Goldfine, 1984; Dowhan, 1997; Popendorf et al., 2011). The abundances of the apolar lipids cholesterol, produced by all eukaryotes, and alkenones, originating from eukaryotic algae, co-vary with the abundances of the algal respiratory quinones $PQ_{9:9}$ and vitamin K1 as well as G-DAG (Figs. VIII.8, VIII.14 and VIII.15). This indicates that algae are the major source of these lipids in the oxic zone of the Black Sea (Table VIII.2). In addition to G-DAGs, algae synthesize P-DAG lipids (Sanina et al., 2004; Suzumura, 2005), and, as a response to phosphorous limitation, also BLs (e.g., Van Mooy et al., 2009). However, BL and P-DAG abundances are not correlated to those of algal biomarkers (Figs. VIII.8, VIII.14 and VIII.15), indicating that they may originate primarily from bacterial sources as previously suggested for other oceanic provinces (cf. Benning et al., 1995; Lin et al., 2006; Schubotz et al., 2009; Van Mooy and Fredricks, 2010).

The detection of $MK_{6:0}$ and $MK_{6:1}$ further indicates thaumarchaeal respiratory activity at this depth (cf. Chapter VII), although the concentrations of these quinones and the contribution to the overall respiratory quinone pool were comparatively little (Fig. VIII.6). Similarly, low abundances of thaumarchaeal biomass in the oxic zone are implicated by minor abundances of intact polar GDGTs (Figs. VIII.8 and VIII.14), which are thought to be predominantly sourced by planktonic *Thaumarchaeota* (e.g. Pitcher et al., 2011a), but have recently been suggested to be also produced by Marine Group II *Euryarchaeota* (Lincoln et al., 2014a).

VIII.4.2.2. Suboxic zone (90 and 120 mbsl): Archaeal ammonia-oxidation, bacterial sulfur-, methane- and nitrite-oxidation

The quinone composition in the suboxic zone is substantially different from that observed in the oxic zone. The predominance of thaumarchaeal quinones (>70 % of total quinones, (Fig. VIII.8) and the decrease in dissolved ammonium concentration (Fig. VIII.3) indicate that archaeal ammonia-oxidation is the major respiratory process in these layers as suggested in an earlier study (cf. Chapter VII). Moreover, the depth profiles of both intact polar GDGTs and the thaumarchaeal quinones $MK_{6:0}$ and $MK_{6:1}$ showed a distinct concentration maximum in the suboxic zone (Figs. VIII.8 and VIII.14) in agreement with similar observations based on the abundances of thaumarchaeal 16S rRNA and *amoA* indicating maximum thaumarchaeotal abundance in the chemocline (ammonia-monooxygenase subunit A) gene biomarkers (Coolen et al., 2007; Lam et al., 2007). The absence of quinones involved in photosynthesis indicates that cyanobacteria and eukaryotic algae do not inhabit the suboxic zone or are metabolically not active.

The UQs detected in the suboxic zone likely originate from aerobic ammonia-, iron-, and sulfur-oxidizing α-, β- and γ-*Proteobacteria* as well as aerobic nitrite- and methane-oxidizing α- and γ-*Proteobacteria* (Table VIII.2; Collins and Green, 1985; Hiraishi, 1999). The occurrence of these biogeochemical processes in the Black Sea chemocline has also been attested by previous geochemical as well as gene and lipid biomarker surveys (e.g., Durisch-Kaiser et al., 2005; Konovalov et al., 2005; Schubert et al., 2006; Wakeham et al., 2007). *Proteobacteria* are probably the producers of the abundant P-DAGs as well as G-DAGs and DPGs (Barridge and Shively, 1968; Short et al., 1969; Makula, 1978; Goldfine, 1984; Fang et al., 2000) detected in the suboxic zone and thus represent a major part of the microbial biomass in this part of the Black Sea water column.

The concentrations of both IPLs and quinones are comparatively low in the samples from the chemocline (Figs. VIII.8 and VIII.14), suggesting low microbial biomass and respiratory activity. This is in contrast to other studies where high microbial activity was proposed to occur at the chemocline (e.g., Wakeham et al., 2007) but in line with decreased microbial cell densities compared to the oxic and anoxic zones as inferred from fluorescence *in situ* hybridization counts (e.g., Pimenov and Neretin, 2006). Since IPLs are tracers for microbial biomass while quinone concentrations are related to biomass and respiratory activity, our results suggest that microbial biomass in the chemocline is dominated by diverse bacteria, whereas respiratory activity is dominated by ammonia-oxidizing *Thaumarchaeota*.

VIII.4.2.3. Photic anoxic zone (120-150 mbsl): Bacterial anoxygenic photosynthesis

Penetration of H_2S-containing water into the photic zone (Fig. VIII.3) may result in bacterial anoxygenic photosynthesis. Indeed, $ChQ_{7:7}$ and the carotenoid isorenieratene (Repeta and Simpson, 1991), which are both diagnostic for anaerobic phototrophic green sulfur bacteria of the family *Chlorobiaceae* (Frydman and Rapoport, 1963; Overmann, 2006), showed distinct concentration maxima in anoxic, sulfidic waters at 150 mbsl (Figs. VIII.6 and VIII.8). This habitat depth is close to the maximum depth for phototrophic growth suggested for the Black Sea based on the optical transparency of seawater (Repeta, 1993). $MK_{7:7}$, which is a major quinone in the chlorosomes of *Chlorobiaceae* (Frydman and Rapoport, 1963; Frigaard et al., 1997), is the only MK that significantly increased in concentration at this depth (b-isomer, Fig. VIII.8), further suggesting a major contribution of these organisms to respiratory activity at the deep chemocline. The abundance of a single *Chlorobium* phylotype at the deep chemocline at depths of up to 145 mbsl has been reported to be a widespread feature of the Black Sea and attributed to extremely low-light adaptation of this particular phylotype (Overmann et al., 1992; Manske et al., 2005; Marschall et al., 2010). The major polar lipids of *Chlorobiaceae* are G-DAG, P-DAG and DPG (Overmann, 2006), which were also abundant at this depth (Figs. VIII.13 and VIII.14). The peak of $ChQ_{7:7}$ at the deep chemocline, the distinctive co-variation with isorenieratene as well as $MK_{7:7}$ and the abundance of characteristic IPLs support the use of $ChQ_{7:7}$ as a biomarker for anaerobic photosynthesis in the environment, which we demonstrate for the first time in the present paper.

VIII.4.2.4. Anoxic zone (150 – 1200 mbsl): Sulfate and nitrate reduction, anammox, and sulfur oxidation

The first appearance of polyunsaturated MKs in the anoxic zone (including the deep chemocline at 150 mbsl) reflects a shift of aerobic and micro-aerobic archaeal and bacterial respiration to mainly bacterial, MK-dependent, anaerobic respiration (Figs. VIII.6 and VIII.8). Likely sources of polyunsaturated MKs in the anoxic zone are diverse sulfate-reducing δ-*Proteobacteria*, such as *Desulfobacter*, *Desulfococcus*, and *Desulfosarcina* spp., which produce predominantly $MK_{7:7}$. Furthermore, *Desulfovibrio* and *Desulfuromonas* synthesize $MK_{6:6}$, and $MK_{8:8}$, respectively, as major quinones (Table VIII.2; Collins and Jones, 1981). Sulfur oxidizing ϵ-*Proteobacteria* of the genus *Sulfurimonas* might represent an additional source of $MK_{6:6}$ in the Black Sea (Fuchsman et al., 2011). Potential sources for $MK_{7:7}$ and $MK_{9:9}$ are sulfate-reducing *Firmicutes* related to the genus *Desulfotomaculum* (e.g., Collins and Jones, 1981). Several of these bacterial clades have been suggested to be responsible to a large extent of dark carbon fixation below the chemocline (Pimenov and Neretin, 2006). The occurrence of quinones of sulfate reducing bacteria in

the anoxic zone is also consistent with the IPL distribution, which is similar to that reported by Schubotz et al. (2009). Bacterial intact polar ether lipids (AEGs and DEGs) which are almost exclusively associated with anaerobic bacteria (e.g., Kim et al., 1970) and particularly sulfate reducers (Table VIII.2; Rütters et al., 2001; Sturt et al., 2004), were detected throughout the anoxic water column (Figs. VIII.13 and VIII.14). Since sulfate reducing and sulfur oxidizing *Proteobacteria* contain a mix of DAG, AEG and DEG core lipids, they are likely also a major source for P-DAGs (e.g., Rütters et al., 2001). Moreover, ornithine lipids were detected in minor abundances in the anoxic zone and might originate from sulfate reducing bacteria such as *Desulfovibrio* spp. (Makula and Finnerty, 1975; Schubotz et al., 2009; Seidel et al., 2013). The association of these IPLs with specific quinones is supported by the correlation of P-DAG and OL abundances with those of $MK_{6:6}$ (a+b), $MK_{8:8}$ (a+b) and $MK_{9:9}$ (b) (Figs. VIII.8, VIII.14 and VIII.15) and concentration maxima of these compounds in the upper anoxic zone (300 mbsl). An activity and abundance maximum of sulfate reducers and sulfur oxidizers in the upper anoxic zone is consistent with the observations that these bacteria first appear beneath the chemocline (Durisch-Kaiser et al., 2005; Lin et al., 2006; Wakeham et al., 2007; Fuchsman et al., 2011) and that sulfur oxidation and sulfate reduction rates are highest in the upper anoxic zone of the Black Sea (Jørgensen et al., 1991; Albert et al., 1995).

Other sources of $MK_{6:6}$ might be *Planctomycetes* (Ward et al., 2006; Kulichevskaya et al., 2007, 2008; Kulichevskaya et al., 2015). Bacteria affiliated with a deeply-branching monophyletic lineage of this phylum perform the reduction of NO_2^- to N_2 by NH_4^+, i.e., anaerobic ammonium oxidation (anammox). Based on the analysis of 16S ribosomal RNA gene markers and the anammox specific ladderane lipids, anammox bacteria have been shown to be mainly present within the suboxic zone (e.g., Kuypers et al., 2003; Wakeham et al., 2007). Moreover, Coolen et al. (2007) and Lam et al. (2007) proposed the co-occurrence and coupling of bacterial anammox and archaeal ammonia-oxidation within the chemocline of the central Black Sea. The quinone profiles at our study site in the southern Black Sea indicate a vertical separation of the depth habitats of ammonia-oxidizing *Thaumarchaeota* and anammox bacteria, with *Thaumarchaeota* being confined to the suboxic zone and anammox bacteria residing within the upper anoxic zone (cf. Table VIII.2), although geochemical coupling of these processes cannot be excluded. High sulfide concentrations appear to inhibit growth of anammox bacteria (Jensen et al., 2008) and thus anammox bacteria are likely restricted to the upper part of the anoxic zone. IPLs detected in the anoxic zone, such as P-DAG, OL and BL, might in part be sourced from anammox bacteria (Moore et al., 2013; Kulichevskaya et al., 2015), but their diagnostic intact polar ladderane lipids were not detected, probably because of their typically low abundance (Jaeschke et al., 2009).

Fully unsaturated and partially saturated MKs with chains lengths of 8 to 11 have been commonly associated with bacteria of the phylum *Actinobacteria* (Table VIII.2; Collins and Jones, 1981; Urakawa et al., 2005). In particular, *Actinobacteria* have been implicated in denitrification, i.e., the heterotrophic reduction of NO_3^- to N_2, within the anoxic zone of the Black Sea (Fuchsman et al., 2011). Quinones with 9 to 11 isoprenoid units are abundant in the anoxic zone of the Black Sea, especially in the deeper part (Fig. VIII.8), and thus indicate a significant contribution of *Actinobacteria* to the metabolic activity, possibly denitrification, in the deep anoxic Black Sea. Furthermore, *Actinobacteria* might be a source of the abundant P-DAGs and G-DAGs observed in the deeper part of the Black Sea water column (Fig. VIII.14).

Late eluting UQ isomers (b-series) occurred only in the anoxic water column and were absent from the oxic and suboxic zones, suggesting production of these compounds by unknown anaerobic bacteria (Fig. VIII.8). Alternatively, lateral intrusions of modified Bosporus water represent a significant mechanism providing dissolved oxygen to the suboxic and upper anoxic zones of the Black Sea (Lewis and Landing, 1991; Tebo, 1991) and might explain the occurrence of UQs in the anoxic water column. These lateral injections of oxygen-enriched waters have been further suggested to cause stabilization of the suboxic zone, balance its redox budget and enable extensive autocatalytic and microbial Mn(II) oxidation by dissolved oxygen in the western and southwestern Black Sea close to our study site (Tebo, 1991; Oguz et al., 2001; Konovalov et al., 2003; Schippers et al., 2005).

Alternatively, the detection of quinones typically associated with aerobic processes, $PQ_{9:9}$ and UQs, in the anoxic water column might be indicative of an allochthonous origin by vertical transport from the oxic zone or lateral transport from the upper continental slope. Sediment trap investigations demonstrated that terrestrial organic matter accumulated during periods of low organic carbon flux associated with high freshwater runoff particularly in the late winter and late spring, and/or by an influx of particles resuspended by storms from the basin margins (Honjo et al., 1987; Hay et al., 1990). Therefore, the high lipid and quinone concentrations in the anoxic zone compared to the oxic and suboxic zones (Figs. VIII.6 and VIII.8) might result from lateral transport of fossil biomass but may also be explained by high productivity *in situ* that is stimulated or sustained by lateral input of fresh organic matter and electron acceptors used by anaerobic microbes, e.g., sulfate reducing bacteria.

1G-Cer contributed up to $15\,\%$ of the total IPLs in the suboxic and anoxic zones (Fig. VIII.13). However, the sources of these lipids, which are typically associated with eukaryotes, below the oxic zone remain unconstrained. Schubotz et al. (2009) suggested an unknown anaerobic bacterial origin for these lipids based on a bacteria-like fatty acid composition of G-Cer in the anoxic zone contrary to a eukaryotic fatty acid compo-

sition observed in the photic zone. The fact that G-Cer abundances in our dataset are not correlated with eukaryotic biomarkers such as $PQ_{9:9}$, vitamin K1, alkenones and cholesterol but with UQs and MKs (Fig. VIII.15) strongly suggest a bacterial origin of these compounds below the oxic zone and thus support the hypothesis of Schubotz et al. (2009).

MPs are characteristic biomarkers for members of the archaeal order *Methanosarcinales* (cf. Chapter VII), which comprise the metabolically most versatile methanogens utilizing CO_2 + H_2, acetate, and methylated compounds as substrates (Kendall and Boone, 2006). Methanogens are likely outcompeted for acetate and H_2 by sulfate reducing bacteria in the anoxic zone of the Black Sea due to thermodynamic constraints (e.g., Abram and Nedwell, 1978; Oremland and Polcin, 1982; Lin et al., 2012). Thus, utilization of non-competitive methylated substrates (Oremland and Polcin, 1982; Oremland et al., 1982) is a likely methanogenic pathway of the *Methanosarcinales* in the Black Sea. Although water column methane concentrations were not measured at our study site, methane is present in significant amounts in the anoxic zone at other sites in the Black Sea (e.g., Reeburgh et al., 1991; Wakeham et al., 2007). It was suggested that most of the methane present in the Black Sea water column derives from the sediments (Reeburgh et al., 1991), but the presence of MP indicates that methylotrophic methanogenesis may also occur within the anoxic water column. However, anaerobic methane oxidizing ANME-2 archaea that are phylogenetically closely related to the *Methanosarcinales* have been detected in the anoxic water column of the Black Sea (Vetriani et al., 2003; Schubert et al., 2006; Wakeham et al., 2007). While the presence of MP in ANME-2 has not been constrained due to a lack of cultured representatives, these methanotrophic archaea might represent an additional source of MP. Intact polar ARs showed a similar profile as MPs and these compounds are thus likely sourced from the same euryarchaeotal sources, *Methanosarcinales* (Koga and Morii, 2005) and ANME (Rossel et al., 2008), but may also be produced by other uncultivated anaerobic planktonic euryarchaeotal groups present in the anoxic zone of the Black Sea (Vetriani et al., 2003).

Other quinones specific for archaea, i.e., fully saturated menaquinones or menaquinone derivatives (cf. Chapter VII), were not detected in the anoxic zone of the Black Sea. This indicates that either most anaerobic planktonic *Cren-* and *Euryarchaeota* do not produce quinones or that these archaea synthesize bacterial-like polyunsaturated quinones similar to those found in extremely halophilic archaea of the order *Halobacteriales* (Collins et al., 1981) and thermophilic archaea of the order *Thermoplasmatales* (cf. Chapter VII), the latter being phylogenetically related to uncultivated planktonic Marine Group II *Euryarchaeota* also found in the Black Sea (e.g., DeLong, 1998; Vetriani et al., 2003).

VIII.4.3. Respiratory quinones and IPLs in the Black Sea sediments

In contrast to the water column, where positive and negative correlations between the investigated quinones and lipids were observed, quinones and lipids in the sediments were exclusively positively correlated (Fig. VIII.15). Moreover, quinones as well as IPLs were correlated to the abundance of cholesterol (Fig. VIII.15), which might be used as a tracer of fossil biomass. This suggests that the lipid biomarker concentrations follow total organic carbon content and thus, that most compounds originate either from fossil detritus or that the microbial abundance and activity *in situ* is strongly dependent on organic matter availability.

Whereas archaeal IPLs only represent minor components in all water column samples, the bacterial to archaeal IPL ratio is much more balanced in the sediments (Fig. VIII.13). This signal is not reflected in the quinone composition, (Fig. VIII.6). Both saturated and polyunsaturated menaquinones, which are potentially produced by archaea (cf. Chapter VII) showed low relative abundances in the sediments, suggesting that the sedimentary archaea do not produce significant amounts of quinones.

In the upper 2-4 mbsf, the mineralization of the organic matter is mainly driven by sulfate reduction as sulfate constitutes the major electron acceptor in Black Sea sediments (Jørgensen et al., 2001). Due to the lack of electron acceptors, fermenters, methanogens and acetogens are likely the only microbes that are active in the sulfate-depleted (methanogenic) zone. Since, acetogenesis, especially with H_2 as the electron donor, is thermodynamically less favorable than methanogenesis (e.g., Lin et al., 2012), homoacetogens are typically outcompeted by methanogens in many habitats (Liu and Whitman, 2008). Since most fermenters have lost the ability to produce quinones (Collins and Jones, 1981; Nowicka and Kruk, 2010) and hydrogenotrophic methanogens do not contain quinones or functional quinone analogs (cf. Chapter VII; Thauer et al., 2008), the quinone abundance and diversity is expected to be low in the methanogenic zone.

VIII.4.3.1. Evidence for preservation of quinones in Unit I sediments

The range of quinone types detected in the sediment was similar to the anoxic water column, but the relative abundances of quinones were significantly different (Fig. VIII.6). $PQ_{9:9}$ was the most abundant quinone, similar to the oxic zone of the water column. Since $PQ_{9:9}$ is not known to be produced by non-photosynthetic and anaerobic microorganisms, the high relative abundance of this quinone indicates that a large fraction of the quinone pool may originate from allochthonous, photic zone-derived organic matter. Moreover, the depth profile of the eukaryotic apolar lipid cholesterol was similar to that of $PQ_{9:9}$ (Figs. VIII.9, VIII.14 and VIII.15) further supporting a fossil origin of $PQ_{9:9}$. The concentration of vitamin K1 was very low in the sediments although the depth

profile was similar to cholesterol and $PQ_{9:9}$ (Figs. VIII.6 and VIII.9), indicating different degradation kinetics of the two quinone types that might be related for example to the different headgroup types or the length of the isoprenoid chain. Similarly, Urakawa et al. (2000) and Urakawa et al. (2005) detected significant amounts of $PQ_{9:9}$ and vitamin K1 in shallow marine sediments and suggested that these quinones originate from phytoplankton detritus. The same likely applies for the *Chlorobiaceae*-specific $ChQ_{7:7}$ at our study site. $ChQ_{7:7}$ and isorenieratene do not follow the same trend in the sediments despite originating from the same biological source (Fig. VIII.9). This observation indicates rapid degradation of $ChQ_{7:7}$ as further exemplified by its strong decrease in abundance within the uppermost sediment (Fig. VIII.14), whereas isorenieratene is well preserved in the sedimentary record of the Black Sea (Fig. VIII.14; cf. Repeta, 1993). Maxima in sedimentary isorenieratene concentrations were interpreted to represent periods of a shallow chemocline position, whereas absence of isorenieratene was assumed to indicate chemocline depths below the euphotic zone (Repeta, 1993; Sinninghe Damsté et al., 1993). Thus, the two peaks observed at approximately 100 cmbsf and in the sapropel layer (ca. 400 cmbsf) at our study site reflect periods of a shallow chemocline with abundant green sulfur bacteria in the Black Sea water column (Fig. VIII.14).

The distribution of UQ and MK isomers differed significantly between the water column and the sediments (see Fig. VIII.7) and suggests either different communities inhabiting the two environments and/or adaptation different adaptation mechanisms, while significant transport of UQ and MK isomers from the water column to the sediments seems unlikely to explain the strongly diverging quinone composition on the sediment (Figs. VIII.7 and VIII.9). Modification of quinone stereochemistry may strongly affect the physicochemical properties of these compounds similar to the influence of fatty acid *cis*/*trans* isomerism on membrane fluidity in bacteria (Guckert et al., 1986; Heipieper et al., 1992; Loffeld and Keweloh, 1996), and may thus represent an adaptation mechanism characteristic for benthic bacteria. In contrast, the *cis*/*trans* ratio of fatty acids has also been used as an index for early diagenesis based on the assumption that *cis*-isomers are preferentially degraded and clay-catalyzed conversion of the *cis* isomers to the *trans* isomers occurs abiotically in the sediments (Van Vleet and Quinn, 1979). Analogously, quinone isomers may represent either life signals of the benthic microbial community or transformation products of allochthonous lipids.

VIII.4.3.2. Evidence for benthic bacterial activity

The co-occurrence of polyunsaturated MKs and P-DEG lipids that we observed throughout the sediment suggests the presence of indigenous sulfate reducing bacteria (Collins and Jones, 1981; Rütters et al., 2001; Sturt et al., 2004). Based on gene analysis, (Leloup

et al., 2007) showed that sulfate-reducing microorganisms including *Deltaproteobacteria*, *Desulfobacteraceae* and *Desulfovibrionales* were predominant in the sulfate reduction zone but also occurred in the methanogenic zone of the northwestern Black Sea. Albert et al. (1995) observed that modeled acetate, lactate, and formate turnover times in central Black Sea surface sediments were generally less than one day, suggesting that sulfate reduction may be limited by the supply of these substrates through fermentation. Moreover, some sulfate reducing bacteria, such as some *Desulfovibrio* and *Desulfobacter* species may also switch to fermentative metabolisms and perform for example disproportionation of thiosulfate (e.g., Krumholz et al., 1997; Rabus et al., 2006). Occurrence of this process in marine sediments has been confirmed by radiotracer experiments and recognized as an important component of the sulfur cycle (Jørgensen, 1990; Jørgensen et al., 1991). Thus, the sulfate reducers inhabiting deep, sulfate-depleted sediments in the Black Sea potentially switch to fermentation as an alternative form of energy conservation, which may explain the abundance of MKs and DEG IPLs in the sulfate-depleted sediments (cf. Fig. VIII.13). An additional explanation for the high abundances of MKs and DEG IPLs is the formation of endospores and/or persistence of dormant microbial populations under unfavorable, e.g., sulfate-limited conditions as previously suggested by (Leloup et al., 2007). These hypotheses are not necessarily exclusive. All bacterial IPLs except for P-DEGs abundant in the surficial sediments were not detected below 40 cmbsf, where sulfate became depleted (Fig. VIII.3). This switch to ether-based lipids would be consistent with the notion that ether-lipids are more stable and less permeable to ions as compared to ester-based analogs, resulting in reduced maintenance energy (Valentine, 2007).

VIII.4.3.3. Evidence for benthic archaeal activity

MPs were present within the top 400 cmbsf, which indicates the presence of *Methanosarcinales* and/or ANME-2 at these depths (Fig. VIII.9). Similar to the anoxic water column, these archaea either produce methane via methylotrophic methanogenesis (*Methanosarcinales*), due to competition for acetate and hydrogen with sulfate-reducers in the presence of abundant sulfate (Oremland and Polcin, 1982), or are associated with the anaerobic oxidation of methane (ANME-2, e.g., Hinrichs et al., 1999; Orphan et al., 2001). The oxidation of methane has been demonstrated to occur in Black Sea sediments (e.g., Reeburgh et al., 1991; Jørgensen et al., 2001) and sulfate and methane profiles revealed patterns typical for the anaerobic oxidation of methane at our study site (Fig. VIII.3; cf. Barker and Fritz, 1981; Whiticar, 1999; Yoshinaga et al., 2014). Thus, it is probable that the MPs observed in the sulfate reduction zone originate at least partly from ANME-2. Analysis of the stable carbon isotopic composition of MPs or the analysis of ANME-2

enrichment cultures for the occurrence of MPs will be helpful for testing their potential for MP synthesis.

Since methanogenesis has been shown to predominantly occur in the limnic sediments (Unit II) below the sulfate-reduction zone (Jørgensen et al., 2004), and MPs were not detected at these depths, *Methanosarcinales* are likely not abundant below the sulfate-reduction zone. Instead, CO_2-reduction by hydrogenotrophic methanogens, e.g., *Methanobacteriales* or *Methanococcales* which do not produce quinones, is more likely to occur in the deep sediments. The $\delta^{13}C_{CH_4}$ values of approximately $-75‰$ observed in the methanogenic zone are also consistent with the range of values characteristically associated with CH_4 produced via CO_2-reduction (Whiticar et al., 1986) assuming $\delta^{13}C_{CO_2}$ of ca. $-20‰$ for the Black Sea sediments (e.g., Knab et al., 2009). The strongly depleted $\delta^{13}C_{CH_4}$ values observed below the sulfate-methane transition zone (ca. 100-200 cmbsf; Fig. VIII.3) likely result from carbon isotope equilibration between methane and CO_2 during anaerobic oxidation of methane under low sulfate concentrations (<0.5 mM, cf. Yoshinaga et al., 2014).

In contrast to the water column, IP-ARs do not follow the same trend as MPs (Figs. VIII.11 and VIII.14, which implies additional benthic archaeal sources for IP-ARs. Sources of IP-ARs in the sulfate-depleted zone might be hydrogenotrophic methanogens such as *Methanobacteriales* and *Methanococcales* (Koga et al., 1993b; Koga and Morii, 2005) or benthic heterotrophic archaea as suggested by Biddle et al. (2006) for deeply buried sediments at the Peru margin.

The abundances of thaumarchaeal quinones ($MK_{6:0}$ and $MK_{6:1}$) and intact GDGTs appear to be decoupled in the sediments, whereas they showed a strong positive correlation in the water column (Fig. VIII.15). Thus, the two compound groups might also have different sources in the sediments as discussed for MPs and IP-ARs. Intact GDGTs have been detected in a variety of sedimentary systems as major IPLs (e.g., Lipp et al., 2008; Lipp and Hinrichs, 2009; Liu et al., 2011), which is consistent with our data (Fig. VIII.13).

Intact GDGTs, particularly 2G-GDGTs, have been associated with ANME-1 archaea at cold methane seeps (Rossel et al., 2008). Additionally, some methanogens, such as members of the order *Methanobacteriales*, are able to synthesize acyclic GDGTs (Koga and Morii, 2005). Similarly to IP-ARs, the isotopic signature of intact GDGTs from deeply buried sediments provided evidence for a heterotrophic benthic archaeal source (Biddle et al., 2006). Additionally, archaeal 16S rRNA surveys have revealed various lineages of uncultured archaea, such as the Miscellaneous Crenarchaeotal Group (MCG), that occur ubiquitously in subsurface habitats (e.g., Biddle et al., 2006; Sørensen and Teske, 2006). The lipid composition of these benthic archaeal lineages remains unconstrained due to a paucity of cultivated representatives. However, GDGT production by these lineages is plausible due to their close phylogenetic relatedness to cultivated, GDGT-producing ther-

mophiles (cf. Pearson and Ingalls, 2013; Schouten et al., 2013a). However, intact GDGTs in sediments might also partly be derived from benthic *Thaumarchaeota*. Although only aerobic growth has been reported for cultured *Thaumarchaeota* (e.g., Könneke et al., 2005; Stahl and de la Torre, 2012), several studies reported that thaumarchaeal phylotypes are present in anoxic subsurface sediments (Inagaki et al., 2006; Roussel et al., 2009; Jørgensen et al., 2012). Jørgensen et al. (2012) suggested that sediment-specific thaumarchaeal lineages might oxidize ammonia with alternative so far unknown electron acceptors or produce oxygen intracellularly, similar to the methane oxidizing bacterium *Candidatus* Methylomirabilis oxyfera (Ettwig et al., 2010). The decoupling of the abundances of thaumarchaeal MKs and IP-GDGTs and the contrasting correlations of IP-AR and IP-GDGT as well as polyunsaturated quinones in the sediment (Fig. VIII.15) suggests, however, that the benthic archaea synthesize either bacterial-like quinones or are devoid of quinones.

Production of CO_2 as well as ammonium and phosphate by a consortium of fermentative and methanogenic microbes typically occurs during the remineralization of sedimentary organic matter (e.g., Megonigal et al., 2003; Burdige, 2006; Burdige and Komada, 2013). We observed highest concentrations of PO_4^{3-} and NH_4^+ in the pore waters at ca. 400 cmbsf near the organic-rich sapropel layer, whereas concentrations above and below this depth showed a decreasing trend, indicating their production at the sapropel (Fig. VIII.3). This provides strong evidence for microbial activity within deep sediments of the Black Sea. Parkes et al. (2000) and Coolen et al. (2002) reported high bacterial cell numbers and enhanced hydrolytic enzyme activity in a Mediterranean sapropel suggestive of high microbial activity in these organic-rich layers. Coolen et al. (2002) further found particularly green non-sulfur bacteria (*Chloroflexus*-like organisms) to be active within the sapropels. *Chloroflexi* synthesize exclusively polyunsaturated MKs (Imhoff and Bias-Imhoff, 1995; Zhi et al., 2014), which may explain the high abundance of these quinones in the sapropel.

VIII.4.3.4. Microbial activity versus preservation of paleo-signals in Unit II sediments

Absolute concentrations of IPLs and quinones were low in Unit II, indicating much less biomass than in the overlying sediments. These sediments were deposited during the last glacial when the Black Sea was a freshwater lake (Ross et al., 1970; Degens and Ross, 1972). The total organic carbon content in these layers is comparably low (Jørgensen et al., 2004) due to well oxygenated conditions during the time of deposition (Ross et al., 1970; Degens and Ross, 1972), potentially explaining the absence of the photosynthetic quinones, especially $PQ_{9:9}$. Since the organic carbon in the deep limnic deposits mostly

consists of terrestrial recalcitrant material (Calvert et al., 1987), it is likely less available to microbes as a carbon and energy source, which might explain the low abundance of IPLs and quinones in Unit II sediments.

We further observed high relative abundances of $ChQ_{7:7}$ in Unit II sediments (Fig. VIII.6), which can hardly be explained by the benthic production of this quinone specific for photosynthetic green sulfur bacteria. It was suggested that the water column was fully oxygenated during the lacustrine phase (e.g., Deuser, 1972) and thus a fossil source from *Chlorobiaceae*, which is the only known source for $ChQ_{7:7}$, is unlikely. Additionally, isorenieratene was not detected in the samples from Unit II and the preservation potential of this compound seems to be much higher as observed for Unit II. The occurrence of $ChQ_{7:7}$ in Unit II sediments thus suggests that there is either a so far unconstrained benthic source or a specific preservation mechanism for this compound.

Apart from microbial life *in situ*, fossilization of IPLs might significantly contribute to the observed signal. Although it is generally assumed that IPLs are degraded quickly after cell death (White et al., 1979; Harvey et al., 1986), more recent studies revealed evidence that the turnover times of IPLs outside living cells are dependent on their structural properties (Logemann et al., 2011). Whereas intact lipids that contain ester-bound moieties are rapidly degraded by microbes independent of the polar head group, significant proportions of ether-lipids, such as archaeal and bacterial diether and archaeal tetraether lipids, may not be degraded during early diagenesis and may thus contribute to the recalcitrant organic matter in deeply buried sediments (Schouten et al., 2010; Logemann et al., 2011; Xie et al., 2013). The turnover times for respiratory quinones have not been studied yet, but incubation experiments by Hedrick and White (1986) indicate rapid changes of the quinone distribution within a few days when anoxic sediments were incubated under aerobic conditions and vice versa. However, particularly the high relatively high abundances of $PQ_{9:9}$ observed in Unit I sediments may attest a recalcitrant character at least to some quinone types. Thus, the quinone and IPL signals in Black Sea sediments likely reflect mixed allochthonous and autochthonous sources.

VIII.5. Conclusions

Our comprehensive analysis of respiratory quinone and membrane lipid distributions in the Black Sea water column demonstrates that this combined approach is capable of resolving the stratification of microbial abundances, community composition and metabolisms along the redox gradients of the southern Black Sea, which are summarized in Fig. VIII.16.

The oxic, photic zone of the Black Sea water column was dominated by high abundances of quinones (UQs, vitamin K1, $PQ_{9:9}$) and IPLs (G-DAG, BL, P-DAG) associated

with oxygenic photosynthesis and aerobic respiration. In contrast, low concentrations of IPLs and respiratory quinones indicated comparatively low biomass and metabolic activity in the suboxic zone at the upper chemocline. Here, high relative abundances of thaumarchaeal menaquinones ($MK_{6:0}$ and $MK_{6:1}$) and low relative abundances of thaumarchaeal IPLs (IP-GDGTs) indicated that respiratory activity but not biomass was dominated by thaumarchaeal ammonia-oxidizers. In contrast, low respiratory activity but high contributions to the total microbial biomass were likely associated with aerobic proteobacterial methane-, iron-, and nitrite-oxidizers (UQs, P-DAGs, G-DAGs).

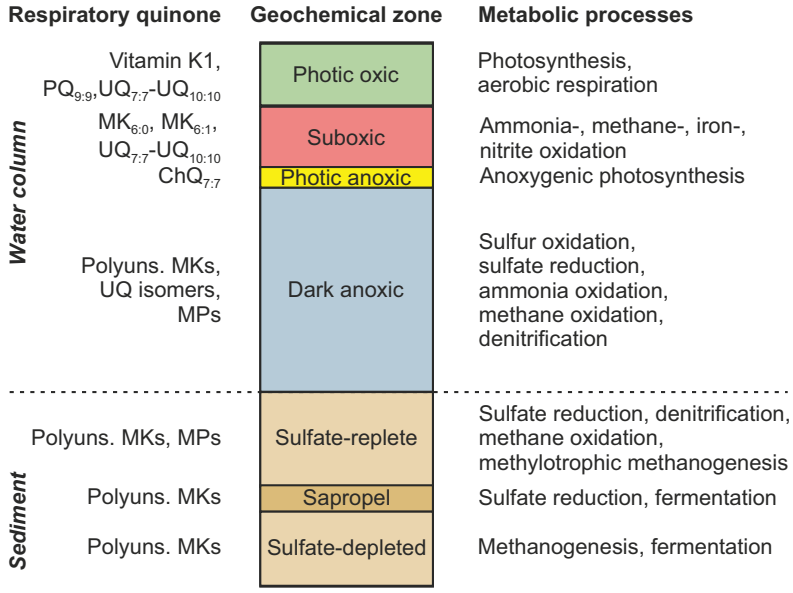

Figure VIII.16. Schematic representation of the distribution of respiratory quinones and associated metabolic processes.in the different geochemical zones of the Black Sea.

A pronounced maximum in $ChQ_{7:7}$ and the pigment isorenieratene indicated metabolically active, extremely low-light adapted *Chlorobiaceae* performing anoxygenic photosynthesis in the lower anoxic chemocline.

High abundances of MKs, distinct UQ isomers and bacterial ether (AEG, DEG) and ester (DAG) IPLs indicated high respiratory activity and biomass in the dark anoxic zone below the chemocline associated with a high diversity of bacterial metabolisms such as sulfate reduction, anammox and denitrification by β-, and ϵ-*Proteobacteria*, *Firmicutes*, *Planctomycetes*, and *Actinobacteria*. Presence of methanogens affiliated with the *Methanosarcinales* and/or methanotrophic archaea of the ANME-2 clade was indicated by characteristic MPs and high abundances of IP-ARs.

Sulfate reduction and sulfate-dependent anaerobic oxidation of methane were the major processes identified in the upper sediment and based on sulfate and methane concentration and $\delta^{13}C_{CH_4}$ profiles, high abundances of bacterial MKs as well as ester and ether lipids and archaeal MPs and IP-ARs. Alternatively, MPs and IP-ARs might

also be sourced by *Methanosarcinales* performing methylotrophic methanogenesis in the presence of sulfate. The sapropel layer located at 4 mbsf was associated with a peak of dissolved ammonium concentration as well as maximum abundances of bacterial and archaeal IPLs and quinones, suggesting intense microbial heterotrophic activity in this organic-matter rich layer. The detection of high abundances of biogenic methane in the deeper sediment and the disappearance of MPs near and below the sapropel indicated that methanogenesis in the deep sediment was not driven by *Methanosarcinales* but by hydrogenotrophic methanogens, e.g. *Methanobacteriales* and *Methanococcales*.

In conclusion, combined membrane lipid and respiratory quinone profiling provides a useful tool to trace abundances and metabolic processes of microbial communities involved in the cycling of carbon, nitrogen, and sulfur in the stratified Black Sea. Thus, it appears as a promising technique for enhancing the quantitative aspect of membrane lipid analyses with process-related information from respiratory quinones.

Acknowledgements

We are grateful to the crew, chief scientist M. Zabel, and the scientific shipboard party of R/V Meteor cruise M84/1 (DARCSEAS I). L. Wörmer, N.I. Goldenstein, C. Zhu, T. Meador, S. Pape, and T. Goldhammer are thanked for supporting sampling and instrumental analyses. We thank F. Schmidt for support with statistical analyses. We thank Dr. Ian Bull (University of Bristol) for providing alkenone standards. This study was funded by the European Research Council under the European Union's Seventh Framework Programme–'Ideas' Specific Programme, ERC grant agreement No. 247153 (Advanced Grant DARCLIFE; PI: K.-U.H.) and by the Deutsche Forschungsgemeinschaft through the Gottfried Wilhelm Leibniz Prize awarded to K.-U.H. (Hi 616-14-1) and instrument grant Inst 144/300-1 (HPLC-qToF system).

Chapter IX

Concluding Remarks

Summary and conclusions

This PhD thesis focused on lipids that form prokaryotic and eukaryotic cell membranes. Signatures of membrane lipids in environmental samples reflect the community composition and the physicochemical and physiological conditions under which microbial community members have existed in the natural habitat (cf. Brocks and Pearson, 2005; Brocks and Banfield, 2009). However, the use of lipids as strict life and chemotaxonomic markers is limited since most lipids found in the environment are common to several phylogenetically related organisms and lipid distribution patterns are a response to multiple environmental variables (cf. Hazel and Williams, 1990). Moreover, the full characterization of lipids in environmental samples and microbial cultures typically requires a combination of analytical approaches due to the structural complexity and the wide range of concentrations (e.g., Lipp and Hinrichs, 2009) resulting in complex workflows for lipid analysis. To fully characterize the environmental lipidome including trace amounts in complex organic sample matrices and to identify new biomarkers, reliable and sensitive methods are of crucial importance. The work presented in this thesis aimed at *(i)* improving the analytical methodology for lipid analysis, *(ii)* expanding the portfolio of lipid biomarkers for the characterization of microbial life in marine environments and *(iii)* investigating the proxy potential of novel lipids as chemotaxonomic makers and as indicator for redox conditions.

In the first research manuscript (**Chapter III**), we described new HPLC-MS-based protocols for the analysis of archaeal and bacterial glycerol ether core lipids due to limitations in sensitivity and inadequate separation of target compounds, such as core iGDGTs and iGDDs, when using the previous generation of methods. The presented

protocols take advantage of new chromatographic possibilities such as small particle sizes (<2 μm) and novel column packing materials. They offer superior chromatographic separation of archaeal and bacterial GDGT core lipids while maintaining an analytical window encompassing the whole spectrum of ether core lipids found in environmental samples. The protocols thus allow a more nuanced exploration of the distribution of these lipids in the environment. Examination of MS^2 data of the compounds eluting as chromatographic shoulders of iGDGTs and iGDDs showed the same fragmentation pattern for pairs comprising shoulder and major peak, suggesting a high degree of structural similarity. The substitution of cycloalkane moieties by double bonds in shoulder peaks was excluded on the basis of a hydrogenation experiment. Thus, the shoulder peaks of the GDGTs likely represent either regioisomers or structural isomers with different biphytane moieties, e.g., different ring positions; further verification is needed, however, to support this hypothesis.

In **Chapter IV**, we introduced an extension of the analytical protocols described in chapter III, which enables the simultaneous acquisition of three paleo SST proxies (TEX_{86}, $U_{37}^{K'}$ and LDI) and six additional proxies such as the archaeol/caldarchaeol ecometric and the methane index for the reconstruction of paleosalinity and past methane hydrate dissociation, respectively. This novel protocol eliminates laborious sample preparation steps and reduces analysis time while at the same time providing increased sensitivity of one order of magnitude compared to conventional GC-based methods. As a proof of concept, we have applied this method to sediments deposited since 21 kyrs BP in the Sea of Marmara. This interval covers large shifts in climate and environmental conditions, such as the Last Glacial Maximum (LGM), the Bølling/Allerød (B/A), the Younger Dryas, sapropel S1 formation and the late Holocene. Reconstructed temperatures differed considerably between the proxies, suggesting that parameters other than temperature additionally affect the distributions of the relevant lipids. For example, changes in the composition of alkenone-producing species at the transition from the LGM to the B/A were inferred from unreasonably high $U_{37}^{K'}$-derived SST values (ca. 20 °C) during the LGM. The species present in the Sea of Marmara before its connection to the Eastern Mediterranean thus likely had a different proxy-environment relationship than today's ubiquitously occurring haptophyte *Emiliania huxleyi*. In contrast, SST_{LDI} and $SST_{TEX_{86}}$ are low during the last glacial and, as expected, show warming at the transition to the B/A. Clearly, the ecological and hydrological changes in the Sea of Marmara had less influence on the relationship between temperature and the distributions of *i*GDGTs and long chain diols. The observations from this study confirmed that considering multiple proxies is crucial to verify the consistency of results between different methods. The novel analytical protocol greatly simplified the overall workflow for the analysis of

the existing organic SST proxies and might further expand their application for paleoenvironmental reconstructions.

The third study (**Chapter V**) showed the identification of fatty acid-substituted iGDGTs (FA-*i*GDGTs) and observed their widespread occurrence in environmental samples. We suggest that these compounds are of diagenetic origin formed by the esterification of free fatty acids and *i*GDGTs. Both compounds appear to be in chemical equilibrium and the concentration of FA-*i*GDGTs is suggested to be dependent on reactant availability, hydrolytic conditions and water activity. Their production might serve as an example for the early cross-linking reactions occurring during early diagenesis of these compounds, leading to their subsequent incorporation into geopolymers.

In **Chapter VI**, we examined the microbial membrane lipid distributions in the brine-seawater interface, the anoxic brine and sediments of the deep-sea hypersaline anoxic Discovery Basin. This system is considered to be uninhabitable for life due to the extremely high $MgCl_2$ concentration, restricting microbial activity to the interface. Based on the detection of taxonomically specific IPLs and core lipids, we confirmed that ammonia oxidizing, extremely halophilic, methanogenic archaea, as well as sulfate-reducing bacteria inhabit the interface, suggesting their influence on carbon, nitrogen and sulfur cycling. Several intact membrane lipids have been identified for the first time in environmental samples, e.g., GN-1G- and NAcG-AR, which were linked to archaeal methanogens belonging to *Methanohalophilus*. Other distinct lipids could be assigned to *Halobacteriales*-like archaea, such as Me-PGP-, SDG- and PG-Ext-Uns-AR as well as core Uns- and Ext-ARs. The presence of marine AOA was indicated by the detection of large quantities of HPH-GDGT, which is only known from *Thaumarchaeota*, whereas abundant phospholipids containing non-isoprenoid diether core lipid structures were linked to sulfate-reducing bacteria.

Although we considered that novel extremophilic microorganisms may be possible at in situ Mg^{2+} concentrations, a more plausible explanation is that microbial metabolism cannot proceed in the brine body and sediments and that the high Mg^{2+} concentrations resulted in excellent preservation of molecular biomarkers. Thus, the sedimentary IPL and core lipid record enabled the study of past microbial life from times before the formation of the basin to modern hypersaline conditions. The changing environmental conditions were consistently reflected in changes in the lipid biomarker distributions. The composition of head groups and unsaturated side chain structures in halophilic archaeal lipids differed distinctly between the brine-seawater interface and surface sediments, suggesting different archaeal communities and/or their adaptation to changing conditions at the interface since the brine formation. The detection of halophilic

archaea-specific IPLs only in the top 23 cm of the sediment confirmed a young age of the brine (<2000 yr). After basin formation but before intrusion of highly concentrated salt solution, methanogenesis and sulfate reduction were major microbial metabolic activities supporting the prevalence of anoxic conditions. The conditions before the basin formation were likely oligotrophic and a sharp lithological transition recorded the collapse of the basin at ca. 35000 yr BP. In these deposits we identified the intact forms of hybrid isoprenoid/branched tetraether lipids. These compounds combine attributes usually considered characteristic of either archaea (phytanyl moiety) or bacteria (methylated alkyl moiety). We hypothesize that the lipids originate from relict benthic communities and they might represent specific adaptations to for example high temperatures together with anoxia.

Chapters VII and VIII focused on the distribution of respiratory quinones in cultivated archaea and their potential as biomarkers for archaeal and bacterial community structure in a case study from the Black Sea. In **Chapter VII**, we investigated the respiratory quinone inventory of 25 cultivated archaeal strains covering the three phyla *Cren-*, *Eury-* and *Thaumarchaeota*. The quinone compositions allowed the differentiation of distinct archaeal clades. For instance, the single quinones in the thaumarchaeal *Nitrosopumilales* were saturated and monounsaturated menaquinones containing six isoprenoid units ($MK_{6:0}$ and $MK_{6:1}$). The thaumarchaeal quinones have been reported for the first time in this study and are promising biomarkers for tracing this globally abundant clade. Other distinct chemotaxonomic markers are thiophene-containing quinones for *Sulfolobales* and methanophenazines, functional quinone analogs, for *Methanosarcinales*. Thus, the structural variations of quinones and their distribution among archaea bear significant chemotaxonomic information that can be used to classify and quantify distinct archaeal orders in the environment. The considerably different quinone inventories of the investigated archaeal strains was attributed to different habitats, adaptive strategies and metabolism of their producers. Moreover, the heterogeneous taxonomic distribution of quinone types among the archaea provided insights into the evolutionary history of quinone biosynthetic pathways. Specifically, the distribution of menaquinones in archaea indicates an ancestral origin of menaquinone biosynthesis in *Crenarchaeota*. In contrast, quinone biosynthesis in *Euryarchaeota* is highly divergent and indicates lateral transfer of polyunsaturated menaquinone biosynthesis from bacteria to *Halobacteriales*. We additionally exemplarily demonstrated the biomarker potential of thaumarchaeal quinones on samples from a water column profile of the Black Sea, where $MK_{6:0}$ and $MK_{6:1}$ trace thaumarchaeal distribution and abundance.

The comprehensive study of the environmental distribution of microbial respiratory quinones and membrane lipids in marine suspended particulate matter and sediments

from the Black Sea (**Chapter VIII**) resolved the stratification of microbial abundance, community composition and diversity of metabolisms along the redox gradients. We used novel, highly sensitive analytical protocols permitting direct and simultaneous detection of quinones and membrane lipids. In total, we identified more than 30 different quinone structures including several novel UQ and MK isomers. The dominant quinones in the oxic zone were ubiquinones, which are associated with aerobic respiration, and phylloquinone (vitamin K1) and plastoquinone, which are both involved in electron transfer of photosystem I and II of cyanobacteria and phototrophic eukaryotes. The main intact polar lipids in the oxygenated surface waters were G-DAG, BL, and P-DAG and could be assigned to the same biological sources as the quinones. Most striking findings appeared in the chemocline. In the upper chemocline, thaumarchaeal MKs ($MK_{6:0}$ and $MK_{6:1}$), which are associated with the aerobic oxidation of ammonium (chapter VII), were the dominant quinones, while low relative abundances of thaumarchaeal IPLs (IP-GDGTs) were observed. This indicated that respiratory activity but not biomass was dominated by thaumarchaeal ammonia-oxidizers. In contrast, based on abundant P-DAGs and G-DAGs, the largest contribution to biomass in these layers was related to aerobic proteobacterial methane-, iron-, and nitrite-oxidizers. In the photic anoxic zone (deep chemocline), distinct peaks of $ChQ_{7:7}$ and isorenieratene indicated metabolically active, extremely-low light adapted *Chlorobiaceae*, which supported the use of $ChQ_{7:7}$ as a diagnostic biomarker for anaerobic photosynthesis in the environment and which we demonstrated for the first time in this study. The high abundance and diversity of quinones and IPLs in the dark, anoxic zone indicated high respiratory activity and large quantity of biomass of denitrifying, ammonium-oxidizing, sulfur-oxidizing and sulfate-reducing bacteria. Another process that could be identified in these depths was the anaerobic oxidation of methane indicated by detection of *Methanosarcinales*-specific MPs.

Based on geochemical profiles of methane and sulfate in combination with polyunsaturated MK, P-DEGs and AEGs as well as MPs and IP-ARs, sulfate reduction and methylotrophic methanogenesis or the anaerobic oxidation of methane were identified as major processes in the upper 4 m of the sediment. In the deeper sediments, in contrast, high concentrations of biogenic methane and the disappearance of MPs suggested that methanogenesis was not driven by *Methanosarcinales* but by other hydrogenotrophic methanogens, e.g., *Methanobacteriales* and *Methanococcales*. In this study, we further considered contributions from fossil planktonic sources to the sedimentary quinone pool, as indicated by the detection of the photosynthetic quinone $PQ_{9:9}$. However, especially in the sediments several so far undescribed UQ and MK isomers were detected and their distribution pattern strongly indicates subsurface production. Based on the distribution of thaumarchaeal quinones ($MK_{6:0}$ and $MK_{6:1}$) and IP-GDGTs in the sediments

and the absence of other typical archaeal quinones (cf. **Chapter VII**), it seems that benthic archaea synthesize either bacterial-like quinones or are devoid of quinones. The results from this last chapter suggest that quinone composition carries information on microbes involved in redox cycling of carbon, sulfur and nitrogen in the water column and potentially also in sediments, which further supports and establishes the use of respiratory quinones as biomarkers for microbial community composition and associated respiratory processes in environmental samples. Thus, respiratory quinone profiling provides additional process-related information to the more quantitative aspect of IPLs.

Results from this last chapter suggest that quinone composition carries information on microbes involved in redox cycling of carbon, sulfur and nitrogen in the water column and potentially also in sediments, which further supports and establishes the use of respiratory quinones as biomarkers for microbial community composition and associated respiratory processes in environmental samples. Thus, respiratory quinone profile provides additional process-related information to the more quantitative aspect of IPLs.

Outlook

The work presented in this thesis contributed to the development of novel analytical protocols for lipid analysis that have significantly expanded the analytical window for microbial lipidomics in complex environmental sample matrices and have paved the way for the discovery of a multitude of novel microbial biomarkers. Some of these lipids bear significant chemotaxonomic information and have a high biomarker potential for the classification and quantification of distinct microbial groups and their associated processes in the environment. However, these investigation raised new questions and several aspects remain unsolved for example regarding exact biological sources and structures of many novel lipids, which need to be addressed by future investigations. Perspectives that have emerged during the course of this PhD project are presented in the following paragraphs.

Further insights into the identities and the significance of GDGT isomers. The structure of previously co-eluting isomers of isoprenoid GDGTs could not be fully validated by MS^2 experiments. To fully characterize these compounds, their isolation via preparative LC and subsequent identification by NMR or detailed analysis of chemical degradation products would be thus required. Since the separation efficiency of preparative LC columns is generally worse compared to analytical columns, the latter would have to be used for isolation. The function of the shoulder compounds remains

also unknown. However, we proposed that different ring positions might result in chromatographic separation of the isomers and Chong et al. (2012) demonstrated that the cyclopentane ring position can have significant influence on membrane packing tightness, lipid conformation, membrane thickness and organization, and headgroup hydration/orientation. Moreover, Elling et al. (2014) observed changes in the distribution of these compounds with growth phase of *N. maritimus*, providing evidence that they are involved in membrane lipid adaption in response to metabolic status. Additionally, high abundances of early-eluting GDGT isomers occurred in some soils, where they are even more abundant than their "regular" counterparts (Pitcher et al., 2009a). This suggests that previously hidden clues regarding source organisms and/or community response to environmental forcing factors may be encoded in the distribution of the isomers but systematic studies on their distribution for example along pH and temperature gradients will be useful as well as further studies of archaeal pure cultures.

Extending the analytical window. The novel HPLC methods extend the analytical window to compounds that are typically analyzed by GC, such as alkenones. This leads to a highly simplified workflow for proxy applications where nine paleoenvironmental proxies can be analyzed simultaneously within one analysis. The analytical window can potentially be further extended to encompass other apolar lipids, such as core DEG, AEG and DAG lipids as well as steroids and hopanoids. Methods capable of measuring and identifying all lipids simultaneously in a single sample are of great advantage for the field of environmental lipidomics and would allow rapid screening of samples and deliver maximum information per unit time.

Constraining the uncertainties of organic SST proxies. Although the organic SST proxies are widely applied and often provide reasonable temperature estimates, concerns regarding where and when they record temperature remain. Multiproxy approaches help to verify the consistency of results between different methods and help to identify additional factors. However, more insights into the physiological responses of the organisms to a changing environment and their effect on the proxies, preferably based on pure culture experiments, are needed for constraining uncertainties. Although alkenone-producing haptophytes have been studied in detail (Epstein et al., 1998; Versteegh et al., 2001; Prahl et al., 2003; Ono et al., 2012, e.g.,), results for GDGT-producing cultures of Thaumarchaeota are still lacking except for an initial study by Elling et al. (2014) that investigated GDGT distributions in response to growth phase. The gained knowledge from more systematic culture-based studies could then be transferred to calibration models using modern analogue environments as suggested by Tierney and Tingley

(2014) to provide more reliable SST estimates in the geologic record.

Sources, identities and fate of novel intact tetraether lipids. In sediments from the Discovery Basin the intact forms of IB- and OB-GDGTs were identified for the first time using novel highly sensitive methods. IB- and OB-core lipids occur ubiquitously in the marine environment indicating important roles of the producers in the environment (Liu et al., 2012b). However, the structures have only been tentatively identified based on inspection of fragment mass spectra and further structural elucidation by NMR analysis of isolated and purified compounds is desirable to prove their exact structures. This will be particularly interesting for IB-GDGTs as they combine archaeal and bacterial traits (Schouten et al., 2000). Information on the stereochemistry of the glycerol could help to constrain a bacterial or archaeal source of these lipids (Sinninghe Damsté et al., 2000) although their distribution in the marine water column (Liu et al., 2014; Xie et al., 2014) as well as in our study from the Discovery Basin suggests a bacterial origin. Moreover, future work exploring the environmental distribution patterns of intact IB- and OB-GDGTs will help to determine their microbial sources and functional role in the source organism.

Systematic investigation of the distribution of quinones in the environment and further validation of their potential as life- and redox-markers. Studies on the environmental distribution of respiratory quinones are scarce and additional work on the behavior of quinones in the marine environment is required before these compounds can be widely applied as rigorous biomarkers. For example, little is known about the origin and fate of quinones in the marine water column. Besides the pioneering study presented in **Chapter VII** of this thesis, their biological sources, transport vectors, and chemical stability during sedimentation are not fully constrained. Moreover, knowledge about the effects of physiological and environmental parameters on quinone distributions is limited. Recently, (Sévin and Sauer, 2014) showed that ubiquinones act as a membrane-stabilizing agents that enhance resistance to osmotic stress. Since membrane stability is an intriguing feature of organisms under energy stress (Valentine, 2007), an important role of quinones in membrane lipid adaptation can be expected. Thus, investigation of the quinone composition of environmentally relevant cultured organisms grown under a range of conditions including nutrient and substrate starvation will be useful for the interpretation of quinone profiles. Moreover, further exploration of quinone distributions in a wide range of environments with contrasting microbial community compositions may help to connect specific metabolisms to lipids with so far unknown biological precursors, and hence to identify or constrain potential source organisms. In order to evaluate the validity of quinones as strict life-markers, degradation experiments

similar to those performed for IPLs (Logemann et al., 2011; Xie et al., 2013) are further required. The development of a method for stable isotope analysis of quinones, e.g., based on high-temperature GC, would enhance the information gained from their distribution as well as enabling the application of stable isotope probing experiments.

Chapter X

Contributions as Co-Author

X.1. Comprehensive glycerol ether lipid fingerprints through a novel reversed phase liquid chromatography–mass spectrometry protocol

Chun Zhu, Julius S. Lipp, Lars Wörmer, **Kevin W. Becker**, Jan Schröder and Kai-Uwe Hinrichs

Published in *Organic Geochemistry*
Vol. 65 (2013), pages 53-62. doi: 10.1016/j.orggeochem.2013.09.012

Organic Geochemistry Group, MARUM – Center for Marine Environmental Sciences & Department of Geosciences, University of Bremen, 28359 Bremen, Germany

* Corresponding author. E-mail: czhu@uni-bremen.de

Abstract
Glycerol ether lipid distributions have been developed as proxies for reconstructing past environmental change or, in their intact polar form, for fingerprinting the viable microbial community composition. However, due to their structural complexity, full characterization of glycerol ether lipids requires separate protocols for the analysis of the polar head groups and the alkyl chain moieties in core ether lipids. As a consequence, the valuable relationship between core ether lipid composition and specific polar head groups is often lost; this limits understanding of the diversity of ether lipids and their utility as biogeochemical proxies. Here, we report a novel reversed phase liquid chromatography–electrospray ionization-mass spectrometry (RP–ESI-MS) protocol that enables the simultaneous analysis of polar head groups (e.g. phosphocholine, phosphoglycerol, phosphoinositol, hexose and dihexose) and alkyl moieties (e.g. alkyl moieties modified with different numbers of cycloalkyl moieties, hydroxyl and alkyl groups and double bonds) in crude lipid extracts without further preparation. The protocol greatly enhances detection of archaeal intact polar lipids (IPLs) and core lipids (CLs) with double bond- and hydroxyl group-bearing alkyl moieties. With these improvements, widely used ratios that describe relative distributions of the core lipids, such as TEX_{86} and ring index, can now be directly determined in specific intact polar lipids (IPL-specific TEX_{86} and ring index). Since IPLs are the putative precursors of the environmentally persistent

core lipids, their detailed examination using this protocol can potentially provide new insights into diagenetic and biological mechanisms inherent to these proxies. In a series of 12 samples from diverse settings, core and IPL-specific TEX_{86} values followed the order: 2G-GDGTs > core GDGTs > 1G-GDGTs > 1G-GDGT-PI and the ring indices followed: 1G-GDGTs ≈ core GDGTs > 2G-GDGTs > 1G-GDGT-P1G > 2G-OH-GDGTs ≈ 1G-OH-GDGTs (1G, monoglycosyl; 2G, diglycosyl; P1G, phosphomonoglycosyl; GDGT, glycerol dialkyl glycerol tetraether).

X.2. Effects of growth phase on the membrane lipid composition of the thaumarchaeon *Nitrosopumilus maritimus*

Felix J. Elling[a], Martin Könneke[a,*], Julius S. Lipp[a], **Kevin W. Becker**[a], Emma J. Gagen[b,+] and Kai-Uwe Hinrichs[a]

Published in *Geochimica et Cosmochimica Acta*
Vol. 141 (2014), pages 579-597. doi: 10.1016/j.gca.2014.07.005

[a]Organic Geochemistry Group, MARUM - Center for Marine Environmental Sciences & Department of Geosciences, University of Bremen, 28359 Bremen, Germany
[b]Lehrstuhl für Mikrobiologie und Archaeenzentrum, Universität Regensburg, 93053 Regensburg, Germany

[+]Present address: E.J. Gagen, School of Earth Sciences, The University of Queensland, St. Lucia, Australia

[*]Corresponding author. E-mail: mkoenneke@marum.de

Abstract
The characteristic glycerol dibiphytanyl glycerol tetraether membrane lipids (GDGTs) of marine ammonia-oxidizing archaea (AOA) are widely used as biomarkers for studying their occurrence and distribution in marine environments and for reconstructing past sea surface temperatures using the TEX_{86} index. Despite an increasing use of GDGT biomarkers in microbial ecology and paleoceanography, the physiological and environmental factors influencing lipid composition in AOA, in particular the cyclization of GDGTs, remain unconstrained. We investigated the effect of metabolic state on the composition of intact polar and core lipids and the resulting TEX_{86} paleothermometer in pure cultures of the marine AOA *Nitrosopumilus maritimus* as a function of growth phase. The cellular lipid content ranged from 0.9 to 1.9 fg $cell^{-1}$ and increased during growth but was lower in the stationary phases, indicating changes in average cell size in response to metabolic status. The relative abundances of monoglycosidic GDGTs increased from 27% in early growth phase to 60% in late stationary phase, while monohydroxylated GDGTs increased only slightly. The proportions of characteristic hexose-phosphohexose GDGTs were up to 7-fold higher during growth than in stationary phase, suggesting

that they are valuable biomarkers for the metabolically active fraction of AOA assemblages in the environment. Methoxy archaeol was identified as a novel, genuine archaeal lipid of yet unknown function; it is one of the most abundant single compounds in the lipidome of *N. maritimus*. TEX_{86} values of individual intact GDGTs and total GDGTs differed substantially, were generally lower during early and late growth phases than in stationary phase, and did not reflect growth temperature. Consequently, our results strongly suggest that biosynthesis is at least partially responsible for the systematic offsets in TEX_{86} values between different intact polar GDGT classes observed previously in environmental samples. Nevertheless, differences in degradation rates of intact polar GDGTs may influence the TEX_{86} index because the intact polar lipid precursors differ for individual core GDGTs and moreover their relative abundances change with growth stage, which may result in distinct release rates of core GDGTs from their polar precursors. Overall, our findings stress the need to accurately describe the factors influencing GDGT cyclization in thaumarchaea and thus paleotemperature reconstructions.

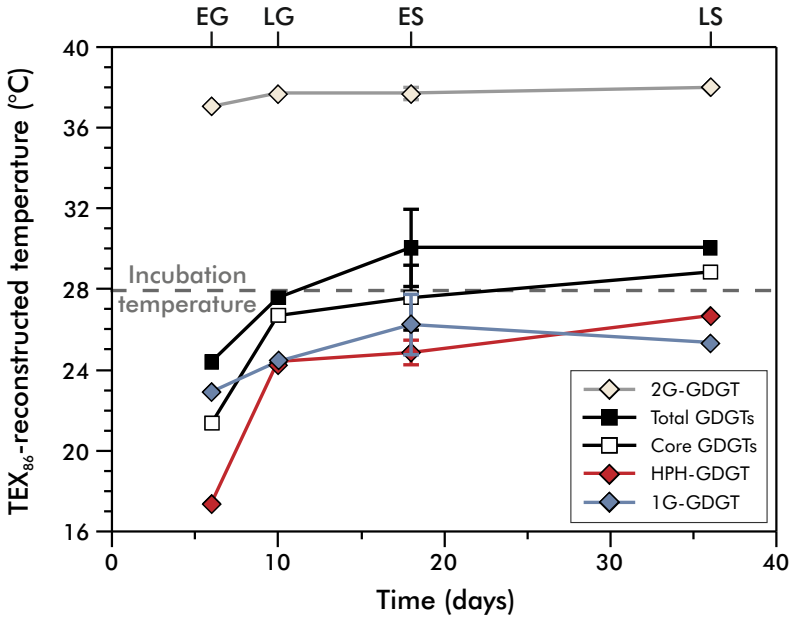

Figure X.1. Reconstructed TEX_{86} temperatures for individual IPLs (diamonds) and core GDGTs in the TLE and total GDGTs derived by hydrolysis (squares) showing temperature increase during batch growth compared to the actual incubation temperature (28 °C, dashed line). Error bars represent the deviation of the mean for triplicate cultures harvested in early stationary phase. EG: Early growth phase; LG: Late growth phase; ES: Early stationary phase; LS: Late stationary phase.

X.3. Comparative analysis of the thaumarchaeal lipidome

Felix J. Elling[a], Martin Könneke[a,*], **Kevin W. Becker**[a], Michaela Stieglmeier[b], Graeme W. Nicol[c], Eva Spieck[d], José R. de la Torre[e], Gerhard Herndl[f,g], Christa Schleper[b] and Kai-Uwe Hinrichs[a]

In preparation for *Applied and Environmental Microbiology*

[a]Organic Geochemistry Group, MARUM - Center for Marine Environmental Sciences & Department of Geosciences, University of Bremen, 28359 Bremen, Germany
[b]Department of Microbial Ecology, University of Vienna, 1090 Vienna, Austria
[c]Institute of Biological and Environmental Sciences, University of Aberdeen, Aberdeen AB24 3UU, United Kingdom
[d]Biozentrum Klein Flottbek, Abteilung für Mikrobiologie und Biotechnologie, Universität Hamburg, 22609 Hamburg, Germany.
[e]Department of Biology, San Francisco State University, San Francisco, CA, USA
[f]Department of Limnology and Oceanography, University of Vienna, 1090 Vienna, Austria
[g]Department of Biological Oceanography, Royal Netherlands Institute for Sea Research, 1790 AB Den Burg, Netherlands

*Corresponding author. E-mail: mkoenneke@marum.de

Abstract
Archaea of the phylum *Thaumarchaeota* are globally distributed and abundant microorganisms mediating the oxidation of ammonia to nitrite in the ocean, soil, as well as in geothermal systems and represent a major source of archaeal lipids in these environments. However, interpretation of environmental lipid profiles is mainly hindered by the lack of comparative and quantitative studies on the membrane lipid composition of cultivated representatives of this phylum. Here, we describe the core and intact polar lipid (IPL) composition of 11 thaumarchaeal pure and enrichment cultures representing all four characterized thaumarchaeal clades. In general, all thaumarchaeal strains synthesize similar lipid types conFsisting of consisting mainly of glycerol dibiphytanyl glycerol tetraethers with monoglycosidic, diglycosidic, phosphoxehose and hexose-phosphoxose headgroups. However, the relative abundances of these lipids as well as their core lipid composition differ significantly among the thaumarchaeal phylo-

genetic subgroups. While the core lipid composition of cultivated *Thaumarchaeota*, such as the content of the characteristic biomarker crenarchaeol, appears to be determined by their phylogenetic affiliation, the IPL composition reflects their habitat or growth conditions. Based on comparison of the thaumarchaeal lipidome with analyses of 21 eury- and crenarchaeal strains and environmental samples from the equatorial North Pacific Ocean, we further demonstrate that the apolar lipid methoxy archaeol is synthesized exclusively by *Thaumarchaeota* and thus represents a diagnostic chemotaxonomic biomarker for this archaeal phylum. The description of the thaumarchaeal lipidome comprised of 100 structurally different lipid types supports the interpretation of archaeal lipid signatures in environmental samples and provides useful characteristics to identify distinct thaumarchaeal clades.

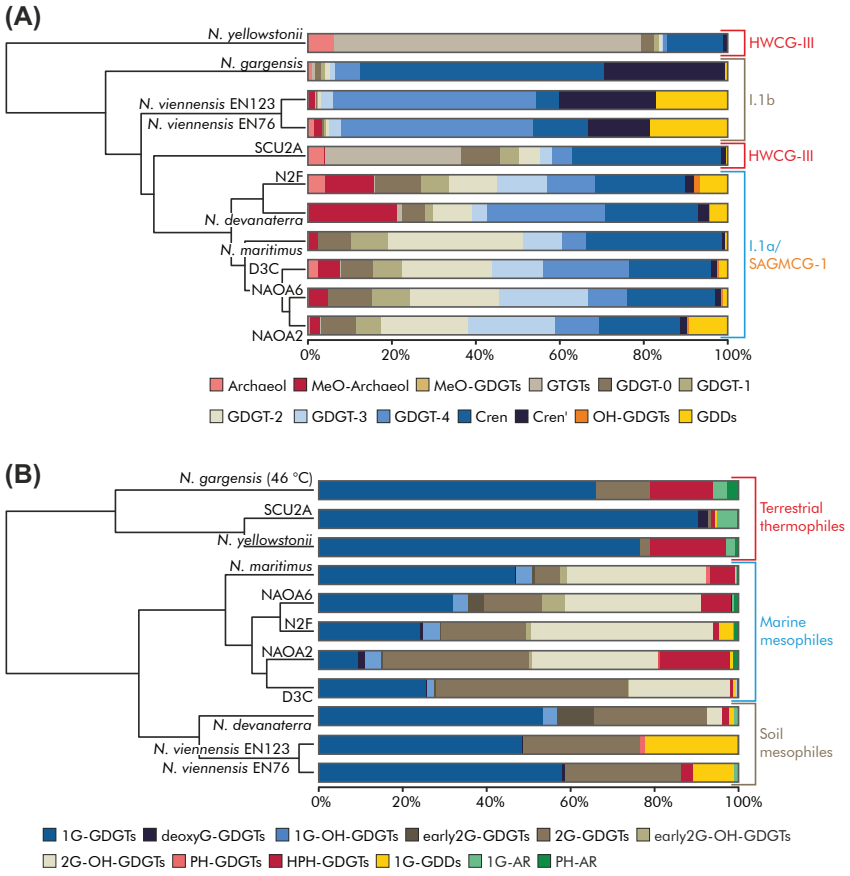

Figure X.2. (A) Cluster analysis of the relative abundances of major core lipid types in eleven thaumarchaeal strains from the four phylogenetic groups I.1a, I.1b, SAGMCG-1 and HWCG-III (calculated using the Euclidean distance metric from full lipid diversity including individual cyclized GTGTs, MeO-GDGTs and GDDs). Cren: crenarchaeol. Cren': crenarchaeol regioisomer. (B) Cluster analysis of the relative abundances of intact polar lipid types in eleven thaumarchaeal strains (calculated using the Euclidean distance metric from full lipid diversity including individual cyclized intact polar GDGTs). Cultures from similar habitats show close relatedness in their intact polar lipid compositions.

References

Abeliovich, A. (2006). The Nitrite Oxidizing Bacteria. English. In: *The Prokaryotes*. Ed. by M. Dworkin, S. Falkow, E. Rosenberg, K.-H. Schleifer, and E. Stackebrandt. Springer New York, pp. 861–872. DOI: 10.1007/0-387-30745-1_41.

Abken, H. J., M. Tietze, J. Brodersen, S. Bäumer, U. Beifuss, and U. Deppenmeier (1998). Isolation and characterization of methanophenazine and function of phenazines in membrane-bound electron transport of *Methanosarcina mazei* Gö1. *Journal of Bacteriology* **180** (8), 2027–2032.

Abram, J. W. and D. B. Nedwell (1978). Inhibition of methanogenesis by sulphate reducing bacteria competing for transferred hydrogen. *Archives of Microbiology* **117** (1), 89–92. DOI: 10.1007/BF00689356.

Aksu, a. E., T. Abrajano, P. J. Mudie, and D. Yasar (1999). Organic geochemical and palynological evidence for terrigenous origin of the organic matter in Aegean Sea sapropel S1. *Marine Geology* **153** (1-4), 303–318.

Aksu, A. E., R. N. Hiscott, M. a. Kaminski, P. J. Mudie, H. Gillespie, T. Abrajano, and D. Yasar (2002). Last glacial Holocene paleoceanography of the Black Sea and Marmara Sea: stable isotopic, foraminiferal and coccolith revidence. *Marine Geology* **190**, 119–149.

Albert, D. B., C. Taylor, and C. S. Martens (1995). Sulfate reduction rates and low molecular weight fatty acid concentations in the water column and surficial sediments of the Black Sea. *Deep-Sea Research I* **42** (7), 1239–1260. DOI: 10.1016/0967-0637(95)00042-5.

Aleem, M. I. H. and D. L. Sewell (1984). Oxidoreductase systems in *Nitrobacter agilis*. In: *Microbial Chemoautotrophy*. Ed. by W. R. Strohl and O. H. Tuovinen. Columbus, OH: Ohio State University Press, pp. 185–210.

Alexander, E., A. Stock, H.-W. Breiner, A. Behnke, J. Bunge, M. M. Yakimov, and T. Stoeck (2009). Microbial eukaryotes in the hypersaline anoxic L'Atalante deep-sea basin. *Environmental Microbiology* **11** (2), 360–381. DOI: 10.1111/j.1462-2920.2008.01777.x.

Ali, M., M. Oshiki, T. Awata, K. Isobe, Z. Kimura, H. Yoshikawa, D. Hira, T. Kindaichi, H. Satoh, T. Fujii, and S. Okabe (2015). Physiological characterization of anaerobic ammonium oxidizing bacterium '*Candidatus* Jettenia caeni'. *Environmental Microbiology*. DOI: 10.1111/1462-2920.12674.

Allen, M. B. (1959). Studies with Cyanidium caldarium, an anomalously pigmented chlorophyte. *Archiv für Mikrobiologie* **32** (3), 270–277. DOI: 10.1007/BF00409348.

Amesz, J. (1973). The function of plastoquinone in photosynthetic electron transport. *Biochimica et Biophysica Acta* **301**, 35–51.

Anraku, Y. (1988). Bacterial electron transport chains. *Annual Review of Biochemistry* **57** (1), 101–132. DOI: 10.1146/annurev.biochem.57.1.101.

Arístegui, J., C. M. Duarte, J. M. Gasol, and L. Alonso-Sáez (2005). Active mesopelagic prokaryotes support high respiration in the subtropical northeast Atlantic Ocean. *Geophysical Research Letters* **32** (3), 1–4. DOI: 10.1029/2004GL021863.

Arístegui, J., J. M. Gasol, C. M. Duarte, and G. J. Herndl (2009). Microbial oceanography of the dark oceanÂ's pelagic realm. *Limnology and Oceanography* **54** (5), 1501–1529. DOI: 10.4319/lo.2009.54.5.1501.

Arpino, P. and G. Ourisson (1971). Interactions between rock and organic matter. Esterification and transesterification induced in sediments by methanol and ethanol. *Analytical Chemistry* **43** (12), 1656–1657. DOI: 10.1021/ac60306a006.

Arrigo, K. R. (2005). Marine microorganisms and global nutrient cycles. *Nature* **437** (7057), 349–355. DOI: 10.1038/nature04159.

Arthur, M. A. and W. E. Dean (1998). Organic-matter production and preservation and evolution of anoxia in the Holocene Black Sea. *Paleoceanography* **13** (4), 395–411. DOI: 10.1029/98PA01161.

Azam, F. (1998). Microbial control of oceanic carbon flux: the plot thickens. *Science*, 694–696.

Baba, T., H. Minamikawa, M. Hato, and T. Handa (2001). Hydration and molecular motions in synthetic phytanyl-chained glycolipid vesicle membranes. *Biophysical journal* **81** (6), 3377–3386. DOI: 10.1016/S0006-3495(01)75970-X.

Bach, W., K. J. Edwards, J. M. Hayes, S. Sievert, J. a. Huber, and M. L. Sogin (2006). Energy in the dark: Fuel for life in the deep ocean and beyond. *Eos, Transactions American Geophysical Union* **87** (7), 73.

Backer, H. and M. Schoell (1972). New Deeps with Brines and Metalliferous Sediments in the Red Sea. *Nature Physical Science* **240**, 153–158. DOI: 10.1038/physci240153a0.

Bahr, A., F. Lamy, H. Arz, H. Kuhlmann, and G. Wefer (2005). Late glacial to Holocene climate and sedimentation history in the NW Black Sea. *Marine Geology* **214**, 309–322. DOI: 10.1016/j.margeo.2004.11.013.

Barker, J. F. and P. Fritz (1981). Carbon isotope fractionation during microbial methane oxidation. *Nature* **293** (5830), 289–291. DOI: 10.1038/293289a0.

Barridge, J. K. and J. M. Shively (1968). Phospholipids of the Thiobacilli. *Journal of Bacteriology* **95** (6), 2182–2185.

Basse, A., C. Zhu, G. J. Versteegh, G. Fischer, K.-U. Hinrichs, and G. Mollenhauer (2014). Distribution of intact and core tetraether lipids in water column profiles of suspended particulate matter off Cape Blanc, NW Africa. *Organic Geochemistry* **72**, 1–13. DOI: 10.1016/j.orggeochem.2014.04.007.

Bauersachs, T., E. N. Speelman, E. C. Hopmans, G.-J. Reichart, S. Schouten, and J. S. S. Damsté (2010). Fossilized glycolipids reveal past oceanic N_2 fixation by heterocystous cyanobacteria. *Proceedings of the National Academy of Sciences of the United States of America* **107** (45), 19190–19194. DOI: 10.1073/pnas.1007526107.

Bauersachs, T., K. Weidenbach, R. A. Schmitz, and L. Schwark (2015). Distribution of glycerol ether lipids in halophilic, methanogenic and hyperthermophilic archaea. *Organic Geochemistry* **83-84**, 101–108. DOI: http://dx.doi.org/10.1016/j.orggeochem.2015.03.009.

Becker, K. W., J. S. Lipp, C. Zhu, X.-L. Liu, and K.-U. Hinrichs (2013). An improved method for the analysis of archaeal and bacterial ether core lipids. *Organic Geochemistry* **61**, 34–44. DOI: 10.1016/j.orggeochem.2013.05.007.

Bekker, M., G. Kramer, A. F. Hartog, M. J. Wagner, C. G. de Koster, K. J. Hellingwerf, and M. J. T. de Mattos (2007). Changes in the redox state and composition of the quinone pool of *Escherichia coli* during aerobic batch-culture growth. *Microbiology* **153**, 1974–1980. DOI: 10.1099/mic.0.2007/006098-0.

Belderson, R. H., N. H. Kenyon, and A. H. Stride (1978). Local submarine salt-karst formation on the Hellenic Outer Ridge , eastern Mediterranean. *Geology* **6**, 716–720. DOI: 10.1130/0091-7613(1978)6<716.

Beney, L. and P. Gervais (2001). Influence of the fluidity of the membrane on the response of microorganisms to environmental stresses. English. *Applied Microbiology and Biotechnology* **57** (1-2), 34–42. DOI: 10.1007/s002530100754.

Benning, C., Z. H. Huang, and D. A. Gage (1995). Accumulation of a novel glycolipid and a betaine lipid in cells of *Rhodobacter sphaeroides* grown under phosphate limitation. *Archives of Biochemistry and Biophysics* **317** (1), 103–111. DOI: 10.1006/abbi.1995.1141.

Bentley, R. and R. Meganathan (1982). Biosynthesis of vitamin K (menaquinone) in Bacteria. *Microbiological Reviews* **46** (3), 241–280.

Biddle, J. F., J. S. Lipp, M. A. Lever, K. G. Lloyd, K. B. Sørensen, R. Anderson, H. F. Fredricks, M. Elvert, T. J. Kelly, D. P. Schrag, M. L. Sogin, J. E. Brenchley, A. Teske, C. H. House, and K.-U. Hinrichs (2006). Heterotrophic Archaea dominate sedimentary subsurface ecosystems off Peru. *Proceedings of the National Academy of Sciences of the United States of America* **103** (10), 3846–3851. DOI: 10.1073/pnas.0600035103.

Blair, N., A. Leu, E. Muñoz, J. Olsen, E. Kwong, and D. Des Marais (1985). Carbon isotopic fractionation in heterotrophic microbial metabolism. *Applied and Environmental Microbiology* **50** (4), 996–1001.

Blöchl, E., R. Rachel, S. Burggraf, D. Hafenbradl, H. W. Jannasch, and K. O. Stetter (1997). *Pyrolobus fumarii*, gen. and sp. nov., represents a novel group of archaea, extending the upper temperature limit for life to 113°C. *Extremophiles* **1** (1), 14–21. DOI: 10.1007/s007920050010.

Blumenberg, M. (2010). Microbial Chemofossils in Specific Marine Hydrothermal and Methane Cold Seep Settings. English. In: *The Vent and Seep Biota SE - 4*. Ed. by S. Kiel. Vol. 33. Topics in Geobiology. Springer Netherlands, pp. 73–106. DOI: 10.1007/978-90-481-9572-5_4.

Boetius, a. (1995). Microbial hydrolytic enzyme activities in deep-sea sediments. *Helgoländer Meeresuntersuchungen* **49** (1-4), 177–187.

Boetius, A., K. Ravenschlag, C. J. Schubert, D. Rickert, F. Widdel, A. Gieseke, R. Amann, B. B. Jørgensen, U. Witte, and O. Pfannkuche (2000). A marine microbial consortium apparently mediating anaerobic oxidation of methane. *Nature* **407** (6804), 623–626. DOI: 10.1038/35036572.

Bohrmann, G. and M. Torres (2006). Gas Hydrates in Marine Sediments. English. In: *Marine Geochemistry SE - 14*. Ed. by H. Schulz and M. Zabel. Springer Berlin Heidelberg, pp. 481–512. DOI: 10.1007/3-540-32144-6_14.

Bolle, M.-P., A. Pardo, K.-U. Hinrichs, T. Adatte, K. Von Salis, S. Burns, G. Keller, and N. Muzylev (2000). The Paleocene–Eocene transition in the marginal northeastern Tethys (Kazakhstan and Uzbekistan). English. *International Journal of Earth Sciences* **89** (2), 390–414. DOI: 10.1007/s005310000092.

Boucher, Y., C. J. Douady, R. T. Papke, D. A. Walsh, M. E. R. Boudreau, C. L. Nesbø, R. J. Case, and W. F. Doolittle (2003). Lateral gene transfer and the origins of prokaryotic groups. *Annual Review of Genetics* **37**, 283–328. DOI: 10.1146/annurev.genet.37.050503.084247.

Boucher, Y., H. Huber, L. Haridon, K. O. Stetter, and W. F. Doolittle (2001). Bacterial Origin for the Isoprenoid Biosynthesis Enzyme HMG-CoA Reductase of the Archaeal Orders Thermoplasmatales and Archaeoglobales. *Molecular Biology and Evolution* **18** (7), 1378–1388.

Boyd, P. W., R. Strzepek, F. Fu, and D. a. Hutchins (2010). Environmental control of open-ocean phytoplankton groups: Now and in the future. *Limnology and Oceanography* **55** (3), 1353–1376. DOI: 10.4319/lo.2010.55.3.1353.

Bradley, A. S., H. Fredricks, K.-U. Hinrichs, and R. E. Summons (2009). Structural diversity of diether lipids in carbonate chimneys at the Lost City Hydrothermal Field. *Organic Geochemistry* **40** (12), 1169–1178. DOI: 10.1016/j.orggeochem.2009.09.004.

Brassell S.C.and Eglinton, G., I. Marlowe, U. Pflaumanmn, and M. Sarnthein (1986). Molecular stratigraphy: a new tool for climatic assessment. *Nature* **320** (13), 129–133.

Brett, M. T. and D. C. Müller-Navarra (1997). The role of highly unsaturated fatty acids in aquatic foodweb processes. *Freshwater Biology* **38**, 483–499. DOI: 10.1046/j.1365-2427.1997.00220.x.

Brettel, K. and W. Leibl (2001). Electron transfer in photosystem I. *Biochimica et Biophysica Acta* **1507**, 100–114.

Brinkhoff, T., G. Muyzer, C. O. Wirsen, and J. Kuever (1999). *Thiomicrospira chilensis* sp. nov., a mesophilic obligately chemolithoautotrophic sulfuroxidizing bacterium isolated from a *Thioploca mat*. *International Journal of Systematic Bacteriology* **49 Pt 2** (1 999), 875–879. DOI: 10.1099/00207713-49-2-875.

Brochier-Armanet, C., B. Boussau, S. Gribaldo, and P. Forterre (2008). Mesophilic Crenarchaeota: proposal for a third archaeal phylum, the Thaumarchaeota. *Nature Reviews Microbiology* **6** (3), 245–252. DOI: 10.1038/nrmicro1852.

Brochier-Armanet, C., P. Forterre, and S. Gribaldo (2011). Phylogeny and evolution of the Archaea: one hundred genomes later. *Current Opinion in Microbiology* **14** (3), 274–281. DOI: 10.1016/j.mib.2011.04.015.

Brock, T. D., K. M. Brock, R. T. Belly, and R. L. Weiss (1972). *Sulfolobus*: A new genus of sulfur-oxidizing bacteria living at low pH and high temperature. *Archiv für Mikrobiologie* **84** (1), 54–68. DOI: 10.1007/BF00408082.

Brocks, J. J. and R. E. Summons (2003). Sedimentary Hydrocarbons, Biomarkers for Early Life. In: *Treatise on Geochemistry*. Ed. by H. Turekian and D. Holland. Oxford: Pergamon, pp. 63–115. DOI: http://dx.doi.org/10.1016/B0-08-043751-6/08127-5.

Brocks, J. J. and A. Pearson (2005). Building the Biomarker Tree of Life. *Reviews in Mineralogy and Geochemistry* **59**, 233–258. DOI: 10.2138/rmg.2005.59.10.

Brocks, J. J. and J. Banfield (2009). Unravelling ancient microbial history with community proteogenomics and lipid geochemistry. *Nature Reviews Microbiology* **7**, 601–609. DOI: 10.1038/nrmicro2167.

Brumsack, H. J. (1989). Geochemistry of Recent TOC-rich sediment from the Gulf of California and the Black Sea. *Geologische Rundschau* **78**, 851–882.

Burdige, D. J. (2006). *Geochemistry of Marine Sediments*. Princeton, USA: Princeton University Press, p. 624.

Burdige, D. J. (2007). Preservation of organic matter in marine sediments: Controls, mechanisms, and an imbalance in sediment organic carbon budgets? *Chemical reviews* **107** (2), 467–485. DOI: 10.1021/cr050347q.

Burdige, D. J. and T. Komada (2013). Using ammonium pore water profiles to assess stoichiometry of deep remineralization processes in methanogenic continental margin sediments. *Geochemistry, Geophysics, Geosystems* **14** (5), 1626–1643. DOI: 10.1002/ggge.20117.

Çağatay, M. N., N. Görür, O. Algan, C. Eastoe, A. Tchapalyga, D. Ongan, T. Kuhn, and I. Kuşcu (2000). Late Glacial–Holocene palaeoceanography of the Sea of Marmara: timing of connections with the Mediterranean and the Black Seas. *Marine Geology* **167** (3â€“4), 191–206. DOI: http://dx.doi.org/10.1016/S0025-3227(00)00031-1.

Çağatay, M. (1999). Geochemistry of the Late Pleistocene-Holocene Sediments of the Black Sea: An Overview. English. In: *Environmental Degradation of the Black Sea: Challenges and Remedies SE - 2*. Ed. by S. BeÅŸiktepe, Ü. Ünlüata, and A. Bologa. Vol. 56. NATO Science Series. Springer Netherlands, pp. 9–22. DOI: 10.1007/978-94-011-4568-8_2.

Calvert, S. E., J. S. Vogel, and J. R. Southon (1987). Carbon accumulation rates and the origin of the Holocene sapropel in the Black Sea. *Geology* **15** (10), 918–921.

Calvert, S. (1983). Geochemistry of Pleistocene sapropels and associated sediments from the Eastern Mediterranean. *Oceanologica Acta* **6** (3), 255–267.

Camerlenghi, A. (1990). Anoxic basins of the eastern Mediterranean: geological framework. *Marine Chemistry* **31** (1-3), 1–19. DOI: 10.1016/0304-4203(90)90028-B.

Camerlenghi, A. and F. McCoy (1990). Physiography and structure of Bacino Bannock (eastern mediterranean). English. *Geo-Marine Letters* **10** (1), 23–30. DOI: 10.1007/BF02431018.

Campbell, K. A. (2006). Hydrocarbon seep and hydrothermal vent paleoenvironments and paleontology: Past developments and future research directions. *Palaeogeography, Palaeoclimatology, Palaeoecology* **232** (2â€“4), 362–407. DOI: http://dx.doi.org/10.1016/j.palaeo.2005.06.018.

Canfield, D. E. and B. Thamdrup (2009). Towards a consistent classification scheme for geochemical environments, or, why we wish the term 'suboxic' would go away. *Geobiology* **7** (4), 385–392. DOI: 10.1111/j.1472-4669.2009.00214.x.

Canfield, D. E., F. J. Stewart, B. Thamdrup, L. De Brabandere, T. Dalsgaard, E. F. Delong, N. P. Revsbech, and O. Ulloa (2010). A cryptic sulfur cycle in oxygen-minimum-zone waters off the Chilean coast. *Science* **330** (6009), 1375–1378. DOI: 10.1126/science.1196889.

Carballeira, N. M., M. Reyes, A. Sostre, H. Huang, M. F. J. M. Verhagen, and M. W. Adams (1997). Unusual fatty acid compositions of the hyperthermophilic archaeon Pyrococcus furiosus and the bacterium *Thermotoga maritima*. *Journal of Bacteriology* **179** (8), 2766–2768.

Cardace, D., J. D. Morris, A. D. Peacock, and D. C. White (2006). Habitability of subseafloor sediments at the Costa Rica convergent margin. In: *Proceedings of the Ocean Drilling Program, Scientific Results Volume 205*. Ed. by J. D. Morris, H. W. Villinger, and A. Klaus. College Station, TX, USA: Ocean Drilling Program.

Carrillo-Hernandez, T., P. Schaeffer, P. Adam, P. Albrecht, S. Derenne, and C. Largeau (2003). Remarkably well-preserved archaeal and bacterial membrane lipids in 140 million year old sediments from the Russian platform (Kashpir Oil Shales, Upper Jurassic). In: *21st International Meeting on Organic Geochemistry, Krakow*. Krakow, pp. 77–78.

Castañeda, I. S., E. Schefuß, J. Pätzold, J. S. Sinninghe Damsté, S. Weldeab, and S. Schouten (2010). Millennial-scale sea surface temperature changes in the eastern Mediterranean (Nile River Delta region) over the last 27,000 years. *Paleoceanography* **25** (1), PA1208. DOI: 10.1029/2009PA001740.

Chaler, R., J. Villanueva, and J. O. Grimalt (2003). N on-linear effects in the determination of paleotemperature U k alkenone ratios by chemical ionization mass spectrometry. *Journal of Chromatography A* **1012**, 87–93.

Chaler, R., J. O. Grimalt, C. Pelejero, and E. Calvo (2000). Sensitivity Effects in $U_{37}^{K'}$ Paleotemperature Estimation by Chemical Ionization Mass Spectrometry. *Analytical Chemistry* **72** (24), 5892–5897.

Chappe, B., P. Albrecht, and W. Michaelis (1982). Polar Lipids of Archaebacteria in Sediments and Petroleums. *Science* **217** (4554), 65–66. DOI: 10.1126/science.217.4554.65.

Chong, P. L.-G., U. Ayesa, V. P. Daswani, and E. C. Hur (2012). On physical properties of tetraether lipid membranes: effects of cyclopentane rings. *Archaea* **2012**, 138439. DOI: 10.1155/2012/138439.

Clarke, C. F., A. C. Rowat, and J. W. Gober (2014). Osmotic stress: Is CoQ a membrane stabilizer? *Nat Chem Biol* **10** (4), 242–243.

Claypool, G. and I. R. Kaplan (1974). The Origin and Distribution of Methane in Marine Sediments. English. In: *Natural Gases in Marine Sediments SE - 8*. Ed. by I. Kaplan. Vol. 3. Marine Science. Springer US, pp. 99–139. DOI: 10.1007/978-1-4684-2757-8_8.

Cline, J. D. (1969). Spectrophotometric determination of hydrogen sulfide in natural waters. *Limnology and Oceanography* **14** (3), 454–458.

Coates, C. S., J. Ziegler, K. Manz, J. Good, B. Kang, S. Milikisiyants, R. Chatterjee, S. Hao, J. H. Golbeck, and K. V. Lakshmi (2013). The structure and function of quinones in biological solar energy transduction: a cyclic voltammetry, EPR, and hyperfine sub-level correlation (HYSCORE) spectroscopy study of model naphthoquinones. *The Journal of Physical Chemistry. B* **117** (24), 7210–7220. DOI: 10.1021/jp401024p.

Collins, M. D. and P. N. Green (1985). Isolation and characterization of a novel coenzyme Q from some methane-oxidizing bacteria. *Biochemical and Biophysical Research Communications* **133** (3), 1125–1131. DOI: 10.1016/0006-291X(85)91253-7.

Collins, M. D. and B. J. Tindall (1987). Occurrence of menaquinones and some novel methylated menaquinones in the alkaliphilic, extremely halophilic archaebacterium *Natronobacterium gregoryi*. *FEMS Microbiology Letters* **43** (3), 307–312. DOI: 10.1016/0378-1097(87)90417-4.

Collins, M. D., H. N. M. Ross, B. J. Tindall, and W. D. Grant (1981). Distribution of isoprenoid quinones in halophilic bacteria. *Journal of Applied Bacteriology* **50** (3), 559–565. DOI: 10.1111/j.1365-2672.1981.tb04258.x.

Collins, M. D. and D. Jones (1981). Distribution of isoprenoid quinone structural types in bacteria and their taxonomic implications. *Microbiological Reviews* **45** (2), 316–354.

Comita, P. B., R. B. Gagosian, H. Pang, and C. E. Costello (1984). Structural elucidation of a unique macrocyclic membrane lipid from a new, extremely thermophilic, deep-sea hydrothermal vent archaebacterium, Methanococcus jannaschii. *The Journal of Biological Chemistry* **259** (24), 15234–15241.

Conrad, R. (1999). Contribution of hydrogen to methane production and control of hydrogen concentrations in methanogenic soils and sediments. *FEMS Microbiology Ecology* **28** (3), 193–202.

Conte, M. H., M.-A. Sicre, C. Rühlemann, J. C. Weber, S. Schulte, D. Schulz-Bull, and T. Blanz (2006). Global temperature calibration of the alkenone unsaturation index (U Kâ€² 37) in surface waters and comparison with surface sediments. *Geochemistry, Geophysics, Geosystems* **7** (2), n/a–n/a. DOI: 10.1029/2005GC001054.

Coolen, M. J. L., B. Abbas, J. van Bleijswijk, E. C. Hopmans, M. M. M. Kuypers, S. G. Wakeham, and J. S. Sinninghe Damsté (2007). Putative ammonia-oxidizing Crenarchaeota in suboxic waters of the Black Sea: a basin-wide ecological study using 16S ribosomal and functional genes and membrane lipids. *Environmental Microbiology* **9** (4), 1001–1016. DOI: 10.1111/j.1462-2920.2006.01227.x.

Coolen, M. J. L., H. Cypionka, A. M. Sass, H. Sass, and J. Overmann (2002). Ongoing modification of Mediterranean Pleistocene sapropels mediated by prokaryotes. *Science* **296** (5577), 2407–2410. DOI: 10.1126/science.1071893.

Cronan, J. E. and E. P. Gelmann (1975). Physical properties of membrane lipids: biological relevance and regulation. *Bacteriological Reviews* **39** (3), 232–256.

Daffonchio, D., S. Borin, T. Brusa, L. Brusetti, P. W. J. J. van der Wielen, H. Bolhuis, M. M. Yakimov, G. D'Auria, L. Giuliano, D. Marty, C. Tamburini, T. J. McGenity, J. E. Hallsworth, A. M. Sass, K. N. Timmis, A. Tselepides, G. J. de Lange, A. Hübner, J. Thomson, S. P. Varnavas, F. Gasparoni, H. W. Gerber, E. Malinverno, C. Corselli, J. Garcin, B. McKew, P. N. Golyshin, N. Lampadariou, P. Polymenakou, D. Calore, S. Cenedese, F. Zanon, and S. Hoog (2006). Stratified prokaryote network in the oxic-anoxic transition of a deep-sea halocline. *Nature* **440** (7081), 203–7. DOI: 10.1038/nature04418.

Dalsgaard, T., B. Thamdrup, and D. E. Canfield (2005). Anaerobic ammonium oxidation (anammox) in the marine environment. *Research in Microbiology* **156** (4), 457–464. DOI: http://dx.doi.org/10.1016/j.resmic.2005.01.011.

Darland, G., T. D. Brock, W. Samsonoff, and S. F. Conti (1970). A thermophilic, acidophilic mycoplasma isolated from a coal refuse pile. *Science* **170** (3965), 1416–1418.

Dawson, K. S., K. H. Freeman, and J. L. Macalady (2012). Molecular characterization of core lipids from halophilic archaea grown under different salinity conditions. *Organic Geochemistry* **48**, 1–8. DOI: 10.1016/j.orggeochem.2012.04.003.

De Jonge, C., E. C. Hopmans, A. Stadnitskaia, W. I. C. Rijpstra, R. Hofland, E. Tegelaar, and J. S. Sinninghe Damsté (2013). Identification of novel penta- and hexamethylated branched glycerol dialkyl glycerol tetraethers in peat using HPLC-MS2, GC-MS and GC-SMB-MS. *Organic Geochemistry* **54**, 78–82. DOI: 10.1016/j.orggeochem.2012.10.004.

De Lange, G. J. and H. L. ten Haven (1983). Recent sapropel formation in the eastern Mediterranean. *Nature* **305** (27), 797–798.

De Lange, G. J., G. Catalano, G. P. Klinkhammer, and G. W. Luther (1990a). The interface between oxic seawater and the anoxic Bannock brine; its sharpness and the consequences for the redox-related cycling of Mn and Ba. *Marine Chemistry* **31** (1-3), 205–217. DOI: 10.1016/0304-4203(90)90039-F.

De Lange, G., J. Middelburg, C. Van der Weijden, G. Catalano, G. Luther, D. Hydes, J. Woittiez, and G. Klinkhammer (1990b). Composition of anoxic hypersaline brines in the Tyro and Bannock Basins, eastern Mediterranean. *Marine Chemistry* **31** (1-3), 63–88. DOI: 10.1016/0304-4203(90)90031-7.

De Rosa, M., S. De Rosa, A. Gambacorta, L. Minale, R. H. Thomson, and R. D. Worthington (1977). Caldariellaquinone, a unique benzo[*b*]thiophen-4,7-quinone from *Caldariella acidophila*, an extremely thermophilic and acidophilic bacterium. *Journal of the Chemical Society, Perkin Transactions 1* **6**, 653–657. DOI: 10.1039/p19770000653.

De Rosa, M., E. Esposito, A. Gambacorta, B. Nicolaus, and J. D. Bu'Lock (1980). Effects of temperature on ether lipid composition of *Caldariella acidophila*. *Phytochemistry* **19** (5), 827–831. DOI: 10.1016/0031-9422(80)85120-X.

De Rosa, M., A. Gambacorta, W. D. Grant, V. Lanzotti, and B. Nicolaus (1988). Polar Lipids and Glycine Betaine from Haloalkaliphilic Archaebacteria. *Microbiology* **134** (1), 205–211. DOI: 10.1099/00221287-134-1-205.

De Rosa, M., A. Gambacorta, B. Nicolaus, and W. D. Grant (1983). A C_{25},C_{25} Diether Core Lipid from Archaebacterial Haloalkaliphiles. *Microbiology* **129** (8), 2333–2337. DOI: 10.1099/00221287-129-8-2333.

De Rosa, M., A. Gambacorta, and A. Gliozzi (1986). Structure, Biosynthesis, and Physicochemical Properties of Archaebacterial Lipids. *Microbiological Reviews* **50** (1), 70–80.

De Rosa, M., A. Gambacorta, B. Nicolaus, H. N. M. Ross, W. D. Grant, and J. D. Bu'Lock (1982). An Asymmetric Archaebacterial Diether Lipid from Alkaliphilic Halophiles. *Microbiology* **128** (2), 343–348. DOI: 10.1099/00221287-128-2-343.

Degens, E. T. and D. A. Ross (1972). Chronology of the Black Sea over the last 25,000 years. *Chemical Geology* **10**, 1–16. DOI: 10.1016/0009-2541(72)90073-3.

DeLong, E. F. (1992). Archaea in coastal marine environments. *Proceedings of the National Academy of Sciences of the United States of America* **89** (12), 5685–5689. DOI: 10.1073/pnas.89.12.5685.

DeLong, E. F. (1998). Everything in moderation: Archaea as 'non-extremophiles'. *Current Opinion in Genetics & Development* **8** (6), 649–654. DOI: 10.1016/S0959-437X(98)80032-4.

DeLong, E. F. (2006). Archaeal mysteries of the deep revealed. *Proceedings of the National Academy of Sciences of the United States of America* **103** (17), 6417–6418. DOI: 10.1073/pnas.0602079103.

Dembitsky, V. M. (1996). Betaine ether-linked glycerolipids: Chemistry and biology. *Progress in Lipid Research* **35** (1), 1–51. DOI: 10.1016/0163-7827(95)00009-7.

DeNiro, M. J. and S. Epstein (1976). You are what you eat (plus a few permil): the carbon isotope cycle in food chains. *Geological Society of America* **6**, 834–835.

DeNiro, M. J. and S. Epstein (1977). Mechanism of carbon isotope fractionation associated with lipid synthesis. *Science* **197** (4300), 261–263.

Deuser, W. G. (1972). Late-Pleistocene and Holocene history of the Black Sea as indicated by stable-isotope studies. *Journal of Geophysical Research* **77** (6), 1071–1077. DOI: 10.1029/JC077i006p01071.

D'Hondt, S., B. Jørgensen, and D. Miller (2003). *Proceedings of the Ocean Drilling Program, Initial Reports, 201*. Tech. rep. College Station, TX, USA: Ocean Drilling Program. DOI: 10.2973/odp.proc.ir.201.2003.

D'Hondt, S., B. B. Jørgensen, D. J. Miller, A. Batzke, R. Blake, B. A. Cragg, H. Cypionka, G. R. Dickens, T. Ferdelman, K.-U. Hinrichs, N. G. Holm, R. Mitterer, A. Spivack, G. Wang, B. Bekins, B. Engelen, K. Ford, G. Gettemy, S. D. Rutherford, H. Sass, C. G. Skilbeck, I. W. Aiello, G. Guèrin, C. H. House, F. Inagaki, P. Meister, T. Naehr, S. Niitsuma, R. J. Parkes, A. Schippers, D. C. Smith, A. Teske, J. Wiegel, C. N. Padilla, and J. L. S. Acosta (2004). Distributions of microbial activities in deep subseafloor sediments. *Science (New York, N.Y.)* **306** (5705), 2216–2221. DOI: 10.1126/science.1101155.

D'Hondt, S., A. J. Spivack, R. Pockalny, T. G. Ferdelman, J. P. Fischer, J. Kallmeyer, L. J. Abrams, D. C. Smith, D. Graham, F. Hasiuk, H. Schrum, and A. M. Stancin (2009). Subseafloor sedimentary life in the South Pacific Gyre. *Proceedings of the National Academy of Sciences* **106** (28), 11651–11656. DOI: 10.1073/pnas.0811793106.

Dietrich, L. E. P., M. M. Tice, and D. K. Newman (2006). The co-evolution of life and Earth. *Current Biology* **16**, 395–400. DOI: 10.1016/j.cub.2006.05.017.

Dietrich, W. and O. Klimmek (2002). The function of methyl-menaquinone-6 and polysulfide reductase membrane anchor (PsrC) in polysulfide respiration of *Wolinella succinogenes*. *European Journal of Biochemistry* **269** (4), 1086–1095. DOI: 10.1046/j.0014-2956.2001.02662.x.

DiSpirito, A. A., W. H. T. Loh, and O. H. Tuovinen (1983). A novel method for the isolation of bacterial quinones and its application to appraise the ubiquinone composition of *Thiobacillus ferrooxidans*. *Archives of Microbiology* **135** (1), 77–80. DOI: 10.1007/BF00419487.

Dowhan, W. (1997). Molecular basis for membrane phospholipid diversity: why are there so many lipids? *Annual review of biochemistry* **66** (1), 199–232. DOI: 10.1146/annurev.biochem.66.1.199.

Dowhan, W. and M. Bogdanov (2002). Functional roles of lipids in membranes. In: *Biochemistry of Lipids, Lipoproteins and Membranes*. Ed. by D. E. Vance and J. E. Vance. Elsevier Science.

Drake, H., K. Küsel, and C. Matthies (2006). Acetogenic Prokaryotes. English. In: *The Prokaryotes SE - 13*. Ed. by M. Dworkin, S. Falkow, E. Rosenberg, K.-H. Schleifer, and E. Stackebrandt. Springer New York, pp. 354–420. DOI: 10.1007/0-387-30742-7_13.

Duarte, C. M., J. J. Middelburg, and N. Caraco (2005). Major role of marine vegetation on the oceanic carbon cycle. *Biogeosciences* **2** (1), 1–8. DOI: 10.5194/bg-2-1-2005.

Ducklow, H. W. (1995). Ocean biogeochemical fluxes: New production and export of organic matter from the upper ocean. *Reviews of Geophysics* **33** (S2), 1271–1276. DOI: 10.1029/95RG00130.

Dunne, J. P., J. L. Sarmiento, and A. Gnanadesikan (2007). A synthesis of global particle export from the surface ocean and cycling through the ocean interior and on the seafloor. *Global Biogeochemical Cycles* **21** (4), n/a–n/a. DOI: 10.1029/2006GB002907.

Dunphy, P. J., D. L. Gutnick, P. G. Phillips, and A. F. Brodie (1968). A new natural naphthoquinone in *Mycobacterium phlei*. *Journal of Biological Chemistry* **243** (2), 398–407.

Durisch-Kaiser, E., L. Klauser, B. Wehrli, and C. Schubert (2005). Evidence of intense archaeal and bacterial methanotrophic activity in the Black Sea water column. *Applied and Environmental Microbiology* **71** (12), 8099–8106. DOI: 10.1128/AEM.71.12.8099-8106.2005.

Eckert, S., H. J. Brumsack, S. Severmann, B. Schnetger, C. März, and H. Fröllje (2013). Establishment of euxinic conditions in the Holocene Black Sea. *Geology* **41**, 431–434. DOI: 10.1130/G33826.1.

Edgcomb, V., W. Orsi, C. Leslin, S. S. Epstein, J. Bunge, S. Jeon, M. M. Yakimov, A. Behnke, and T. Stoeck (2009). Protistan community patterns within the brine and halocline of deep hypersaline anoxic basins in the eastern Mediterranean Sea. *Extremophiles : life under extreme conditions* **13** (1), 151–67. DOI: 10.1007/s00792-008-0206-2.

Edwards, K. J. (2004). Performing Real-Time PCR. In: *Real-Time PCR: An Essential Guide*. Ed. by K. Edwards, J. Logan, and N. Saunders. Norfolk, UK: Horizon Bioscience, pp. 71–83.

Eglinton, G. and M. Calvin (1967). Chemical fossils. *Scientific American* **216**, 32–43.

Eglinton, G., P. M. Scott, T. Belsky, A. L. Burlingame, and M. Calvin (1964). Hydrocarbons of Biological Origin from a One-Billion-Year-Old Sediment. *Science* **145** (3629), 263–264. DOI: 10.1126/science.145.3629.263.

Eglinton, T. I. and G. Eglinton (2008). Molecular proxies for paleoclimatology. *Earth and Planetary Science Letters* **275** (1-2), 1–16. DOI: 10.1016/j.epsl.2008.07.012.

Elferink, M. G. L., J. G. D. Wit, A. J. M. Driessen, and W. N. Konings (1994). Stability and proton-permeability of liposomes composed of archaeal tertraether lipids. *Biochimica et Biophysica Acta* **1193**, 247–254. DOI: 10.1016/0005-2736(94)90160-0.

Elling, F. J., M. Könneke, J. S. Lipp, K. W. Becker, E. J. Gagen, and K.-U. Hinrichs (2014). Effects of growth phase on the membrane lipid composition of the thaumarchaeon *Nitrosopumilus maritimus* and their implications for archaeal lipid distributions in the marine environment. *Geochimica et Cosmochimica Acta* **141**, 579–597. DOI: 10.1016/j.gca.2014.07.005.

Eltgroth, M. L., R. L. Watwood, and G. V. Wolfe (2005). Production and cellular localization of neutral long-chain lipids in the Haptophyte algae Isochrysis galbana and Emiliania huxleyi. *Journal of Phycology* **41** (5), 1000–1009. DOI: 10.1111/j.1529-8817.2005.00128.x.

Elvert, M., A. Boetius, K. Knittel, and B. B. Jørgensen (2003). Characterization of specific membrane fatty acids as chemotaxonomic markers for sulfate-reducing bacteria involved in anaerobic oxidation of methane. *Geomicrobiology Journal* **20** (4), 403–419. DOI: 10.1080/01490450303894.

Elvert, M., E. Suess, and M. J. Whiticar (1999). Anaerobic methane oxidation associated with marine gas hydrates: superlight C-isotopes from saturated and unsaturated C20 and C25 irregular isoprenoids. *Naturwissenschaften* **86** (6), 295–300. DOI: 10.1007/s001140050619.

Epstein, B. L., S. D'Hondt, J. G. Quinn, J. Zhang, and P. E. Hargraves (1998). An effect of dissolved nutrient concentrations on alkenone-based temperature estimates. *Paleoceanography* **13** (2), 122–126. DOI: 10.1029/97PA03358.

Escala, M., A. Rosell-Melé, and P. Masqué (2007). Rapid screening of glycerol dialkyl glycerol tetraethers in continental Eurasia samples using HPLC/APCI-ion trap mass spectrometry. *Organic Geochemistry* **38** (1), 161–164. DOI: 10.1016/j.orggeochem.2006.08.013.

Ettwig, K. F., M. K. Butler, D. Le Paslier, E. Pelletier, S. Mangenot, M. M. M. Kuypers, F. Schreiber, B. E. Dutilh, J. Zedelius, D. de Beer, J. Gloerich, H. J. C. T. Wessels, T. van Alen, F. Luesken, M. L. Wu, K. T. van de Pas-Schoonen, H. J. M. Op den Camp, E. M. Janssen-Megens, K.-J. Francoijs, H. Stunnenberg, J. Weissenbach, M. S. M. Jetten, and M. Strous (2010). Nitrite-driven anaerobic methane oxidation by oxygenic bacteria. *Nature* **464** (7288), 543–548. DOI: 10.1038/nature08883.

Falkowski, P. G. (1998). Biogeochemical Controls and Feedbacks on Ocean Primary Production. *Science* **281**, 200–206. DOI: 10.1126/science.281.5374.200.

Falkowski, P. G., T. Fenchel, and E. F. Delong (2008). The microbial engines that drive Earth's biogeochemical cycles. *Science* **320** (3), 1034–1039. DOI: 10.1126/science.1153213.

Fang, J., M. J. Barcelona, and J. D. Semrau (2000). Characterization of methanotrophic bacteria on the basis of intact phospholipid profiles. *FEMS Microbiology Letters* **189** (1), 67–72. DOI: 10.1111/j.1574-6968.2000.tb09207.x.

Ferris, F. G., W. S. Fyfe, and T. J. Beveridge (1988). Metallic ion binding by Bacillus subtilis: Implications for the fossilization of microorganisms. *Geology* **16** (2), 149–152. DOI: 10.1130/0091-7613(1988)016<0149:MIBBBS>2.3.CO;2.

Field, C. B. (1998). Primary Production of the Biosphere: Integrating Terrestrial and Oceanic Components. *Science* **281** (July), 237–240. DOI: 10.1126/science.281.5374.237.

Filker, S., A. Stock, H.-W. Breiner, V. Edgcomb, W. Orsi, M. M. Yakimov, and T. Stoeck (2013). Environmental selection of protistan plankton communities in hypersaline anoxic deep-sea basins, Eastern Mediterranean Sea. *MicrobiologyOpen* **2** (1), 54–63. DOI: 10.1002/mbo3.56.

Fisher, C., H. Roberts, E. Cordes, and B. Bernard (2007). Cold Seeps and Associated Communities of the Gulf of Mexico. *Oceanography* **20** (4), 118–129. DOI: 10.5670/oceanog.2007.12.

Fontugne, M. R. and S. E. Calvert (1992). Late Pleistocene Variability of the Carbon Isotopic Composition of Organic Matter in the Eastern Mediterranean: Monitor of Changes in Carbon Sources and Atmospheric CO2 Concentrations. *Paleoceanography* **7** (1), 1–20. DOI: 10.1029/91PA02674.

Franzmann, P., E. Stackebrandt, K. Sanderson, J. Volkman, D. Cameron, P. Stevenson, T. Mcmeekin, and H. Burton (1988). *Halobacterium lacusprofundi* sp. nov., a Halophilic Bacterium Isolated from Deep Lake, Antarctica. *Systematic and Applied Microbiology* **11** (1), 20–27. DOI: 10.1016/S0723-2020(88)80044-4.

Frigaard, N. U., S. Takaichi, M. Hirota, K. Shimada, and K. Matsuura (1997). Quinones in chlorosomes of green sulfur bacteria and their role in the redox-dependent fluorescence studied in chlorosome-like bacteriochlorophyll c aggregates. *Archives of Microbiology* **167**, 343–349. DOI: 10.1007/s002030050453.

Froelich, P. N., G. P. Klinkhammer, M. L. Bender, N. A. Luedtke, G. R. Heath, D. Cullen, P. Dauphin, D. Hammond, B. Hartman, and V. Maynard (1979). Early oxidation of organic matter in pelagic sediments of the eastern equatorial Atlantic: suhoxic diagenesis. *Geochimica et Cosmochimica Actamica*.

Fry, J. C., R. J. Parkes, B. a. Cragg, A. J. Weightman, and G. Webster (2008). Prokaryotic biodiversity and activity in the deep subseafloor biosphere. *FEMS Microbiology Ecology* **66** (2), 181–196. DOI: 10.1111/j.1574-6941.2008.00566.x.

Frydman, B. and H. Rapoport (1963). Non-chlorophyllous pigments of *Chlorobium Thiosulfatophilum* chlorobiumquinone. *Journal of the American Chemical Society* **85** (6), 823–825. DOI: 10.1021/ja00889a044.

Fuchsman, C. A., J. B. Kirkpatrick, W. J. Brazelton, J. W. Murray, and J. T. Staley (2011). Metabolic strategies of free-living and aggregate-associated bacterial communities inferred from biologic and chemical profiles in the Black Sea suboxic zone. *FEMS Microbiology Ecology* **78**, 586–603. DOI: 10.1111/j.1574-6941.2011.01189.x.

Fuhrman, J. A., K. McCallum, and A. A. Davis (1992). Novel major archaebacterial group from marine plankton. *Nature* **356** (6365), 148–149. DOI: 10.1038/356148a0.

Fusi, N., A. Negri, P. Tarbini, and M. B. Cita (1996). Marine geology of the Medriff Corridor , Mediterranean Ridge. *The Island Arc* **5**, 420–439.

Gabriel, J. L. and P. L. G. Chong (2000). Molecular modeling of archaebacterial bipolar tetraether lipid membranes. *Chemistry and Physics of Lipids* **105** (2), 193–200. DOI: 10.1016/S0009-3084(00)00126-2.

Gaines, S. M., G. Eglinton, and J. Rullkötter (2009). *Echoes of life: what fossil molecules reveal about earth history*. Oxford [etc.]: Oxford University Press.

Gattinger, A., M. Schloter, and J. C. Munch (2002). Phospholipid etherlipid and phospholipid fatty acid fingerprints in selected euryarchaeotal monocultures for taxonomic profiling. *FEMS Microbiology Letters* **213** (1), 133–139. DOI: 10.1111/j.1574-6968.2002.tb11297.x.

Geiger, O., V. Röhrs, B. Weissenmayer, T. M. Finan, and J. E. Thomas-Oates (1999). The regulator gene phoB mediates phosphate stress-controlled synthesis of the membrane lipid diacylglyceryl-*N,N,N*-trimethylhomoserine in *Rhizobium* (*Sinorhizobium*) *meliloti*. *Molecular Microbiology* **32** (1), 63–73.

Geiger, O., N. González-Silva, I. M. López-Lara, and C. Sohlenkamp (2010). Amino acid-containing membrane lipids in bacteria. *Progress in Lipid Research* **49** (1), 46–60. DOI: 10.1016/j.plipres.2009.08.002.

Geyer, R., A. D. Peacock, D. C. White, C. Lytle, and G. J. V. Berkel (2004). Atmospheric pressure chemical ionization and atmospheric pressure photoionization for simultaneous mass spectrometric analysis of microbial respiratory ubiquinones and menaquinones. *Journal of Mass Spectrometry* **39**, 922–929. DOI: 10.1002/jms.670.

Gibson, J. A. E., M. R. Miller, N. W. Davies, G. P. Neill, D. S. Nichols, and J. K. Volkman (2005). Unsaturated diether lipids in the psychrotrophic archaeon *Halorubrum lacusprofundi*. *Systematic and Applied Microbiology* **28** (1), 19–26. DOI: 10.1016/j.syapm.2004.09.004.

Gliozzi, A., G. Paoli, M. De Rosa, and A. Gambacorta (1983). Effect of isoprenoid cyclization on the transition temperature of lipids in thermophilic archaebacteria. *Biochimica et Biophysica Acta* **735**, 234–242.

Gliozzi, A., A. Relini, and P. L.-G. Chong (2002). Structure and permeability properties of biomimetic membranes of bolaform archaeal tetraether lipids. *Journal of Membrane Science* **206** (1-2), 131–147. DOI: 10.1016/S0376-7388(01)00771-2.

Goldfine, H. and P.-O. Hagen (1968). *N*-Methyl Groups in Bacterial Lipids. *Journal of Bacteriology* **95** (2), 367–375.

Goldfine, H. (1984). Bacterial membranes and lipid packing theory. *Journal of Lipid Research* **25** (13), 1501–1507.

Goldfine, H. and T. A. Langworthy (1988). A growing interest in bacterial ether lipids. *Trends in Biochemical Sciences* **13** (6), 217–221. DOI: http://dx.doi.org/10.1016/0968-0004(88)90087-4.

Gräther, O. and D. Arigoni (1995). Detection of regioisomeric macrocyclic tetraethers in the lipids of *Methanobacterium thermoautotrophicum* and other archaeal organisms. *Journal of the Chemical Society, Chemical Communications* (4), 405–406. DOI: 10.1039/c39950000405.

Grauel, A.-L., A. Leider, M.-L. S. Goudeau, I. a. Müller, S. M. Bernasconi, K.-U. Hinrichs, G. J. de Lange, K. A. Zonneveld, and G. J. Versteegh (2013). What do SST proxies really tell us? A high-resolution multiproxy ($U^{K'}_{37}$, TEX^{H}_{86} and foraminifera $\delta^{18}O$) study in the Gulf of Taranto, central Mediterranean Sea. *Quaternary Science Reviews* **73**, 115–131. DOI: 10.1016/j.quascirev.2013.05.007.

Gray, H. B. and W. R. Ellis (1994). Electron transfer. In: *Bioinorganic Chemistry*. Ed. by I. Bertini, H. B. Gray, S. J. Lippard, and J. S. Valentine. Mill Valley, CA, USA: University Science Books, pp. 315–363.

Grimalt, J. O., E. Calvo, and C. Pelejero (2001). Sea surface paleotemperature errors in $U^{K'}_{37}$ estimation due to alkenone measurements near the limit of detection. *Paleoceanography* **16** (2), 226–232. DOI: 10.1029/1999PA000440.

Grossi, V., D. Mollex, A. Vinçon-Laugier, F. Hakil, M. Pacton, and C. Cravo-Laureau (2015). Mono- and dialkyl glycerol ether lipids in anaerobic bacteria: biosynthetic insights from the mesophilic sulfate-reducer Desulfatibacillum alkenivorans PF2803 T. *Applied and Environmental Microbiology* **81** (9), AEM.03794–14. DOI: 10.1128/AEM.03794-14.

Guckert, J. (1985). Phospholipid, ester-linked fatty acid profiles as reproducible assays for changes in prokaryotic community structure of estuarine sediments. *FEMS Microbiology Letters* **31** (3), 147–158. DOI: 10.1016/0378-1097(85)90016-3.

Guckert, J. B., M. a. Hood, and D. C. White (1986). Phospholipid ester-linked fatty acid profile changes during nutrient deprivation of *Vibrio Cholerae*: Increases in the *trans/cis* ratio and proportions of cyclopropyl fatty acids. *Applied and Environmental Microbiology* **52** (4), 794–801.

Guillard, R. R. L. and J. H. Ryther (1962). Studies of marine planktonic diatoms. I. Cyclotella nana Hustedt, and Detonula confervacea (cleve) Gran. *Canadian Journal of Microbiology* **8** (2), 229–239. DOI: 10.1139/m62-029.

Hall, P. O. J. and R. C. Aller (1992). Rapid, Small-Volume, Flow Injection Analysis for CO_2 and NH_4^+ in Marine and Freshwaters. *Limnology and Oceanography* **37** (5), 1113–1119.

Hallsworth, J. E., S. Heim, and K. N. Timmis (2003). Chaotropic solutes cause water stress in Pseudomonas putida. *Environmental Microbiology* **5** (12), 1270–1280. DOI: 10.1111/j.1462-2920.2003.00478.x.

Hallsworth, J. E., M. M. Yakimov, P. N. Golyshin, J. L. M. Gillion, G. D'Auria, F. de Lima Alves, V. La Cono, M. Genovese, B. A. McKew, S. L. Hayes, G. Harris, L. Giuliano, K. N. Timmis, and T. J. McGenity (2007). Limits of life in $MgCl_2$-containing environments: chaotropicity defines the window. *Environmental Microbiology* **9** (3), 801–813. DOI: 10.1111/j.1462-2920.2006.01212.x.

Harvey, H. R., R. D. Fallon, and J. S. Patton (1986). The effect of organic matter and oxygen on the degradation of bacterial membrane lipids in marine sediments. *Geochimica et Cosmochimica Acta* **50** (5), 795–804. DOI: 10.1016/0016-7037(86)90355-8.

Harwood, J. L. (1998). Membrane Lipids in Algae. In: *Lipids in phothosynthesis: Structure, Function and Genetics*. Ed. by S. Paul-André and M. Norio. Vol. 6. Dordrecht, The Netherlands: Springer, pp. 53–64. DOI: 10.1007/0-306-48087-5.

Hasegawa, Y., N. Kawada, and Y. Nosoh (1980). Change in chemical composition of membrane of Bacillus caldotenax after shifting the growth temperature. English. *Archives of Microbiology* **126** (2), 103–108. DOI: 10.1007/BF00511214.

Hatzenpichler, R., E. V. Lebedeva, E. Spieck, K. Stoecker, A. Richter, H. Daims, and M. Wagner (2008). A moderately thermophilic ammonia-oxidizing crenarchaeote from a hot spring. *Proceedings of the National Academy of Sciences of the United States of America* **105** (6), 2134–2139. DOI: 10.1073/pnas.0708857105.

Hay, B. J., M. a. Arthur, W. E. Dean, E. D. Neff, and S. Honjo (1991). Sediment deposition in the Late Holocene abyssal Black Sea with climatic and chronological implications. *Deep Sea Research Part A. Oceanographic Research Papers* **38**, S1211–S1235. DOI: 10.1016/S0198-0149(10)80031-7.

Hay, B. J., S. Honjo, S. Kempe, V. A. Ittekkot, E. T. Degens, T. Konuk, and E. Izdar (1990). Interannual variability in particle flux in the southwestern Black Sea. *Deep Sea Research Part A. Oceanographic Research Papers* **37** (6), 911–928. DOI: 10.1016/0198-0149(90)90103-3.

Hayes, J. (1993). Factors controlling ^{13}C contents of sedimentary organic compounds: Principles and evidence. *Marine Geology* **113** (1-2), 111–125. DOI: 10.1016/0025-3227(93)90153-M.

Hayes, J. M. (2001). Fractionation of Carbon and Hydrogen Isotopes in Biosynthetic Processes. *Reviews in Mineralogy and Geochemistry* **43** (1), 225–277. DOI: 10.2138/gsrmg.43.1.225.

Hazel, J. R. and E. E. Williams (1990). The role of alterations in membrane lipid composition in enabling physiological adaptation of organisms to their physical environment. *Progress in lipid research* **29**, 167–227. DOI: 10.1016/0163-7827(90)90002-3.

Hedges, J. I. and R. G. Keil (1995). Sedimentary organic matter preservation: an assessment and speculative synthesis. *Marine Chemistry* **49** (2-3), 81–115. DOI: 10.1016/0304-4203(95)00008-F.

Hedrick, D. B. and D. C. White (1986). Microbial respiratory quinones in the environment. *Journal of Microbiological Methods* **5** (5-6), 243–254. DOI: 10.1016/0167-7012(86)90049-7.

Hefter, J. (2008). Analysis of Alkenone Unsaturation Indices with Fast Gas Chromatography/Time-of-Flight Mass Spectrometry. *Analytical Chemistry* **80** (6). PMID: 18288817, 2161–2170. DOI: 10.1021/ac702194m.

Heipieper, H. J., R. Diefenbach, and H. Keweloh (1992). Conversion of *cis* unsaturated fatty acids to *trans*, a possible mechanism for the protection of phenol-degrading *Pseudomonas putida* P8 from substrate toxicity. *Applied and Environmental Microbiology* **58** (6), 1847–1852.

Hensel, R., K. Matussek, K. Michalke, L. Tacke, B. J. Tindall, M. Kohlhoff, B. Siebers, and J. Dielenschneider (1997). *Sulfophobococcus zilligii* gen. nov., spec. nov. a Novel Hyperthermophilic Archaeum Isolated from Hot Alkaline Springs of Iceland. *Systematic and Applied Microbiology* **20** (1), 102–110. DOI: 10.1016/S0723-2020(97)80054-9.

Herbert, T. D. (2003). 6.15 - Alkenone Paleotemperature Determinations. In: *Treatise on Geochemistry*. Ed. by K. Turekian and H. Holland. Oxford: Pergamon, pp. 391–432. DOI: http://dx.doi.org/10.1016/B0-08-043751-6/06115-6.

Hernández-Sánchez, M., E. Woodward, K. Taylor, G. M. Henderson, and R. Pancost (2014). Variations in GDGT distributions through the water column in the South East Atlantic Ocean. *Geochimica et Cosmochimica Acta* **132**, 337–348. DOI: 10.1016/j.gca.2014.02.009.

Herndl, G. J., T. Reinthaler, E. Teira, H. van Aken, C. Veth, A. Pernthaler, and J. Pernthaler (2005). Contribution of Archaea to total prokaryotic production in the deep Atlantic Ocean. *Applied and Environmental Microbiology* **71** (5), 2303–2309. DOI: 10.1128/AEM.71.5.2303-2309.2005.

Heuer, V. B., J. W. Pohlman, M. E. Torres, M. Elvert, and K.-U. Hinrichs (2009). The stable carbon isotope biogeochemistry of acetate and other dissolved carbon species in deep subseafloor sediments at the northern Cascadia Margin. *Geochimica et Cosmochimica Acta* **73** (11), 3323–3336. DOI: 10.1016/j.gca.2009.03.001.

Hinrichs, K. and A. Boetius (2002). The Anaerobic Oxidation of Methane : New Insights in Microbial Ecology and Biogeochemistry, 457–477.

Hinrichs, K.-U. and F. Inagaki (2012). Biogeochemistry. Downsizing the deep biosphere. *Science (New York, N.Y.)* **338** (6104), 204–5. DOI: 10.1126/science.1229296.

Hinrichs, K.-U., J. M. Hayes, S. P. Sylva, P. G. Brewer, and E. F. DeLong (1999). Methane-consuming archaebacteria in marine sediments. *Nature* **398** (6730), 802–805. DOI: 10.1038/19751.

Hiraishi, A. (1999). Isoprenoid quinones as biomarkers of microbial populations in the environment. *Journal of Bioscience and Bioengineering* **88** (5), 449–460. DOI: 10.1016/S1389-1723(00)87658-6.

Hiraishi, A. and K. Kato (1999). Quinone profiles in lake sediments: Implications for microbial diversity and community structures. *The Journal of General and Applied Microbiology* **45** (5), 221–227. DOI: 10.2323/jgam.45.221.

Hiraishi, A., M. Iwasaki, T. Kawagishi, N. Yoshida, T. Narihiro, and K. Kato (2003). Significance of lipoquinones as quantitative biomarkers of bacterial populations in the environment. *Microbes and Environments* **18** (2), 89–93. DOI: 10.1264/jsme2.18.89.

Hiratsuka, T., K. Furihata, J. Ishikawa, H. Yamashita, N. Itoh, H. Seto, and T. Dairi (2008). An alternative menaquinone biosynthetic pathway operating in microorganisms. *Science* **321** (5896), 1670–1673. DOI: 10.1126/science.1160446.

Hoefs, M., S. Schouten, J. W. De Leeuw, L. L. King, S. G. Wakeham, and J. S. Sinninghe Damsté (1997). Ether lipids of planktonic archaea in the marine water column. *Applied and Environmental Microbiology* **63** (8), 3090–3095.

Hoefs, M. J. L., G. J. M. Versteegh, W. I. C. Rijpstra, J. W. de Leeuw, and J. S. S. Damsté (1998). Postdepositional oxic degradation of alkenones: Implications for the measurement of palaeo sea surface temperatures. *Paleoceanography* **13** (1), 42–49. DOI: 10.1029/97PA02893.

Hoehler, T. M., D. B. Albert, M. J. Alperin, and C. S. Martens (1999). Acetogenesis from CO2 in an anoxic marine sediment. *Limnology and Oceanography* **44** (3), 662–667. DOI: 10.4319/lo.1999.44.3.0662.

Hoehler, T. M., M. J. Alperin, D. B. Albert, and C. S. Martens (1994). Field and laboratory studies of methane oxidation in an anoxic marine sediment: Evidence for a methanogen-sulfate reducer consortium. *Global Biogeochemical Cycles* **8** (4), 451–463. DOI: 10.1029/94GB01800.

Holländer, R. (1976). Correlation of the function of demethylmenaquinone in bacterial electron transport with its redox potential. *FEBS Letters* **72** (1), 98–100. DOI: 10.1016/0014-5793(76)80821-6.

Hölzl, G. and P. Dörmann (2007). Structure and function of glycoglycerolipids in plants and bacteria. *Progress in Lipid Research* **46** (5), 225–243. DOI: 10.1016/j.plipres.2007.05.001.

Honjo, S., B. J. Hay, S. Manganini, V. L. Asper, E. T. Degens, V. Ittekkot, S. Kempe, E. Izdar, Y. T. Konuk, and H. A. Benli (1987). Seasonal cyclicity of lithogenic particle fluxes at a Southern Black Sea sediment trap station. In: *Particle Flux in the Ocean*. Ed. by E. Degens, E. Izdar, and S. Honjo. Hamburg, Germany: Universität Hamburg, pp. 19–40.

Hooper, A. B., R. H. Erickson, and K. R. Terry (1972). Electron transport systems of Nitrosomonas: isolation of a membrane-envelope fraction. *Journal of Bacteriology* **110** (1), 430–438.

Hopmans, E. C., S. Schouten, R. D. Pancost, M. T. J. van der Meer, and J. S. Sinninghe Damsté (2000). Analysis of intact tetraether lipids in archaeal cell material and sediments by high performance liquid chromatography/atmospheric pressure chemical ionization mass spectrometry. *Rapid Communications in Mass Spectrometry* **14** (7), 585–589. DOI: 10.1002/(SICI)1097-0231(20000415)14:7<585::AID-RCM913>3.0.CO;2-N.

Hopmans, E. C., J. W. H. Weijers, E. Schefuß, L. Herfort, J. S. Sinninghe Damsté, and S. Schouten (2004). A novel proxy for terrestrial organic matter in sediments based on branched and isoprenoid tetraether lipids. *Earth and Planetary Science Letters* **224** (1-2), 107–116. DOI: 10.1016/j.epsl.2004.05.012.

House, C. H., J. Schopf, and K. O. Stetter (2003). Carbon isotopic fractionation by Archaeans and other thermophilic prokaryotes. *Organic Geochemistry* **34** (3), 345–356. DOI: 10.1016/S0146-6380(02)00237-1.

Huber, H. and K. O. Stetter (2006). Thermoplasmatales. In: *The Prokaryotes, Volume 3: Archaea. Bacteria: Firmicutes, Actinomycetes*. Ed. by M. Dworkin, S. Falkow, E. Rosenberg, K.-H. Schleifer, and E. Stackebrandt, pp. 101–112. DOI: 10.1007/0-387-30743-5_7.

Huber, H., M. Thomm, H. König, G. Thies, and K. O. Stetter (1982). *Methanococcus thermolithotrophicus*, a novel thermophilic lithotrophic methanogen. *Archives of Microbiology* **132** (1), 47–50. DOI: 10.1007/BF00690816.

Huber, R., T. Wilharm, D. Huber, A. Trincone, S. Burggraf, H. König, R. Reinhard, I. Rockinger, H. Fricke, and K. O. Stetter (1992). *Aquifex pyrophilus* gen. nov. sp. nov., Represents a Novel Group of Marine Hyperthermophilic Hydrogen-Oxidizing Bacteria. *Systematic and Applied Microbiology* **15** (3), 340–351. DOI: http://dx.doi.org/10.1016/S0723-2020(11)80206-7.

Hügler, M. and S. M. Sievert (2011). Beyond the Calvin cycle: autotrophic carbon fixation in the ocean. *Annual Review of Marine Science* **3**, 261–289. DOI: 10.1146/annurev-marine-120709-142712.

Huguet, C., S. Fietz, and A. Rosell-Melé (2013). Global distribution patterns of hydroxy glycerol dialkyl glycerol tetraethers. *Organic Geochemistry* **57**, 107–118. DOI: 10.1016/j.orggeochem.2013.01.010.

Huguet, C., G. J. de Lange, Ö. Gustafsson, J. J. Middelburg, J. S. Sinninghe Damsté, and S. Schouten (2008). Selective preservation of soil organic matter in oxidized marine sediments (Madeira Abyssal Plain). *Geochimica et Cosmochimica Acta* **72** (24), 6061–6068. DOI: 10.1016/j.gca.2008.09.021.

Huguet, C., E. C. Hopmans, W. Febo-Ayala, D. H. Thompson, J. S. Sinninghe Damsté, and S. Schouten (2006). An improved method to determine the absolute abundance of glycerol dibiphytanyl glycerol tetraether lipids. *Organic Geochemistry* **37** (9), 1036–1041. DOI: 10.1016/j.orggeochem.2006.05.008.

Huguet, C., J.-H. Kim, G. J. de Lange, J. S. Sinninghe Damsté, and S. Schouten (2009). Effects of long term oxic degradation on the , TEX_{86} and BIT organic proxies. *Organic Geochemistry* **40** (12), 1188–1194. DOI: 10.1016/j.orggeochem.2009.09.003.

Huguet, C., A. Schimmelmann, R. Thunell, L. J. Lourens, J. S. Sinninghe Damsté, and S. Schouten (2007). A study of the TEX_{86} paleothermometer in the water column and sediments of the Santa Barbara Basin, California. *Paleoceanography* **22** (3), PA3203. DOI: 10.1029/2006PA001310.

Imhoff, J. and U. Bias-Imhoff (1995). Lipids, quinones and fatty acids of anoxygenic phototrophic bacteria. In: *Anoxygenic Photosynthetic Bacteria*. Ed. by R. Blankenship, M. Madigan, and C. Bauer. Dordrecht, The Netherlands: Kluwer Academic Publishers, pp. 179–205.

Inagaki, F., K. Hinrichs, and Y. Kubo (2013). the Expedition 337 Scientists: Deep coalbed biosphere off Shimokita-microbial processes and hydrocarbon system associated with deeply buried coalbed in the ocean. *IODP Prel Report* **337**.

Inagaki, F., T. Nunoura, S. Nakagawa, A. Teske, M. Lever, A. Lauer, M. Suzuki, K. Takai, M. Delwiche, F. S. Colwell, K. H. Nealson, K. Horikoshi, S. D'Hondt, and B. B. Jørgensen (2006). Biogeographical distribution and diversity of microbes in methane hydrate-bearing deep marine sediments on the Pacific Ocean Margin. *Proceedings of the National Academy of Sciences of the United States of America* **103** (8), 2815–2820. DOI: 10.1073/pnas.0511033103.

Ingalls, A. E., C. Huguet, and L. T. Truxal (2012). Distribution of intact and core membrane lipids of archaeal glycerol dialkyl glycerol tetraethers among size-fractionated particulate organic matter in Hood Canal, Puget Sound. *Applied and Environmental Microbiology* **78** (5), 1480–1490. DOI: 10.1128/AEM.07016-11.

Ingalls, A. E., S. R. Shah, R. L. Hansman, L. I. Aluwihare, G. M. Santos, E. R. M. Druffel, and A. Pearson (2006). Quantifying archaeal community autotrophy in the mesopelagic ocean using natural radiocarbon. *Proceedings of the National Academy of Sciences of the United States of America* **103** (17), 6442–6447. DOI: 10.1073/pnas.0510157103.

IPCC (2014). *Climate Change 2014: Impacts, Adaptation, and Vulnerability. Part A: Global and Sectoral Aspects. Contribution of Working Group II to the Fifth Assessment Report of the Intergovernmental Panel on Climate Change [Field, C.B., V.R. Barros, D.J. Dokken, K.J.* Cambridge, United Kingdom and New York, NY, USA: Cambridge University Press, p. 1132.

Iverson, V., R. M. Morris, C. D. Frazar, C. T. Berthiaume, R. L. Morales, and E. V. Armbrust (2012). Untangling genomes from metagenomes: revealing an uncultured class of marine Euryarchaeota. *Science* **335** (6068), 587–590. DOI: 10.1126/science.1212665.

Iwasaki, M. and A. Hiraishi (1998). A New Approach to Numerical Analyses of Microbial Quinone Profiles in the Environment. *Microbes and Environments* **13** (2), 67–76. DOI: 10.1264/jsme2.13.67.

Jaeschke, A., C. Rooks, M. Trimmer, J. C. Nicholls, E. C. Hopmans, S. Schouten, and J. S. Sinninghe Damsté (2009). Comparison of ladderane phospholipid and core lipids as indicators for anaerobic ammonium oxidation (anammox) in marine sediments. *Geochimica et Cosmochimica Acta* **73** (7), 2077–2088. DOI: 10.1016/j.gca.2009.01.013.

Jahn, U., R. Summons, H. Sturt, E. Grosjean, and H. Huber (2004). Composition of the lipids of *Nanoarchaeum equitans* and their origin from its host *Ignicoccus* sp. strain KIN4/I. *Archives of Microbiology* **182** (5), 404–413. DOI: 10.1007/s00203-004-0725-x.

Jannasch, H. W., C. O. Wirsen, and S. J. Molyneaux (1991). Chemoautotrophic sulfur-oxidizing bacteria from the Black Sea. *Deep Sea Research Part A. Oceanographic Research Papers* **38**, S1105–S1120. DOI: 10.1016/S0198-0149(10)80026-3.

Jannasch, H. W. (1991). Microbial Processes in the Black Sea Water Column and Top Sediment: An Overview. In: *Black Sea Oceanography*. Ed. by E. Ä°zdar and J. W. Murray. Dordrecht, The Netherlands: Springer, pp. 271–286. DOI: 10.1007/978-94-011-2608-3.

Jensen, M. M., M. M. M. Kuypers, G. Lavik, and B. Thamdrup (2008). Rates and regulation of anaerobic ammonium oxidation and denitrification in the Black Sea. *Limnology and Oceanography* **53** (1), 23–36. DOI: 10.4319/lo.2008.53.1.0023.

Jones, W. J. and G. U. Holzer (1991). The Polar and Neutral Lipid Composition of Methanosphaera stadtmanae. *Systematic and Applied Microbiology* **14** (2), 130–134. DOI: http://dx.doi.org/10.1016/S0723-2020(11)80290-0.

Jongsma, D., A. R. Fortuin, W. Huson, S. R. Troelstra, G. T. Klaver, J. M. Peters, D. van Harten, G. J. de Lange, and L. ten Haven (1983). Discovery of an anoxic basin within the Strabo Trench, eastern Mediterranean. *Nature* **305** (5937), 795–797. DOI: 10.1038/305795a0.

Jørgensen, B. B. (1990). A thiosulfate shunt in the sulfur cycle of marine sediments. *Science* **249** (4965), 152–154. DOI: 10.1126/science.249.4965.152.

Jørgensen, B. B. and A. Boetius (2007). Feast and famine–microbial life in the deep-sea bed. *Nature reviews. Microbiology* **5** (10), 770–81. DOI: 10.1038/nrmicro1745.

Jørgensen, B. B., M. E. Böttcher, H. Lüschen, L. N. Neretin, and I. I. Volkov (2004). Anaerobic methane oxidation and a deep H_2S sink generate isotopically heavy sulfides in Black Sea sediments. *Geochimica et Cosmochimica Acta* **68** (9), 2095–2118. DOI: 10.1016/j.gca.2003.07.017.

Jørgensen, B. B., H. Fossing, C. O. Wirsen, and H. W. Jannasch (1991). Sulfide oxidation in the anoxic Black Sea chemocline. *Deep Sea Research Part A. Oceanographic Research Papers* **38**, S1083–S1103. DOI: 10.1016/S0198-0149(10)80025-1.

Jørgensen, B. B., A. Weber, and J. Zopfi (2001). Sulfate reduction and anaerobic methane oxidation in Black Sea sediments. *Deep Sea Research Part I: Oceanographic Research Papers* **48**, 2097–2120. DOI: 10.1016/S0967-0637(01)00007-3.

Jørgensen, S. L., B. Hannisdal, A. Lanzén, T. Baumberger, K. Flesland, R. Fonseca, L. Øvreås, I. H. Steen, I. H. Thorseth, R. B. Pedersen, and C. Schleper (2012). Correlating microbial community profiles with geochemical data in highly stratified sediments from the Arctic Mid-Ocean Ridge. *Proceedings of the National Academy of Sciences of the United States of America* **109** (42), 2846–2855. DOI: 10.1073/pnas.1207574109.

Kaiser, P., R. Geyer, P. Surmann, and H. Fuhrmann (2012). LC-MS method for screening unknown microbial carotenoids and isoprenoid quinones. *Journal of Microbiological Methods* **88** (1), 28–34. DOI: 10.1016/j.mimet.2011.10.001.

Kamekura, M. and M. Kates (1999). Structural diversity of lipids in members of Halobacteriaceae. *Bioscience, Biotechnology, and Biochemistry* **63** (6), 969–972.

Kamio, Y., S. Kanegasaki, and H. Takahashi (1969). Occurrence of plasmalogens bacteria in anaerobic. *The Journal of General and Applied Microbiology* **15** (4), 439–451. DOI: 10.2323/jgam.15.439.

Karl, D. M. and G. A. Knauer (1991). Microbial production and particle flux in the upper 350 m of the Black Sea. *Deep Sea Research Part A. Oceanographic Research Papers* **38**, S921–S942. DOI: 10.1016/S0198-0149(10)80017-2.

Karner, M. B., E. F. DeLong, and D. M. Karl (2001). Archaeal dominance in the mesopelagic zone of the Pacific Ocean. *Nature* **409** (6819), 507–510. DOI: 10.1038/35054051.

Karstensen, J., L. Stramma, and M. Visbeck (2008). Oxygen minimum zones in the eastern tropical Atlantic and Pacific oceans. *Progress in Oceanography* **77** (4), 331–350. DOI: 10.1016/j.pocean.2007.05.009.

Kastens, K. A. and F. N. Spiess (1984). Dissolution and collapse features on the eastern Mediterranean Ridge. *Marine Geology* **56** (1â€“4), 181–193. DOI: http://dx.doi.org/10.1016/0025-3227(84)90012-4.

Kates, M., M. K. Wassef, and D. J. Kushner (1968). Radioisotopic studies on the biosynthesis of the glyceryl diether lipids of Halobacterium cutirubrum. *Canadian Journal of Biochemistry* **46** (8), 971–977. DOI: 10.1139/o68-145.

Kates, M., L. S. Yengoyan, and P. S. Sastry (1965). A diether analog of phosphatidyl glycerophosphate in Halobacterium cutirubrum. *Biochimica et Biophysica Acta (BBA) - Lipids and Lipid Metabolism* **98** (2), 252–268. DOI: http://dx.doi.org/10.1016/0005-2760(65)90119-0.

Kates, M. (1993a). Biology of halophilic bacteria, Part II – Membrane lipids of extreme halophiles: biosynthesis, function and evolutionary significance. *Experientia* **49** (12). Ed. by M. Kates D. J. Kushner and A. T. Matheson, 1027–1036. DOI: 10.1007/BF01929909.

Kates, M. (1993b). Membrane lipids of archaea. In: *The Biochemistry of Archaea (Archaebacteria)*. Ed. by M. Kates D. J. Kushner and A. T. Matheson. Amsterdam, The Netherlands: Elsevier Science, pp. 261–295.

Kato, M., M. Sakai, K. Adachi, H. Ikemoto, and H. Sano (1996). Distribution of betaine lipids in marine algae. *Phytochemistry* **42** (5), 1341–1345. DOI: 10.1016/0031-9422(96)00115-X.

Kawahara, K., H. Kuraishi, and U. Zähringer (1999). Chemical structure and function of glycosphingolipids of *Sphingomonas* spp and their distribution among members of the α-4 subclass of Proteobacteria. English. *Journal of Industrial Microbiology and Biotechnology* **23** (4-5), 408–413. DOI: 10.1038/sj.jim.2900708.

Keeling, R. E., A. Körtzinger, and N. Gruber (2010). Ocean deoxygenation in a warming world. *Annual review of marine science* **2**, 199–229. DOI: 10.1146/annurev.marine.010908.163855.

Keller, M., F. J. Braun, R. Dirmeier, D. Hafenbradl, S. Burggraf, R. Rachel, and K. O. Stetter (1995). *Thermococcus alcaliphilus* sp. nov., a new hyperthermophilic archaeum growing on polysulfide at alkaline pH. *Archives of Microbiology* **164** (6), 390–395. DOI: 10.1007/BF02529736.

Kellermann, M. Y. (2012). "Lipid biomolecules reveal patterns of microbial metabolism in extreme environments". PhD Thesis. University of Bremen.

Kelley, D. S., J. A. Baross, and J. R. Delaney (2002). Volcanoes, fluids, and life at mid-ocean ridge spreading centers. *Annual Review of Earth and Planetary Sciences* **30** (1), 385–491. DOI: 10.1146/annurev.earth.30.091201.141331.

Kendall, M. and D. Boone (2006). The order Methanosarcinales. In: *The Prokaryotes, Volume 3: Archaea. Bacteria: Firmicutes, Actinomycetes*. Ed. by M. Dworkin, S. Falkow, E. Rosenberg, K.-H. Schleifer, and E. Stackebrandt. New York, USA: Springer, pp. 244–256.

Killops, S. D. and V. J. Killops (2013). *Introduction to organic geochemistry*. John Wiley & Sons.

Kim, J.-H., C. Huguet, K. A. F. Zonneveld, G. J. M. Versteegh, W. Roeder, J. S. Sinninghe Damsté, and S. Schouten (2009). An experimental field study to test the stability of lipids used for the TEX_{86} and $U^{K'}_{37}$ palaeothermometers. *Geochimica et Cosmochimica Acta* **73** (10), 2888–2898. DOI: 10.1016/j.gca.2009.02.030.

Kim, J.-H., S. Schouten, E. C. Hopmans, B. Donner, and J. S. Sinninghe Damsté (2008). Global sediment core-top calibration of the TEX_{86} paleothermometer in the ocean. *Geochimica et Cosmochimica Acta* **72** (4), 1154–1173. DOI: 10.1016/j.gca.2007.12.010.

Kim, J.-H., J. van der Meer, S. Schouten, P. Helmke, V. Willmott, F. Sangiorgi, N. Koç, E. C. Hopmans, and J. S. Sinninghe Damsté (2010). New indices and calibrations derived from the distribution of crenarchaeal isoprenoid tetraether lipids: Implications for past sea surface temperature reconstructions. *Geochimica et Cosmochimica Acta* **74** (16), 4639–4654. DOI: 10.1016/j.gca.2010.05.027.

Kim, K. C., Y. Kamio, and H. Takahashi (1970). Glyceryl ether phospholipid in anaerobic bacteria. *The Journal of General and Applied Microbiology* **16** (4), 321–325. DOI: 10.2323/jgam.16.4_321.

Knab, N. J., B. A. Cragg, E. R. C. Hornibrook, L. Holmkvist, R. D. Pancost, C. Borowski, R. J. Parkes, and B. B. Jorgensen (2009). Regulation of anaerobic methane oxidation in sediments of the Black Sea. *Biogeosciences* **6**, 1505–1518. DOI: 10.5194/bgd-5-2305-2008.

Knappy, C. S. and B. J. Keely (2012). Novel glycerol dialkanol triols in sediments: transformation products of glycerol dibiphytanyl glycerol tetraether lipids or biosynthetic intermediates? *Chemical Communications* **48** (6), 841–843. DOI: 10.1039/c1cc15841d.

Knappy, C. S., C. E. M. Nunn, H. W. Morgan, and B. J. Keely (2011). The major lipid cores of the archaeon Ignisphaera aggregans: implications for the phylogeny and biosynthesis of glycerol monoalkyl glycerol tetraether isoprenoid lipids. *Extremophiles* **15** (4), 517–528. DOI: 10.1007/s00792-011-0382-3.

Knappy, C. S., J. P. J. Chong, and B. J. Keely (2009). Rapid discrimination of archaeal tetraether lipid cores by liquid chromatography-tandem mass spectrometry. *Journal of the American Society for Mass Spectrometry* **20** (1), 51–59. DOI: 10.1016/j.jasms.2008.09.015.

Knappy, C., P. Yao, M. Pickering, and B. Keely (2014). Identification of homoglycerol- and dihomoglycerol-containing isoprenoid tetraether lipid cores in aquatic sediments and a soil. *Organic Geochemistry* **76**, 146–156. DOI: 10.1016/j.orggeochem.2014.06.003.

Knudsen, E., E. Jantzen, K. Bryn, J. G. Ormerod, and R. Sirevåg (1982). Quantitative and structural characteristics of lipids in *Chlorobium* and *Chloroflexus*. *Archives of Microbiology* **132** (2), 149–154. DOI: 10.1007/BF00508721.

Koga, Y. and H. Morii (2005). Recent advances in structural research on ether lipids from Archaea including comparative and physiological aspects. *Bioscience, Biotechnology, and Biochemistry* **69** (11), 2019–2034. DOI: 10.1271/bbb.69.2019.

Koga, Y. (2011). Early evolution of membrane lipids: how did the lipid divide occur? *Journal of Molecular Evolution* **72** (3), 274–282. DOI: 10.1007/s00239-011-9428-5.

Koga, Y., M. Akagawa-Matsushita, M. Ohga, and M. Nishihara (1993a). Taxonomic significance of the distribution of component parts of polar ether lipids in methanogens. *Systematic and Applied Microbiology* **16** (3), 342–351. DOI: 10.1016/S0723-2020(11)80264-X.

Koga, Y., H. Morii, M. Akagawa-Matsushita, and M. Oohga (1998). Correlation of Polar Lipid Composition with 16S rRNA Phylogeny in Methanogens. Further Analysis of Lipid Component Parts. *Bioscience, Biotechnology, and Biochemistry* **62** (2), 230–236. DOI: 10.1271/bbb.62.230.

Koga, Y., M. Nishihara, H. Morii, and M. Akagawa-Matsushita (1993b). Ether polar lipids of methanogenic bacteria: structures, comparative aspects, and biosyntheses. *Microbiological Reviews* **57** (1), 164–182.

Komatsu, H. and P. L. G. Chong (1998). Low permeability of liposomal membranes composed of bipolar tetraether lipids from thermoacidophilic archaebacterium *Sulfolobus acidocaldarius*. *Biochemistry* **37** (97), 107–115. DOI: 10.1021/bi972163e.

Könneke, M., A. E. Bernhard, J. R. de la Torre, C. B. Walker, J. B. Waterbury, and D. A. Stahl (2005). Isolation of an autotrophic ammonia-oxidizing marine archaeon. *Nature* **437** (7058), 543–546. DOI: 10.1038/nature03911.

Könneke, M., J. S. Lipp, and K.-U. Hinrichs (2012). Carbon isotope fractionation by the marine ammonia-oxidizing archaeon *Nitrosopumilus maritimus*. *Organic Geochemistry* **48**, 21–24. DOI: 10.1016/j.orggeochem.2012.04.007.

Könneke, M., D. M. Schubert, P. C. Brown, M. Hügler, S. Standfest, T. Schwander, L. Schada von Borzyskowski, T. J. Erb, D. A. Stahl, and I. A. Berg (2014). Ammonia-oxidizing archaea use the most energy-efficient aerobic pathway for CO_2 fixation. *Proceedings of the National Academy of Sciences of the United States of America* **111** (22), 8239–8244. DOI: 10.1073/pnas.1402028111.

Konovalov, S. K., G. W. I. Luther, G. E. Friederich, D. B. Nuzzio, B. M. Tebo, J. W. Murray, T. Oguz, B. Glazer, and R. E. Trouwborst (2003). Lateral injection of oxygen with the Bosporus plume-fingers of oxidizing potential in the Black Sea. *Limnology and Oceanography* **48** (6), 2369–2376. DOI: 10.4319/lo.2003.48.6.2369.

Konovalov, S., J. Murray, and G. Luther (2005). Basic Processes of Black Sea Biogeochemistry. *Oceanography* **18** (2), 24–35. DOI: 10.5670/oceanog.2005.39.

Konovalov, S., A. Samodurov, T. Oguz, and L. Ivanov (2004). Parameterization of iron and manganese cycling in the Black Sea suboxic and anoxic environment. *Deep-Sea Research Part I: Oceanographic Research Papers* **51**, 2027–2045. DOI: 10.1016/j.dsr.2004.08.005.

Koonin, E. V., K. S. Makarova, and L. Aravind (2001). Horizontal gene transfer in prokaryotes: quantification and classification. *Annual Review of Microbiology* **55**, 709–742. DOI: 10.1146/annurev.micro.55.1.709.

Kröger, A. and V. Dadák (1969). On the Role of Quinones in Bacterial Electron Transport. The Respiratory System of *Bacillus megaterium*. *European Journal of Biochemistry* **11** (2), 328–340. DOI: 10.1111/j.1432-1033.1969.tb00776.x.

Krumholz, L. R., J. P. McKinley, G. A. Ulrich, and J. M. Suflita (1997). Confined subsurface microbial communities in Cretaceous rock. *Nature* **386** (6620), 64–66. DOI: 10.1038/386064a0.

Krümmel, A. and H. Harms (1982). Effect of organic matter on growth and cell yield of ammonia-oxidizing bacteria. *Archives of Microbiology* **133** (1), 50–54. DOI: 10.1007/BF00943769.

Kulichevskaya, I. S., A. A. Ivanova, E. N. Detkova, W. I. C. Rijpstra, J. S. Sinninghe Damsté, and S. N. Dedysh (2015). *Planctomicrobium piriforme* gen. nov., sp. nov., a Stalked Planctomycete from a Littoral Wetland of a Boreal Lake. *International Journal of Systematic and Evolutionary Microbiology*. DOI: 10.1099/ijs.0.000154.

Kulichevskaya, I. S., A. O. Ivanova, O. I. Baulina, P. L. E. Bodelier, J. S. S. Damsté, and S. N. Dedysh (2008). *Singulisphaera acidiphila* gen. nov., sp. nov., a non-filamentous, *Isosphaera*-like planctomycete from acidic northern wetlands. *International Journal of Systematic and Evolutionary Microbiology* **58** (5), 1186–1193. DOI: 10.1099/ijs.0.65593-0.

Kulichevskaya, I. S., A. O. Ivanova, S. E. Belova, O. I. Baulina, P. L. E. Bodelier, W. I. C. Rijpstra, J. S. Sinninghe Damsté, G. A. Zavarzin, and S. N. Dedysh (2007). *Schlesneria paludicola* gen. nov., sp. nov., the first acidophilic member of the order Planctomycetales, from *Sphagnum*-dominated

boreal wetlands. *International Journal of Systematic and Evolutionary Microbiology* **57** (11), 2680–2687. DOI: 10.1099/ijs.0.65157-0.

Kunihiro, T., B. Veuger, D. Vasquez-Cardenas, L. Pozzato, M. Le Guitton, K. Moriya, M. Kuwae, K. Omori, H. T. S. Boschker, and D. van Oevelen (2014). Phospholipid-derived fatty acids and quinones as markers for bacterial biomass and community structure in marine sediments. *PloS One* **9** (4), e96219. DOI: 10.1371/journal.pone.0096219.

Kushwaha, S. C., M. Kates, G. Juez, F. Rodriguez-Valera, and D. J. Kushner (1982). Polar lipids of an extremely halophilic bacterial strain (R-4) isolated from salt ponds in Spain. *Biochimica et Biophysica Acta (BBA) - Lipids and Lipid Metabolism* **711** (1), 19–25. DOI: http://dx.doi.org/10.1016/0005-2760(82)90004-2.

Kuypers, M. M., P. Blokker, J. Erbacher, H. Kinkel, R. D. Pancost, S. Schouten, and J. S. Sinninghe Damsté (2001). Massive expansion of marine archaea during a mid-Cretaceous oceanic anoxic event. *Science* **293** (5527), 92–95. DOI: 10.1126/science.1058424.

Kuypers, M. M. M., P. Blokker, E. C. Hopmans, H. Kinkel, R. D. Pancost, S. Schouten, and J. S. Sinninghe Damsté (2002). Archaeal remains dominate marine organic matter from the early Albian oceanic anoxic event 1b. *Palaeogeography, Palaeoclimatology, Palaeoecology* **185** (1-2), 211–234. DOI: 10.1016/S0031-0182(02)00301-2.

Kuypers, M. M. M., G. Lavik, D. Woebken, M. Schmid, B. M. Fuchs, R. Amann, B. B. Jørgensen, and M. S. M. Jetten (2005). Massive nitrogen loss from the Benguela upwelling system through anaerobic ammonium oxidation. *Proceedings of the National Academy of Sciences of the United States of America of the United States of America* **102** (18), 6478–6483. DOI: 10.1073/pnas.0502088102.

Kuypers, M. M. M., A. O. Sliekers, G. Lavik, M. Schmid, B. B. Jørgensen, J. G. Kuenen, J. S. Sinninghe Damsté, M. Strous, and M. S. M. Jetten (2003). Anaerobic ammonium oxidation by anammox bacteria in the Black Sea. *Nature* **422**, 608–611. DOI: 10.1038/nature01472.

Kvenvolden, K. A. and T. J. McDonald (1986). *Organic Geochemistry on JOIDES Resolution - An essay*. College Station, TX, United States: Ocean Drilling Program, Texas A&M University, p. 97. DOI: 10.2973/odp.tn.6.1986.

Kwiecien, O., H. W. Arz, F. Lamy, S. Wulf, A. Bahr, U. Röhl, and G. H. Haug (2008). Estimated reservoir ages of the Black Sea since the last glacial. *Radiocarbon* **50** (1), 99–118.

La Cono, V., F. Smedile, G. Bortoluzzi, E. Arcadi, G. Maimone, E. Messina, M. Borghini, E. Oliveri, S. Mazzola, S. L'Haridon, L. Toffin, L. Genovese, M. Ferrer, L. Giuliano, P. N. Golyshin, and M. M. Yakimov (2011). Unveiling microbial life in new deep-sea hypersaline Lake Thetis. Part I: Prokaryotes and environmental settings. *Environmental Microbiology* **13** (8), 2250–2268. DOI: 10.1111/j.1462-2920.2011.02478.x.

Lam, P., M. M. Jensen, G. Lavik, D. F. McGinnis, B. Müller, C. J. Schubert, R. Amann, B. Thamdrup, and M. M. M. Kuypers (2007). Linking crenarchaeal and bacterial nitrification to anammox in the Black Sea. *Proceedings of the National Academy of Sciences of the United States of America* **104** (17), 7104–7109. DOI: 10.1073/pnas.0611081104.

Langworthy, T. A. (1977). Long-chain diglycerol tetraethers from *Thermoplasma acidophilum*. *Biochimica et Biophysics Acta* **487**, 37–50.

Langworthy, T. A. (1982). Lipids of bacteria living in extreme environments. In: *Current Topics in Membranes and Transport, Membrane lipids of prokaryotes 17*. Ed. by S. Razin and S. Rottem. Academic press, pp. 45–77.

Langworthy, T. A., W. R. Mayberry, and P. F. Smith (1974). Long-chain glycerol diether and polyol dialkyl glycerol triether lipids of *Sulfolobus acidocaldarius*. *Journal of Bacteriology* **119** (1), 106–116.

Langworthy, T. A., P. F. Smith, and W. R. Mayberry (1972). Lipids of Thermoplasma acidophilum. *Journal of Bacteriology* **112** (3), 1193–2000.

Langworthy, T. A. Langworthy, G. Holzer, J. G. Zeikus, and T. G. Tornabene (1983). Iso- and Anteiso-Branched Glycerol Diethers of the Thermophilic Anaerobe *Thermodesulfotobacterium commune*. *Systematic and Applied Microbiology* **4** (1), 1–17.

LaRock, P. A., R. D. Lauer, J. R. Schwarz, K. K. Watanabe, and D. A. Wiesenburg (1979). Microbial Biomass and Activity Distribution in an Anoxic, Hypersaline Basin. *Applied and Environmental Microbiology* **37** (3), 466–470.

Lavik, G., T. Stührmann, V. Brüchert, A. Van der Plas, V. Mohrholz, P. Lam, M. Mussmann, B. M. Fuchs, R. Amann, U. Lass, and M. M. M. Kuypers (2009). Detoxification of sulphidic African shelf waters by blooming chemolithotrophs. *Nature* **457** (7229), 581–584. DOI: 10.1038/nature07588.

Lee, K. E., J.-H. Kim, I. Wilke, P. Helmke, and S. Schouten (2008). A study of the alkenone, TEX_{86}, and planktonic foraminifera in the Benguela Upwelling System: Implications for past sea surface temperature estimates. *Geochemistry, Geophysics, Geosystems* **9** (10), Q10019. DOI: 10.1029/2008GC002056.

Lehtovirta-Morley, L. E., D. T. Verhamme, G. W. Nicol, and J. I. Prosser (2013). Effect of nitrification inhibitors on the growth and activity of *Nitrosotalea devanaterra* in culture and soil. *Soil Biology and Biochemistry* **62**, 129–133. DOI: 10.1016/j.soilbio.2013.01.020.

Leider, A., K.-U. Hinrichs, G. Mollenhauer, and G. J. M. Versteegh (2010). Core-top calibration of the lipid-based $U^{K'}_{37}$ and TEX_{86} temperature proxies on the southern Italian shelf (SW Adriatic Sea, Gulf of Taranto). *Earth and Planetary Science Letters* **300** (1-2), 112–124. DOI: 10.1016/j.epsl.2010.09.042.

Leloup, J., A. Loy, N. J. Knab, C. Borowski, M. Wagner, and B. B. Jørgensen (2007). Diversity and abundance of sulfate-reducing microorganisms in the sulfate and methane zones of a marine sediment, Black Sea. *Environmental Microbiology* **9**, 131–142. DOI: 10.1111/j.1462-2920.2006.01122.x.

Lever, M. A. (2013). Functional gene surveys from ocean drilling expeditions - a review and perspective. *FEMS Microbiology Ecology* **84** (1), 1–23. DOI: 10.1111/1574-6941.12051.

Lewis, B. and W. Landing (1991). The biogeochemistry of manganese and iron in the Black Sea. *Deep Sea Research Part A. Oceanographic Research Papers* **38**, S773–S803. DOI: 10.1016/S0198-0149(10)80009-3.

Lin, L.-H., J. Hall, J. Lippmann-Pipke, J. A. Ward, B. Sherwood Lollar, M. DeFlaun, R. Rothmel, D. Moser, T. M. Gihring, B. Mislowack, and T. C. Onstott (2005). Radiolytic H_2 in continental crust: Nuclear power for deep subsurface microbial communities. *Geochemistry, Geophysics, Geosystems* **6** (7), n/a–n/a. DOI: 10.1029/2004GC000907.

Lin, X., S. G. Wakeham, I. F. Putnam, Y. M. Astor, M. I. Scranton, A. Y. Chistoserdov, and G. T. Taylor (2006). Comparison of vertical distributions of prokaryotic assemblages in the anoxic Cariaco Basin and Black Sea by use of fluorescence in situ hybridization. *Applied and Environmental Microbiology* **72** (4), 2679–2690. DOI: 10.1128/AEM.72.4.2679-2690.2006.

Lin, Y.-S., V. B. Heuer, T. Goldhammer, M. Y. Kellermann, M. Zabel, and K.-U. Hinrichs (2012). Towards constraining H2 concentration in subseafloor sediment: A proposal for combined analysis by two distinct approaches. *Geochimica et Cosmochimica Acta* **77**, 186–201. DOI: 10.1016/j.gca.2011.11.008.

Lin, Y.-S., J. S. Lipp, M. Y. Yoshinaga, S.-H. Lin, M. Elvert, and K.-U. Hinrichs (2010). Intramolecular stable carbon isotopic analysis of archaeal glycosyl tetraether lipids. *Rapid Communications in Mass Spectrometry* **24** (19), 2817–2826. DOI: 10.1002/rcm.4707.

Lincoln, S. A., B. Wai, J. M. Eppley, M. J. Church, R. E. Summons, and E. F. DeLong (2014a). Planktonic Euryarchaeota are a significant source of archaeal tetraether lipids in the ocean. *Proceedings of the National Academy of Sciences of the United States of America* **111** (27), 9858–9863. DOI: 10.1073/pnas.1409439111.

Lincoln, S. A., B. Wai, J. M. Eppley, M. J. Church, R. E. Summons, and E. F. DeLong (2014b). Reply to Schouten et al.: Marine Group II planktonic Euryarchaeota are significant contributors to tetraether lipids in the ocean. *Proceedings of the National Academy of Sciences of the United States of America* **111** (41), 4286. DOI: 10.1073/pnas.1416736111.

Lipp, J. S. and K.-U. Hinrichs (2009). Structural diversity and fate of intact polar lipids in marine sediments. *Geochimica et Cosmochimica Acta* **73** (22), 6816–6833. DOI: 10.1016/j.gca.2009.08.003.

Lipp, J. S., Y. Morono, F. Inagaki, and K.-U. Hinrichs (2008). Significant contribution of Archaea to extant biomass in marine subsurface sediments. *Nature* **454** (7207), 991–994. DOI: 10.1038/nature07174.

Litchfield, C. D. (1998). Survival strategies for microorganisms in hypersaline environments and their relevance to life on early Mars. *Meteoritics & Planetary Science* **33** (4), 813–819. DOI: 10.1111/j.1945-5100.1998.tb01688.x.

Liu, X.-L. (2011). "Glycerol ether lipids in sediments: sources, diversity and implications". PhD Thesis. University of Bremen.

Liu, X.-L., A. Leider, A. Gillespie, J. Gröger, G. J. Versteegh, and K.-U. Hinrichs (2010). Identification of polar lipid precursors of the ubiquitous branched GDGT orphan lipids in a peat bog in Northern Germany. *Organic Geochemistry* **41** (7), 653–660. DOI: 10.1016/j.orggeochem.2010.04.004.

Liu, X.-L., J. S. Lipp, J. M. Schröder, R. E. Summons, and K.-U. Hinrichs (2012a). Isoprenoid glycerol dialkanol diethers: A series of novel archaeal lipids in marine sediments. *Organic Geochemistry* **43**, 50–55. DOI: 10.1016/j.orggeochem.2011.11.002.

Liu, X.-L., J. S. Lipp, J. H. Simpson, Y.-S. Lin, R. E. Summons, and K.-U. Hinrichs (2012b). Mono- and dihydroxyl glycerol dibiphytanyl glycerol tetraethers in marine sediments: Identification of both core and intact polar lipid forms. *Geochimica et Cosmochimica Acta* **89**, 102–115. DOI: 10.1016/j.gca.2012.04.053.

Liu, X., J. S. Lipp, and K.-U. Hinrichs (2011). Distribution of intact and core GDGTs in marine sediments. *Organic Geochemistry* **42** (4), 368–375. DOI: 10.1016/j.orggeochem.2011.02.003.

Liu, X.-L., R. E. Summons, and K.-U. Hinrichs (2012c). Extending the known range of glycerol ether lipids in the environment: structural assignments based on tandem mass spectral fragmentation patterns. *Rapid Communications in Mass Spectrometry* **26** (19), 2295–2302. DOI: 10.1002/rcm.6355.

Liu, X.-L., C. Zhu, S. G. Wakeham, and K.-U. Hinrichs (2014). In situ production of branched glycerol dialkyl glycerol tetraethers in anoxic marine water columns. *Marine Chemistry* **166**, 1–8. DOI: 10.1016/j.marchem.2014.08.008.

Liu, Y. and W. B. Whitman (2008). Metabolic, phylogenetic, and ecological diversity of the methanogenic archaea. *Annals of the New York Academy of Sciences* **1125**, 171–189. DOI: 10.1196/annals.1419.019.

Lloyd, K. G., M. K. May, R. T. Kevorkian, and A. D. Steen (2013). Meta-analysis of quantification methods shows that archaea and bacteria have similar abundances in the subseafloor. *Applied and Environmental Microbiology* **79** (24), 7790–7799. DOI: 10.1128/AEM.02090-13.

Loffeld, B. and H. Keweloh (1996). *cis/trans* isomerization of unsaturated fatty acids as possible control mechanism of membrane fluidity in *Pseudomonas putida* P8. *Lipids* **31** (8), 811–815.

Logemann, J., J. Graue, J. Köster, B. Engelen, J. Rullkötter, and H. Cypionka (2011). A laboratory experiment of intact polar lipid degradation in sandy sediments. *Biogeosciences* **8** (9), 2547–2560. DOI: 10.5194/bg-8-2547-2011.

Lombard, J., P. López-García, and D. Moreira (2012). An ACP-independent fatty acid synthesis pathway in Archaea: implications for the origin of phospholipids. *Molecular Biology and Evolution* **29** (11), 3261–3265. DOI: 10.1093/molbev/mss160.

Londry, K. L., K. G. Dawson, H. D. Grover, R. E. Summons, and A. S. Bradley (2008). Stable carbon isotope fractionation between substrates and products of *Methanosarcina barkeri*. *Organic Geochemistry* **39** (5), 608–621. DOI: 10.1016/j.orggeochem.2008.03.002.

Lopes dos Santos, R. a., M. I. Spooner, T. T. Barrows, P. De Deckker, J. S. Sinninghe Damsté, and S. Schouten (2013). Comparison of organic ($U^{K'}_{37}$, TEX^{H}_{86} , LDI) and faunal proxies (foraminiferal assemblages) for reconstruction of late Quaternary sea surface temperature variability from offshore southeastern Australia. *Paleoceanography* **28** (3), 377–387. DOI: 10.1002/palo.20035.

López, J. F. and J. O. Grimalt (2004). Phenyl- and cyclopentylimino derivatization for double bond location in unsaturated C_{37}-C_{40} alkenones by GC-MS. *Journal of the American Society for Mass Spectrometry* **15** (8), 1161–72. DOI: 10.1016/j.jasms.2004.04.024.

López-García, P. and D. Moreira (2008). Tracking microbial biodiversity through molecular and genomic ecology. *Research in Microbiology* **159** (1), 67–73. DOI: http://dx.doi.org/10.1016/j.resmic.2007.11.019.

López-Lara, I. M., C. Sohlenkamp, and O. Geiger (2003). Membrane Lipids in Plant-Associated Bacteria: Their Biosyntheses and Possible Functions. *Molecular Plant-Microbe Interactions* **16** (7), 567–579. DOI: 10.1094/MPMI.2003.16.7.567.

Madigan, M. T., J. M. Martinko, and J. Parker (2011). *Brock Biology of Microorganisms*. Upper Saddle River, NJ: Pearson Education.

Makula, R. A. and W. R. Finnerty (1975). Isolation and characterization of an ornithine-containing lipid from *Desulfovibrio gigas*. *Journal of Bacteriology* **123** (2), 523–529.

Makula, R. A. (1978). Phospholipid composition of methane-utilizing bacteria. *Journal of Bacteriology* **134** (3), 771–777.

Mancuso, C. A., G. Odham, G. Westerdahl, J. N. Reeve, and D. C. White (1985). C_{15}, C_{20}, and C_{25} isoprenoid homologues in glycerol diether phospholipids of methanogenic archaebacteria. *Journal of Lipid Research* **26** (9), 1120–1125.

Manske, A. K., J. Glaeser, M. M. M. Kuypers, and J. Overmann (2005). Physiology and phylogeny of green sulfur bacteria forming a monospecific phototrophic assemblage at a depth of 100 meters in the Black Sea. *Applied and Environmental Microbiology* **71** (12), 8049–8060. DOI: 10.1128/AEM.71.12.8049-8060.2005.

Marschall, E., M. Jogler, U. Henßge, and J. Overmann (2010). Large-scale distribution and activity patterns of an extremely low-light-adapted population of green sulfur bacteria in the Black Sea. *Environmental Microbiology* **12** (5), 1348–1362. DOI: 10.1111/j.1462-2920.2010.02178.x.

Martens-Habbena, W., P. M. Berube, H. Urakawa, J. R. de la Torre, and D. A. Stahl (2009). Ammonia oxidation kinetics determine niche separation of nitrifying Archaea and Bacteria. *Nature* **461** (7266), 976–979. DOI: 10.1038/nature08465.

Martin, W. F. (2012). Hydrogen, metals, bifurcating electrons, and proton gradients: the early evolution of biological energy conservation. *FEBS Letters* **586** (5), 485–493. DOI: 10.1016/j.febslet.2011.09.031.

Mathai, J. C., G. D. Sprott, and M. L. Zeidel (2001). Molecular mechanisms of water and solute transport across archaebacterial lipid membranes. *The Journal of Biological Chemistry* **276** (29), 27266–27271. DOI: 10.1074/jbc.M103265200.

Mauclaire, L., K. Zepp, P. Meister, and J. McKenzie (2004). Direct in situ detection of cells in deep-sea sediment cores from the Peru Margin (ODP Leg 201, Site 1229). *Geobiology* **2** (4), 217–223. DOI: 10.1111/j.1472-4677.2004.00035.x.

McCollom, T. M. and E. L. Shock (1997). Geochemical constraints on chemolithoautotrophic metabolism by microorganisms in seafloor hydrothermal systems. *Geochimica et Cosmochimica Acta* **61** (20), 4375–4391. DOI: http://dx.doi.org/10.1016/S0016-7037(97)00241-X.

McCollom, T. M. and J. S. Seewald (2007). Abiotic Synthesis of Organic Compounds in Deep-Sea Hydrothermal Environments. *Chemical Reviews* **107** (2), 382–401. DOI: 10.1021/cr0503660.

Meador, T. B., M. Bowles, C. S. Lazar, C. Zhu, A. Teske, and K.-U. Hinrichs (2014a). The archaeal lipidome in estuarine sediment dominated by members of the Miscellaneous Crenarchaeotal Group. *Environmental Microbiology*, n/a–n/a. DOI: 10.1111/1462-2920.12716.

Meador, T. B., E. J. Gagen, M. E. Loscar, T. Goldhammer, M. Y. Yoshinaga, J. Wendt, M. Thomm, and K.-U. Hinrichs (2014b). *Thermococcus kodakarensis* modulates its polar membrane lipids and elemental composition according to growth stage and phosphate availability. *Frontiers in Microbiology* **5**, 10. DOI: 10.3389/fmicb.2014.00010.

Megonigal, J. P., M. E. Hines, and V. P. T. (2003). Anaerobic metabolism: Linkages to trace gases and aerobic processes. In: *Treatise on Geochemistry*. Ed. by H. D. Holland and K. K. Turekian. Oxford, UK: Pergamon, pp. 317–424.

Ménot, G. and E. Bard (2010). Geochemical evidence for a large methane release during the last deglaciation from Marmara Sea sediments. *Geochimica et Cosmochimica Acta* **74** (5), 1537–1550. DOI: 10.1016/j.gca.2009.11.022.

Menzel, D., E. C. Hopmans, S. Schouten, and J. S. Sinninghe Damsté (2006). Membrane tetraether lipids of planktonic Crenarchaeota in Pliocene sapropels of the eastern Mediterranean Sea. *Palaeogeography, Palaeoclimatology, Palaeoecology* **239** (1-2), 1–15. DOI: 10.1016/j.palaeo.2006.01.002.

Mesbah, N. M. and J. Wiegel (2008). Life at extreme limits: The anaerobic halophilic alkalithermophiles. *Annals of the New York Academy of Sciences* **1125**, 44–57. DOI: 10.1196/annals.1419.028.

Michaelis, W. and P. Albrecht (1979). Molecular fossils of archaebacteria in kerogen. *Naturwissenschaften* **66** (8), 420–422. DOI: 10.1007/BF00368078.

Mitchell, P. (1961). Coupling of phosphorylation to electron and hydrogen transfer by a chemiosmotic type of mechanism. *Nature* **191**, 144–148. DOI: 10.1038/191144a0.

Mollenhauer, G., T. I. Eglinton, N. Ohkouchi, R. R. Schneider, P. J. Müller, P. M. Grootes, and J. Rullkötter (2003). Asynchronous alkenone and foraminifera records from the Benguela Upwelling System. *Geochimica et Cosmochimica Acta* **67** (12), 2157–2171. DOI: http://dx.doi.org/10.1016/S0016-7037(03)00168-6.

Moore, E. K., E. C. Hopmans, W. I. C. Rijpstra, L. Villanueva, S. N. Dedysh, I. S. Kulichevskaya, H. Wienk, F. Schoutsen, and J. S. Sinninghe Damsté (2013). Novel mono-, di-, and trimethylornithine membrane lipids in northern wetland planctomycetes. *Applied and Environmental Microbiology* **79** (22), 6874–6884. DOI: 10.1128/AEM.02169-13.

Morii, H., H. Yagi, H. Akutsu, N. Nomura, Y. Sako, and Y. Koga (1999). A novel phosphoglycolipid archaetidyl(glucosyl)inositol with two sesterterpanyl chains from the aerobic hyperthermophilic archaeon *Aeropyrum pernix* K1. *Biochimica et Biophysica Acta* **1436** (3), 426–436. DOI: 10.1016/S0005-2760(98)00157-X.

Morii, H., T. Eguchi, M. Nishihara, K. Kakinuma, H. König, and Y. Koga (1998). A novel ether core lipid with H-shaped C_{80}-isoprenoid hydrocarbon chain from the hyperthermophilic methanogen *Methanothermus fervidus*. *Biochimica et Biophysica Acta* **1390**, 339–345.

Morono, Y., T. Terada, N. Masui, and F. Inagaki (2009). Discriminative detection and enumeration of microbial life in marine subsurface sediments. *The ISME journal* **3** (5), 503–511. DOI: 10.1038/ismej.2009.1.

Müller, P. J., G. Kirst, G. Ruhland, I. von Storch, and A. Rosell-Melé (1998a). Calibration of the alkenone paleotemperature index U37Kâ€² based on core-tops from the eastern South Atlantic and the global ocean (60Â°N-60Â°S). *Geochimica et Cosmochimica Acta* **62** (10), 1757–1772. DOI: http://dx.doi.org/10.1016/S0016-7037(98)00097-0.

Müller, P., G. Kirst Kirst Ruhland, I. von Storch, and A. Rosell-Melé (1998b). Calibration of the alkenone paleotemperature index UK37 based on core-tops from the eastern South Atlantic and the global ocean (60°N-60°S). *Geochimica et Cosmochimica Acta* **62** (10), 1757–1772.

Murray, J. W. and E. Yakushev (2006). The suboxic transition zone in the Black Sea. In: *Past and Present Water Column Anoxia*. Ed. by L. N. Neretin. Springer, pp. 105–138.

Murray, J. W., H. W. Jannasch, S. Honjo, R. F. Anderson, W. S. Reeburgh, Z. Top, G. E. Friederich, L. A. Codispoti, and E. Izdar (1989). Unexpected changes in the oxic/anoxic interface in the Black Sea. *Nature* **338**, 411–413. DOI: 10.1038/338411a0.

Namwong, S., S. Tanasupawat, T. Kudo, and T. Itoh (2011). *Haloarcula salaria* sp. nov. and *Haloarcula tradensis* sp. nov., isolated from salt in Thai fish sauce. *International Journal of Systematic and Evolutionary Microbiology* **61**, 231–236. DOI: 10.1099/ijs.0.021790-0.

Nealson, K., C. Myers, and B. Wimpee (1991). Isolation and identification of manganese-reducing bacteria and estimates of microbial Mn(IV)-reducing potential in the Black Sea. *Deep Sea Research Part A. Oceanographic Research Papers* **38**, S907–S920. DOI: 10.1016/S0198-0149(10)80016-0.

Nelson, K. E., R. A. Clayton, S. R. Gill, M. L. Gwinn, R. J. Dodson, D. H. Haft, E. K. Hickey, J. D. Peterson, W. C. Nelson, K. A. Ketchum, L. McDonald, T. R. Utterback, J. A. Malek, K. D. Linher, M. M. Garrett, A. M. Stewart, M. D. Cotton, M. S. Pratt, C. A. Phillips, D. Richardson, J. Heidelberg, G. G. Sutton, R. D. Fleischmann, J. A. Eisen, O. White, S. L. Salzberg, H. O. Smith, J. C. Venter, and C. M. Fraser (1999). Evidence for lateral gene transfer between Archaea and Bacteria from genome sequence of *Thermotoga maritima*. *Nature* **399** (6734), 323–329. DOI: 10.1038/20601.

Nelson-Sathi, S., T. Dagan, G. Landan, A. Janssen, M. Steel, J. O. McInerney, U. Deppenmeier, and W. F. Martin (2012). Acquisition of 1,000 eubacterial genes physiologically transformed a methanogen at the origin of Haloarchaea. *Proceedings of the National Academy of Sciences of the United States of America* **109** (50), 20537–20542. DOI: 10.1073/pnas.1209119109.

Nelson-Sathi, S., F. L. Sousa, M. Roettger, N. Lozada-Chávez, T. Thiergart, A. Janssen, D. Bryant, G. Landan, P. Schönheit, B. Siebers, J. O. McInerney, and W. F. Martin (2014). Origins of major archaeal clades correspond to gene acquisitions from bacteria. *Nature* **517**, 77–80. DOI: 10.1038/nature13805.

Newman, D. K. and J. F. Banfield (2002). Geomicrobiology: how molecular-scale interactions underpin biogeochemical systems. *Science* **296**, 1071–1077. DOI: 10.1126/science.1010716.

Ngugi, D. K., J. Blom, I. Alam, M. Rashid, W. Ba-Alawi, G. Zhang, T. Hikmawan, Y. Guan, A. Antunes, R. Siam, H. El Dorry, V. Bajic, and U. Stingl (2015). Comparative genomics reveals adaptations of a halotolerant thaumarchaeon in the interfaces of brine pools in the Red Sea. *The ISME Journal* **9** (2), 396–411. DOI: 10.1038/ismej.2014.137.

Nichols, D. S., M. R. Miller, N. W. Davies, A. Goodchild, M. Raftery, and R. Cavicchioli (2004). Cold adaptation in the antarctic archaeon *Methanococcoides burtonii* involves membrane lipid unsaturation. *Journal of Bacteriology* **186** (24), 8508–8515. DOI: 10.1128/JB.186.24.8508.

Nichols, P. D. and P. D. Franzmann (1992). Unsaturated diether phospholipids in the Antartic methanogen *Methanococcoides burtonii*. *FEMS Microbiology Letters* **98** (1-3), 205–208. DOI: 10.1111/j.1574-6968.1992.tb05515.x.

Nichols, P. D., P. M. Shaw, C. A. Mancuso, and P. D. Franzmann (1993). Analysis of archaeal phospholipid-derived di- and tetraether lipids by high temperature capillary gas chromatography. *Journal of Microbiological Methods* **18** (1), 1–9. DOI: 10.1016/0167-7012(93)90066-Q.

Nicolaus, B., A. Trincone, L. Lama, G. Palmieri, and A. Gambacorta (1992). Quinone composition in *Sulfolobus solfataricus* grown under different conditions. *Systematic and Applied Microbiology* **15** (1), 18–20. DOI: 10.1016/S0723-2020(11)80131-1.

Nishida, F., M. Nishijima, K. Mochida, H. Sano, N. Nomura, Y. Sako, and T. Maruyama (1999). Isoprenoid quinones in an aerobic hyperthermophilic archaeon, *Aeropyrum pernix*. *FEMS Microbiology Letters* **174** (2), 339–346. DOI: 10.1111/j.1574-6968.1999.tb13588.x.

Nishihara, M., S. Nagahama, M. Ohga, and Y. Koga (2000). Straight-chain fatty alcohols in the hyperthermophilic archaeon *Pyrococcus furiosus*. *Extremophiles* **4** (5), 275–277. DOI: 10.1007/s007920070013.

Nitschke, W., D. Kramer, A. Riedel, and U. Liebl (1995). From naphtho- to benzoquinones - (r)evolutionary reorganizations of electron transfer chains. In: *Photosynthesis: From Light to Biosphere*. Ed. by P. Mathis. Dordrecht, The Netherlands: Kluwer Academic, pp. 945–950.

Novitsky, J. A. (1986). Degradation of Dead Microbial Biomass in a Marine Sediment. *Applied and Environmental Microbiology* **52** (3), 504–509.

Nowicka, B. and J. Kruk (2010). Occurrence, biosynthesis and function of isoprenoid quinones. *Biochimica et Biophysica Acta* **1797** (9), 1587–1605. DOI: 10.1016/j.bbabio.2010.06.007.

Oguz, T., J. W. Murray, and A. E. Callahan (2001). Modeling redox cycling across the suboxic-anoxic interface zone in the Black Sea. *Deep-Sea Research Part I: Oceanographic Research Papers* **48** (3), 761–787. DOI: 10.1016/S0967-0637(00)00054-6.

Ohkouchi, N., T. I. Eglinton, L. D. Keigwin, and J. M. Hayes (2002). Spatial and temporal offsets between proxy records in a sediment drift. *Science* **298** (5596), 1224–7. DOI: 10.1126/science.1075287.

Okayama, S. (1976). Redox potential of plastoquinone A in spinach chloroplasts. *Biochimica et Biophysica Acta* **440**, 331–336. DOI: 10.1016/0005-2728(76)90067-0.

Oliver, J. D. and R. R. Colwell (1973). Extractable Lipids of Gram-Negative Marine Bacteria: Phospholipid Composition. *Journal of Bacteriology* **114** (3), 897–908.

Olsen, I. and E. Jantzen (2001). Sphingolipids in bacteria and fungi. *Anaerobe* **7** (2), 103–112. DOI: 10.1006/anae.2001.0376.

Ono, M., K. E. N. Sawada, Y. Shiraiwa, and M. Kubota (2012). Changes in alkenone and alkenoate distributions during acclimatization to salinity change in Isochrysis galbana: Implication for alkenone-based paleosalinity and paleothermometry. *GEOCHEMICAL JOURNAL* **46** (3), 235–247. DOI: 10.2343/geochemj.2.0203.

Orcutt, B. N., D. E. LaRowe, J. F. Biddle, F. S. Colwell, B. T. Glazer, B. K. Reese, J. B. Kirkpatrick, L. L. Lapham, H. J. Mills, J. B. Sylvan, S. D. Wankel, and C. G. Wheat (2013). Microbial activity in the marine deep biosphere: progress and prospects. *Frontiers in Microbiology* **4**, 189. DOI: 10.3389/fmicb.2013.00189.

Oremland, R. S. and S. Polcin (1982). Methanogenesis and Sulfate Reduction: Competitive and Noncompetitive Substrates in Estuarine Sediments. *Applied and Environmental Microbiology* **44** (6), 1270–1276.

Oremland, R. S., L. M. Marsh, and S. Polcin (1982). Methane production and simultaneous sulphate reduction in anoxic, salt marsh sediments. *Nature* **296** (5853), 143–145. DOI: 10.1038/296143a0.

Oren, A. (1983). *Halobacterium sodomense* sp. nov. a Dead Sea Halobacterium with an Extremely High Magnesium Requirement. *International Journal of Systematic Bacteriology* **33** (2), 381–386.

Oren, A. (1999). Bioenergetic Aspects of Halophilism. *Microbiology and Molecular Biology Reviews* **63** (2), 334–348.

Oren, A. (2002a). Diversity of halophilic microorganisms: Environments, phylogeny, physiology, and applications. *Journal of Industrial Microbiology & Biotechnology* **28** (1), 56–63. DOI: 10.1038/sj.jim.7000176.

Oren, A. (2002b). Molecular ecology of extremely halophilic Archaea and Bacteria. *FEMS Microbiology Ecology* **39** (1), 1–7. DOI: 10.1111/j.1574-6941.2002.tb00900.x.

Oren, A. (2008). Microbial life at high salt concentrations: phylogenetic and metabolic diversity. *Saline systems* **4**. DOI: 10.1186/1746-1448-4-2.

Orphan, V. J., C. H. House, K. U. Hinrichs, K. D. McKeegan, and E. F. DeLong (2001). Methane-consuming archaea revealed by directly coupled isotopic and phylogenetic analysis. *Science* **293** (5529), 484–487. DOI: 10.1126/science.1061338.

Ourisson, G., M. Rohmer, and K. Poralla (1987). Prokaryotic Hopanoids and other Polyterpenoid Sterol Surrogates. *Annual Review of Microbiology* **41** (1), 301–333. DOI: 10.1146/annurev.mi.41.100187.001505.

Overmann, J. (2006). The Family Chlorobiaceae. In: *The Prokaryotes. Volume 7: Proteobacteria: Delta, Epsilon Subclass.* Ed. by M. Dworkin, S. Falkow, E. Rosenberg, K.-H. Schleifer, and E. Stackebrandt. New York, USA: Springer, pp. 359–378. DOI: 10.1007/0-387-30747-8_13.

Overmann, J., H. Cypionka, and N. Pfennig (1992). An extremely low-light adapted phototrophic sulfur bacterium from the Black Sea. *Limnology and Oceanography* **37** (1), 150–155. DOI: 10.4319/lo.1992.37.1.0150.

Pace, N. R. (1997). A molecular view of microbial diversity and the biosphere. *Science* **276** (5313), 734–740. DOI: 10.1126/science.276.5313.734.

Pancost, R., E. Hopmans, and J. Sinninghe Damsté (2001). Archaeal lipids in Mediterranean cold seeps: molecular proxies for anaerobic methane oxidation. *Geochimica et Cosmochimica Acta* **65** (10), 1611–1627. DOI: 10.1016/S0016-7037(00)00562-7.

Pancost, R. D., J. M. Coleman, G. D. Love, A. Chatzi, I. Bouloubassi, and C. E. Snape (2008). Kerogen-bound glycerol dialkyl tetraether lipids released by hydropyrolysis of marine sediments: A bias against incorporation of sedimentary organisms? *Organic Geochemistry* **39** (9), 1359–1371. DOI: 10.1016/j.orggeochem.2008.05.002.

Paper, W., U. Jahn, M. J. Hohn, M. Kronner, D. J. Näther, T. Burghardt, R. Rachel, K. O. Stetter, and H. Huber (2007). *Ignicoccus hospitalis* sp. nov., the host of *'Nanoarchaeum equitans'*. *International Journal of Systematic and Evolutionary Microbiology* **57** (4), 803–808. DOI: 10.1099/ijs.0.64721-0.

Parkes, R. J., B. A. Cragg, S. J. Bale, J. M. Getlifff, K. Goodman, P. A. Rochelle, J. C. Fry, A. J. Weightman, and S. M. Harvey (1994). Deep bacterial biosphere in Pacific Ocean sediments. *Nature* **371** (6496), 410–413.

Parkes, R. J., B. A. Cragg, J. C. Fry, R. A. Herbert, J. W. T. Wimpenny, J. A. Allen, and M. Whitfield (1990). Bacterial Biomass and Activity in Deep Sediment Layers from the Peru Margin [and Discussion]. *Philosophical Transactions of the Royal Society of London. Series A, Mathematical and Physical Sciences* **331** (1616), 139–153. DOI: 10.2307/53658.

Parkes, R. J., B. A. Cragg, and P. Wellsbury (2000). Recent studies on bacterial populations and processes in subseafloor sediments: A review. *Hydrogeology Journal* **8**, 11–28. DOI: 10.1007/PL00010971.

Paulmier, a. and D. Ruiz-Pino (2009). Oxygen minimum zones (OMZs) in the modern ocean. *Progress in Oceanography* **80** (3-4), 113–128. DOI: 10.1016/j.pocean.2008.08.001.

Pearson, A. (2010). Handbook of Hydrocarbon and Lipid Microbiology. Ed. by K. N. Timmis. DOI: 10.1007/978-3-540-77587-4.

Pearson, A. (2014). *Lipidomics for Geochemistry*. Ed. by P. G. Falkowski and K. H. Freeman. 2nd ed. Vol. 12. London, UK: Elsevier Ltd., pp. 291–336. DOI: 10.1016/B978-0-08-095975-7.01022-6.

Pearson, A., Z. Huang, A. E. Ingalls, C. S. Romanek, J. Wiegel, K. H. Freeman, R. H. Smittenberg, and C. L. Zhang (2004). Nonmarine crenarchaeol in Nevada hot springs. *Applied and Environmental Microbiology* **70** (9), 5229–5237. DOI: 10.1128/AEM.70.9.5229-5237.2004.

Pearson, A. (2008). Who lives in the sea floor? *Nature* **454** (7207), 952–953. DOI: 10.1038/454952a.

Pearson, A. and A. E. Ingalls (2013). Assessing the Use of Archaeal Lipids as Marine Environmental Proxies. *Annual Review of Earth and Planetary Sciences* **41** (1), 359–384. DOI: 10.1146/annurev-earth-050212-123947.

Peretó, J., P. López-García, and D. Moreira (2004). Ancestral lipid biosynthesis and early membrane evolution. *Trends in biochemical sciences* **29** (9), 469–77. DOI: 10.1016/j.tibs.2004.07.002.

Perry, K. A., J. E. Kostka, G. W. Luther, and K. H. Nealson (1993). Mediation of sulfur speciation by a Black Sea facultative anaerobe. *Science* **259** (1990), 801–803. DOI: 10.1126/science.259.5096.801.

Pester, M., C. Schleper, and M. Wagner (2011). The Thaumarchaeota: an emerging view of their phylogeny and ecophysiology. *Current Opinion in Microbiology* **14** (3), 300–306. DOI: 10.1016/j.mib.2011.04.007.

Peterse, F., J.-H. Kim, S. Schouten, D. K. Kristensen, N. Koç, and J. S. Sinninghe Damsté (2009). Constraints on the application of the MBT/CBT palaeothermometer at high latitude environments (Svalbard, Norway). *Organic Geochemistry* **40** (6), 692–699. DOI: 10.1016/j.orggeochem.2009.03.004.

Pikuta, E. V., R. B. Hoover, and J. Tang (2007). Microbial extremophiles at the limits of life. *Critical reviews in microbiology* **33**, 183–209. DOI: 10.1080/10408410701451948.

Pimenov, N. and L. Neretin (2006). Composition and activities of microbial communities involved in carbon, sulfur, nitrogen and manganese cycling in the oxic/anoxic interface of the Black Sea. In: *Past and Present Water Column Anoxia*. Ed. by L. N. Neretin. Berlin, Germany: Springer, pp. 501–521.

Pitcher, A. (2011). "Intact polar lipids of ammonia-oxidizing Archaea: Structural diversity and application in molecular ecology". PhD thesis. Universiteit Utrecht.

Pitcher, A., E. C. Hopmans, A. C. Mosier, S.-J. Park, S.-K. Rhee, C. A. Francis, S. Schouten, and J. S. Sinninghe Damsté (2011a). Core and intact polar glycerol dibiphytanyl glycerol tetraether lipids of ammonia-oxidizing archaea enriched from marine and estuarine sediments. *Applied and Environmental Microbiology* **77** (10), 3468–3477. DOI: 10.1128/AEM.02758-10.

Pitcher, A., E. C. Hopmans, S. Schouten, and J. S. Sinninghe Damsté (2009a). Separation of core and intact polar archaeal tetraether lipids using silica columns: Insights into living and fossil biomass contributions. *Organic Geochemistry* **40** (1), 12–19. DOI: 10.1016/j.orggeochem.2008.09.008.

Pitcher, A., S. Schouten, and J. S. Sinninghe Damsté (2009b). In situ production of crenarchaeol in two California hot springs. *Applied and Environmental Microbiology* **75** (13), 4443–4451. DOI: 10.1128/AEM.02591-08.

Pitcher, A., L. Villanueva, E. C. Hopmans, S. Schouten, G.-J. Reichart, and J. S. Sinninghe Damsté (2011b). Niche segregation of ammonia-oxidizing archaea and anammox bacteria in the Arabian Sea oxygen minimum zone. *The ISME Journal* **5** (12), 1896–1904. DOI: 10.1038/ismej.2011.60.

Polymenakou, P. N., E. G. Stephanou, A. Tselepides, and S. Bertilsson (2007). Organic Matter Preservation and Microbial Community Accumulations in Deep-Hypersaline Anoxic Basins. *Geomicrobiology Journal* **24** (1), 19–29. DOI: 10.1080/01490450601134283.

Popendorf, K. J., T. Tanaka, M. Pujo-Pay, A. Lagaria, C. Courties, P. Conan, L. Oriol, L. E. Sofen, T. Moutin, and B. A. S. Van Mooy (2011). Gradients in intact polar diacylglycerolipids across the Mediterranean Sea are related to phosphate availability. *Biogeosciences* **8** (12), 3733–3745. DOI: 10.5194/bg-8-3733-2011.

Powls, R., E. Redfearn, and S. Trippett (1968). The structure of chlorobiumquinone. *Biochemical and Biophysical Research Communications* **33** (3), 408–411.

Poynter, J. and G. Eglinton (1991). The biomarker concept – strengths and weaknesses. *Fresenius' Journal of Analytical Chemistry* **339** (10), 725–731. DOI: 10.1007/BF00321733.

Prahl, F. G. and S. G. Wakeham (1987). Calibration of unsaturation patterns in long-chain ketone compositions for palaeotemperature assessment. *Nature* **330** (6146), 367–369. DOI: 10.1038/330367a0.

Prahl, F. G., M. a. Sparrow, and G. V. Wolfe (2003). Physiological impacts on alkenone paleothermometry. *Paleoceanography* **18** (2), n/a–n/a. DOI: 10.1029/2002PA000803.

Prahl, F. G., L. A. Muehlhausen, and D. L. Zahnle (1988). Further evaluation of long-chain alkenones as indicators of paleoceanographic conditions. *Geochimica et Cosmochimica Acta* **52** (9), 2303–2310. DOI: http://dx.doi.org/10.1016/0016-7037(88)90132-9.

Presley, B. and I. Kaplan (1968). Changes in dissolved sulfate, calcium and carbonate from interstitial water of near-shore sediments. *Geochimica et Cosmochimica Acta* **32** (10), 1037–1048. DOI: 10.1016/0016-7037(68)90106-3.

Quay, P., R. Sonnerup, T. Westby, J. Stutsman, and A. McNichol (2003). Changes in the $^{13}C/^{12}C$ of dissolved inorganic carbon in the ocean as a tracer of anthropogenic CO_2 uptake. *Global Biogeochemical Cycles* **17** (1), 4–20. DOI: 10.1029/2001GB001817.

Quinn, P. J. (2012). Lipid–lipid interactions in bilayer membranes: Married couples and casual liaisons. *Progress in Lipid Research* **51** (3), 179–198. DOI: http://dx.doi.org/10.1016/j.plipres.2012.01.001.

Rabus, R., T. A. Hansen, and F. Widdel (2006). Dissimilatory Sulfate and Sulfur-Reducing Prokaryotes. In: *The Prokaryotes. Volume 2: Ecophysiology and Biochemistry*. Ed. by M. Dworki, S. Falkow, E. Rosenberg, K.-H. Schleifer, and E. Stackebrandt. New York, USA: Springer, pp. 659–768. DOI: 10.1007/0-387-30742-7_22.

Rampen, S. W., V. Willmott, J.-H. Kim, E. Uliana, G. Mollenhauer, E. Schefuß, J. S. Sinninghe Damsté, and S. Schouten (2012). Long chain 1,13- and 1,15-diols as a potential proxy for palaeotemperature reconstruction. *Geochimica et Cosmochimica Acta* **84**, 204–216. DOI: 10.1016/j.gca.2012.01.024.

Raven, J. A. (2009). Contributions of anoxygenic and oxygenic phototrophy and chemolithotrophy to carbon and oxygen fluxes in aquatic environments. **1**, 1–16. DOI: 10.3354/ame01315.

Rechka, J. and J. Maxwell (1988). Characterisation of alkenone temperature indicators in sediments and organisms. *Organic Geochemistry* **13** (4-6), 727–734. DOI: 10.1016/0146-6380(88)90094-0.

Redfearn, E. and R. Powls (1968). Quinones of green photosynthetic bacteria. *Bioochemical Journal* **106**, 50.

Redfield, A. C. (1958). The biological control of chemical factors in the environment. *American Scientist* **46** (3), 205–221.

Reeburgh, W. S., B. B. Ward, S. C. Whalen, K. A. Sandbeck, K. A. Kilpatrickt, and L. J. Kerkhof (1991). Black Sea methane geochemistry. *Deep Sea Research Part A. Oceanographic Research Papers* **38**, S1189–S1210. DOI: 10.1016/S0198-0149(10)80030-5.

Reno, M. L., N. L. Held, C. J. Fields, P. V. Burke, and R. W. Whitaker (2009). Biogeography of the *Sulfolobus islandicus* pan-genome. *Proceedings of the National Academy of Sciences of the United States of America* **106** (44), 18873–18873. DOI: 10.1073/pnas.0911400106.

Repeta, D. J. and D. J. Simpson (1991). The distribution and recycling of chlorophyll, bacteriochlorophyll and carotenoids in the Black Sea. *Deep Sea Research Part A. Oceanographic Research Papers* **38**, S969–S984. DOI: 10.1016/S0198-0149(10)80019-6.

Repeta, D. J. (1993). A high resolution historical record of Holocene anoxygenic primary production in the Black Sea. *Geochimica et Cosmochimica Acta* **57** (17), 4337–4342. DOI: 10.1016/0016-7037(93)90334-S.

Riedinger, N., B. Brunner, Y.-S. Lin, A. Voßmeyer, T. G. Ferdelman, and B. B. Jørgensen (2010). Methane at the sediment–water transition in Black Sea sediments. *Chemical Geology* **274** (1-2), 29–37. DOI: 10.1016/j.chemgeo.2010.03.010.

Rodrigo-Gámiz, M., F. Martinez-Ruiz, S. Rampen, S. S., and J. Sinninghe Damsté (2014). Sea surface temperature variations in the western Mediterranean Sea over the last 20 kyr: A dual-organic proxy ($U^{K'}_{37}$ and LDI) approach. *Paleoceanography* **29** (2), 87–98. DOI: 10.1002/2013PA002466.

Rontani, J.-F., F. G. Prahl, and J. K. Volkman (2006). Characterization of unusual alkenones and alkyl alkenoates by electron ionization gas chromatography/mass spectrometry. *Rapid communications in mass spectrometry : RCM* **20** (4), 583–8. DOI: 10.1002/rcm.2346.

Rosell-Melé, A., E. Bard, K.-C. Emeis, J. O. Grimalt, P. Müller, R. Schneider, I. Bouloubassi, B. Epstein, K. Fahl, A. Fluegge, K. Freeman, M. Goñi, U. Güntner, D. Hartz, S. Hellebust, T. Herbert, M. Ikehara, R. Ishiwatari, K. Kawamura, F. Kenig, J. de Leeuw, S. Lehman, L. Mejanelle, N. Ohkouchi, R. D. Pancost, C. Pelejero, F. Prahl, J. Quinn, J.-F. Rontani, F. Rostek,

J. Rullkötter, J. Sachs, T. Blanz, K. Sawada, D. Schulz-Bull, E. Sikes, C. Sonzogni, Y. Ternois, G. Versteegh, J. K. Volkman, and S. Wakeham (2001). Precision of the current methods to measure the alkenone proxy $U_{37}^{K'}$ and absolute alkenone abundance in sediments: Results of an interlaboratory comparison study. *Geochemistry, Geophysics, Geosystems* **2** (7), n/a–n/a. DOI: 10.1029/2000GC000141.

Rosell-Mele, A., J. F. Carter, A. T. Parry, and G. Eglinton (1995). Determination of the UK37 index in geological samples. *Analytical Chemistry* **67** (7), 1283–1289. DOI: 10.1021/ac00103a021.

Ross, D. A., E. T. Degens, and J. Macilvaine (1970). Black sea: Recent sedimentary history. *Science* **170** (3954), 163–165. DOI: 10.1126/science.170.3954.163.

Rossel, P. E., M. Elvert, A. Ramette, A. Boetius, and K.-U. Hinrichs (2011). Factors controlling the distribution of anaerobic methanotrophic communities in marine environments: Evidence from intact polar membrane lipids. *Geochimica et Cosmochimica Acta* **75** (1), 164–184. DOI: 10.1016/j.gca.2010.09.031.

Rossel, P. E., J. S. Lipp, H. F. Fredricks, J. Arnds, A. Boetius, M. Elvert, and K.-U. Hinrichs (2008). Intact polar lipids of anaerobic methanotrophic archaea and associated bacteria. *Organic Geochemistry* **39** (8), 992–999. DOI: 10.1016/j.orggeochem.2008.02.021.

Rothschild, L. J. and R. L. Mancinelli (2001). Life in extreme environments. *Nature* **409** (6823), 1092–1101. DOI: 10.1038/35059215.

Roussel, E. G., A. L. Sauvadet, C. Chaduteau, Y. Fouquet, J. L. Charlou, D. Prieur, and M. A. Cambon Bonavita (2009). Archaeal communities associated with shallow to deep subseafloor sediments of the New Caledonia Basin. *Environmental Microbiology* **11** (9), 2446–2462. DOI: 10.1111/j.1462-2920.2009.01976.x.

Ruepp, A., W. Graml, M. L. Santos-Martinez, K. K. Koretke, C. Volker, H. W. Mewes, D. Frishman, S. Stocker, A. N. Lupas, and W. Baumeister (2000). The genome sequence of the thermoacidophilic scavenger *Thermoplasma acidophilum*. *Nature* **407** (6803), 508–513. DOI: 10.1038/35035069.

Russell, N. J. (1989). Adaptive modifications in membranes of halotolerant and halophilic microorganisms. *Journal of Bioenergetics and Bomembranes* **21** (1), 93–113. DOI: 10.1007/BF00762214.

Russell, N. J., R. I. Evans, P. F. ter Steeg, J. Hellemons, A. Verheul, and T. Abee (1995). Membranes as a target for stress adaptation. *International Journal of Food Microbiology* **28** (2), 255–261.

Rütters, H., H. Sass, H. Cypionka, and J. Rullkötter (2001). Monoalkylether phospholipids in the sulfate-reducing bacteria *Desulfosarcina variabilis* and *Desulforhabdus amnigenus*. *Archives of Microbiology* **176** (6), 435–442. DOI: 10.1007/s002030100343.

Rütters, H., H. Sass, H. Cypionka, and J. Rullkötter (2002). Phospholipid analysis as a tool to study complex microbial communities in marine sediments. *Journal of Microbiological Methods* **48** (2-3), 149–160. DOI: 10.1016/S0167-7012(01)00319-0.

Ryan, W. B. F., C. O. Major, G. Lericolais, and S. L. Goldstein (2003). Catastrophic flooding of the Black Sea. *Annual Review of Earth and Planetary Sciences* **31** (1), 525–554. DOI: 10.1146/annurev.earth.31.100901.141249.

Ryan, W. B. F., W. C. Pitman III, C. O. Major, K. Shimkus, V. Moskalenko, G. A. Jones, P. Dimitrov, N. Gorür, M. Sakinç, and H. Yüce (1997). An abrupt drowning of the Black Sea shelf. *Marine Geology* **138** (1â€“2), 119–126. DOI: http://dx.doi.org/10.1016/S0025-3227(97)00007-8.

Sáenz, J. P., E. Sezgin, P. Schwille, and K. Simons (2012). Functional convergence of hopanoids and sterols in membrane ordering. *Proceedings of the National Academy of Sciences of the United States of America* **109** (35), 14236–14240. DOI: 10.1073/pnas.1212141109.

Sakata, S., J. M. Hayes, A. R. McTaggart, R. A. Evans, K. J. Leckrone, and R. K. Togasaki (1997). Carbon isotopic fractionation associated with lipid biosynthesis by a cyanobacterium: Relevance for interpretation of biomarker records. *Geochimica et Cosmochimica Acta* **61** (24), 5379–5389. DOI: http://dx.doi.org/10.1016/S0016-7037(97)00314-1.

Sanina, N. M., S. N. Goncharova, and E. Y. Kostetsky (2004). Fatty acid composition of individual polar lipid classes from marine macrophytes. *Phytochemistry* **65** (6), 721–730. DOI: 10.1016/j.phytochem.2004.01.013.

Sass, A. M., B. A. McKew, H. Sass, J. Fichtel, K. N. Timmis, and T. J. McGenity (2008). Diversity of Bacillus-like organisms isolated from deep-sea hypersaline anoxic sediments. *Saline systems* **4**. DOI: 10.1186/1746-1448-4-8.

Schäfer, G., S. Anemüller, R. Moll, M. Gleissner, and C. L. Schmidt (1993). Has *Sulfolobus* an Archaic Respiratory System? Structure, Function and Genes of its Components. *Systematic and Applied Microbiology* **16** (4), 544–555. DOI: 10.1016/S0723-2020(11)80324-3.

Schäfer, G., M. Engelhard, and V. Müller (1999). Bioenergetics of the Archaea. *Microbiology and Molecular Biology Reviews* **63** (3), 570–620.

Schattenhofer, M., B. M. Fuchs, R. Amann, M. V. Zubkov, G. A. Tarran, and J. Pernthaler (2009). Latitudinal distribution of prokaryotic picoplankton populations in the Atlantic Ocean. *Environmental Microbiology* **11** (8), 2078–2093. DOI: 10.1111/j.1462-2920.2009.01929.x.

Schippers, A., L. N. Neretin, J. Kallmeyer, T. G. Ferdelman, B. A. Cragg, R. J. Parkes, and B. B. Jørgensen (2005). Prokaryotic cells of the deep sub-seafloor biosphere identified as living bacteria. *Nature* **433** (7028), 861–864. DOI: 10.1038/nature03302.

Schnorf, U. (1966). "Der Einfluss von Substituenten auf Redoxpotential und Wuchsstoffeigenschaften von Chinonen". PhD Thesis. Eidgenössische Technische Hochschule, Zürich. DOI: 10.3929/ethz-a-000090587.

Schoell, M. (1988). Multiple origins of methane in the Earth. *Chemical Geology* **71** (1â€“3), 1–10. DOI: http://dx.doi.org/10.1016/0009-2541(88)90101-5.

Schoepp-Cothenet, B., C. Lieutaud, F. Baymann, A. Verméglio, T. Friedrich, D. M. Kramer, and W. Nitschke (2009). Menaquinone as pool quinone in a purple bacterium. *Proceedings of the National Academy of Sciences of the United States of America* **106** (21), 8549–8554. DOI: 10.1073/pnas.0813173106.

Schoepp-Cothenet, B., R. van Lis, A. Atteia, F. Baymann, L. Capowiez, A.-L. Ducluzeau, S. Duval, F. ten Brink, M. J. Russell, and W. Nitschke (2013). On the universal core of bioenergetics. *Biochimica et Biophysica Acta* **1827** (2), 79–93. DOI: 10.1016/j.bbabio.2012.09.005.

Schouten, S., M. J. L. Hoefs, M. P. Koopmans, H.-j. Bosch, J. S. Sinninghe Damsté, and J. S. S. Damste (1998). Structural characterization, occurrence and fate of archaeal ether-bound acyclic and cyclic biphytanes and corresponding diols in sediments. *Organic Geochemistry* **29** (5-7), 1305–1319. DOI: 10.1016/S0146-6380(98)00131-4.

Schouten, S., E. C. Hopmans, and J. S. Sinninghe Damsté (2004). The effect of maturity and depositional redox conditions on archaeal tetraether lipid palaeothermometry. *Organic Geochemistry* **35** (5), 567–571. DOI: 10.1016/j.orggeochem.2004.01.012.

Schouten, S., E. C. Hopmans, and J. S. Sinninghe Damsté (2013a). The organic geochemistry of glycerol dialkyl glycerol tetraether lipids: A review. *Organic Geochemistry* **54**, 19–61. DOI: 10.1016/j.orggeochem.2012.09.006.

Schouten, S., E. C. Hopmans, M. Baas, H. Boumann, S. Standfest, M. Könneke, D. A. Stahl, and J. S. Sinninghe Damsté (2008). Intact Membrane Lipids of "*Candidatus* Nitrosopumilus maritimus," a Cultivated Representative of the Cosmopolitan Mesophilic Group I Crenarchaeota. *Applied and Environmental Microbiology* **74** (8), 2433–2440. DOI: 10.1128/AEM.01709-07.

Schouten, S., E. C. Hopmans, R. D. Pancost, and J. S. Sinninghe Damsté (2000). Widespread occurrence of structurally diverse tetraether membrane lipids: evidence for the ubiquitous presence of low-temperature relatives of hyperthermophiles. *Proceedings of the National Academy of Sciences of the United States of America* **97** (26), 14421–14426. DOI: 10.1073/pnas.97.26.14421.

Schouten, S., E. C. Hopmans, A. Rosell-Melé, A. Pearson, P. Adam, T. Bauersachs, E. Bard, S. M. Bernasconi, T. S. Bianchi, J. J. Brocks, L. T. Carlson, I. S. Castañeda, S. Derenne, A. D. Selver, K. Dutta, T. Eglinton, C. Fosse, V. Galy, K. Grice, K.-U. Hinrichs, Y. Huang, A. Huguet, C. Huguet, S. Hurley, A. Ingalls, G. Jia, B. Keely, C. Knappy, M. Kondo, S. Krishnan, S. Lincoln, J. Lipp, K. Mangelsdorf, A. Martínez-García, G. Ménot, A. Mets, G. Mollenhauer, N. Ohkouchi, J. Ossebaar, M. Pagani, R. D. Pancost, E. J. Pearson, F. Peterse, G.-J. Reichart, P. Schaeffer, G. Schmitt, L. Schwark, S. R. Shah, R. W. Smith, R. H. Smittenberg, R. E. Summons, Y. Takano, H. M. Talbot, K. W. R. Taylor, R. Tarozo, M. Uchida, B. E. van Dongen, B. A. S. Van Mooy, J. Wang, C. Warren, J. W. H. Weijers, J. P. Werne, M. Woltering, S. Xie, M. Yamamoto, H. Yang, C. L. Zhang, Y. Zhang, M. Zhao, and J. S. Sinninghe Damsté (2013b). An interlaboratory study of TEX_{86} and BIT analysis of sediments, extracts, and standard mixtures. *Geochemistry, Geophysics, Geosystems* **14** (12), 5263–5285. DOI: 10.1002/2013GC004904.

Schouten, S., E. C. Hopmans, E. Schefuß, and J. S. Sinninghe Damsté (2002). Distributional variations in marine crenarchaeotal membrane lipids: a new tool for reconstructing ancient sea water temperatures? *Earth and Planetary Science Letters* **204** (1-2), 265–274. DOI: 10.1016/S0012-821X(02)00979-2.

Schouten, S., E. C. Hopmans, J. van der Meer, A. Mets, E. Bard, T. S. Bianchi, A. Diefendorf, M. Escala, K. H. Freeman, Y. Furukawa, C. Huguet, A. Ingalls, G. Ménot-Combes, A. J. Nederbragt, M. Oba, A. Pearson, E. J. Pearson, A. Rosell-Melé, P. Schaeffer, S. R. Shah, T. M. Shanahan, R. W. Smith, R. Smittenberg, H. M. Talbot, M. Uchida, B. A. S. Van Mooy, M. Yamamoto, Z. Zhang, and J. S. Sinninghe Damsté (2009). An interlaboratory study of TEX_{86} and BIT analysis using high-performance liquid chromatography-mass spectrometry. *Geochemistry, Geophysics, Geosystems* **10** (3), Q03012. DOI: 10.1029/2008GC002221.

Schouten, S., C. Huguet, E. C. Hopmans, M. V. M. Kienhuis, and J. S. S. Damsté (2007). Analytical methodology for TEX_{86} paleothermometry by high-performance liquid chromatography/atmospheric pressure chemical ionization-mass spectrometry. *Analytical Chemistry* **79** (7), 2940–2944. DOI: 10.1021/ac062339v.

Schouten, S., J. J. Middelburg, E. C. Hopmans, and J. S. Sinninghe Damsté (2010). Fossilization and degradation of intact polar lipids in deep subsurface sediments: A theoretical approach. *Geochimica et Cosmochimica Acta* **74** (13), 3806–3814. DOI: 10.1016/j.gca.2010.03.029.

Schouten, S., A. Pitcher, E. C. Hopmans, L. Villanueva, J. van Bleijswijk, and J. S. Sinninghe Damsté (2012). Intact polar and core glycerol dibiphytanyl glycerol tetraether lipids in the Arabian Sea oxygen minimum zone: I. Selective preservation and degradation in the water column and consequences for the TEX_{86}. *Geochimica et Cosmochimica Acta* **98**, 228–243. DOI: 10.1016/j.gca.2012.05.002.

Schrenk, M. O., J. a. Huber, and K. J. Edwards (2010). Microbial provinces in the subseafloor. *Annual review of marine science* **2**, 279–304. DOI: 10.1146/annurev-marine-120308-081000.

Schröder, J. M. (2015). "Intact pooar lipids in marine sediments: improving analytical pprotocol and assassess planktonik and benthic sources". PhD Thesis. University of Bremen.

Schubert, C. J., M. J. L. Coolen, L. N. Neretin, A. Schippers, B. Abbas, E. Durisch-Kaiser, B. Wehrli, E. C. Hopmans, J. S. S. Damsté, S. Wakeham, and M. M. M. Kuypers (2006). Aerobic and anaerobic methanotrophs in the Black Sea water column. *Environmental Microbiology* **8** (10), 1844–1856. DOI: 10.1111/j.1462-2920.2006.01079.x.

Schubotz, F., D. R. Meyer-Dombard, A. S. Bradley, H. F. Fredricks, K.-U. Hinrichs, E. L. Shock, and R. E. Summons (2013). Spatial and temporal variability of biomarkers and microbial diversity reveal metabolic and community flexibility in streamer biofilm communities in the Lower Geyser Basin, Yellowstone National Park. *Geobiology* **11** (6), 549–569. DOI: 10.1111/gbi.12051.

Schubotz, F., J. S. Lipp, M. Elvert, and K.-U. Hinrichs (2011). Stable carbon isotopic compositions of intact polar lipids reveal complex carbon flow patterns among hydrocarbon degrading

microbial communities at the Chapopote asphalt volcano. *Geochimica et Cosmochimica Acta* **75** (16), 4399–4415. DOI: 10.1016/j.gca.2011.05.018.

Schubotz, F., S. G. Wakeham, J. S. Lipp, H. F. Fredricks, and K.-U. Hinrichs (2009). Detection of microbial biomass by intact polar membrane lipid analysis in the water column and surface sediments of the Black Sea. *Environmental Microbiology* **11** (10), 2720–2734. DOI: 10.1111/j.1462-2920.2009.01999.x.

Schulz, H.-M., A. Schöner, and K.-C. Emeis (2000). Long-chain alkenone patterns in the Baltic sea–an ocean-freshwater transition. *Geochimica et Cosmochimica Acta* **64** (3), 469–477. DOI: http://dx.doi.org/10.1016/S0016-7037(99)00332-4.

Schütz, M., M. Brugna, E. Lebrun, F. Baymann, R. Huber, K. O. Stetter, G. Hauska, R. Toci, D. Lemesle-Meunier, P. Tron, C. Schmidt, and W. Nitschke (2000). Early evolution of cytochrome *bc* complexes. *Journal of Molecular Biology* **300** (4), 663–675. DOI: 10.1006/jmbi.2000.3915.

Seidel, M., J. Graue, B. Engelen, J. Köster, H. Sass, and J. Rullkötter (2012). Advection and diffusion determine vertical distribution of microbial communities in intertidal sediments as revealed by combined biogeochemical and molecular biological analysis. *Organic Geochemistry* **52**, 114–129. DOI: 10.1016/j.orggeochem.2012.08.015.

Seidel, M., H. Rütters, J. Rullkötter, and H. Sass (2013). Phosphate-free ornithine lipid contents in *Desulfovibrio* spp. respond to growth temperature. *Organic Geochemistry* **59**, 133–142. DOI: 10.1016/j.orggeochem.2013.04.004.

Sévin, D. C. and U. Sauer (2014). Ubiquinone accumulation improves osmotic-stress tolerance in *Escherichia coli*. *Nature Chemical Biology* **10** (4), 266–272. DOI: 10.1038/nchembio.1437.

Shah, S. R., G. Mollenhauer, N. Ohkouchi, T. I. Eglinton, and A. Pearson (2008). Origins of archaeal tetraether lipids in sediments: Insights from radiocarbon analysis. *Geochimica et Cosmochimica Acta* **72** (18), 4577–4594. DOI: 10.1016/j.gca.2008.06.021.

Shimada, H., N. Nemoto, Y. Shida, T. Oshima, and A. Yamagishi (2008). Effects of pH and temperature on the composition of polar lipids in *Thermoplasma acidophilum* HO-62. *Journal of Bacteriology* **190** (15), 5404–5411. DOI: 10.1128/JB.00415-08.

Shimada, H., Y. Shida, N. Nemoto, T. Oshima, and A. Yamagishi (2001). Quinone profiles of *Thermoplasma acidophilum* HO-62. *Journal of Bacteriology* **183** (4), 1462–1465. DOI: 10.1128/JB.183.4.1462-1465.2001.

Shively, J. M. and A. A. Benson (1967). Phospholipids of *Thiobacillus thiooxidans*. *Journal of Bacteriology* **94** (5), 1679–1683.

Shokes, R. F., P. K. Trabant, B. J. Presley, and D. F. Reid (1977). Anoxic, hypersaline basin in the northern gulf of Mexico. *Science* **196** (4297), 1443–1446. DOI: 10.1126/science.196.4297.1443.

Short, S. A., D. C. White, and M. I. Aleem (1969). Phospholipid metabolism in *Ferrobacillus ferrooxidans*. *Journal of Bacteriology* **99** (1), 142–150.

Simon, J. (2002). Enzymology and bioenergetics of respiratory nitrite ammonification. *FEMS Microbiology Reviews* **26** (3), 285–309. DOI: 10.1111/j.1574-6976.2002.tb00616.x.

Sinninghe Damsté, J. S., S. G. Wakeham, M. E. Kohnen, J. M. Hayes, and J. W. de Leeuw (1993). A 6,000-year sedimentary molecular record of chemocline excursions in the Black Sea. *Nature* **362** (6423), 827–829. DOI: 10.1038/362827a0.

Sinninghe Damsté, J. S., E. C. Hopmans, R. D. Pancost, S. Schouten, and J. A. J. Geenevasen (2000). Newly discovered non-isoprenoid glycerol dialkyl glycerol tetraether lipids in sediments. *Chemical Communications* (17), 1683–1684. DOI: 10.1039/b004517i.

Sinninghe Damsté, J. S., W. I. C. Rijpstra, E. C. Hopmans, M.-Y. Jung, J.-G. Kim, S.-K. Rhee, M. Stieglmeier, and C. Schleper (2012). Intact polar and core glycerol dibiphytanyl glycerol tetraether lipids of group I.1a and I.1b *Thaumarchaeota* in soil. *Applied and Environmental Microbiology* **78** (19), 6866–6874. DOI: 10.1128/AEM.01681-12.

Sinninghe Damsté, J. S., W. I. C. Rijpstra, E. C. Hopmans, S. Schouten, M. Balk, and A. J. M. Stams (2007). Structural characterization of diabolic acid-based tetraester, tetraether and mixed ether/ester, membrane-spanning lipids of bacteria from the order *Thermotogales*. *Archives of Microbiology* **188** (6), 629–641. DOI: 10.1007/s00203-007-0284-z.

Sinninghe Damsté, J. S., W. I. C. Rijpstra, E. C. Hopmans, J. W. H. Weijers, B. U. Foesel, J. Overmann, and S. N. Dedysh (2011). 13,16-Dimethyl octacosanedioic acid (iso-diabolic acid), a common membrane-spanning lipid of Acidobacteria subdivisions 1 and 3. *Applied and environmental microbiology* **77** (12), 4147–54. DOI: 10.1128/AEM.00466-11.

Sinninghe Damsté, J. S., S. Schouten, E. C. Hopmans, A. C. T. van Duin, and J. A. J. Geenevasen (2002). Crenarchaeol: the characteristic core glycerol dibiphytanyl glycerol tetraether membrane lipid of cosmopolitan pelagic crenarchaeota. *The Journal of Lipid Research* **43** (10), 1641–1651. DOI: 10.1194/jlr.M200148-JLR200.

Sittig, M. and H. Schlesner (1993). Chemotaxonomic Investigation of Various Prosthecate and/or Budding Bacteria. *Systematic and Applied Microbiology* **16** (1), 92–103. DOI: 10.1016/S0723-2020(11)80253-5.

Smith, D., G. Eglinton, and R. Morris (1983). Occurrence of long-chain alkan-diols and alkan-15-one-1-ols in a quaternary sapropel from the Eastern Mediterranean. English. *Lipids* **18** (12), 902–905. DOI: 10.1007/BF02534571.

Smith, M., P. De Deckker, J. Rogers, J. Brocks, J. Hope, S. Schmidt, R. Lopes dos Santos, and S. Schouten (2013). Comparison of UK37, TEXH86 and LDI temperature proxies for reconstruction of south-east Australian ocean temperatures. *Organic Geochemistry* **64**, 94–104. DOI: 10.1016/j.orggeochem.2013.08.015.

Sojo, V., A. Pomiankowski, and N. Lane (2014). A bioenergetic basis for membrane divergence in Archaea and Bacteria. *PLoS Biology* **12** (8), e1001926. DOI: 10.1371/journal.pbio.1001926.

Sørensen, K. B. and A. Teske (2006). Stratified communities of active Archaea in deep marine subsurface sediments. *Applied and Environmental Microbiology* **72** (7), 4596–4603. DOI: 10.1128/AEM.00562-06.

Sørensen, P. G., R. P. Cox, and M. Miller (2008). Chlorosome lipids from *Chlorobium tepidum*: Characterization and quantification of polar lipids and wax esters. *Photosynthesis Research* **95** (2-3), 191–196. DOI: 10.1007/s11120-007-9242-5.

Sorokin, Y. I. (2002). *The Black Sea: Ecology and Oceanography*. Leiden, The Netherlands: Backhuys Publishers, p. 875.

Sorokin, Y. I., P. Y. Sorokin, V. A. Avdeev, D. Y. Sorokin, and S. V. Ilchenko (1995). Biomass, production and activity of bacteria in the Black Sea, with special reference to chemosynthesis and the sulfur cycle. *Hydrobiologia* **308**, 61–76. DOI: 10.1007/BF00037788.

Sousa, F. L., T. Thiergart, G. Landan, S. Nelson-Sathi, I. A. C. Pereira, J. F. Allen, N. Lane, and W. F. Martin (2013). Early bioenergetic evolution. *Philosophical Transactions of the Royal Society of London. Series B, Biological Sciences* **368** (1622), 20130088. DOI: 10.1098/rstb.2013.0088.

Spang, A., R. Hatzenpichler, C. Brochier-Armanet, T. Rattei, P. Tischler, E. Spieck, W. Streit, D. A. Stahl, M. Wagner, and C. Schleper (2010). Distinct gene set in two different lineages of ammonia-oxidizing archaea supports the phylum Thaumarchaeota. *Trends in Microbiology* **18** (8), 331–340. DOI: 10.1016/j.tim.2010.06.003.

Spang, A., J. H. Saw, S. L. Jørgensen, K. Zaremba-Niedzwiedzka, J. Martijn, A. E. Lind, R. van Eijk, C. Schleper, L. Guy, and T. J. G. Ettema (2015). Complex archaea that bridge the gap between prokaryotes and eukaryotes. *Nature*. DOI: 10.1038/nature14447.

Sperling, M., G. Schmiedl, C. Hemleben, K. Emeis, H. Erlenkeuser, and P. Grootes (2003). Black Sea impact on the formation of eastern Mediterranean sapropel S1? Evidence from the Marmara Sea. *Palaeogeography, Palaeoclimatology, Palaeoecology* **190**, 9–21. DOI: 10.1016/S0031-0182(02)00596-5.

Sprott, G. D., C. J. Dicaire, C. G. Choquet, G. B. Patel, and I. Ekiel (1993). Hydroxydiether Lipid Structures in *Methanosarcina* spp. and *Methanococcus voltae*. *Applied and Environmental Microbiology* **59** (3), 912–914.

Sprott, G. D., M. Meloche, and J. C. Richards (1991). Proportions of diether, macrocyclic diether, and tetraether lipids in *Methanococcus jannaschii* grown at different temperatures. *Journal of Bacteriology* **173** (12), 3907–3910.

Stadnitskaia, A., I. Bouloubassi, M. Elvert, K.-U. Hinrichs, and J. S. Sinninghe Damsté (2008). Extended hydroxyarchaeol, a novel lipid biomarker for anaerobic methanotrophy in cold seepage habitats. *Organic Geochemistry* **39** (8), 1007–1014. DOI: http://dx.doi.org/10.1016/j.orggeochem.2008.04.019.

Stahl, D. A. and J. R. de la Torre (2012). Physiology and Diversity of Ammonia-Oxidizing Archaea. *Annual Review of Microbiology* **66** (1), 83–101. DOI: 10.1146/annurev-micro-092611-150128.

Stams, A. J. M. and C. M. Plugge (2009). Electron transfer in syntrophic communities of anaerobic bacteria and archaea. *Nature Reviews Microbiology* **7** (8), 568–577. DOI: 10.1038/nrmicro2166.

Stanley, D. J. and C. Blanpied (1980). Late Quaternary water exchange between the eastern Mediterranean and the Black Sea. *Nature* **285** (5766), 537–541.

Stevens, H. and O. Ulloa (2008). Bacterial diversity in the oxygen minimum zone of the eastern tropical South Pacific. *Environmental Microbiology* **10** (5), 1244–1259. DOI: 10.1111/j.1462-2920.2007.01539.x.

Stewart, F. J., O. Ulloa, and E. F. DeLong (2012). Microbial metatranscriptomics in a permanent marine oxygen minimum zone. *Environmental Microbiology* **14** (1), 23–40. DOI: 10.1111/j.1462-2920.2010.02400.x.

Stiehl, T., J. Rullkötter, and A. Nissenbaum (2005). Molecular and isotopic characterization of lipids in cultured halophilic microorganisms from the Dead Sea and comparison with the sediment record of this hypersaline lake. *Organic Geochemistry* **36** (9), 1242–1251. DOI: 10.1016/j.orggeochem.2005.05.002.

Stock, A., H.-W. Breiner, M. Pachiadaki, V. Edgcomb, S. Filker, V. La Cono, M. M. Yakimov, and T. Stoeck (2012). Microbial eukaryote life in the new hypersaline deep-sea basin Thetis. *Extremophiles : life under extreme conditions* **16** (1), 21–34. DOI: 10.1007/s00792-011-0401-4.

Stramma, L., S. Schmidtko, L. a. Levin, and G. C. Johnson (2010). Ocean oxygen minima expansions and their biological impacts. *Deep-Sea Research Part I: Oceanographic Research Papers* **57** (4), 587–595. DOI: 10.1016/j.dsr.2010.01.005.

Sturt, H. F., R. E. Summons, K. Smith, M. Elvert, and K.-U. Hinrichs (2004). Intact polar membrane lipids in prokaryotes and sediments deciphered by high-performance liquid chromatography/electrospray ionization multistage mass spectrometry - new biomarkers for biogeochemistry and microbial ecology. *Rapid Communications in Mass Spectrometry* **18** (6), 617–628. DOI: 10.1002/rcm.1378.

Summons, R. E., A. S. Bradley, L. L. Jahnke, and J. R. Waldbauer (2006). Steroids, triterpenoids and molecular oxygen. *Philosophical transactions of the Royal Society of London. Series B, Biological sciences* **361** (May), 951–968. DOI: 10.1098/rstb.2006.1837.

Suutari, M. and S. Laakso (1994). Microbial Fatty Acids and Thermal Adaptation. *Critical Reviews in Microbiology* **20** (4), 285–328. DOI: 10.3109/10408419409113560.

Suzumura, M. (2005). Phospholipids in marine environments: A review. *Talanta* **66** (2 SPEC. ISS.), 422–434. DOI: 10.1016/j.talanta.2004.12.008.

Tarui, M., N. Tanaka, K. Tomura, M. Ohga, H. Morii, and Y. Koga (2007). Lipid component parts analysis of the hyperthermophilic sulfate-reducing archaeon *Archaeoglobus fulgidus*. *Journal of UOEH* **29** (2), 131–139.

Taylor, K. W. R., M. Huber, C. J. Hollis, M. T. Hernandez-Sanchez, and R. D. Pancost (2013). Re-evaluating modern and Palaeogene GDGT distributions: Implications for SST reconstructions. *Global and Planetary Change* **108**, 158–174. DOI: 10.1016/j.gloplacha.2013.06.011.

Tebo, B. M. (1991). Manganese(II) oxidation in the suboxic zone of the Black Sea. *Deep Sea Research Part A. Oceanographic Research Papers* **38** (1), S883–S905. DOI: 10.1016/S0198-0149(10)80015-9.

Teske, A. and K. B. Sørensen (2008). Uncultured archaea in deep marine subsurface sediments: have we caught them all? *The ISME journal* **2** (1), 3–18. DOI: 10.1038/ismej.2007.90.

Teske, A. P. (2006). Microbial communities of deep marine subsurface sediments: Molecular and cultivation surveys. *Geomicrobiology Journal* **23** (6), 357–368. DOI: 10.1080/01490450600875613.

Thamdrup, B., T. Dalsgaard, M. M. Jensen, O. Ulloa, L. Farías, and R. Escribano (2006). Anaerobic ammonium oxidation in the oxygen-deficient waters off northern Chile. *Limnology and Oceanography* **51** (5), 2145–2156. DOI: 10.4319/lo.2006.51.5.2145.

Thauer, R. K., A.-K. Kaster, H. Seedorf, W. Buckel, and R. Hedderich (2008). Methanogenic archaea: ecologically relevant differences in energy conservation. *Nature Reviews Microbiology* **6** (8), 579–591. DOI: 10.1038/nrmicro1931.

Thiel, V., A. Jenisch, G. Landmann, A. Reimer, and W. Michaelis (1997). Unusual distributions of long-chain alkenones and tetrahymanol from the highly alkaline Lake Van, Turkey. *Geochimica et Cosmochimica Acta* **61** (10), 2053–2064. DOI: http://dx.doi.org/10.1016/S0016-7037(97)00038-0.

Thurl, S., W. Witke, I. Buhrow, and W. Schäfer (1986). Different types of quinones from sulphur-dependent archaebacteria. *Biological Chemistry Hoppe-Seyler* **367** (3), 191–197. DOI: 10.1515/bchm3.1986.367.1.191.

Thurl, S. and W. Schäfer (1988). Lipids from the sulphur-dependent archaebacterium *Thermoproteus tenax*. *Biochimica et Biophysica Acta* **961** (2), 253–261. DOI: 10.1016/0005-2760(88)90120-8.

Thurl, S., I. Buhrow, and W. Schäfer (1985). New types of menaquinones from the thermophilic archaebacterium *Thermoproteus tenax*. *Biological Chemistry Hoppe-Seyler* **366** (2), 1079–1084. DOI: 10.1515/bchm3.1985.366.2.1079.

Tierney, J. E. and J. M. Russell (2009). Distributions of branched GDGTs in a tropical lake system: Implications for lacustrine application of the MBT/CBT paleoproxy. *Organic Geochemistry* **40** (9), 1032–1036. DOI: http://dx.doi.org/10.1016/j.orggeochem.2009.04.014.

Tierney, J. E. and M. P. Tingley (2014). A Bayesian, spatially-varying calibration model for the TEX_{86} proxy. *Geochimica et Cosmochimica Acta* **127**, 83–106. DOI: 10.1016/j.gca.2013.11.026.

Tietze, M., A. Beuchle, I. Lamla, N. Orth, M. Dehler, G. Greiner, and U. Beifuss (2003). Redox potentials of methanophenazine and CoB-S-S-CoM, factors involved in electron transport in Methanogenic archaea. *Chembiochem* **4** (4), 333–335. DOI: 10.1002/cbic.200390053.

Tindall, B. J., K. O. Stetter, and M. D. Collins (1989). A novel, fully saturated menaquinone from the thermophilic, sulphate-reducing archaebacterium *Archaeoglobus fulgidus*. *Microbiology* **135** (3), 693–696. DOI: 10.1099/00221287-135-3-693.

Tindall, B. J., V. Wray, R. Huber, and M. D. Collins (1991). A novel, fully saturated cyclic menaquinone in the archaebacterium *Pyrobaculum organotrophum*. *Systematic and Applied Microbiology* **14** (3), 218–221. DOI: 10.1016/S0723-2020(11)80371-1.

Tissot, B. and D. Welte (1978). *Petroleum formation and occurrence: a new approach to oil and gas exploration*. Springer-Verlag,New York, NY.

Tompkins, R. E. and L. E. Shephard (1979). Orca Basin: Depositional processes, geotechnical properties and clay mineralogy of Holocene sediments within an anoxic hypersaline basin, northwest Gulf of Mexico. *Marine Geology* **33** (3-4), 221–238. DOI: 10.1016/0025-3227(79)90082-3.

Toney, J. L., Y. Huang, S. C. Fritz, P. a. Baker, E. Grimm, and P. Nyren (2010). Climatic and environmental controls on the occurrence and distributions of long chain alkenones in lakes of the interior United States. *Geochimica et Cosmochimica Acta* **74** (5), 1563–1578. DOI: 10.1016/j.gca.2009.11.021.

Tornabene, T. G., T. A. Langworthy, G. Holzer, and J. Oró (1979). Squalenes, phytanes and other isoprenoids as major neutral lipids of methanogenic and thermoacidophilic "archaebacteria". *Journal of Molecular Evolution* **13** (1), 73–83. DOI: 10.1007/BF01732755.

Tourna, M., M. Stieglmeier, A. Spang, M. Könneke, A. Schintlmeister, T. Urich, M. Engel, M. Schloter, M. Wagner, A. Richter, and C. Schleper (2011). *Nitrososphaera viennensis*, an ammonia oxidizing archaeon from soil. *Proceedings of the National Academy of Sciences of the United States of America* **108** (20), 8420–8425. DOI: 10.1073/pnas.1013488108.

Trincone, A., V. Lanzotti, B. Nicolaus, W. Zillig, M. De Rosa, and A. Gambacorta (1989). Comparative Lipid Composition of Aerobically and Anaerobically Grown *Desulfurolobus ambivalens*, an Autotrophic Thermophilic Archaeobacterium. *Microbiology* **135** (10), 2751–2757. DOI: 10.1099/00221287-135-10-2751.

Trincone, A., B. Nicolaus, G. Palmieri, M. De Rosa, R. Huber, G. Huber, K. O. Stetter, and A. Gambacorta (1992). Distribution of complex and core lipids within new hyperthermophilic members of the *Archaea* domain. *Systematic and Applied Microbiology* **15** (1), 11–17. DOI: 10.1016/S0723-2020(11)80130-X.

Turich, C., K. H. Freeman, M. A. Bruns, M. Conte, A. D. Jones, and S. G. Wakeham (2007). Lipids of marine Archaea: Patterns and provenance in the water-column and sediments. *Geochimica et Cosmochimica Acta* **71** (13), 3272–3291. DOI: 10.1016/j.gca.2007.04.013.

Uda, I., A. Sugai, Y. H. Itoh, and T. Itoh (2001). Variation in molecular species of polar lipids from Thermoplasma acidophilum depends on growth temperature. *Lipids* **36** (1), 103–105. DOI: 10.1007/s11745-001-0914-2.

Urakawa, H., T. Yoshida, M. Nishimura, and K. Ohwada (2000). Characterization of depth-related population variation in microbial communities of a coastal marine sediment using 16S rDNA-based approaches and quinone profiling. *Environmental Microbiology* **2** (5), 542–554. DOI: 10.1046/j.1462-2920.2000.00137.x.

Urakawa, H., T. Yoshida, M. Nishimura, and K. Ohwada (2001). Characterization of microbial communities in marine surface sediments by terminal-restriction fragment length polymorphism (T-RFLP) analysis and quinone profiling. *Marine Ecology Progress Series* **220**, 47–57. DOI: 10.3354/meps220047.

Urakawa, H., T. Yoshida, M. Nishimura, and K. Ohwada (2005). Characterization of depth-related changes and site-specific differences of microbial communities in marine sediments using quinone profiles. *Fisheries Science* **71** (1), 174–182. DOI: 10.1111/j.1444-2906.2005.00945.x.

Valentine, D. L. (2007). Adaptations to energy stress dictate the ecology and evolution of the Archaea. *Nature Reviews Microbiology* **5** (4), 316–323. DOI: 10.1038/nrmicro1619.

Valentine, D. L. (2009). Isotopic remembrance of metabolism past. *Proceedings of the National Academy of Sciences of the United States of America* **106** (31), 12565–12566. DOI: 10.1073/pnas.0906428106.

Valentine, D. L. (2011). Emerging Topics in Marine Methane Biogeochemistry. *Annual Review of Marine Science* **3** (1), 147–171. DOI: 10.1146/annurev-marine-120709-142734.

Van Cappellen, P., E. Viollier, A. Roychoudhury, L. Clark, E. Ingall, K. Lowe, and T. Dichristina (1998). Biogeochemical Cycles of Manganese and Iron at the Oxic–Anoxic Transition of a Stratified Marine Basin (Orca Basin, Gulf of Mexico). *Environmental Science & Technology* **32** (19), 2931–2939. DOI: 10.1021/es980307m.

Van der Wielen, P. W. J. J., H. Bolhuis, S. Borin, D. Daffonchio, C. Corselli, L. Giuliano, G. D'Auria, G. J. de Lange, A. Huebner, S. P. Varnavas, J. Thomson, C. Tamburini, D. Marty, T. J. McGenity, and K. N. Timmis (2005). The enigma of prokaryotic life in deep hypersaline anoxic basins. *Science* **307** (5706), 121–123. DOI: 10.1126/science.1103569.

Van Mooy, B. A. S. and H. F. Fredricks (2010). Bacterial and eukaryotic intact polar lipids in the eastern subtropical South Pacific: Water-column distribution, planktonic sources, and fatty

acid composition. *Geochimica et Cosmochimica Acta* **74** (22), 6499–6516. DOI: 10.1016/j.gca.2010.08.026.

Van Mooy, B. A. S., H. F. Fredricks, B. E. Pedler, S. T. Dyhrman, D. M. Karl, M. Koblízek, M. W. Lomas, T. J. Mincer, L. R. Moore, T. Moutin, M. S. Rappé, and E. A. Webb (2009). Phytoplankton in the ocean use non-phosphorus lipids in response to phosphorus scarcity. *Nature* **458** (7234), 69–72. DOI: 10.1038/nature07659.

Van Mooy, B. A. S., G. Rocap, H. F. Fredricks, C. T. Evans, and A. H. Devol (2006). Sulfolipids dramatically decrease phosphorus demand by picocyanobacteria in oligotrophic marine environments. *Proceedings of the National Academy of Sciences of the United States of America* **103** (23), 8607–8612. DOI: 10.1073/pnas.0600540103.

Van Vleet, E. S. and J. G. Quinn (1979). Early diagenesis of fatty acids and isoprenoid alcohols in estuarine and coastal sediments. *Geochimica et Cosmochimica Acta* **43** (3), 289–303. DOI: 10.1016/0016-7037(79)90195-9.

Vardi, A., B. A. S. Van Mooy, H. F. Fredricks, K. J. Popendorf, J. E. Ossolinski, L. Haramaty, and K. D. Bidle (2009). Viral Glycosphingolipids Induce Lytic Infection and Cell Death in Marine Phytoplankton. *Science* **326** (5954), 861–865. DOI: 10.1126/science.1177322.

Ventosa, A., J. J. Nieto, and A. Oren (1998). Biology of Moderately Halophilic Aerobic Bacteria. *Microbiology and Molecular Biology Reviews* **62** (2), 504–544.

Versteegh, G. J. M. and J. W. de Leeuw (1997). Potential palaeoenvironmental information of C_{24} to C_{36} mid-chain diols, keto-ols and mid-chain hydroxy fatty acids; a critical review. *Organic Geochemistry* **27** (97), 1–13.

Versteegh, G. J. M., R. Riegman, J. W. D. Leeuw, and J. H. F. F. Jansen (2001). $U_{37}^{K'}$ values for Isochrysis galbana as a function of culture temperature, light intensity and nutrient concentrations. *Organic Geochemistry* **32**, 785–794.

Vetriani, C., H. V. Tran, and L. J. Kerkhof (2003). Fingerprinting microbial assemblages from the oxic/anoxic chemocline of the Black Sea. *Applied and Environmental Microbiology* **69** (11), 6481–6488. DOI: 10.1128/AEM.69.11.6481.

Vidal, L., G. Ménot, C. Joly, H. Bruneton, F. Rostek, M. N. Çağatay, C. Major, and E. Bard (2010). Hydrology in the Sea of Marmara during the last 23 ka: Implications for timing of Black Sea connections and sapropel deposition. *Paleoceanography* **25** (1), PA1205. DOI: 10.1029/2009PA001735.

Vidal, M., C. M. Duarte, and S. Agusti (1999). Dissolved organic nitrogen and phosphorus pools and fluxes in the central Atlantic Ocean. *Limnology and Oceanography* **44** (1), 106–115. DOI: 10.4319/lo.1999.44.1.0106.

Villanueva, J. and J. O. Grimalt (1997). Gas Chromatographic Tuning of the $U_{37}^{K'}$ Paleothermometer. *Analytical Chemistry* **69** (16), 3329–3332. DOI: 10.1021/ac9700383.

Villanueva, J., C. Pelejero, and J. O. Grimalt (1997). Clean-up procedures for the unbiased estimation of C_{37} alkenone sea surface temperatures and terrigenous n-alkane inputs in paleoceanography. *Journal of Chromatography A* **757** (1â€“2), 145–151. DOI: http://dx.doi.org/10.1016/S0021-9673(96)00669-3.

Villanueva, L., J. del Campo, R. Guerrero, and R. Geyer (2010). Intact phospholipid and quinone biomarkers to assess microbial diversity and redox state in microbial mats. *Microbial Ecology* **60** (1), 226–238. DOI: 10.1007/s00248-010-9645-2.

Völkl, P., R. Huber, E. Drobner, R. Rachel, S. Burggraf, A. Trincone, and K. O. Stetter (1993). *Pyrobaculum aerophilum* sp. nov., a novel nitrate-reducing hyperthermophilic archaeum. *Applied and Environmental Microbiology* **59** (9), 2918–2926.

Volkman, J. K., S. M. Barrett, S. I. Blackburn, M. P. Mansour, E. L. Sikes, and F. Gelin (1998). Microalgal biomarkers: A review of recent research developments. *Organic Geochemistry* **29** (5â€“7), 1163–1179. DOI: http://dx.doi.org/10.1016/S0146-6380(98)00062-X.

Volkman, J. K., S. M. Barrett, G. A. Dunstan, and S. W. Jeffrey (1992). C_{30}-C_{32} alkyl diois and unsaturated alcohols in microalgae of the class Eustigmatophyceae. *Organic Geochemistry* **18** (1), 131–138.

Vreeland, R. H. (1987). Mechanisms of halotolerance in microorganisms. *Critical reviews in microbiology* **14** (4), 311–356. DOI: 10.3109/10408418709104443.

Wagner, G. C., R. J. Kassner, and M. D. Kamen (1974). Redox Potentials of Certain Vitamins K: Implications for a Role in Sulfite Reduction by Obligately Anaerobic Bacteria. *Proceedings of the National Academy of Sciences of the United States of America* **71** (2), 253–256. DOI: 10.1073/pnas.71.2.253.

Wakeham, S. G., R. Amann, K. H. Freeman, E. C. Hopmans, B. B. Jørgensen, I. F. Putnam, S. Schouten, J. S. Sinninghe Damsté, H. M. Talbot, and D. Woebken (2007). Microbial ecology of the stratified water column of the Black Sea as revealed by a comprehensive biomarker study. *Organic Geochemistry* **38** (12), 2070–2097. DOI: 10.1016/j.orggeochem.2007.08.003.

Waldbauer, J. R., L. S. Sherman, D. Y. Sumner, and R. E. Summons (2009). Late Archean molecular fossils from the Transvaal Supergroup record the antiquity of microbial diversity and aerobiosis. *Precambrian Research* **169**, 28–47. DOI: 10.1016/j.precamres.2008.10.011.

Walker, C. B., J. R. de la Torre, M. G. Klotz, H. Urakawa, N. Pinel, D. J. Arp, C. Brochier-Armanet, P. S. G. Chain, P. P. Chan, A. Gollabgir, J. Hemp, M. Hügler, E. A. Karr, M. Könneke, M. Shin, T. J. Lawton, T. Lowe, W. Martens-Habbena, L. A. Sayavedra-Soto, D. Lang, S. M. Sievert, A. C. Rosenzweig, G. Manning, and D. A. Stahl (2010). *Nitrosopumilus maritimus* genome reveals unique mechanisms for nitrification and autotrophy in globally distributed marine crenarchaea. *Proceedings of the National Academy of Sciences of the United States of America* **107** (19), 8818–8823. DOI: 10.1073/pnas.0913533107.

Wallmann, K., F. Aghib, D. Castradori, M. Cita, E. Suess, J. Greinert, and D. Rickert (2002). Sedimentation and formation of secondary minerals in the hypersaline Discovery Basin, eastern Mediterranean. *Marine Geology* **186** (1-2), 9–28. DOI: 10.1016/S0025-3227(02)00170-6.

Wallmann, K., E. Suess, G. H. Westbrook, G. Winckler, and M. B. Cita (1997). Salty brines on the Mediterranean sea floor. *Nature* **387** (6628), 31–32.

Walsh, D. A., E. Zaikova, C. G. Howes, Y. C. Song, J. J. Wright, S. G. Tringe, P. D. Tortell, and S. J. Hallam (2009). Metagenome of a versatile chemolithoautotroph from expanding oceanic dead zones. *Science* **326** (5952), 578–582. DOI: 10.1126/science.1175309.

Ward, N., J. T. Staley, J. A. Fuerst, S. Giovannoni, and E. Schlesner, H. Stackebrandt (2006). The order Planctomycetales, including the genera Planctomyces, Pirellula, Gemmata and Isosphaera and the Candidatus genera Brocadia, Kuenenia and Scalindua. In: *The Prokaryotes, Volume 3: Archaea. Bacteria: Firmicutes, Actinomycetes*. Ed. by M. Dworkin, S. Falkow, E. Rosenberg, K.-H. Schleifer, and E. Stackebrandt. New York, USA: Springer, pp. 757–793.

Webster, G., L. C. Watt, J. Rinna, J. C. Fry, R. P. Evershed, R. J. Parkes, and A. J. Weightman (2006). A comparison of stable-isotope probing of DNA and phospholipid fatty acids to study prokaryotic functional diversity in sulfate-reducing marine sediment enrichment slurries. *Environmental Microbiology* **8** (9), 1575–1589. DOI: 10.1111/j.1462-2920.2006.01048.x.

Wefer, G. (2010). *Dynamische Erde-Zukunftsaufgaben der Geowissenschaften: Strategieschrift*. MARUM, Univ. Bremen.

Wei, Y., J. Wang, J. Liu, L. Dong, L. Li, H. Wang, P. Wang, M. Zhao, and C. L. Zhang (2011). Spatial variations in archaeal lipids of surface water and core-top sediments in the South china sea and their implications for paleoclimate studies. *Applied and Environmental Microbiology* **77** (21), 7479–7489. DOI: 10.1128/AEM.00580-11.

Weijers, J. W. H., S. Schouten, E. C. Hopmans, J. A. J. Geenevasen, O. R. P. David, J. M. Coleman, R. D. Pancost, and J. S. Sinninghe Damsté (2006). Membrane lipids of mesophilic anaerobic bacteria thriving in peats have typical archaeal traits. *Environmental Microbiology* **8** (4), 648–657. DOI: 10.1111/j.1462-2920.2005.00941.x.

Weijers, J. W. H., S. Schouten, J. C. van den Donker, E. C. Hopmans, and J. S. Sinninghe Damsté (2007). Environmental controls on bacterial tetraether membrane lipid distribution in soils. *Geochimica et Cosmochimica Acta* **71** (3), 703–713. DOI: 10.1016/j.gca.2006.10.003.

Wellsbury, P., K. Goodman, T. Barth, B. A. Cragg, S. P. Barnes, and R. J. Parkes (1997). Deep marine biosphere fuelled by increasing organic matter availability during burial and heating. *Nature* **388**, 573–576.

White, D. C., W. M. Davis, J. S. Nickels, J. D. King, and R. J. Bobbie (1979). Determination of the sedimentary microbial biomass by extractible lipid phosphate. *Oecologia* **40** (1), 51–62. DOI: 10.1007/BF00388810.

Whiticar, M. J., E. Faber, and M. Schoell (1986). Biogenic methane formation in marine and freshwater environments: CO_2 reduction vs. acetate fermentation–Isotope evidence. *Geochimica et Cosmochimica Acta* **50** (5), 693–709. DOI: 10.1016/0016-7037(86)90346-7.

Whiticar, M. J. (1999). Carbon and hydrogen isotope systematics of bacterial formation and oxidation of methane. *Chemical Geology* **161** (1-3), 291–314. DOI: 10.1016/S0009-2541(99)00092-3.

Whittaker, M., D. Bergmann, D. Arciero, and A. B. Hooper (2000). Electron transfer during the oxidation of ammonia by the chemolithotrophic bacterium *Nitrosomonas europaea*. *Biochimica et Biophysica Acta* **1459** (2-3), 346–355. DOI: 10.1016/S0005-2728(00)00171-7.

Widdel, F. and F. Bak (1992). Gram-negative mesophilic sulfate-reducing bacteria. In: *The Prokaryotes. A Handbook on the Biology of Bacteria: Ecophysiology, Isolation, Identification, Application.* Ed. by A. Ballows, H. G. Trüper, M. Dworkin, W. Harder, and K.-H. Schleifer. 2nd ed. New York: Springer, pp. 3352–3378.

Wissenbach, U., A. Kröger, and G. Unden (1990). The specific functions of menaquinone and demethylmenaquinone in anaerobic respiration with fumarate, dimethylsulfoxide, trimethylamine N-oxide and nitrate by *Escherichia coli*. *Archives of Microbiology* **154** (1), 60–66. DOI: 10.1007/BF00249179.

Woese, C. R. and G. E. Fox (1977). Phylogenetic structure of the prokaryotic domain: the primary kingdoms. *Proceedings of the National Academy of Sciences of the United States of America* **74** (11), 5088–5090. DOI: 10.1073/pnas.74.11.5088.

Woese, C. R., O. Kandler, and M. L. Wheelis (1990). Towards a natural system of organisms: proposal for the domains Archaea, Bacteria, and Eucarya. *Proceedings of the National Academy of Sciences of the United States of America* **87** (12), 4576–4579. DOI: 10.1073/pnas.87.12.4576.

Wörmer, L., J. S. Lipp, J. M. Schröder, and K.-U. Hinrichs (2013). Application of two new LC–ESI–MS methods for improved detection of intact polar lipids (IPLs) in environmental samples. *Organic Geochemistry* **59**, 10–21. DOI: 10.1016/j.orggeochem.2013.03.004.

Wright, J. J., K. M. Konwar, and S. J. Hallam (2012). Microbial ecology of expanding oxygen minimum zones. *Nature Reviews Microbiology* **10** (6), 381–394. DOI: 10.1038/nrmicro2778.

Wuchter, C., B. Abbas, M. J. L. Coolen, L. Herfort, J. van Bleijswijk, P. Timmers, M. Strous, E. Teira, G. J. Herndl, J. J. Middelburg, S. Schouten, and J. S. Sinninghe Damsté (2006). Archaeal nitrification in the ocean. *Proceedings of the National Academy of Sciences of the United States of America* **103** (33), 12317–12322. DOI: 10.1073/pnas.0600756103.

Wuchter, C., S. Schouten, M. J. L. Coolen, and J. S. Sinninghe Damsté (2004). Temperature-dependent variation in the distribution of tetraether membrane lipids of marine Crenarchaeota: Implications for TEX_{86} paleothermometry. *Paleoceanography* **19** (4), PA4028. DOI: 10.1029/2004PA001041.

Xie, S., J. S. Lipp, G. Wegener, T. G. Ferdelman, and K.-U. Hinrichs (2013). Turnover of microbial lipids in the deep biosphere and growth of benthic archaeal populations. *Proceedings of the National Academy of Sciences of the United States of America* **110** (15), 6010–6014. DOI: 10.1073/pnas.1218569110.

Xie, S., X.-L. Liu, F. Schubotz, S. G. Wakeham, and K.-U. Hinrichs (2014). Distribution of glycerol ether lipids in the oxygen minimum zone of the Eastern Tropical North Pacific Ocean. *Organic Geochemistry* **71**, 60–71. DOI: 10.1016/j.orggeochem.2014.04.006.

Yakimov, M. M., V. La Cono, R. Denaro, G. D'Auria, F. Decembrini, K. N. Timmis, P. N. Golyshin, and L. Giuliano (2007). Primary producing prokaryotic communities of brine, interface and seawater above the halocline of deep anoxic lake L'Atalante, Eastern Mediterranean Sea. *The ISME journal* **1** (8), 743–755. DOI: 10.1038/ismej.2007.83.

Yakimov, M. M., V. La Cono, G. L. Spada, G. Bortoluzzi, E. Messina, F. Smedile, E. Arcadi, M. Borghini, M. Ferrer, P. Schmitt-Kopplin, N. Hertkorn, J. A. Cray, J. E. Hallsworth, P. N. Golyshin, and L. Giuliano (2015). Microbial community of the deep-sea brine Lake *Kryos* seawater-brine interface is active below the chaotropicity limit of life as revealed by recovery of mRNA. *Environmental Microbiology* **17**, 364–382. DOI: 10.1111/1462-2920.12587.

Yamauchi, K., K. Doi, Y. Yoshida, and M. Kinoshita (1993). Archaebacterial lipids: highly proton-impermeable membranes from 1,2-diphytanyl-sn-glycero-3-phosphocoline. *Biochimica et Biophysica Acta* **1146** (2), 178–182. DOI: 10.1016/0005-2736(93)90353-2.

Yoshinaga, M. Y., E. J. Gagen, L. Wörmer, N. K. Broda, T. B. Meador, J. Wendt, M. Thomm, and K.-U. Hinrichs (2015a). *Methanothermobacter thermautotrophicus* modulates its membrane lipids in response to hydrogen and nutrient availability. *Frontiers in Microbiology* **6**, 5. DOI: 10.3389/fmicb.2015.00005.

Yoshinaga, M. Y., T. Holler, T. Goldhammer, G. Wegener, J. W. Pohlman, B. Brunner, M. M. M. Kuypers, K.-U. Hinrichs, and M. Elvert (2014). Carbon isotope equilibration during sulphate-limited anaerobic oxidation of methane. *Nature Geoscience* **7** (3), 190–194. DOI: 10.1038/ngeo2069.

Yoshinaga, M. Y., M. Y. Kellermann, P. E. Rossel, F. Schubotz, J. S. Lipp, and K.-U. Hinrichs (2011). Systematic fragmentation patterns of archaeal intact polar lipids by high-performance liquid chromatography/electrospray ionization ion-trap mass spectrometry. *Rapid communications in mass spectrometry* **25** (23), 3563–3574. DOI: 10.1002/rcm.5251.

Yoshinaga, M. Y., C. S. Lazar, M. Elvert, Y.-S. Lin, C. Zhu, V. B. Heuer, A. Teske, and K.-U. Hinrichs (2015b). Possible roles of uncultured archaea in carbon cycling in methane-seep sediments. *Geochimica et Cosmochimica Acta* **164**, 35–52. DOI: http://dx.doi.org/10.1016/j.gca.2015.05.003.

You, L., B. Zhang, and Y. J. Tang (2014). Application of stable isotope-assisted metabolomics for cell metabolism studies. *Metabolites* **4** (2), 142–65. DOI: 10.3390/metabo4020142.

Zabel, M. and Cruise Participants (2013). *RV METEOR, Cruise Report M84/L1, Biogeochemistry and methane hydrates of the Black Sea; Oceanography of the Mediterranean; Shelf sedimentation and cold water carbonates*. DFG Senatskommission für Ozeanographie, p. 39. DOI: 10.2312/cr_m84_1.

Zabel, M., A. Boetius, K.-C. Emeis, T. G. Ferdelman, and V. Spieß (2008). *Cruise Report M76/L1, M76/L2, M76/L3a+b, PROSA Process studies in the eastern South Atlantic*. DFG Senatskommission für Ozeanographie. DOI: 10.2312/cr_m76.

Zech, R., L. Gao, R. Tarozo, and Y. Huang (2012). Branched glycerol dialkyl glycerol tetraethers in Pleistocene loess-paleosol sequences: Three case studies. *Organic Geochemistry* **53**, 38–44. DOI: 10.1016/j.orggeochem.2012.09.005.

Zhang, C. L., J. Wang, Y. Wei, C. Zhu, L. Huang, and H. Dong (2011). Production of branched tetraether lipids in the lower pearl river and estuary: Effects of extraction methods and impact on bGDGT proxies. *Frontiers in Microbiology* **2** (January), 274. DOI: 10.3389/fmicb.2011.00274.

Zhang, Y.-M. and C. O. Rock (2008). Membrane lipid homeostasis in bacteria. *Nature Reviews Microbiology* **6** (3), 222–233. DOI: 10.1038/nrmicro1839.

Zhi, X.-Y. Y., J.-C. C. Yao, S.-K. K. Tang, Y. Huang, H.-W. W. Li, and W.-J. J. Li (2014). The futalosine pathway played an important role in menaquinone biosynthesis during early prokaryote evolution. *Genome Biology and Evolution* **6** (1), 149–160. DOI: 10.1093/gbe/evu007.

Zhu, C., J. S. Lipp, L. Wörmer, K. W. Becker, J. Schröder, and K.-U. Hinrichs (2013a). Comprehensive glycerol ether lipid fingerprints through a novel reversed phase liquid chromatography-mass spectrometry protocol. *Organic Geochemistry* **65**, 53–62. DOI: 10.1016/j.orggeochem.2013.09.012.

Zhu, C., T. B. Meador, W. Dummann, and K.-U. Hinrichs (2014a). Identification of unusual butanetriol dialkyl glycerol tetraether and pentanetriol dialkyl glycerol tetraether lipids in marine sediments. *Rapid Communications in Mass Spectrometry* **28** (4), 332–338. DOI: 10.1002/rcm.6792.

Zhu, C., M. Y. Yoshinaga, C. A. Peters, X.-L. Liu, M. Elvert, and K.-U. Hinrichs (2014b). Identification and significance of unsaturated archaeal tetraether lipids in marine sediments. *Rapid Communications in Mass Spectrometry* **28** (10), 1144–1152. DOI: 10.1002/rcm.6887.

Zhu, R., T. W. Evans, L. Wörmer, Y.-S. Lin, C. Zhu, and K.-U. Hinrichs (2013b). Improved sensitivity of sedimentary phospholipid analysis resulting from a novel extract cleanup strategy. *Organic Geochemistry* **65**, 46–52. DOI: 10.1016/j.orggeochem.2013.10.002.

Zhuang, G. (2014). "Methylotrophic methanogenesis and potential methylated substrates in marine sediment". PhD Thesis.

Zink, K.-G., D. Leythaeuser, M. Melkonian, and L. Schwark (2001). Temperature dependency of long-chain alkenone distributions in recent to fossil limnic sediments and in lake waters1. *Geochimica et Cosmochimica Acta* **65** (2), 253–265. DOI: http://dx.doi.org/10.1016/S0016-7037(00)00509-3.

Zink, K.-G., H. Wilkes, U. Disko, M. Elvert, and B. Horsfield (2003). Intact phospholipids-microbial "life markers" in marine deep subsurface sediments. *Organic Geochemistry* **34** (6), 755–769. DOI: 10.1016/S0146-6380(03)00041-X.

Ziveri, P., C. Grandi, A. Stefanetti, and M. B. Cita (1995). Biogenic fluxes in Bannock Basin: first results from a sediment trap study (November 1991 - May 1992). Italian. *Rendiconti Lincei* **6** (2), 131–145. DOI: 10.1007/BF03001662.

N a m e : ..... Datum .....

Anschrift : .....

E r k l ä r u n g

Hiermit versichere ich, dass ich

1. die Arbeit ohne unerlaubte fremde Hilfe angefertigt habe,

2. keine anderen als die von mir angegebenen Quellen und Hilfsmittel benutzt habe und

3. die den benutzten Werken wörtlich oder inhaltlich entnommenen Stellen als solche kenntlich gemacht habe.

_____, den .....

(Unterschrift)